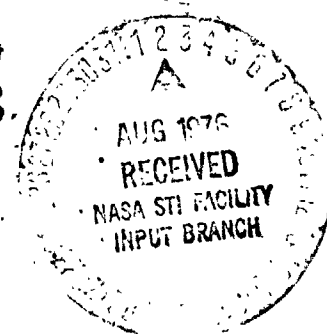


NASA TM-X-71159

X-662-76-154

PREPRINT

THE STRUCTURE AND CONTENT OF THE GALAXY AND GALACTIC GAMMA RAYS



JUNE 1976



**GODDARD SPACE FLIGHT CENTER
GREENBELT, MARYLAND**

(NASA-TM-X-71159) THE STRUCTURE AND CONTENT
OF THE GALAXY AND GALACTIC GAMMA RAYS (NASA)
416 p HC \$11.00 CSCL 03B

N76-29110
THRU
N76-29132
Unclas
45966

G3/90

THE STRUCTURE AND CONTENT OF THE GALAXY
AND
GALACTIC GAMMA RAYS

The proceedings of an international symposium held at
NASA's Goddard Space Flight Center, Greenbelt, Maryland
June 2-4, 1976

PREFACE

The following papers in this preprint include all of the invited papers from the Second International Gamma-Ray Symposium held at NASA Goddard Space Flight Center, June 2-4, 1976 entitled "The Structure and Content of the Galaxy and Galactic Gamma-Rays".

A glance at the contents of this preprint will show that this was not just a γ -ray symposium, but in reality a symposium on galactic structure drawing on all branches of galactic astronomy with emphasis on the implications of the new γ -ray observations. The following papers are not just reviews; they include much new and previously unpublished material including (1) the first reported results from the COS-B γ -ray satellite presented by our European colleagues, (2) new SAS-2 results on γ -ray pulsars, Cygnus X-3 and new maps of the galactic diffuse flux, (3) very recent data from CO surveys of the galaxy, (4) new high resolution radio surveys of external galaxies, (5) new results on the galactic distribution of pulsars and (6) new theoretical work on galactic γ -ray emission. For this reason, the committee felt the need to make this preprint available shortly after the symposium in order to provide the astrophysical community with this new work well before the proceedings are published in final book form by NASA.

Other copies of this preprint will be available on a limited basis by writing one of the committee members.

Carl E. Fichtel
Floyd W. Stecker
NASA/Goddard Space Flight Center
Greenbelt, Maryland 20771
June 1976

ORGANIZING COMMITTEE

C. Crannell

C. Fichtel*

F. Jones

D. Kniffen

F. Stecker*

D. Thompson

J. Trombka

*Co-Chairmen

AGENDA FOR GAMMA RAY SYMPOSIUM

"THE STRUCTURE AND CONTENT OF THE GALAXY AND GALACTIC GAMMA RAYS"

<u>June 2, 1976</u>	<u>Page</u>
Introductory Remarks - Floyd Stecker	
Welcome - John F. Clark, Director NASA/Goddard Space Flight Center	vii
Morning Chairman: Raymond Wills, European Space Research and Technology Centre, Noordwijk, The Netherlands	
SAS-2 Galactic Gamma Ray Results-I - David Thompson NASA/Goddard Space Flight Center	1
SAS-2 Galactic Gamma Ray Results-II - Robert Hartman NASA/Goddard Space Flight Center	12
The COS-B Experiment and Mission - Boudewijn Swanenburg, Huygens Laboratorium, The Netherlands	23
COS-B Intensity Profiles of High-Energy Gamma Radiation From the Galaxy	
Part 1, Galactic Disk - Jacques Paul, CEN Saclay, France	39
Part 2, Localized Sources - Hans Mayer Hasselwander Max Planck Institut, W. Germany	45
The Time Structure of the Gamma-Ray Emission from the Crab and Vela Pulsars - Rosolino Buccheri, Universita di Palermo, Italy	52
Afternoon Chairman: George F. Pieper, NASA/Goddard Space Flight Center	
Low and Medium Energy Gamma Rays - Gerald Share, U. S. Naval Research Laboratory, Washington, D. C., U.S.A.	65
Very High Energy Gamma Rays - Jonathan Grindlay, Center for Astrophysics, Cambridge, Mass., U.S.A.	84
Pulsar Theory and Cosmic Ray Origin, Peter Sturrock, Institute of Plasma Research, Stanford University, Stanford, CA, U.S.A.	108

	<u>Page</u>
Gamma Ray Pulsars - Hakki Ugelman Middle East Technical University, Ankara, Turkey	118
Contributed "hot topic" papers	126

June 3, 1976

Morning Chairman: Maurice Shapiro, U. S. Naval Research Laboratory, Washington, D. C. U.S.A.	
Density Wave Theory - William Roberts, Jr., University of Virginia, Charlottesville, Va., U.S.A.	128
Observations of Molecular Clouds - Nicholas Scoville, University of Massachusetts, Amherst, Mass., U.S.A.	163
Galactic Atomic and Ionized Hydrogen - W. Butler Burton, National Radio Astronomy Obs., Charlottesville, Va., U.S.A.	177
Nonthermal Radio (Synchrotron) - John Baldwin Cavendish Laboratory, Cambridge, England	206
Infrared Astronomy and High Energy Astrophysics - Giovanni Fazio, Center for Astrophysics, Cambridge, Mass., U.S. A.	222
Afternoon Chairman: Arnold Wolfendale, University of Durham, England	
Ultraviolet Observations of Local Gas - Edward Jenkins, Princeton University, Princeton, N. J., U.S.A.	239
Small Scale Local Gamma Ray Features - Jean-Loup Puget, Observatoire de Meudon, France	255
Diffuse Galactic Gamma Ray Lines - Richard Lingenfelter, University of California, Los Angeles, CA, U.S.A.	264
Contributed "hot topic" papers	286

June 4, 1976

Page

Morning Chairman: Bernard Peters, Danish Space Research
Institute, Lyngby, Denmark

Continued presentation of "hot topic" papers 288

Supernova Origin of Cosmic Rays - David Arnett, 289
University of Illinois, Urbana, Illinois, U.S.A.

Galactic Distribution of Pulsars - John Seiradakis 299
Max-Planck-Institut, Bonn, Fed. Republic of Germany

Cosmic Ray Propagation and Containment - Eugene Parker, 320
University of Chicago, Chicago, Ill., U.S.A.

Gamma Rays and Large-Scale Galactic Structure - (1) - 341
Donald Kniffen, NASA/Goddard Space Flight Center

Afternoon Chairman: Livio Scarsi, Universita di Palermo,
Palermo, Italy

Gamma Rays and Large-Scale Galactic Structure - (2) - 357
Floyd Stecker, NASA/Goddard Space Flight Center

Summary and Panel Discussion - Giovanni Bignami,
University of Milan, Italy; Edward Chupp, University
of New Hampshire, U.S.A.; Carl Fichtel, NASA/Goddard
Space Flight Center, U.S.A.; Kenneth Greisen, Cornell
University, U.S.A.; Eugene Parker, University of
Chicago, U.S.A.; Volkes Schönfelder, Max-Planck-Institut,
West Germany; Evry Shatzman, Obs. de Meudon, France;
Jack Trombka, NASA/Goddard Space Flight Center, U.S.A.;
Raymond Wills, European Space Research and Technology
Center, The Netherlands.

Concluding Remarks - Carl Fichtel

Goddard Colloquium

Gamma Rays and the Structure of our Galaxy -
Kenneth Greisen, Cornell University, U.S.A.

Registered Participants of γ -Ray Symposium 392

WELCOME

John F. Clark, Director
NASA/Goddard Space Flight Center
Greenbelt, Md. 20771

It gives me great pleasure to welcome you to Goddard Space Flight Center to participate in our second international Gamma-Ray Symposium. We are all happy to see that so many distinguished members of the international scientific community are with us today.

There has been a deep interest in γ -ray astronomy at Goddard since shortly after Goddard was formed--not only because it was realized that the space age permitted this new astronomical window to be opened, but also because of the great significance of γ -ray astronomy which arises from its very direct relationship to the largest transfers of energy occurring in astrophysical processes.

At the time of the first international γ -ray symposium held here at Goddard just over three years ago, shortly after the launch of SAS-2, I expressed the hope that it would be the first of many fruitful international γ -ray symposia. That hope has become reality. In the following year, our colleagues at the European Space Agency held a symposium at Frascati in preparation for COS-B, the first results from which we will hear about this morning. ESA has also planned a symposium in the near future which, we are certain, will also be very successful.

The progress in γ -ray astronomy over the last three years has been very encouraging. The first fairly definitive results are now beginning to emerge particularly in regard to the galactic plane, and, as they do, great interest is evolving in the interrelationship between galactic structure, cosmic ray origin, the cosmic ray distribution in the galaxy, and γ -rays. Point sources are also beginning to emerge with one of the great surprises being the identification of several γ -ray pulsars with their radio counterparts. We are, of course, pleased at the active role that Goddard has been playing in both the observational and theoretical aspects of this work.

Our meeting this week will be of a somewhat different nature than the first symposium. It will address itself primarily to a particular task, namely that of determining the relationship of the new galactic γ -ray results to the overall problem of the structure, content, and dynamics of the galaxy. To this end, distinguished colleagues from other scientific disciplines of observational and theoretical astronomy

and astrophysics have been invited to report and review recent advances in these fields which also bear on these problems. We are confident that the interaction of knowledgeable scientists in these various fields will greatly further progress in determining the nature of our galaxy and its contents, both through dialogue and inspiration. Periods of free discussion and a panel discussion have been planned to further that dialogue.

The recent NASA report on the "Outlook for Space" to the year 2000 lists many questions which it is hoped that both NASA and the world space community will help answer and γ -ray astronomy should be prominently involved in the solution of these problems. To this end, this symposium, together with the one sponsored by ESLAB toward the end of this year should act as strong catalysts to stimulate even further continued strong research in this very important scientific field.

On that note for the future, I would once again like to thank you all for coming, welcome you to Goddard, and wish you the greatest success in your present work.

N76-29111

SAS-2 GALACTIC GAMMA RAY RESULTS I

D. J. Thompson, C. E. Fichtel, R. C. Hartman,
D. A. Kniffen, G. F. Bignami*, R. C. Lamb**

NASA/Goddard Space Flight Center
Laboratory for High Energy Astrophysics
Greenbelt, Maryland 20771

H. Ügelman, M. E. Özel, T. Tümer

Middle East Technical University
Physics Department
Ankara, Turkey

ABSTRACT

Continuing analysis of the data from the SAS-2 high energy γ -ray experiment has produced an improved picture of the sky at photon energies above 35 MeV. On a large scale, the diffuse emission from the galactic plane is the dominant feature observed by SAS-2. This galactic plane emission is most intense between galactic longitude 310° and 45° , corresponding to a region within 7 kpc of the galactic center. Within the high-intensity region, SAS-2 observes peaks around galactic longitudes 315° , 330° , 345° , 0° , and 35° . These peaks appear to be correlated with such galactic features and components as molecular hydrogen, atomic hydrogen, magnetic fields, cosmic ray concentrations, and photon fields.

*NAS-NRC Postdoctoral Research Associate 1973-75.

**On faculty leave from Iowa State University during 1975-76.

1. Introduction. Because high-energy γ -rays can be produced by a variety of mechanisms, observations of galactic γ -radiation can provide information about many different galactic components. γ -rays originating from neutral pions produced in collisions between cosmic ray nucleons and interstellar matter, for example, are related directly to the product of the cosmic ray and matter densities. Bremsstrahlung γ -rays represent a probe of the cosmic ray electron and interstellar matter distributions, while inverse Compton γ -rays relate the cosmic ray electrons to the photon fields in the galaxy. By combining the γ -ray measurements with other observations related to these galactic components, it may be possible to obtain a more complete picture of the galaxy than would be possible with any single set of observations alone. In simplest terms, then, the goal of this paper will be to present the SAS-2 results in their current form and to try to indicate how these γ -ray observations may be related to other constituents of the galaxy.

2. Experimental. The SAS-2 experiment, the calibration procedure, and the methods of data analysis have all been described by Derdeyn et al. (1972) and Fichtel et al. (1975). The detector is a digitized, wire-grid spark chamber which uses as a triggering telescope an anti-coincidence scintillator dome, a set of scintillators, and a set of Cerenkov detectors. The energy threshold is somewhat less than 30 MeV, photon energies can be measured up to approximately 200 MeV, and an integral intensity can be obtained above 200 MeV. The two-dimensional angular resolution for γ -ray energies above 100 MeV is between 3° and 4° , depending on the incident spectrum.

Results from most of the SAS-2 observations along the galactic plane have been published previously (Fichtel et al., 1975). Since the time that these results were compiled, however, a number of changes have taken place to give improvements in the results: (1) New orbit-attitude solutions have been obtained for portions of the data. These solutions have provided greater accuracy for portions of the data already analyzed and have allowed the analysis of additional data for which no orbit-attitude information was previously available. (2) Some additional telemetry data became available. (3) A slightly different method of computing arrival directions for individual γ -rays was incorporated into the data analysis system. (4) Some inconsistencies in data analysis procedures between different observing periods were removed.

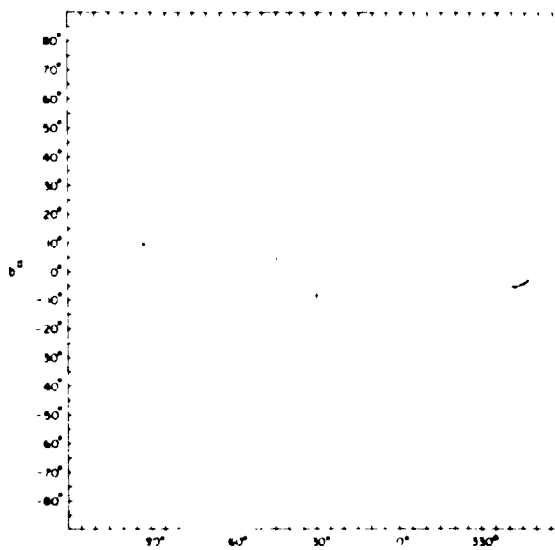
Two important features of these improvements should be emphasized. First, none of the adjustments change any of the large-scale features of the results. At most, these modifications enhance the statistics

for certain regions of the SAS-2 exposure and alter slightly the small-scale picture of the γ -ray sky. Second, at present not all of these changes have been included in the SAS-2 data base. Work is continuing on incorporating these changes. The reader is cautioned that the SAS-2 results presented here are not in final form, although the regions around the galactic center and the galactic anticenter have been updated.

3. Results of the Large-Scale SAS-2 Observations. One of the most graphic ways of viewing the γ -ray sky is shown in the map of γ -ray flux contours in figure 1. A description of the construction of this map will indicate its values and limitations. The entire celestial sphere is divided into 20736 bins of equal solid angle. The bins are separated by 2.5° in galactic longitude throughout the sky. The latitude bins have widths adjusted to maintain the equal solid angle. At the galactic equator, the bins have a latitude width of about 0.7° . For each bin, the number of detected photons within the bin is divided by an exposure parameter (the sensitivity of the observations at that bin) to yield a γ -ray intensity. The intensities obtained in this way are smoothed by combining bins, and contours of equal intensity are then drawn using the centroids of the bins to represent the bin positions. Because of this smoothing procedure, this sky map is most useful for examining large-scale features. Any single feature observed in this plot has a positional uncertainty of $\pm 2^\circ$.

As can be seen in the figure, the SAS-2 observations used for this plot cover about half the galactic plane in longitude and a range of galactic latitudes from well below the plane to the north galactic pole. The lowest γ -ray intensity contour lies at a value about three

Figure 1. Contour map of γ -ray intensities observed by SAS-2 at energies above 100 MeV. The dashed line shows the limits of the SAS-2 exposure. In units of 10^{-4} photons $\text{cm}^{-2} \text{s}^{-1} \text{sr}^{-1}$, the contours are 5.1, 4.0, 3.0, 2.1, 1.3, and 0.7. The highest and lowest contours are darker than the others.



times greater than the diffuse flux observations by SAS-2 (Fichtel et al., 1975). Only γ -rays with measured energies greater than 100 MeV were used. Clearly, at this intensity level, the only significant features in the γ -ray sky are ones associated with our own galaxy.

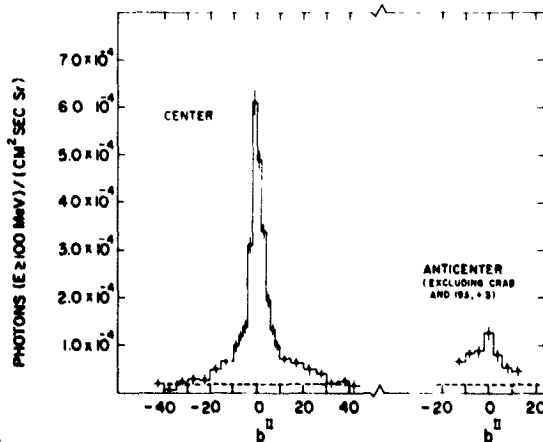
In terms of γ -ray emission, the galactic plane can be roughly divided into two regions. The section of the plane between galactic longitudes 310° and 45° , surrounding the galactic center, is an intense ridge. The entire range stands out above all other parts of the γ -ray sky, but prominent peaks and valleys are visible within the region. The remainder of the galactic plane resembles the section in figure 1 between 45° and 120° longitude. The plane stands out clearly above the diffuse background, but at a significantly lower level than the central region.

Within the intense central region of the plane, four peaks are visible on the contour plot, centered on longitudes 315° , 330° , 0° , and 35° . The single most intense region observed by SAS-2 is the section of the plane around 330° . On a finer resolution scale, what appears as an elongated peak in figure 1 is actually two separate intense peaks, one centered on 330° and the other centered on 345° . In terms of galactic structure, the entire intense region encompasses the part of the galaxy within about 7 kpc of the galactic center. The discussion of how these observations may be related to other components of the galaxy will be postponed until section 4.

The parts of figure 1 away from the central ridge also show some features, the most prominent of which appears at galactic longitudes centered on 75° - 80° . While this excess is not as intense as any of the peaks around the galactic center, it does stand out from the parts of the plane on either side. Other apparent features between 50° and 120° are all of low statistical significance, as is the small region at galactic latitude -35° . By contrast, the excess extending from the galactic plane up to latitudes about $+15^\circ$ above the galactic center lies in a region of high exposure by SAS-2 and may very well be significant.

Figure 2 shows the SAS-2 data above 100 MeV summed as a function of galactic latitude for the regions around the galactic center and the

Figure 2. Distribution of γ -rays with measured energies greater than 100 MeV as a function of galactic latitude. Data from the center cover $330^\circ < l < 30^\circ$. Data from the anticenter exclude the Crab, Vela, and (193,+3) sources. The diffuse background is shown as a dashed line.



galactic anticenter. As in figure 1, the dominance of the galactic emission over the diffuse radiation is clear, even for the anticenter region where the plane is relatively weaker. In the center region, the data has been largely updated with the changes discussed in section 2. The principal features of these results are the same as discussed by Fichtel et al. (1975). The latitude distribution in the center longitude range is broader than would be expected from the detector resolution alone. Two components, a narrow one with the detector resolution and a broader one with a gaussian 1σ of 6° to 7° are needed to give a good fit to the data. The resolution-limited component represents at least half the total radiation. This narrow component must originate either from localized sources or from features with a width comparable to the galactic disk thickness at a distance greater than 2 kpc. The broader component could originate either from the nearby galactic disk or from a more distant component with a greater thickness. In the anticenter direction, the observed γ -radiation has a distribution significantly broader than the detector resolution, suggesting that most of this radiation originates in nearby regions, as would be expected from the position of the solar system in the galaxy.

One additional aspect of the latitude distribution deserves mention. In the galactic center region, the intensity is somewhat higher on the positive side of the plane than on the negative side. In the anticenter region, the intensity is higher on the negative side of the plane than on the positive side. These excesses are also visible in figure 1 and the anticenter flux contour plot of Hartman et al. (1976). Although these regions of greater intensity are difficult to localize, their general position suggests an identification with the local distribution of stars and gas known as Gould's Belt.

The distribution of high-energy γ -ray emission as a function of galactic longitude is one of the most useful observations for relating γ -ray results to galactic structure. Figure 3 shows the SAS-2 data summed between $-10^\circ < b^{II} < +10^\circ$ in longitude bins 2.5° wide. Two important considerations concerning this data are: First, the 2.5° bin size is smaller than the SAS-2 resolution for γ -ray energies above 100 MeV. Even a point source will appear with finite width on this plot. Second, not all the data shown here have been updated with the changes discussed in section 2, particularly in regions away from the galactic center. Even though these changes are not expected to alter any large-scale features, any individual point may show a noticeable adjustment in the final analysis. In short, no single bin on this present longitude plot should be taken by itself as decisive.

Figure 3 emphasizes many of the features of the galactic plane which were visible in figures 1 and 2: the dominance of the plane itself above the diffuse background, the strong contrast between the

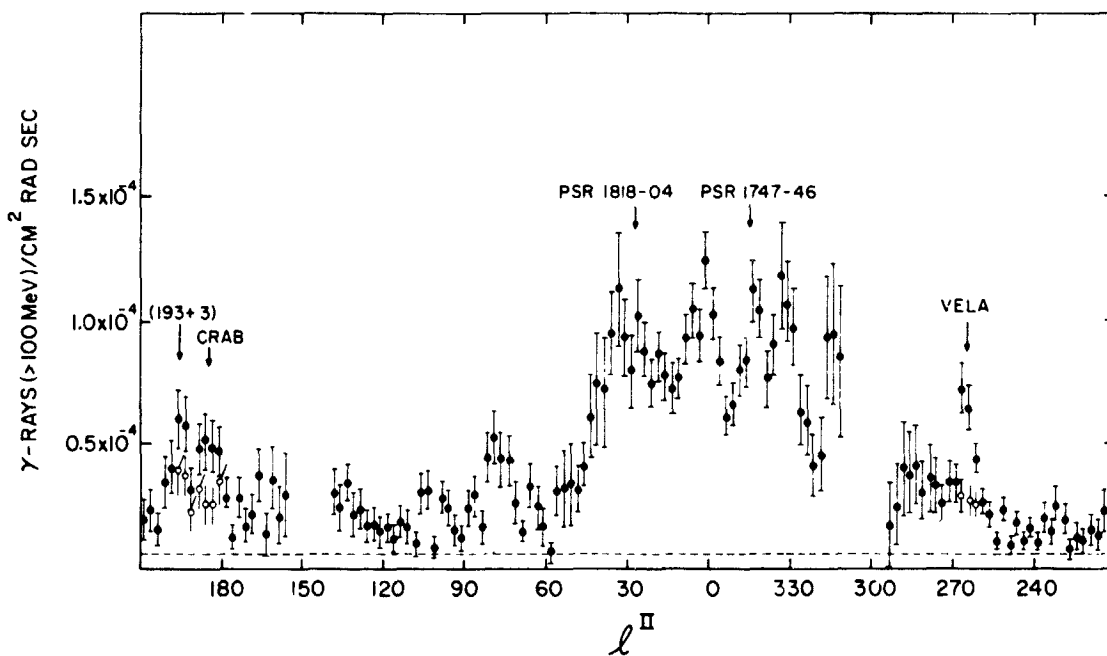


Figure 3. Distribution of high-energy (> 100 MeV) γ -rays along the galactic plane. The SAS-2 data are summed from $b^{\text{II}} = -10^\circ$ to $b^{\text{II}} = +10^\circ$. The diffuse background is shown as a dashed line. Arrows mark the locations of localized sources. The open circles give the estimated galactic emission with localized sources subtracted. Error bars shown are statistical only. An additional uncertainty of about 10% should be attached to the overall normalization.

galactic center region and the rest of the galactic plane, and the non-uniformity of the high-intensity region around the galactic center. In the part of the plane away from the galactic center, four peaks above the general plane emission can be seen. Those associated with the Crab (Kniffen et al., 1974) and the Vela supernova remnant (Thompson et al., 1975) have been discussed in detail previously. The regions around longitudes 75° and 195° have not been definitely identified with known sources (Fichtel et al., 1975), but available evidence points to their being localized rather than extended sources (Kniffen et al., 1975; Hartman et al., 1976).

In the region of strong γ -ray emission between 310° and 45° , five peaks stand out. These peaks are centered on longitudes 315° , 330° , 345° , 0° , and 35° . From figure 1, all of the peaks could be seen to lie on the galactic plane itself, within uncertainties. Because the peak near 315° lies relatively close to the limit of the SAS-2

exposure, its overall significance is the smallest of the five. The peaks at 330° and 345° are sufficiently narrow to be consistent with the detector resolution, implying that they must be distant large-scale features or intense localized sources. The fact that these peaks lie in a direction not far from the galactic center suggests a large scale rather than discrete origin for two reasons. First, the inner section of the galaxy is the region most likely to contain the cosmic rays and matter which produce diffuse galactic γ -rays. Second, unless a discrete source were extremely intense, it would have to be relatively nearby in order to be seen against the general galactic background. This effect is illustrated by the locations of two candidate γ -ray pulsars in the general region around the center (PSR 1747-46 and PSR 1818-04; Ugelman et al., 1976). Although these are identified γ -ray sources, they contribute less than 10% of the intensity in any one bin in figure 3. The enhancement in the longitude distribution around the 0° direction itself appears to be slightly broader than the detector resolution. While this effect may not be statistically significant, it suggests the possibility of an extended source in the galactic center direction.

4. Discussion. Any attempt to interpret the galactic γ -ray emission in terms of a model faces the difficulty that the galactic components which produce γ -rays (cosmic rays, interstellar matter, magnetic fields) are interrelated. Many different approaches to the problem can therefore be considered. Bignami et al. (1975) have used the spiral pattern deduced from 21 cm data in the galaxy as the basis for the matter and cosmic ray distributions. Stecker et al. (1975) started with the distribution of molecular hydrogen in the galaxy estimated from 2.6 mm carbon monoxide emission. Fuchs et al. (1975) developed a model based on the magnetic field configuration in the galaxy. Paul et al. (1975) used radio measurements of the synchrotron radiation to estimate the cosmic ray and matter distribution. Cowsik and Voges (1975) studied the possible inverse Compton component of the radiation by using a model for the starlight distribution in the galaxy. All of these models have had some success in interpreting either part or all of the SAS-2 γ -ray observations. Instead of reviewing such models in detail or proposing a new model, this discussion will attempt to show how the γ -ray results themselves motivated the various approaches.

One of the key questions in studying the galactic emission is the production mechanism for the γ -radiation. The available data (Samimi et al., 1974; Fichtel et al., 1975; Sood et al., 1975) suggest that the dominant source of high energy (> 100 MeV) γ -rays is neutral pion decay, while the dominant source of medium energy (< 50 MeV) γ -rays has a spectrum such as that expected from inverse Compton scattering or electron bremsstrahlung. The high-energy radiation then reflects the product of the matter density and the nucleonic cosmic ray density along a given line of sight. In order to calculate

the medium energy component, knowledge is needed of the cosmic ray electron density, the matter density, and the photon density as a function of position in the galaxy. Some information is also needed about the degree of association or coupling between the various components. No single aspect of this problem can be considered to be definitively understood at present, and one of the special advantages of γ -ray astronomy lies in its unique ability to probe the galactic cosmic ray distributions in conjunction with other galactic components.

In studying the spatial distribution of the observed γ -radiation, as summarized in figures 1, 2, and 3, the most important features are: (1) the broad relatively flat excess around the galactic center and the contrast between this excess and the anticenter regions; (2) the specific non-uniformities within the high-intensity central sector; and (3) the resolution-limited and broader components of the latitude distribution in the galactic center region. Each of these features contains important information about the distribution in the galaxy of the components responsible for the γ radiation.

The center to anticenter intensity ratio does not appear to be explainable strictly in terms of the galactic interstellar matter distribution. The neutral hydrogen distribution as measured by 21 cm radio observations shows far less contrast than the γ -ray observations. The 2.6 mm observations of CO, considered to be a tracer of molecular hydrogen, do show a strong contrast as a function of galactic radius, but the peak of this distribution lies at a radius between 4 and 6 kpc from the galactic center. Such a distribution alone could not account for the high-intensity ridge extending from 310° to 45° (Stecker et al., 1975). The failure of the galactic matter distributions to explain the γ -ray distribution is a strong argument that the cosmic rays which interact with the matter are themselves not uniform in the galaxy--an argument which supports the galactic origin for the bulk of the cosmic rays.

If it is assumed that the expansive pressures of the kinetic motion of the gas, the cosmic rays, and the magnetic fields in the galaxy can only be contained by the mass of the gas, then some degree of correlation would be expected between the matter density, the magnetic field and the cosmic ray density, at least on a large scale (Bignami et al., 1975). This approach suggests that the synchrotron emission from cosmic ray electrons interacting with the magnetic fields might show some of the same features as the γ -ray emission originating from cosmic ray nucleons interacting with interstellar matter (Paul et al., 1974). A comparison of figure 1 with the 150 Mhz map of Landecker and Wielebinski (1970), reproduced in figure 4, shows that this is indeed the case. In particular, the synchrotron measurements show the same strong center to anticenter contrast as seen in the SAS-2 results. On a galaxy-wide scale, then, these radio measurements seem to support

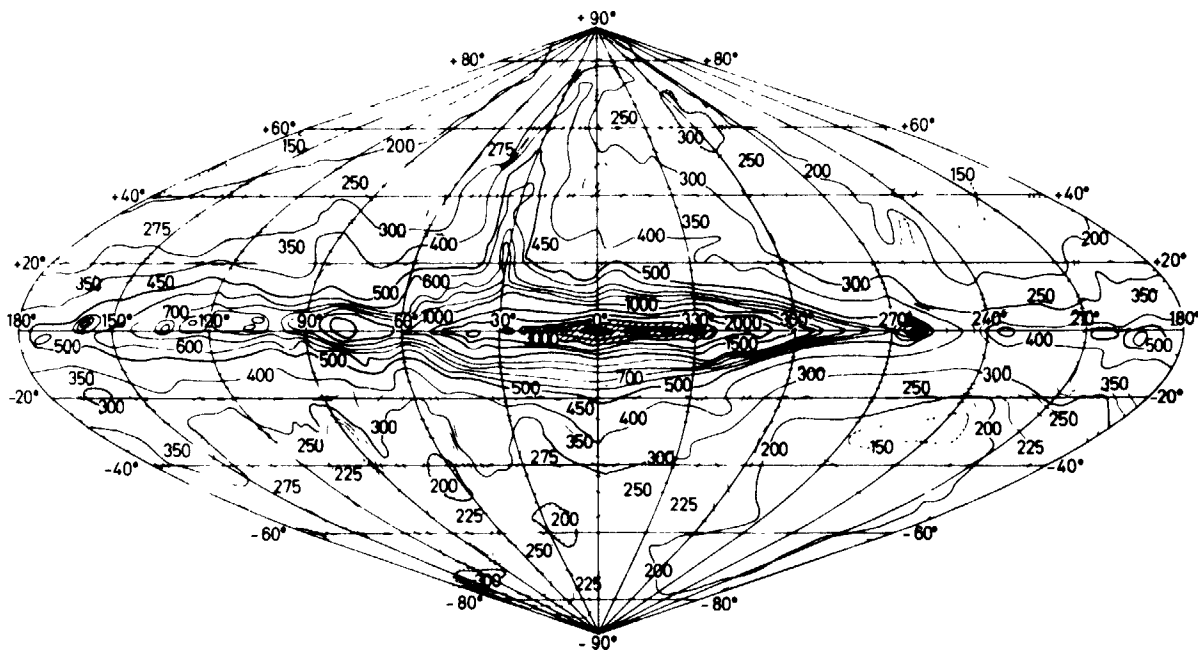


Figure 4. Map of 150 MHz brightness temperatures in galactic coordinates (Landecker and Wielebinski, 1970).

the concept of coupling between the matter density, the magnetic field, and the cosmic ray density.

The five strong peaks in the γ -ray data surrounding the galactic center offer additional clues to the origin of this high-energy radiation. Under the general assumption that ours is a spiral galaxy (although the pitch angle of the spiral may be small in some regions), a peak in the γ -ray data implies a long line of sight through a region of high emissivity, such as along a spiral feature. The direction of the 35° peak, for example, would be tangent to a galactic arm at a radius of about 6 kpc. This direction is roughly coincident with the observed peak in the molecular hydrogen distribution and with one of the arms which has been observed in 21 cm neutral hydrogen measurements. The fact that this is the only strong peak observed between the galactic center and 45° longitude is a strong motivation for considering the molecular hydrogen as the principal source of the γ -radiation.

Because relatively little is known about conditions at the center of the galaxy, the somewhat broadened peak close to the galactic center may have several origins. Radio observations indicate that neutral and molecular hydrogen are not particularly abundant over the

general galactic center region. If this γ -ray peak is attributed to cosmic ray -- matter interactions, then either the cosmic ray intensity would have to be much higher in the galactic center than in other parts of the galaxy or the matter would have to be in some unseen form such as ionized gas. The fact that the galactic center is a strong source of radio, infrared, and X-ray emission suggests the possibility of discrete source contributions, although the intensity appears rather large to be explained by any one γ -ray source at such a large distance. Another possibility is an inverse Compton contribution resulting from an increase in the cosmic ray electron density and the starlight density toward the galactic center. Such a component would be strongly peaked toward 0° longitude, as shown for example by Cowsik and Voges (1975). The central peak in the SAS-2 longitude distribution could also be made up of several components. Until more is learned about the galactic center region, it will be difficult to determine whether this γ -ray excess has an origin similar to the other peaks in the data or whether it represents a unique γ -ray source.

The three peaks observed between 310° and the galactic center direction all coincide with spiral arm features in the Simonson (1976) picture of the galaxy, based on 21 cm measurements and the density wave theory. Because the observed densities of neutral hydrogen in these arms are not extremely high, a strong correlation between the cosmic ray density and the matter density in this region would be necessary in order to explain the results solely in terms of these features (Bignami et al., 1976). In the absence of any CO measurements of this region of the sky to indicate where molecular hydrogen might be concentrated, one possibility would be to assume some sort of symmetry with the opposite side of the galactic center. The molecular hydrogen might then be found at the position of the 330° feature. Some other explanation would then be needed for the other two peaks in this region. An alternative possibility, suggested by Fichtel et al. (1976), is that the molecular hydrogen densities are high, as observed around the 35° direction, but that the cosmic rays are more strongly coupled to the diffuse neutral hydrogen than to the high-density clouds of molecular hydrogen. One additional observation which might tend to support such a concept is the 150 MHz sky map (Landecker and Wielebinski, 1970), which shows the 310° to 45° segment of the galactic plane to be an intense source of synchrotron radiation, with an additionally intense ridge between 330° and 0° longitude. As mentioned before, this radio observation would suggest a strong coupling between the cosmic ray electrons and the magnetic field, with an implied coupling to the distributed matter in the same region.

Finally, the two component nature of the observed γ -ray latitude distribution is a somewhat unexplored subject. The most likely explanation of the broad component of the latitude distribution toward the galactic center is that this radiation is originating from regions

close enough to the solar system that the galactic disk itself appears broader than the detector resolution, while the resolution-limited component originates from more distant parts of the galactic plane. A small contribution to the broad component could come from an extension of the cosmic ray disk above the disk defined by interstellar matter, although Bignami et al. (1975) have shown that a broader cosmic ray disk would have little effect. Another small contributor to the broad latitude component could be inverse Compton γ -rays produced by cosmic ray electrons and starlight or 3° K radiation, since both stars and cosmic ray electrons are thought to extend above the interstellar gas disk. Additional work on the SAS-2 data, studying only the broad latitude component, may reveal additional information about the nature and origin of this radiation.

In summary, the SAS-2 results have shown that high energy γ -rays are an excellent tracer of the components and structure of the galaxy. The γ -ray evidence for a galactic origin of cosmic rays is strong, and the combination of γ -ray data with measurements at other wavelengths provides useful information about the dynamic processes coupling the matter, magnetic fields, and cosmic rays in the galaxy. As more γ -ray data and more data from other sources become available, some of the prospects and possibilities which have been raised by SAS-2 should become a greatly improved picture of our galaxy.

REFERENCES

- Bignami, G. F., Fichtel, C. E., Kniffen, D. A., and Thompson, D. J. 1975, Ap. J. 199, 54.
- Cowsik, R. and Voges, W. 1975, Proc. 14th International Cosmic Ray Conf. 1, 74.
- Derdeyn, S. M., Ehrmann, C. H., Fichtel, C. E., Kniffen, D. A., and Ross, R. W. 1972, Nucl. Instr. and Methods 98, 557.
- Dodds, D., Strong, A. W., and Wolfendale, A. W. 1974, Nature, 250, 716.
- Fichtel, C. E., Hartman, R. C., Kniffen, D. A., Thompson, D. J., Bignami, G. F., Ügelman, H., Üzel, M. E., and Tümer, T., 1975, Ap. J. 198, 163.
- Fichtel, C. E., Kniffen, D. A., Thompson, D. J., Bignami, G. F., and Cheung, C. Y. 1976, Ap. J., in press.
- Fuchs, B., Schlickeiser, R., and Thielheim, K. O., 1975, Proc. 14th International Cosmic Ray Conference 1, 83.
- Hartman, R. C., Fichtel, C. E., Kniffen, D. A., Thompson, D. J., Bignami, G. F., Lamb, R. C., Ügelman, H., Üzel, M. E., and Tümer, T., 1976, Proc. Goddard Gamma-Ray Symposium (this conference).
- Kniffen, D. A., Hartman, R. C., Thompson, D. J., Bignami, G. F., Fichtel, C. E., Ügelman, H., and Tümer, T., 1974, Nature, 251, 397.
- Kniffen, D. A., Bignami, G. F., Fichtel, C. E., Hartman, R. C., Ügelman, H., Thompson, D. J., Üzel, M. E., and Tümer, T., Proc. 14th International Cosmic Ray Conf., 1, 100.
- Landecker, T. L. and Wielebinski, R., 1970, Aust. Jour. Phys. Astrophys., Suppl. 16.
- Ügelman, H. B., Fichtel, C. E., Kniffen, D. A., and Thompson, D. J. 1976, Ap. J., in press.
- Paul, J., Casse, M. and Cesarsky, C. J., 1974, Proc. 9th ESLAB Symposium, ESRO SP-106, 246.

N 76-29112

SAS-2 GALACTIC GAMMA RAY RESULTS II. LOCALIZED SOURCES

R.C. Hartman, C.E. Fichtel, D.A. Kniffen, R.C. Lamb^{**}, D.J. Thompson
NASA/Goddard Space Flight Center
Laboratory for High Energy Astrophysics
Greenbelt, Maryland 20771

C.F. Bignami^{*}
Universita di Milano, Milano, Italy

H. Ögelman, M. Özel, and T. Tümer
Middle East Technical University, Ankara, Turkey

ABSTRACT

Gamma-ray emission has been detected from the radio pulsars PSR1818-04 and PSR1747-46, in addition to the previously reported gamma-ray emission from the Crab and Vela pulsars. Since the Crab pulsar is the only one observed in the optical and X-ray bands, these gamma-ray observations suggest a uniquely gamma-ray phenomenon occurring in a fraction of the radio pulsars. Using distance estimates of Taylor and Manchester (1975), we find that PSR1818-04 has a gamma-ray luminosity comparable to that of the Crab pulsar, while the luminosities of PSR1747-46 and the Vela pulsar are approximately an order of magnitude lower. This survey of SAS-2 data for pulsar correlations has also yielded upper limits to gamma-ray luminosity for 71 other radio pulsars. For five of the closest pulsars, upper limits for gamma-ray luminosity are found to be at least three orders of magnitude lower than that of the Crab pulsar.

The gamma-ray enhancement around galactic coordinates $l^{\text{II}} = 193^\circ$, $b^{\text{II}} = +4^\circ$ is probably not associated with the recently discovered Milky Way satellite galaxy (Simonson, 1975), since its position seems to be incompatible and its intensity appears to be unreasonably high. The enhancement near the galactic plane in the Cygnus region, while consistent with the location of a galactic spiral arm feature, is sufficiently well-localized to be compatible with a point-like source.

* NAS-NRC Postdoctoral Research Associate 1973-75

** On faculty leave from Iowa State University during 1975-76

1. Introduction. Three years ago, at the time of the Denver Cosmic Ray Conference, there was only one confirmed gamma-ray point source observation of high statistical weight, the Crab Nebula. There were some results from balloon-borne experiments which indicated excesses of three or even four standard deviation significance; however, with the exception of observations of the Crab pulsar, none of those results were convincingly confirmed.

At the present time, analysis of the SAS-2 data is nearing completion. In addition to the general galactic plane emission discussed in the previous paper, the SAS-2 gamma-ray telescope also recorded a number of localized regions of enhanced gamma-ray emission, all within about 10° of the galactic plane.

2. Results. In the general direction of the galactic anticenter, two enhancements are seen in the SAS-2 data above the background, about 12° apart. This region has recently been re-analyzed, as discussed in the previous paper, with the result shown in Figure 1. The two enhancements are clearly separated. One of them is obviously associated with the Crab Nebula, since a large portion of its emission is pulsed at the period of the Crab pulsar. In deriving a total intensity for the Crab source, some uncertainty

is encountered in estimating the diffuse background to be subtracted. The background estimate which has been used includes regions both above and below the galactic plane, and yields a Crab intensity of $(3.2 \pm 0.9) \times 10^{-6} \text{ cm}^{-2} \text{ s}^{-1}$ above 100 MeV. It is now clear (Fichtel et al., 1975; Kniffen et al., 1975) that there is a higher diffuse flux south of the galactic plane than on the north side. Since the Crab is south of the galactic plane, it is possible that a higher background should be used for the total intensity calculation, which would result in a somewhat lower value, but still within the quoted errors. Figure 2 shows the result of folding individual event times at the predicted radio pulsar period. The gamma-ray emission is found to be strongly pulsed, with

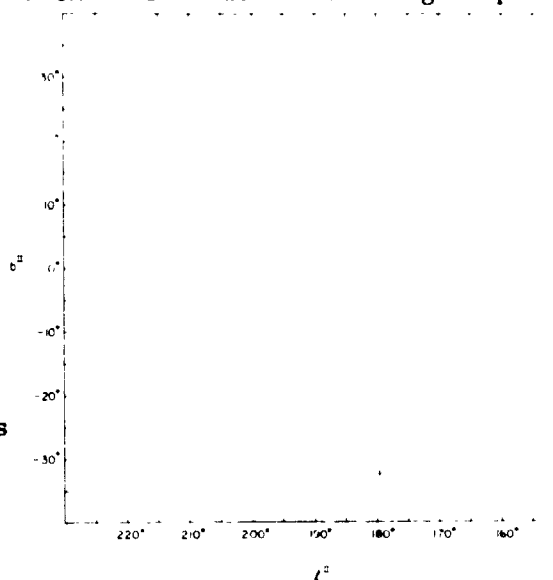


Figure 1. Contour plot of the intensity of gamma rays with energy $> 100 \text{ MeV}$ from the galactic anticenter region. The contour lines represent 75%, 60%, 45%, 30% and 15% of the maximum value, $3 \times 10^{-4} \text{ cm}^{-2} \text{ sr}^{-1} \text{ s}^{-1}$.

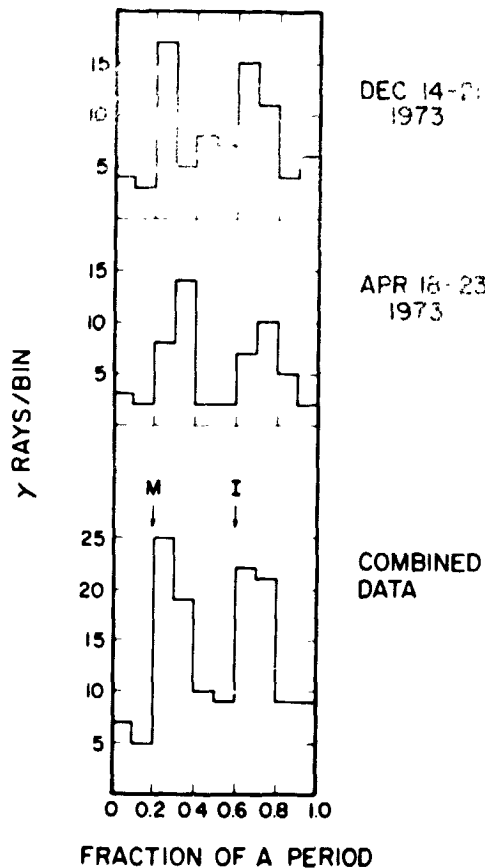


Figure 2. Phase plot for gamma rays ($E > 35$ MeV) from the Crab Pulsar (NP0531+21). The arrows marked M and I indicate the positions of the main radio pulse and inter-pulse.

may be 1000 or more in the 1.5 - 10 keV band (Rappaport et al., 1974).

The energy spectrum of the Vela source is essentially the same as that of the galactic plane, within the detector ability to see a difference. Furthermore, the pulsed fraction is independent of energy, again within the detector limitations. For all energies combined, the pulsed fraction is $70^{+14}_{-12}\%$. The total flux above 35 MeV is $(15.1 \pm 2.4) \times 10^{-6} \text{ cm}^{-2} \text{ s}^{-1}$, and above 100 MeV is $(6.3 \pm 1.1) \times 10^{-6} \text{ cm}^{-2} \text{ s}^{-1}$.

structure and phase similar to those seen in radio, optical and X-ray bands. The pulsed intensity is $(2.2 \pm 0.7) \times 10^{-6} \text{ cm}^{-2} \text{ s}^{-1}$ above 100 MeV. Thus the pulsed emission accounts for most, if not all, of the enhancement seen in the Crab region. The spectrum of the Crab gamma rays is consistent with a power-law extrapolation from X-ray energies, for both the pulsed and total intensities.

The strongest source observed by SAS-2 is associated with the Vela supernova remnant. The surprising discovery (Thompson et al., 1975) is that a major part of the Vela gamma-ray flux is pulsed at the radio period, although no pulsation is observed in the optical range, and no confirmed observation of pulsation has been made in the X-ray range. Still more intriguing is the fact that the gamma radiation is double-pulsed and that neither pulse is in the phase with the single radio pulse. Figure 3 shows the dramatic difference in the pulsed behavior of the Crab and Vela pulsars in the radio, optical, X-ray and gamma-ray energy ranges. Although the Vela pulsar is a brighter gamma-ray source than the Crab as seen from the Earth, the gamma-ray luminosity of the Crab pulsar is about eight times that of the Vela pulsar above 100 MeV. In contrast, the luminosity ratio $L_{\text{CRAB}}/L_{\text{VELA}}$ in the X-ray region is at least 80 (Fritz et al., 1971; Harnden and Gorenstein, 1973) at 1 keV, and

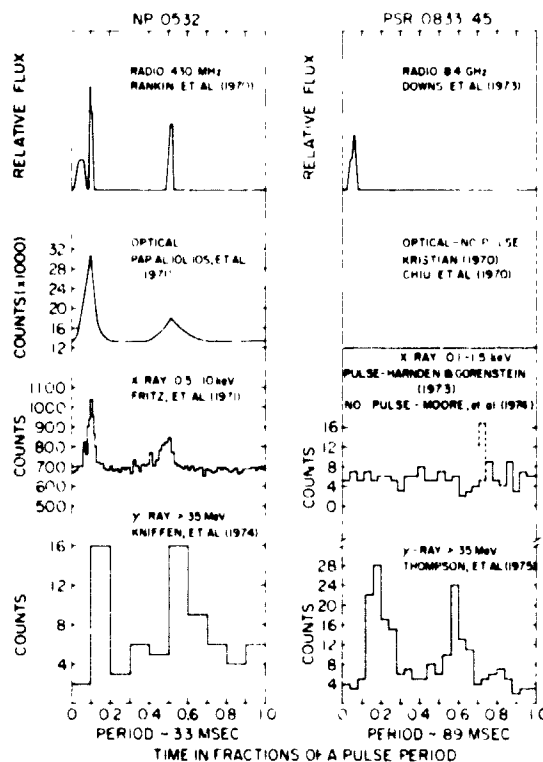
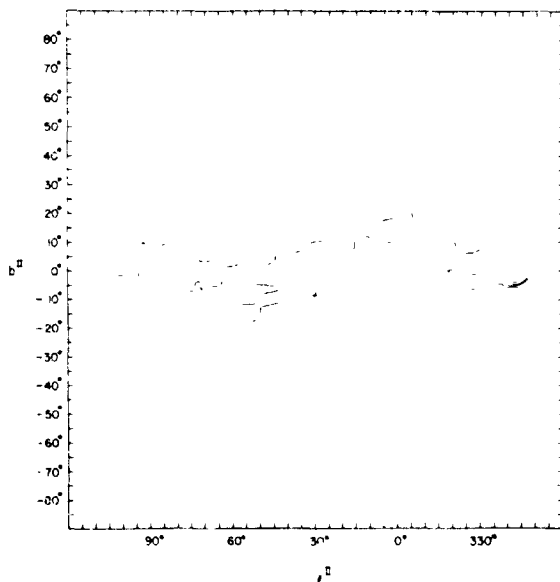


Figure 3. Comparison of Crab and Vela pulsar phase plots in radio, optical, X-ray and gamma-ray bands.

Thompson (1975) has proposed a model for the Vela pulsar in which the radio emission originates near the polar surface of a neutron star which has its magnetic dipole axis roughly perpendicular to its spin axis. The gamma-ray emission then arises from synchrotron radiation in the region where the polar field lines reach the speed-of-light cylinder. In each case the photons are emitted roughly along the magnetic field lines, and the spiral shape of the field lines produces the observed 13 millisecond delay between the radio pulse and the gamma-ray pulse. The double-pulsed gamma-ray structure is explained by assuming that the gamma rays are emitted in a broader cone than the radio emission, and that we observe gamma-ray emission from both magnetic poles, but radio emission from only one pole. Obviously, this picture does not apply to the Crab Pulsar. Its different phase structure and spectrum indicate that a different mechanism is probably responsible for its gamma-ray emission.

The observation of gamma rays from the Vela pulsar, which is not seen in the optical or X-ray regions, suggests that other radio pulsars might be observable at gamma-ray energies. Of the 147 known radio pulsars, 134 were within the region of the sky observed by SAS-2. For 59 of these, however, the period and period derivative were not known with sufficient accuracy to give adequate phase information during the

SAS-2 observations. This leaves 75 pulsars available for study, two of which have already been discussed, the Crab and Vela pulsars. For the remaining 73, a search has been made for gamma-ray pulsation at the predicted radio periods. In two cases, phase distributions were obtained which are relatively improbable. The phase plot for PSR 1818-04, with a period of about 0.6 sec., is shown in Figure 4. The position of the radio pulse is shown by the arrow marked "R".



The chance that a distribution like this might occur randomly in one of the 73 pulsars is about 0.3%. The contour plot shown in Figure 5 indicates an enhancement, not significant by itself, in the appropriate region for this pulsar. The pulsed flux above 35 MeV found for PSR1818-04 is $(2.0 \pm 0.5) \times 10^{-6} \text{ cm}^{-2} \text{ s}^{-1}$.

The phase plot in Figure 6 is for gamma rays from the region around the pulsar 1747-46, which has a period of 0.742 sec. There is a chance probability of about 0.6% of seeing it in one of 73 distributions. Since PSR1747 lies 10° south of the galactic plane, at a galactic longitude of 345° , it is feasible to look for an enhancement in the total gamma-ray flux from that region. The contour plot in Figure 5 shows a bump in the proper region; a more careful analysis, using a band of latitudes from -6° to -14° to estimate background, yields a 3σ positive

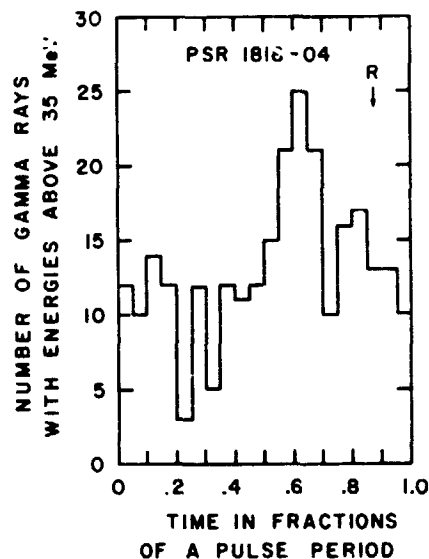
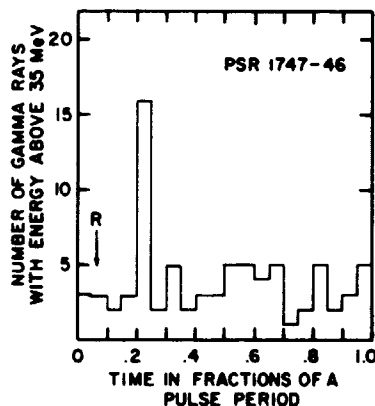


Figure 4. Phase plot for gamma-rays ($E > 35 \text{ MeV}$) from PSR 1818-04. The arrow marked R is the position of the observed radio pulse.

Figure 5. Contour plot of the intensity of gamma rays with energy $> 100 \text{ MeV}$ for galactic longitudes between 270° and 90° . The contour lines represent 31%, 63%, 47%, 33%, 21% and 11% of the maximum, which is $6.3 \times 10^{-4} \text{ cm}^{-2} \text{ sr}^{-1} \text{ s}^{-1}$.

Figure 6. Phase plot for gamma rays ($E > 35$ MeV) from PSR1747-46. The arrow marked R indicates the position of the observed radio pulse.



result. This independent evidence enhances the significance of the pulsed result.

The total flux obtained for PSR1747-46 is $(1.6 \pm 0.6) \times 10^{-6} \text{ cm}^{-2} \text{ s}^{-1}$ above 100 MeV. For pulsed flux above 100 MeV we find a value of $(6.5 \pm 3.3) \times 10^{-7} \text{ cm}^{-2} \text{ s}^{-1}$, based on only six events. Above 35 MeV, the pulsed flux is $(2.4 \pm 0.7) \times 10^{-6} \text{ cm}^{-2} \text{ s}^{-1}$. We note that the delay between the radio pulse and the gamma-ray pulse is 115 ± 20 milliseconds, or 0.16 ± 0.03 of a pulse period. This delay is very close to that between the radio pulse and the closer of the two gamma-ray pulses for the Vela pulsar of 0.15 ± 0.02 period.

Thus we now have strong evidence of four radio gamma-ray pulsars, only one of which, the youngest, is detectable at optical and X-ray energies. Several obvious questions immediately come to mind. For instance, what fraction of the energy lost by the pulsar goes into gamma radiation? If we know the period and its derivative, and assume a moment of inertia of 10^{45} g cm^2 , we can estimate the pulsar's rotational energy loss rate from

$$\frac{dE_R}{dt} = I \Omega \dot{\Omega} = \frac{4 \pi^2 I \dot{P}}{P^3}$$

where Ω , $\dot{\Omega}$, P and \dot{P} are the angular frequency and period and their time derivatives, and I is the moment of inertia.

For the gamma rays, we assume a radiating cone of 1 sr and a typical energy of 100 MeV, with the result shown in Figure 7. We see that the Crab and Vela pulsars are apparently radiating only 10^{-3} to 10^{-4} of their energy in gamma rays. Pulsars 1747 and 1818, however, seem to be radiating a major fraction of their energy in this range. The apparent excess of the gamma-ray luminosity over the energy loss rate for PSR1818 is attributable to large uncertainties in both the

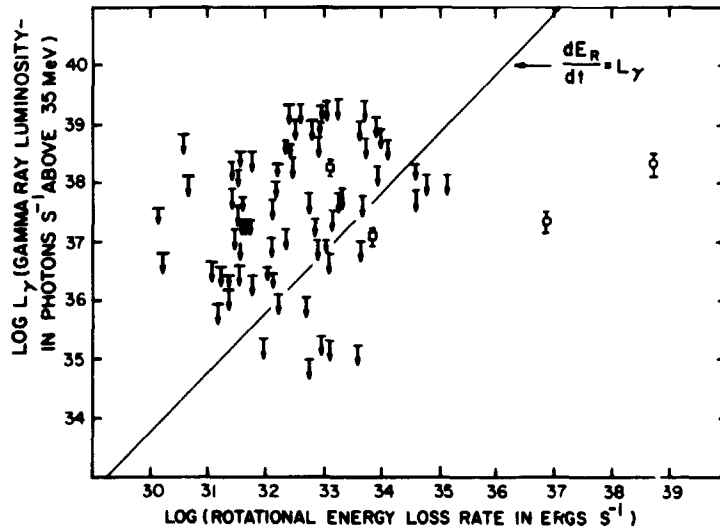


Figure 7. Observed gamma-ray luminosities and upper limits as a function of pulsar rotational energy loss rates, from Taylor and Manchester (1975). Open circles are the Crab (Kniffen et al., 1974) and Vela pulsar (Thompson et al., 1975) observations. The open boxes are for PSR1747-46 and PSR1818-04. Distance estimates from Taylor and Manchester (1975) were used in calculating luminosities. Error bars reflect only gamma-ray flux uncertainties. The line indicates the condition in which all pulsar rotational energy loss appears in the form of gamma rays.

pulsar moment of inertia and the width of the gamma-ray emission cone.

We can also compare the pulsar luminosities and upper limits with apparent ages $P/2\dot{P}$, as shown in Figure 8. No simple relationship is obvious between gamma-ray luminosity and apparent age; however it is worthwhile to note that all four of the pulsars for which gamma-ray pulsations have been observed show ages less than about 10^6 years, while most of the pulsars included in the study have ages greater than 10^6 years. This suggests, although not conclusively, that gamma-ray luminosity decreases rapidly for pulsars older than 10^6 years, as is the case for radio luminosity.

If gamma-ray emission is a fairly general property of pulsars, as now seems possible, it is natural to ask what portion of the gamma-ray luminosity of the Galaxy is attributable to pulsars. Since no gamma-ray pulsars are presently seen with ages greater than about 10^6 years, we use that figure as the pulsar gamma-ray lifetime. If pulsars are created in the Galaxy at the rate of one every 100 years, and each radiates for 10^6 years a gamma-ray luminosity of 10^{37} photons s^{-1} above 35 MeV, we find a contribution of $10^{41} s^{-1}$, or about 5% of the luminosity of the Galaxy due to cosmic-ray interactions.

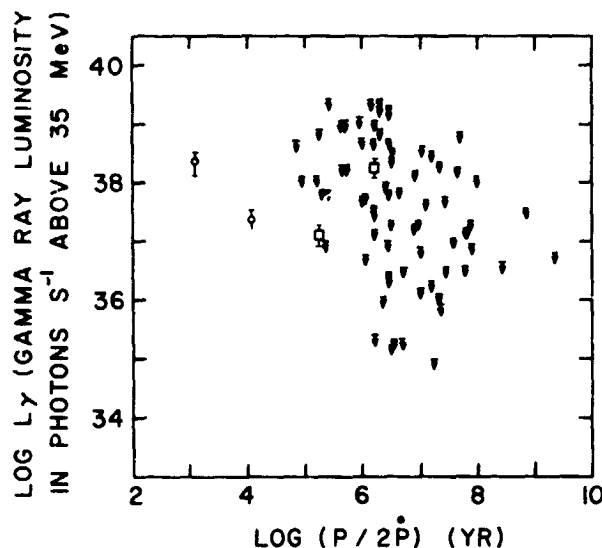


Figure 8. Observed gamma-ray luminosities and upper limits as a function of apparent age $P/2P$. See caption for Figure 7.

One region of enhanced gamma-ray intensity has been observed with SAS-2 which has not been clearly identified with any known object. In the region of the galactic anticenter, there is a major flux enhancement centered at approximate galactic coordinates $l^{II} = 193^\circ$, $b^{II} = +4^\circ$. This source has an intensity comparable to that of the Crab for energies above 100 MeV. However, it appears on the basis of limited statistics to have a somewhat flatter spectrum, since it stands out most prominently as a localized source for energies above 100 MeV. Lamb, Thompson and Fichtel (1975) have investigated the possibility that this source might be associated with the recently discovered (Simonson, 1975) satellite galaxy near the Milky Way. They concluded that the association is unlikely, for two reasons: first, the position obtained for the gamma-ray source is at least five standard deviations from the position given by Simonson (1975); second, from Simonson's (1975) estimates of the distance and mass of the new galaxy, it appears that its cosmic-ray density would have to be nearly two orders of magnitude greater than is observed locally if its emission is assumed to be due to cosmic ray interactions. Several supernova remnants are known in the same general direction as the unidentified gamma-ray enhancement, but the closest, IC443, is more than 4° , or at least 5σ , from the gamma-ray source.

Very recently we have found evidence for possible periodicity in this source, with a period of about one minute. This possibility was first noticed by examining the time intervals between individual gamma rays from the source. Figure 9 lists all pairs of events near $l^{II} = 193^\circ$, $b^{II} = +4^\circ$ which occurred during single SAS-2 orbits (The SAS-2 telescope was recording celestial gamma rays for about 60% of each 95 minute orbit) during one week of observation. It was noted that the

shorter intervals all appear to be approximate multiples of the shortest interval, 57.7 seconds. By assigning integer factors of multiplication a better value of the hypothetical period was found, as shown in Figure 9. The probability that this indication of periodicity is a chance regularity is estimated to be 1 or 2 per cent. A folding search of the three observing intervals, each one week long, showed evidence for periodicity, but the intervals showed slightly different periods, consistent with a period increasing at a rate of 2.2×10^{-9} . Figure 10 shows the resulting phase plot. In view of the number of trials used, and the added degree of freedom in assuming a non-zero P , we feel that the evidence for this periodicity is not statistically compelling, but must await confirmation. However, this unidentified object, which presently appears to be a uniquely gamma-ray phenomenon, is certainly one of the important experimental problems in gamma-ray astronomy.

CLOSE PAIRS FROM DEC 14-21, 1972 DATA

PAIR NO	Δt (SEC)	ASSUMED MULTIPLE M	$\Delta t/M$ (SEC)	CALCULATED MULTIPLE
1	756.7	13	58.2	12.94
2	652.8	11	59.3	11.16
3	1271.5	22	57.8	21.74
4	57.7	1	57.8	0.99
5	117.2	3	59.1	3.03
6	347.1	6	57.9	5.93
7	133.4	2	66.7	2.28
8	300.1	5	60.1	5.13
9	519.2	9	57.7	8.88
10	1568.2	27	58.1	26.81
11	122.4	2	61.2	2.09
12	939.8	16	58.7	16.06
TOTAL	6846.1	117	58.5	

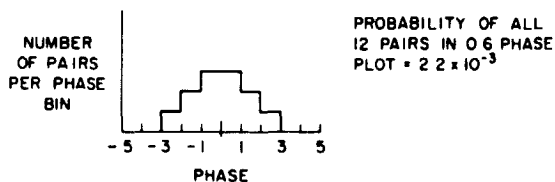


Figure 9. Time intervals between pairs of gamma-ray events from near $\ell^{II} = 193^\circ$, $b^{II} = +4^\circ$ which occurred within single SAS-2 orbits (45 minute intervals).

The final source we will mention is in the Cygnus region, near the galactic plane at a galactic longitude of about 75° . It has been pointed out previously that this enhancement, which is clearly seen in the contour map of Figure 5, is in about the same position as the local spiral arm seen in 21 cm radio measurements, and therefore might be a galactic arm feature rather than a point source. Reanalysis of one of the two weeks of observation indicates, however, that the enhancement is compatible with a point-like source, and is considerably narrower in longitude than the calculated width of about 15° for a galactic arm feature in this direction (e.g. Bignami et al., 1975). If a galactic arm feature is 200 pc thick normal to the galactic plane, and is 1 - 2 kpc away, its observed latitude extent would be $5^\circ - 10^\circ$, which is also probably incompatible with the observations.

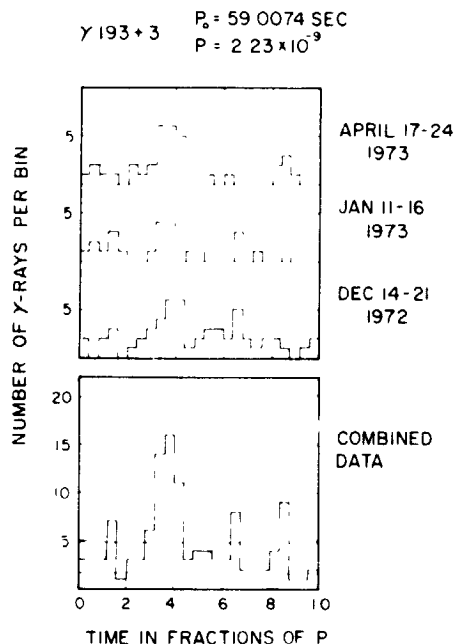


Figure 10. Phase plot for the gamma-ray source at $l^{\text{II}} = 193^\circ$, $b^{\text{II}} = +4^\circ$, assuming a period increasing with the indicated \dot{P} .

The observed position is consistent with that of Cygnus X-3, a prominent X-ray source modulated with a 4.8 hr. period. The period and phase of the X-ray modulation are known sufficiently precisely to make a fold of the SAS-2 data at this period meaningful. However, this period is almost exactly 3 times the orbital period of the SAS-2 satellite and care is required in order to avoid a possible spurious indication of periodicity. Figure 11 shows the result of folding the SAS-2 data at the known X-ray period of 4.8 hr. The bottom part of the figure includes all of the data from the week of observation, $\sim 90\%$ of which are gamma rays not associated with the Cygnus X-3 region. The small modulation seen in this data is the direct result of the nearness of the orbital period to one-third of the folding period. In the upper part of Figure 11 only those gamma-ray events near Cygnus X-3 are shown. There is clear indication of a 4.8 hr. modulation in these gamma rays with a minimum near the minimum predicted from the X-ray data. The probability of finding this behavior by a random fluctuation of a uniform time distribution is about 0.1%

The SAS-2 observations have also produced upper limits on gamma-ray fluxes from a number of interesting astrophysical objects. In general, for objects away from the galactic plane these limits are around $10^{-6}\ \text{cm}^{-2}\ \text{s}^{-1}$ for gamma rays above 100 MeV. Objects in this group include Cen A, Cas A, Tycho SNR, M87, M31, Sco X-1, Cyg X-1,

Cyg X-2, LMC, SMC, and Jupiter. We note that our upper limit on Cen A does not contradict the Compton-synchrotron model recently proposed by Grindlay (1975) for that object.

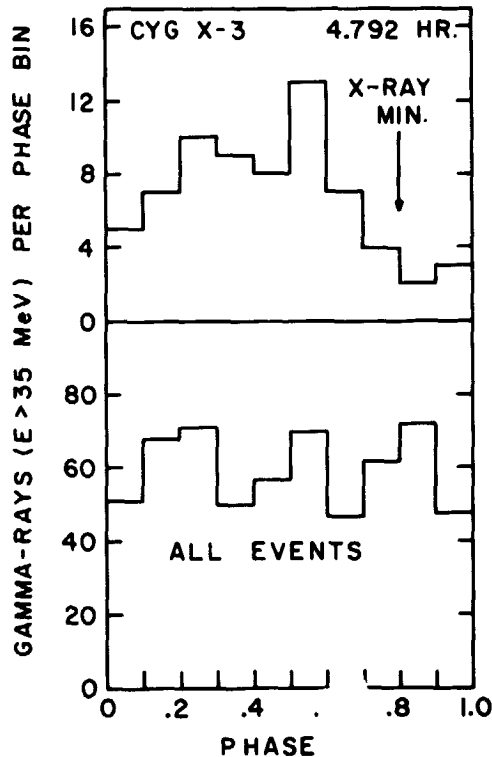


Figure 11. (a) Phase plot for gamma rays from the region around Cygnus X-3, folded at the 4.782 hour period observed in X-rays from Cygnus X-3; (b) Phase plot for all gamma rays observed during the same observation interval. The small modulation at three times the Cygnus X-3 frequency is due to the fact that the SAS-2 orbital period was almost exactly one-third of the Cygnus X-3 period. A distribution similar to this would be expected in Figure 11 (a) if no 4.792 hour modulation is present.

3. Summary. SAS-2 has provided evidence for gamma-ray emission from four radio pulsars (the Crab and Vela pulsars, PSR1747-46 and PSR 1818-04). Three of the four have not been observed to pulse at optical or X-ray energies. We have made a tentative identification of Cygnus X-3 as a gamma-ray source, with intensity modulated at the 4.8 hour period observed in X-rays. Finally, a strong gamma-ray source seen near the galactic anticenter has not been identified with any known object.

Past experience in astrophysics has shown that every time a new frequency band has been investigated, totally new and unexpected objects and processes have been discovered. Gamma-ray astronomy is apparently beginning to demonstrate this principle again.

4. References.

- Bignami, G.F., Fichtel, C.E., Kniffen, D.A., and Thompson, D.J. 1975, Ap.J. 199, 54.
- Fichtel, C.E., Hartman, R.C., Kniffen, D.A., Thompson, D.J., Bignami, G.F., Ogelman, H., Ozel, M.E., and Tümer, T. 1975, 14th International Cosmic Ray Conference, Munich 1, 29.
- Fritz, G., Meekins, J.F., Chubb, G.A., Friedman, H., and Henry, R.C. 1971, Ap.J. 164, L55.
- Grindlay, J.E. 1975, Ap.J. 199, 49.
- Harnden, F.R., Jr. and Gorenstein, P. 1973, Nature 241, 107.
- Kniffen, D.A., Hartman, R.C., Thompson, D.J., Bignami, G.F., Fichtel, C.E., Ogelman, H., and Tümer, T. 1974, Nature 251, 397.
- Kniffen, D.A., Bignami, G.F., Fichtel, C.E., Hartman, R.C., Ogelman, H.B., Thompson, D.J., Ozel, M.E., and Tümer, T. 1975, 14th International Cosmic Ray Conference, Munich 1, 100.
- Lamb, R.C., Thompson, D.J., and Fichtel, C.E. 1975, NASA/Goddard Space Flight Center Preprint X-662-75-321.
- Rappaport, S., Bradt, H., Doxsey, R., Levine, A., and Spada, G. 1974, Nature 251, 471.
- Simonson, S.C. III 1975, Ap.J. Lett. 201, L103.
- Taylor, J.H., and Manchester, R.N. 1975, Astron. J. 80, 794.
- Thompson, D.J., Fichtel, C.E., Kniffen, D.A., and Ogelman, H.B. 1975, Ap. J. 200, L79.
- Thompson, D.J. 1975, Ap.J. 201, L117.

N76-29113

PRELIMINARY RESULTS FROM THE
EUROPEAN SPACE AGENCY'S
COS-B SATELLITE FOR
GAMMA-RAY ASTRONOMY

The Caravane Collaboration

Presentations to the Symposium:

'THE STRUCTURE AND CONTENT OF THE GALAXY AND
COSMIC GAMMA RAYS'

held at

The National Aeronautics and Space Administration
Goddard Spaceflight Centre

2-4 June 1976

Preliminary results from the European Space Agency's
COS-B satellite for Gamma Ray Astronomy

The Caravane Collaboration

K. Bennett⁶, G.F. Bignami², G. Boella², R. Buccheri³,
J.J. Burger⁶, A. Cuccia³, W. Hermsen¹, J. Higdon¹,
G. Kanbach⁴, L. Koch⁵, G.G. Lichti⁶, J. Masnou⁵,
H.A. Mayer-Hasselwander⁴, J.A. Paul⁵, L. Scarsi³,
P.G. Shukla⁵, B.N. Swanenburg¹, B.G. Taylor⁶ and
R.D. Wills⁶.

1. Cosmic-Ray Working Group, Huygens Laboratorium, Leiden,
The Netherlands.
2. Laboratorio di Fisica Cosmica e Tecnologie Relative del CNR,
Istituto di Scienze Fisiche dell'Università di Milano, Italy.
3. Istituto Fisica, Università di Palermo, Italy.
4. Max Planck Institut für Physik und Astrophysik, Institut für
Extraterrestrische Physik, Garching bei München, Germany.
5. Service d'Electronique Physique, Centre d'Etudes Nucléaires
de Saclay, Gif-sur-Yvette, France.
6. Space Science Department, European Space Research and
Technology Centre, Noordwijk, The Netherlands.

Foreword.

The idea of a European mission for gamma-ray astronomy was first considered about ten years ago when an ESRO feasibility study was undertaken. Five University and Research Institutes the: Max Planck Institute, Garching, Cosmic Ray Working Group, Leiden, Istituto di Scienze Fisiche, University of Milan, Centre d'Etudes Nucléaires, Saclay and the Physical Laboratory, University of Southampton forming the Caravane Collaboration, then developed the mission requirements and instrument characteristics. In May 1969, the Caravane Collaboration approached ESRO with a letter of intent, proposing that they produce the experiment for the proposed COS-B satellite and in July 1969, the ESRO council formally approved the inclusion of COS-B in the organisation's scientific programme.

Many scientists were involved already at this stage, but it is appropriate here that particular mention be made of the senior members of the collaboration responsible for bringing the idea of a gamma-ray mission to life:

H.C. van de Hulst, G.W. Hutchinson, J. Labeyrie, R. Lüst,
G.P. Occhialini, C. Occhialini-Dilworth and K. Pinkau.

In 1970 the Southampton group had to withdraw from the collaboration and the remaining members invited the Space Science Department of ESTEC, lead by Dr. E.A. Trendelenburg to join the collaboration. At about the same time, the University of Palermo, joined the Milan group for the provision of the X-ray detector.

During the course of the next five years many scientists no longer directly involved made vital contributions to the COS-B programme namely:

R.D. Andresen, I. Arens, P. Coffaro, M. Gorisse,
E. Pfeffermann, A. Scheepmaker, G. Sironi and W.H. Voges

Supporting the scientists were the engineers technicians and programmers of the institutes without whom the project could not have continued, including:

Messrs. R. Duc, N. Heinecke, T. Hydra, P. Keirle, G. Kettenring,
E. Leimann, P. Mussio, R. Roger and Mme F. Soroka.

The authors can not do better than to quote the words of H.C. van de Hulst, the chairman of the COS-B Steering Committee, in an article written prior to the launch of the satellite in August 1975:

"....I wish to thank each member of the Collaboration for his contribution, members whose unrelenting input and caution in safeguarding the technical and scientific quality of the experiment are the best guarantee of ultimate success".

COS-B has now achieved ten months of life in orbit and is repaying all the time and effort expended over almost the last decade.

THE COS-B EXPERIMENT AND MISSION

The Caravane Collaboration

ABSTRACT

The COS-B satellite carries a single experiment, capable of detecting gamma rays with energies greater than 30 MeV. Its objectives are to study the spatial, energy and time characteristics of high-energy radiation of galactic and extragalactic origin. The capability to search for gamma-ray pulsations is enhanced by the inclusion in the payload of a proportional counter sensitive to X-rays of 2-12 KeV.

The experiment has been calibrated using particle accelerators. The results of these measurements are presented and the performance of the system in orbit is discussed.

1. Introduction. The European Space Agency's satellite COS-B was launched from NASA's Western Test Range on 9 August 1975. Its mission is to study in detail the sources of extraterrestrial gamma radiation of energy above about 30 MeV. The principal objectives of this study are:

1. To investigate the spatial structure and energy spectrum of gamma-ray emission from the galactic plane.
2. To examine known or postulated localised sources of gamma radiation, to determine the energy spectrum of sufficiently strong sources and to search for time variations (long and short term) in their intensities.
3. To measure the flux and energy spectrum of the diffuse radiation from high galactic latitudes.

Two further objectives, defined during the development stages of the program, are a study of the long-term variability of X-ray sources (Boella et al, 1974a) and a high time-resolution study of cosmic gamma-ray bursts (Boella et al 1975).

COS-B carries a single large experiment, which was designed, constructed and tested under the responsibility of a collaboration of research laboratories known as the Caravane Collaboration, whose members are listed in Table 1. The definition of the observation program and the analysis of the data are also collaborative activities.

TABLE 1
THE CARAVANE COLLABORATION

Max Planck Institut für Physik und Astrophysik, Institut für
Extraterrestrische Physik, Garching-bei-München

Service d'Electronique Physique, Centre d'Etudes Nucléaires de Saclay

Cosmic Ray Working Group, Huygens Laboratory, Leiden

Laboratorio di Fisica Cosmica e Tecnologia Relative,
Istituto di Scienze Fisische dell'Università di Milano

Istituto Fisica, Università di Palermo

Space Science Department, ESA, Noordwijk

2. Instrumentation. The experiment has been described in detail by Bignami et al (1975). A sectional view of the central detector is shown in Figure 1. It features a 240 x 240 mm² 16-gap wire-matrix spark chamber (SC) with magnetic-core read out. Interleaved between the gaps are 12 tungsten plates giving a total thickness of 0.5 radiation length for the conversion of incident photons to electron pairs. The top gap and the bottom 3 gaps have no tungsten immediately above them.

The chamber is triggered by a coincidence pulse from a three-element telescope. The field of view of the telescope is defined by the 30 mm-thick plexiglas directional Cherenkov counter C (Andresen et al, 1974b) and the 10 mm-thick plastic scintillation counter B2, each of which is divided into four quadrants. The 4 mm-thick plastic scintillator B1 (Andresen et al, 1974a) above counter C provides a measurement of the number of particles leaving the bottom of the spark chamber. The 10 mm-thick plastic-scintillator guard counter A, surrounding the spark chamber and upper part of the telescope, is placed in anticoincidence to reject triggers due to incident charged particles.

Beneath the telescope is the energy calorimeter consisting of a caesium-iodide scintillator E, 4.7 radiation length thick, to absorb the secondary particles produced by the incident photons and a plastic scintillator D to provide information on high-energy events for which this absorption is incomplete.

Alongside the gamma-ray detector is mounted a proportional counter, sensitive to X-rays in the energy range 2-12 KeV, to provide synchronisation for possible pulsations of gamma-ray emission from

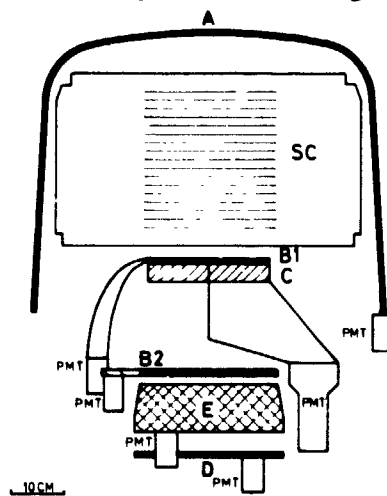


Fig. 1: Sectional view of the COS-B experiment. Identification of the units is given in the text.

sources known to pulsate at X-ray wavelengths (Boella et al 1974b). The relative times of arrival of individual X-ray photons are recorded with a precision of 0.2 ms.

3. The satellite and its orbit. COS-B is configured as a cylinder 1.40 m diameter and 1.13 m long, with the main experiment package occupying the central region as shown in the cutaway view of Figure 2.



Fig. 2: Cutaway view of the COS-B satellite. Key to subsystems:

1. Anticoincidence Counter
2. Spark Chamber
3. Triggering telescope
4. Energy calorimeter
5. Pulsar synchroniser
6. Structure
7. Superinsulation
8. Sun and Earth-albedo sensors (attitude measurement)
9. Spin thruster
10. Precession thruster (attitude control)
11. Nitrogen tank (attitude control)
12. Neon tank (spark chamber gas flushing)
13. Solar-cell array
14. Electronics

The pulsar synchroniser is mounted on the equatorial equipment platform with its optical axis parallel to that of the main experiment. All experiment electronics units and spacecraft subsystems are mounted above or below this platform in order to minimise the amount of material in the field of view and to reduce the probability of the experiment being triggered by background induced by charged-particle interactions in these units. The total mass at launch was 278 kg of which the experiment units comprise 118 kg.

The satellite is spin-stabilised at about 10 rpm about its axis of symmetry, which coincides with the optical axis of the gamma-ray detector. A nitrogen-gas attitude-control system is used to point the experiment in the desired direction. Sun and earth sensors provide data from which the attitude can be reconstituted with a precision of better than 0.5° .

The initial elements of the COS-B orbit, and their latest available values are given in Table 2. The eccentric orbit was preferred over a low orbit because the loss of observation time due to earth occultation is much less. The orbital plane is inclined at 90° to the earth's equator with the argument of perigee in the fourth quadrant which ensures that for most of the operational part of the orbit the satellite is in sight of one of the ESTRACK ground stations. This provides for a high data recovery, without the use of an on-board tape recorder. Regions of the celestial sphere which are close to the

TABLE 2

COS-B ORBITAL PARAMETERS

Date (Y, M, D)	1975-08-08	1976-03-30
Orbit number	1	154
Altitude of perigee (km)	346	2624
Altitude of apogee (km)	99103	96828
Semi-major axis (km)	56103	56104
Eccentricity	0.880	0.840
Inclination (deg.)	90.15	93.08
R.A. of ascending node (deg.)	43.72	42.43
Argument of perigee (deg.)	344.68	325.19
Period (h,m)	36-44	36-44

direction of the line of apsides are difficult or impossible to observe due to the entry of the earth into the field of view or because the earth-aspect angle is outside the range of operation of the albedo sensors for most of the orbit. The right ascension of the ascending node was chosen so that these regions contained only target directions of lowest scientific interest.

The position of the satellite at any time may be reconstituted from tracking data with a precision of 75 km. This is compatible with the 250 μ s relative accuracy of the on-board clock and, allowing for uncertainties in the propagation delay, permits the determination of the absolute Universal times of gamma-ray or X-ray events in either the satellite or the solar-barycentric frame of reference with an uncertainty of better than 1 ms.

4. Observation program and orbital operations. Routine experiment operations began on 17 August 1975 when the satellite was directed towards its first target, the Crab Nebula, with the instrument axis pointing at the pulsar NP 0532. Table 3 shows the subsequent program of observations and the relative sky coverage achieved so far is as shown in Figure 3. At the present time the satellite is pointed towards Virgo, midway between 3C273 and M87. It is intended that in the next six months the observations of Vela and the anticentre will be repeated and as much as possible of the parts of the galactic disc not yet studied will be observed. A study of either the Large or the Small Magellanic Cloud is also foreseen.

TABLE 3
COS-B OBSERVATION PROGRAM

Beginning of observation	Target	Galactic Coordinates	
		l ^{II}	b ^{II}
Orbit 6 1975-08-17	NP0532	185 ^o	-6 ^o
26 1975-09-17	GX5-1	5 ^o	-1 ^o
48 1975-10-20	Vela X	264 ^o	-3 ^o
60 1975-11-08	Vela X-1	263 ^o	4 ^o
73 1975-11-28	Cygnus	74 ^o	0 ^o
90 1975-12-24	Cen X-3	292 ^o	0 ^o
110 1976-01-23	Cen A	309 ^o	19 ^o
130 1976-02-23	Cir X-1	322 ^o	0 ^o
150 1976-03-24	3U 1832-05	26 ^o	1 ^o
170 1976-04-24	Aquila	45 ^o	0 ^o
190 1976-05-24	Virgo	286 ^o	69 ^o

Scheduling of observations is constrained by limitations on solar-aspect angle, attitude-sensor coverage and entry of the earth into the field of view, but takes account of scientific priorities and, where possible, the known plans of other satellite, balloon or ground-based astronomy experiments. The standard period of one month for each observation was chosen to provide good statistics and is also the minimum necessary to achieve the full capability of the attitude-reconstitution software.

The experiment is only operated outside the radiation belts, i.e. about 80% of the time. Occasionally the observation is reduced due to automatic switch-off caused by fluctuations of the boundary of the radiation belts or by solar-flare events. About 45 min. per orbit is devoted to calibration of the detectors, using either cosmic-ray protons or an In-Flight-Test system with electronic stimulation and light-emitting diodes. During alternate orbits a calibration of the pulsar synchroniser is made using an Am ²⁴¹-Sr target source.

The satellite carries a gas-flushing system to permit emptying and refilling of the spark chamber. This has been used at 6- to 8-week intervals to forestall progressive deterioration of spark-chamber performance due to poisoning of the gas. At this rate of usage, the supply of gas carried is more than sufficient for the nominal two-year lifetime.

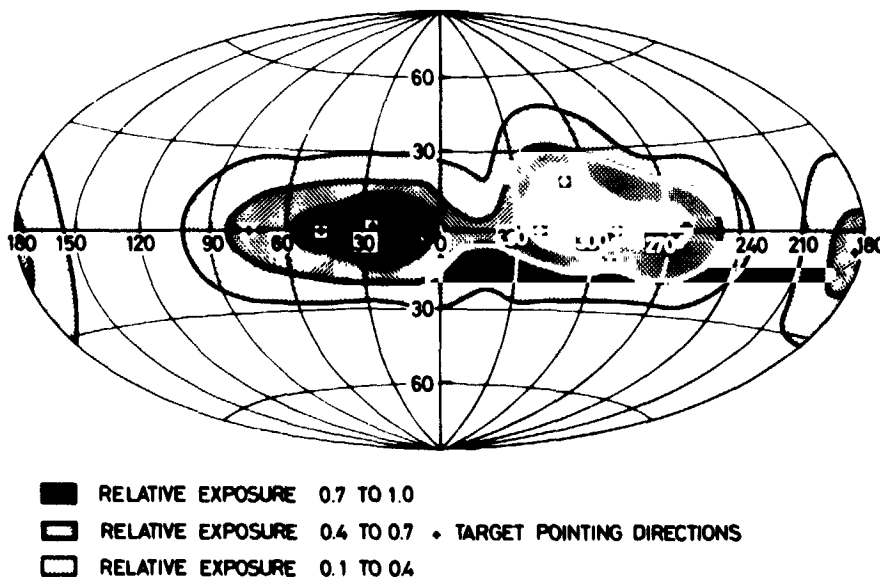


Fig. 3: Relative sky coverage between 17 August 1975 and 23 May 1976 (galactic coordinates).

Data are received by the ESTRACK ground stations at Redu (Belgium) and Fairbanks (Alaska). The subsequent paths of data processing are summarised in Figure 4. The recorded data are despatched at regular intervals to the European Space Operations Centre (ESOC), Darmstadt where they form the basis of the final data processing. In addition, data recorded at Redu can be transmitted to the Operations Centre in ESOC, either in real time or, by playing back the tape, at the end of a pass. Real-time data are used for monitoring the correct functioning of spacecraft and experiment subsystems, especially during telecommanding operations.

From the data played back to ESOC a fraction, averaging about 20% of all data acquired, is made available to the experimenters' "Fast Routine Facility". In this facility the Collaboration has set up programs for a preliminary analysis of this sample of data, using predicted orbit, attitude and time information provided by ESOC. This permits a thorough check of the performance of the experiment, providing the possibility of a fast feedback to keep the equipment in the optimum operational mode. In addition preliminary scientific conclusions can be reached (Bennett et al, 1976), which can be taken into account in planning the future observation program well in advance of the analysis of the final data.

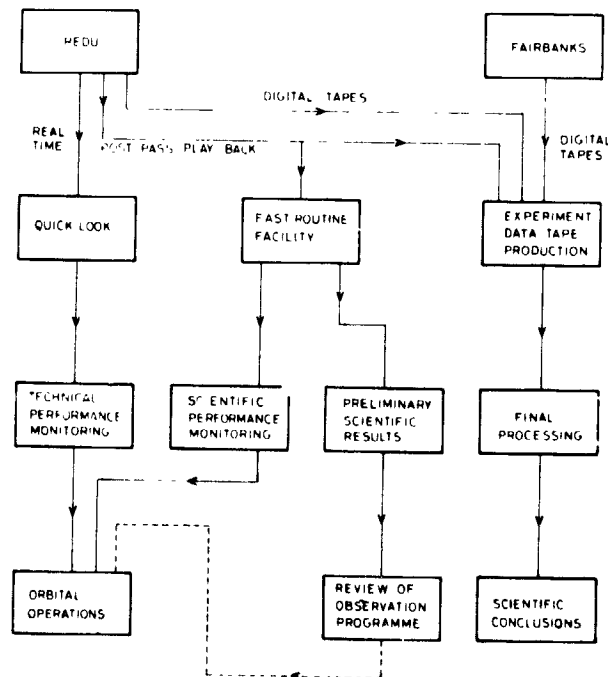


Fig. 4: Overall flow chart of data processing

5. Calibration and in-flight performance. The characteristics of the experiment were determined before launch by exposing the instrument to beams of gamma rays and charged particles at particle accelerators. The data acquired were analysed using the same computer programs that are used for flight-data analysis. An automatic spark-chamber picture-analysis program classifies the events and assigns the addresses of set cores to electron tracks from which the directions of incidence of the gamma-ray photons are reconstituted. Analysis of the data from proton and electron exposures showed that acceptance of only events in which an electron pair is recognized in both projections (class 22 events) gives a high confidence that little background is included but does imply rejecting some genuine gamma rays. For many purposes, where the signal can be identified by another criterion, e.g. spatial localisation or time pulsation, events showing a pair in only one projection (class 2 events) may also be used.

Both the engineering model and the flight model were calibrated in tagged photon beams with energies between 20 MeV and 6 GeV at DESY, Hamburg. (Christ et al, 1974). Measurements were made at a selection of photon energies and directions of incidence (Bennett et al, 1974) and the results were smoothed and interpolated to provide the sensitivities used in the analysis of the flight data. The effective area of the engineering model for recognition of gamma rays as class 2 or class 22 events is shown in Figure 5. The efficiency for class 22 only events is about 30% lower. The data from the calibration of

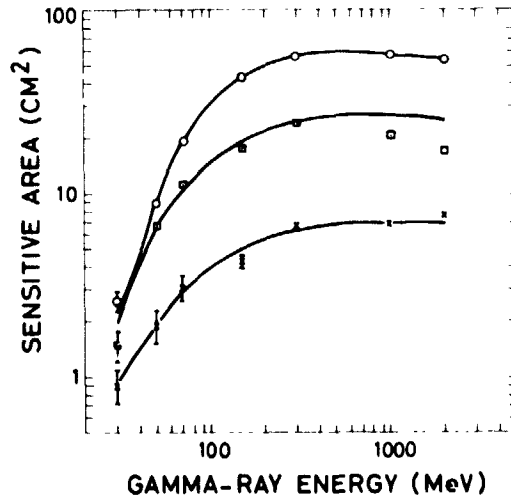


Fig. 5: Effective sensitive area of the engineering model for detecting and recognising gamma rays. Measurements are shown by circles (0°), squares (15°), crosses (30° incidence) and the solid lines represent the interpolations used in the analysis of flight data.

the flight model are currently being analysed. First indications are that the results are not much different from those of the engineering model.

The angular resolution has been characterized by the half angle of a cone, centered on the observed source direction, within which 68% of the reconstituted directions lie. This parameter is shown in Figure 6 for the engineering model. Observation of the point source in Vela, which will be presented in a following paper, confirms that, at least at higher energies, the flight model is similar to the engineering model.

An important characteristic of the experiment is its capability to measure gamma-ray energy over a wide dynamic range. The energy can be derived from measurements of track length in the spark chamber and from the energy loss as measured by the counter pulse heights. The method is still being optimised using data from the accelerator calibration of the flight model. For incidence parallel to the axis an energy resolution of about 50% (FWHM) is achievable in the energy range 70 to 500 MeV.

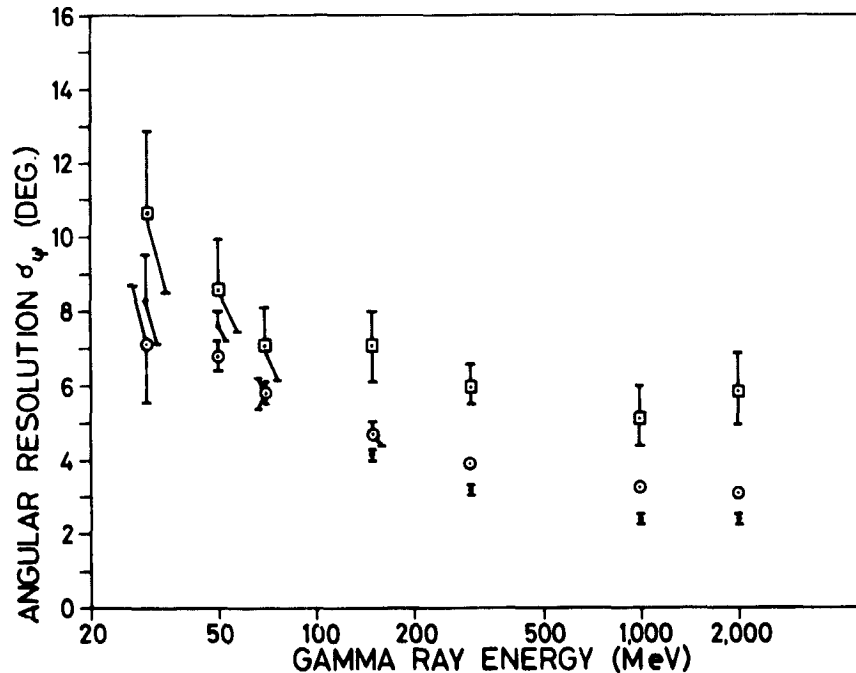


Fig. 6: Angular resolution of the engineering model as a function of energy for selected events incident parallel to the axis (closed circles) and at 15° (open circles) and 30° (squares) to the axis.

The charged-particle environment in the eccentric orbit required special care to be taken in suppressing background triggers. From the accelerator tests and a balloon flight it was concluded that the expected trigger rate would be compatible with the telemetry capability. This prediction proved to be justified, with trigger rates between 0.15 and 0.25 s⁻¹ (depending on the triggering mode). The majority of residual background triggers can be rejected from the data by very simple criteria on the spark-chamber pictures. Although the automatic spark-chamber analysis program has been very highly refined there are still occasions when the track assignment or event classification can be improved upon by human intervention. A system is available which uses a mini-computer with interactive display to permit such intervention and it is intended to use it to monitor the performance of the automatic analysis and to apply corrections where necessary to those events that have been automatically selected as the best candidates for gamma-ray events.

The performance of the complete system (hardware plus software) can be expected to vary with time, especially due to aging of the spark-chamber gas. A check on this has been made by dividing the first two observation periods into shorter intervals of time and measuring for each the counting rates of selected gamma rays in different energy intervals. This has shown that over a period of a month the total efficiency does not vary by more than about 10%. Day-to-day monitoring of spark-chamber performance is possible using the real-time display facilities in the Control Centre. A display of the first gamma-ray event seen on this system is shown in Figure 7.

In the accompanying papers results are presented that are based on analysis using the calibration data and analysis methods described above. For the following reasons these results are preliminary:

- the calibration used may not reflect exactly the performance of the flight unit
- the automatic analysis without human correction leaves a non-negligible background
- not all data acquired for the observations discussed have been received.

As a result, absolute values should be treated with caution. None of the conclusions derived are affected by these limitations. However the combined effect of the quoted uncertainties prohibits at present the drawing of conclusions on energy spectra in most cases.

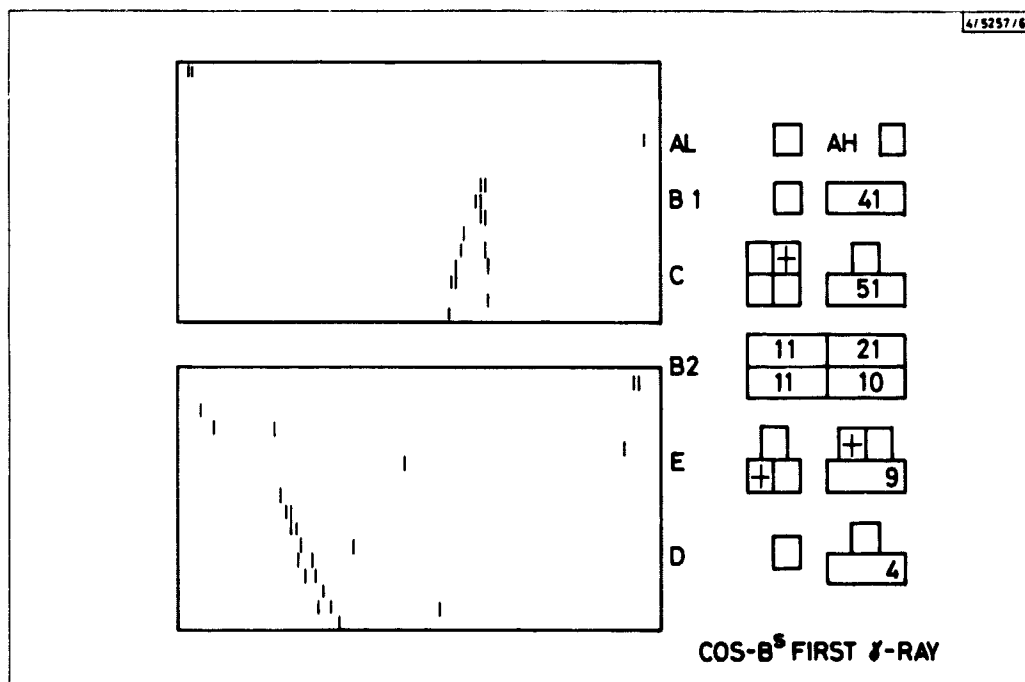


Fig. 7: Real-time display of spark-chamber "picture" for the first event accepted as a gamma-ray event. (This display has only half the resolution of the spark chamber.)

References

Andresen, R.D., Arens, I., Taylor, B.G. and Wills, R.D., 1974a, Nucl. Inst. and Meths. 115, 531.

Andresen, R.D., Arens, I., Taylor, B.G. and Wills, R.D., 1974b, Nucl. Inst. and Meths., 120, 85

Bennett, K., Burger, J.J., Gorisse, M., Mayer-Hasselwander, H.A., Paul, J.A., Pfeiffermann, E., Shukla, P.G., Stiglitz, R., Swanenburg, B.N., Taylor, B.G. and Wills, R.D., 1974, Proc. 9th ESLAB Symposium (Frascati), ESRO SP-106, 323

Bennett, K., Bignami, G.F., Boella, G., Buccheri, R., Gorisse, M., Hermsen, W., Kanbach K., Lichti, G.G., Mayer-Hasselwander, H.A., Paul, J.A., Scarsi, L., Swanenburg, B.N., Taylor B.G. and Wills, R.D., 1976, to be published in Astron. and Astrophysics.

Bignami, G.F., Boella, G., Burger, J.J., Keirle, P., Mayer-Hasselwander, H.A., Paul, J.A., Pfeiffermann, E., Scarsi, L., Swanenburg, B.N., Taylor, B.G., Voges, W. and Wills, R.D., 1975, Space Sci. Instr. 1, 245

Boella, G., Buccheri, R., Coffaro, P., Molteni, D. and Scarsi, L., 1974a, Proc. 9th ESLAB Symposium (Frascati), ESRO SP-106, 345

Boella, G., Buccheri, R., Burger, J.J., Coffaro, P. and Paul, J., 1974b, Proc. 9th ESLAB Symposium (Frascati), ESRO SP-106, 353.

Boella, G., Gorisse, M., Paul, J., Taylor, B.G. and Wills, R.D., 1975, Space Sci. Inst. 1, 269

Christ, H., Peters, F., Bignami, G.F., Burger, J.J., Hermsen, W., Paul, J.A., Pfeiffermann, E., Taylor, B.G., Voges, W.H. and Wills, R.D., 1974, Nucl. Inst. and Meths., 116, 477

N76-29114

COS-B OBSERVATIONS OF THE HIGH ENERGY GAMMA
RADIATION FROM THE GALACTIC DISC

The Caravane Collaboration

ABSTRACT

During the first months of operation, COS-B has observed galactic high-energy gamma rays from the galactic disc. In the galactic centre and Vela regions the disc emission distribution has been measured. From these data the existence of a local (< 1 kpc) and a distant (> 3 kpc) emitting region is apparent in the general direction of the inner galaxy.

1. Introduction. During the first three months of operation the COS-B experiment has observed approximately one fourth of the galactic disc including the galactic-centre region, the galactic anticentre and the Vela region. A completely automatic analysis of the events recorded during these observations reveals a galactic gamma-ray emission from the three regions. In the anticentre and Vela regions localized sources of gamma-ray emission are present. The study of these discrete gamma-ray sources is described in an accompanying paper.

The presence of localised sources complicates the observation of the diffuse galactic emission, especially in the anticentre region, where the contribution of the galactic background cannot at present be resolved from the discrete sources. The reduction of the effective sensitive area for photons incident at large angles limits the significance of the events recorded at the edges of the observation zones. For this presentation, our survey of the galactic emission is then restricted to the Vela region ($244^\circ < \text{LII} < 284^\circ$) and to the galactic centre region ($350^\circ < \text{LII} < 20^\circ$).

The exact nature of the origin of the high-energy gamma rays from the Galaxy is still questionable in spite of the large number of interpretations of the SAS-2 data. (For a review see for instance Paul, Cassé and Cesarsky, 1976). Most of these interpretations indicate that the galactic gamma rays originate in the galactic disc and especially in the interstellar gas layer - the scale height of the galactic disc, the observed width of the galactic emission and the angular resolution of the gamma ray detector provide limits to the distance of the emitting regions. For example an emitting region located in a disc ~ 200 pc thick would appear to be about 4° wide if its distance from the Sun is 3 kpc. It has been suggested (Fichtel et al, 1975) that towards the galactic centre (within $\pm 30^\circ$ longitude) the high-energy gamma-ray emission (>100 MeV) is represented by the sum of a wide contribution from the nearby Sagittarius arm and a narrow component coming from distant regions. At other galactic longitudes only a wide component has been observed. A high-resolution observation of the galactic gamma ray emission (>15 MeV) indicates that a dominant part of the gamma radiation emitted from the direction of the galactic centre may be confined to a $\sim 3^\circ$ wide band lying along the galactic equator (Samimi, Share and Kinzer, 1974) suggesting a source location more distant than 4 kpc.

High-resolution observations can be achieved by the COS-B experiment if high-energy events are selected. For example, the angular resolution of the experiment is about 3° for photons of 300 MeV (Bennett et al, 1974). With such a resolution a line emission as thin as 4° may be resolved. The long exposure time achieved during our galactic-disc survey enables us to take advantage of the better angular resolution at high energy.

For the purpose of this paper only those gamma-ray events are considered for which the tracks of the electron pair are separately identified in two projections. Applying this selection assures that the instrumental background can be neglected with respect to the galactic emission. However the detection efficiency is not accurately known at present, so that the quoted intensities should be considered to be preliminary.

2. Observations. Figure 1 shows the latitude profile of the galactic emission in the galactic longitude interval $244^\circ < l_{II} < 284^\circ$ for the energy ranges 70-2000 MeV and 300-2000 MeV. The contribution of the Vela source has been excluded from both distributions by ignoring a circular region centered at the position of the Vela pulsar and with a radius equal to 9° (range 70-2000 MeV) or 6° (range 300-2000 MeV).

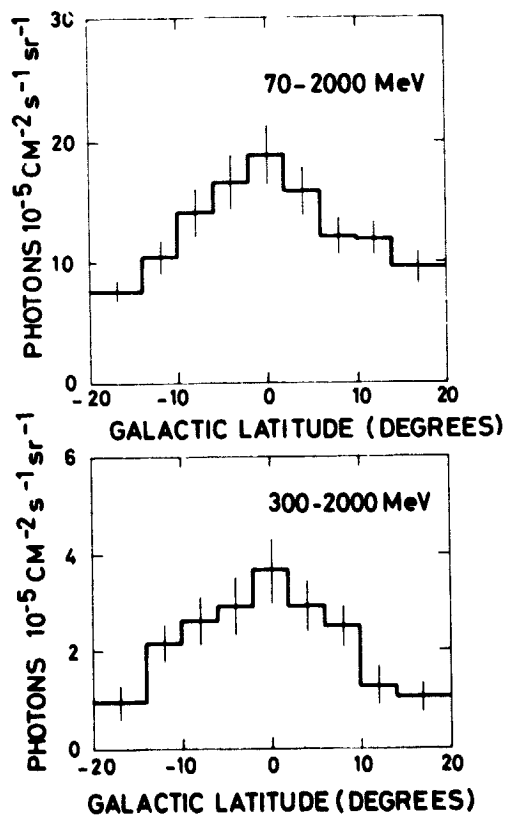


Fig. 1 Latitude profile of the gamma ray emission summed from $244^\circ < l_{II} < 284^\circ$ excluding the contribution of the Vela source. The error bars reflect only the statistical uncertainties.

The better angular resolution in the 300-2000 MeV range does not reveal more structure. The observed distribution width of about 20° suggests that at $l_{II} = 270^\circ$ the galactic high-energy gamma rays originate in regions less than 1 kpc distant.

Figure 2 shows the latitude profile of the galactic emission in the galactic longitude interval $350^\circ < l_{II} < 20^\circ$ for the energy ranges 70-2000 MeV and 300-2000 MeV. The difference between the two profiles is consistent with the variation of angular resolution with energy. The data imply the existence of a wide component and a narrow one. The measured thickness of the narrow component ($< 4^\circ$ above 300 MeV) is compatible with a thin line emission. The wide component is

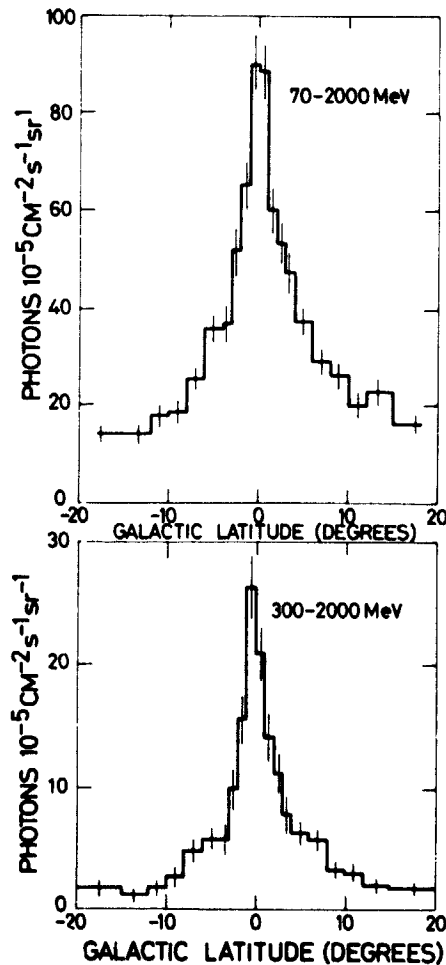


Fig. 2 Latitude profile of the gamma ray emission summed from $l_{II} = 350^\circ$ to $l_{II} = 20^\circ$.

reminiscent of the disc profile in the Vela region. This result suggests that most of the gamma rays recorded in the latitude intervals $-10^\circ < b_{II} < -2^\circ$ and $2^\circ < b_{II} < 10^\circ$ originate in close-by regions (≤ 1 kpc) while a large fraction of those observed in the range $-2^\circ < b_{II} < 2^\circ$ come from distant regions, at least >3 kpc if one assumes that the scale height of the emitting region is 100 pc. A more quantitative analysis is required to resolve the possible contribution from intermediate distances.

The sensitivity of our survey permits the investigation of the galactic structure in more detail. Figure 3 shows the longitude distributions of the two components separately. The longitude distribution of the close-by component (curve b) is reminiscent of the distribution of the predicted contribution from the interstellar medium within 1 kpc of the Sun as deduced from interstellar reddening by Puget et al (1975).

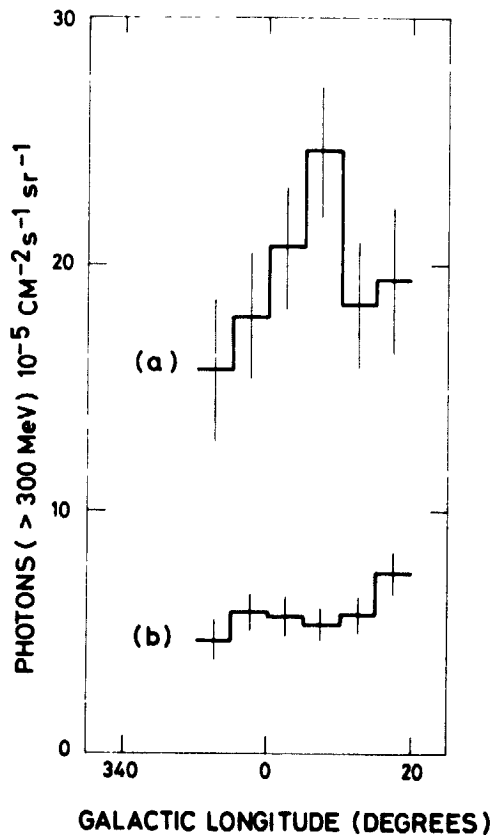


Fig. 3 Longitude profile of the gamma ray emission in the energy range 300-2000 MeV summed from $-2^\circ < b_{II} < 2^\circ$ (curve a) and from $-10^\circ < b_{II} < -2^\circ$ and $2^\circ < b_{II} < 10^\circ$ (curve b).

The distribution of the distant component (curve a) reaches a maximum for $5^\circ < l^{\text{II}} < 10^\circ$. While this may be taken as a hint of some structure in the inner region of the galaxy, the data definitely exclude a peaking of this high-energy radiation at $l^{\text{II}} = 0$.

3. Conclusion. In spite of the rather incomplete survey of the galactic disc presented here, the following conclusions are derived:

- i) most of the galactic high-energy gamma rays originate
 - a) from close by regions whose latitude-profile widths are compatible with a distance ≤ 1 kpc, or
 - b) from distant regions compatible with a thin line source indicating a distance > 3 kpc.
- ii) Such distant regions are not observed at $l^{\text{II}} \sim 270^\circ$ indicating that the contribution of the outer galaxy is very weak.

References

- Bennett, K., Burger, J.J., Gorisse, M., Mayer-Hasselwander, H.A., Paul, J.A., Pfeffermann, E., Shukla, P.G., Stiglitz, R., Swanenburg, B.N., Taylor, B.G. and Wills, R.D., 1974, Proc. 9th ESLAB Symposium (Frascati), ESRO SP-106, 323.
- Fichtel, C.E., Hartman, R.C., Kniffen, D.A., Thompson, D.J., Bignami, G.F., Ögelman, H., Özel, M.F. and Tümer, T., 1975, Ap. J. 198, 163.
- Paul, J., Cassé, M. and Cesarsky, C.J., 1976, Ap. J. to be published in the July 15, 1976 Ap. J.
- Puget, J.L., Ryter, C., Serra, G. and Bignami, G., 1975, Proc. 14th Inter. Cosmic Ray Conference 1, 52.
- Samimi, J., Share, G.H. and Kinzer, R.L., 1974
Proceedings of the 9th ESLAB Symposium, ESRO SP-106, 211.

' N76-29115

COS-B OBSERVATIONS OF LOCALISED SOURCES OF GAMMA-RAY EMISSION

The Caravane Collaboration

ABSTRACT

In October 1975 the high-energy gamma ray flux from the Vela pulsar was measured by COS-B to be 1.6 to 2.1 times higher than the flux measured by SAS-2 in 1973.

The existence is confirmed of a second region of enhanced radiation in the galactic anticentre in addition to that from the from the Crab pulsar.

1. Introduction. COS-B data from the first three observation periods, galactic anticentre, galactic centre and Vela region, have been analysed by the automatic processing sequence. This comprises spark chamber picture recognition and classification and derivation of the direction of incidence and energy for each event recognized as a gamma ray. Intensity skymaps were produced for selected event classes and energy ranges.

Since only the purely automatic picture recognition process is used for the present analysis there remains a residual background in these skymaps. Although for the gamma classes 2 and 22 used for this analysis the background is higher than for class 22 alone, the possibility to use the calibration data already available for class 2 and 22 makes it preferable to use these data.

In Figure 1 the data from the first three observation periods for gamma rays of energy greater than 100 MeV are plotted as line fluxes derived by integrating intensities from -10° to $+10^\circ$ galactic latitude. The error bars indicate statistical errors. The striking feature is the high peak observed in the Vela region.

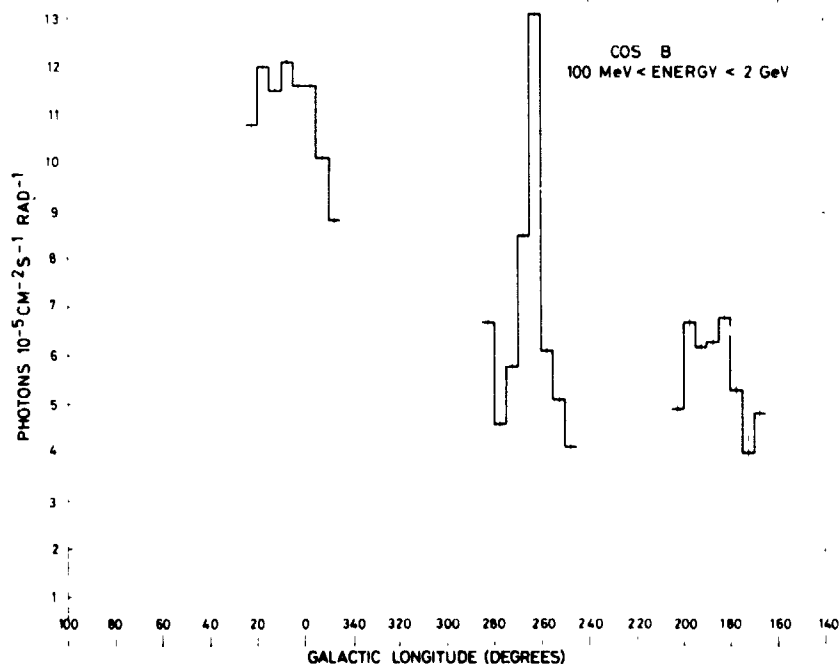


Fig. 1 Observed flux for three observation periods integrated over the latitude range -10° to $+10^\circ$ for the energy range 100 MeV to 2 GeV, derived by automatic analysis without background subtraction. Statistical errors are indicated.

2. Vela. Figure 2 shows a latitude profile across the galactic plane integrated over 22° of longitude centred on the Vela pulsar. To make use of the better angular resolution the 300 to 2000 MeV energy band is used for this latitude profile. In this profile it is seen that the peak coincides within 0.5 degree with the position of the Vela radio pulsar (PSR 0833-45) at $b^{\text{II}} = -2.8^\circ$. The width of the peak is consistent with that expected from the angular resolution as determined from the calibration for this energy range. It is therefore evident that most of the source flux is emitted from a source much less extended than the supernova remnant which has a diameter of 5 degrees. Final evidence for the identification of this gamma ray point source with the radio pulsar will be provided in a following paper on pulsation analysis.

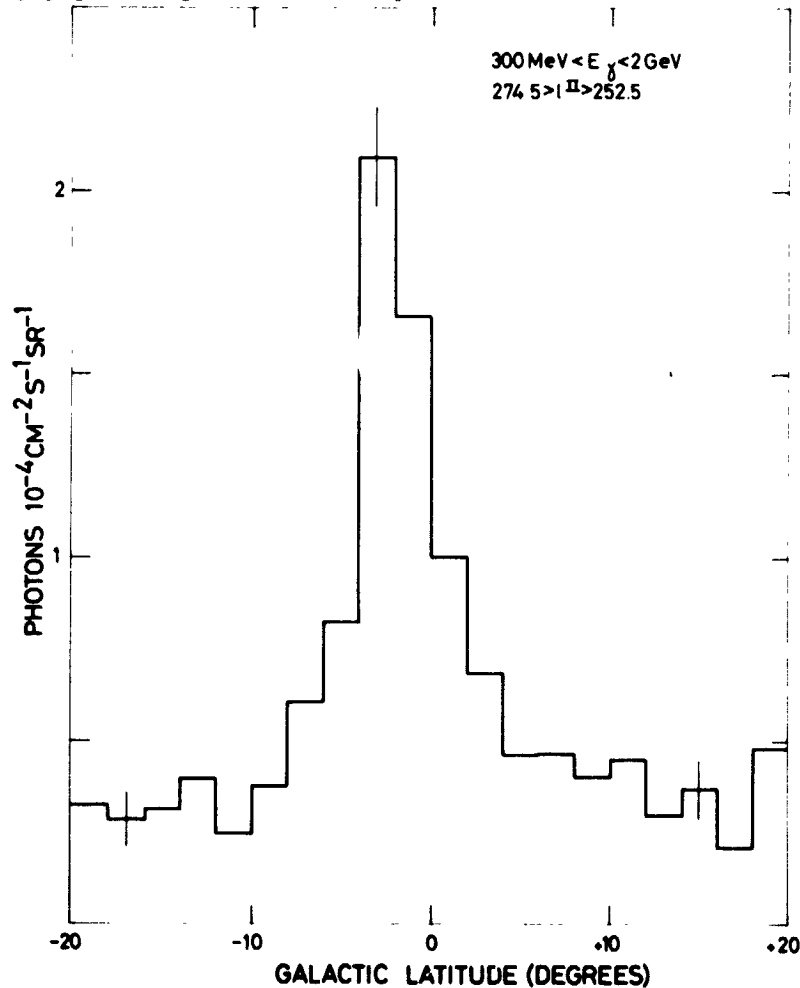


Fig. 2 Latitude profile in the Vela region for the energy range 300 MeV to 2 GeV. (Analysis and errors as for Figure 1).

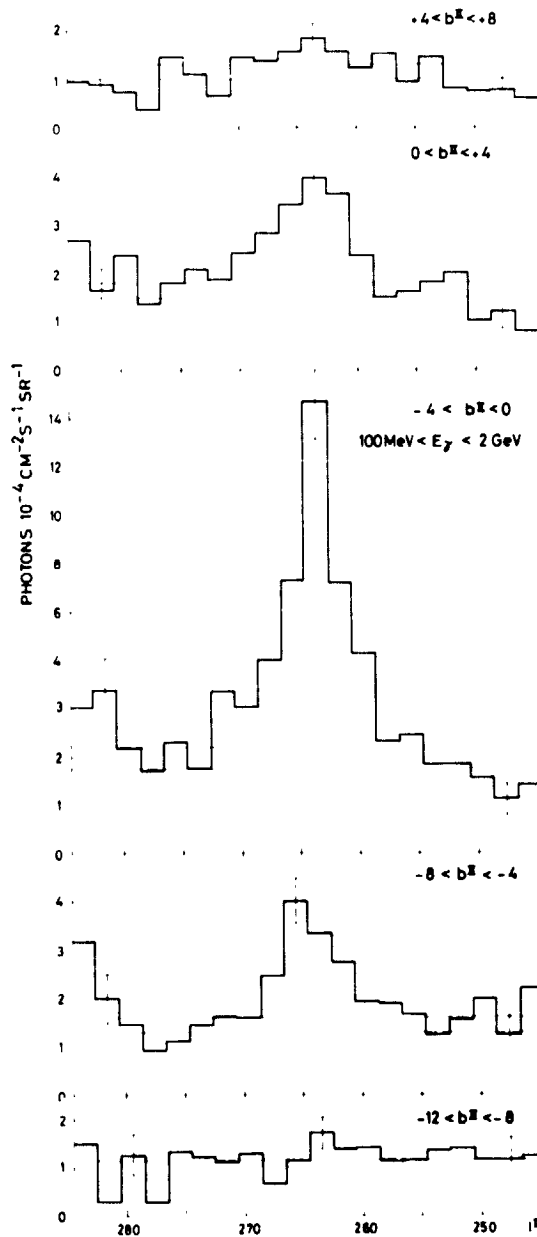


Fig. 3 Longitude scans for the Vela region in five latitude bands for the energy range 100 MeV to 2 GeV. (Analysis and errors as for Figure 1).

It is worthwhile to remark that the Vela observation period was divided into two parts, one with the experiment axis pointed to the Vela pulsar ($l^{II} = 264^{\circ}$, $b^{II} = -3^{\circ}$) the other with the axis directed to the binary system 3U0900-40, ($l^{II} = 263^{\circ}$, $b^{II} = +4^{\circ}$). Analysis of these two periods gave consistent results and prove the correctness of the applied analysis procedure concerning the reconstitution of arrival directions.

Longitude scans for different latitude intervals are presented in Figure 3 for energy greater than 100 MeV. These clearly indicate the source contribution above the galactic disc and background. In order to separate the intensity of the Vela point source from the underlying galactic disc and background components, a maximum and minimum background level in each scan has been assigned and the excess flux above these levels has been attributed to the point source leading to the flux values given in Table 1. Comparing these limits with the measurement of SAS-2 (Thompson et al, 1975) we find that our values are 1.6 to 2.1 times higher.

TABLE 1

Energy Range	COS-B	SAS-2
	100-2000 MeV	>100 MeV
Flux Upper limit ($\text{cm}^{-2} \text{s}^{-1}$)	1.3×10^{-5}	$(6.3 \pm 1.1) \times 10^{-6}$
Flux Lower limit ($\text{cm}^{-2} \text{s}^{-1}$)	1.0×10^{-5}	

This factor is too large to be accounted for by error in the COS-B calibration or analysis. This is supported by a comparison of the COS-B measurement of the narrow line component from the galactic centre region with the flux derived from the measurements of SAS-2; the COS-B flux comes out about 15% lower than the SAS-2 figure.

It is interesting to note that a glitch in the pulsar period took place about one month prior to the COS-B observation (Manchester, Goss and Hamilton, 1976; the previous glitch occurred about 1.5 yr before the SAS-2 observation. The increased rotational energy loss after the glitch cannot simply explain the increased γ luminosity. If the two phenomena are related the gamma ray emission, absorption or beaming process must be extremely sensitive to changes in rotational parameters.

No change in intensity (greater than 20%) is apparent in the 39 days of observation. A second observation is scheduled for August 1976 with the aim of gaining insight into the long-term behaviour of the Vela luminosity.

3. The Galactic Anticentre Region. In Figure 1 the COS-B data show a relatively weak and wider peak in the anticentre, as compared with the Vela region. From the detailed sky map it was seen that this enhancement has broad maxima centred at two positions, one being $l_{II} = 185^\circ$, $b_{II} = -6^\circ$, the Crab Pulsar, the other being the location $l_{II} = 195^\circ$, $b_{II} = +5^\circ$ for which enhanced radiation has been already reported by Kniffen et al (1975). More detailed longitude and latitude profiles centered at each of the two positions are given in Figures 4 and 5.

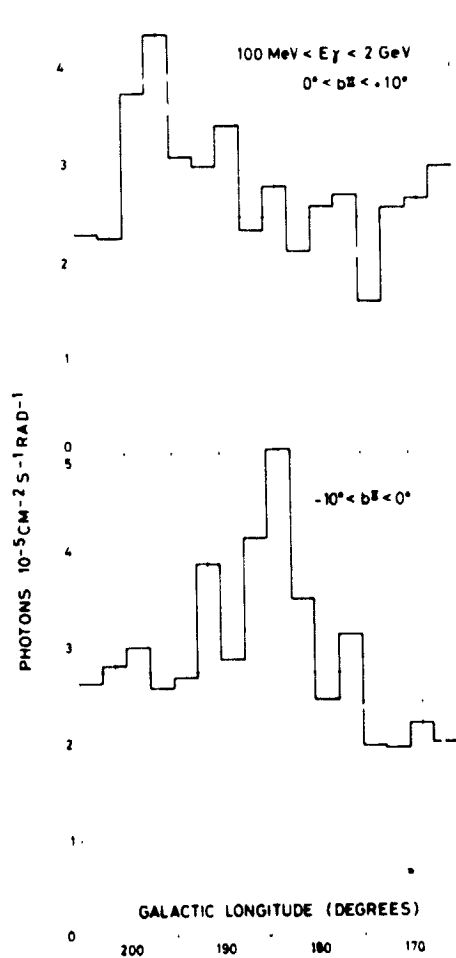


Fig. 4 Integrated fluxes in two latitude bands in the anticentre region for the energy range 100 MeV - 2 GeV. (Analysis and errors as for Figure 1).

Figure 4 shows longitude profiles, one north the other south of the galactic equator, integrated over 10° of latitude. The profiles show similar asymmetric peaks. In Figure 5 latitude profiles are shown; we again find distinct asymmetric peaks with maxima at the location of Crab and at $l_{II} = 5^\circ$. The larger statistical errors in the latter region are due to the reduced sensitivity since this region is about 14° from the experiment axis.

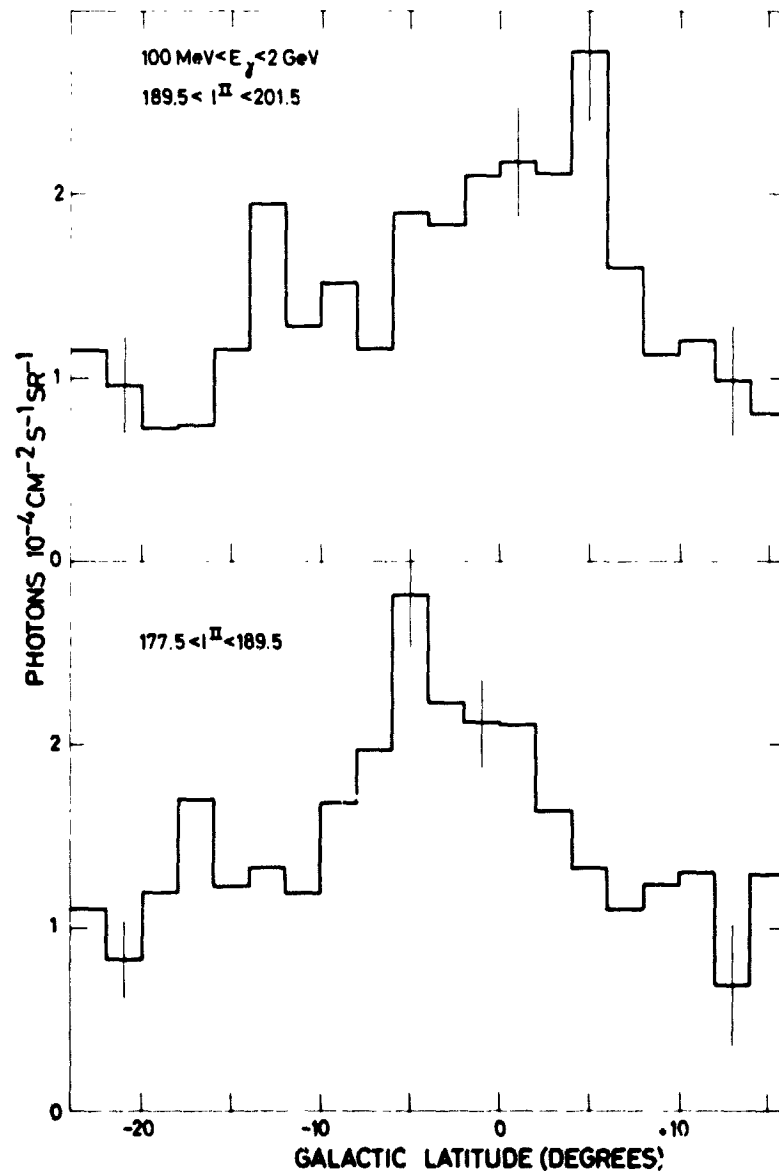


Fig. 5 Latitude profiles for the anticentric region centered on the longitudes $l_{II} = 185^\circ$ and $l_{II} = 195^\circ$. (Analysis and errors as for Figure 1).

Using a method similar to that for the Vela source, the magnitude of the enhancement from the region $-10^\circ < b_{II} < 0^\circ$ and $177.5^\circ < l_{II} < 192.5^\circ$ (Crab) is found to be $(3.0 \pm 0.5) \times 10^{-6} \text{ cm}^{-2} \text{ s}^{-1}$. The flux determined for the region $0^\circ < b_{II} < 10^\circ$ and $187.5^\circ < l_{II} < 202.5^\circ$ is $2.2 \times 10^{-6} \text{ cm}^{-2} \text{ s}^{-1}$ with similar uncertainties.

The statistical uncertainties in the present data do not allow a detailed investigation of the structure of the emission region. The peak at $l_{II} = 195^\circ$, $b_{II} = 5^\circ$ is consistent with a point source but an extended object cannot be ruled out.

It is planned to look in this region again with COS-B in October 1976 with the optical axis nearer to the region $l_{II} = 195^\circ$, $b_{II} = 5^\circ$. These data may help resolve the uncertain nature of the emission in this complex region of the sky.

References

- Kniffen, D.A., Bignami, G.F., Fichtel, C.E., Hartman, R.C., Ögelman, H., Thompson, D.J., Ozel, M.E. and Tumer, T., 1975, Proc. 14th Internat. Cosmic Ray Conf. (Munich), 1, 100.
- Manchester, R.N., Goss, W.M., and Hamilton, P.A., 1976, Nature, 259, 291.
- Thompson, D.J., Fichtel, C.E., Kniffen, D.A. and Ögelman, H.B., 1975, Ap. J. (letters), 200, L79.

N76-29116

THE TIME STRUCTURE OF THE GAMMA-RAY EMISSION FROM THE CRAB
AND VELA PULSARS

The Caravane Collaboration

ABSTRACT

High-resolution data on the pulsed gamma-ray emission from the Crab and Vela pulsars are presented. The light curves of these two pulsars at gamma-ray energies show striking similarities.

The measured pulsed intensity from Vela at energies greater than 50 MeV was found to be $\sim 1.3 \times 10^{-5} \text{ cm}^{-2}\text{s}^{-1}$. The energy spectrum is not consistent with a power law.

1. Introduction. The objective of studying the short-period temporal behaviour of possible gamma-ray emission from sources known to have time structure at longer wavelengths was included when the COS-B mission was defined. At that time, some 50 radio pulsars were known and one, NP-0532, the Crab pulsar, had been observed to emit pulsed radiation in X-rays and possibly gamma rays (Vasseur et al, 1971, Leray et al, 1972). The number of radio pulsars known now is about 150 and two, possibly four, gamma ray pulsars have been detected (Browning, Ramsden and Wright 1971, Albats et al 1972, McBreen et al 1973, Albats et al 1974, Thompson et al 1975, Ugelman et al 1976).

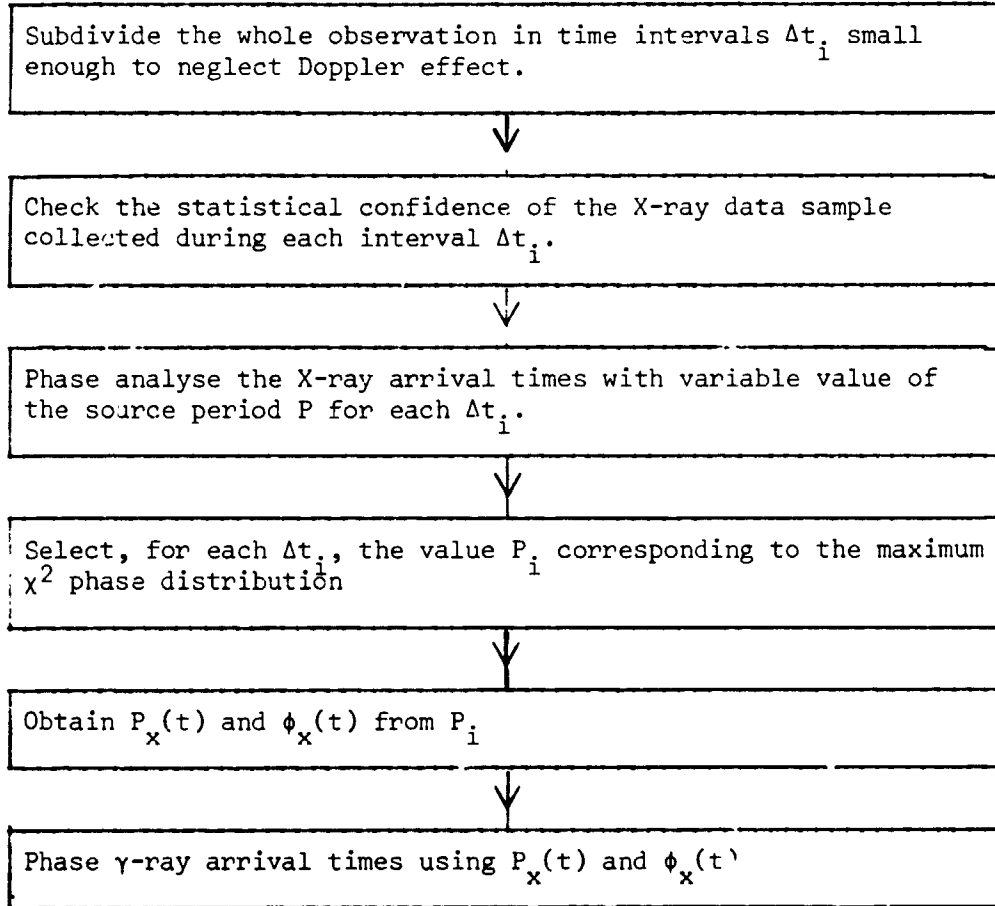
Apart from the intrinsic interest in the temporal properties per se, the detection and correlation of a characteristic time structure can be decisive for the identification of weak gamma-ray point sources buried in, for example, the galactic plane.

The low intensity of gamma rays above 30 MeV requires long observation times ($\sim 10^6$ secs.) to provide sufficient statistic to extract temporal patterns from the background. Under these conditions, a phase analysis down to 1 ms or less with the solar barycentric system as reference frame, would require a stability of the on-board clock and a knowledge of the satellite orbital elements beyond the expected scope of the COS-B programme. Hence a small X-ray detector, referred to as the pulsar synchroniser (PS), with an effective area of 80 cm^2 sensitive to X-rays in the interval 2-12 KeV was included in the payload (Boella et al, 1974). The arrival times of the X- and γ -quanta at the satellite would be determined by sampling the spacecraft clock to 0.2 ms increments. This detector would provide a convenient counting rate capability so that the period and phase of X-ray pulsars of intensity down to 0.1 of the pulsed emission from the Crab could be obtained in the satellite reference frame in intervals of about one hour, within which Doppler effects due to the motion of the earth and satellite could be neglected. With this information the search for pulsations in the gamma-ray emission could be undertaken.

In fact, it has been possible to determine the satellite position to better than 20 km, a factor ~ 4 better than expected and the on-board clock has achieved a stability of 1 in 10^9 over three hours, ten times better than specified. The on-board time can be related to UTC to better than 1 ms. Thus COS-B is able to perform a gamma ray phase analysis both by synchronising with the X-ray data from the pulsar synchroniser in the satellite reference frame and by using the solar-system barycentre as a reference frame.

2. Description of the procedures used for the pulsar analysis

The following block-diagram outlines the phase analysis by the synchronisation method:



The validity of the method was checked by a study in which the experimental conditions of COS-B were simulated. That part of the X-ray analysis relative to the extraction of the pulsating pattern in each of the synchronisation intervals Δt_i has been tested on experimental and Monte-Carlo simulated data in order to check the confidence of the algorithm used (Boella et al 1974).

For the Solar-System Barycentre analysis the two steps were (a) transformation of photon arrival times at the barycentre - using the ephemeris (kindly supplied by Lincoln Lab. through the courtesy of Dr. Henry Helmken (SAO)) and the position of the satellite and

(b) computation of residual phases at the barycentre. In the case of NP 0532 the solar-barycentric period and phase have been derived from the X-ray analysis through the synchronisation method. For PSR 0833 a "period model" has been used as obtained from radio observations by Manchester, Goss and Hamilton (1976) and Reichley and Downs (private communication). Absolute radio phase values are not yet available for comparison.

3. NP 0532 observations. COS-B observed NP-0532, the Crab Nebula and the region of the galactic anticentre from 17 August to 17 September 1975. The X-ray light curve is shown in Figure 1 for the entire observation period excluding intervals when the data were disturbed. The pulsed fraction of X-ray emission in the range 2-12 keV, accounting for the instrumental background is 8.5%, which is compatible with the results of Ducros et al (1970).

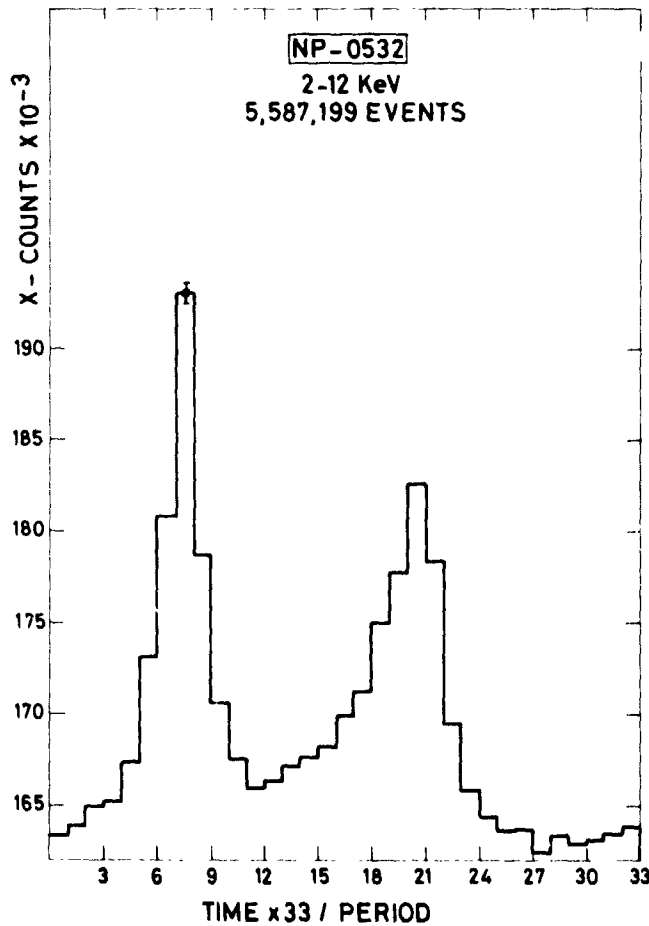


Fig. 1
X-ray light curve
of the Crab pulsar
NP 0532 obtained
for the period 17 Sep-
tember 1975. The
pulsar period of
33.1 ms is divided
into bins of
 ~ 1 ms.

Figure 2 shows, superimposed on the X-ray light curve, the gamma-ray light curve derived by the synchronization method for class 2 and 22 events for energies ≥ 50 MeV and for reconstituted directions within an acceptance cone of half-angle $\theta_{\max} = 6^\circ$ centred on the pointing direction, for all intervals when both X-ray and gamma-ray data were available simultaneously ($\sim 50\%$ of the operational time). The very strong similarity of the X- and gamma-ray light-curves is evident.

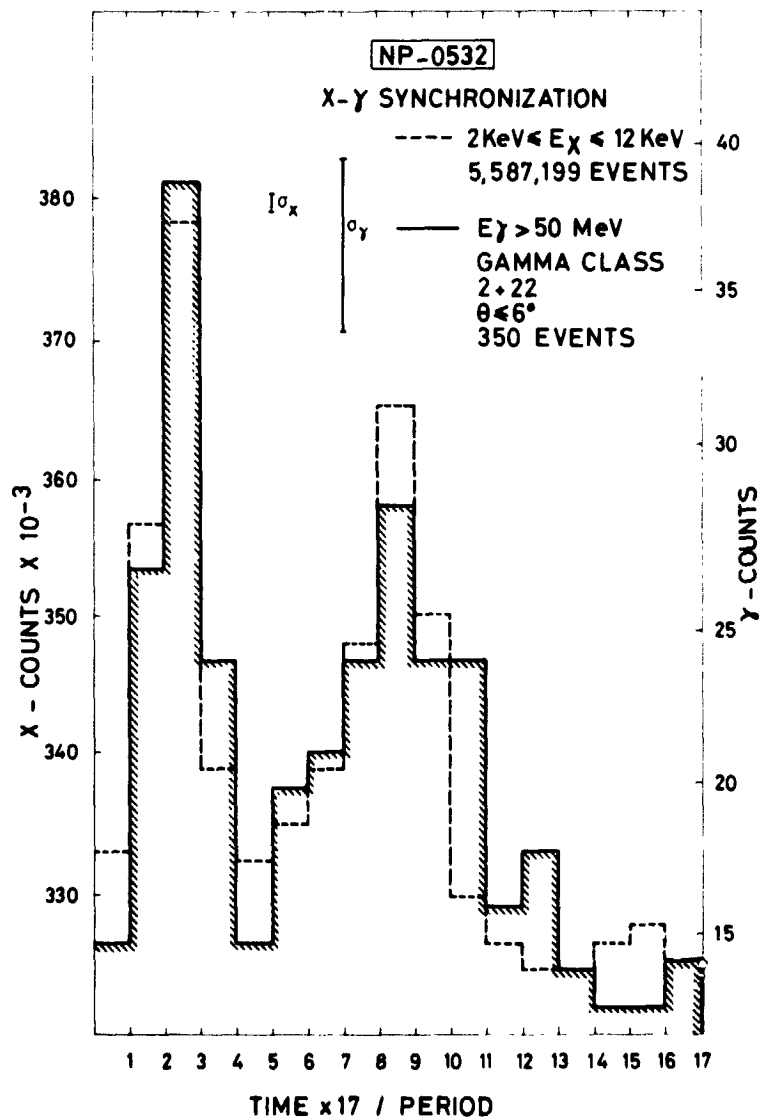


Fig. 2 Gamma-ray light curve of NP 0532, obtained by the synchronization method, compared with the X-ray light curve. The pulsar period is divided into bins of ~ 2 ms.

Figure 3 shows the gamma-ray light curve derived by the solar-barycentric analysis for class 2 and 22 events with energies ≥ 50 MeV and within $\theta_{\max} = 8^\circ$. This analysis used radio data supplied by Rankin (private communication) updated by phase information obtained from the PS. All available gamma-ray data over the completed observation period have been used. The separation of the two peaks is 13.5 ms, while the main- and interpulse have 1.5 ms and 3.0 ms widths at half height respectively. The lower limit for the pulsed fraction for $E_\gamma \geq 50$ MeV derived from Figure 3 is $\sim 35\%$, with the background level taken as the average of bins 47 to 66. It must be noted that the unpulsed fraction includes any continuous component from the source, a contribution from the general gamma-ray emission from the anticentre region and instrumental background.

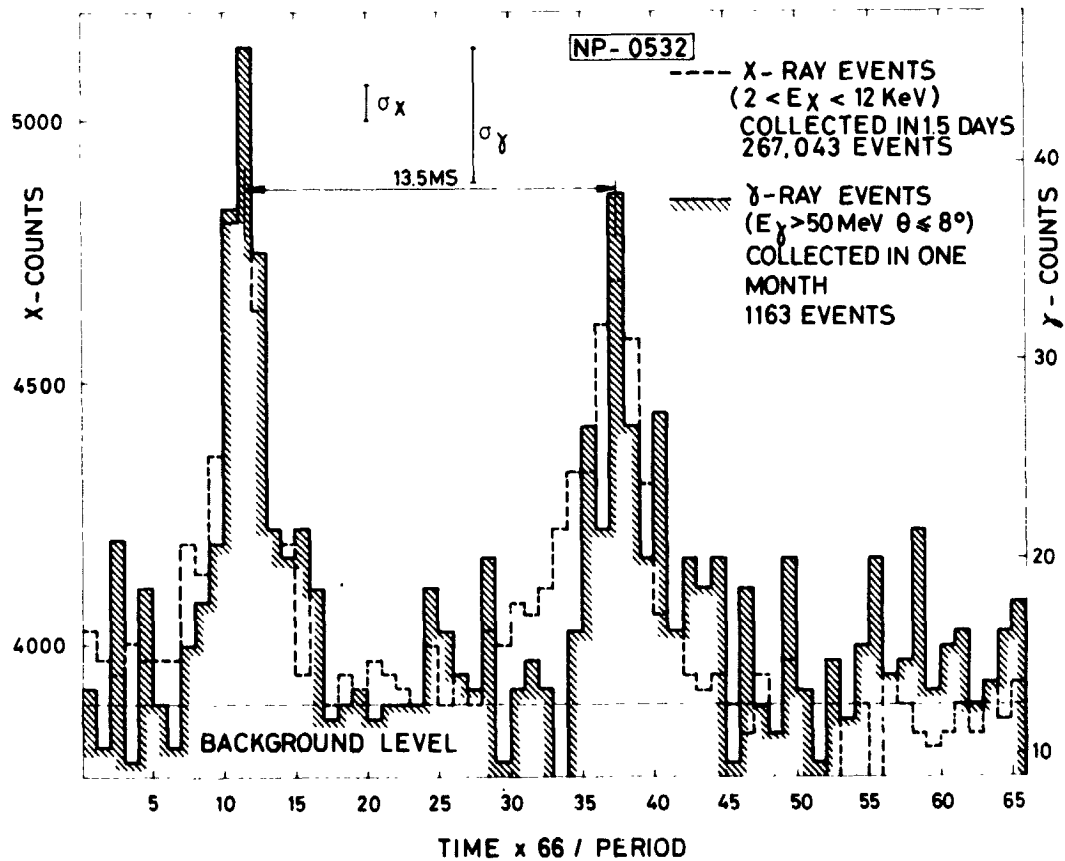


Fig. 3 Gamma-ray light curve of NP 0532, obtained by solar system barycentric analysis, compared with the X-ray light curve. The pulsar period is divided into bins of ~ 0.5 ms.

So far, only 36 h of X-ray data have been analysed by this method. The X-ray light-curve obtained is superimposed on the gamma-ray light-curve in Figure 3. The overall similarity of Figures 2 and 3 gives confidence for the application of the barycentric analysis for pulsars not exhibiting temporal structure observable by the PS.

4. PSR 0833-45 observations. COS-B observed the neighbourhood of the Vela supernova remnant, with the experiment axis directed to PSR 0833-45 from 20 October to 8 November and to 3U0900-40 from 8 November to 20 November 1975. Since the pulsar emits little or no pulsed X-radiation (Rappaport et al, 1974), the synchronization method cannot be applied and gamma-ray light curves can only be obtained through the barycentric method. The barycentric analysis has been carried out separately for the two periods, based on the radio data. Only the first period has been analysed in detail.

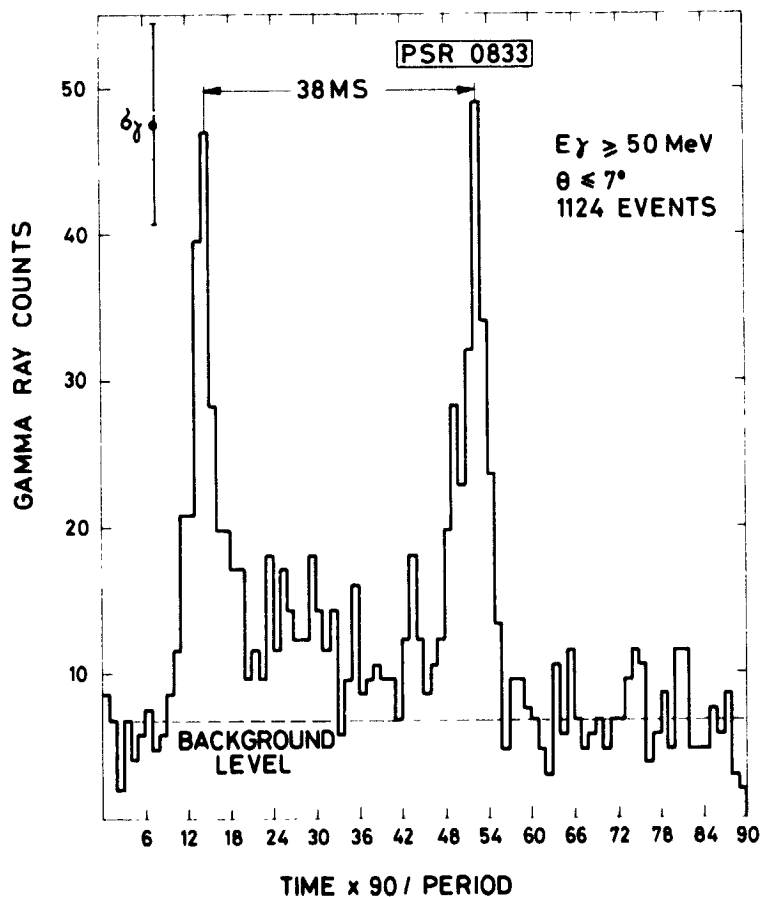


Fig. 4 Gamma-ray light curve of PSR 0833, obtained through solar system barycentric analysis, for the period 20 October to 8 November 1975. The pulsar period of 89.2 ms is divided into bins of ~ 1 ms.

Figure 4 is an example of the gamma-ray light curve for class 2 and 22 events of $E_{\gamma} > 50$ MeV and for $\theta_{\max} = 7^{\circ}$. This result clearly establishes details of the pulsed gamma-ray emission. The separation of the two peaks is 38 ms, while the main- and interpulse have 3 ms and 6 ms widths at half height respectively. These widths are in contrast with the measurements of Thompson et al (1975), who reports widths of 14 ms.

A series of light-curves for various selections on energy and arrival direction has been produced. From these, Figure 5 has been derived which shows the number of gamma rays above the background (average of bins 67 to 90) in the phase plot as a function of θ_{\max} for five energy intervals. The number of pulsed gamma rays reaches a maximum at higher acceptance angles as the energy is decreased, consistent with the variation of angular resolution with energy. The curves through the data points have been fitted qualitatively. The

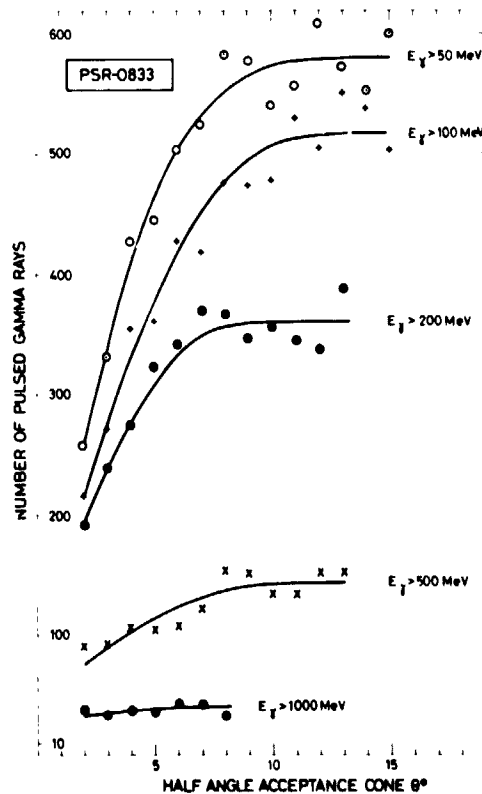


Fig. 5 The number of pulsed gamma rays, i.e. those in the light curve peaks above the background level, shown as a function of the half angle of the acceptance cone for reconstituted gamma-ray arrival directions centred on PSR 0833, for five energy intervals.

asymptotic value of the number of pulsed events for each energy has been taken and, correcting for the energy dependence of the sensitivity of the instrument, the integral energy spectrum shown in Figure 6 was obtained. Over the energy range from 50 to 1000 MeV, the spectrum is not consistent with a power law. The pulsed flux above 50 MeV is $1.3 \times 10^{-5} \text{ cm}^{-2}\text{s}^{-1}$ and above 100 MeV is $1.0 \times 10^{-5} \text{ cm}^{-2}\text{s}^{-1}$.

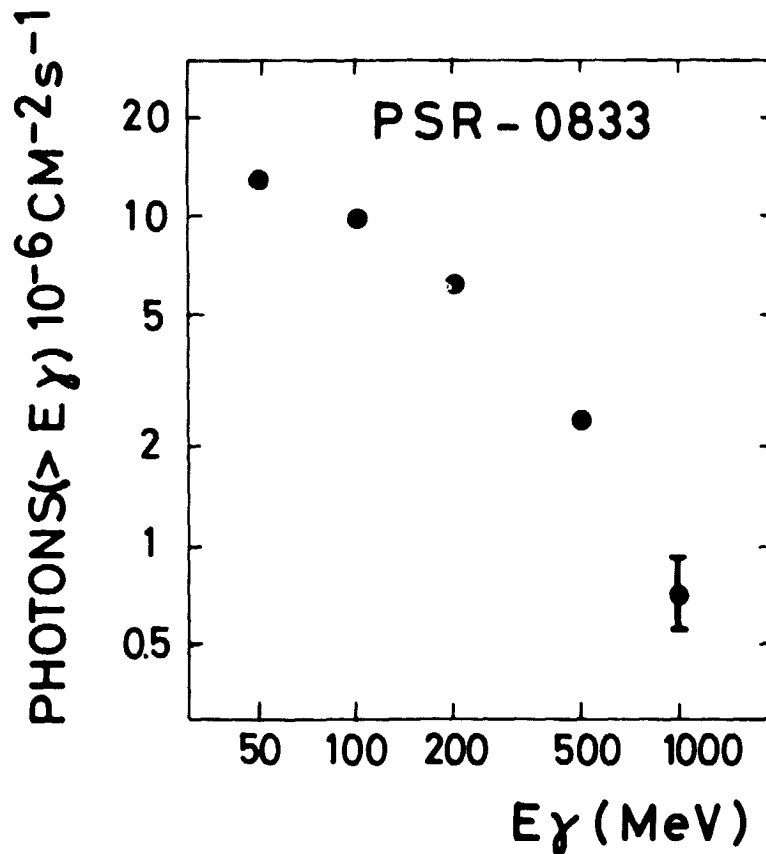


Fig. 6 The integral energy spectrum for the pulsed component of the gamma-ray emission from PSR 0833. The statistical error at 1 GeV (40 counts) is indicated. The data have not been corrected for the finite energy resolution, which may result in uncertainties $\sim 20\%$ in energy assignment. The intensity for $E_\gamma \geq 50 \text{ MeV}$ is $1.3 \times 10^{-5} \text{ photons cm}^{-2} \text{ s}^{-1}$.

The pulsed fraction of gamma rays for above 50 MeV and above 500 MeV as a function of acceptance angle is plotted in Figure 7. The diagram shows that the lower limit of the pulsed fraction is approximately 85%. The unpulsed fraction contains any non-varying component from the pulsar, the supernova remnant, the galactic plane and instrumental background. Given this pulsed fraction, the pulsed flux is consistent with the total flux quoted in the previous paper.

Comparing these measurements with those of Thompson et al (1975), we conclude that the pulsed luminosity has increased significantly (by about a factor of 2). It is uncertain whether the apparent change in pulse widths is related to this change in luminosity.

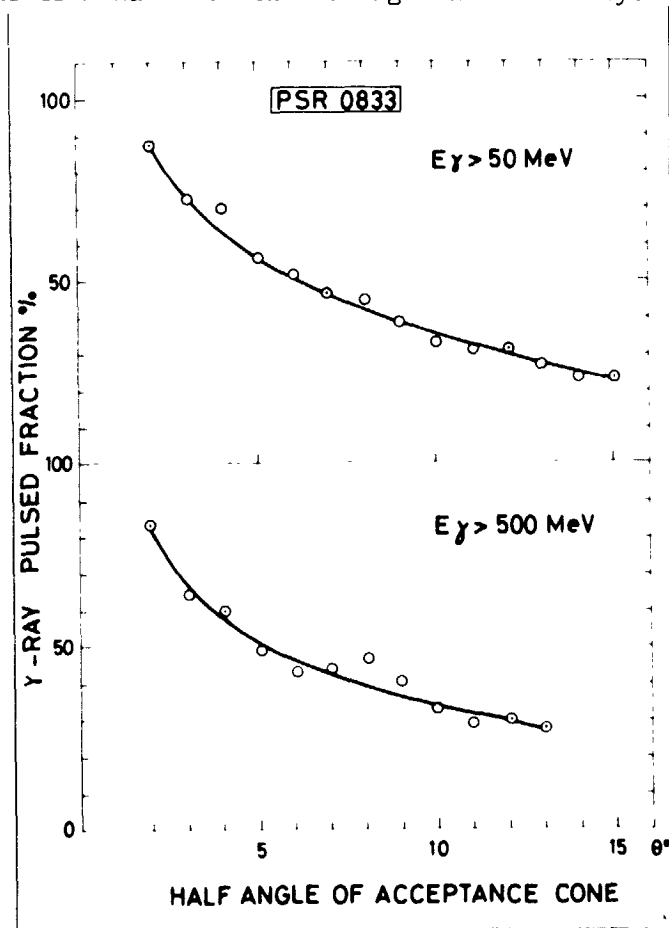


Fig. 7 The pulsed fraction of gamma rays recorded as a function of the half angle of the acceptance cone for reconstituted gamma-ray arrival directions centred on PSR-0833 for $E_\gamma > 50$ and > 500 MeV. The lower limit to the pulsed fraction is $\sim 85\%$.

5. Comparison of NP-0532 and PSR 0833-45. Figure 8 shows the gamma-ray light curves for $E_\gamma > 50$ MeV and $E_\gamma > 200$ MeV derived by solar barycentric analysis for the complete observation period of NP 0532 and for the second period 8-28 November on PSR 0833-45. For both

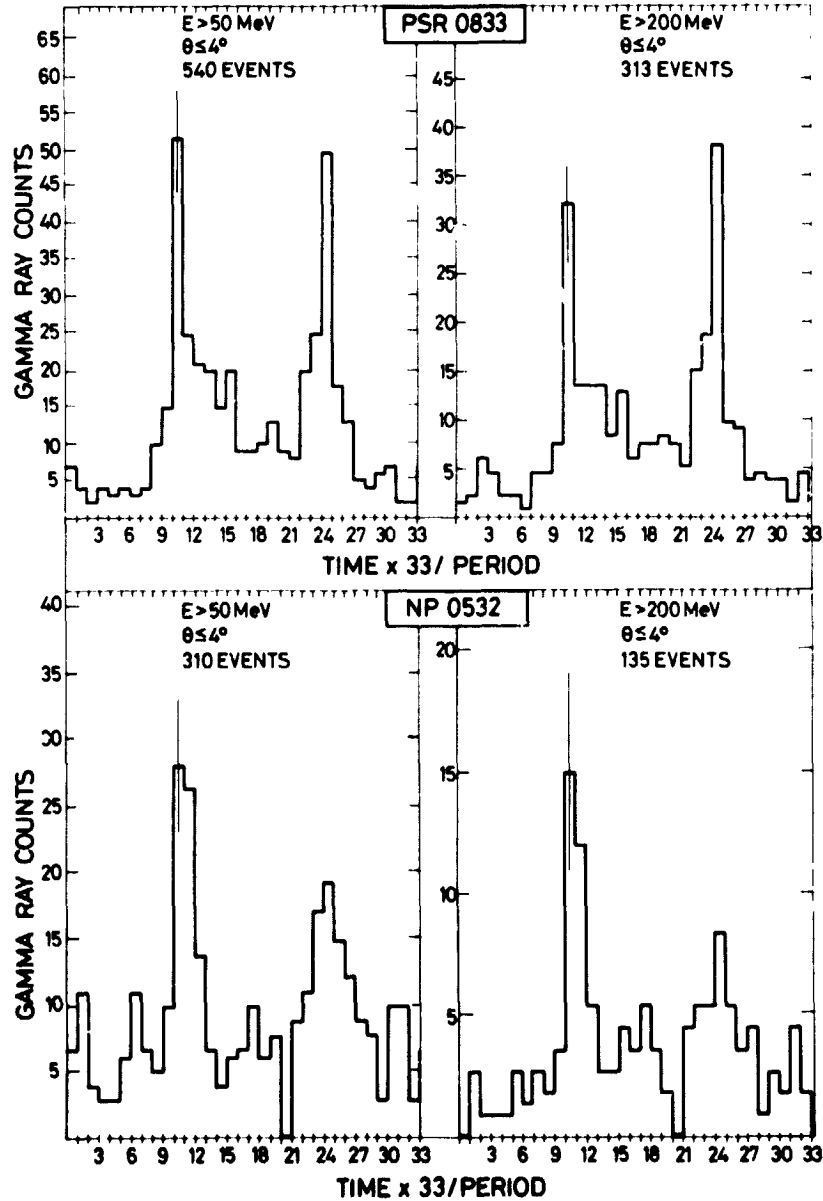


Fig. 8 The gamma-ray light curves of PSR 0833 (8-28 November 1975) and NP 0532 (17 August - 17 September 1975) compared at $E_\gamma > 50$ and 200 MeV, with the periods of both the pulsars divided into 33 time bins.

pulsars the structure is dominated by two narrow pulses separated by 0.42 of the period. This structure is practically the same for the two energies shown.

In the light of the extreme difference of these two pulsars at longer wavelengths and their striking similarity at gamma-ray energies, it is tempting to suggest that the pulsar process manifests itself directly in the gamma-ray emission and that the radiation at lower energies reflects more complicated processes.

References

- Albats, P., Frye, G.M. jr, Zych, A.D., Mace, O.B., Hopper, V.D. and Thomas, J.A. 1972, *Nature* 240, 221.
- Albats, P., Frye, G.M. jr, Thomson, G.B., Hopper, V.D., Mace, O.B., Thomas, J.A. and Staib, J.A. 1974, *Nature*, 251, 400.
- Boella, G., Buccheri, R., Burger, J.J., Coffaro, P and Paul, J., 1974, Proc. 9th ESLAB Symposium (Frascati) ESRO SP-106, 353.
- Browning, R., Ramsden, D. and Wright, P.J., 1971, *Nature Phys Sci.*, 232, 99.
- Ducros, G., Ducros, R., Rocchia, R. and Tarrius, A., 1970, *Nature*, 227, 153.
- Leray, J.P., Vasseur, J., Paul, J., Parlier, B., Forichon, M., Agrinier, B., Boella, G., Maraschi, L., Treves, A., Buccheri, R., Cuccia, A., and Scarsi, L., 1972, *Astron. and Astrophys.*, 216, 443.
- Manchester, R.N., Goss, W.H. and Hamilton, P.A., 1976, *Nature*, 259, 291.
- McBreen B., Ball, S.E., Campbell, M., Greisen, K. and Koch, D., 1973, *Ap. J.*, 184, 571.
- Ogelman, H., Fichtel, C.E., Kniffen, D.A. and Thompson D.J., 1976, preprint.
- Rappaport, S., Bradt, H., Doxsey, R., Levine, A. and Spada, G., 1974, *Nature*, 251, 471.
- Thompson, D.J., Fichtel, C.E., Kniffen, D.A. and Ogelman, H.B., 1975, *Ap. J.*, (Letters), 200, L79.
- Vasseur, J., Paul, J., Parlier, B., Leray, J.P., Forichon, M., Agrinier, B., Boella, G., Maraschi, L., Treves, A., Buccheri, R., Cuccia, A. and Scarsi, L., 1971, *Nature Phys. Sci.*, 203, 46.

Acknowledgements

The success of this mission owes much to the dedicated efforts of the JOC-B Project Staff lead by Mr. G. Altmann at ESTEC, Noordwijk, The Netherlands and the operations and data processing staffs at ESOC, Darmstadt, Federal Republic of Germany. For their efforts in the provision of the experiment hardware, the individual institutes of the Collaboration are indebted to the engineers of their contractors, namely:

Dr. W. Brunner of M.B.B. and Dr. E. Hübner of Siemens (Spark Chamber), Messrs. W. Drtil and R. Zohl of A.F.G.-Telefunken (Triggering Telescope), Messrs. E.H. Stogsdill, P. Christon and R. McConaughey of Ball Brothers Research Corporation (Energy Calorimeter) and Messrs. A. Bonanni and A. Jacopini of Laben (Experiment Electronics and Pulsar Synchroniser).

N 76-29117

"LOW-AND-MEDIUM ENERGY GALACTIC GAMMA-RAY OBSERVATIONS"

Gerald H. Share, E.O. Hulburt Center for Space Research,
Naval Research Laboratory, Washington, D.C. 20375

ABSTRACT

Observation of 0.2-100 MeV diffuse gamma radiation emitted from the Galaxy can provide information on the intensities of 5-50 MeV/nucleon cosmic-rays and >50 MeV electrons in interstellar space. Recent measurements of gamma-rays emitted from the galactic center region provide evidence for a diffuse continuum between 10 and 100 MeV which is dominant over the π^- -decay emission generated in high-energy nuclear collisions. The intensities of the recently reported nuclear-line gamma rays, also observed in the direction of the galactic center, require the presence of intense fluxes of low-energy cosmic-rays in the inner Galaxy if the gamma-rays are produced on a galactic scale. Current detection techniques for 0.1-100 MeV gamma-ray measurements are summarized and their capabilities for measuring the diffuse galactic emission are evaluated. Significant improvement in our knowledge of low-and-medium energy galactic gamma radiation can be expected within the next few years.

1. Introduction. In this Symposium we are primarily interested in large scale features of our Galaxy, such as the spatial distribution of interstellar matter and energetic particles. Diffuse gamma radiation emitted from the Galaxy provides us with information which either supplements or is not obtainable from the more traditional disciplines of astronomy.

Observations of galactic gamma radiation in the hundred MeV energy region from SAS-2 and COS-B have been summarized earlier in these Proceedings. These high-energy photons are generated in the interactions of particles with kinetic energies $\gtrsim 500$ MeV. Although discrete gamma-ray sources, such as the Crab Nebula and the Vela Pulsar contribute to the enhanced emission from along the galactic plane, it is likely that most of this radiation is produced in interactions of high-energy cosmic-ray protons and alpha particles with interstellar matter. These interactions produce the characteristic π^0 -decay γ -ray spectrum which peaks near 70 MeV, and above which energy more than 80% of the emission occurs. For this reason, >100 MeV gamma rays can provide information on the fluxes of GeV cosmic-ray nuclei and on the densities of interstellar gas in regions of the Galaxy distant from Earth.

In this paper the status of the observations of lower energy ($E < 100$ MeV) galactic gamma radiation is summarized. These low-and-medium energy gamma rays provide us, in like manner, with information on the fluxes of two other components of the galactic cosmic radiation, electrons with energies $\gtrsim 50$ MeV and nuclei with energies between 5 and 50 MeV/nucleon. The electrons can generate continuum gamma radiation from bremsstrahlung interactions on interstellar gas or from "inverse" Compton scattering on interstellar starlight. The low-energy nuclei produce nuclear-line emission in inelastic collisions with interstellar gas.

The next section discusses the low-and-medium energy gamma-ray observations which have been made in the general vicinity of the galactic center ($|b^{\text{II}}| < 10^\circ; -30^\circ \lesssim l^{\text{II}} < +30^\circ$), where the intensity is expected to be greatest. Future investigations will aim at achieving better sensitivities so that low-and-medium energy gamma-ray emission can be mapped from other extended regions of the Galaxy as

well. The last section treats the detection techniques that will be in use in the next few years and the anticipated improvements in the measurements.

2. Observational Status.

A. Detection Techniques. Before presenting the observations which have been made to date, it will be helpful to first describe the instruments used. Although the SAS-2 multiplate spark chamber (Fichtel et al. 1975a) is most sensitive at energies above 100 MeV it responds to photons down to ~35 MeV. At these energies the angular resolution is considerably degraded but some spectral information on diffuse galactic emission is available.

An experiment which provides both good angular resolution ($\approx 2^\circ$) and good energy resolution ($\pm 15\%$) in the 15-100 MeV range is the emulsion wide-gap spark chamber array which Bob Kinzer, Carl Noggle, Nat Seeman and I developed at NRL (Share et al. 1974). A drawing of the configuration flown during a 1971 exposure to the galactic center region is shown in Figure 1. Gamma rays convert in the stack of nuclear emulsions (E) producing electron pairs which are detected by a counter telescope consisting of a proportional counter (P) and two plastic scintillation counters (B). The plastic scintillation counters (A) reject charged cosmic radiation. Use of a combination absorption - Čerenkov counter (C) limits detectable gamma-ray energies to ≈ 200 MeV. The trajectories of the electron pairs are photographed in a wide-gap spark chamber permitting the tracks to be located in the emulsion where precise measurements can be made near the point at which the gamma rays converted.

The third instrument, shown in Figure 2, was developed at the Smithsonian Astrophysical Observatory (Helmken and Hoffman 1970) and flown in 1971. It consists of a telescope arrangement using plastic scintillators and a gas Čerenkov counter. Although it has excellent background rejection properties and is sensitive down to ~15 MeV, it has rather poor angular resolution, $\approx 25^\circ$, and provides no spectral information.

The fourth instrument is shown in Figure 3 and was designed at Rice University to detect gamma rays of much lower energy, from ~50 keV to ~10 MeV (Walraven et al., 1975). It consists of a 5 cm thick NaI crystal, with a sensitive area of ~180 cm², which is shielded by other NaI crystals and collimated to an aperture of ~13° FWHM.

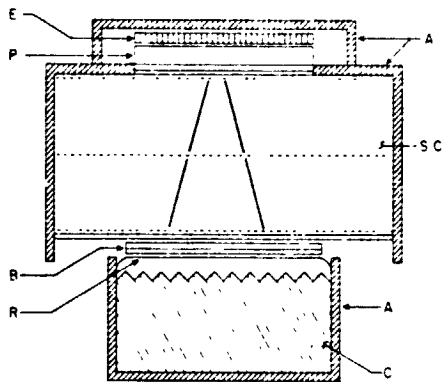


Fig. 1 NRL Emulsion-Spark-Chamber Telescope (≥ 15 MeV)

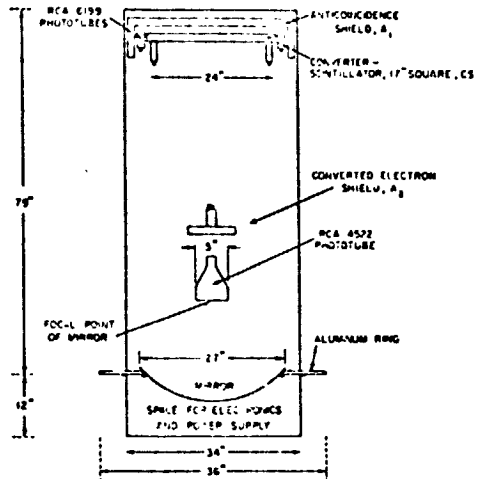


Fig. 2 SAO Čerenkov Telescope (≥ 15 MeV)

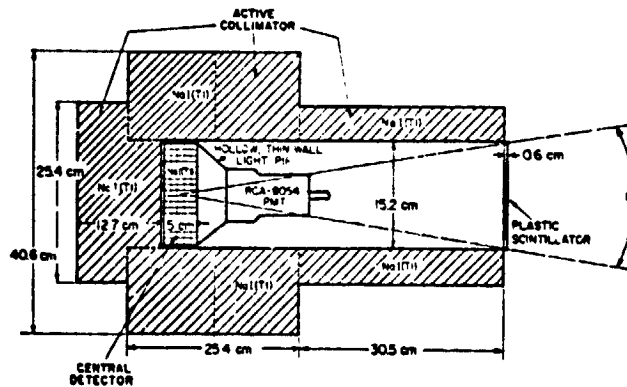


Fig. 3 Rice Actively Shielded Scintillator (0.1-10 MeV)

B. Summary of the Observations. Much of the data from these experiments relating to galactic observations have already been published. What I have attempted to do is to combine these results with some theoretical studies in order to appraise the status of our knowledge of the 0.1-100 MeV diffuse emission from the galactic plane. The summary takes the form of the differential spectrum, shown in Figure 4, of the radiation emitted from the direction of the galactic center ($|b^{II}| < 10^\circ$; $-30^\circ < l^{II} < 30^\circ$). From the shape of the spectrum, especially at energies > 100 MeV, we can determine the relative contributions that processes such as high energy proton interactions and electron bremsstrahlung make to the total gamma-ray flux. This determination is critical to the interpretation of the longitude distribution of galactic gamma rays which is discussed later in the Symposium by Floyd Stecker and Don Kniffen.

Shown at high energies are the data obtained by the group at Imperial College, London (Sood et al. 1975). The measurement between 600 and 1400 MeV was 4σ over background in the latitude interval $|b^{II}| < 4^\circ$, while the other points are 2σ upper limits. Recent extended balloon-borne exposures with this same experiment promise significant improvement in these high-energy measurements (G.K. Rochester 1976, private communication). In addition, forthcoming results from COS-B should provide good quality spectral data up to ~ 2 GeV (Bennett et al. 1974).

The data from SAS-2 have been adapted from the integral spectrum given by Fichtel et al. (1975a). Caution must be taken in using such a subtraction procedure, the large errors shown reflect this uncertainty. As suggested by Cowsik and Voges (1975) a "direct" differential representation of the SAS-2 galactic energy data, similar to that given for the diffuse cosmic background in the same paper, is desirable.

The points designated as NRL-Mashhad have been derived from an analysis of data obtained during a 1971 exposure with the emulsion-spark chamber system shown in Figure 1 (Share et al. 1974; Samimi et al. 1974). The emulsion analysis which has been performed recently at the Ferdowsi University, Mashhad, Iran is almost completed. The spectral data shown in the Figure were obtained in collaboration with Robert Kinzer and Jalal Samimi and have not been presented before in this form. They have been derived using only γ -ray events > 100 MeV for which both

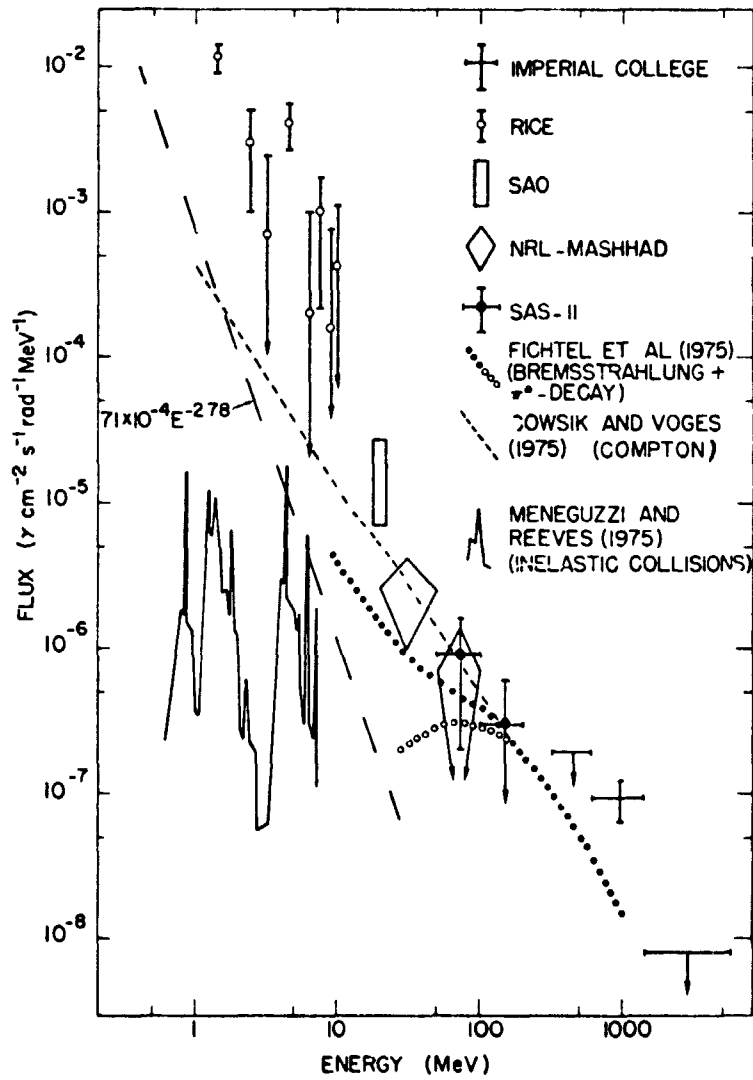


Fig. 4 Differential measurements of galactic γ -ray emission ($|b^{II}| < 10^\circ$; $|l^{II}| < 30^\circ$) compared with calculations.

members of the electron pair were energetic enough to leave the stack of emulsions and to be recorded in the spark chamber. Final results from a complete analysis will be presented in a forthcoming publication. The differential intensities were found by subtracting the contribution of atmospheric background (determined from data taken at $|b_{ll}| > 6^\circ$) from the γ -ray spectrum observed within $\pm 3^\circ$ of the galactic equator for longitudes $-30^\circ \leq l \leq 30^\circ$. The limited statistics in both the galactic and background spectra yield large errors after subtraction.

Because of the important energy range over which it was made, data obtained using the SAO Čerenkov telescope have been included, even though only an integral measurement was made. The conversion to a differential intensity yields a large uncertainty which is reflected in the errors given.

Before discussing the low-energy data, it is well to reflect on the measurements above 10 MeV. Various systematic uncertainties, such as exposures to differing sections of the galactic plane near the galactic center are present, in addition to the statistical uncertainties shown. With this in mind, the agreement between experiments is reasonable. Shown for comparison are the calculated differential spectra of galactic gamma-rays produced by electron bremsstrahlung and Compton collisions, and by cosmic-ray interactions on interstellar matter. The bremsstrahlung and π^0 -decay intensities are from the calculations of Fichtel et al. (1975b) for a galactic longitude of 335° . The π^0 intensity dominates over bremsstrahlung for energies above 100 MeV. However, as suggested by Ramaty and Westergard (1976), the bremsstrahlung contribution could be significantly greater if the cosmic-ray electrons are stopped before they can escape from the Galaxy (closed Galaxy model). The Compton spectrum shown was calculated by Cowsik and Voges (1975) and indicates that the Compton process dominates the galactic gamma-ray emission even at energies above 100 MeV. However, other estimates of the Compton source strength are significantly lower (Shukla and Paul 1976; Dodds et al. 1975).

The data in their present fragmentary form provide an indication of the dominant production mechanisms for gamma rays < 100 MeV. The NRL-Mashhad observations, taken together with those from SAS-2 are consistent with a continuum produced primarily by electron bremsstrahlung or Compton collisions.

The data plotted below 10 MeV from the Rice observations (Haymes, et al. 1975) were obtained during an exposure centered on the hard X-ray source GX 1+4. Continuum emission up to ~800 keV was observed from this region of the galactic plane; it is likely that much, if not all, of it is emitted from the hard X-ray source. However, for purposes of comparison I have chosen to plot the extrapolation of this continuum spectrum ($dN/dE = 7.1 \times 10^{-4} E^{-2.78}$) to higher energies assuming that the gamma rays are emitted from a diffuse source along the plane. There is some evidence in the Rice data for such diffuse emission. A brief exposure to the longitude range from 339° - 352° along the plane during a background portion of the flight also showed an enhancement over background measurements taken at higher latitudes. In addition, the continuum intensity measured in an earlier Rice experiment (Johnson and Haymes 1973) was about a factor of two larger than the current measurement; this is consistent with a diffuse interpretation because of the larger aperture of the earlier experiment.

Some of the higher energy data points observed by the Rice group above 1 MeV are also plotted, assuming a diffuse origin, in order to indicate the level of sensitivity of the current measurements in this energy range. Most of the data points >800 keV are consistent with zero; however evidence was found for features which can be attributed to nuclear line emission. This evidence is illustrated in Figure 5 which is taken from Haymes et al.

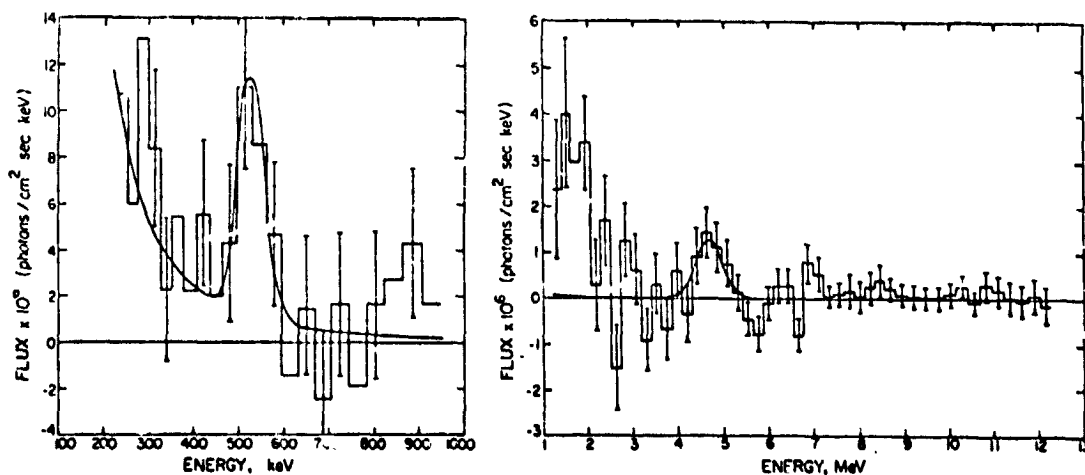


Fig. 5 Spectral data obtained by Haymes et al. (1975) giving evidence for nuclear line features emitted from the galactic center region.

(1975). The features at ~0.5 MeV and ~4.5 MeV can be attributed to positron annihilation and emission from the excited state of ^{12}C , respectively, while the broad enhancement from 1.2 to 2 MeV could be due to a combination of lines from ^{56}Fe , ^{24}Mg , ^{20}Ne , ^{29}Si . If confirmed these line features represent the first observation of nuclear gamma rays emitted from outside our solar system.

Returning to Figure 4 we can compare the intensity of these features, assuming a diffuse origin from the galactic plane, with recent calculations by Meneguzzi and Reeves (1975; see also Rygg and Fishman 1973). I've plotted their results for an assumed E^{-3} differential spectrum in kinetic energy for cosmic ray nuclei in the 5-50 MeV/nucleon range by normalizing to their calculated π^0 -decay gamma ray intensity. Although the expected features agree with the observations, the calculated intensity is about two orders of magnitude below the observations, requiring either that the cosmic ray intensities are significantly higher or that the features come from localized sources such as supernova remnants.

A detailed discussion of galactic nuclear line features is found in Richard Lingenfelter's paper in these Proceedings. It is of importance to note in Figure 4 that both narrow and broad features are expected. The broad features arise from Doppler broadening of γ -rays emitted from heavy cosmic ray nuclei excited in collisions with ambient hydrogen gas. With this in mind, I wish to question the interpretation by Fishman and Clayton (1972) of a possible line feature at ~478 keV, observed by Johnson and Haymes (1973), as being produced by excited ^7Li in the cosmic radiation. Any feature produced in this way would be severely broadened and not show evidence for a narrow line profile. Even the narrow features, arising from cosmic-ray proton excitation of nuclei in the ambient gas may show significant broadening (e.g., ~80 keV FWHM in the 4.43 MeV line of ^{12}C).

3. Future Observations. There is considerable activity at present devoted to the development of suitable instrumentation for observing low-and-medium energy gamma radiation. For the purpose of observing diffuse emission from the galactic plane, an optimum instrument would be one having a reasonably broad field of view (~25° FWHM) and an angular resolution of about 1°. This would enable the galactic diffuse emission to be not only resolved simultaneously from the background but would also permit

variations of the diffuse emission to be mapped and resolved from any point sources. Energy resolution in the range >10 MeV is not critical, a resolution of $\sim 25\%$ FWHM should be adequate to distinguish the various processes contributing to the diffuse emission. Below 10 MeV, better energy resolution is critical in order to identify and distinguish the lines which may be emitted. In the near future, it is perhaps not essential to attain the excellent resolution (~ 2.5 keV FWHM) characteristic of Germanium detectors. High sensitivity crystal detectors with moderate energy resolution ($\sim 3\%-8\%$) can perform a large part of the pioneering activity in this field. (This is especially true because many of the nuclear lines are expected to be significantly Doppler broadened). Future detection systems will probably employ arrays of large volume (~ 150 cm³) intrinsic Germanium detectors capable of achieving both high sensitivity and excellent energy resolution.

It is clear from the results obtained from SAS-1, SAS-2 and COS-B, that long term observations are important for making high sensitivity measurements and for detecting transient phenomena which can complicate measurements of a diffuse intensity. It is probably more important for the observations >10 MeV to be performed above any overlying atmosphere than it is for observations <10 MeV. This is true because the intrinsic background of the high energy detectors is much lower than the background produced in the overlying atmosphere as viewed from high altitude balloons. The reverse is true for energies <10 MeV. In fact there are significant advantages that balloon-borne low-energy gamma-ray detectors have, e.g., a stable background environment which is free from the high intensity radiation fields that most satellites periodically encounter.

The prospects for long duration balloon observations are growing. In the past most flights have been limited to durations of ~ 8 hours, except for the semi-annual wind turn-around periods, when durations of 40 hours have been achieved. Recent innovations such as transatlantic balloon flights, as the one launched last year from Sicily, offer flight durations of 5-7 days. Even longer durations of up to two to three months will be possible with the successful development of large superpressure balloons expected within the next one or two years.

With these general considerations in mind, I wish to summarize the current status of instrument development in

the low-and-medium energy gamma-ray domain and also the sensitivities for detecting diffuse galactic emission that can be achieved in the next few years. Table 1 lists the types of instruments that are currently in operation, or being planned, which are known to me. Within each category there may be one or more variations developed by different groups. My purpose here is not to provide an all inclusive listing, but one which is just representative. Typical properties of currently used detectors are also given in the Table.

The Rice detector shown in Figure 3 falls into the first category of actively shielded and collimated crystals. Another example of this type is the UCSD-MIT detector (Matteson et al. 1974) which will be launched on board the HEAO-A satellite in the Spring of 1977. This instrument is shown in Figure 6. It consists of a cluster of detectors with different apertures and energy ranges of operation. The most sensitive element for detecting the diffuse galactic γ -ray emission is the central detector with its 40° field of view. The four point source detectors (20° aperture) will be helpful in distinguishing discrete sources. The block of CsI shown in the Figure is used as a shutter, primarily for measurements of the diffuse cosmic background.

A second type of shielded scintillator is also listed in the Table. This type has a large aperture and uses an occulter to identify point sources of radiation; it therefore is not designed for observation of extended sources. Groups at Toulouse (Mandrou et al. 1975) and the University of New Hampshire (Chupp 1975, private communication) are currently employing this technique.

High-energy resolution germanium detectors make up the next group. Significant progress is being made in the utilization of large volume detectors such as the instrument developed at Toulouse (Vedrenne 1976, private communication) which employs a 140 cm^3 diode. This instrument will be flown within the next year from Brazil to study the nuclear line emission from the galactic center region. Shown in Figure 7 is the array of four 40 cm^3 Ge(Li) detectors developed for balloon observations by the Jet Propulsion Laboratories (Jacobson et al. 1975). The detectors are actively shielded and collimated by cylindrical crystals of CsI. This configuration is similar to the one being developed for the HEAO-C satellite which has four 60 cm^3 diodes (Hicks and Jacobson, 1974).

Table 1

Typical Properties of Low-and-Medium Energy γ -Ray Detectors

Detector	Energy Range MeV	Area cm ²	Aperture (FWHM) °	Efficiency (%)	Resolution Energy	Resolution (FWHM) Angle
Actively shielded and collimated inorganic scintillators	~0.1-10	100-300	10° - 30°	~50 @ 1 MeV ~20 @ 5 MeV	~60 keV @ .7 MeV ~110 keV @ 5 MeV	10° - 30°
Actively shielded inorganic scintillators with shutter/occluder	~0.1-10	100-300	~80°	~50 @ 1 MeV ~20 @ 5 MeV	~60 keV @ .7 MeV ~180 keV @ 5 MeV	~20°
Actively shielded germanium detectors	~0.1-10	40-50	20° - 60°	~12 @ 1 MeV ~5 @ 5 MeV	2.5 keV @ 1 MeV	20° - 60°
Semi-actively shielded Compton detector	0.5-20	500	~2°	~12 @ 1 MeV ~5 @ 5 MeV ~3 @ 10 MeV	~150 keV @ 1 MeV	~2°
Double Compton telescope	0.5-20	4000-10000	70° - 100°	2-3 @ 1 MeV 3-5 @ 5 MeV 2-3 @ 10 MeV	14-40%	15° - 30°
Large-area low-mass multiplate chambers	≥5 MeV	500-10000	~60°	2 @ 10 MeV 10 @ 100 MeV	~100%	10°-20° @ 20 MeV ~3° @ 100 MeV
Heavy-gas wide-gap spark chamber (conceptual)	≥5 MeV	~3000	~60°	0.5 @ 10 MeV 2 @ 100 MeV	~50%	~4° @ 10 MeV ~2° @ 20 MeV
Emulsion spark chamber	≥15 MeV	650	~60°	2 @ 20 MeV 15 @ 100 MeV	~30%	~2° @ 20 MeV ~1° @ 100 MeV

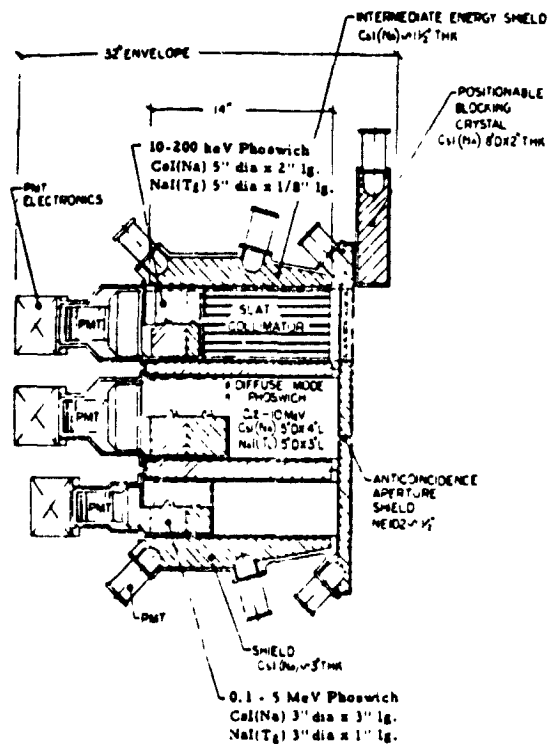


Fig. 6 The γ -ray detector on EAO-A.

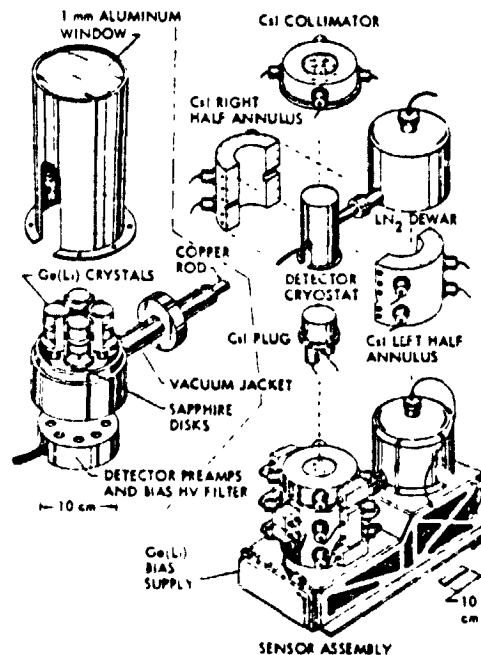


Fig. 7 The JPL balloon-borne Germanium array.

This will not be the first germanium detector to be placed in orbit. The group at Lockheed flew two 50 cm³ Ge(Li) detectors on a polar orbiting satellite in 1972 (Nakano et al. 1974). Other laboratories with experiments using Germanium include a Sandia-Bell Lab collaboration (Leventhal 1976, private communication) and Goddard (Cline 1976, private communication).

The next two types of instruments operate in a higher energy range. Both make use of the Compton effect for detecting incident gamma radiation, but they are significantly different in their concept and operation. Shown in Figure 8 is the semi-actively shielded Compton detector built in a collaboration between Milan and Southampton (Maccagni et al. 1975). An $\sim 2^\circ$ field of view is provided by the lead-slats and lead-scintillator shielding. This type of shielding represents significant cost savings over inorganic crystals, but its background

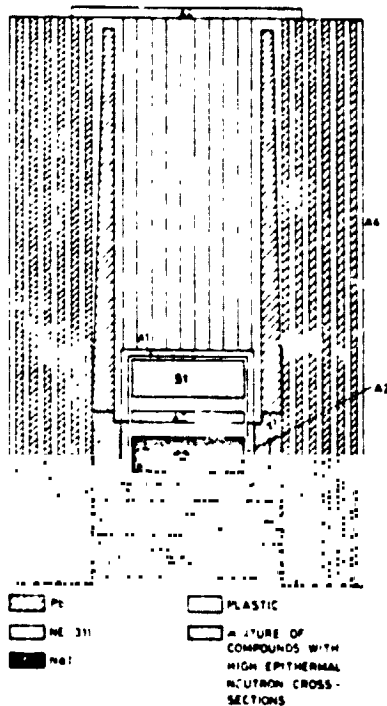


Fig. 8 The Southampton-Milan shielded Compton detector.

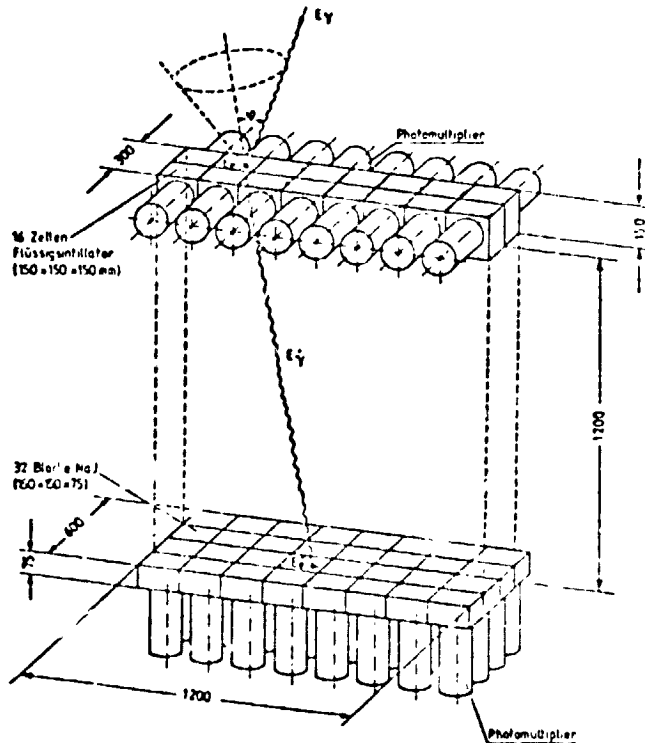


Fig. 9 The large area Compton telescope designed at the Max Planck Institute.

rejection still needs to be demonstrated under flight conditions. The narrow field of view primarily limits this system to observation of point sources.

The double Compton telescopes developed independently at Munich (Schönfelder et al. 1973) and at the University of California at Riverside (Herzo et al. 1975) represent the first attempts to develop an imaging system in this difficult energy domain. The Riverside system utilizes several tanks of liquid scintillator which also make it a sensitive detector for solar neutrons. A modified and significantly enlarged Compton telescope is currently being constructed at Munich (Graml et al. 1975). It is shown in Figure 9 and consists of sixteen separate detecting elements in each plane. The use of NaI in the bottom plane greatly improves the instrument's energy resolution and sensitivity.

The last three detectors listed in the Table are all imaging systems designed for higher gamma-ray energies. The large-area low-mass multiplate chambers are basically

C-2

the same as the systems designed for photons >50 MeV except for the emphasis on reducing the scattering of the pair produced electrons, primarily by incorporating thinner converting plates. The instrument shown in Figure 10, which was designed at the Moscow Engineering Physics Institute (Galper et al. 1975), illustrates some of the characteristics of this low-mass design. The conversion plates are a factor of ~ 4 thinner than those used in COS-B. In addition thin-window proportional counters (designated by C) are used as triggering elements. The angular resolution attainable with this instrument should be about a factor of two better than achieved by COS-B based on the reduction of scattering material; it is therefore difficult to understand how a resolution of 3° at 17 MeV can be achieved as claimed by the authors. Other instruments for investigating this same energy domain, but having considerably larger sensitive areas have been developed by the Case-Western Melbourne collaboration (Jenkins et al. 1974), by the Saclay-Toulouse collaboration (Bonfand et al. 1975) and by the group at Goddard (D. Kniffen 1975, private communication).

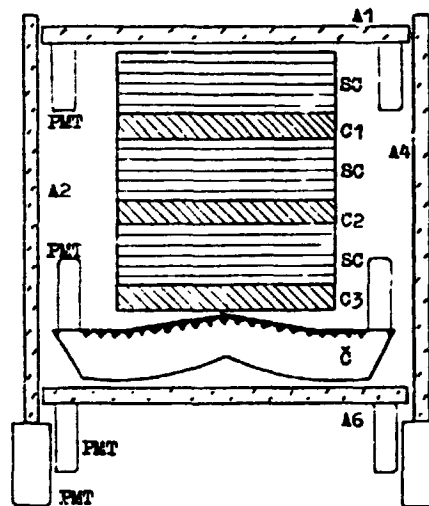


Fig. 10 Diagram of the low-mass γ -ray telescope developed at the Moscow Engineering Physics Institute.

The next type of instrument is only conceptual (Kinzer et al. 1970; see also Kniffen 1971) but, if developed, it should provide a significant improvement in angular resolution in its energy range without having the difficulties inherent in the emulsion spark chamber design listed last in the Table. In this concept, the gamma rays convert in a heavy noble gas, e.g., xenon, of a wide-gap spark chamber. This permits measurements to be made on the directions of pair electrons before they are scattered appreciably. The limiting feature of this instrument is its low conversion efficiency and high operating voltage. Perhaps, though, with the age of the Space Shuttle near, it may be worth further appraisal.

I've already discussed the operation of the emulsion wide-gap spark chamber array developed at NRL (see Figure 1). A modified instrument, with sensitivity extending to ~ 1 GeV (Samimi et al. 1974) was recently flown and obtained ten hours of exposure to the galactic center region. From this exposure ~ 500 galactic gamma rays will be mapped at a resolution of $1^\circ - 2^\circ$. The analysis which is proceeding at NRL and the Ferdowsi University at Mashhad, Iran, is arduous; but as is evident from the Table, no other operating system can approach this angular resolution in the 10-100 MeV range. This resolution is also critical for identifying any point sources which contribute to the diffuse galactic emission.

It is reasonable to ask at this point what we can anticipate learning from low-and-medium energy galactic gamma-ray observations within the next few years. The graph shown in Figure 11 attempts to answer this question

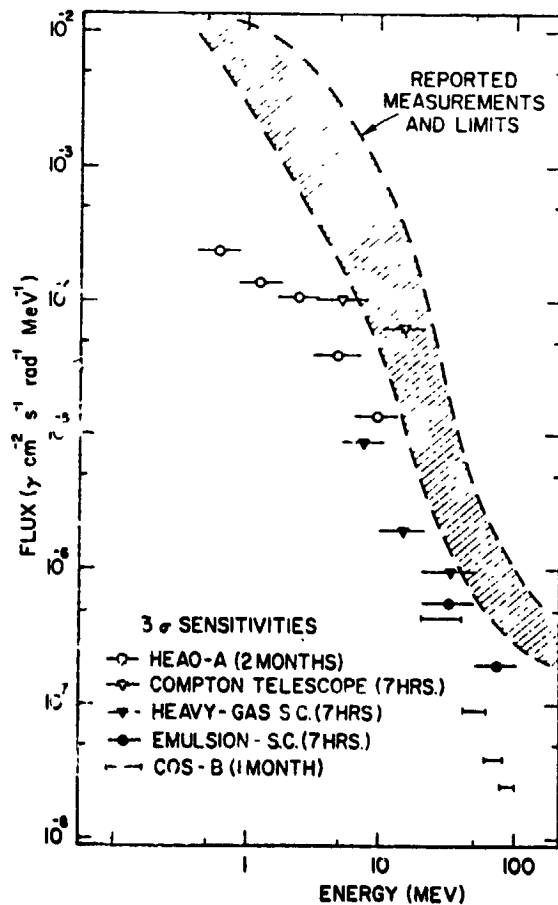


Fig. 11 Comparison of galactic γ -ray sensitivities achievable in the next few years with current measurements.

for the continuum emission >1 MeV. The shaded area shows the range of current measurements made in the direction of the galactic center (including limits) as depicted in Figure 4. The points give estimates of the 3σ sensitivities of current instruments as adapted from publications or communications. No limits are given on the Figure for the large area multiplate chambers, but I'd estimate their sensitivities to be somewhat better than those plotted for the emulsion-spark chambers. For purposes of comparison, I've included an estimate of the sensitivity of the conceptual heavy-gas spark chamber. It is also important to keep in mind that systematic uncertainties in the HEAO-A measurements, due to the rapidly changing background environment, can significantly degrade the plotted sensitivities.

Even with these reservations, it is clear that much will be learned about diffuse galactic emission in the 1-100 MeV region in the next few years. The relative contribution of electron initiated processes, such as Bremsstrahlung and Compton interactions, to the total galactic γ -ray emission will be well known. In addition, initial mapping of these low-energy components will enable the spatial distribution to be determined to a level approaching that obtained from SAS-2 for higher energy photons.

A similar comparison can be made between the reported nuclear-line intensities and sensitivities attainable within the next few years. This comparison is shown in Table 2. The observed intensities are adapted from the work of Haymes et al. 1975 on the assumption that these features are emitted on a galactic scale. The limits have been adapted from sensitivities estimated by the different experimenters. It is clear, once again, the advantage that comes from extended observations, such as are available with the HEAO-A detector. The sensitivity obtainable with the large area Compton telescopes is also worthy of note; however, their limited energy resolution may be a significant liability for future line observations.

The sensitivities available during a single day's exposure with the current generation of germanium detectors are just sufficient to detect the reported line features. The increased exposure available, with long duration balloon flights and satellites improves their capabilities significantly as can be seen in the Table. However, we

Table 2

ESTIMATED SENSITIVITIES TO GALACTIC γ -RAY LINES
($\times 10^{-3} \text{ CM}^{-2}\text{S}^{-1}\text{RAD}^{-1}$)

EXPERIMENT	0.5 MeV	0.9 MeV	1.2-2 MeV	4.5 MeV
1. DOUBLE COMPTON TELESCOPE (7 HRS)				
A) RIVERSIDE (HERZO ET AL. 1975)	-	-	-	0.4
B) MUNICH (SCHONFELDER, PRIVATE COMM.)	-	-	-	0.1
2. HEAO-A SCINTILLATOR (2 MONTHS) (MATTESON ET AL. 1974)	0.04	0.03	0.09	0.03
3. SHIELDED GE(LI)				
A) BALLOON - 7 HRS (JACOBSON ET AL. 1975)	1.0	2.0	-	2.
B) HEAO-C (HICKS AND JACOBSON 1974)	0.02	0.05	-	0.15
OBSERVED INTENSITY (HAYMES ET AL. 1975)	3.5±1.0	1.6±1.4	11.5±2.6	4.2±1.2

must remember that these sensitivities are estimated under the assumption that the intrinsic line width of the radiation is less than the detector's resolution (~2.5 keV). This is not the case with many of the lines (e.g., Doppler broadening of the 4.43 MeV ^{12}C line is expected to be ~80 keV).

References.

- Bennett, K., Burger, J.J., Gorisse, M., Mayer-Basselwanger, H.A., Paul, J., Pfeffermann, E., Shukla, P.G., Stiglitz, R., Swanenburg, B.N., Taylor, B.G., and Wills, R.D. 1974, Proc. 9th ESLAB Symp., ESRO SP-106, 323.
- Bonfand, E., Parlier, B., Forichon, M., Mouglin, B., Leconte, A., Courtois, J.C., Agrinier, B., Andrejo, J., Niel, M., Lavigne, M., and Vedrenne, G. 1975, Proc. 14th Int. Cosmic Ray Conf., 9, 3141.
- Cowsik, R., and Voges, W. 1975, Proc. 14th Int. Cosmic Ray Conf., 1, 74.
- Dodds, D., Strong, A.W., Wolfendale, A.W., Wdowczyk, J. 1975, J. Phys. A., 8, 624.
- Fichtel, C.E., Hartman, R.C., Kniffen, D.A., Thompson, D.J., Bignami, G.F., Ögelman, H., Özel, M.F., and Tümer, T. 1975a, Ap. J., 198, 163.
- Fichtel, C.E., Kniffen, D.A., Thompson, D.J., Bignami, G.F., Cheung, C.Y. 1975b, NASA preprint X-662-75-246.
- Fishman, G.J., and Clayton, D.D. 1972, Ap. J., 178, 337.
- Galper, A.M., Grigoryev, V.A., Kirillov-Ugryumov, V.G., Kotov, Yu. D., Kulakov, Ye. V., Smirnov, Yu. V., and Yurov, V.N. 1975, Proc. 14th Int. Cosmic Ray Conf., 9, 3143.
- Graml, F., Mitchell, E., Zasche, D., Daugherty, J., Schönfelder, V., and Maier, M.R. 1975, Proc. 14th Int. Cosmic Ray Conf., 9, 3129.
- Haymes, R.C., Walraven, G.D., Meegan, C.A., Hall, R.D., Djuth, F.T., and Shelton, D.H. 1975, Ap. J., 201, 593.
- Helmken, H., and Hoffman, J. 1970, Nucl. Inst. Meth., 80, 125.
- Helmken, H.F., and Hoffman, J.A. 1973, Nature Phys. Sci., 243, 6.
- Herzo, D., Koga, R., Millard, W.A., Moon, S., Ryan, J., Wilson, R., Zych, A.D., and White, R.S. 1975, Nucl. Inst. and Meth., 123, 583.

- Hicks, D.B., and Jacobson, A.A. 1974, IEEE Trans. Nucl. Sci., NS-21, 169.
- Jacobson, A.S., Bishop, R.J., Culp, G.W., Jung, L., Mahoney, W.A., and Willett, J.B. 1975, Nucl. Inst. and Meth., 127, 115.
- Jenkins, T., Albats, P., Frye, G., Kolman, R., Schindler, S., Schreiner, R., Thomson, G., and Mace, O. 1974, Proc. 9th ESLAB Symp., ESRO SP-106, 171.
- Johnson, W.N. III, and Haymes, R.C. 1973, Ap. J., 184, 103.
- Kinzer, R.L., Noggle, R.C., Seeman, N., and Share, G.H. 1970, Bull. Amer. Phys. Soc., 15, 613.
- Kniffen, D. 1971 in Cosmic Gamma Rays by F.W. Stecker (Washington, D.C.: U.S. Gov't Printing Office), p. 237.
- Maccagni, D., Paizis, C., P rotti, F., Piccinotti, G., Stiglitz, R., Dean, A.J., Martin, S.J., and Ramsden, D. 1975, Proc. 14th Int. Cosmic Ray Conf., 9, 3135.
- Mandrou, P., Niel, M., Nrabonne, J., and Sabaud, C. 1975, Preprint to be published in Nucl. Inst. and Meth.
- Matteson, J.L., Pelling, R.M., and Peterson, L.E. 1974, Proc. 9th ESLAB Symp., ESRO SP-106, 177.
- Meneguzzi, M., and Reeves, H. 1975, preprint to be published in Ast. and Ap.
- Nakano, G.H., Imhof, W.L., and Johnson, R.G. 1974, IEEE Trans. Nucl. Sci., NS-21, 159.
- Ramaty, R., and Westergard, N.J. 1976, NASA preprint X-660-76-19.
- Rygg, T.A., and Fishman, G.J. 1973, Proc. 13th Int. Cosmic Ray Conf., 1, 472.
- Samimi, J., Share, G.H., and Kinzer, R.L. 1974 Proc. 9th ESLAB Symp., ESRO SP-106, 211.
- Schönfelder, V., Hirner, A., and Schneider, K. 1973, Nucl. Inst. and Meth., 107, 385.

Share, G.H., Kinzer, R.L. and Seeman, N. 1974, Ap. J.,
187, 45.

Shukla, P.G., and Paul J. 1976, preprint submitted to Ap. J.

Sood, R.K., Bennett, K., Clayton, P.G., And Rochester, G.K.
1975, Proc. 14th Int. Cosmic Ray Conf., 1, 35.

Walraven, G.D., Hall, R.D., Meegan, C.A., Coleman, P.L.,
Shelton, D.H., and Haymes, R.C. 1975, Ap. J., 202, 502.

N 76-29118

VERY HIGH ENERGY GAMMA RAY ASTRONOMY

Jonathan E. Grindlay

Center For Astrophysics, Harvard and Smithsonian Observatories
Cambridge, Massachusetts 02138

ABSTRACT

Recent results in ground based very high energy ($>10^{11}$ eV) gamma ray astronomy are reviewed. The various modes of the atmospheric Cerenkov technique are described, and the importance of cosmic ray rejection methods is stressed. The positive detections (at $\geq 10^{12}$ eV) of the Crab pulsar that suggest a very flat spectrum and time-variable pulse phase are discussed. Observations of other pulsars (particularly Vela) suggest these features may be general. Evidence that a 4.8 hr modulated effect was detected at $E_\gamma > 10^{12}$ eV from Cyg X-3 is strengthened in that the exact period originally proposed agrees well with a recent determination of the X-ray period. The southern sky observations are reviewed, and the significance of the detection of an active galaxy (NGC 5128) is considered for source models and future observations.

VERY HIGH ENERGY GAMMA RAY ASTRONOMY

J. E. GRINDLAY
Center for Astrophysics
Harvard College Observatory and Smithsonian Astrophysical Observatory

I. INTRODUCTION

Gamma ray astronomy at very high energies ($\gtrsim 10^{11}$ eV) was last reviewed by Fazio (1973). Accordingly, the present review will be confined largely to results reported since this time. These results have been particularly exciting in that the first sources of very high energy gamma rays have now been detected by several groups using different techniques.

The spectrum of observable electromagnetic radiation from cosmic sources outside the solar system now extends all the way through photon energies of $\gtrsim 10^{12}$ eV. This is some 3 orders of magnitude above the gamma ray energies accessible to current satellite detectors. Thus, for a source like the Crab pulsar NP 0532, the integral photon flux is more than 3 orders of magnitude lower and detection systems with extremely large area-time factors are required. In fact, for NP 0532 the pulsed flux we shall summarize is only about 1 photon/hour if it were recorded by a detector measuring 100 m by 100 m square! Such incredibly low fluxes at these highest energies are possible to detect with systems that detect the extensive air showers (EAS) that are produced in the earth's atmosphere by single primary gamma rays with energies $> 10^8$ eV. For primary energies $\gtrsim 10^{11}$ eV, there are enough (~ 300)

electrons in the shower with energies above the threshold for Cerenkov radiation in the atmosphere that the EAS initiated by a single gamma ray may be detected entirely by optical techniques (Jelley 1958). The disk of optical Cerenkov photons (~ 150 m radius, ~ 2 m thickness) produced in such a shower is sufficiently dense (~ 5 photons/ m^2) that it may be detected as a ~ 10 nsec light flash with a photomultiplier at the focus of a large optical light collector such as the 10 m reflector at Mt. Hopkins Observatory.

The atmospheric Cerenkov technique has been further developed recently by several groups seeking to improve the sensitivity of the early searches for very high energy gamma ray sources. We shall briefly review these experiments and the recent modifications of the Cerenkov technique. These experiments have finally yielded rather convincing evidence for the detection of at least two gamma ray sources above 10^{12} eV. In reviewing these results, it will be clear that the astrophysical implications of these very high energy gamma ray sources for models of several classes of object are already quite profound. It is especially interesting, for example, that one of these sources is an active radio galaxy (Cen A). If nuclei of active galaxies are generally very high energy gamma ray sources, then perhaps QSO's will be detectable with further increases in sensitivity. Detection of quasars in turn would permit testing the cosmological interpretation of QSO red shifts since objects more distant than 3C273 ($z \cong 0.16$) could be attenuated by $(\gamma - \nu)$ pair production of the gamma rays on the optical photon background. Alternatively, it should be pointed out that since the ($\sim 10^{12}$ eV) gamma ray mean free path for

attenuation by either $\gamma-\gamma$ or $\gamma-p$ interactions is so long, essentially all objects but the most distant quasars are potentially observable.

II. Observational Techniques

The simplest type of Cerenkov receiver, consisting of one or more (in coincidence) optical reflectors pointed directly at a suspected source, has been used in most of the searches for very high energy gamma rays (e.g., Chudakov et al. 1965, Long et al. 1965, Fazio et al. 1968, Weekes et al. 1972, Porter et al. 1974, Stepanian et al. 1975, and Erickson et al. 1976). These "single beam" detectors were pointed directly at the suspected sources, since the optical Cerenkov radiation expected in the gamma ray-initiated EAS (γ -EAS) is calculated to be (Rieke 1969) collimated about the primary direction to within $\sim 1^\circ$. In actual fact, most of the searches mentioned above employed the drift scan technique where the detectors were pointed such that the earth's rotation caused the object to transit through the (typically $\sim 1^\circ$) detector field of view. In many of the observations of Weekes et al. (1972), as well as others we shall describe below, the candidate source (as well as background) was tracked for maximum exposure. In none of these observations was there active rejection of the background of cosmic ray-initiated EAS (p -EAS); gamma rays from the source direction were sought as an increase in the total detected rate.

The absolute sensitivity of these various experiments is based on calculations of the Cerenkov light pool expected for γ -EAS. However, even the most complete calculations of the electromagnetic cascade and light distributions (Rieke 1969)

including as well as the effects of the geomagnetic field (Weekes and Rieke 1974) are uncertain to within a factor of ~ 2 . Since the results are quite strongly dependent on the exact detector configuration (i. e. atmospheric depth, field of view, etc.) it is similarly difficult to make relative comparisons of the sensitivity of the various systems. In general, since the detector is operated at a threshold such that the background is entirely due to the flux $F_p \sim K E_p^{-1.6}$ of cosmic rays (p-EAS) above energy threshold $E_0 \sim E_p$, the detectability of a gamma ray flux or S/N will vary as $\sim E^{-\alpha} / \sqrt{F_p} \sim E^{-\alpha + 0.8}$ where α is the integral spectral index of the gamma ray source. Thus, for $\alpha > 0.8$ the maximum sensitivity should be possible for the lowest gamma ray energy thresholds or the largest optical collector area (directly proportional to E_0). This was, of course, the philosophy behind the single 10 m. reflector at Mt. Hopkins with $E_0 \sim 1 \times 10^{11}$ eV. It is interesting, however, that the sources detected so far have turned out to (probably) have flat spectra with $\alpha < 0.8$ and thus maximum detectability at the highest energies in the $10^{11} - 10^{13}$ eV range. Apart from the 10 m. reflector results (Weekes et al. 1972), the energy threshold for all the other single beam searches mentioned above was $\sim 10^{12}$ eV. The effective collection area in all cases was $\sim 2 \times 10^8$ cm². In addition to the several uncertainties mentioned, the actual values of these parameters are also strongly dependent on zenith angle, sky brightness and atmospheric transparency.

When the first single beam observations (e.g. Chudakov et al. (1965), Fazio et al. 1968) yielded gamma ray upper limits of $\leq 1\%$ of the detected cosmic ray flux (typically $\sim 10 - 100 \text{ min}^{-1}$), it became clear that some degree of background rejection was needed. Mongain et al. (1968) attempted to select γ -EAS by using a fast ($\sim 3 \text{ nsec}$) coincidence system to favor detection of Cerenkov light from the first few interaction lengths of the shower, since the γ -EAS develop faster than p-EAS. The light from

this portion of the shower is "focussed" (due to increasing index of refraction) in an annulus of radius ~ 120 m and duration < 3 nsec. Although this technique preferentially selects ν -EAS, and in fact positive effects were reported (e.g. O'Mongain et al. 1968, Jennings et al. 1974), the background p-EAS were still not actively rejected. Apart from the "fast annulus" mentioned, ν -EAS are expected (Zatsepin and Cerenkov 1962) to have a flatter lateral photon distribution than p-EAS, which will be more strongly peaked at the core. Tornabene (1976) has set up an array of Cerenkov detectors and by multi-coincidence fast timing (Tornabene and Cusimano 1968), the EAS core location, arrival direction and Cerenkov front curvature may be determined as well as the photon lateral distribution. EAS with peaked distributions at the core may thus be rejected from the analysis for gamma ray events. This "multiple beam" technique has the advantage that the individual detectors may have large ($\sim 5^\circ$) fields of view and a source may be "tracked" with a series of drift scans. It suffers, however, from the systematic difficulty that in a single EAS the lateral distribution can be quite different from the average due to the effects of fluctuations (i. e. the Cerenkov disk can be "spotty") and thus the core density and location are uncertain. Nevertheless, this technique is among the most promising and positive results have been obtained which we shall describe below.

Other multiple beam techniques have been described by Grindlay et al. (1974, 1976). These have employed multiple photomultiplier detectors at the focus of the Mt. Hopkins 10 m reflector. Since the angular distribution of ν -EAS (especially) will be broadened by geomagnetic effects, a class of EAS were selected by a 3-fold coincidence of a 1° triangle of phototubes. Another configuration of 6 phototubes surrounding a central detector (all with $\sim 1^\circ$ beams) on the reflector optical axis was used to isolate a class of roughly circular shower spots by an anti-coincidence of the center with the

surrounding channels. Cosmic ray showers would generally be incident off-axis and produce elongated Cerenkov images. This technique was not as sensitive as the first, however, since the effective detection area must be smaller since gamma rays must be incident within ~ 50 m of the reflector for their Cerenkov image to appear circular (within $\sim 1^\circ$).

We conclude our discussion of Cerenkov detection techniques with the so-called "double beam" technique for actively rejecting p-EAS (Grindlay 1971a, 1972; Grindlay et al. 1976 and references therein). This method embodies several of the distinguishing features of γ -EAS already mentioned - the fast timing and relatively broad vs. peaked lateral distributions. However, the main feature (originally suggested by experiment (Grindlay 1971b)) is the detection of the penetrating cores in p-EAS by identifying structure in the angular distribution of the Cerenkov light. The angular structure shows up as follows. Whereas the peak detection of background Cerenkov flashes by two reflectors (with $\sim 1^\circ$ beams) separated by, say, ~ 70 m occurs when the reflectors are inclined towards each other by $\sim 0.3^\circ$, an enhanced (over the optical beam response) rate is observed as the angle is increased, but not decreased. Furthermore, this relative increase is greatest in the ultraviolet, suggesting the radiating particles are comparatively close to the detector and the $1/\lambda^2$ Cerenkov spectrum suffers less atmospheric absorption than at the primary peak of the angular distribution. The natural interpretation of these data was (Grindlay 1971a) that the primary peak was due to the large number of electrons at the p-EAS maximum and the UV component due to penetrating particles, primarily muons, on axis near the core and detected at the characteristic Cerenkov opening angle of $\sim 1^\circ$. This hypothesis was supported by detailed Monte Carlo calculations of p-EAS (proton through iron primaries) and the Cerenkov production of the penetrating particles. The calculated angular distribution shown in Figure 1 (Grindlay 1974) agrees well with the observations.

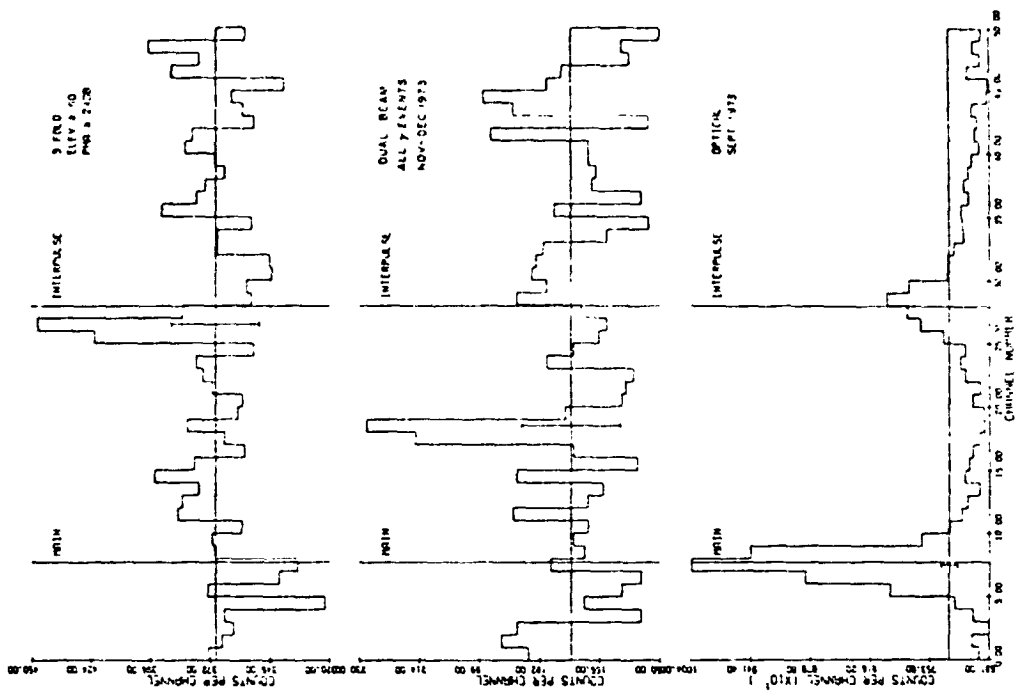


Fig. 2. NIP0372 phase histograms. Multibeam 3-fold coincidence events in January 1971 (top); non-retorted double beam events in December 1973 (middle); optical pulses recorded with 1.5 m fibre optic telescope and Gamma Ray Lab. recording system in September 1973 (bottom).

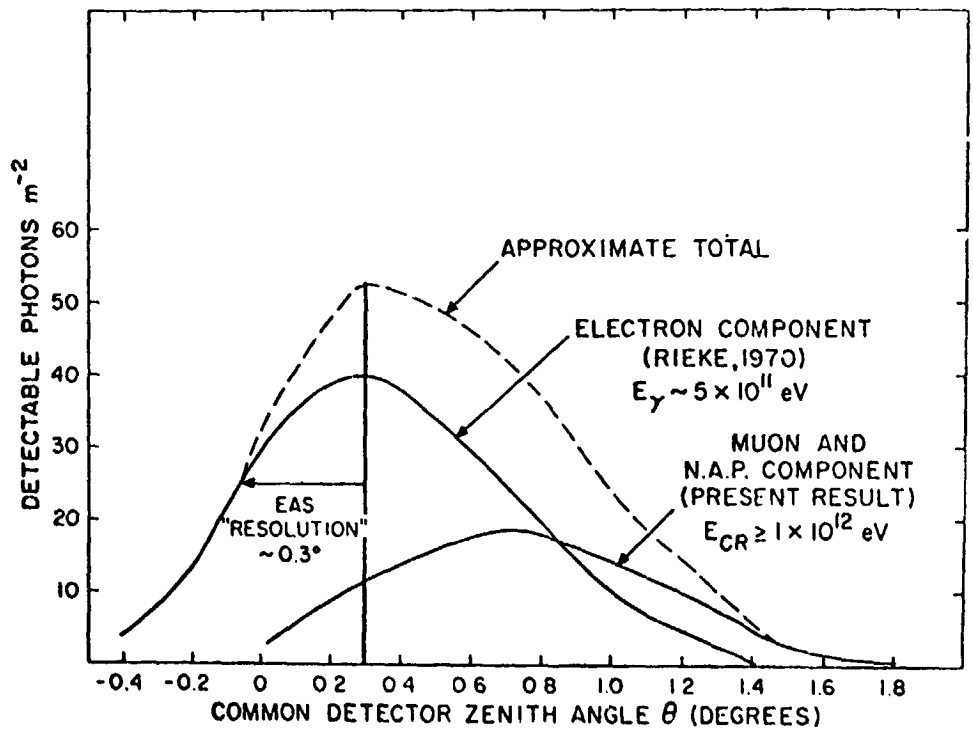


Fig. 1. Calculated Čerenkov angular distributions at $R = 40$ m from EAS axis at 2300 m as detected by $\sim 1^\circ$ light receivers.

Thus, p-EAS may be actively rejected by detection of the penetrating muon cores which are not expected in the (nearly) pure electromagnetic cascades of γ -EAS. This requires an array of at least 3 spaced Cerenkov detectors: two originally detect the EAS at its maximum while the third, through an appropriately delayed coincidence, searches for emission from the muon core. Such a system can be pointed at a suspected source either in the drift scan mode (Grindlay 1972) or continuously tracking (Grindlay et al. 1975a, 1976). The double beam technique is restricted to gamma ray energy thresholds $> 3 \times 10^{11}$ eV (for sufficient muon numbers). In general, the other multiple beam techniques mentioned are also restricted to threshold energies above the minimum values because of the importance of fluctuations.

Finally, we note that all the coincidence techniques described here usually employed random coincidence controls. A number of the single beam observations (Fazio et al. 1968, Charman et al. 1969, Weekes et al. 1972) have also used servo systems such that the phototube current or pulse rate remained constant as sky brightness changed. While this introduces additional noise, it is essential for non-coincidence experiments (e.g. Weekes et al. 1972).

III. Observational Results

A. Crab Nebula and Pulsar NP0532

We begin with the Crab in our discussion of results since this object has been observed by all groups and the pulsar NP0532 has now been detected in several of these observations. Since the review by Fazio (1973), the principal results on the Crab have been obtained at Mt. Hopkins by the SAO group using the multibeam and double beam techniques (Grindlay et al. 1974, 1976; Helmken et al. 1975). These observations were all conducted with ~~the 10m reflector alone (multiple beam) or in coincidence with~~ a remote 1.5m reflector (double beam). All observations were done in a tracking mode on NP0532 in an effort to observe a pulsed flux; background was not measured off source to determine a steady flux. The final results have been described by Grindlay et al. (1976) and only a summary will be given here. In Figure 2 the phase histograms of selected γ -EAS show the Crab pulsations at about the 5σ level. The phase of each EAS arrival time (recorded within 100 μ sec of absolute U. T.) was computed by interpolation between phases calculated for the optical pulse every 30 min. The accuracy of both the data recording and analysis systems was repeatedly verified by recording the optical pulsations of NP0532 with the 1.5m Tillinghast Telescope at Mt. Hopkins (adjacent to the 10m reflector) and the gamma ray data recording system. The

optical phase histogram is also given in Figure 2 (lower section) and the predicted vs. observed phases of both the main and secondary pulses are in close agreement.

The most striking feature of these results is that the gamma ray pulsations at $E_0 \geq 8 \times 10^{11}$ eV are time variable. In December 1973, the pulsar was detected at $\sim 5\sigma$ by the double beam observations (Figure 2, middle) in ~ 24 hours of exposure on 5 nights. The phase of the pulsations is about 6 msec after the main pulse phase, and in a region of the light curve that is increasingly "filled in" with increasing photon energy. Pulse features at this phase have also been detected occasionally at radio and X-ray energies (see Grindlay et al. 1976 for refs.). In January 1974, however, the pulsations were detected ($\sim 3\sigma$ confidence level) again in just a single peak but at a phase ~ 2 msec before the phase of the optical secondary pulse. The effect was present only in the highest pulse height data or for $E_0 > 10^{12}$ eV, whereas the double beam pulses were evident over the entire (factor of ~ 10) pulse height range above the threshold $\sim 8 \times 10^{11}$ eV. Thus, these results provide strong evidence for a very flat spectral component (consistent with $F(>E) \sim A E^0$) of the NP0532 spectrum at the highest energies that is almost certainly not (by virtue of its shape and time variability) an extrapolation of the "low energy" spectrum through ~ 100 meV. We return to further discussion of this spectrum below.

These SAO results have been supported by several other groups. Jennings et al. (1974) reported a $\sim 3\sigma$ pulsed effect at $\geq 10^{12}$ eV that was peculiar in that two peaks (with the ~ 13 msec separation of the optical pulses) were detected at a phase ~ 14 msec before the optical phase. It should be noted that these observations were all conducted after the major Crab glitch of September 1969. In January 1972, Porter et al. (1974) reported a $\sim 4\sigma$ pulsed effect ($E_0 \geq 5 \times 10^{12}$ eV) at the phase of the optical secondary pulse. The effect appeared to be variable on time scales of several days and was in fact only detected on the first 2 of 3 nights in January and not in February 1972. The observations were conducted with a coincidence wide-angle single beam Cerenkov system at Mt. Hopkins, and it is interesting to note that the phase is in good agreement with the double beam observations (Grindlay 1972 and Grindlay et al. 1976) obtained in November - December 1971. It is also interesting to note that these observations all were within several months of a minor glitch of the pulsar in early October 1971.

In December 1973, on some of the very same nights (e.g. 3 December) as the Mt. Hopkins observations, Tornabene (1976) was recording on the Crab with his multi-detector Cerenkov system for locating EAS cores and lateral distributions as described

above. While his analysis is still incomplete, he reports that he has detected a relatively strong effect from NP0532 at energies $\gtrsim 10^{12} - 10^{13}$ eV. Preliminary phase analysis of the γ -EAS events indicates the effect may be entirely pulsed at either the ~ 6 msec delayed interpulse or near the optical pulse phases as in Figure 2. This is a very important result (and final analysis is awaited) and obtained with a very different technique which would provide additional confirmation of the very high energy pulsed flux from NP0532 as well as its variability.

Finally, in February and March 1975, Erickson et al. (1976) have also recently found evidence for the detection of NP0532 at $E \gtrsim 10^{13}$ eV. They used a coincidence single beam system in which two multi-mirror reflectors were co-aligned on the Crab in a tracking mode. Events were defined by requiring the equivalent of 4-fold (out of 16) coincidences, but no active cosmic ray rejection was available in the analysis. A phase analysis of the detected events on 5 nights yielded $\sim 3\sigma$ peaks either just before the optical secondary pulse (March 15) or at ~ 5 msec after the optical main pulse (March 14 and 17). No pulsations were detected on either February 10 or March 4, which were shortly after another major Crab period glitch on February 4, 1975 (Lohsen 1975).

We have plotted many of these Cerenkov results in the spectral plot of Figure 3, which also shows the extrapolation of the NP0532 spectrum through ~ 1 GeV (McBreen et al. 1973). The result of Tornabene is not yet final and therefore not shown; we estimate it would be near the point F on the plot. While probably only the double beam results and the wide angle results of Porter et al. (1974) (and possible Tornabene's results) are statistically very significant, all of the results taken together present an unquestionable detection of NP0532 at energies $\gtrsim 10^{12}$ eV. If this detection is accepted (as the many independent observations require), it is also very likely that the pulsar spectrum at these energies is either flat or conceivably even has a positive slope (!) above 10^{11} eV. It is also necessary to accept the fact that this spectral component of the pulsar is time variable in both amplitude and phase.

There is evidence, of course, for changes in the pulsar emission that may directly relate to this high energy gamma ray variability. The possible association of detection at the several phases with glitches has been mentioned above. The detections of December 1973 followed a period^{of} enhanced (on a broad decline) radio emission (Rankin et al. 1974). This possible association of detectable pulsations and general pulsar variability suggests that the enhanced position effects reported by Fazio et al. (1972) following the 1969 September and 1971 August and October glitches could in fact

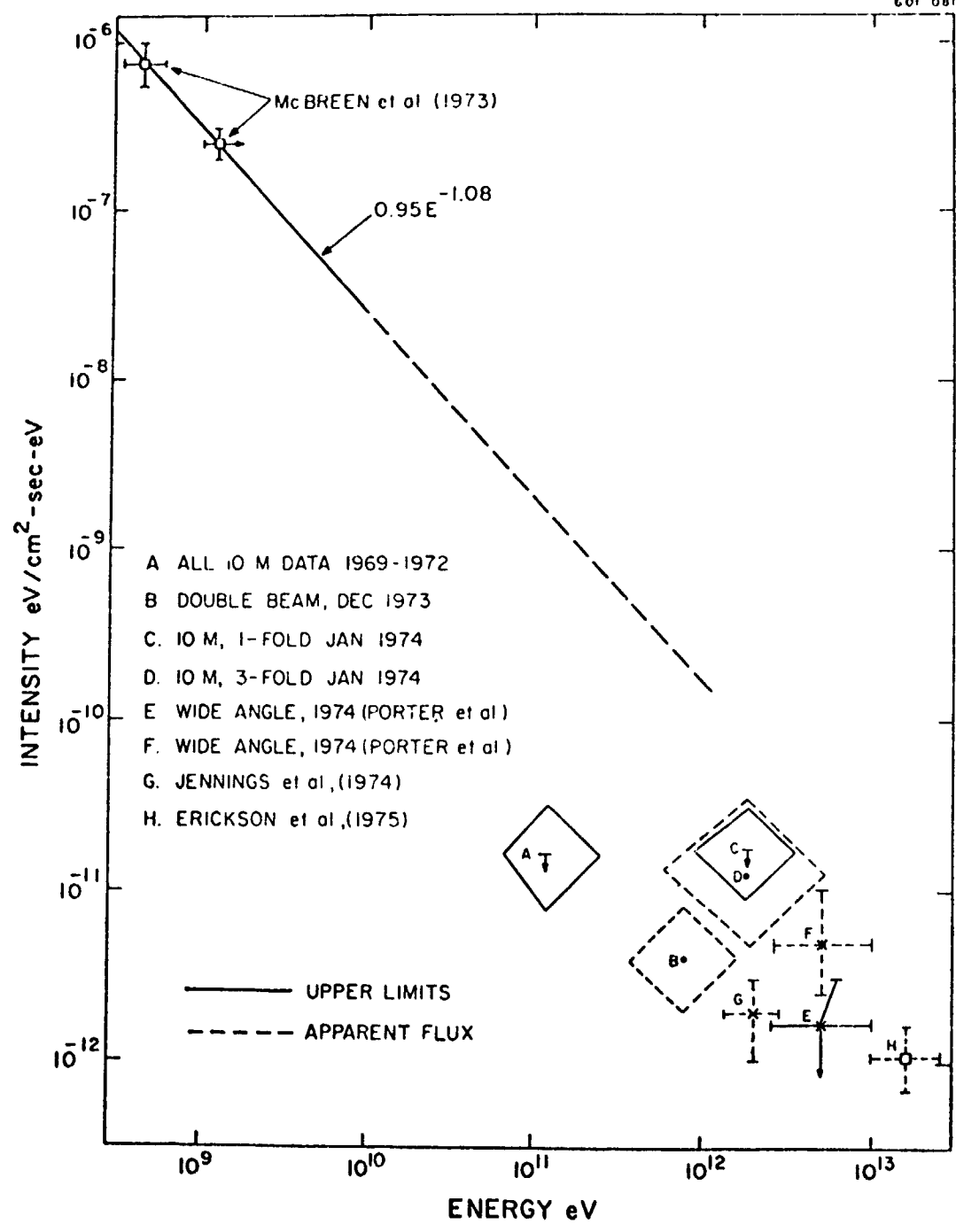


Fig. 3. Spectral distribution of recent Cerenkov results on NP0532 pulsations.

have been pulsed with variable phase. However for this not to have been evident in the pulsation analysis, the phase variability must be on a time scale of several days such that pulsations were smoothed out in the less-sensitive single beam data. Although time scales of days are in fact indicated for the phase variations described above, the apparently flat pulsed spectrum would tend to argue against a largely pulsed origin for the short-term enhancement at $\sim 10^{11}$ eV. In any case, these lowest energy Cerenkov results are significant mostly for limiting the minimum value of the average magnetic field in the Crab nebula to $B_{\perp} \geq 5 \times 10^{-4}$ gauss. This value was recently calculated by the author using the Compton-synchrotron model of Grindlay and Hoffman (1971) and the most recent X-ray data summarized by Wolfe and Novick (1976), who also derived an upper limit of $B_{\perp} \leq 8 \times 10^{-4}$ gauss from the variation of X-ray size. Thus the high energy gamma ray observations of extended objects like the Crab nebula (in which Compton-synchrotron processes may occur) can limit or establish the source magnetic fields. In the Crab, the best value appears to be $\sim 6 \times 10^{-4}$ gauss, or near the equipartition value.

B. Results of Northern Sky Observations

We have emphasized the Crab results since these are the most significant detections of the northern sky observations. A large number of other candidate sources have also been observed, although for none has the exposure been more than a fraction of that on the Crab. Results on a list of 27 objects, primarily supernova remnants, radio galaxies and quasars, have been reported by Weekes et al. (1972). Most of these were surveyed with the drift scan technique though several were tracked with the 10m reflector. All observations were done with the single beam technique, and no significant positive effects were found. Although useful limits on magnetic fields were obtained for several in addition to the Crab.

A total of 41 objects have been observed by the group at the Crimean Observatory (Stepanian et al. 1975) using a drift scan technique. While these observations were "single beam" in that no cosmic ray rejection was employed and the detectors were pointed directly at the position through which the source would transit, two separate 2-fold coincidence detectors (1.5m reflectors) were used. These were offset in right ascension by 2.5° so that the candidate source would transit through the two systems sequentially, thus allowing a check on sky transparency independent of sky brightness or source contributions. These authors have derived the actual distribution of rate fluctuations and found the data are well described (within a few percent) by normal sta-

tistics near the zenith. Such checks are especially important for all Cerenkov observations in which source and background are compared. In general, coincidence experiments - even without servoing the phototube singles rate or current on sky brightness - give experimental fluctuations within a few percent of Poisson values (c. f. also discussion of southern sky results below and Grindlay et al. (1975a)) whereas single channel systems (e.g. Weekes et al. 1972) yield $\sigma_{\text{exp}}/\sigma_{\text{theor}} \approx 1.15$.

Three possible sources ($\geq 3\sigma$) at $E_0 \geq 2 \times 10^{12}$ eV are reported by the Crimean group. These are unidentified regions near $\alpha = 05^{\text{h}} 15^{\text{m}}$, $\delta = +1^\circ$ and $\alpha = 01^{\text{h}} 11^{\text{m}}$, $\delta = +62^\circ$. The first of these may be associated with a source at ~ 100 meV reported by Frye (1973). The second of these, which the authors claim to be time variable as it was ^{not} detected by Mt. Hopkins observations (Weekes 1973) between two periods of possible detection. Clearly further observations are needed. The third source reported is Cyg X-3, an X-ray source with a 4.8 hour period that has been detected up to hard X-ray energies (Pietsch et al. 1976). The drift scans in 1972-1973 on this object yielded $\sim 3.5\sigma$ evidence for emission from Cyg X-3 at the X-ray phases 0.3 and 0.9. The sum of several drift scans obtained at these phases is shown in Figure 4. These data are from just ^{the} one of the two offset (in r. a.) detector systems which was at the lowest energy threshold. No effect was seen in the other system at a factor of ~ 2 higher energy, suggesting that if the source was actually detected, its spectrum (unlike the Crab) must be very steep (with integral spectral index ≥ 3.2). This would imply detection at the high energy cutoff of the spectrum. Unfortunately, Stapanian et al. (1975) do not give an estimate of the flux to which the effect in Figure 4 corresponds so comparison with other measurements is difficult. It is curious, though, that the detection of Cyg X-3 claimed by the same group (Vladimirsky et al. 1973) at the time of the 1972 September radio outburst was also only detected in the low energy system and yet the flux (given as 2×10^{-10} photons/cm²sec) is significantly above an extrapolation of the X-ray spectrum. Apparently during the outbursts at least a two component spectrum is required. Tracking observations of Cyg X-3, with fields of view increased to 2° , were conducted from July - November 1974 (Vladimirsky et al. 1975). In August (only) a

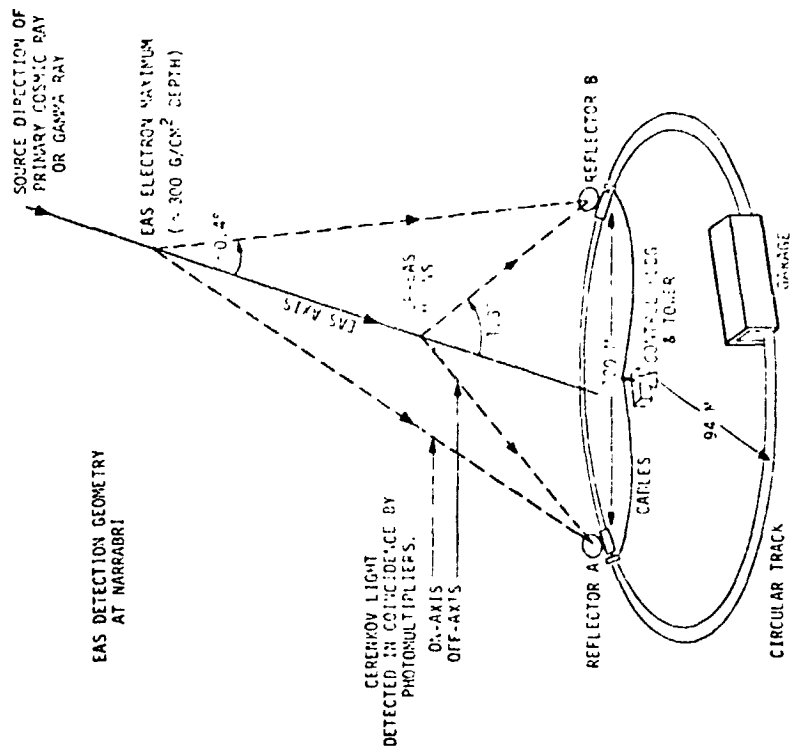


Fig. 5. Geometry of Cerenkov detection of EAS by double beam technique. Application shown is at 7 m optical reflectors of Narrabri Observatory, NSW, Australia.

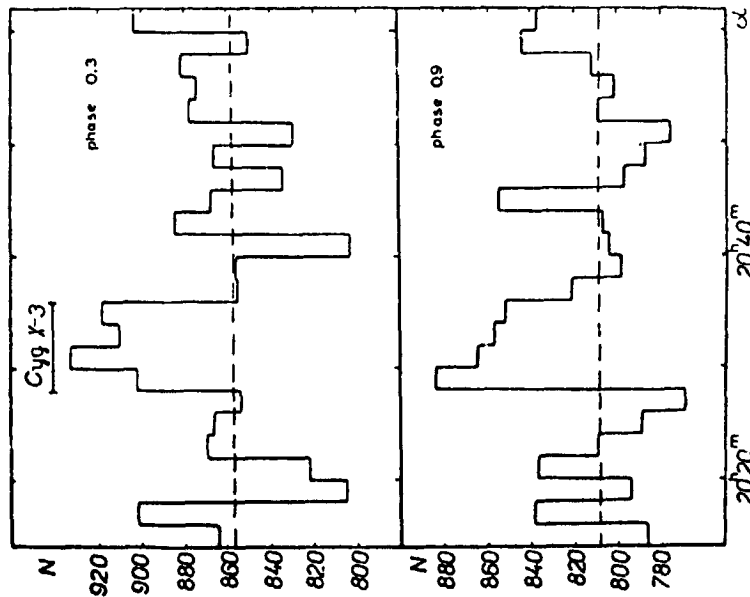


Fig. 4. Time profile of counting rate obtained for Cyg X-3 (by first section data) (a) for X-ray source phase is 0.30 ± 0.025 (b) for X-ray source phase is 0.900 ± 0.025 \pm denotes the right ascension.

REPRODUCIBILITY OF THE ORIGINAL PAGE IS POOR

significant effect ($\sim 4.4\sigma$) was detected, which was primarily at phase 0.35 of the 4.8 hour period. It is especially interesting that the authors find the phase of the 1972-1973 effect would agree with that for 1974 if a period 0.199682 days is used since that is very close to the current best determination (Parsignault et al. 1976) of the X-ray period. This object deserves much further study by other Cerenkov detection groups as well, since there is now (this conference) evidence that Cyg X-3 has been detected at ~ 100 meV.

A systematic sky survey of a large area of sky is needed to search for previously unsuspected sources of very high energy gamma rays. Such a program was described by Weekes et al. (1975), and a survey of the entire sky north of declination 0° is in progress. A large fraction has now been covered, with some areas scanned several times. Unfortunately, data analysis is just beginning and results are not yet available. One important addition to the system described by Weekes et al. (1975) was made: a double beam system has been included. Two 1.5m reflectors at 188m separation from the 10m reflector were operated in 2-fold coincidence with 2 pairs of detectors at the focus of the 10m reflector. The reflectors were pointed towards each other such that EAS were originally detected at their electron maxima. Then, as in all the double beam observations, a third reflector (in this case located near the center of the baseline) was operated in coincidence with each of the original 2-fold coincidence outputs. This channel, biased to detect the penetrating minor component in the UV, then provided the cosmic ray rejection with an efficiency of $\sim 70\%$. In addition to completing the planned survey, a number of observations of the Cyg X-3 region will be conducted.

C. Results of Southern Sky Observations

Since the center of the Galaxy passes directly overhead at Southern latitudes (-30°), ground-based Cerenkov observations of the galactic center source region identified at ~ 100 MeV (e.g. Fichtel et al. 1975) are particularly attractive. An opportunity to conduct such observations, as well as of a number of other potential very high energy sources for the first time, became available in 1972. A group at the University of Sydney, Australia

had conducted Cerenkov observations (including an upper limit on the Crab steady flux) in 1968 using the two 7m aperture optical reflectors of the stellar intensity interferometer at Narrabri NSW (Hanbury Brown et al. 1969). A collaborative observation program between this group and SAO was arranged in 1971 since it was recognized that the computer-controlled Narrabri reflectors were ideally suited for tracking-mode double beam observations. The reflectors and data recording system were thus converted to accommodate the double beam observations and a program of observations of 11 candidate sources was carried out in April - July 1972, April - June 1973 and March - April 1974. A complete description of this program and the results has been given by Grindlay et al. (1975b) and we shall give only a brief summary here.

All the observations were conducted with the reflectors separated by 120m and tracking the source under computer control while maintaining the double beam pointing geometry as shown in Figure 5. The rejection efficiency against p-EAS achieved by the off-axis photomultipliers was $\sim 60\%$ and the total EAS detection rate was $\sim 1 \text{ sec}^{-1}$. Candidate source objects were tracked in between observations of \sim half the duration in which comparison sky regions ($\geq 2^\circ$ in r. a. to either side of the source) were tracked over the identical ranges of track and elevation angle as the source. The comparison regions were selected for identical sky brightness and hence singles rate as the source so no servo of photomultiplier voltages was required.

No significant effects were detected from the galactic center or from possible point sources reported at $\sim 100 \text{ MeV}$ (Frye et al. 1971). The upper limit for emission from within $\sim 1^\circ$ of the galactic center was $F (\geq 3 \times 10^{11} \text{ eV}) < 8 \times 10^{-11} \text{ photons cm}^{-2} \text{ sec}^{-1}$ and is a factor of ~ 3 above an extrapolation of a π^0 spectrum from the $\sim 100 \text{ MeV}$ results. This result also requires that any flat inverse Compton component of the galactic center (or plane) flux not extend to $> 10^{11} \text{ eV}$ without a break in the spectrum. Interesting results were obtained on the three pulsars observed. All showed a "steady source" excess of $> 2\sigma$ above background, with MP1451-68 actually $\sim 3\sigma$ positive. However upon analyzing the data for pulsations at the predicted periods and summing all the data in phase, only the Vela pulsar yielded evidence for pulsed emission, and this only in 1972. A $\sim 4\sigma$ (single) peak was evident in

the data at a phase within 3 msec before or after (de-dispersed) radio pulse phase (Grindlay et al 1975b). This single peak contrasts with the double peaked pulse structure found at ~ 100 MeV (Thompson et al. 1975) though it is similar to the Crab pulsar at ~ 100 MeV at comparable energies (Figure 2). Thus it is striking that just as the Crab and Vela pulsars show almost identical double pulsed light curves at ~ 100 MeV, they may also be very similar (single pulse) at very high energies. Since a very much smaller effect, and only at the highest Cerenkov pulse heights (or primary energies), was detected in the 1973 observations, the Vela spectrum may be like the Crab pulsar also in being very flat and time variable. Unfortunately, the single 4σ detection (1972) of Vela renders these results much less certain statistically than for the Crab. However one may speculate that if pulsars produce very high energy gamma ray sources with variable phase, then perhaps the "steady" effects on MP1451-68 (and, though only $\sim 2\sigma$, also on PSR1749-28) are actually pulsed with phase variations occurring within a few days.

The final result we shall summarize was obtained on the radio galaxy Cen A (NGC5128). This is the closest (~ 5 mpc) of 3 active galaxies (including the QSO 3C273) observed and is especially interesting for its compact source structure in the nucleus detected through hard X-ray energies. The source was detected at $2-3\sigma$ in each of the 3 observing periods for a total detection at the $\sim 4.6\sigma$ level of an average flux

$$F (\geq 3 \times 10^{11} \text{ eV}) \approx 4.4 \times 10^{-11} \text{ photons cm}^{-2} \text{ sec}^{-1}$$

Complete details are given by Grindlay et al. (1975a). About half of the data were recorded with pulse height (spectral) information, and the spectrum of the observed gamma ray flux is consistent with a spectrum that is flatter than the background cosmic ray spectrum up to a break at $\sim 3 \times 10^{12}$ eV. Such a spectrum and indeed the entire detected flux can be understood in terms of a Compton-synchrotron model of the nucleus of NGC5128 (Grindlay 1975) where the $\sim 10^{12}$ eV gamma rays are produced by inverse Compton scattering of an X-ray synchrotron electron spectrum (through electron energies $\sim 10^{13}$ eV) on the optical - X-ray synchrotron photons. The synchrotron

spectra were calculated assuming the compact sources are self-absorbed in the radio regime. The very high energy gamma ray flux then provides the additional constraint necessary to solve for both the source angular diameter and magnetic field. The complete source spectrum model requires a two component source whose diameters are then calculated to be $\sim .01$ pc and 0.2 pc and magnetic fields ~ 2 gauss and $\sim .01$ gauss, respectively. The high energy gamma rays are produced in the larger component, which may be a cosmic ray source surrounding the smaller source in the nucleus of NGC5128.

IV. Conclusion

After a long beginning it now seems that ground-based gamma ray astronomy has begun to yield positive results of great astrophysical interest. The early upper limits on steady emission from objects such as the Crab nebula were themselves of fundamental importance for establishing limits to pion production and the necessity of continuing acceleration of electrons (Cludakov et al. 1965) and for important limits on the magnetic field (Weekes et al. 1972) in the Crab. Now with solid evidence for pulsed emission from NP0532 at $> 10^{12}$ eV that is variable in phase, pulsar emission and particle acceleration theories are additionally constrained. Consideration of these theories suggests, for example, (Grindlay et al. 1976) that the very high energy pulsed spectrum may arise from bremsstrahlung of a cosmic ray beam (accelerated off the neutron star) as it traverses relatively dense matter accumulated at the "force balance" radius (Roberts and Sturrock 1973) relatively far from the star (thereby also escaping pair conversion in the magnetic field). The possible association of NP0532 emission (at $> 10^{11}$ eV) and pulsar glitch activity might then be understood, since glitches may arise when matter from this force balance shell is released into the nebula.

The results obtained by the Crimean group, particularly on Cyg X-3, are of great interest. If the Cyg X-3 variable emission, primarily at X-ray phase ~ 0.3 , can be confirmed, it is of major significance for theories of this very unusual X-ray source. None of the currently proposed theories for this object would directly predict 10^{12} eV gamma rays. A gamma ray flux

could arise from (presumably by inverse Compton or bremsstrahlung processes) production of $\sim 10^{12}$ eV cosmic rays in this type of source. The evidence for the reality of the periodic $> 10^{12}$ eV emission from Cyg X-3 reported by Vladimirsky et al. (1975) is greatly strengthened by the fact that the trial best-fit period they proposed ($0^d.199682$) now turns out to be the best-fit X-ray period (Parsignault et al. 1976).

The most important result of the southern sky observations is, of course, the detection of $> 10^{11}$ eV gamma rays from the first extragalactic source, Cen A. This result and the model (Grindlay 1975) which accounts for the flux and entire NGC5128 spectrum by inverse Compton scattering in compact synchrotron sources in the nucleus, provides new insight into the physics of active galaxies. The results suggest other objects of this type may also be detected. The other key results of the Australian observations were the possible detection of pulsed emission from the Vela pulsar PSR0833-45 with pulse profile and variability similar to that of the Crab pulsar, and the lack of detectable emission from the galactic center or galactic plane.

It is useful to summarize the major conclusions reached by very high energy gamma ray astronomy to date:

- 1) Gamma ray sources above 10^{11} eV appear to be point sources or compact objects which may be usually time variable and are accelerating cosmic rays. The physical conditions (i. e. magnetic fields, energy densities, etc.) in these objects are revealed by the very high energy gamma ray fluxes or upper limits.

- 2) Pulsars, at least the Crab and possibly Vela and others, produce very high energy spectra of pulsed gamma rays that are variable in phase and amplitudes. These spectra are almost certainly not an extrapolation of the low energy pulsar spectrum and may arise from the primary particles (rather than their cascades) accelerated by the pulsar.

- 3) All of the possible source fluxes reported are $\leq 5\%$ (usually $< 1\%$) of the background cosmic ray rate detected. While the strongest classes of sources may not yet have been detected, the high background problem and

results to date point out the necessity that future observations be double beam, multi-beam, or in some way actively reject the cosmic ray background.

The final point should be re-emphasized. Despite the very promising progress achieved in ground-based gamma ray astronomy, a major increase in sensitivity is needed. It is very likely that an extension of the double beam technique to a multi-reflector EAS array could achieve this.

REFERENCES

- Charman, W.N., Jelley, J.V. and Drever, R.W.P. 1969. Proc. 11th Intl. Conf. on Cosmic Rays (Budapest) OG-11.
- Chudakov, A.E., Dadykin, V.L., Zatsepin, V.I., and Nesterova, N.M. 1965. Cosmic Rays (Proc. P.N. Lebedev Inst.), 26, 99.
- Erickson, R.A., Fickle, R.K. and Lamb, R.C. 1976. Ap.J., in press.
- Fazio, G.G., Helmken, H.F., O'Mongain, E. and Weekes, T.C. 1972. Ap.J. (Letters), 175, L117.
- Fazio, G.G., Helmken, H.F., Rieke, G.H. and Weekes, T.C. 1968. Nature, 220, 892.
- Fazio, G.G. 1973. Gamma Ray Astrophysics, NASA, SP-339, P.153.
- Fichtel, C.E., Hartman, R.C., Kniffen, D.A., Thompson, D.J., Bignami, G.F., Ogelman, H., Ozel, M.F. and Turner, T. 1975. Proc. 14th Intl. Cosmic Ray Conf (Munich), 1, 29.
- Frye, G.M., Albats, P.A., Zych, A.D., Staib, J.A., Hopper, V.D., Rawlinson, W.R. and Thomas, J.A. 1971. Nature, 233, 466.
- Frye, G. 1973. IAU Symp. No. 55 (Madrid).
- Grindlay, J.E. 1971a. Smithsonian Astro. Obs. Special Report, No. 334.
- _____ 1971b. Nuovo Cimento, 2B, 119.
- _____ 1972. Ap.J. (Letters), 174, L9.
- _____ 1974. Phys. Rev. D, 11, 517.
- _____ 1975. Ap.J., 199, 49. Grindlay, J.E. and Hoffmann, J.A. 1971, Ap. Letters, 8, 209.
- Grindlay, J.E., Helmken, H.F. and Weekes, T.C. 1974. ESLAB Symposium on Gamma Ray Astronomy, Frascati (Italy), 301.
- _____ 1976. Ap.J., to be published Oct. 15, 1976.
- Grindlay, J.E., Helmken, H.F., Brown, R.H. Davis, J. and Allen, L.R. 1975a. Ap.J. (Letters), 197, L9.
- _____ 1975b. Ap.J., 201, 82. Hanbury Brown, R., Davis, J. and Allen, L.R. 1969, M.N.R.A.S., 146, 399.
- Helmken, H.F., Grindlay, J.E. and Weekes, T.C. 1975. Proc. 14th Intl. Cosmic Ray Conf. (Munich), 1, 123.
- Jelley, J.V. 1958. Cerenkov Radiation and Its Applications (New York: Pergamon Press).

- Jennings, D.M. White, G., Porter, N.A., O'Mongain, E., Fegan, D.J.,
and White, J. 1974. Nuovo Cimento, 20B, 71.
- Lohsen, E. 1975. Nature, 258, 689.
- Long, C.D., McBreen, B., Porter, N.A. and Weekes, T.C. 1965.
Proc. 9th Intl. Cosmic Ray Conf. (London), 1, 318.
- McBreen, B., Ball, S.E. Jr., Campbell, M., Greisen, K. and Koch, D.
1973. Ap.J., 184, 571.
- O'Mongain, E.P., Porter, N.A., White, J., Fegan, D.J., Jennings, D.M.,
and Lawless, B.G. 1968. Nature, 219, 1348.
- Parsignault, D.R., Schreier, E., Grindlay, J., and Gursky, H. 1976.
Ap.J. (Letters), in press.
- Pietsch, W., Kendiziorra, E., Stanbert, R., and Trumper, J. 1976.
Ap.J. (Letters), 203, L67.
- Porter, N.A., Delaney, T., and Weekes, T.C. 1974. ESLAB Symposium
on Gamma Ray Astronomy, Frascati (Italy), 295.
- Rankin, J.M., Payne, R.R. and Campbell, D.B. 1974. Ap.J. (Letters), 193,
L71.
- Rieke, G.H. 1969. Smithsonian Astro. Obs. Special Report, No. 301.
- Roberts, D.H. and Sturrock, P.A. 1973. Ap.J., 181, 161.
- Stepanian, A.A., Vladimirovsky, B.M., Neshpor, Yu.I. and Fomin, V.P.
1975. Astrophys. and Space Sci., 38, 267.
- Thompson, D.J., Fichtel, C.E., Kniffen, D.A. and Ogelman, H. 1975.
Ap.J. (Letters), 200, L79.
- Tornabene, H.S. 1976. Contributed paper, this conference.
- Tornabene, H.S. and Cusimano, F.J. 1968. Can. J. Phys., 46, S81.
- Vladimirovsky, B.M., Stepanian, A.A. and Fomin, V.P. 1973. Proc. 13th
Intl. Cosmic Ray Conf. (Denver), 1, 456.
- Vladimirovsky, B.M., Neshpor, Yu.I., Stepanian, A.A. and Fomin, V.P.
1975. Proc. 14th Intl. Cosmic Ray Conf. (Munich), 1, 118.
- Weekes, T.C., Fazio, G.G., Helmken, H.F., O'Mongain, E.P. and
Rieke, G.H. 1972. Ap.J., 174, 165.
- Weekes, T.C. 1973. Proc. 13th Intl. Cosmic Ray Conf. (Denver)1, 446.

- Weekes, T. C. and Rieke, G. H. 1974. ESLAB Symposium on Gamma Ray Astronomy, Frascati (Italy), 287.
- Weekes, T. C., Helmken, H. F. and Horine, E. 1975. Proc. 14th intl. Cosmic Ray Conf. (Munich), 1, 133.
- Wolfe, R. and Novick, R. 1976. Nature, in press.
- Zatsepin, V. I. and Chudakov, A. E. 1962. Soviet Phys - JETP, 15, 1126.

N76-29119

RADIATION MECHANISMS AND MAGNETOSPHERIC STRUCTURE OF PULSARS*

P.A. Sturrock and K.B. Baker, Institute for Plasma Research,
Stanford University, Stanford, California 94305

ABSTRACT

This article outlines the chain of thought which has led to a model of pulsars now being investigated at Stanford. Key early considerations were those which led to the identification of pulsars with neutron stars and the Goldreich-Julian model of pulsar magnetospheres. Another important step was the recognition that, in a pulsar magnetosphere, a high-energy gamma ray may annihilate to produce an electron-positron pair. Arguments advanced by Scargle and Pacini suggest that pulsar magnetospheres may contain large masses of plasma, a suggestion which has important implications concerning the structure of the magnetosphere.

Observational data seems to support a magnetosphere model based on the Scargle-Pacini idea rather than the Goldreich-Julian model. The cascade process resulting from pair creation enables one to interpret the x-ray emission from the Crab and Vela pulsars as synchrotron radiation. On the other hand, the optical radiation from the Crab pulsar is best understood as coherent curvature radiation. Radio emission is interpreted as curvature radiation produced by charge bunches moving along magnetic field lines. Certain tests of this model are proposed.

*Presented by P.A. Sturrock

1. Introduction. I am very sorry that Franco Pacini could not be here today to give this talk. Franco would no doubt have had much to say about the origin of cosmic rays. By contrast, I have very little to say on this topic, and I shall be concerned primarily with the problem of the magnetospheric structure of pulsars and of radiation mechanisms.

I think virtually all scientists now believe that pulsars are rotating neutron stars, but in the early days there was a competing hypothesis that they were pulsing white dwarfs. Some of you may be curious to ask, "What ever happened to white dwarfs?". Table 1 will show you why white dwarfs were ousted in favor of neutron stars.

IS A PULSAR A NEUTRON STAR OR A WHITE DWARF?

	NS	WD
1. PERIOD IN RANGE .03 SEC to 3.7 SEC	✓	X
2. PERIOD STABLE TO 1 PART IN 10^9	✓	?
3. PERIOD INCREASES	✓	X?
4. NO OPTICAL PHOTOSPHERIC RADIATION	✓	X
5. TWO PULSARS IN SUPERNOVA REMNANTS	✓	X

TABLE 1

It is believed that white dwarfs could not vibrate as rapidly as .03 seconds. It is believed that white dwarfs would not have a stability of the oscillation as good as one part in 10^9 . If pulsars were pulsing white dwarfs, we would expect their period to decrease because stars become denser with age just as we all do. One would expect to be able to observe the objects (or some of them) by their photospheric emission. One would not expect to find pulsars in supernova remnants if they were white dwarfs. Now, of course, one fact will not destroy a theory or a theorist, but an array of five facts as good as these will bring any theorist into line.

Once that argument was settled and it was accepted that pulsars are neutron stars, the next question was where the radiation is produced. There were, and perhaps still are, two schools of thought. One school proposes that the radiation is produced at the light cylinder. T. Gold was one of the first and published a paper in 1969 (Gold, 1969) developing the idea of streams of plasma flowing out along field lines. (Figure 1.) When they get to the light

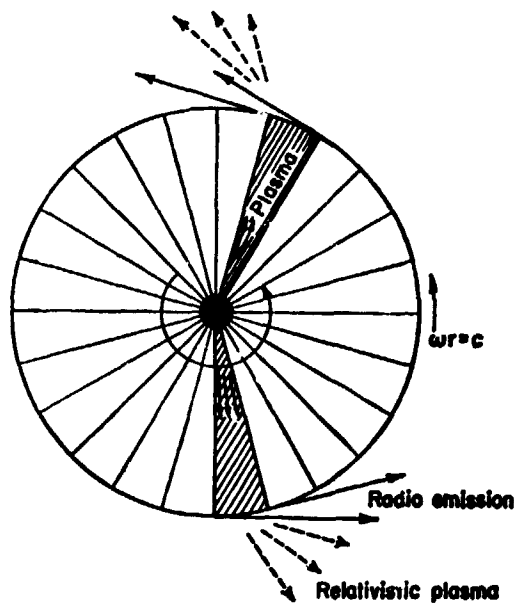


FIGURE 1. Light-cylinder model for emission of radio energy and relativistic gas. The neutron star has a corotating magnetosphere reaching out to the circle at which ωr , the peripheral speed, is close to the speed of light. Plasma emitted on the surface by nonthermal processes will be accelerated to relativistic speeds and flung out of the magnetosphere (Gold, 1969).

cylinder where $\omega r = c$, they must be moving at the speed of light and they will beam radiation in the forward direction. An improved model was developed by Professor Smith, who is now the director of the Royal Greenwich Observatory, in 1971 (Smith, 1971, 1973). However, I have not seen much published from this school in recent years. Some of my colleagues feel that this particular question is now settled: that radiation is not produced at the light cylinder, it really is produced near the polar cap. This school of thought began with two radio observers Radhakrishnan and Cooke (1969), who also published in 1969. Their diagram in their first paper is shown in Figure 2. It is assumed that radiation is produced at two cones at the magnetic polar caps. So there are in fact two lighthouse beams which swing around with the star. If an observer is lucky, he may be in the line of fire of one of these beams and see one pulse per rotation. If he is extremely lucky, so that the rotation axis is almost orthogonal to the magnetic axis, then he may see two pulses. There are in fact a few pulsars which do show both the pulse and what is called an "interpulse".

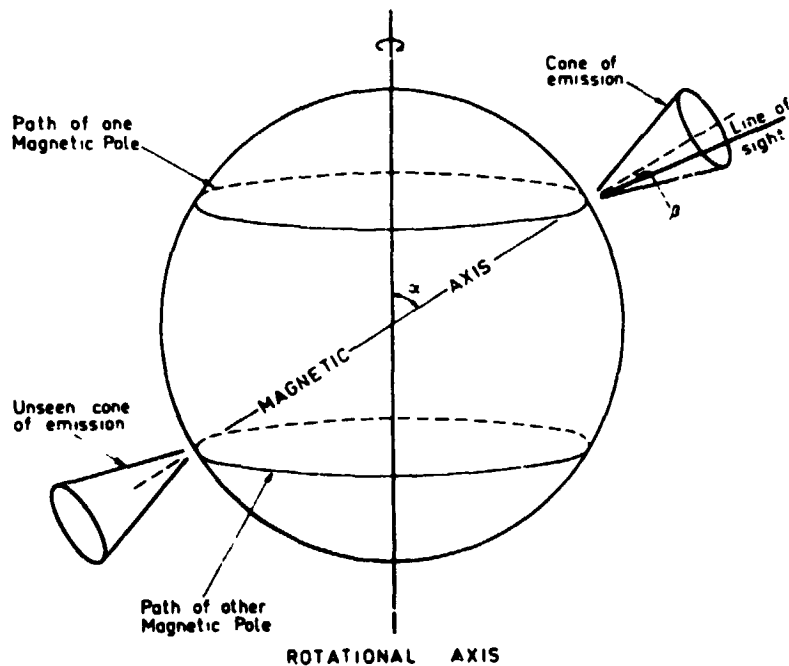


FIGURE 2. The geometry of polar-cap model: Close-up view of neutron star with emission regions near the surface at the magnetic poles. The dipole field lines give a preferred direction to each part of the emission region producing the linear sweep of polarization observed in a radio pulse (Radakrishnan and Cooke, 1969).

Also in 1969, a very important paper was published by Goldreich and Julian (1969). (It is a rare theoretical paper which leads to an editorial in the New York Times.) This paper outlined a model for the structure of a pulsar magnetosphere. The authors showed that the electric fields produced by induction are so strong that there must be plasma in the vicinity of the star drawn off by field emission. They concluded that the magnetic field lines could be closed only out to the light cylinder and must be open beyond that point. The plasma flow constitutes a "pulsar wind", similar to the solar wind.

2. Magnetospheric Structure. So here were two excellent ideas: that of Radhakrishnan and Cooke and that of Goldreich and Julian, which together led to a prediction. One could calculate the expected pulse width of the beam produced at the polar cap of a pulsar and compare it with the observational data. However, when this is done, there is no fit between the mean pulse-width expected for a given period on the basis of that model and what is actually observed (Figure 3).

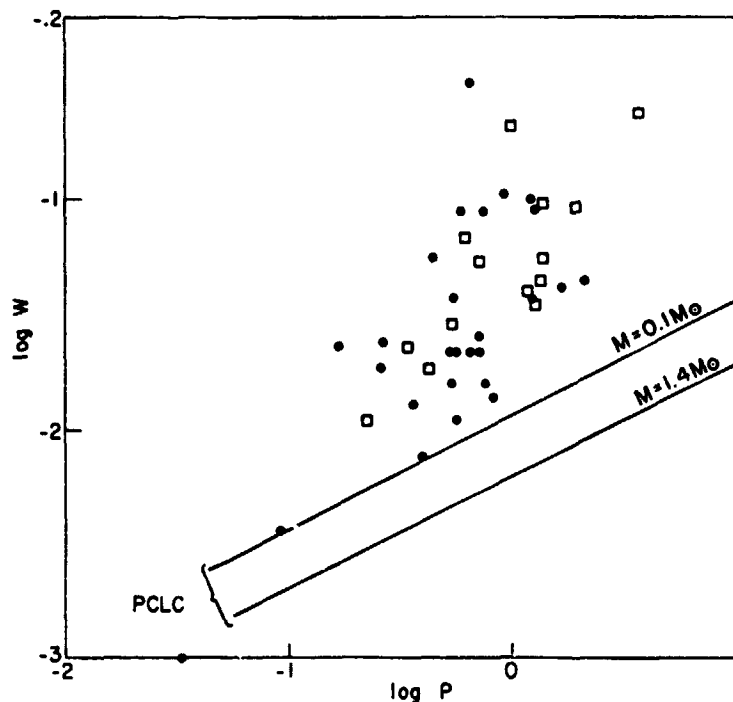


FIGURE 3. Pulse width W versus period P distribution of pulsars. The curves show the mean expected relationship for the PCLC model (polar-cap radiation, lines opening at the light cylinder) for the star masses indicated.

This seems to imply that one of the two ideas is incorrect. Either radiation is not produced as proposed by Radhakrishnan and Cooke, or the magnetosphere does not have the structure proposed by Goldreich and Julian. I think the answer to that question comes by considering the braking index of a pulsar. The torque exerted on a pulsar will, we expect, vary as a power of the rotation frequency:

$$\Theta = -I \frac{d\omega}{dt} \propto \omega^n \quad (2.)$$

We can in fact determine n from observational data if we know the period, the derivative of the period and the second derivative of the period, which we do for the Crab:

$$n = \frac{\omega \ddot{\omega}}{\dot{\omega}^2} \quad (2.)$$

Goldreich and Julian made the definite prediction that $n = 3$. Data for the Crab is still not certain, but it seems to be in the range 2.2 to 2.6 (Boynton et al., 1972).

In any case, it seems that there is a clear-cut discrepancy between prediction and observational data, suggesting that the idea of Radhakrishnan and Cooke may be correct, but that of Goldreich and Julian is somehow probably incorrect. Where did it go wrong? A possible suggestion arose out of a paper published by Scargle and Pacini (1971). They noted that the 1969 glitch of the Crab pulsar was apparently associated both with the disturbance of a wisp in the Crab nebula and with a change in the dispersion measure. They proposed, therefore (contrary to most current thoughts), that a glitch is a magnetospheric phenomenon involving an instability which itself involves a large mass of plasma trapped in a pulsar magnetic field. Their estimate was that mass must be about 10^{21} grams. Dave Roberts and I looked into this possibility and we found that such a large mass could probably not be contained in the pulsar magnetosphere. Either gravitational force or centrifugal force would disrupt the equilibrium situation unless there was a singular situation with the gas collecting at the "force-balance" or "corotation" position where gravitational and centrifugal forces just balance. Suppose that gas were to be ejected into the magnetic field either by evaporation from the star or by ionization of neutral gas being accreted by the star. If a lot of gas collects and cools down at small radii, it will fall to the surface. If, on the other hand, it collects at large radii, it will pull open the field lines, the end result being that the largest closed field line comes at the force-balance radius rather than at the light cylinder.

We can express this radius (of the Y-type neutral point) in terms of the mass of the star and the period of the star:

$$\omega^2 R_{FB} = \frac{GM}{R_{FB}^2}, \quad (2.3)$$

which leads to

$$R_{FB} = 10^{-2.9} M^{1/3} P^{2/3}. \quad (2.4)$$

In the inner region, the magnetic field is approximately dipolar and drops off as r^{-3} , but once the field lines open up the field will drop off as r^{-2} . This change in the magnetospheric structure also produces a change in the braking index (Roberts and Sturrock, 1972), which we calculated to be $n = 2.33$. This value is in reasonable agreement with the known data. The opening of the field lines at R_{FB} also means a larger polar cap, and hence a different dependence of the pulse width on the period (Roberts and Sturrock, 1972):

$$\omega = 10^{1.1} M^{-1/6} R^{1/2} P^{2/3}. \quad (2.5)$$

This expression involves the mass of the star, but for masses in the

range $.1 M_{\odot}$ to $1.4 M_{\odot}$, there is a reasonable fit with the data (Figure 4). We note that different orientations of the spin axis and magnetic axis can give rise to values of the pulse period either larger or smaller than the value given by equation (2.5).

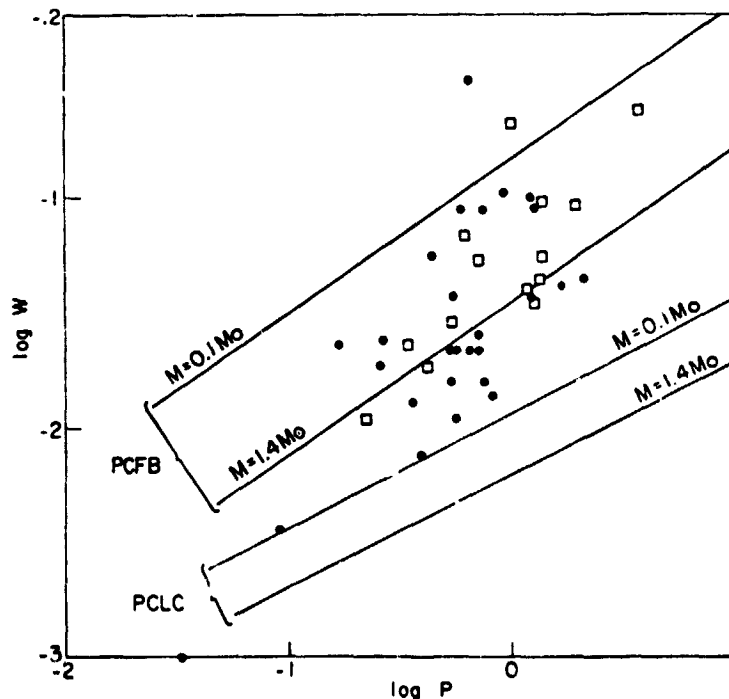


FIGURE 4. Pulse width W versus period P distribution of pulsars. The curves repeat those of Figure 3, and also show the mean expected relationship for the PCFB model (polar-cap radiation, lines opening at the force-balance radius) for the star masses indicated.

3. Radiation. Now I want to turn to the more important question: Where and how is the radiation produced, and how intense is it? First I would draw your attention to the fact that a wind such as the solar wind will cause magnetic field lines to spiral in the equatorial plane. A field pattern such as this has non-zero curl, so that there must be currents flowing to maintain this field pattern. If these currents are flowing along field lines, they must originate in or flow into the polar caps. For the simple case that the dipole axis is parallel to the spin axis, at each polar cap there will be an inflow of current at the center and an outflow at the edges or vice-versa. If intense currents are leaving the polar caps, one expects that electric fields somehow develop in that region to draw off the currents. We can estimate the current and the charge density

and hence estimate the voltage required: for the Crab pulsar, which probably has a field strength of order 10^{12} gauss and has a rotation period of about 33 ms, we find that the voltage must be of order 10^{16} volts. If any ions leave part of the polar cap, they may accelerate to that enormously high voltage, and if they escape into interstellar space, they might contribute significantly to the cosmic ray intensity. On the other hand, electrons will radiate, because they are moving along curved magnetic field lines and have a smaller mass, and the radiation reaction becomes so intense as to limit the electron energy to about 10^{14} volts. Hence if half the rotational power goes to driving the ion flow and the other half goes to driving the electron flow, almost all the power that goes into driving electrons will go into an intense flux of gamma rays of energy about 10^{12} eV.

Our model has now advanced to the point that we have a structure for the magnetosphere and we have an elementary picture of where the acceleration occurs. But what we now find is that we have produced an intense source of very high energy gamma rays. Perhaps participants in this conference may be happy about that, but radio astronomers are really not satisfied because they assert that all pulsars produce radio emission. In addition, one pulsar produces optical emission, and perhaps two produce x-rays, whereas the only radiation produced by the model at this stage is a flux of gamma rays.

The missing link (Sturrock, 1971) is believed to be the following: - If a high-energy gamma ray is moving transverse to an intense magnetic field, it will annihilate to produce an electron-positron pair. The gamma ray energies in the Crab, for example, are so high and the field strength is so high, that this annihilation will occur extremely rapidly. When it occurs, there are two important consequences. One is the production of secondary particles - electrons and positrons - moving with non-zero pitch angles which therefore will emit by the synchrotron process. This may give rise to the optical or x-ray or gamma ray part of the spectrum. The important point is that whereas we began with a stream of charge of just one sign (electrons), we now have a stream with particles of opposite sign - positrons. Some of these will tend to move back towards the surface of the star under the action of the electric field, and this will create a two-stream situation which plasma physicists know is potentially unstable. If the instability should occur, it will give rise to bunching of the charges, and it is precisely this that one needs to give rise to radio emission because single particles flowing along curved field lines will give negligible radio emission, but bunches of charge will give significant radio emission.

One may estimate the spectrum to be expected from this model (Roberts et al., 1973). With quite a reasonable assumption about the degree of bunching of the electron beam, one can fit the radio data.

The simplest estimate of the x-ray spectrum gives a $\nu^{-1/2}$ law, but when one takes full account of the cascade process, this becomes modified to a ν^{-1} law which is a better fit to the observed data. The estimates are fairly sensitive to the mass of the star. However, an important point is that the model does not allow gamma rays of energy 10^{12} eV to escape from the polar cap regions. Hence the observations by Grindlay (1972) are hard to understand. Second, the emission is self-absorbed at 2 or 3 keV energy, so that there is no way to explain the optical emission on the basis of this model. In fact the optical pulse shape has such a sharp cusp that it must be produced by particles of energy 10^8 eV or more. This means the magnetic field strength must be less than 10^6 gauss if the radiation is being produced by the synchrotron mechanism. But the field has this low a value only near the light cylinder. The difficulty with assuming the radiation to be produced near the light cylinder is again that the cusp is so sharp that it would require emission in a very small region of the light cylinder. I am not saying these requirements cannot be met, but there is no current model that satisfactorily meets them.

One way out of this difficulty was proposed by Steve Turk, a student who worked with me who unfortunately died three years ago. His suggestion is that each primary electron gives rise to a stream of gamma rays, each gamma ray producing an electron-positron pair, so that a string of secondary particles form near each primary electron. A very small separation of these particles, due to a quite small electric field, will mean that the electrons and positrons will behave independently so that one can obtain coherent radiation in this model even in the optical part of the spectrum. Hence we propose that the optical radiation from the Crab may be coherent curvature radiation. The observational data yields a spectrum which peaks at little less than 10^{15} Hz, at a luminosity of about 10^{18} ergs per Hz per second. One can fit this data approximately with a star of mass 0.4 solar mass, which is also the mass indicated by the power budget of the Crab nebula (Sturrock et al., 1975).

4. Discussion. To conclude, we shall review the properties which we attribute to pair creation.

(a) We believe that pair creation explains the period-age distribution. The point is that as a star slows down, it eventually reaches a period (for a given field strength and mass) for which pair creation will no longer occur. In that case, we believe that bunching will no longer occur so that there will no longer be radio emission (Sturrock et al., 1976).

(b) We attribute the coherent RF radiation to pair creation, as discussed earlier.

(c) We believe that the optical radiation from the Crab is coherent and is due essentially to pair creation process.

(d) We believe that x-ray emission from the Crab and the Vela pulsars is due to pair creation. [I would add that, if the new observations of radiation from 1747 and 1818 are correct, this gamma-ray emission (which is of fairly low energy) may be due to pair creation.]

(e) Based on analysis of the radio data, which is not unambiguous, there appears to be a large flux of low energy particles into the Crab nebula. The current model does lead to a large particle flux (mainly of positrons and electrons) into the nebula.

(f) The precursor of the Crab may be due to the possibility that radio emission occurs not only where electrons leave the polar cap (EPZ), but also where ions leave the polar cap (IPZ). The Crab is the only pulsar spinning rapidly enough for pair creation to occur in the IPZ, so it is the only pulsar for which this process would occur. This interpretation suggests an explanation of the curious fact that the Crab is the only pulsar with a precursor.

There are still some observations to be made that I think would help to resolve some of the remaining outstanding equations. I think it is most desirable to try to determine whether the optical and the x-ray parts of the spectra of the Crab pulsar are continuous or whether they are quite distinct. This can be determined by trying to extend the optical spectrum into the UV or by trying to extend the x-ray spectrum to lower energies. It also would be valuable to try to determine the polarization of the x-ray emission from the Crab pulsar because the model I am proposing suggests that the E-vector of the x-ray emission should be orthogonal to the E-vector for the optical emission. On the other hand, if they are both produced by the same process (say if they are both synchrotron radiation), then they should both have electric vectors in the same direction.

REFERENCES

- Boynnton, P.E., Groth, E.J., Hutchinson, D.P., Nanos, Jr., G.P., Partridge, R.B., and Wilkinson, D.T. 1972, Ap. J., 175, 217.
Gold, T. 1969, Nature, 221, 25.
Goldreich, P., and Julian, W.H. 1969, Ap. J., 157, 869.
Grindlay, J.E. 1972, Ap. J. Letters, 174, L9.
Radhakrishnan, V., and Cooke, D.J. 1969, Astrophys. Letters, 3, 225.
Roberts, D.H., and Sturrock, P.A. 1972, Ap. J. Letters, 173, L33.
Roberts, D.H., Sturrock, P.A., and Turk, J.S. 1973, Ann. N.Y. Acad. Sci., 224, 206.
Scargle, J.D., and Pacini, F. 1971, Nature Phys. Sci., 232, 144.

Smith, F.G. 1971, Nature Phys. Sci., 231, 191.
Smith, F.G. 1973, Nature, 243, 207.
Sturrock, P.A., Petrosian, V., and Turk, J.S. 1975, Ap. J., 196, 73.
Sturrock, P.A., Baker, K., and Turk, J.S. 1976, Ap. J., 206, 273.

N76-29120

GAMMA RAY PULSARS

H. Ügelman, S. Ayasli, and A. Hacinliyan
Middle East Technical University
Ankara, Turkey

ABSTRACT

Recent data from the high energy γ -ray experiment have revealed the existence of four pulsars emitting photons above 35 MeV. An attempt is made to explain the γ -ray emission from these pulsars in terms of an electron-photon cascade that develops in the magnetosphere of the pulsar. Although there is very little material above the surface of the pulsar, the very intense magnetic fields (10^{12} gauss) correspond to many radiation lengths which cause electrons to emit photons via magnetic bremsstrahlung and these photons to pair produce. The cascade develops until the mean photon energy drops below the pair production threshold which happens to be in the γ -ray range; at this stage the photons break out from the source.

1. Introduction. Initial results of the SAS-2 γ -ray telescope have shown that two of the outstanding γ -ray sources in the galactic plane survey were the pulsars PSR 0531+21 (Crab) and PSR 0833-45 (Vela) (Kniffen et al., 1974; Thompson et al., 1975). Subsequently, a more extensive search of the SAS-2 data for pulsed emission from some 75 more radio pulsars has yielded positive fluxes with chance occurrences less than 10^{-4} for PSR 1747-46 and PSR 1818-04 (Ogelman et al., 1976).

Among these four γ -ray emitting pulsars that cover an age span of 10^3 to 10^6 years only the youngest one, Crab nebula pulsar, exhibits emission in other parts of the electromagnetic spectrum, in addition to the radio and gamma ray region. Thus, it appears that γ -ray emission around the 35 MeV region is a fundamental emission feature of pulsars. In this paper we attempt to show that this feature is a consequence of the co-existence of intense magnetic and electric fields that can produce energetic electrons near the pulsar surface.

Since γ -rays in the energy range under discussion are commonly considered to be the signature of high energy protons interacting with the ambient medium and producing π^0 mesons which in turn decay into γ -rays, we may consider the applicability of this process to the pulsars for the production of gamma rays. There are two strong objections to this alternate explanation. One is the fact that above the surface of the pulsar there is very little material to cause interactions of the high energy protons that may be accelerated in the electric fields near the surface. The density of current producing charges is estimated to be near 10^{13} cm^{-3} even for the fastest pulsars. This magnitude of density integrated to the speed of light cylinder only yields about 10 micrograms cm^{-2} of material above the surface which is of the order of 10^{-6} to 10^{-7} interaction mean free paths for protons. The second objection lies in the fact that even if sufficient material was found for protons to interact, such as the surface of the neutron star, the efficiency of the π^0 production process requires some 10^{39} to 10^{40} protons s^{-1} to account for the γ -ray flux of an object such as Crab nebula pulsar. This is about a factor of 10^6 larger than the estimated primary electron flux.

Turning back to the material starved, electromagnetically rich pulsar magnetosphere we can speculate on how one may get special emphasis in the emission around gamma ray region. As an analogy let us consider observations of secondary γ -rays below the earth's atmosphere. If we perform such an experiment we may notice a preference of γ -rays around the 10 to 100 MeV region. Although the details of the interactions are complex we can guess the reasons behind the energy preference. Initially we start on top of the atmosphere with energetic particles. The atmosphere is many interacting mean free paths thick to the cosmic rays. The high energy protons quickly interact, producing

mesons which then decay right away into electrons, positrons and γ -rays thereby starting an electromagnetic cascade. The electrons predominantly lose their energy by bremsstrahlung to photons of comparable energy and create electrons with about half their energy; the electromagnetic cascade thus multiplies and grows. When the average electron energy drops below 80 MeV the electrons predominantly start losing their energy by ionization and at around 20 MeV the photons through Compton process. At this stage the electron and photon components can no longer sustain each other, the shower stops growing. Furthermore around 10-50 MeV region the photons have a minimum in their absorption curve which allows them to penetrate deeper into the atmosphere.

A similar situation exists in the pulsar magnetosphere with the source and observer reversed. Energetic electrons accelerated near the surface have to emerge out of the intense magnetic fields of the magnetosphere. In doing so they create an electromagnetic shower, the photons of which eventually break out of the surface. To understand more about the shower let us review the electromagnetic processes that take place in intense magnetic fields.

2. High Energy Electromagnetic Processes in Intense Magnetic Fields. Typical parameters of electrons and magnetic fields in the astrophysical setting put the encountered electromagnetic conversion processes into the classical relativistic regime. However, the surface fields of 10^{12} gauss of pulsars and electric fields that can yield electrons with energies greater than 10^9 eV force us to treat this phenomenon with the proper quantum electrodynamical considerations. Following Erber (1966) we define the dimension less parameter T that characterizes the transition probabilities.

$$T = \left(\frac{E}{mc^2} \right) \left(\frac{B_{\perp}}{B_{cr}} \right) \quad (1)$$

where E is the energy of the electron or the photon, B_{\perp} is the perpendicular component of the field to the direction of the particle and B_{cr} is the natural quantum measure of the field strength:

$$B_{cr} \equiv \frac{m^2 c^3}{e \hbar} = 4.414 \times 10^{13} \text{ gauss} \quad (2)$$

The measure of the dominance region of the electromagnetic process is also characterized by this parameter. For the case $T \ll 1$ we are in the classical relativistic regime and for the $T \gg 1$ region we are in the quantum electrodynamic regime. In the $T \gg 1$ region we can have pair production of photons which eventually disappears as $T \ll 1$.

Furthermore, the peak of the emitted photon spectrum for an electron of energy E is given by:

$$\epsilon_{\gamma\max} = E \left(\frac{3T}{2 + 3T} \right) \quad (3)$$

For $T \gg 1$, $\epsilon_{\gamma} \sim E$ and for $T \ll 1$, $\epsilon_{\gamma} \sim 3ET/2$.

With some simplifying assumptions that will alter the high energy portion of the spectrum, the magnetic bremsstrahlung spectral distribution of an electron with energy E is given by:

$$I(E, \epsilon_{\gamma}, B) = \sqrt{\frac{3\alpha}{2\pi}} \left(\frac{mc}{\hbar c} \right) \left(\frac{T}{E} \right) \left(1 - \frac{\epsilon_{\gamma}}{E} \right) K(2\zeta) \quad (4)$$

where

$$\zeta = \frac{\epsilon_{\gamma}}{(E - \epsilon_{\gamma})3T} \quad (5)$$

and K 's are the incomplete Bessel function integrals that also appear in classical relativistic synchrotron radiation.

We may notice that the intrinsic rate of magnetic bremsstrahlung is measured by $mc^2/\hbar c$ which is of the order of 10^{14} eV/cm. The total energy loss rates integrated over the photon spectrum can be expressed as (Erber, 1966):

$$\frac{d\epsilon}{dx} = 6.43 \times 10^{13} g(T) \text{ eV cm}^{-1} \quad (6)$$

$$g(r) \approx \begin{cases} .556 T^{2/3} & T \gg 1 \\ T^2(1 - 5.95 T) & T \ll 1 \end{cases} \quad (7)$$

To get a feeling for this process we may notice that an electron of energy E in the $T \gg 1$ regime will lose half of its energy in a distance of $0.11 E^{1/3} (\text{eV}) H^{-2/3} (\text{gauss}) \text{ cm}$, and in doing so it will typically radiate one photon with half of its energy. The situation is reminiscent of an energetic electron radiating bremsstrahlung photons in the Coulomb field of the nucleus.

If we examine pair production by energetic photons in magnetic fields we again see the important effect of T parameter. The photon attenuation coefficient $\alpha(T)$ can be expressed as:

$$\alpha(\tau) = \frac{1}{2} \left(\frac{\alpha}{\kappa_c} \right) \left(\frac{B_{\perp}}{B_{cr}} \right) T(\tau) \quad (8)$$

where $T(\tau)$ can be approximated by:

$$T(\tau) \approx \begin{cases} 0.76 \tau^{-1/3} & \tau \gg 1 \\ 0.46 \exp\left(-\frac{8}{3\tau}\right) & \tau \ll 1 \end{cases} \quad (9)$$

The maximum of $\alpha(\tau)$ occurs at $\tau = 12$, or $\epsilon_{\gamma} = 12 mc^2 B_{cr} / B$

For a typical pulsar field of 10^{12} gauss, this maximum corresponds to 270 MeV. At this energy the pulsar magnetosphere corresponds to some 10^{11} radiation lengths of material, or the equivalent of 5×10^5 kilometers of lead! Even though the attenuation length grows exponentially as τ decreases, the pulsar magnetosphere is so "thick" that along the equatorial plane, it will cause all photons above a few MeV to pair produce before emerging out. Near the poles this threshold energy is increased by about a factor of $\csc \theta$ due to the reduction of the perpendicular component of the magnetic field, thereby allowing higher energy photons to emerge.

3. Production of Electromagnetic Cascades in Pulsar Magnetospheres. Various authors have realized the importance of the above mentioned electromagnetic processes in the pulsar magnetospheres and have invoked them to produce coherent bunches of electrons and photons to explain the microwave and optical radiation from these objects (Sturrock, 1971; Ruderman and Sutherland, 1975; Sturrock et al., 1975).

In general the complicated relationship and geometry between the rotation axis ω , the magnetic field B and the resulting E field in a pulsar differ extensively between different models. In this paper we ignore the details and assume that energetic electrons are produced near the pulsar surface and try to estimate the subsequent radiation produced by these electrons and the propagation of this radiation through the pulsar magnetosphere. In particular we would like to trace the outlines of the cascade shower process that will develop as the energetic electrons radiate photons that in turn produce electron-positron pairs.

In the electromagnetic conversion processes discussed above the relevant component of B for the radiation process is perpendicular to the direction of motion, therefore it seems important to know what the

$\vec{E} \cdot \vec{B}$ term is what accelerates the electrons. If electrons are going along field lines, they emit curvature radiation instead of magnetic bremsstrahlung. However, even electrons accelerated in a typical pulsar can lose their energy by curvature radiation to photons around 10^9 eV energy (Ruderman and Sutherland, 1975). These photons that travel in straight lines subsequently encounter the perpendicular component of B as they travel in the curved lines of force. Once they pair produce, the electron-positron pair also feels this component of B in their radiation process. Henceforth, in our discussion, as a first approximation we shall ignore the geometry of the field lines and assume that the component of B perpendicular to the direction of motion is comparable to B. We can then perturb our general conclusions for the polar region by decreasing the effective value of B.

Qualitatively we can describe the cascade in the following way: An energetic electron in $\tau \gg 1$ regime ($E \gg 20$ MeV for $H 10^{12}$ gauss) will lose half of its energy in a distance:

$$\Delta x_{1/2} \approx 10^{-6} \left(\frac{B}{10^{12}} \right)^{-2/3} \left(\frac{E}{10^9} \right)^{1/3} \text{ cm} \quad (11)$$

Where B is in gauss and E is in eV. It loses this energy by typically emitting one photon with energy $E/2$. The radiated photon, if still in the pair production regime, will create an electron-positron pair with each particle containing half of the photon's energy. For a photon of 10^9 eV energy in 10^{12} gauss field, the mean free path against pair production is about 5×10^{-6} cm. Subsequently these electrons and positrons will again radiate one-half their energy as a single photon and so forth. When the mean energy of the electron drops down to a value that corresponds to $\tau \sim 1$ ($E \sim 22$ MeV for $B \sim 10^{12}$ gauss), it starts losing its energy mostly by radiating photons of $\tau \sim 0.6$ which pair produce electron-positrons with $\tau \sim 0.3$. The next generation of photons has τ around 0.1 and they can easily break out of the surface even if this energy is greater than the pair production threshold of $2 m_e c^2$.

Effectively then the maximum of the shower occurs when the mean energy of the electromagnetic component is degraded $\tau = 0.1$ to 0.3 range. Since the photon component of the shower is attenuated at larger distances as compared to the electrons, this maximum will not be a strict spatial maximum but in the steady state implies a concentration of electrons in the above energy range that radiates photons in the corresponding energy range. The extent in height of this cascade is small compared with the distance over which B changes appreciably, hence we can treat the problem as occurring at a constant B value.

We have carried out numerical calculations of the resulting photon spectrum when we let a mono-energetic beam of electrons with

$E = 10^9$ eV pass through a uniform magnetic field of 10^{12} gauss. The results are shown in Figure 1. The ordinate gives the resulting photon spectrum in units of energy per unit photon energy interval produced by a single electron. The three different curves labeled 1, 10 and 30 reflect the spectra after the corresponding number of iterations where each iteration is a distance step of 10^{-6} cm. If we continue this iteration process and follow the photons out to large distances, the portion above 5 MeV should decrease more and the cascade photons that are produced should increase uniformly the intensity level below this energy. We could approximate the resulting photon spectra by:

$$\frac{d\epsilon}{d\epsilon_\gamma} \sim \begin{cases} \frac{E_0}{\epsilon_{cr}} & \epsilon_\gamma < \epsilon_{cr} \\ 0 & \epsilon_\gamma > \epsilon_{cr} \end{cases} \quad (12)$$

where the critical energy ϵ_{cr} is given by:

$$\epsilon_{cr} \sim 0.2 M_e c^2 \left(\frac{B_{cr}}{B_\perp} \right) \quad (13)$$

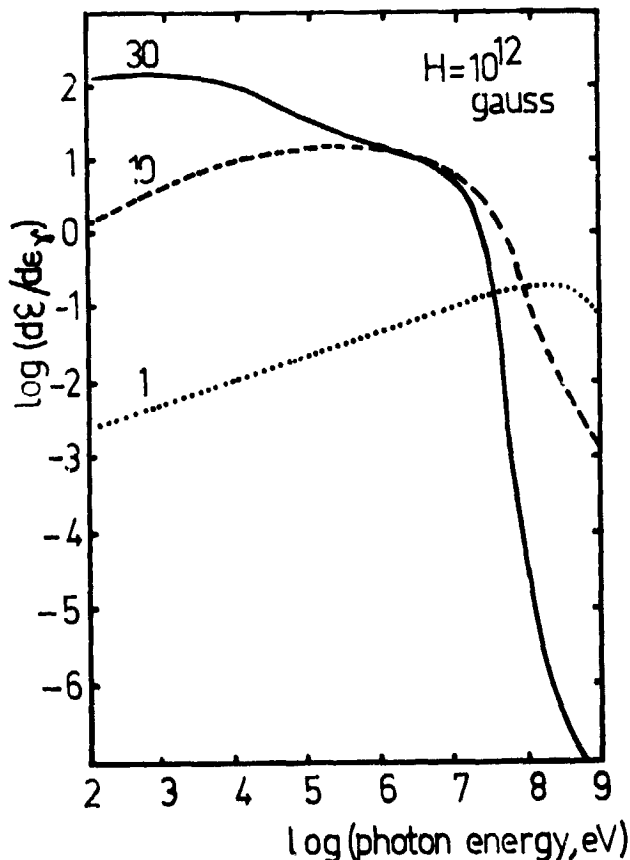


Figure 1. Numerical calculations on the photon spectrum of a shower initiated by 10^9 eV electron in a field of 10^{12} gauss. The curves labeled 1, 10 and 30 are the number of iteration steps in units of 10^{-6} cm.

4. Discussion. There are several factors that will change the idealized calculations of the previous sections. One factor is assumption of the mono-energetic electron beam. In reality there will be a spectrum of electrons accelerated by the pulsar. However, as long as this spectrum implies the existence of electrons above ϵ_{cr} , the conclusions of the previous sections do not change. The second factor is the possibility of the reacceleration of the electrons as they lose energy. A third factor is the geometry of the field lines. We can include this effect approximately by considering the fact ϵ_{cr} will increase as $\csc \theta$ where θ is the angle of propagation with respect to the poles. For example, in the case of the canonical pulsar with $B = 10^{12}$ gauss, ϵ_{cr} is about 5 MeV but within a cone of 6° from the poles. Gamma rays above 50 MeV will be able to break through the pulsar. For the case of $B = 10^{11}$ gauss, $\epsilon_{cr} \sim 50$ MeV, and 500 MeV photons can emerge from the poles within the 6° cone.

In short, gamma rays in the 10^6 to 10^9 eV region are the photons that can break out of the pulsar magnetic fields as well as being photons that correspond to the shower maximum produced by an energetic electron.

The shape of the photon spectrum implies that most of the energy will be radiated away by the gamma rays near the critical energy. Experimentally this fact is certainly supported by PSR 0833-45, PSR 1747-46 and PSR 1818-04 which radiate a factor of 3.5×10^5 , 2.2×10^5 and 3.5×10^5 more respectively in gamma rays above 35 MeV than in the radio region, the only other region an emission has been detected. In the case of the Crab nebula pulsar PSR 0532+ 21 the ratio of the gamma ray to radio luminosity is again 3.1×10^5 , however Crab pulsar shows additional emission in the optical and X-ray regions which must be explained by some other mechanism. Although the Radio luminosity itself needs other coherent emission processes, it is interesting to note that in all the observed gamma ray pulsars the ratio of gamma ray luminosity to radio luminosity is around 3×10^5 .

In conclusion, if the general results of this work are correct, pulsars radiate predominantly in the 10^6 to 10^9 eV range. Although the radio emission is only a trivial part of the energy loss, in understanding pulsars it has received an unfair share of the effort.

REFERENCES

Erber, T. 1966, Rev. Mod. Phys. 38, 626.

Kniffen, D. A., Hartman, R. C., Thompson, D. J., Bignami, G. F.,
Fichtel, C. E., Ügelman, H., and Tümer, T. 1974, Nature 251,
397.

Ügelman, H. B., Fichtel, C. E., Kniffen, D. A., and Thompson, D. J.,
1976 Ap. J. (to be published)

Ruderman, M. A. and Sutherland, P. C. 1975, Ap. J. 196, 51.

Sturrock, P. A. 1971, Ap. J. 164, 529.

Sturrock, P. A., Petrosian, V., and Turk, J. S. 1975, Ap. J. 196, 73.

Thompson, D. J., Fichtel, C. E., Kniffen, D. A., and Ügelman, H. B.
1975, Ap. J. (Letters), 200, L79.

CONTRIBUTED PAPERS

June 2, 1976 P.M.

1. 3-30 MeV Gamma Rays From the Crab, Stephen White, Physics Department, University of California, Riverside CA 92502.

Reference: 3-30 MeV Gamma Rays From the Crab, IGPP-UCR-76-7, Preprint of Institute of Geophysics and Planetary Physics, University of California, Riverside (1976)

2. Ultra High Energy Gamma Rays from the Crab Nebula, Hugh Tornabene, Bowie State College, Bowie, Maryland 20715.

No preprint is available.

3. Gamma Rays from Pulsars, Arnold Wolfendale, Physics Department, University of Durham, South Road, Durham, U.K.

Preprint: Gamma Rays From Pulsars, C. Dahanayake, D. Dodds, and A. W. Wolfendale, Physics Department, University of Durham, England

4. Geminga, Giovanni Bignami, Università di Milano, Istituto di Scienze Fisiche, Aldo Pontromeli, via Celoria 16, Milano, Italy 20133.

Reference: Search for a Correlation Between the New Satellite Galaxy and an Unidentified Gamma Ray Source, G. F. Bignami, T. Macaccaro, C. Paizis, to be published in Astron. and Astrophys.

5. Search for Nuclear Gamma Ray Lines from Nova Cigni, Marvin Leventhal, Bell Telephone Labs., Murray Hill, N. J. 07974

Reference: D. D. Clayton and F. Hoyle, Astrophysical Journal (Letters) 187, L101-L103, Feb. 1, 1974.

6. OSO-7 Hard X-Ray Observations of Diffuse Galactic X-Ray Emission, William Wheaton, Center for Space Research, M.I.T., Cambridge, Mass. 02139

Reference: William A. Wheaton, Thesis UCSD, 1976.

7. Preliminary Results on Background Gamma Ray Lines Observed at Balloon Altitudes, A. S. Jacobson, J. C. Ling, W. A. Mahoney and J. B. Willett, 183-901 Jet Propulsion Laboratory, California Inst. of Technology, Pasadena, CA 91103.

Reference: Measurement of the Terrestrial and Extraterrestrial 0.511 MeV Gamma Rays With a High Energy Resolution Instrument at Balloon Altitude over Palestine Texas, J. C. Ling, W. A. Mahoney, J. B. Willett, and A. S. Jacobson, to be submitted to the J. Geophys. Res. 1976.

N 76 - 291 21

"DENSITY WAVE THEORY"

WILLIAM W. ROBERTS, JR., Department of Applied Mathematics And Computer Science, University of Virginia, Charlottesville, Virginia 22901

ABSTRACT

The prospect that density waves and galactic shock waves are present on the large-scale in disk-shaped galaxies has received support in recent years from both theoretical and observational studies. Large-scale galactic shock waves in the interstellar gas are suggested to play an important governing role in star formation, molecule formation, and the degree of development of spiral structure. Through the dynamics of the interstellar gas and the galactic shock wave phenomenon, a new insight into the physical basis underlying the morphological classification system of galaxies is suggested.

INTRODUCTION

In this symposium a primary focus is the structure, content, and dynamics of our Galaxy as revealed by various galactic constituents and tracers - HI, CO, OH, H₂, young stars, HII regions, supernova remnants, pulsars, γ - radiation, synchrotron radiation, and others. Some of these constituents help to make up the overall gaseous component of our Galaxy, while others have their formation and large-scale distribution directly related to the large-scale dynamics of the gaseous component. In this review on Density Wave Theory strong emphasis will therefore be directed toward the gaseous component and the important role it can play. Our Galaxy is thought not to be greatly different from external spiral galaxies we see; and this review will focus from time to time on external spirals to help us theoretically view our own Galaxy.

In many external galaxies the optical appearance of the disk reveals the presence of luminous spiral arms. If the spiral arms were material arms and were composed of the same material for a substantial portion of the lifetime of the galaxy, the differential rotation inherent in the disk would tend to overwind the arms into nearly circular forms instead of the spirals observed. Partly because of this winding dilemma associated with material arms, a wave interpretation of large-scale spiral structure seems necessary. In the wave interpretation the enhanced luminosity of a spiral arm is believed to originate in the very young, newly formed stars whose births from interstellar clouds have been triggered by the passage of the crest of a spiral density wave.

STELLAR DENSITY WAVES

The density wave viewpoint originated with Bertil Lindblad (1963; also see Lindblad and Langebartel, 1953) and has been developed toward a coherent density wave theory by C.C. Lin and his associates and others (see Lin, 1971). Gravitational forces are considered as dominant forces, with magnetic forces also playing a role but of secondary importance. The fundamental spatial coherence of the wave pattern is provided by the orderly underlying spiral gravitational field of the collective distribution of old to moderately-old disk stars participating in the wave pattern. Lin and Shu (1964, 1966) find that this self gravitation of the material participating in the wave-pattern can

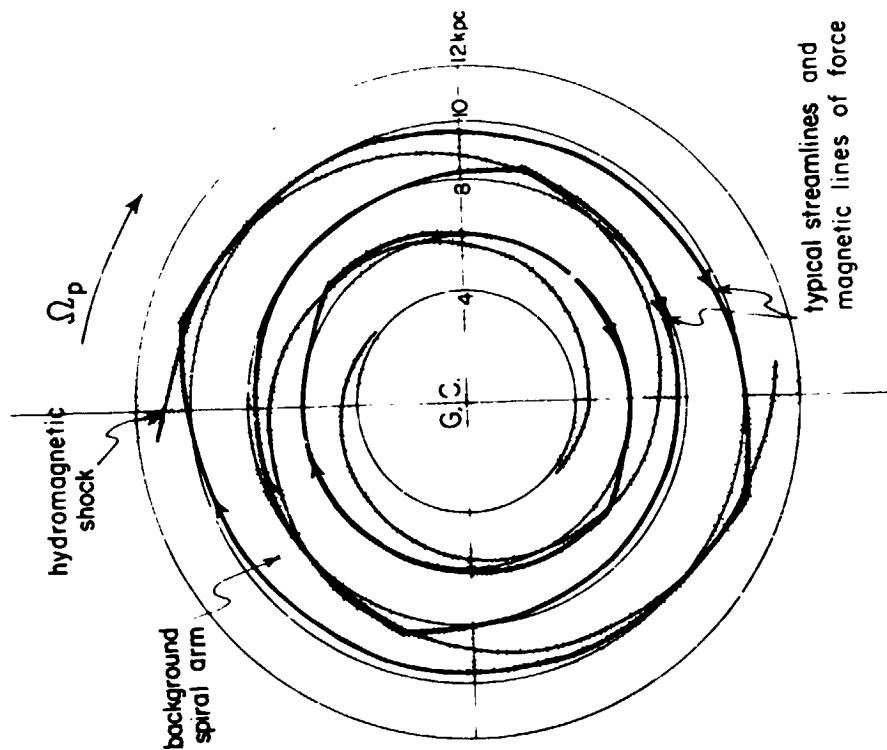


Figure 2. Sketch of the background spiral pattern and the gas response in the density wave model. A shock forms in the background spiral arm. Each gas streamline appears as a sharp-pointed oval with a sharp turning point at each shock (from Roberts, 1969).

Figure 1. Photographic simulation of a background stellar density wave pattern of 5% amplitude. (Kindly prepared by Mr. James M. Huntley)

go a long way toward helping to sustain it. On the other hand Toomre (1969) shows that a group of spiral waves would still propagate in the radial direction and eventually disappear in several rotations of the galaxy. Thus one of the intriguing problems at the present time is how to account for the origin and permanence of spiral structure. Fortunately this problem is receiving the attention of a number of researchers at the present time, and a variety of promising sources have already been found for the generation of spiral structure (see Lin, 1970; Toomre and Toomre, 1972; Lynden-Bell and Kalnajs, 1972; van der Kruit et. al., 1972; Feldman and Lin, 1973; Mark, 1974, 1976 a,b,c,d,; Lin and Lau, 1975; and Lau, Lin, and Mark, 1976).

The mass concentration in a density wave is believed to constitute only a small perturbation on an otherwise rather smooth stellar disk. For this reason the theory for stellar density waves has evolved primarily as a small amplitude linear theory. Figure 1 provides a photographic simulation of a stellar density wave of 5% amplitude superposed on a stellar disk whose axisymmetric distribution is computed from the mass model of Vandervoort (1970) for our Galaxy. Here the resulting background wave pattern of old to moderately-old stars is hardly visible and such background patterns would most certainly be difficult to detect in real galaxies.

GALACTIC SHOCK WAVES

On the other hand, the response of the interstellar gas to the small background spiral gravitational field associated with such stellar density wave pattern is in fact found to be a rather large response in which shock waves form along the arms of the background pattern (Roberts 1969, also see Fujimoto 1966). Figure 2 illustrates the location of the shock formed along the background arms. Undergoing rapid basic rotation about the galactic center, the gas flows along the arrowed streamlines through the slower rotating wave pattern from one shock to the next. It is mainly the spiral gravitational field of the background pattern coupled with rotation along with the effect of pressure and the variation in streamtube cross section that drives the gaseous response and forms the shock. The galactic magnetic field and the cosmic ray particles which interact with the magnetic field also constrain the gas motion. In the model here, a galactic magnetic field is embedded in the gas (Roberts and Yuan, 1970), and the shock that forms is a hydromagnetic shock wave. Because of the enormous size of the galaxy, the magnetic field is essentially "frozen into" the gas, and the arrowed streamlines represent the gas streamlines as well as the magnetic lines of force.

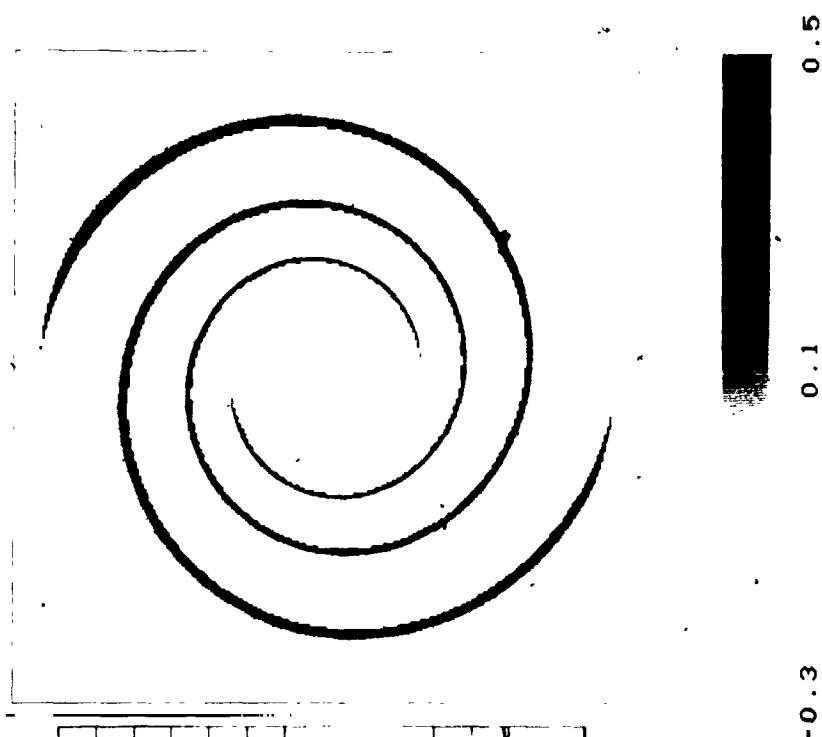


Figure 3. Gas density distribution along a typical streamlane in the density wave model. The potential minimum corresponds to the center of the background spiral arm. Allowing a typical time of 30 million years for the formation and evolution of the relatively massive stars, the region of newly-born stars and H II regions lies just outside the shock and sharp H I peak (from Roberts, 1969).

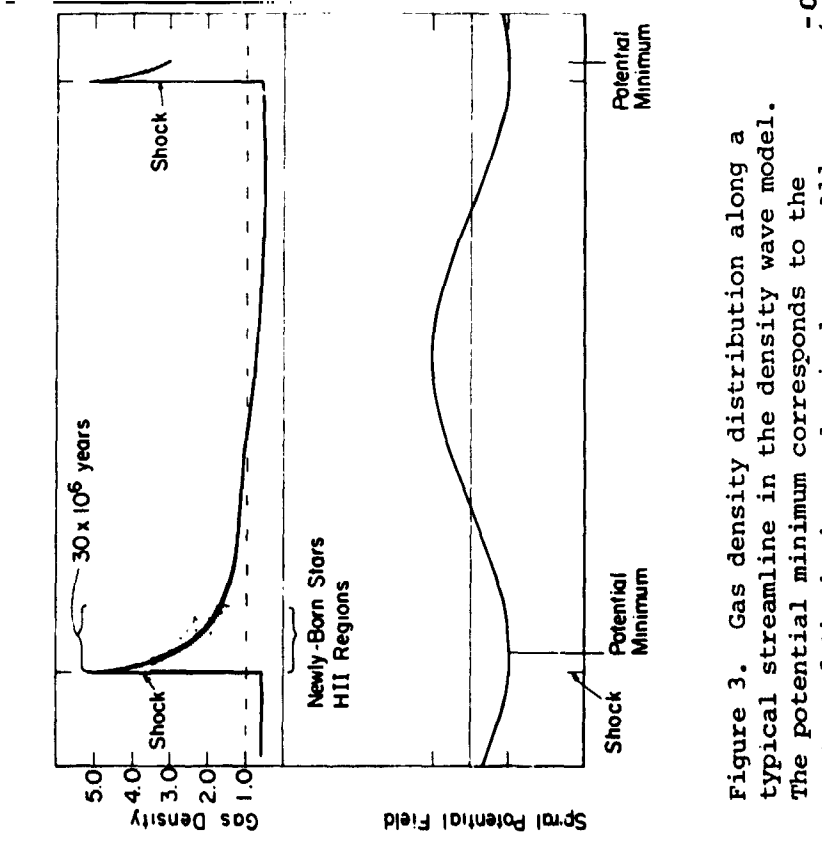


Figure 4. Photographic simulation of the gas density distribution with the formation of a galactic shock wave in the density wave model (from Roberts, 1969). (Kindly prepared by Mr. James M. Huntley)

Figure 3 provides a sketch of the nonlinear response of the gas density distribution along a streamline. The gaseous response has a rather narrow peak induced by the shock wave which forms in the potential well of the background stellar density wave arm. A photographic simulation of the gas density distribution over the face of the model disk is provided in Figure 4. The ridge of the light distribution traces out the shock and the gas density ridge. The surface density response of a particular component in a galaxy is roughly proportional to the inverse square of the characteristic speed. Since the effective acoustic speed of the interstellar gas is typically only one-third to one-fourth of the root mean square random velocity of the disk stars, it is not difficult to see how the same mild spiral gravitational field which induces only a small fractional variation of the disk stars (Figure 1) can drive a very large density response in the interstellar gas toward the formation of shock waves (Figure 4).

The formation of such large amplitude spiral waves in the gas is not greatly sensitive to the form of the background forcing field adopted to drive the gas. For example, in a time dependent study of the gas response to a bar-like oval distortion, Sanders and Huntley (1976) find a large amplitude wave pattern of a rather similar character to that in Figures 2-4, but with rather open spiral arms. Figure 5 shows a photographic simulation of the gas density distribution in two different cases of mild bar-like forcing.

GAS CLOUD COLLAPSE AND STAR FORMATION

Galactic shock waves may well form a possible triggering mechanism for the gravitational collapse of gas clouds, leading to star formation and the formation of other tracers along spiral arms. Figure 3 illustrates this possible star formation mechanism. Gas flows into this shock and compression region from left to right. Before reaching the shock, some of the large clouds and cloud complexes may be on the verge of gravitational collapse. A sudden compression of the clouds in the shock could conceivably trigger the gravitational collapse of some of the largest gas clouds. As the gas leaves the shock region, it is rather quickly decompressed, and star formation ceases.

On the small scale the main obstacle to star formation is that most of the interstellar gas clouds would not be even remotely bound by their self gravitation if the clouds were isolated entities placed in a vacuum. Random motion can act as a "pressure" in that it provides support against the gravitational field of the Galaxy; however, there are difficulties in visualizing how the "effective pressure" is transmitted on a small scale to trigger the gravitational collapse of clouds. This

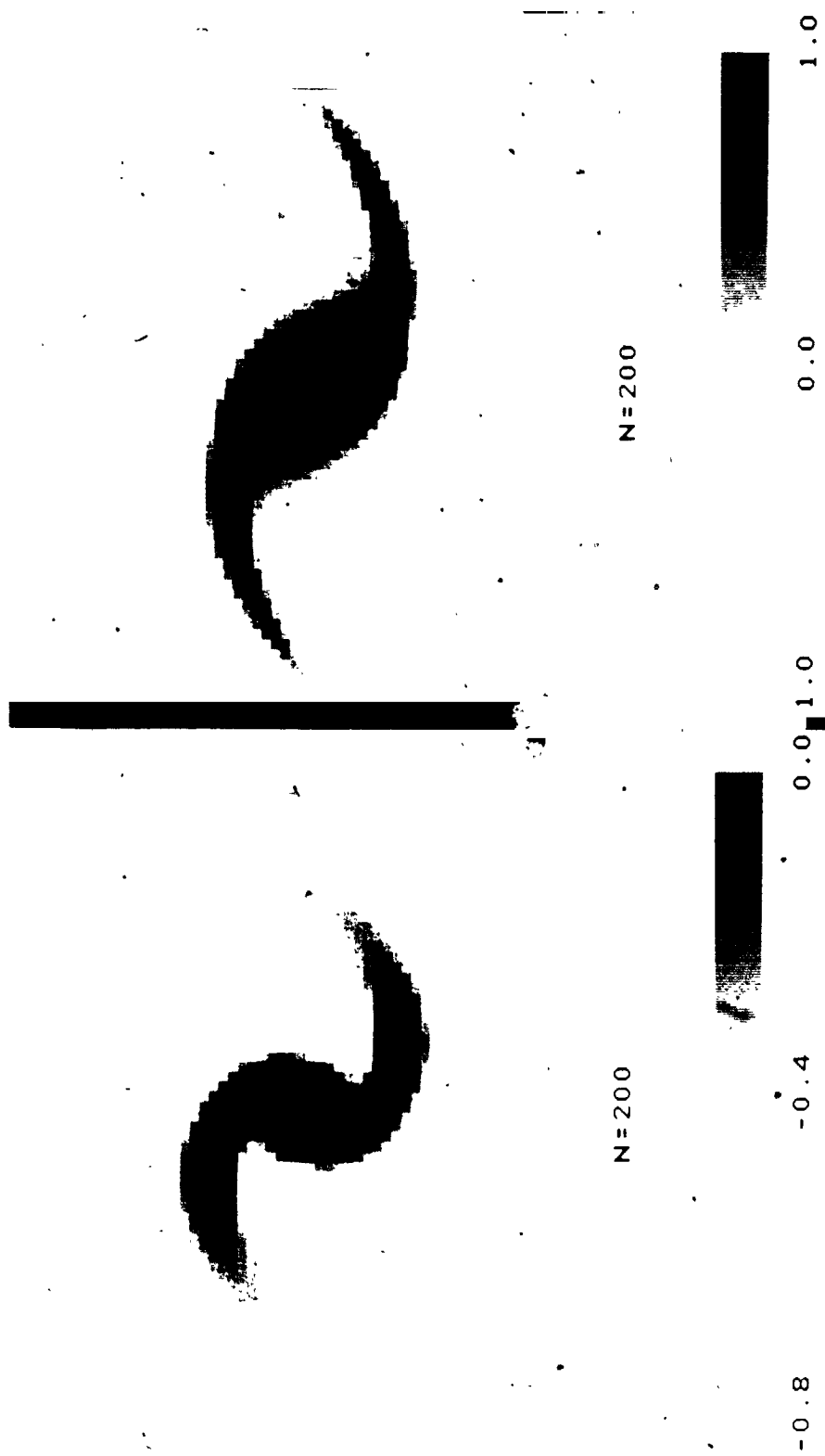


Figure 5a.

Figure 5b.

Photographic simulation of the gas density distribution in response to a mild bar-like oval distortion. Figure 5a. Inner and outer Lindblad resonance and corotation are contained within the model gaseous disk. Figure 5b. Only inner Lindblad resonance is contained within the gaseous disk (from Sanders and Huntley, 1976).

obstacle is now largely removed through recent work by a number of researchers who show that the nearly neutral component of the interstellar medium may consist of two gaseous phases in rough pressure equilibrium with one another. These two phases are identified with the observed cold, dense clouds at temperatures of 20 -200°K and with an unobserved hot, rarefied intercloud medium at temperatures of perhaps 10⁴°K.

In a study of gas flow based on the two-phase concept (Shu, et al., 1972) galactic shocks are found to be initiated by the "hot" intercloud medium. For the case of 5% spiral field it is found that the total variation of pressure along a streamline at the solar circle exceeds the range of pressures consistent with the thermal stability of both cloud and intercloud phases, and phase transitions occur in the flow. Inside the shock layer, the transient pressure tends to achieve a value higher than the maximum pressure, p_{\max} , consistent with thermal stability of the intercloud medium and this forces a transition of some of the "hot" intercloud gas into the "cold" cloud phase. On the other hand, in the interarm region the pressure tends to drop to a value lower than the minimum pressure, p_{\min} , consistent with thermal stability of the cloud medium, and this forces a reverse transition of some of the "cold" cloud gas into the "hot" intercloud phase. As the pressure tends to drop below p_{\min} in the interarm region, the evaporation of cloud material to the intercloud phase helps to maintain a constant pressure environment for the remaining clouds.

In this picture, the clouds are viewed as embedded bodies which expand or contract to adjust to changes of the ambient pressure of the intercloud medium; and the increase in pressure across the galactic shock occurring in the "hot" intercloud phase is in turn transmitted to the "cold" clouds, leading to star formation. Due to the greater compressibility of the gas in the two phase model and the nonlinear nature of self gravity, the critical mass for the gravitational collapse of a gas cloud is substantially reduced from that estimated for an isothermal gas by a factor greater than 10. This decrease of the threshold for gravitational collapse coupled with the effect of the galactic shock as a possible triggering mechanism help to explain why the regions of active star formation can be delineated so sharply in certain external galaxies.

In a study of the time scales relevant to cloud formation and star formation Biermann, et al. (1972) follow the phase transition process by a simple numerical model of thermal evolution in cases for different strengths of compression and magnetic field, and for different rates of heavy element depletion onto grains (also see Mufson, 1974, 1975). Through this work they reconfirm that the transition to the cool stable cloud phase may occur within 10⁶ years and that stars may form within approximately 5 x 10⁶ years in agreement with the time estimates for M 51 by Mathewson, et. al. (1972) and for M 81 by Rots (1975).

Woodward (1976) further enhances the theoretical picture through studies of shock-driven implosions of interstellar clouds toward star formation (also see Sawa 1975). Shu (1974) considers the Parker (magnetic Rayleigh-Taylor) instability for an interstellar medium composed of thermal gas, magnetic field, and cosmic ray particles and investigates the tendency of the gas to drain down magnetic field lines into dense pockets of concentration. Mouschovias, Shu, and Woodward (1974) suggest further that the initiation of this instability in the interstellar medium by the passage of a galactic shock may play a strong role in the formation of large cloud complexes, OB associations, and giant H II regions.

STRONG SHOCKS WITH NARROW REGIONS OF HIGH GAS COMPRESSION;
WEAK SHOCKS WITH BROAD REGIONS OF LOW GAS COMPRESSION

For a wave of given amplitude, the strength of the shock and the degree of compression of the gas vary as the square of the ratio w_{\perp}/a where w_{\perp} is the total (unperturbed plus perturbed) velocity component of the gas normal to a spiral arm and a is the effective acoustic speed of the interstellar gas. If the two-component model of the interstellar medium is adopted, a is unlikely to be very different from the sound speed associated with the intercloud medium $\sim 7 - 12 \text{ km s}^{-1}$ and a mean value of a in this range might be dictated by the atomic physics of all spiral galaxies. On the other hand, w_{\perp} oscillates along a streamline about its unperturbed value $w_{\perp 0}$ because of the forcing of the spiral gravitational field of fractional amplitude F . Shocks form if F is sufficiently large as to force w_{\perp} to achieve transonic values. There are actually two regimes: (1) $w_{\perp 0} > a$ and (2) $w_{\perp 0} < a$. For (1) $w_{\perp 0} > a$, most of the gas on the streamline is moving at supersonic speeds while only a small portion is moving subsonically. The shocks which form in this ($w_{\perp 0} > a$) situation tend to be strong and give rise to narrow regions of high gas compression. For regime (2) $w_{\perp 0} < a$, most of the gas on the streamline is moving subsonically while only a small portion travels supersonically. In this ($w_{\perp 0} < a$) situation the shocks tend to be weak and yield rather broad regions of relatively low gas compression (see Shu, et. al., 1973). Therefore the strength of the shock and compression of the gas and the consequent theoretical differentiation between spiral structure with narrow "filamentary" arms and broad "massive" arms seem to be critically dependent on the quantity

$$w_{\perp 0} = (\Omega - \frac{\Omega}{p}) \tilde{\omega} \cdot \sin i \quad (1)$$

where i is the pitch angle of the wave pattern which is determinable from the dispersion relation of the linear density wave theory once the



Figure 7. Photograph of the sample galaxy NGC 3031 (M81) taken from the Hubble Atlas. The well-developed "filamentary" spiral arms are thought to be a consequence of the strong shocks possible in this galaxy (from Roberts, et. al., 1975).

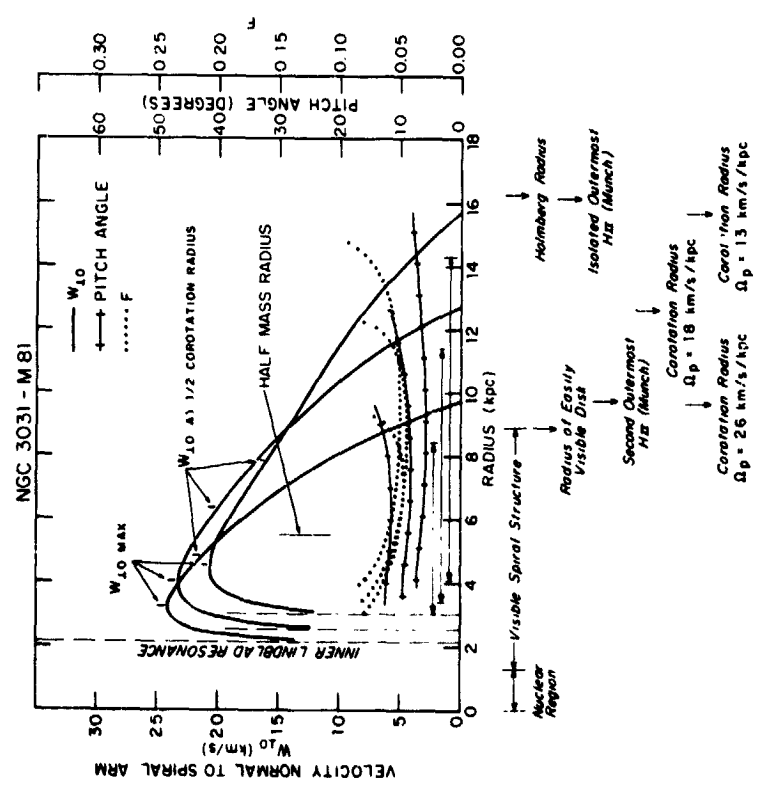


Figure 6. Characteristics of the density wave model for the sample galaxy NGC 3031 (M81). w_{10} , i , and F are sketched for each of three choices of the corotation radius. Since w_{10} is so large, potentially strong shocks and correspondingly well-developed spiral arms are possible (from Roberts, et. al., 1975).

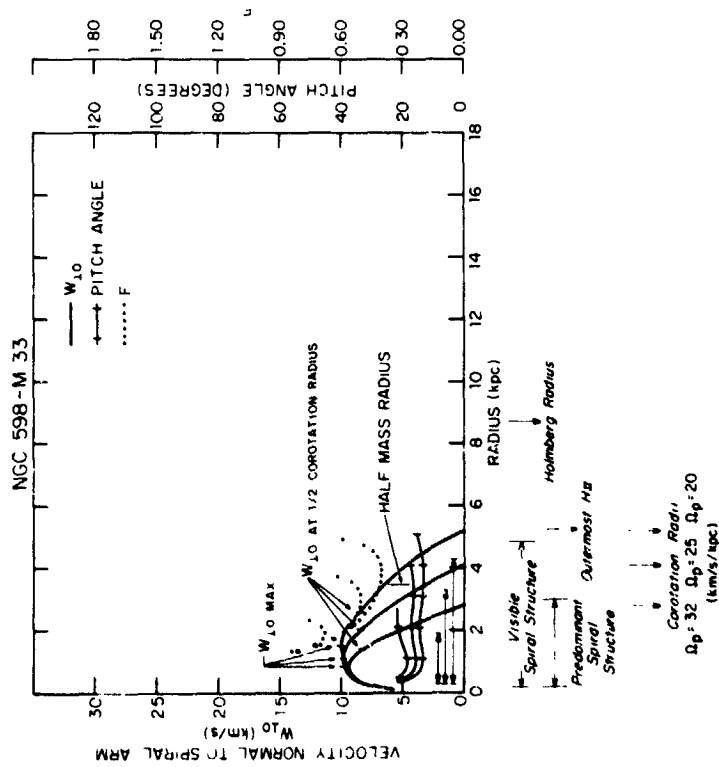
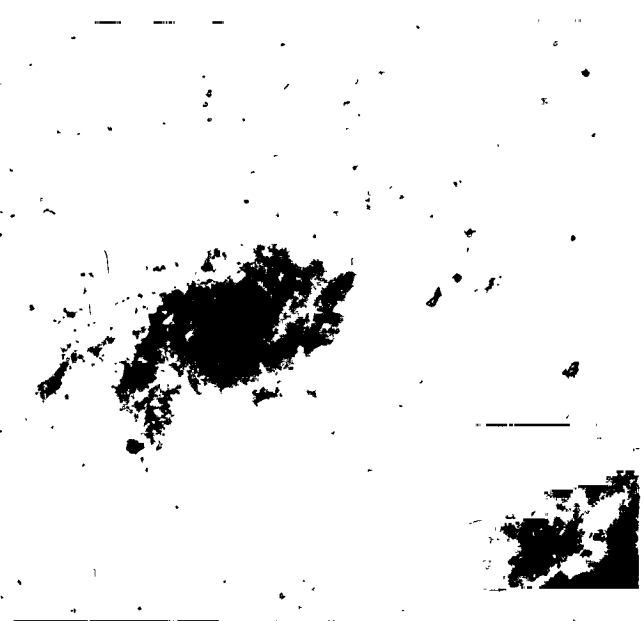


Figure 8. Characteristics of the density wave model for the sample galaxy NGC 598 (M33). w_{10} , i , and F are sketched for each of three choices of the corotation radius. Since w_{10} is so small, only weak shocks, if any at all, could exist (from Roberts, et. al., 1975).

Figure 9. Photograph of the sample galaxy NGC 598 (M33) taken from the Hubble Atlas. The poorly-developed spiral structure is thought to be a consequence of the result that only weak shocks, if any at all, are possible in this galaxy (from Roberts, et. al., 1975).



pattern speed, Ω_p , is specified.

INSIGHT INTO THE PHYSICAL BASIS UNDERLYING THE MORPHOLOGICAL CLASSIFICATION SYSTEM OF GALAXIES

A semiempirical study of the density wave patterns predicted in the models of twenty-four external galaxies is made by Roberts, Roberts, and Shu (1974, 1975; also see Shu, Stachnik, and Vost, 1971). Figure 6 provides the theoretical curves of $w_{\perp 0}$, i , and F characterizing the density wave pattern calculated for one sample galaxy NGC3031 (M81). The superposition of three sets of curves for three possible choices of the corotation radius illustrates that the magnitude of $w_{\perp 0}$ over its extent, and particularly at half corotation, is not overly sensitive to the location of corotation. For NGC3031 the characteristically high levels reached by $w_{\perp 0}$ signify that potentially strong galactic shocks are possible together with a high degree of development of spiral structure with narrow "filamentary" arms.

A photograph of the sample galaxy, NGC3031 (M81), with its typically "filamentary" spiral arms taken from the Hubble Atlas (Sandage 1961) is shown in Figure 7. This well-developed spiral structure with narrow, "filamentary" spiral arms is thought to be a consequence of the rather strong shocks possible in this galaxy. Superposed is the computed wave pattern, based on the curve of theoretical pitch angle i for $\Omega_p = 26$ km/s/kpc in Figure 6.

The theoretical curves of $w_{\perp 0}$, i , and F for another sample galaxy NGC 598 (M33) are provided in Figure 8. The characteristically low levels of $w_{\perp 0}$ signify that only weak shocks, if any at all, would be possible. Consequently the corresponding spiral structure would be expected to be poorly-developed, perhaps with broad "massive" spiral arms of a fuzzy and patchy nature.

A photograph of the sample galaxy, NGC598(M33), with its characteristically "massive" spiral arms taken from the Hubble Atlas is shown in Figure 9. This poorly-developed spiral structure with rather broad, "massive" spiral arms is thought to be a consequence of the result that only very weak shocks, if any at all, are possible in this galaxy. Superposed is the computed wave pattern, based on the curve of theoretical pitch angle i for $\Omega_p = 32$ km/s/kpc in figure 8.

The results for the two sample galaxies in Figures 6-9 suggest that the two parameters $w_{\perp 0}$ and i may play a major role in determining the degree of development of spiral structure in a galaxy as well as its Hubble type. This role is illustrated in Figures 10 and 11

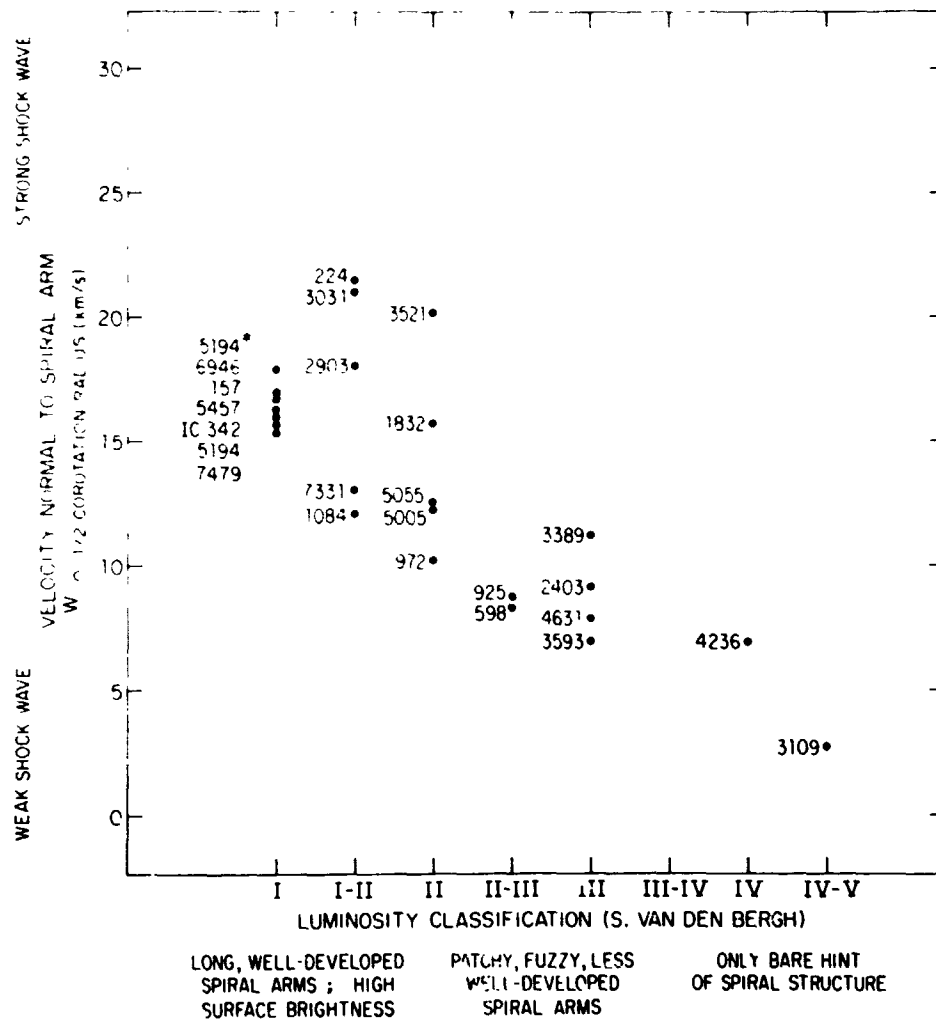


Figure 10. w_{10} and Luminosity Class. Trend for a sample of twenty-four external galaxies indicative of a possible correlation between w_{10} - the velocity component of basic rotation normal to a spiral arm - and shock strength on the one hand, and luminosity classification and degree of development of spiral structure on the other. Those galaxies, in which potentially strong shock waves are possible, are found to exhibit long, well-developed spiral arms. Those galaxies, in which weak shock waves are predicted, are found to exhibit poorly-developed spiral structure (from Roberts, et. al., 1975).

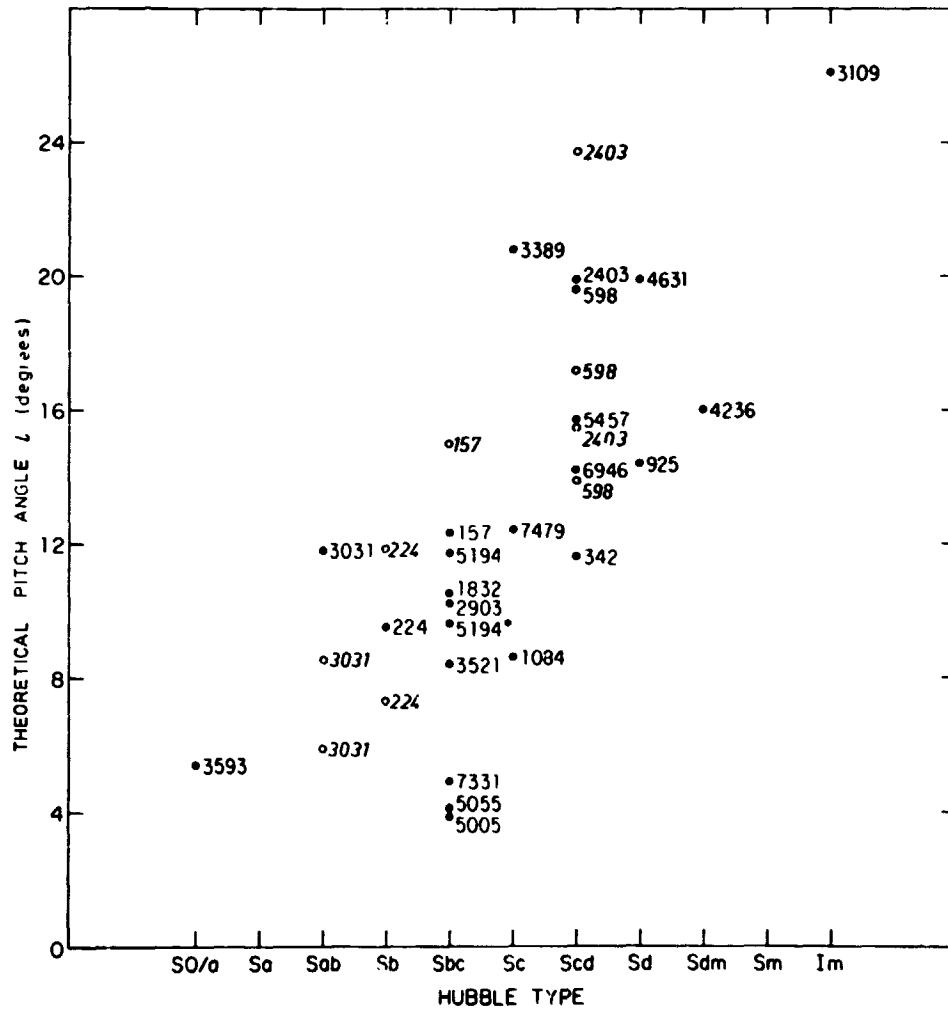


Figure 11. Theoretical Pitch Angle i and Hubble Type. Those galaxies whose models predict wave patterns with very tightly-wound spiral arms of small pitch angle i are the galaxies observed to be of relatively early Hubble type SO/a - Sbc. Those galaxies whose models predict more open and loosely-wound spiral arms with large pitch angle i are the galaxies observed to be of relatively late Hubble type Sc - Im (from Roberts, et. al., 1975).

where, for the computed density wave patterns in the theoretical models of twenty-four external galaxies, $w_{\perp 0}$ (and potential shock strength) and the theoretical pitch angle of the wave pattern are well correlated with luminosity class and Hubble type respectively. In Figure 10, high $w_{\perp 0}$ and potentially strong shocks with narrow regions of high gas compression are found to correspond to galaxies with long well-developed "filamentary" spiral arms; low $w_{\perp 0}$ and weak shocks with broad regions of relatively low gas compression are associated with galaxies with short, patchy "massive" spiral arms. In Figure 11, the computed wave patterns with small theoretical pitch angle i correspond to relatively early Hubble types, SO/a - Sbc; whereas the wave patterns with large theoretical pitch angle i correspond to relatively late Hubble types, Sc - Im. Since the theoretical pitch angle i is dependent on the choice of corotation radius in a galaxy, the correlation in Figure 11 is equivalent to saying that the theoretical wave pattern obtained by choosing the corotation radius according to the criteria in Roberts, et. al. (1975) agrees reasonably well with the observed spiral pattern for each galaxy in the sample.

Through the correlations in Figures 10 and 11, a new insight is suggested into the physical basis for the morphological classification system of galaxies. By showing that typical values of $w_{\perp 0}$ and i (say at half the corotation radius) can be expressed as:

$$w_{\perp 0} = (GM/\tilde{\omega}_c)^{1/2} f(\tilde{\omega}_{.5M}/\tilde{\omega}_c) \quad (2)$$

$$\sin i = g(\tilde{\omega}_{.5M}/\tilde{\omega}_c) \quad (3)$$

where f and g are functions whose forms are specified once the equilibrium disk has been specified except for scale factors, Roberts, et. al. (1975) identify what they believe to be the two fundamental physical parameters which underlie the accepted type-luminosity classification system of galaxies (van den Bergh, 1960 a, b): namely, (1) the total mass of the galaxy, divided by a characteristic dimension, $GM/\tilde{\omega}_c$, and (2) the concentration of mass toward the galactic center, $\tilde{\omega}_{.5M}/\tilde{\omega}_c$. These two fundamental parameters govern $w_{\perp 0}$ and the potential strength of galactic shocks in the interstellar gas as well as the geometry of the spiral wave pattern.

Figure 12 shows for example the dependence of $w_{\perp 0}$ and the potential shock strength on these two fundamental parameters. The black dots indicate the locations of the twenty-four galaxies of the sample plus our own Galaxy with respect to the $w_{\perp 0}$ surface. A galaxy with a mass distribution of moderate central concentration, as evidenced by the parameter $\tilde{\omega}_{.5M}/\tilde{\omega}_c$ being near the value of 0.5, is found to lie near the ridge of the $w_{\perp 0}$ surface. Such a galaxy is capable of forming rather strong shock waves (even with small to moderate forcing F) and is therefore capable of exhibiting well-developed "filamentary" spiral

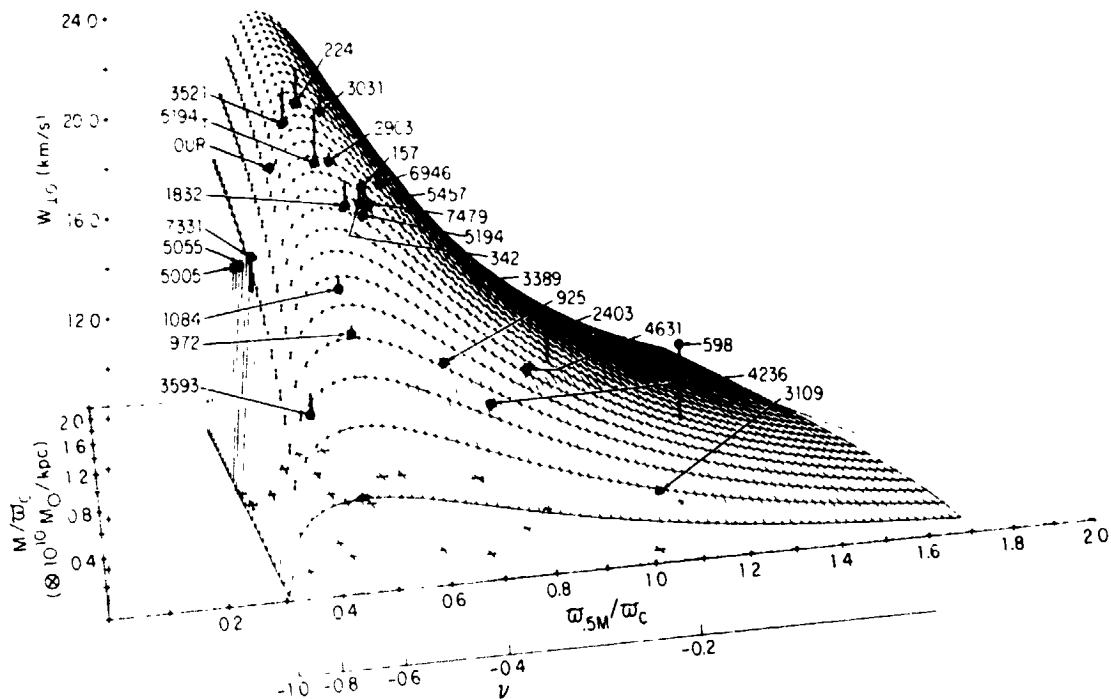


Figure 12. Theoretical categorization of disk-spiral galaxies; a representation of an ensemble of cases spanning a two-dimensional parameter space of the two fundamental parameters: $M/\tilde{\omega}_c$, $\tilde{\omega}_{5M}/\tilde{\omega}_c$. w_{10} evaluated at half corotation generates a w_{10} surface which measures the strength of the galactic shock possible over all cases of the ensemble. Superposed are twenty-four external galaxies plus our own. Those galaxies with a moderate concentration of central mass lie near the ridge of the w_{10} surface; these galaxies can have the strongest shocks (e.g. NGC3031-M81). Those galaxies with a low central mass concentration lie well below the ridge and are predicted to have only weak shocks, if any at all (e.g. NGC598-M33) (from Roberts, et. al., 1975).

structure. The larger the mass of the galaxy, the higher along the ridge it can manifest itself, and the stronger the shocks possible. On the other hand, a galaxy with a mass distribution of very low central concentration, as evidenced by the parameter, $\tilde{\omega}_{5M}/\tilde{\omega}_c$, being substantially larger than 0.5, would lie along the surface at a level well below the ridge. A galaxy in this range is capable of forming only weak

shocks, if any at all (even with large forcing F); and the corresponding spiral structure is expected to be poorly-developed and more "massive." The three coordinates in this representation are ideal in the sense that they are distance independent parameters, and any uncertainty that may be present in the estimate of distance of a galaxy does not enter here.

Some attention should be directed to the forcing amplitude F which in the density wave theory measures the amplitude of the background stellar density wave driving the gas. In those galaxies with high levels of w_{+0} , the potentially strong shocks and high gas compressions can be attained even for rather small (e.g. 5%) to moderate forcing amplitudes F . The larger F is, the stronger the shocks and gas compressions which can be attained. However with zero or negligible forcing, such potentially strong shocks and compressions could not be realized even for galaxies with high levels of w_{+0} . Unfortunately within the present framework of the theory the amplitude of the background driving wave F can be calculated only to within an arbitrary multiplicative scale factor. Of course, the real forcing of the gas in galaxies could be much more complex and even more difficult to calculate if various other driving and excitation mechanisms should enter to help drive the gas.

Empirical estimates of mean compression strengths reached in the spiral arms of eleven of the galaxies in the above sample are inferred observationally by van der Kruit (1973) from high spatial resolution 21 - cm continuum studies with the Westerbork Radio Synthesis Telescope. What is indeed interesting is that F and other possible complexities do not seem to play an overwhelming role because a comparison of the w_{+0} levels in Figures 10 and 12 with van der Kruit's mean compression strengths shows general agreement. Through observations of emission line strengths in the disks of 12 late-type galaxies, Jensen Strom and Strom (1976) find that radial changes in disk gas composition across the face of a galaxy can largely be understood in terms of this density wave picture and can be directly related to variations in the strength of the gas compression (and w_{+0}) and the frequency of compression with each passage through a spiral wave crest $2(\Omega - \Omega_p)$.

INTERNAL STRUCTURE AND TEMPORAL SEQUENCE ACROSS A SPIRAL ARM

In Figure 12 our Galaxy is located near the ridge of the w_{+0} surface. Unfortunately, from our vantage point within the Milky Way System, it is extremely difficult to view clearly and decipher the large scale structure of our own Galaxy. Consequently before focusing on our Galaxy it might be instructive to view in some depth one or two

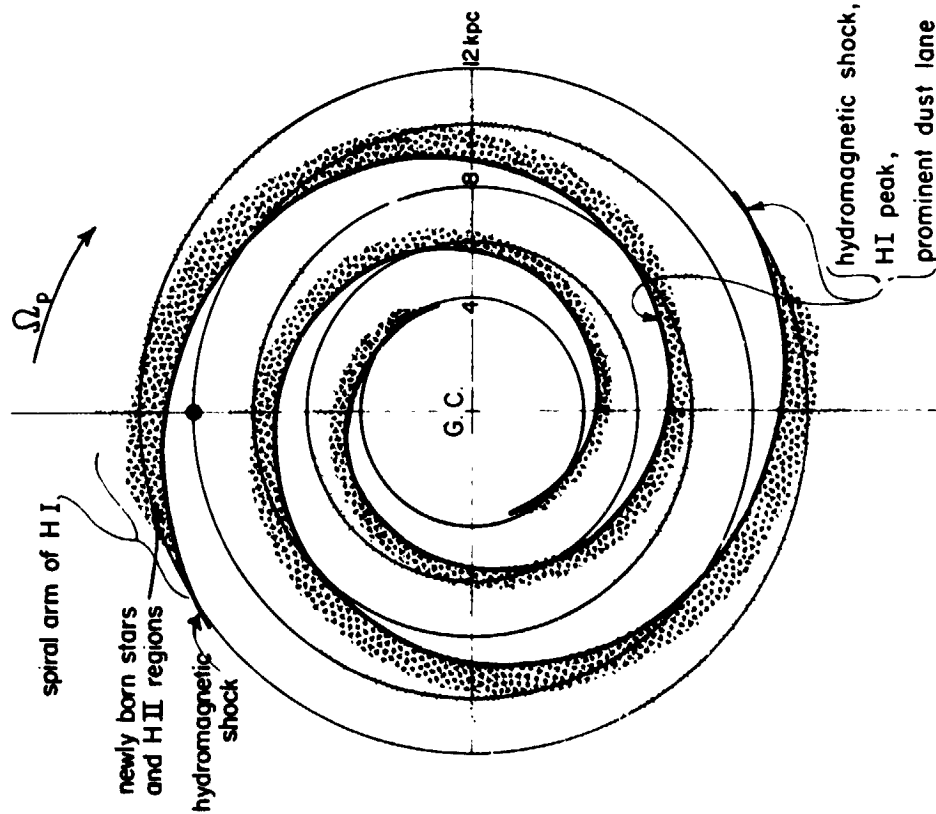


Figure 13. Internal Structure and Temporal Sequence across a Spiral Arm triggered by the formation of a strong shock wave in the density wave picture (from Roberts, 1969; and Roberts and Yuan, 1970).



Figure 14. Photographic simulation of the lane of newly-formed stars just outside the trailing spiral shock wave (from Roberts, 1969; and Roberts and Yuan, 1970). (Kindly prepared by Mr. James M. Huntley)

external spirals which are located on the w_{10} surface near our own Galaxy in Figure 12 and for which detailed observational studies are available.

One important feature to focus on is the predicted internal structure of a spiral arm. This is illustrated by the sketch in Figure 13. With the formation of a galactic shock, the gas density peaks along a narrow front, and the magnetic field frozen into the gas, and possibly the dust particles as well, share in this compression. Therefore, a shock, a sharp H I peak, a narrow dust lane, and the strongest magnetic fields are all expected to lie in a narrow lane on the inside edge of the bright optical arm of young stars and H II regions triggered by the shock. Figure 14 provides a photographic simulation of the lane of young stars distributed in a Poisson distribution outside the shock. To be sure complexities most certainly arise from a number of sources ranging from local processes within the shock region governing the interaction of clouds with the intercloud medium, e.g. through turbulent viscosity (Sawa, 1975) and governing the post-triggered collapse of gas clouds (Woodward, 1976) to the effects of spiral arm drift and age dependent spreading of the newly-formed stars (Biermann and Tinsley, 1974; and Wielen, 1975). Therefore Figures 13 and 14 are meant to provide only a qualitative overview of the temporal sequence of physical phenomena expected in the density wave theory across a spiral arm in the region interior to corotation.

THE SAMPLE GALAXY NGC 5194 (M 51) - OBSERVATIONAL STUDIES

Recent observational results from the Westerbork telescope in the Netherlands indicate that NGC5194 (M 51) - a galaxy located on the w_{10} surface near our own Galaxy in Figure 12 - is one striking example which exhibits features suggested in this wave picture. Figure 15a shows a map of M51 and its companion NGC5195 presented as a series of intensity profiles from the survey at 1415 MHz by Mathewson, et. al. (1972). The most striking feature of the radio map is the clear delineation of two radio spiral arms. Most of the spiral arm emission does not arise in supernova remnants that lie in the bright optical arms, but rather more than half of the total emission of M 51 is contained in the narrow radio spiral arms. The inner portions of the radio arms are unresolved by the aerial beam and this implies that they are less than 250 pc in width. Linear polarization is detected in their emission which indicates that their origin is due to the synchrotron mechanism. Connected with this phenomenon of synchrotron emission is the strong dependence of the radio emissivity on the strength of the magnetic field which in the density wave theory is predicted to be strongest in the compression region at the shock and dust lane.

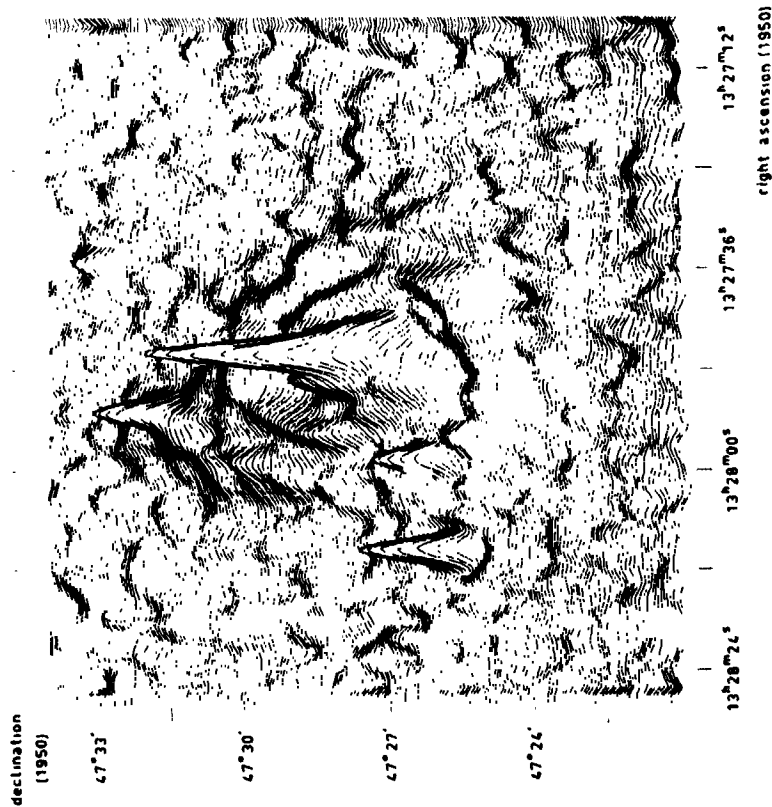


Figure 15a.

Figure 15a. Map of the 1415 MHz emission in M 51 presented as a series of intensity profiles. Two rather striking radio spiral arms stand out. Figure 15b. The ridge of the radio spiral arms in synchrotron emission lies well along the dust lanes generally on the inner sides of the optical spiral arms (from Mathewson, et. al., 1972).

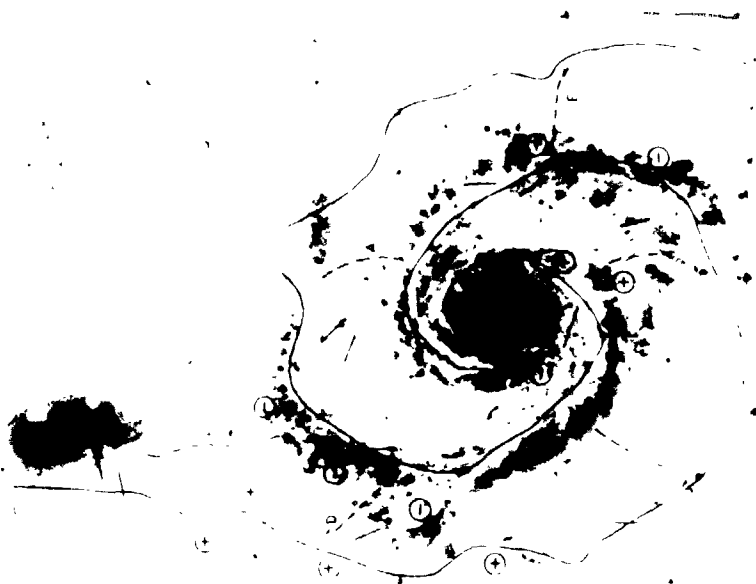


Figure 15b.

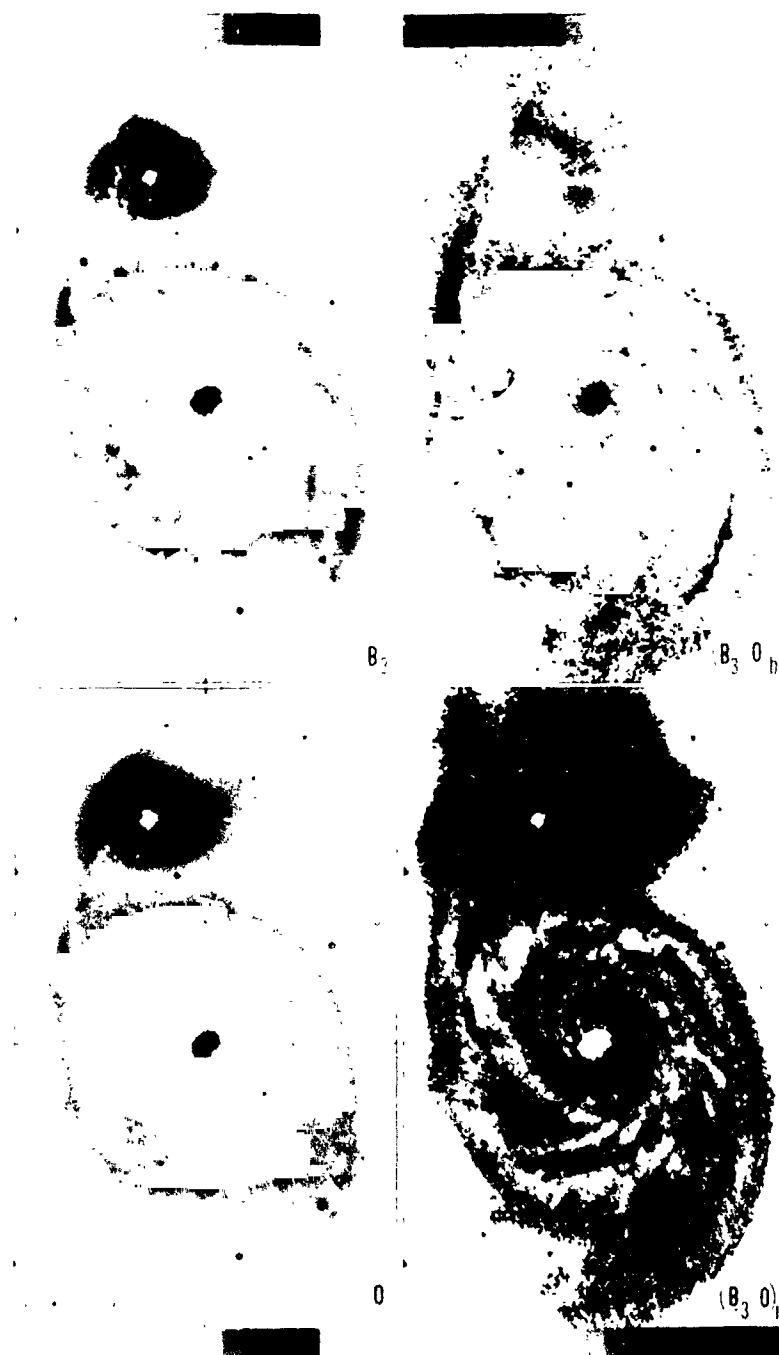


Figure 16. Surface Brightness and Color Index Maps of M 51. In the lower left panel, the spiral pattern is interpreted as an azimuthal density variation in the old stellar disk population, as identifiable in a background stellar density wave (from Schweizer, 1976).

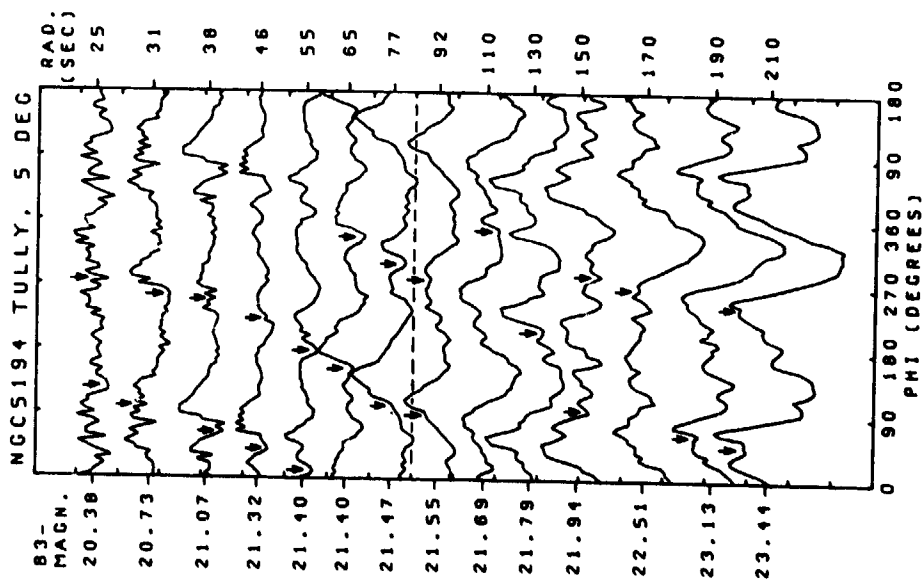


Figure 17. Azimuthal surface brightness profiles of M 51 in the B3 passband. The strong dust lanes (arrows) often found on the inside edge of the arm profiles are actually shifted a little onto the rising inside slope (from Schweizer, 1976).



Figure 18. Two projections of a three dimensional map of surface brightness of M 51 and its companion NGC 5195 in a yellow-green passband. The spiral arms are visible winding up the slopes of the mountain of total surface brightness (from Burkhead, 1976).

The ridge line of the 1415 MHz emission from the radio spiral arms is determined by Mathewson, et. al. (1972) and this ridge line is shown in Figure 15b superposed on an optical photograph of M 51 and NGC5195. Here it is apparent that the ridge of the radio spiral arms in synchrotron emission and the strongest magnetic fields lie well along the dust lanes generally on the inner sides of the optical spiral arms.

Through a study of the detailed surface photometry of six galaxies including M 51, Schweizer (1976) detects background spiral patterns in the old stellar disk population. He identifies the arms of these broad patterns as background stellar density wave arms. Figure 16 shows his surface brightness and color index maps for M 51. The red arms which stand out in the O passband (lower left panel) are composed mainly of old giants underlying the old stellar disk, and these are the arms in M 51 identified by Schweizer for the first time as background stellar density wave arms. The blue arms which stand out in the B3 passband (upper left panel) are representative of the young population I stars.

In his identification of the background density wave arms, Schweizer makes use of a sequence of azimuthal surface-brightness profiles at different radii, shown for M 51 in Figure 17. It is interesting to note that most of the strong dust lanes (marked by arrows) are not only located on the inside edge of the arm profiles but are also often shifted a little onto the rising inside slope of the profiles. In fact in the outer parts of M 51 some appear even right on top of the arm profiles. Schweizer argues that the rise of surface brightness of the arm profiles inside the dust lanes must be largely due to the old disk stars which participate in the background density wave arms.

In another view, Figure 18 shows two projections of a three dimensional map of surface brightness of M 51 and its companion NGC5195 computed by Burkhead (1976) from a combination of photographic plates weighted toward yellow-green (centered about 5300 Å). Here, the spiral arms of M 51 might well be characterized as narrow roadways slowly winding up the sides of the steep mountain of total surface brightness (not unlike the wave arms in Figure 1).

THE SAMPLE GALAXY NGC 3031 (M 81) - OBSERVATIONAL STUDIES

Another rather striking galaxy - on the w_{40} surface near our own Galaxy in Figure 12 - for which high resolution 21-cm line observations have been possible is the galaxy NGC3031 (M81). Figure 19 contains a radio photograph from Rots and Shane (1975) of the observed density distribution of neutral hydrogen in M81. Although there is a great deal of detailed structure, two major arms of neutral hydrogen seem to stand out as rather prominent spiral features. These H I arms

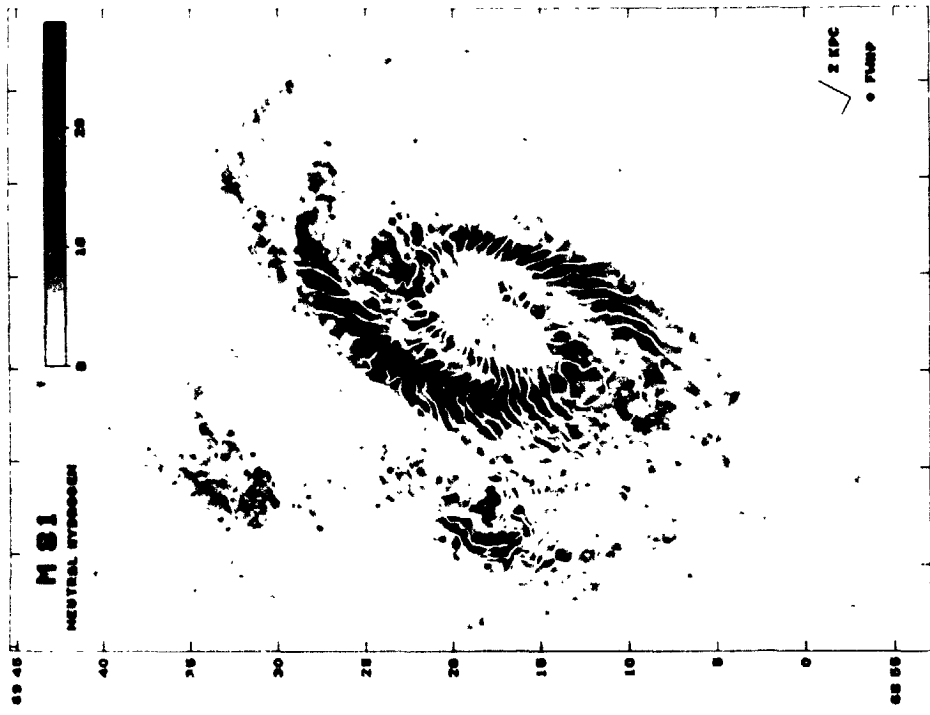


Figure 19. Radiograph of the density distribution of neutral hydrogen in NGC 3031 (M 81). Two major arms of H I stand out as rather prominent features (from Rots and Shane, 1975).

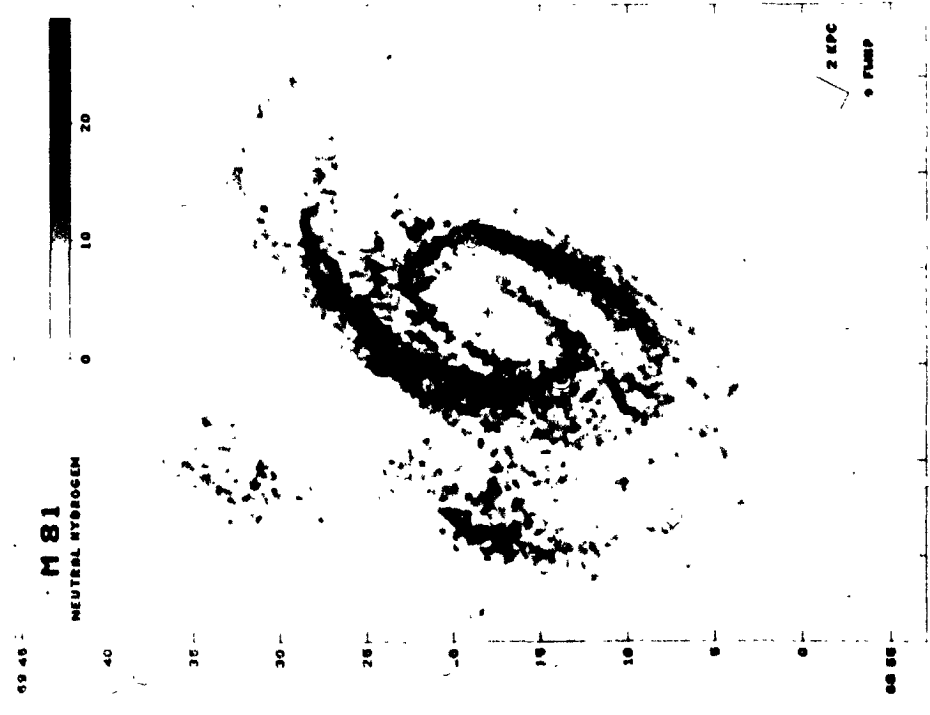


Figure 20. Observed velocity field of M 81. A sequence of crests and troughs in the velocity contours is apparent near the arms, particularly the eastern arm (from Rots, 1975).

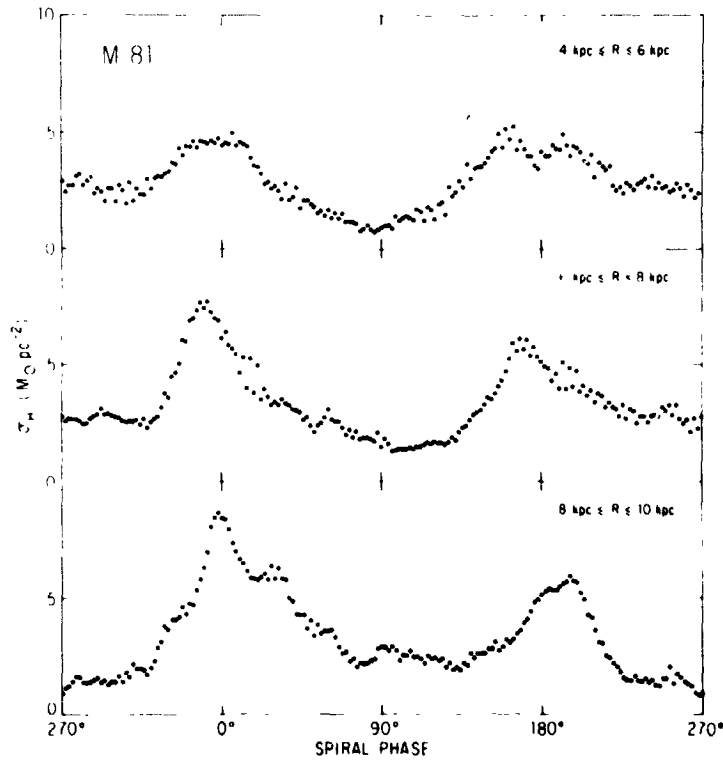


Figure 21. H I surface density as a function of spiral phase about the disk of M 81. The three panels show different radius ranges. The concentration of neutral hydrogen into spiral arms is quite clear with the arm peaks substantially narrower than the interarm troughs (from Rots, 1975).

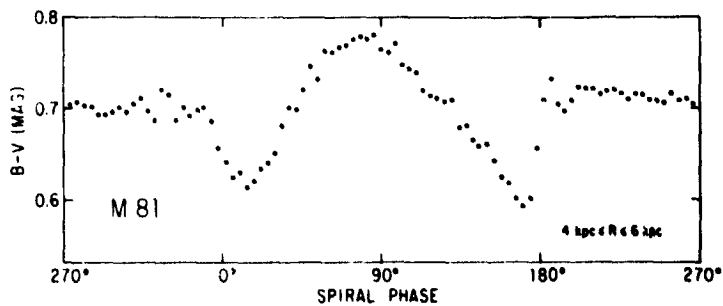


Figure 22. B - V color as a function of spiral phase about the disk of M 81. This plot can be directly compared with the upper panel in Figure 21. The arm ridges where the H I is most compressed (Figure 21) correspond to the bluer regions (troughs in Figure 22) where young stars may be forming with prominence (from Rots, 1975).

are also closely coincident with the optical arms and the dust. Figure 20 shows the observed velocity field, determined by Rots (1975), superposed on the radio photograph.

Figure 21 from Rots (1975) shows the H I surface density distribution as a function of the spiral phase around three circular bands in M 81, each 2 kpc wide. The concentration of neutral hydrogen in the spiral arms is clearly visible, with the eastern arm around 0° in spiral phase and the western arm around 180° . Moreover the density distribution appears to be of such a nature that the arm peaks are substantially narrower than the interarm troughs, altogether indicative of nonlinear wave phenomena.

Rots also plots the average B - V color in the circular band between 4 and 6 kpc as a function of spiral phase, and this is shown in Figure 22. In view of the H I distribution in the upper panel of Figure 21, a correlation seems to exist between H I and color in the sense that the higher is the surface density of H I, the bluer the color. Indeed the blue regions delineated by the troughs here appear even narrower than the corresponding arm peaks of H I (in the 4 to 6 kpc band) in Figure 21. If these regions of bluer color are interpreted to represent relative increases in the number of young stars forming from the gas, then it would appear that star formation is occurring with prominence only in the limited regions of the H I spiral arms. Rots finds that there actually is a time lag between the highest density of very young stars and the maximum H I surface density of the order of 10^6 to 15^6 , which corresponds to an order of 10 million years, in the sense that the stars are forming with most prominence just outside the ridge of the H I arm from gas that has already just entered and been compressed within this ridge region. This observed time lag between the H I peak and the concentration of young stars across the spiral arms of M 81 is just the temporal sequence expected in the theory between the shock and H I peak and the region of highest concentration of young stars and H II regions. Consequently, these observational results on M 81 suggest that this galaxy is another example which exhibits features predicted in the wave picture.

Visser (1975a) applies the theoretical picture to simulate the nonlinear, large-scale gas flow in M 81. Figure 23 illustrates the theoretically-calculated field of line of sight velocities superposed on a 20" photograph of M 81. The overall trend of loci of equal heliocentric velocities indicates the general rotation of M 81, while the crests and troughs of the contours reflect the systematic motions predicted along the wave arms. With the inclusion of the effect of beam smearing as shown in Figure 24 (Visser 1975b), which is an unavoidable effect inherent in observations, substantial progress toward a deeper understanding of M 81 is possible through a comparison of the smoothed theoretical velocity field (Figure 24) and the observed velocity field (Figure 20).

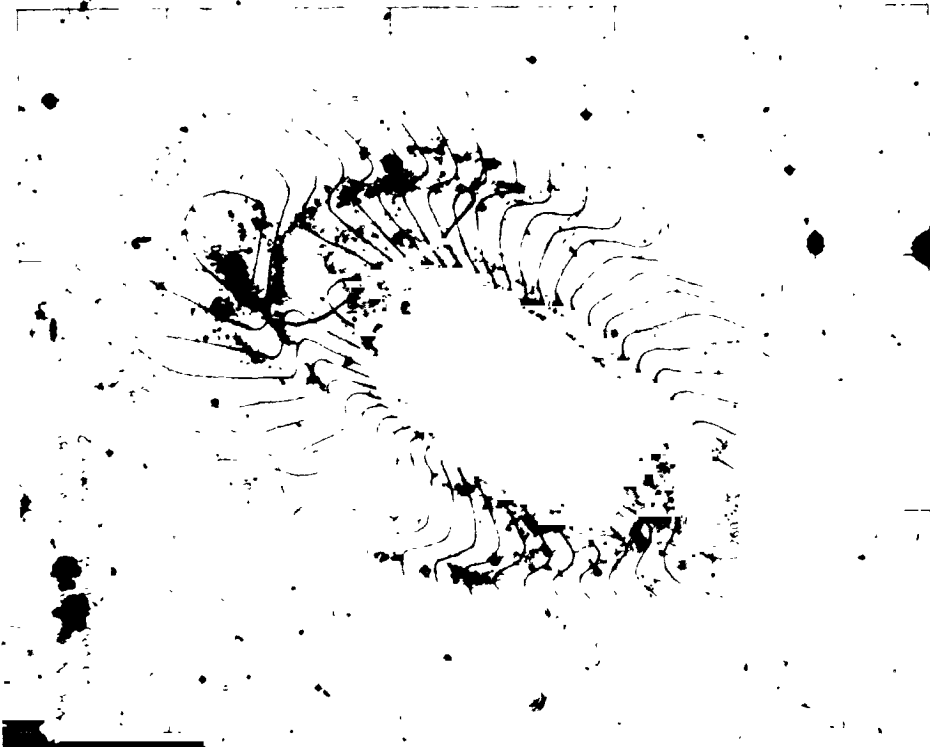


Figure 23. Theoretical velocity field of M 81 with the presence of shock waves, superposed on a 200" photograph (from Visser, 1975a).

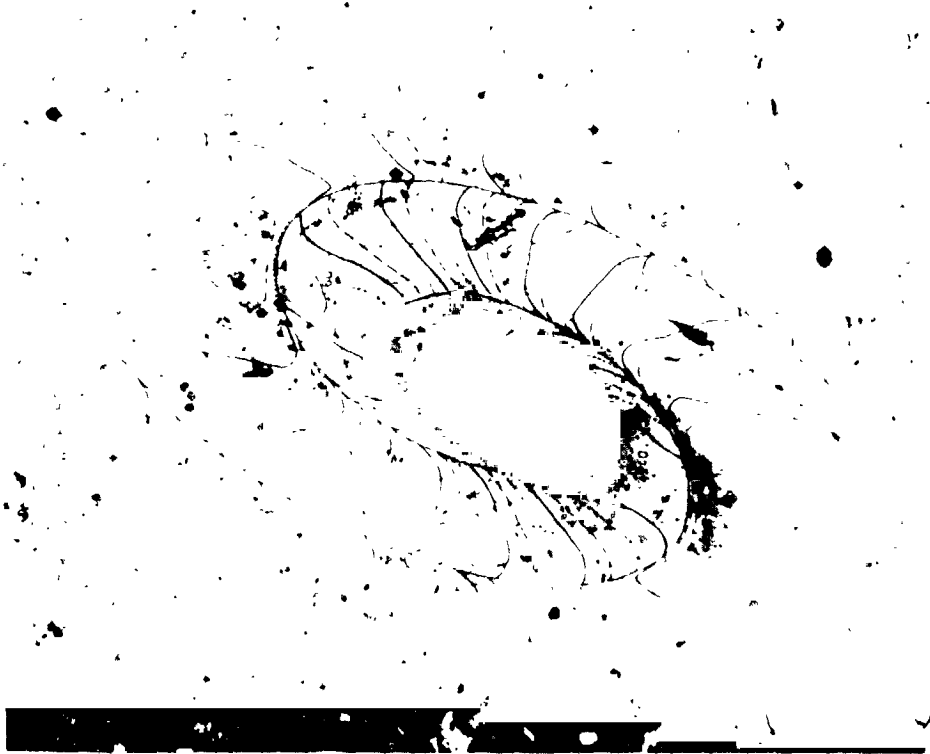


Figure 24. Smoothed theoretical velocity field of M 81 after the effect of beam smearing is taken into account (from Visser, 1975b).

OUR GALAXY

We now turn to focus on our own Milky Way System. Hopefully these concepts of density wave theory which seem to be playing an important role in M 51 and M 81 - two extragalactic systems for which we enjoy a birds eye view - can be borrowed and applied to help us better understand our own Galaxy.

Figure 25 provides curves of w_{10} for two possible choices of corotation radius in our Galaxy (see Burton, 1976). Because of the high levels attained by w_{10} , potentially strong shocks and high gas compressions are possible in the inner parts of the Galaxy, and these have been calculated even for small to moderate forcing F (e.g. Roberts, 1969; Shu, et. al. 1972). Simultaneously the frequency of compression $2(\Omega - \Omega_p)$ with each passage through a spiral wave crest is also substantially higher in the inner parts due to the differential rotation inherent in the galactic disk. Both these effects - the potential strength of gas compression and the frequency of compression - tend to make the conditions for star formation and molecule formation rather favorable in the inner parts of the Galaxy, perhaps inwards as far as inner Lindblad resonance about 4 kpc where the spiral wave is thought to terminate (also see Shu 1975; and Oort, 1973, and Segalovitz, 1975, for application to M 81).

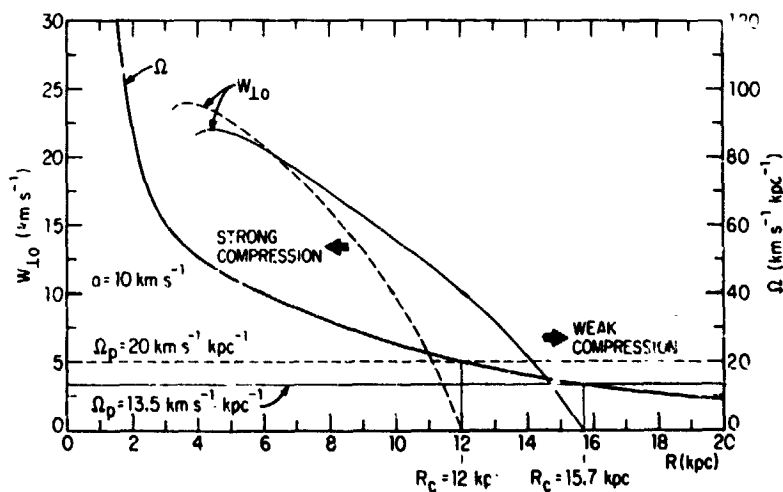


Figure 25. Characteristics of the Density Wave Picture for our Galaxy. Strong shocks and high gas compressions are possible (and have been calculated) in the inner parts where $w_{10} > a$. The frequency of gas compression in shocks is also high in the inner parts. These factors suggest that the conditions for shock-triggered star formation and molecule formation may be favorable in the inner parts of our Galaxy (see Burton, 1976).

Both $w_{\perp 0}$ (and potential shock strength) and the frequency of compression $2(\Omega - \Omega_p)$ decrease with increasing radius in the Galaxy. Moreover, in the outer regions over the range of radii near the solar circle where the intrinsic frequency ν of the density wave satisfies the relation

$$\nu^2 - \alpha^2 = n^{-2}, \quad (4)$$

ultraharmonic resonances can occur in the gas (Shu, et. al., 1973). Here α is the intrinsic acoustic speed of the gas, and $n = +2, +3, +4, \dots$. Such ultraharmonic resonances tend to produce secondary compressions and secondary arm structures in the gas. These secondary features bear some resemblance to the secondary arms, spurs, and feathers often observed (with a birds eye view) in the outer parts of many external spirals. However their presence more than anything else probably confuses any coherence that the overall spiral structure might otherwise have in these outer regions. For larger radii outside the solar circle toward corotation where $w_{\perp 0} < \alpha$, only very weak shocks, if any at all, are possible together with broad regions of relatively low gas compression. Therefore in these outer regions where there may be a lack of coherence as well as a lack of sufficient gas compression the conditions for efficient and coherent star formation and molecule formation may be rather unfavorable except in unusual local environments.

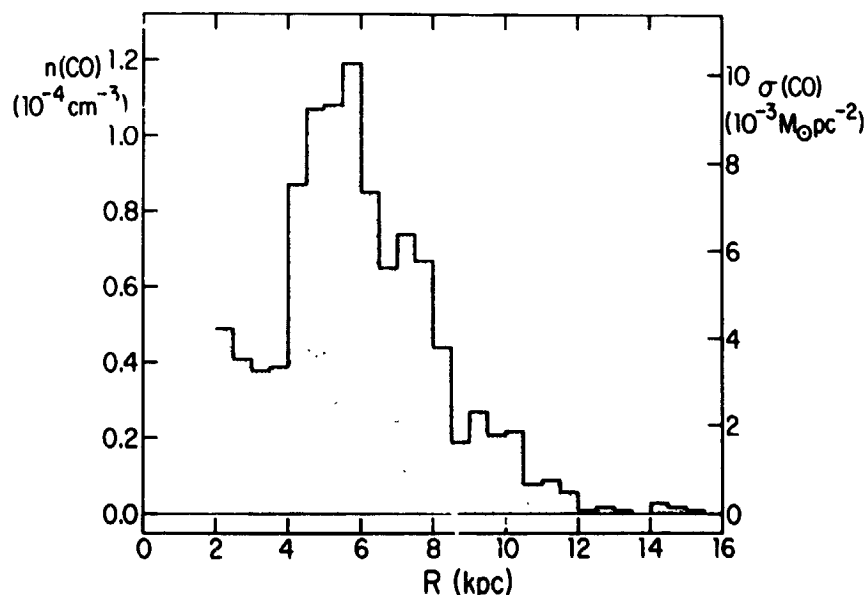


Figure 26. Radial distribution in the Galaxy of $^{12}\text{C}^{16}\text{O}$ volume densities at $b = 0^\circ$ (lefthand ordinate) and of the projected $^{12}\text{C}^{16}\text{O}$ surface densities (righthand ordinate) (from Gordon and Burton, 1976).

Figure 26 shows the radial abundance distribution of the carbon monoxide molecule in our Galaxy found by Gordon and Burton (1976). By relating the CO densities to those of molecular hydrogen on the basis of solar abundances, Gordon and Burton further derive the radial abundance distribution of H_2 in the Galaxy. This is shown in Figure 27 together with their deduced distribution for total interstellar nucleons (also see Stecker, Solomon, Scoville, and Ryter, 1975). They find that the abundance distributions for CO and H_2 are more concentrated than that of the H I toward the inner parts of our Galaxy as well as more concentrated than that of the H I toward the galactic plane. This separation of the peak concentrations of CO and H_2 from that of the H I suggests that there exists a factor other than the average neutral hydrogen gas density which controls the present day formation of molecules (and perhaps young stars) in the Galaxy. If we adopt the density

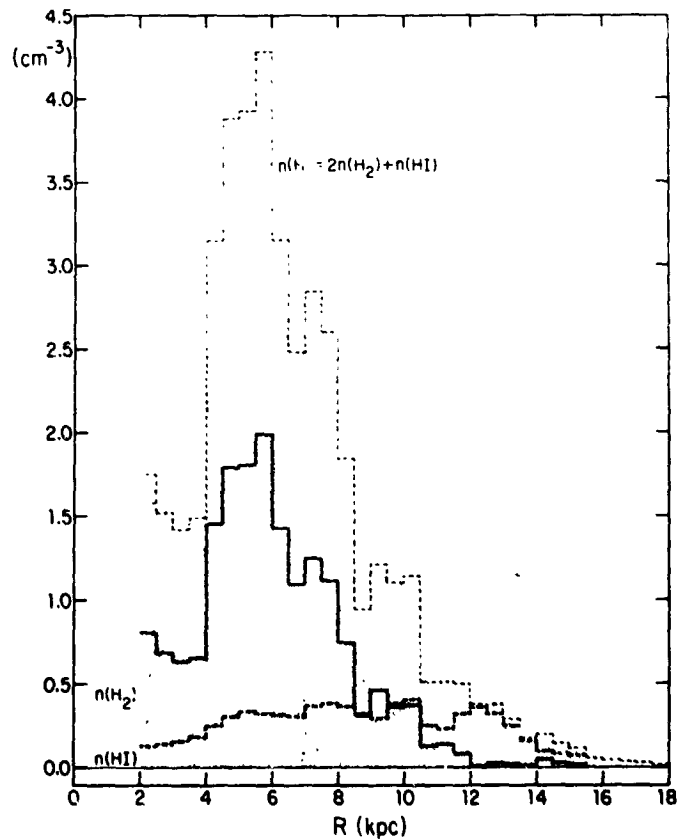


Figure 27. Radial distribution in the plane of the Galaxy of volume densities of atomic and molecular hydrogen. The distribution of the sum $2 n(\text{H}_2) + n(\text{H I})$ indicates the overall distribution of interstellar nucleons (from Gordon and Burton, 1976).

wave picture where the present day formation of molecules (as well as young stars) occurs in part as a result of compression in a galactic shock wave, it is possible to account for this striking separation as a consequence of: (1) the inward increase of the gas density compression (and $w_{\perp 0}$) and (2) the inward increase of the frequency $2(\Omega - \Omega_p)$ at which the interstellar gas is periodically compressed. Because stellar density waves are absorbed at inner Lindblad resonance and cannot propagate inside this region, substantial molecule formation by the wave mechanism is not expected inside 4 kpc.

Similar morphological characteristics also seem to distinguish the distributions of a number of other constituents and tracers - H II regions, supernova remnants, pulsars, γ -radiation, synchrotron radiation, and other molecules - from that of the neutral hydrogen (see Burton, 1976). It is intriguing to consider the prospect that the compression wave mechanism, if strong enough, might play an important role in the formation and large-scale distribution of many of these constituents and tracers as well.

Optical observations of the spiral structure of our Galaxy are confined to the realm of a few kiloparsecs in radius about the Sun. For this reason the current picture of the large-scale spiral structure rests primarily on radio observations of the 21-cm line of neutral hydrogen. Unfortunately from our vantage point within our Milky Way System, we have difficulty in seeing the forest because of the trees.

As Burton (1972) has demonstrated, it is extremely difficult, if not impossible, to interpret a profile of the 21-cm line of neutral hydrogen unambiguously, particularly with both the gas density and the gas velocity varying along the line of sight. Of course in the density wave theory a relation between density and velocity does exist. However, because of the uncertainty in the choice of specific values for the parameters of the model and because of uncertainties in the physical properties and state of the H I gas and the interstellar medium (with multi phases, multi components, turbulence, complicated cloud structures, etc...), the interpretation of line profiles is still very difficult.

Despite these uncertainties Simonson (1976) works toward a simulation of large-scale spiral structure by constructing a model based on density wave kinematics that reproduces many of the main features of the 21-cm H I observations. Figure 28 provides a synthetic optical photograph of his simulated model of our Galaxy as revealed through the 21-cm line profiles. A basically two-armed spiral pattern with a pitch angle of 6° - 8° is apparent between the 4 kpc dispersion ring and the solar circle. Near the solar circle, two additional arms originate, and the pattern outside is multiple-armed.

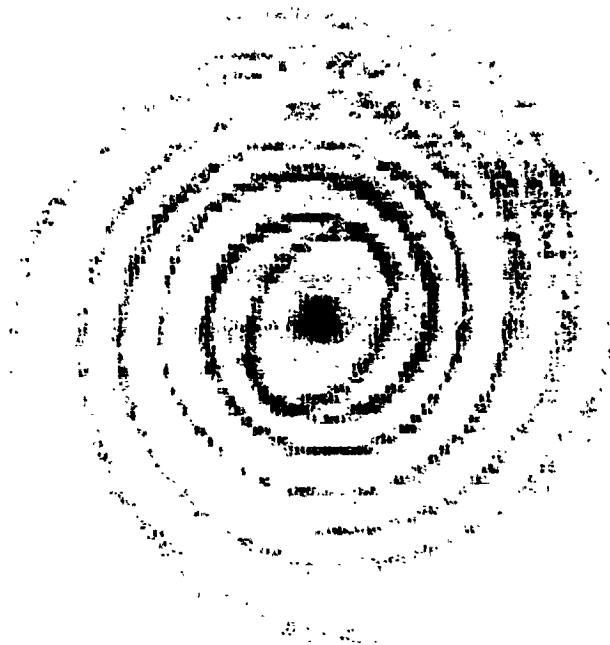


Figure 28. Synthetic Optical Photograph of a simulated model of our Galaxy using density wave kinematics as deduced from 21-cm line profiles of neutral hydrogen (from Simonson, 1976).

PERSPECTIVE TOWARD THE FUTURE

Toward the future the outlook is optimistic. Definitive scientific research generally motivates further scientific research, no matter what the discipline. Most certainly of great benefit will be current and future observational studies and theoretical work on the various constituents and tracers delineating the structure, content, and dynamics of our Galaxy as well as extragalactic systems - H I, CO, OH, and H₂, young stars, H II regions, supernova remnants, pulsars, γ -radiation, synchrotron radiation, and others.

Already there are many exciting problems ripe for the challenge of future investigations. Answers are needed to such questions as: Does our galaxy indeed possess spiral structure, which many extragalactic systems seem to be capable of exhibiting for our birds eye viewing?

If so, how coherent is it and why do the present CO observations for example not show a better delineation of spiral structure in our Galaxy? From our vantage point, how severely do we suffer from not seeing the forest because of the trees? Although the abundance distribution of CO does drop off within the inner 4 kpc in our Galaxy in qualitative agreement with the compression wave mechanism, why does the CO not drop off more abruptly there? Might the compression wave mechanism be capable of penetrating to a sufficient distance inside 4 kpc to account for this low level of CO present, or need there be other sources? Indeed these are only a few of the intriguing questions and problems that could be mentioned; there are many others.

At the present time, theoretical results and developments are progressing well on many fronts; exciting new observational results are springing forth and theoreticians and observationalists alike have the opportunity to learn a great deal more and broaden our present understanding. The interaction between theory and observations is extremely important for the purpose of providing new challenges to current theory and to current observational techniques toward their better and better refinement.

I would like to thank Martin Burkhead, Butler Burton, Jim Huntley, Arnold Rots, Francois Schweizer, Chris Simonson, and Herman Visser for graciously sending me a number of the photographs included in this review, in many cases prior to publication. I would also like to thank Jim Huntley for kindly preparing the photographic simulations. This work was supported in part by the National Science Foundation under grant AST72-05124 A03.

REFERENCES

- Biermann, P., Kippenhahn, R., Tscharnuter, W., and Yorke, H., 1972, Astron. & Astrophys., 19, 113.
- Biermann, P., and Tinsley, B.M., 1974, Publ. Astron. Soc. Pacific, 86, 791.
- Burkhead, M., 1976 (private communication).
- Burton, W.B., 1972, Astron. & Astrophys., 19, 51.
- _____, 1976, Ann. Rev. Astron. & Astrophys., 14.
- Feldman, S.I., and Lin, C.C., 1973, Stud. Appl. Math., Vol. 52, 1.
- Fujimoto, M., 1966, in IAU Symp. No. 29, p. 453.
- Gordon, M.A., and Burton, W.B., 1976, Ap.J. (in preparation).
- Jensen, E.B., Strom, K.M., and Strom, S.E., 1976 (in preparation).
- Lau, Y.Y., Lin, C.C., and Mark, J. W.-K., 1976 (in preparation).

- Lin, C.C., 1970, in Proc. IAU Symp. No. 38, 377.
 _____, 1971, in Highlights of Astr., 2 (D. Reidel Publishing Co., Dordrecht Holland), 88.
- Lin, C.C., and Shu, F.H., 1964, Ap.J., 140, 646.
 _____, 1966, Proc. Nat. Acad. Sci., 55, 229.
- Lin, C.C., and Lau, Y.Y., 1975, SIAM J. APPL. MATH., 29, 2, 352.
- Lindblad, B. (1963) Stockholm Obs. Ann. 22,
 Lindblad, B. and Langebartel, R.G. (1953) Stockholm Obs. Ann. 17,
 6.
- Lynden-Bell, D., and Kalnajs, A.J., 1972, MNRAS, 157, 1.
- Mark, J.W.-K., 1974, Ap.J. 193, 539.
 _____, 1976a, Ap.J. 203, 81.
 _____, 1976b, Ap.J. (May issue).
 _____, 1976c, Ap.J. (June issue).
 _____, 1976d, Ap.J. (in preparation).
- Mathewson, D.S., Kruit, P.C. van der, and Brouw, W.N., 1972,
Astron. & Astrophys., 17, 468.
- Mouschovias, T.Ch., Shu, F.H., and Woodward, P.R., 1974, Astron.
 & Astrophys., 27, 73.
- Mufson, S.L., 1974, Ap.J. 193, 561.
 _____, 1975, Ap.J., 202, 372.
- Cort, J.H., 1973, I.A.U. Symp. No. 58.
- Roberts, W.W., 1969, Ap.J., 158, 123.
- Roberts, W.W., Roberts, M.S., and Shu, F.H., 1974, in IAU Symp.
 No. 58, 439.
 _____, 1975, Ap.J., 196,
 381.
- Roberts, W.W., and Yuan, C., 1970, Ap.J., 161, 877.
- Rots, A.H., 1975, Astron. & Astrophys., 45, 43.
- Rots, A.H., and Shane, W.W., 1975, Astron & Astrophys., 45, 25.
- Sandage, A.R., 1961, The Hubble Atlas of Galaxies (Washington,
 D.C.,: Carnegie Institution of Washington).
- Sanders, R.H., and Huntley, J.M., 1976, Ap.J. (in preparation).
- Sawa, T., 1975, Sci. Reports Tohoku Univ. Series I, LVIII, 13.
- Schweizer, F., 1976, Ap.J. (in preparation).
- Segalovitz, A., 1975, Astron. & Astrophys. 40, 401.
- Shu, F.H., 1974, Astron & Astrophys., 33, 55.
 _____, 1975, Proc. Colloquium on Spiral Galaxies, Bures
 Sur Yvette, 309.
- Shu, F.H., Milione, V., Gebel, W., Yuan, C., Goldsmith, D.W.,
 and Roberts, W.W., 1972, Ap.J., 173, 557.
- Shu, F.H., Milione, V., and Roberts, W.W., 1973, Ap.J., 183,
 819.
- Shu, F.H., Stachnik, R.V., and Yost, J.C., 1971, Ap.J., 166,
 465.
- Simnson, S.C. III, 1976, Astron. & Astrophys., 46, 261.
- Stecker, F.W., Solomon, P.M., Scoville, N.Z., and Ryter, C.E.,
 1975, Ap.J., 201, 90.

- Toomre, A., 1969, Ap.J., 158, 899.
- Toomre, A., and Toomre, J., 1972, Ap.J., 178, 623.
- van den Bergh, S., 1960a, Ap.J., 131, 215.
- _____, 1960b, Ap.J., 131, 558.
- van der Kruit, P.C., 1973, Astron. & Astrophys. 29, 263.
- van der Kruit, P.C., Oort, J.H., and Mathewson, D.S., 1972, Astron. & Astrophys., 21, 169.
- Vandervoort, P.O., 1970, Ap.J., 161, 67.
- Visser, H.C.D., 1975a, in Symp. on Galactic Dynamics (Bures-sur-Yvette, France), 211.
- _____, 1975b (private communication).
- Wielen, R. 1975, Conf. Optical Observing Programs (Bochum, Germany), 59.
- Woodward, P.R., 1976, Ap.J. (in preparation).

N76-29122

THE GALACTIC DISTRIBUTION (IN RADIUS AND Z) OF INTERSTELLAR
MOLECULAR HYDROGEN

N. Z. Scoville, Dept. of Physics and Astronomy, University
of Massachusetts, Amherst, MA 01002

P. M. Solomon and D. B. Sanders, Dept. of Earth and Space
Sciences, State University of New York, Stony Brook, NY
11794

ABSTRACT

New observations of the galactic longitude and latitude distributions of $\lambda = 2.6$ mm CO emission are presented. Analysis of this spectral line data yields the large scale distribution of molecular clouds in the galactic disk and their z-distribution out of the disk. Strong maxima in the number of molecular clouds occur in the galactic nucleus and at galactic radii 4-8 kpc. The peak at 4-8 kpc correlates well with a region of enhanced 100 Mev γ -ray emissivity. This correlation strongly supports the conclusion of Stecker et al. (1975) that the γ -rays are produced as a result of cosmic ray interactions in molecular H_2 clouds rather than HI. One important implication of this is that the interstellar magnetic field lines to which cosmic rays are confined, must therefore not be excluded from these dense clouds.

The width of the cloud layer perpendicular to galactic plane between half density points is 105 ± 15 pc near the 5.5 kpc peak. The total mass of molecular gas in the interior of the galaxy exceeds that of atomic hydrogen and is $3 \cdot 10^6 M_{\odot}$ based on these observations.

Until just the last year there was little appreciation of the possibility that clouds of molecular H_2 rather than atomic hydrogen might constitute the dominant contribution to the interstellar mass. The importance of the H_2 gas on a galactic scale was overlooked, essentially because it was impossible to detect from the ground. The rotational and vibrational transitions of H_2 are weak infrared quadrupole lines; and observations of the ultraviolet resonance lines are limited to clouds of low visual extinction (< 1 mag) in front of nearby O and B stars (e.g. Spitzer et al. 1973). Our knowledge of H_2 in selected, more opaque, and more distant gas clouds has instead been deduced from observations of relatively rare trace molecules like CO, CS, and HCN which have fundamental rotation lines at $\lambda = 1.3$ mm.

Recently observations of the CO $J = 1 \rightarrow 0$ line at 2.6 mm have been extended to surveys of this emission throughout the galactic plane (Scoville and Solomon 1975, and Burton, Gordon, Bania, and Lockman 1975). Scoville and Solomon (1975) used their CO observations to deduce the overall distribution and mass of molecular hydrogen in the galaxy. The relevance of these studies to observations of galactic γ -rays (Fichtel et al. 1975) rests on our early conclusion that within the region of the galaxy interior to the solar circle molecular hydrogen not HI is the dominant constituent of the interstellar medium. (Spitzer et al. 1975) have pointed out that the distribution of molecular hydrogen derived from the CO observations is very similar to the "missing" interstellar matter distribution required to account for the observed rise in γ -ray emission at galactic radii 4 to 8 kpc. The consistent conclusion of both analyses is that at the peak in the molecular cloud distribution ($\bar{r} = 5.5$ kpc) perhaps 90% of the interstellar gas is H_2 and as one moves outward in the galaxy the ratio H_2/HI decreases until at the solar circle the two abundances are about equal.

In the following, we first review CO data obtained in the galactic plane ($b = 0$) from which one derives the radial distribution of CO (and H_2) outside the galactic nucleus. Then some of our most recent observations pertaining to the z -distribution of molecular clouds are discussed. Because the CO emission from the galactic center shows quite different characteristics from that seen elsewhere in the galactic plane, we have devoted a separate section (§4) to analysis of the emission seen at $l < 3^\circ$. And finally we are then able in §5 to estimate the mass and surface density contained in interstellar molecular

hydrogen by integrating the radial distribution function (§2) over galactic radius and z (§3).

1. Considerations for Interpretation of CO Observations

It is in no way obvious that the CO intensities we have observed at different positions in the galaxy should be a proportional indicator of gas column densities. Very generally the line is found to be optically thick and in clouds having high gas density the intensities will, in fact, correlate with gas temperatures not with gas densities. On the basis of ^{12}CO data alone it is impossible to tell in what fraction of the clouds observed in the plane the CO is thermalized. Our limited ^{13}CO data obtained at three positions indicates that the CO is probably not thermalized in roughly half the clouds.

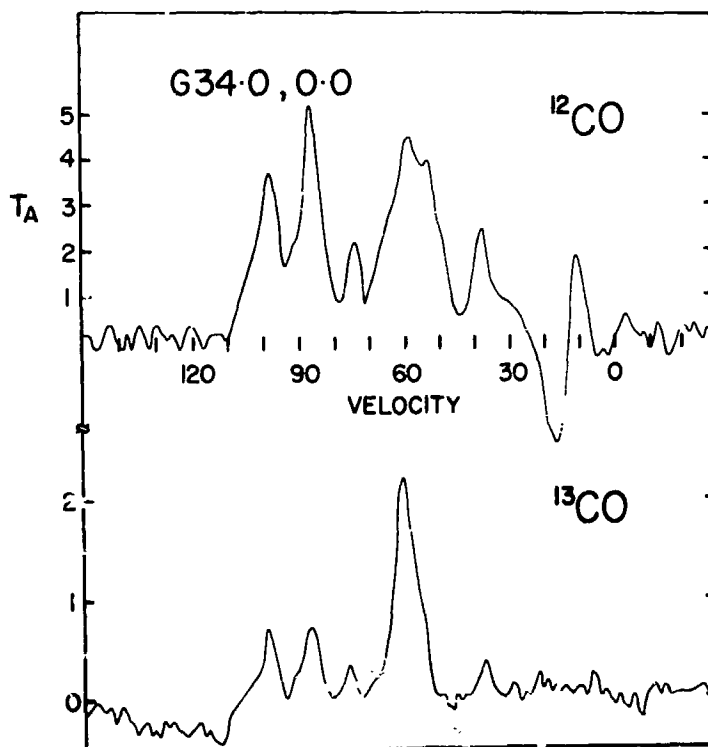


Figure 1: CO and ^{13}CO spectra are shown for the direction $l=34^\circ$, $b=0^\circ$. Note that there are at least five discrete features in the CO spectra, each of which has a counterpart in ^{13}CO . The negative dip at $v=20$ km/sec in the CO spectra is caused by the presence of CO emission at that velocity in the reference position 3° above the galactic plane. The intensity units are Rayleigh-Jeans antenna temperatures $^\circ\text{K}$.

The first figure shows emission of $^{12}\text{C}^{16}\text{O}$ and the rarer isotope $^{13}\text{C}^{16}\text{O}$ obtained at the position $l = 34^\circ$, $b = 0^\circ$. The closest approach of this line of sight to the galactic center occurs at galactic radius 5.5 kpc near the molecular cloud maximum. The discrepancy between the observed intensity ratios $^{13}\text{CO}/^{12}\text{CO}$ (ranging from 1/2 to 1/6 amongst the five features seen in Figure 1) and the much lower value of the interstellar abundance ratio $[^{13}\text{CO}/^{12}\text{CO}] = 1/40$ (Wannier et al 1976) imply that these ^{12}CO lines are optically thick with $\tau > 6$. It must be an important consideration that the CO lines are optically thick and the observed brightness temperatures are, therefore, equal to the excitation temperature characterizing the relative $J = 1$ and $J = 0$ level populations.

This excitation temperature is determined by the rate of collisions of H_2 with CO, by spontaneous radiative decay ($A_{10} = 6 \cdot 10^{-8} \text{ sec}^{-1}$) and by stimulated radiative absorption and emission. In the event that a cloud has $n_{\text{H}_2} < 3000 \text{ cm}^{-3}$, the collisions by themselves would not be sufficient to thermalize the CO levels. However, if in this same region, the CO lines are optically thick, a line photon will be absorbed and scattered approximately τ times before it escapes the cloud. Thus one may visualize that when this "radiation trapping" occurs, each collisional excitation is replicated approximately τ times and the observed excitation temperature will be in some manner proportional to τ . In a more technical treatment of the excitation which solves the full equations of statistical equilibrium for CO (Scoville and Solomon 1974), we have found that for a large regime giving subthermal excitation of optically thick CO,

$$T_B \approx T_{\text{excitation}} \propto (n_{\text{H}_2} \cdot n_{\text{CO}})^{0.4} \quad (1)$$

Therefore, if the abundance ratio $n_{\text{CO}}/n_{\text{H}_2}$ from cloud to cloud is constant,

$$T_B \propto n_{\text{H}_2}^{0.8} \quad (2)$$

As the densities increase and $T_{\text{excitation}} = T_K$, then T_B gradually loses its dependence on n_{H_2} altogether and develops a linear dependence on T_K .

In most of the clouds outside of the galactic nucleus (§4), we feel that the densities are insufficient for complete thermalization and therefore an intuition which associates increased CO intensity with increased gas density seems reasonable though it is hardly proven.

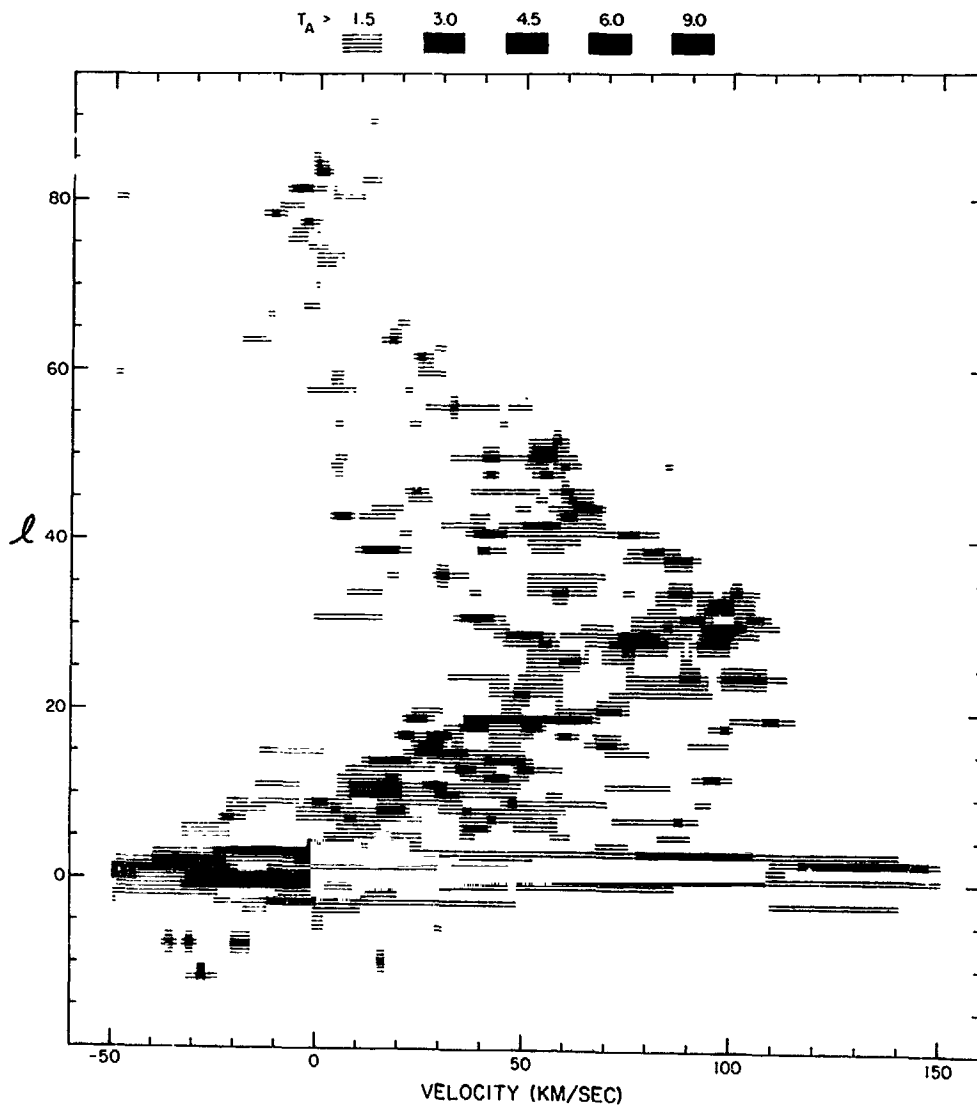


Figure 2: The intensity of CO emission along the galactic equator is shown as a function of longitude and velocity. Molecular emission tends toward lower longitudes and more positive radial velocities as compared with 21 cm (see Kerr 1969), indicating that the molecules are concentrated toward the center of the Galaxy. A version of this figure spanning more velocities ($\pm 300 \text{ km s}^{-1}$), and therefore containing the full range found in the galactic center, may be found in Scoville (1975).

C-3

2. The Radial Distribution of Molecular Gas

The entire run of data from our earlier observations in the galactic plane ($l = -10^\circ$ to $+90^\circ$ sampled once every degree with a 1 arcmin beam) can be displayed in a single longitude-velocity diagram (Figure 2). In this representation a single spectrum observation constitutes a horizontal line of shading. One sees both intense, high velocity emission arising from molecular clouds in the galactic center ($\bar{r} < 300$ pc; see Scoville, Solomon, and Jefferts 1974) and many individual, less intense features which were sampled in the galactic plane outside the center.

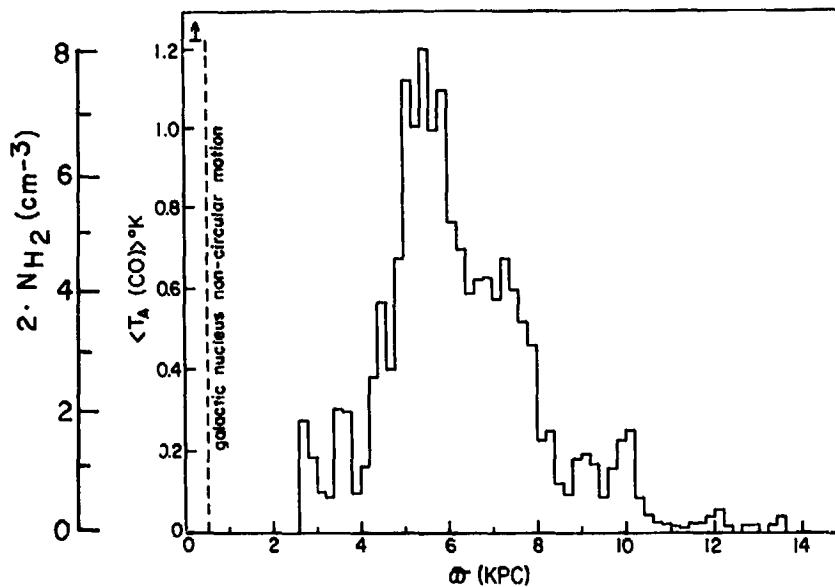


Figure 3: The mean CO antenna temperature as a function of radius in the Galaxy \bar{r} was calculated using the Schmidt (1965) rotation law to transform l, v in Figure 2 to \bar{r} . We use only data at $l > 10^\circ$ in order to exclude the galactic center where much of the gas clearly is not in pure rotation. Note the sharp peak in CO at radius of 5.5 kpc and dramatic falloff toward the Sun and beyond. The vertical scale may also be converted to H_2 surface density through a normalization to $25 M_\odot \text{pc}^{-2}$ at the 5.5 kpc peak (see §5).

A more useful representation of the CO emission for comparison with γ -ray observations is obtained by using the Schmidt rotation law to transform from the l, v coordinates

of Figure 2 to galactic radius (Figure 3). This figure provides our best indication of the molecular gas distribution in the galactic plane outside $\bar{a} = 3$ kpc. The vertical scale of Figure 3 may be approximately transformed from $\langle T_A \rangle$ to n_{H_2} by setting $n_{H_2} = 4 \text{ cm}^{-3}$ at the 5.5 kpc peak (Scoville and Solomon 1975). This H_2 distribution matches well that of other population I components excepting atomic hydrogen (see Figure 4). It is very similar to the distribution of discrete HII regions (Mezger 1970), diffuse ionized gas (Westerhout 1958 and Lockman 1976), and is consistent with the pulsar distribution (Sieradakis, this symposium and Hulse and Taylor 1976). And most important

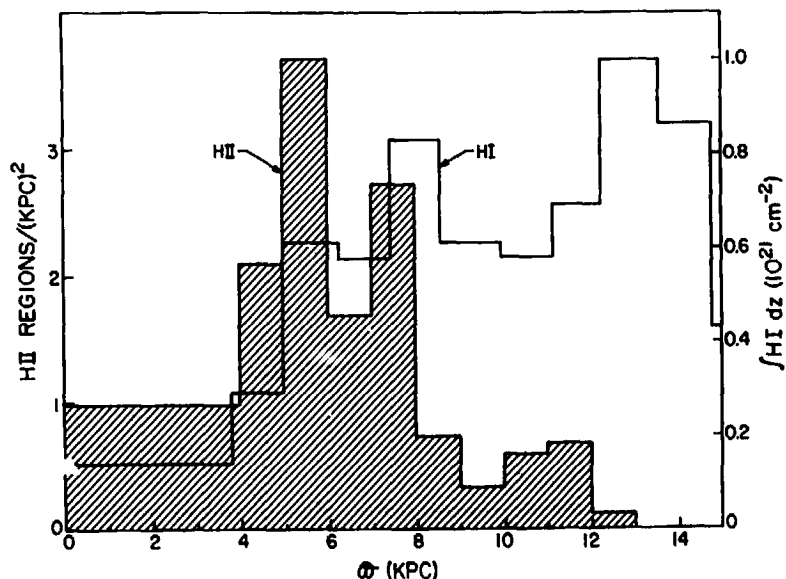


Figure 4: The surface density in giant HII regions (shaded area, Mezger 1970) and free-free continuum radiation (see Figure 16 in Westerhout 1958) show a remarkable similarity to the radial distribution of CO (Fig. 3). In contrast the HI surface density varies little with galactic radius (Van Woerden 1965).

for the discussion at hand, the H_2 distribution is identical to the γ -ray emissivity (Stecker et al. 1975) within observational errors and the uncertainty involved in unfolding the γ -ray longitude distribution. All of these results have been confirmed by the finer spaced, higher sensitivity CO observations of Gordon and Burton (1976) at $b = 0$ and our most recent, higher sensitivity observations in l and b

(Solomon, Scoville, and Sanders 1976).

3. The Thickness of the Molecular Gas Disk

A major shortcoming of the published CO observations when making a comparison with γ -ray data is that the 1 arcminute CO beam observed only the galactic plane, whereas the γ -ray data has a much lower angular resolution - including contributions from over 5° degrees of latitude. Our newest observations and those of Cohen (1976) are, therefore, especially addressed to estimating the thickness of the molecular cloud layer. We have observed along strips perpendicular to the galactic plane from $b = -1$ to $+1^\circ$ every even degree of longitude in the range $l = 0^\circ$ to 50° . Though we have yet to fully analyze these new observations, samples in the form of integrated line intensities are shown in Figures 5 and 6 and tabulated in Table 1.

Interpreting the intensity integral as a proportional indicator of the molecular column densities we may use this data for estimating both the thickness and the central latitude of the clouds. The full width in latitude to half-intensity varies from 0.7° to 1.0° (excluding $l = 0^\circ$). The mean latitude of this emission significantly deviates from the galactic plane in the longitude range 20° to 40° where $\langle b \rangle \approx -0.2$ and most of the emission integral is contributed by gas in the 4-8 kpc ring. This amounts to a displacement $\langle Z \rangle$ of 40 pc below the plane. From the latitude thickness of the emission observed near the terminal velocity* at many longitudes $l = 10 - 50^\circ$ we have estimated that half-density points on either side of the plane are separated by 105 ± 15 pc at radii 4 - 8 kpc. This is in agreement with the crude value of 130 pc found in our earlier survey (Scoville and Solomon 1975) and the estimate of 118 pc found by Burton and Gordon (1976) from data at $l = 21^\circ$. A more sophisticated analysis of the data at all longitudes is planned in order to search for systematic variations of the scale height with galactic radius (Solomon, Scoville, and Sanders 1976).

Perhaps a most relevant quantity against which one should compare the γ -ray observations is the double integral of the line intensity over all velocities and over galactic latitude (last column of Table 1). That the longitude

*Emission at the highest positive velocity in each line-of-sight with $l < 90^\circ$ is produced at the point of closest approach to the galactic center. Therefore, the distance to gas producing emission at these "terminal" velocities is unambiguous.

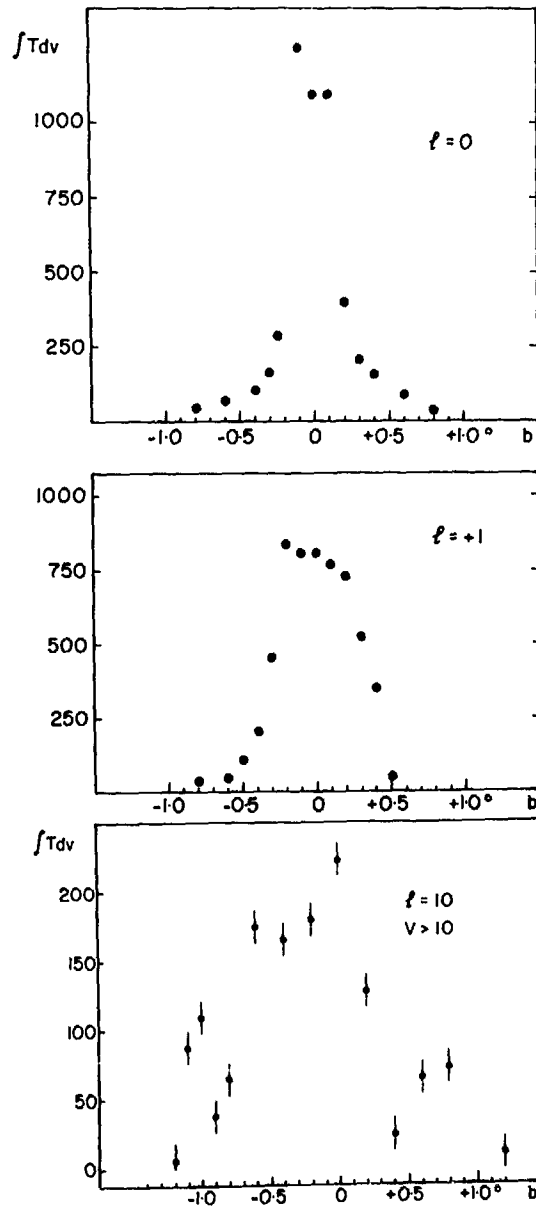


Figure 5: The distribution of integrated CO intensity $\int T_A dV$ in $^{\circ}\text{K}\cdot\text{Km s}^{-1}$ is shown perpendicular to the galactic plane at $l = 0, 1, \text{ and } 10^{\circ}$.

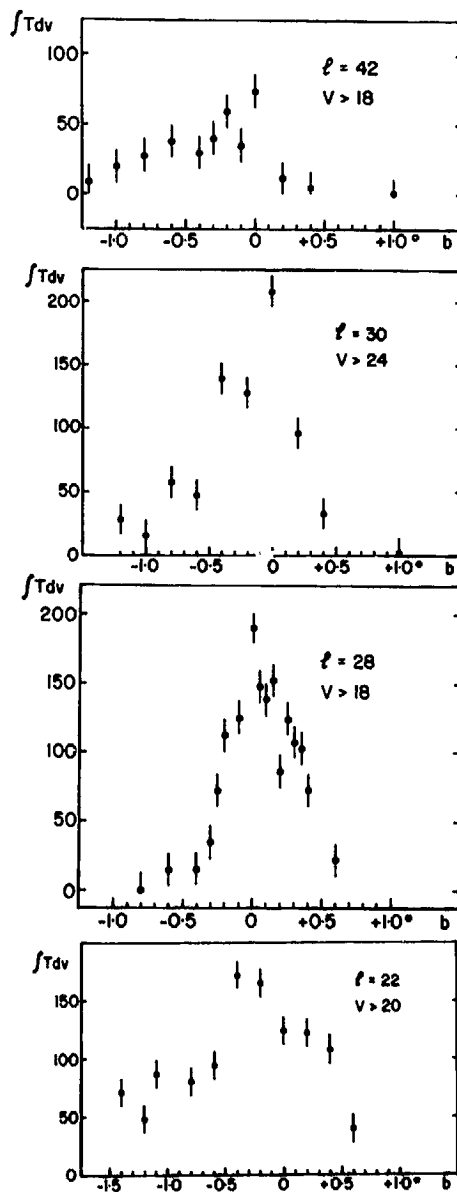


Figure 6: The distribution of integrated CO intensity $\int T_A dv$ in $^{\circ}\text{K}\cdot\text{Km s}^{-1}$ is shown perpendicular to the galactic plane at $\ell = 22^{\circ}$, 38° , 42° , and 50° .

Table 1

Sample Data on the Latitude Distribution of CO Emission

ℓ	$\int T_A dV$ at $b = 0^\circ$ ($K \cdot km s^{-1}$)	$\langle b \rangle$ ($^\circ$)	$\int db \int T_A dV$ ($10^{30} \cdot K \cdot km s^{-1}$)
0°	1200	0	29
1°	775	0	31
10°	200	-0.2	15
22°	170	-0.3	13
30°	200	-0.1	7.4
36°	110	-0.2	4.4
42°	70	-0.3	3
50°	37	-0.1	1

dependence of this double integral is similar to the longitude distribution of 100 Mev γ -ray emission argues most persuasively in favor of the γ -rays being produced within molecular clouds. Indeed this is perhaps the most direct, straightforward comparison one can make. The alternative of comparing the radial distributions of γ -ray and CO emissivities which we have used in the past requires an assumption of azimuthal symmetry about the galactic origin. For a mere comparison of the two observations, the unfolding of both sets of data (in different ways) does not gain anything.

4. The Galactic Center

One enigma in the comparison between CO and γ -ray emissions still remains. Within the inner 3° of longitude about $\ell = 0^\circ$ there is a system of very dense, massive clouds. Here the integrated CO emission is therefore 2-3 times the value at $\ell = 10$ to 30° (Figure 7 and Figure 5) yet the γ -ray emission varies less than 50% over the same longitudes. In interpreting the CO emission elsewhere in the galactic plane, it was convenient to imagine that all clouds had a similar kinetic temperature which was slightly above the observed brightness temperatures. One could justify this assumption

observationally on the basis that all lines observed were weak (most had $T_A < 4^\circ\text{K}$). However, in the galactic center clouds the assumption is clearly not valid inasmuch as several of the CO features have $T_A \geq 20^\circ\text{K}$. In this region there are also several infrared sources (eg. Hoffman et al. 1971) of sufficiently high luminosity to heat the dust and gas to $\geq 30^\circ\text{K}$. And if the CO transition is close to thermalization, a change in T_K can bring about an equal change in the observed $T_A(\text{CO})$ without any change required in n_{H_2} (see §1). We therefore judge that the increase in CO emission going from $l > 3^\circ$ to $l < 3^\circ$ does not accurately reflect column density variation but instead is due largely to kinetic temperature changes. We have previously obtained the total mass $4 \cdot 10^7 - 10^8 M_\odot$ of H_2 inside $l = 3^\circ$ from analysis of detailed CO and ^{13}CO observations there (Scoville et al. 1974).

5. Molecular Cloud Densities and Mass

An important feature of the molecular hydrogen distribution, as deduced from the CO observations, is the extreme concentration of gas into clouds. The fraction of space filled by clouds is approximately 0.007 near the peak in the 4-8 kpc region with a mean molecular hydrogen density within the clouds of 670 cm^{-3} corresponding to a smoothed-out density of $2-5 \text{ cm}^{-3}$ (see Figure 3 and Scoville and Solomon 1975). The corresponding number derived by Gordon and Burton (1976) is 2 cm^{-3} .

The relative abundance of CO within clouds is $[\text{CO}/\text{H}_2] \approx 3 \cdot 10^{-5}$. This abundance ratio must itself depend on the density and opacity of the cloud. Low density or low opacity clouds of the type observed by the Capernicus satellite (cf. Jenkins in this symposium) have a much lower $[\text{CO}/\text{H}_2] \sim 10^{-8}$ and therefore have much weaker CO emission per H_2 molecule. The mass of H_2 in these low opacity clouds is an additional component to that determined through millimeter wave CO surveys.

Combination of the measured width and density estimate ($4 \text{ H}_2 \text{ cm}^{-3}$) yield a mass density of $25 M_\odot \text{ pc}^{-2}$ at 5.5 kpc (see Figure 3). And integrating this surface density function over the galactic disk, we find a total mass of $3 \cdot 10^9 M_\odot$ in interstellar H_2 interior to the solar circle.

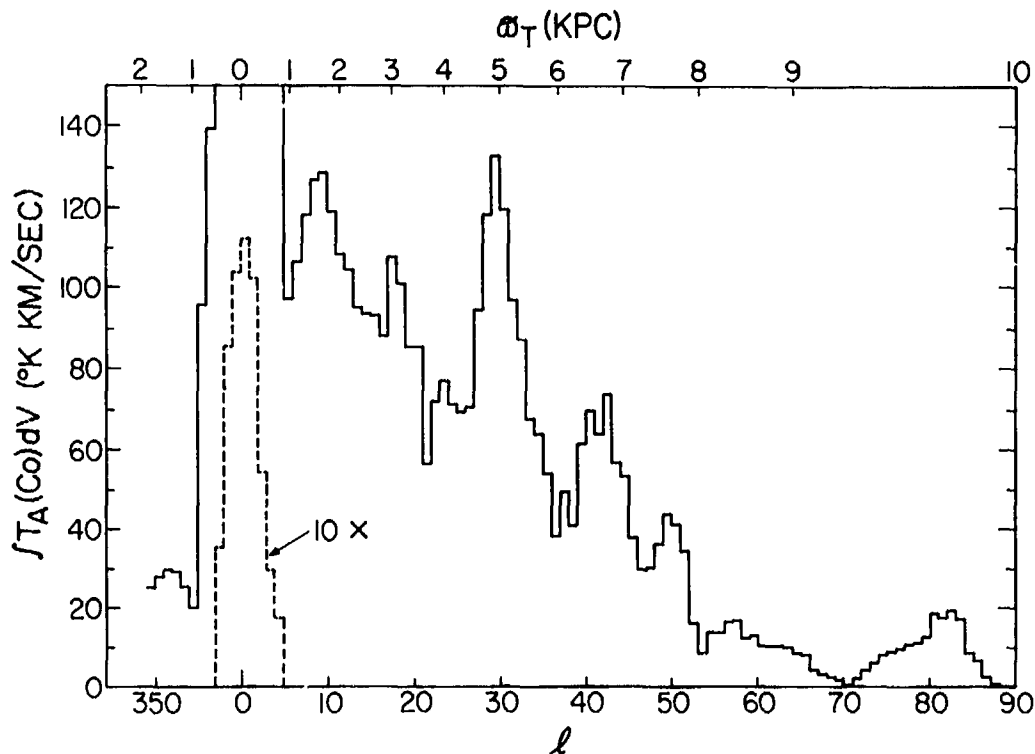


Figure 7: The very strong emission from the galactic center may be appreciated in this graph of integrated intensity as a function of galactic longitude at $b = 0$.

This is Contribution #232 of the Five College Observatories. The research of Nicholas Scoville is partially supported by NSF Grant MPS73-04949.

REFERENCES

- Burton, W. B., Gordon, M. A., Bania, T. M., and Lockman, F. J. 1975, Ap. J., 202, 10.
- Burton, W. B. and Gordon, M. A. 1976 (preprint).
- Cohen, R. 1976, Ph.D. Thesis, Columbia University.
- Fichtel, C. E., Hartman, R. C., Kniffen, D. A., Thompson, D. J., Bignanni, G. F., Ögelman, H., Özel, M. F., and

- Tümer, T. 1975, Ap. J., 198, 163.
- Gordon, M.A. and Burton, W. B. 1976 (preprint).
- Hoffman, W. F., Frederick, C. L., and Emery, F. J. 1971, Ap. J. (Letters), 164, L23.
- Lockman, F. J. 1976, Ap. J. (in press), 15 October.
- Mezger, P. G. 1970, IAU Symposium 38, The Sprial Structure of Our Galaxy, ed. W. Becker and G. Contopoulos (Dordrecht: Reidel), p. 107.
- Scoville, N. Z., Solomon, P. M., and Jefferts, K. B. 1974, Ap. J. (Letters), 187, L63.
- Scoville, N. Z. and Solomon, P. M. 1974, Ap. J. (Letters), 187, L67.
- Scoville, N. Z. and Solomon, P. M. 1975, Ap. J. (Letters), 199, L105.
- Scoville, N. Z. 1975, Symposium on HII Regions, ed. D. Downs and T. L. Wilson (Kleinwalsertal), p. 513.
- Solomon, P. M., Scoville, N. Z., and Sanders, D. B. 1976 (in preparation).
- Spitzer, L., Drake, J. F., Jenkins, E. B., Morton, D. C., Rogerson, J. B., and York, D. G. 1973, Ap. J. (Letters), 181, L116.
- Stecker, F. W., Solomon, P. M., Scoville, N. Z., and Ryter, C. E. 1975, Ap. J., 201, 90.
- Taylor, J. H. and Hulse, R. A. 1976, Ap. J. (in press).
- Van Woerden, H. 1965, Trans. IAU, 12A, 789.
- Wannier, P. G., Penzias, A. A., Linke, R. A., and Wilson, R. W. 1976, Ap. J., 204, 26.
- Westerhout, G. 1958, B.A.N., 14, 215.

N 76 - 291 23

REMARKS ON THE OVERALL DISTRIBUTION OF HYDROGEN IN THE GALACTIC DISK

W. B. Burton, National Radio Astronomy Observatory,* Green Bank,
West Virginia 24944

ABSTRACT

Several current problems concerning the overall distribution of hydrogen in the Galaxy are discussed in general terms. These problems include the degree of saturation characterizing low-latitude emission observations of HI, and the optical-depth corrections to the derived column and volume densities; the amount of fine-scale velocity and spatial structure diluted by the instrumental limitations of the presently available surveys; and the general problem of detailed mapping of the HI in the Galaxy. Comparison is made between the distribution of HI and that of CO and several other galactic tracers. Atomic hydrogen is unique in its distribution, instead of being typical of many Population I constituents. The galactic disk as defined by atomic hydrogen has a diameter fully twice as large as that defined by the ionized and molecular states of hydrogen, as well as by other molecules, supernova remnants, pulsars, γ -radiation, synchrotron radiation, and the youngest stars. It is also less confined to the galactic equator than most of the other constituents. The degree of small-scale structure apparent in the molecular observations is much greater than in the HI observations. Parameters describing the small-scale structure have been determined using Monte Carlo techniques to simulate the observations.

* Operated by Associated Universities, Inc., under contract with the National Science Foundation.

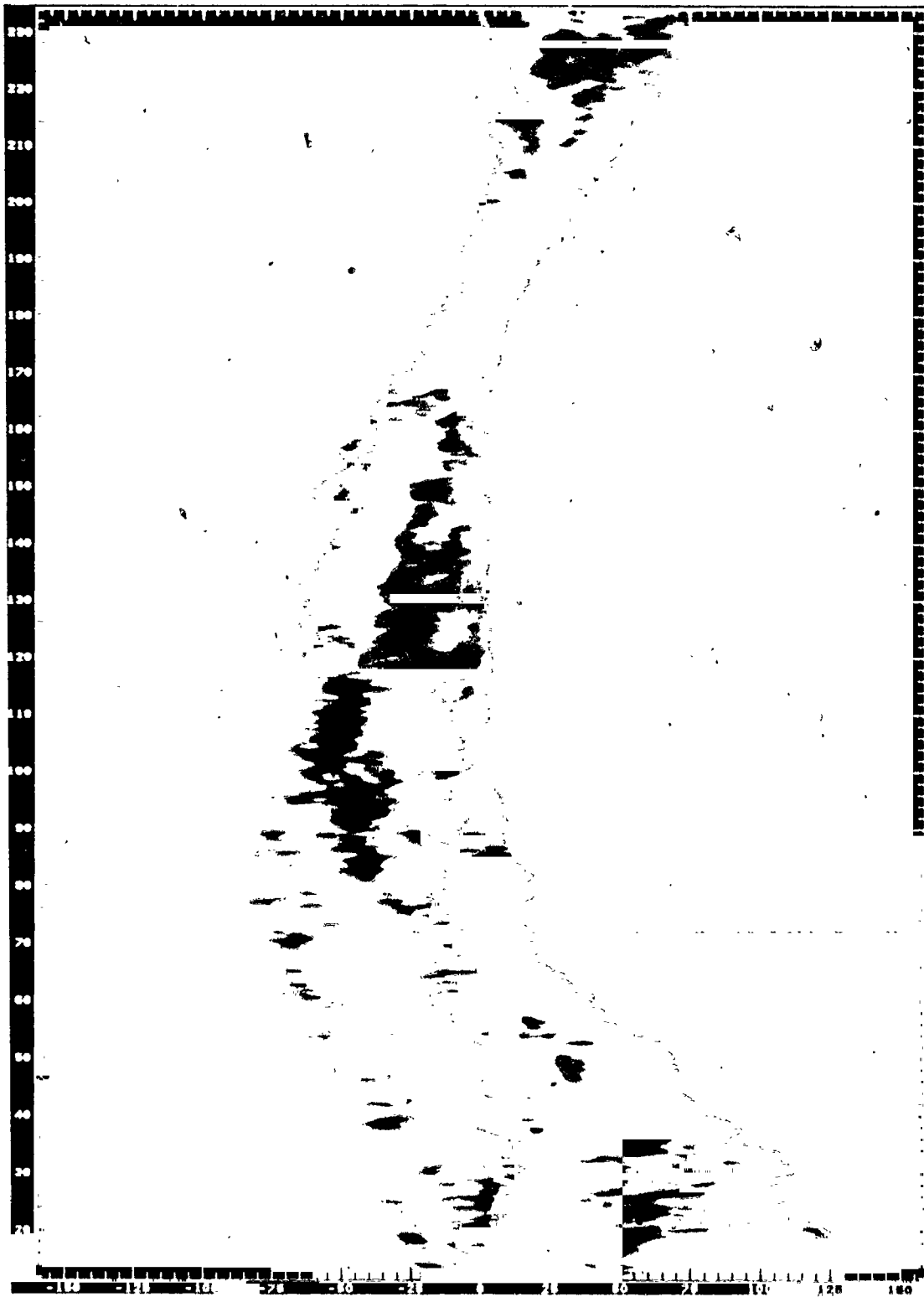
1. Observations of the $\lambda 21$ -cm Line of Atomic Hydrogen. A spectral line of wavelength 21 cm is produced by the well-known hyperfine transition of neutral atomic hydrogen (HI). Observations of this line give intensity, usually expressed as either antenna or brightness temperature, as a function of frequency Doppler-shifted from the line's natural frequency of 1420.406 MHz. The measured frequency shifts are converted to radial velocities ($1 \text{ km s}^{-1} = -4.74 \text{ kHz}$ at $\lambda 21 \text{ cm}$) usually expressed, in Milky Way studies, with respect to the local standard of rest. Observational parameters of the major low-latitude HI surveys have been tabulated by Kerr (1968), by Burton (1974a,b), and--for the central region of the Galaxy--by Simonson (1974).

Observations from Westerhout's (1973) high-resolution survey of the galactic disk are represented in Figure 1 and show HI emission from the portion of the galactic equator accessible to the NRAO 91-m telescope. These observations illustrate the ubiquitous distribution of atomic hydrogen in the Galaxy. HI emission can be observed easily in any direction on the sky, and, although transformation from the observed velocity distribution to a spatial arrangement is very difficult, no region in the galactic disk has been identified as empty of HI.

2. Motions Affecting the $\lambda 21$ -cm Line. A number of mechanisms broaden the 21-cm line from its negligibly small natural width of $10^{-16} \text{ km s}^{-1}$. The overall width of the HI line is determined at low latitudes by differential galactic rotation and is typically 150 km s^{-1} . To an approximation valid to first order over most of the Galaxy, the motions of material are such that the linear rotational velocity, $\Theta(R)$, depends only on distance, R , from the galactic center. The rotation curve for $R < R_0$ has been gotten from 21-cm observations. The method (reviewed by Burton 1974a) involves measuring the terminal velocities, v_t , contributed by material on the locus of subcentral points, where $R = R_{\min} = R_0 |\sin \ell|$, and where the linear rotational velocity is directed entirely along the line-of-sight. The observationally derived rotation curve is $\Theta(R_0 |\sin \ell|) = |v_t| + \Theta_0 |\sin \ell|$, where Θ_0 and R_0 refer to the observer's location.

Terminal velocities derived from 21-cm measurements at $b = 0^\circ$, $\Delta \ell = 0.2$, are plotted in Figure 2. The line in the figure represents the terminal velocities predicted by the smooth rotation curve tabulated by Gordon and Burton (1976). Deviations of the observed terminal velocities from this line should be attributed to deviations from circular rotation (see Shane and Bieger-Smith 1966). The deviations

Figure 1. Grey-scale representation of HI emission intensities in longitude-velocity coordinates at $b = 0^\circ$, $11^\circ < \ell < 234^\circ$, constructed from Westerhout's (1973) observations.



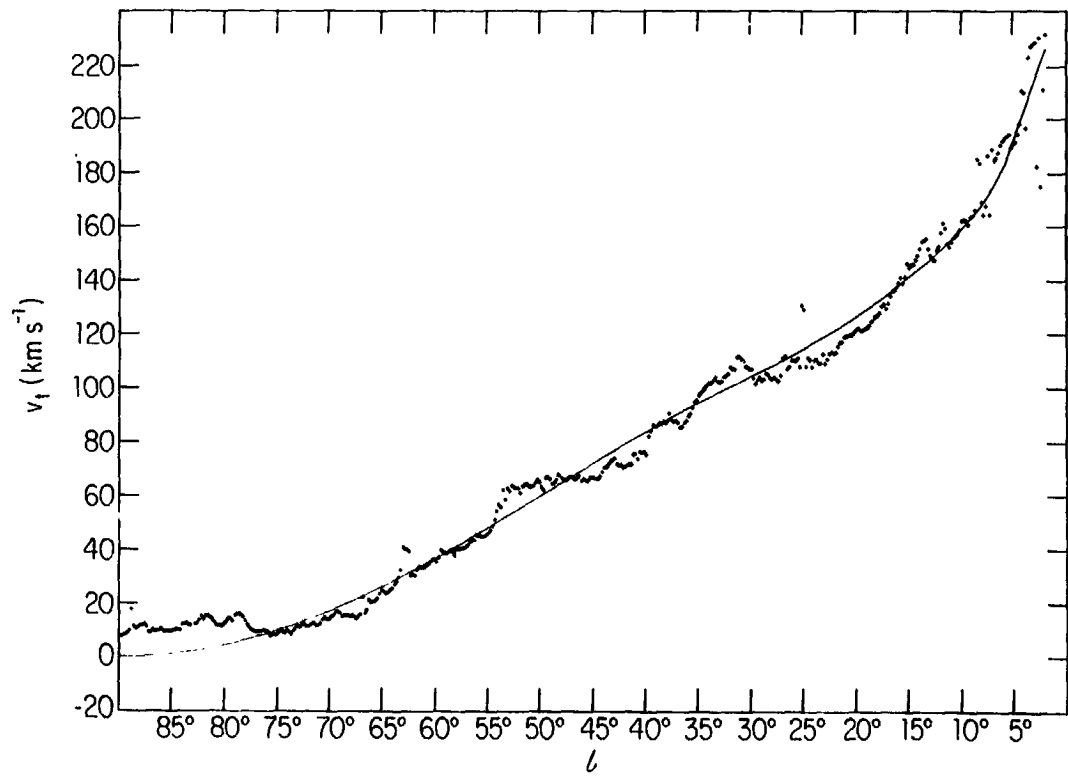
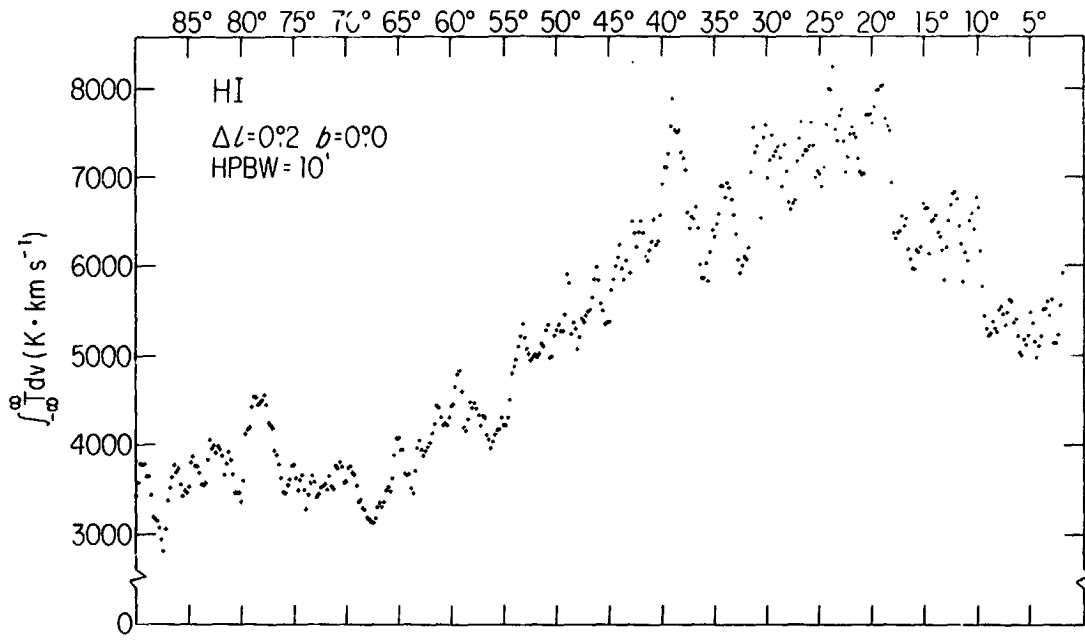
which are not systematic over more than a degree or two of longitude can mostly be associated with known HII regions. The deviations which show a systematic trend over more than several degrees are apparently streaming motions induced by the gravitational torque of large-scale density fluctuations in the overall galactic mass distribution (Barbanis and Woltjer 1967, Yuan 1969, Burton and Shane 1970, Burton 1971). Indeed, these irregularities provide the most convincing direct evidence for the validity in our Galaxy of the density-wave theory. Other arguments motivated by the 21-cm observations are less direct. The density-wave itself has not been directly studied since the expected 5% mass variation (Lin et al. 1969) in the old to moderately old disk stars is not detectable with present techniques. Some of the observational consequences of this theory for our Galaxy have been reviewed recently by Burton (1973; 1974a,b; 1976), Wielen (1974), W. W. Roberts (1975), and Kaplan and Pikel'ner (1974).

If it is correct that the two major perturbations in the v_t longitude variation are due to motions induced by spiral arms, then the locations of these perturbations at $l \approx 52^\circ$ and $l \approx 35^\circ$ provide the tangent directions to two spiral arms. This quite circumstantial evidence seems to be the best from 21-cm observations for the existence of spiral arms in our Galaxy, at least in the portion of it at $R < R_0$.

The terminal velocities derived from observations in the longitude quadrant $270^\circ < l < 360^\circ$ show irregularities somewhat differently placed, although of about the same amplitude, as those found from the northern-hemisphere observations. There is also a well-known systematic difference between the two sides of the Galaxy of about 7 km s^{-1} over the subcentral-point region between $R = 5$ and 8 kpc (Kerr 1969). Manabe and Miyamoto (1975) discuss attempts to find a dynamical explanation of this kinematic asymmetry.

Streaming motions of the sort which influence the terminal velocities are known from a wide variety of observations to be common throughout the Galaxy. Although the amplitude of these motions, $\sim 5\text{--}8 \text{ km s}^{-1}$, is only about two or three percent of the rotational velocity of the Galaxy, their occurrence nevertheless has a profound influence on the appearance of the observed 21-cm profiles. Thus the shape of any observed HI profile can be modelled, with no fluctuations in the hydrogen density, by suitable--and plausible--adjustments to

Figure 2. Upper panel: Variation with longitude of the total-velocity integrals $\int Tdv$ calculated from the HI observations of Westerhout (1976). Lower panel: Variation with longitude of the terminal velocities, representing material along the locus $R_0 \sin l$. The full-drawn line corresponds to the perturbation-free rotation curve tabulated by Gordon and Burton (1976). →



the galactic velocity field (Burton 1971, 1972; Tuve and Lundsager 1972). Although density fluctuations are bound to be present, the kinematic irregularities of the sort known to be present throughout the Galaxy play a predominant role in determining the shape of the observed profiles.

3. Detailed Mapping of the HI Spatial Distribution. One of the major results sought from observations of HI emission is a transformation of features in the observed intensity-velocity profiles to the corresponding spatial distribution of HI density in the Galaxy. The procedures involved in making this transformation require that the profiles be decomposed into physically significant individual features, that these features are contributed directly by density concentrations in space, and that the velocity field is well enough known in advance that accurate kinematic distances can be derived. These requirements are very difficult to satisfy. Isolation of individual features in the heavily blended low-latitude profiles is itself in general a tedious chore, producing results which in many cases are somewhat tentative. Even after the separation is accomplished (obviously a necessary first step to detailed mapping), the relative contributions of the various physical parameters to the separated profile features remain problematic. If the motions are gravitationally induced in the sense of the linear density-wave theory, the resulting spectral feature will furthermore in general occur at a velocity in the profile different from that corresponding to the center of HI mass of the structural feature (Burton 1972). If the motions are those predicted by the non-linear density-wave theory, one structural feature can contribute multiple peaks to the intensity-velocity profile (W. W. Roberts 1972). Variations in the effective HI temperature can also influence the appearance of the line profiles; structural features could even appear as minima instead of as peaks in the profiles in some directions in the not implausible situation that cold clouds are concentrated near minima of the gravitational potential. Line profiles also show some features which result simply from the geometry of the transformation from space to velocity coordinates (Burton 1971). Examples of such model-independent features apparent in Figure 1 include the intensity-ridge near $v = 0 \text{ km s}^{-1}$ at $l < 90^\circ$, the persistently enhanced intensities near the maximum velocities at $l < 90^\circ$, the pseudo-feature centered on $l \sim 75^\circ$, and the enhanced intensities near $l = 180^\circ$.

These procedural difficulties do not mean that the structural characteristics of low-latitude HI are inaccessible, although it does seem important that the definiteness of the 21-cm derived picture of our Galaxy's spiral structure not be over-rated. In general a grand-design of a spiral nature in the overall HI distribution is not yet established. In particular there is little comprehensive evidence for a spiral structure of HI concentrations at $R < R_0$, where because of the double-valuedness of the velocity-distance relationship, the procedural difficulties become more important. Values applicable on a galactic

scale for the spiral arm tilt angle, radial separation, and arm-interarm density contrast are indirectly available from 21-cm observations, although the specific values depend on the validity of working hypotheses, on extrapolation over large portions of the Galaxy, or on theoretical justifications. It is also not clear how representative the solar region ($r \approx 1$ kpc) is of the Galaxy as a whole. Thus there is no consensus (but many opinions) on the location of the Sun with respect to the nearest spiral arms; specification of our location in the overall galactic design is important if, as seems plausible, the parameters of the interstellar medium are regulated by passage of a spiral density wave and the associated compression zone. It is worth noting, however, that the mapping difficulties are primarily procedural. The kinematic irregularities characteristic of our galaxy are remarkably less severe than those commonly found in other spiral galaxies (see e.g., Bottinelli 1971). Similarly, the Galaxy is found to be quite symmetric on a large scale (relative to the situation pertaining in many other spiral galaxies) when comparison of the total velocity extent, or of the total integrated emission, is made between data measured at $b > 0^\circ$ with that at $b < 0^\circ$, or when data at $0^\circ < \ell < 180^\circ$ is compared with that at $180^\circ < \ell < 360^\circ$.

4. HI Column and Volume Densities Near the Galactic Plane. The HI column density is given by $N_{\text{HI}} = 1.823 \times 10^{18} \int T_k \tau(v) dv \text{ cm}^{-2}$ and is in general not a measured quantity because the kinetic gas temperature, T_k , and the optical-depth profile, $\tau(v)$, generally are not measurable. Only in the case of a profile optically thin at all velocities does N_{HI} become directly measurable through the profile integral $\int T_B(v) dv$, since in this case the observed brightness temperature profile, $T_B(v) = T_k (1 - \exp(-\tau(v)))$, is $\approx T_k \tau(v)$. The volume density smoothed over a path of length Δr is gotten from $\int T_B(v) dv / \Delta r$. Densities derived under the assumption of spectral thinness will underestimate the true amount of HI. The degree of saturation depends strongly on the characteristics of the space-to-velocity transformation inherent in the observations, and thus on longitude and latitude. In the limiting case of complete saturation, $T_B(v) = T_k$, and $\int T_B(v) dv / \Delta r = T_k \left| \frac{\Delta v}{\Delta r} \right|$, where Δv is the velocity extent of the portion of the profile considered. The arrangement of the geometrical parameter $\left| \frac{dv}{dr} \right|$ in the galactic disk is what determines, through "velocity-crowding", the model-independent profile features mentioned in the preceding section. For example, as $\ell \rightarrow 0^\circ$, $\frac{dv}{dr} \rightarrow 0^\circ$ over most of the line of sight; the increasing saturation results in the decreasing values of the total profile integrals plotted in Figures 2 and 3 at low ℓ . The condition of optical thinness is probably encountered only for certain velocity segments of most 21-cm profiles observed near the galactic plane, although at higher latitudes, $\tau(v) < 1$ is a realistic first approximation.

The spatial distribution at $|b| \leq 10^\circ$ of the profile integrals derived from observations made by Weaver and Williams (1973) is plotted in Figure 3. At these latitudes, $\tau(v) \approx 1$ is not uncommon, so that

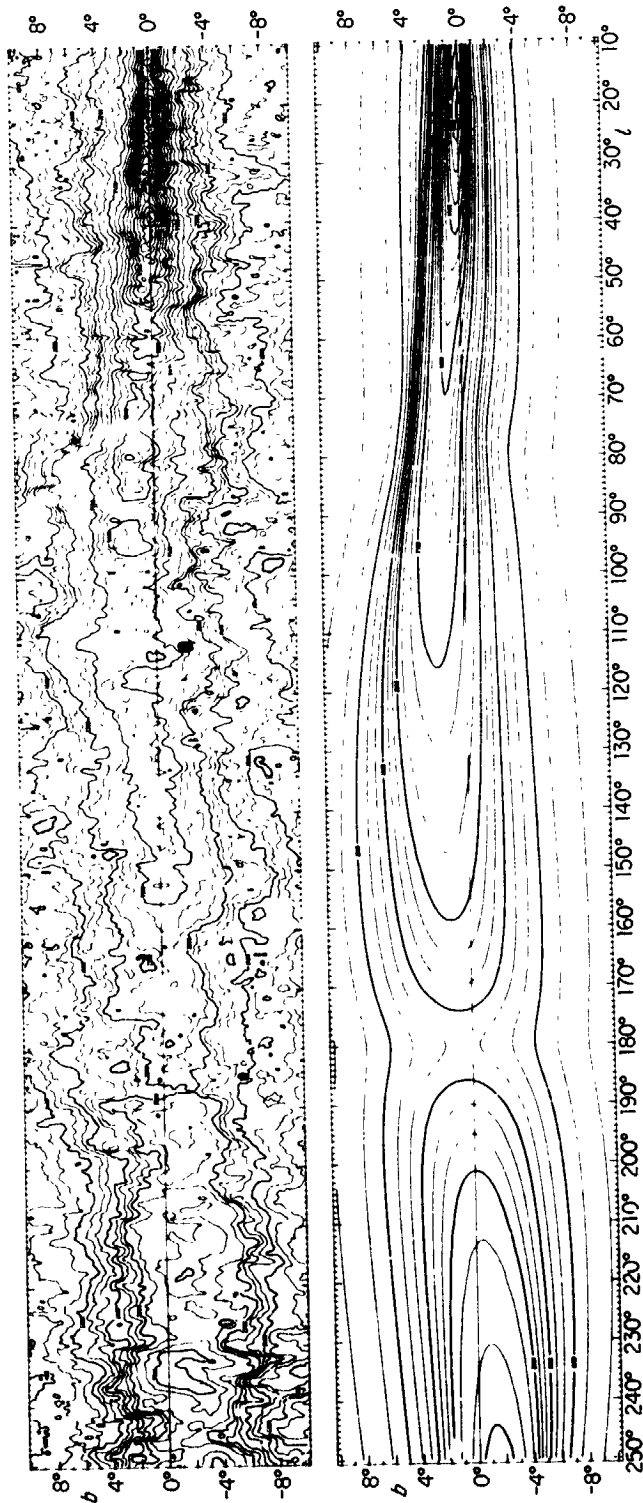


Figure 3. Upper panel: Arrangement on the plane of the sky of the total-velocity integrals $\int Tdv$ calculated from the HI observations of Weaver and Williams (1973). Lower panel: Arrangement on the plane of the sky of the total-velocity integrals $\int Tdv$ calculated from synthetic HI profiles. The parameters describing the model HI gas and its distribution are those given by Baker and Burton (1975).

optical depth effects become important. An estimate of the degree of saturation in fact characterizing the low-latitude HI profiles can be found from the controlled conditions inherent in synthetic profiles. Many aspects of the projection on the plane of the sky of HI emission observed at low latitudes are approximately reproduced by synthetic profiles accounting for the radiative transfer effect of a smooth distribution of gas with $T_k = 120$ K, a peak density $n_{\text{HI}} = 0.33 \text{ cm}^{-3}$, rotating according to a basic rotation curve corresponding to the smooth line in Figure 2, with the z -distribution given by Baker and Burton (1975). The total-velocity integrals from such synthetic profiles are shown in the lower panel of Figure 3. The overall distribution of the synthetic-profile integrals is approximately the same as the observed overall distribution of the total-velocity integrals plotted in Figure

3. Thus the saturation characteristics known for the model profiles can be used to determine corrections which should be applied to the observed profile integrals to give volume and column densities.

The volume density $n_{\text{HI}}(R)$ and the line-of-sight column density $N_{\text{HI}}(\ell)$, corrected for the effects of partial saturation, are plotted in Figure 4. These quantities refer to the locus of latitudes where the total profile integral in the Figure 3 observations is largest. The correction for partial saturation is greater at $R < R_0$ because of the double-valued nature there of the velocity-space relationship. The (beam-smoothed) density of the neutral hydrogen gas remains roughly con-

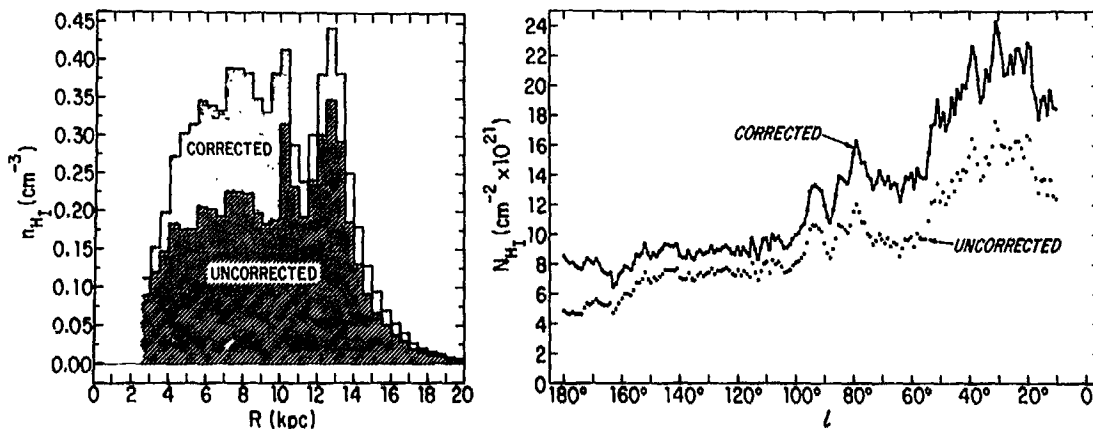


Figure 4. Large-scale distribution of HI volume and column densities in the Galaxy. The densities labelled "corrected" contain an adjustment for optical-depth effects determined from the controlled conditions inherent in model-fitting. The values refer to the latitudes of maximum $\int Tdv$ of the observations in Figure 3. Substantial densities of HI exist at $R > 10$ kpc and at $l > 90^\circ$, contrary to the situation pertaining for many other disk-population constituents.

stant over the major part of the galactic disk. This is in marked contrast with the distribution of total mass density, which increases strongly toward the galactic center. The HI decrease in the inner parts is a characteristic the Galaxy shares in common with all other spiral galaxies for which projected HI surface densities have been measured (M. S. Roberts 1974). In particular, the corrected $n_{\text{HI}}(R)$ distribution for our Galaxy has quite the same form as that observed in the nearby spirals M31 (M. S. Roberts 1974) and M81 (Rots 1975).

5. Beam Dilution in Low-Latitude HI Profiles. Although HI emission measurements sample long lengths of path through the galactic layer, the heavily blended nature of the profiles is such that individual small-scale structure is evident at low latitudes only in special cases. The bulk of the information on the details of the interstellar medium is derived from observations of the solar neighborhood. This limitation is arbitrary, being imposed on most optical measurements by extinction and, at $\lambda 21$ cm, by the relative simplicity of high-latitude profiles. Analyses of high-latitude profiles routinely allow for a wide range of temperatures, densities, and sizes of emitting HI regions (see reviews by Heiles 1974 and by Verschuur 1974).

All of the major surveys of HI galactic disk emission have been made with beamwidths varying from about 12' (300-foot telescope) to $\sim 1^\circ$ (60-foot telescope), and with velocity resolutions generally about 2 km s^{-1} . These beamwidths correspond at a distance of 5 kpc to lengths of 17 pc and 87 pc, respectively. It is not yet completely clear to what extent the limitations of angular and spectral resolution have affected the analyses of these surveys. The limitations imposed by the angular resolution seem the more important. Thus very little additional structure appears in a conventional beam if the spectral resolution is increased beyond 2 km s^{-1} . This practical limitation on the necessary spectral resolution is illustrated by Figure 5, where profiles are plotted which were measured with a velocity resolution of 0.17 km s^{-1} (Lockman and Burton 1976). No fine-scale structure is revealed by these measurements. Indeed, HI spectral features observed at low latitudes rarely have dispersions less than $\sim 3 \text{ km s}^{-1}$; thus, as is generally the case in radio spectroscopy, the widths of individual features are greater than those expected solely from thermal broadening. Unresolved turbulent elements would contribute to the broadening of apparently isolated features.

Substantial additional structure is revealed by measurements made with angular resolution higher than that used in the previously available surveys of HI emission. The newly resurfaced Arecibo 1000-foot telescope offers a 3.5' beamwidth at $\lambda 21$ cm. A comparison is made in Figure 6 between observations made with a 37' beam (Weaver and Williams 1973) and ones made of the same region of the sky, and with the same resolution in velocity, with the Arecibo telescope (Baker and Burton 1976). Although there are many low-latitude structures with angular

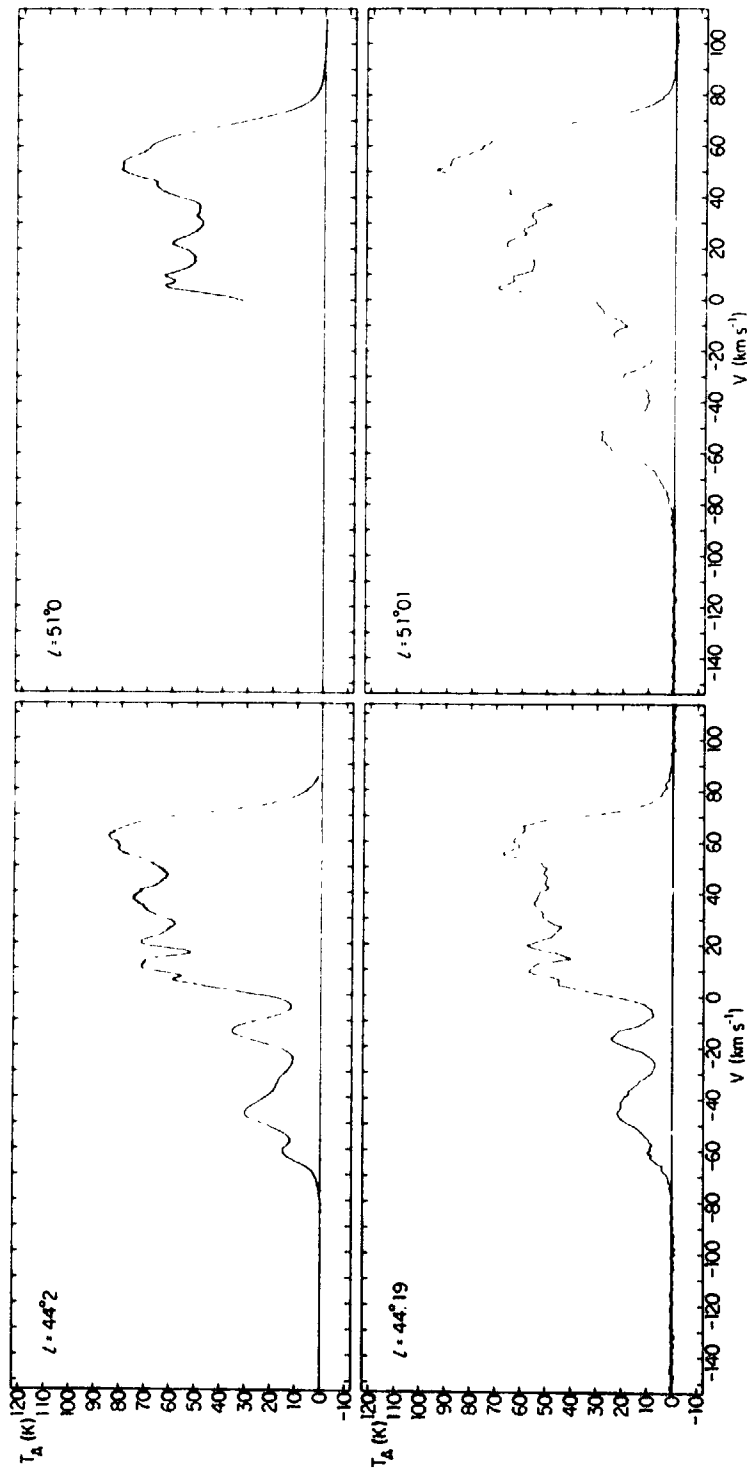
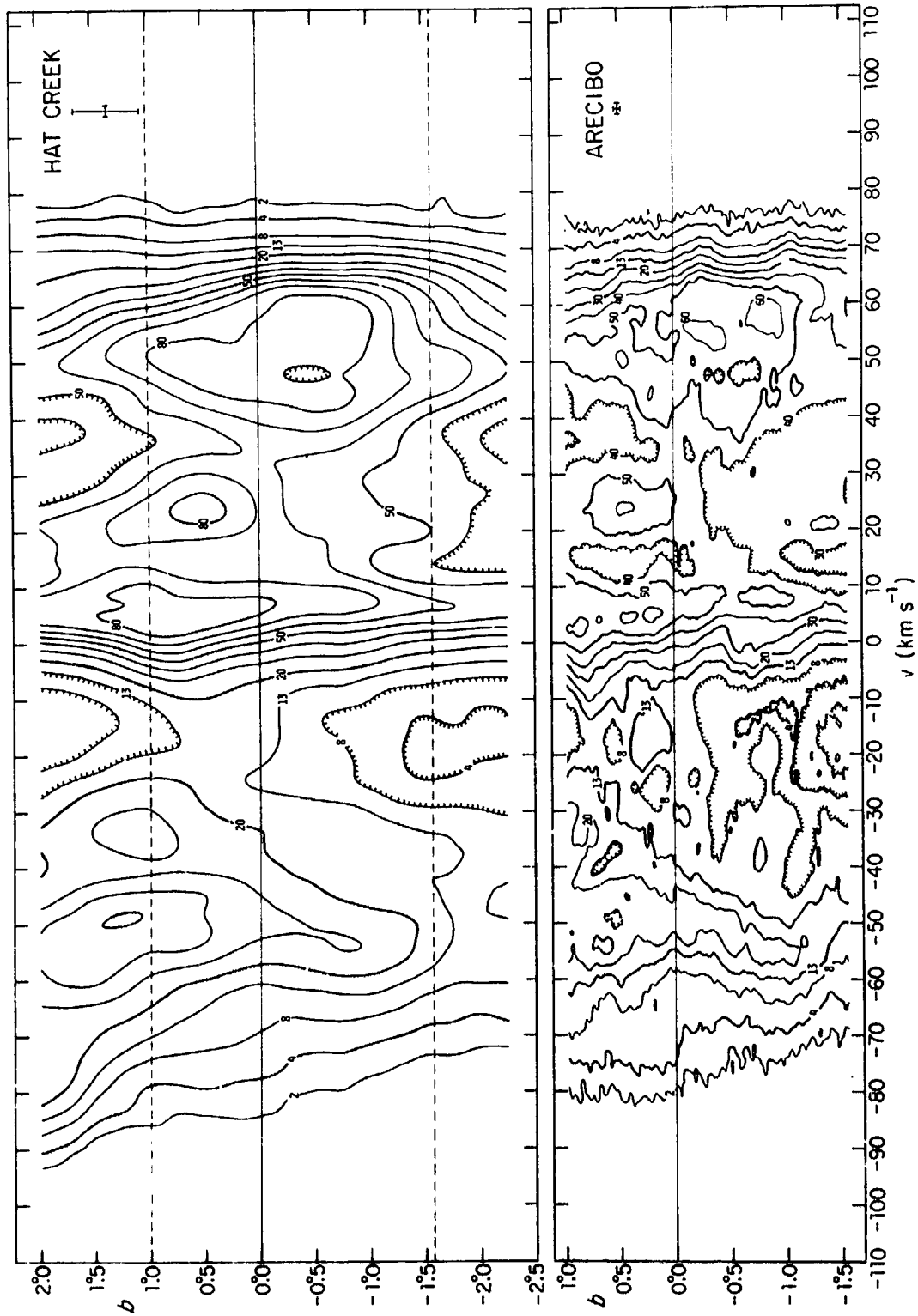


Figure 5. Upper panel: HI profiles observed in the galactic plane at the indicated longitudes with the very high spectral resolution of 0.17 km s^{-1} , using the NRAO 43-m telescope characterized at $\lambda 21 \text{ cm}$ by a $20'$ beamwidth (Lockman and Burton 1976). These profiles show no more detail than corresponding ones observed with the same beamwidth and a spectral resolution of $\sim 2 \text{ km s}^{-1}$. Lower panel: HI profiles observed with 1 km s^{-1} spectral resolution but with the $3.5'$ beamwidth of the Arecibo 1000-foot telescope (Baker and Burton 1976).



←

Figure 6. Comparison showing the widespread occurrence of small-scale HI structures. Upper panel: Latitude-velocity distribution at $l = 52^\circ$ constructed from the 21-cm observations of the Hat Creek survey of Weaver and Williams (1973). The 37' beamwidth and 2.1 km s^{-1} velocity resolution are indicated by the cross in the upper right-hand corner. Lower panel: Latitude-velocity distribution at $l = 52^\circ$ constructed from observations made using the Arecibo 1000-foot telescope (Baker and Burton 1976). The profiles entering the lower panel were smoothed to the same spectral resolution as those in the upper panel. The 3'.5 beamwidth reveals substantial additional structure. At a distance of 5 kpc, representative for low-latitude investigations, 3'.5 subtends a length of 5 pc.

scales greater than 1° (see also Figure 1 and the upper panel of Figure 2), these structures show much fine-scale internal structure. An extensive series of Arecibo observations will provide direct measures (or at least limits) of length-scales of HI emission regions and complexes (Baker and Burton 1976).*

Aspects of this problem have been considered in a less direct way by Baker and Burton (1975). They emphasized that the cold, opaque HI regions revealed in large numbers by absorption measurements (see e.g., Radhakrishnan 1974), which are made against distant continuum sources of vanishingly small angular size, must be strongly beam-diluted in the emission profiles. Otherwise the emission profiles would be saturated; they are observed to be (effectively) optically thin.

6. The Galactic Distribution of Carbon Monoxide and, by Implication, of Molecular Hydrogen. Although 21-cm observations of atomic hydrogen show HI to be an ubiquitous tracer of a number of galactic characteristics, they cannot give the true amount and distribution of interstellar hydrogen. This is partly because cool HI is under-represented in the 21-cm observations, but it is much more important that large amounts of molecular hydrogen do not contribute at all to the 21-cm line. H_2 is the most stable low-temperature form of the most abundant element in the interstellar medium, and undoubtedly predominates over all other material in optically opaque, cool, compressed regions where the molecule is shielded against photo-dissociation after formation on grain surfaces (Solomon and Wickramasinghe 1969, Hollenbach *et al.*

* The National Astronomy and Ionosphere Center is operated by Cornell University under contract with the National Science Foundation. The observations in Figures 5 and 6 represent a preliminary reduction; in particular, the intensity scale is uncalibrated.

1971). H_2 has no observable transition in the radio or in the optical windows. Direct observations of H_2 Lyman absorption bands in the ultraviolet spectra of reddened stars have been made first from rockets (Carruthers 1970) and extensively from the Copernicus satellite (Spitzer *et al.* 1973, Spitzer and Jenkins 1975). Ultraviolet extinction due to interstellar dust limits such observations to material within a kpc or so of the Sun. CO, the next most abundant interstellar molecule, is also concentrated to cool, dense regions where it is self-shielded against radiative dissociation. The most important source of excitation of the CO line involves collisions with H_2 (Goldreich and Kwan 1974, Scoville and Solomon 1974). Thus the observable abundance distribution of CO provides by implication some aspects of the distribution of H_2 .

Observations made along the galactic equator of the $J = 1 \rightarrow 0$ rotational transition of ^{12}CO at ~ 2.6 mm (115 GHz) are shown in Figure 7. The NRAO 11-m telescope has at this wavelength a beamwidth of $65''$; however the effective resolution of Figure 7 is set by the $\sim 12'$ longitude interval between spectra, which is the same as the $12'$ beamwidth of the 91-m telescope at ~ 21 cm characterizing Figure 1. Certain salient characteristics of the CO distribution which distinguish it from the HI distribution are apparent from these observations (see Scoville and Solomon 1975, Burton *et al.* 1975, and Gordon and Burton 1976a).

The most striking difference between the overall HI distribution and that of CO is that the CO flux is much more confined to the inner Galaxy. The relative radial abundance of CO is shown in Figure 8. The mean radius of the distribution is $\bar{R} = 5.9$ kpc; 66% of the accumulated emission originates between 4 and 8 kpc, where the abundance has fallen to its half-maximum level. The abundance distribution is skew, falling off less sharply at $R > 7$ kpc than at $R < 5$ kpc. At $R > 10$ kpc, generally corresponding to the portion of Figure 7 at $l > 0^\circ$, $v < 0$ km s $^{-1}$, very little CO is observed outside of the galactic nucleus. In addition, the CO disk is substantially thinner in the z-direction than the HI disk (see Figure 9).

The radial distributions of several other galactic tracers which can be observed along transgalactic paths are also plotted in Figure 8. Within the uncertainties of the observations, the galactic radial distribution of molecules, distributed ionized hydrogen, giant HII regions, supernova-remnants, pulsars, γ -radiation, and synchrotron radiation are roughly equivalent. The extent of the galactic disk is for HI approximately twice as large as the extent measured for these other tracers. It is clear that the chemical composition and physical state of the interstellar medium show great variations even on a galactic scale. It is necessary to distinguish between compressed material, confined to the inner Galaxy and representing recent or current phenomena, and

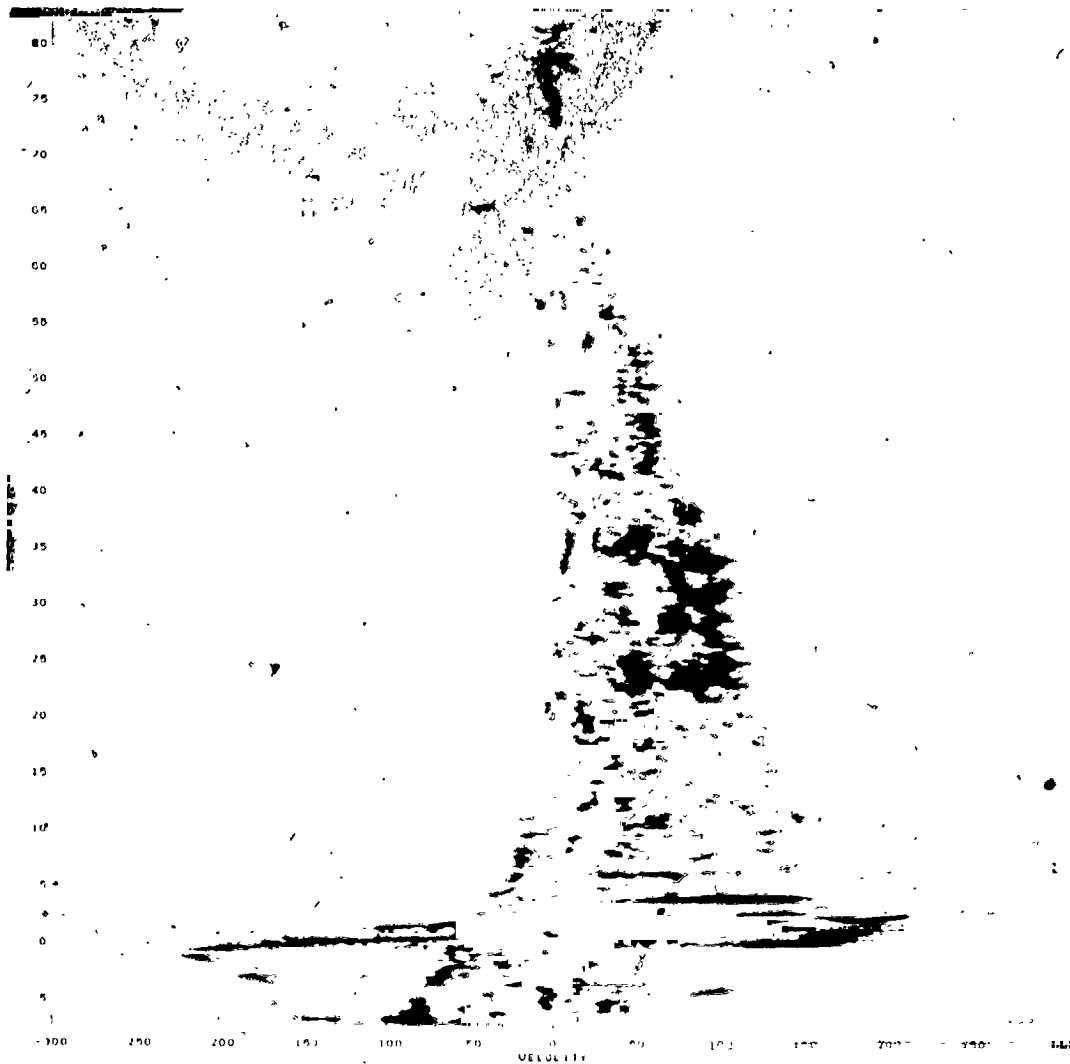


Figure 7. Longitude-velocity arrangement of $^{12}\text{C}^{16}\text{O}$ emission observed along the galactic equator. Little CO emission is seen in the portions of this figure corresponding to $R > 9$ kpc (except for the exceptional Cygnus region) and to $R < 4$ kpc) except for the exceptional 3-kpc arm and the intense nuclear sources). The observations at $l < 10^\circ$ are due to Bania (1976), those at $10^\circ < l < 36^\circ$ to Gordon and Burton (1976), and those at $l > 36^\circ$ to Burton and Gordon (1976b).

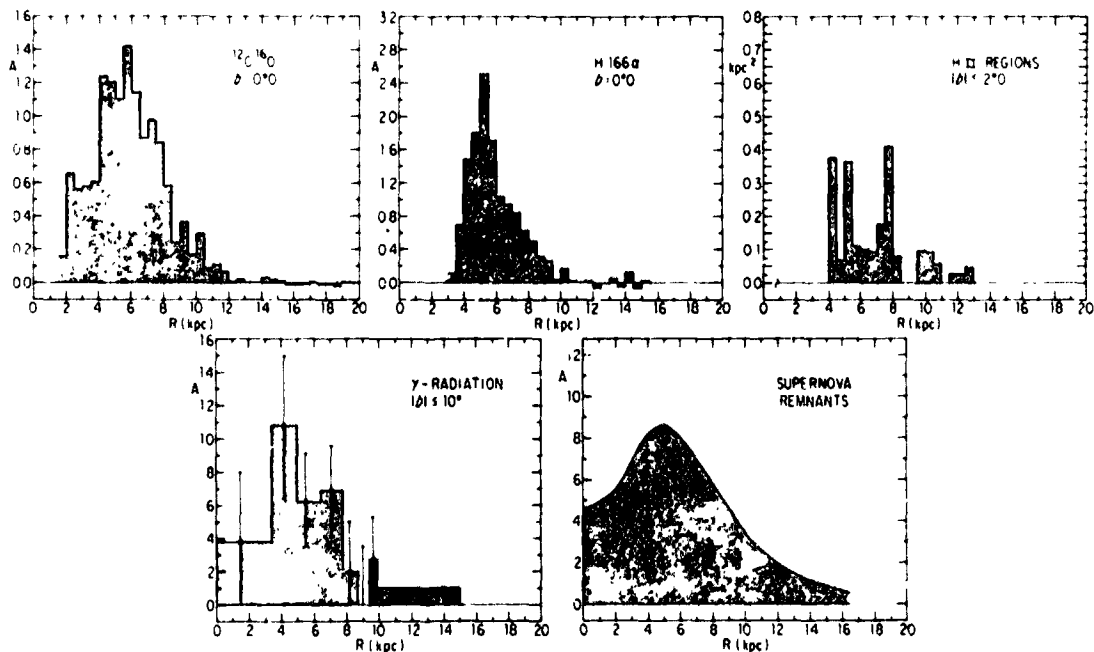


Figure 8. Radial distributions of several constituents of the galactic disk. The CO distribution is from Gordon and Burton (1976), the H166 α distribution is from Lockman (1976), and that for the giant HII regions from a compilation by Burton et al. (1975); only data at $l > 0^\circ$ enter these distributions. The γ -ray distribution (Strong 1975) and that for supernova remnants (Kodaira 1974) utilize data from both sides of the Sun-center line and from a wider latitude range; these distributions are probably less accurate than the upper three, especially in view of the lack of direct kinematic information. The vertical axes labelled A refer to abundances on an arbitrary relative scale.

atomic hydrogen, whose fundamental distribution extends to much larger distances. Instead of being the prototype for the distribution of the constituents of extreme Population I, the distribution of atomic hydrogen seems unique (see Burton et al. 1975, Burton 1976, Stecker 1976). The general picture emerging for our Galaxy is in these respects consistent with the morphological information available for external galaxies.

There is so far no straightforward, comprehensive, or conclusive evidence for spirality on a galactic scale of any of the inner-Galaxy tracers. Probably of the distributions considered that of CO is the most basic representative of the compressed Population I. Extensive and detailed observational material should become available for CO within the next few years. If the inner Galaxy is characterized by a grand design of a spiral form, it is reasonable to expect that this would be

demonstrated by observations of CO because of the high angular resolution at 2.6 mm, the relatively low characteristic velocity dispersion, the abundance of CO, the accessibility of long lengths of path, and the expected confinement to rather narrow zones of high compression. Figures 8 and 11 show that the CO apparently is not confined to the narrow zones which are predicted to trace the compression due to the passage

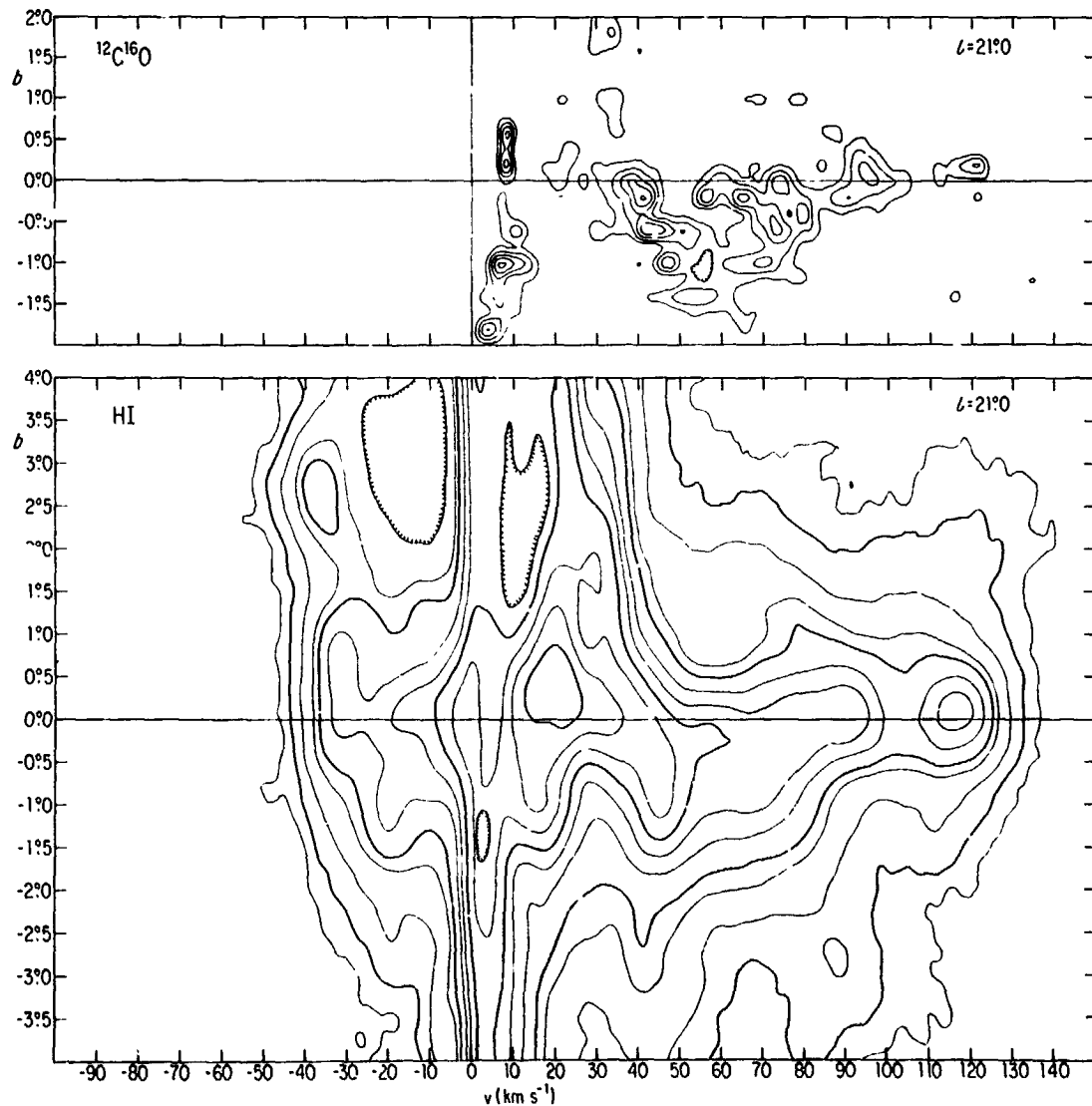


Figure 9. Comparison of CO and HI latitude-velocity distributions in the direction $l = 21^\circ$, showing that the z-thickness of the neutral hydrogen layer is about twice that of the carbon monoxide layer (Burton and Gordon 1976a). The HI observations are from the survey of Weaver and Williams (1973).

of a galactic density-wave. It is particularly puzzling that the run with longitude of terminal velocities, calculated from the CO observations and plotted in the lower panel of Figure 11, shows large-scale irregularities of the same form as those found for the HI and plotted in Figure 2. If the CO kinematics were governed by a galactic shock, then it seems reasonable to expect that this would be indicated by terminal-velocity perturbations of larger amplitude and narrower extent in longitude than found for the neutral gas. Bash and Peters (1976) have recently considered several consequences of the CO terminal velocity variation.

Another important difference between the Figure 1 HI observations and the Figure 7 CO observations concerns the amount of small-scale structure apparent. Although much detail may be unresolved in the HI ob-

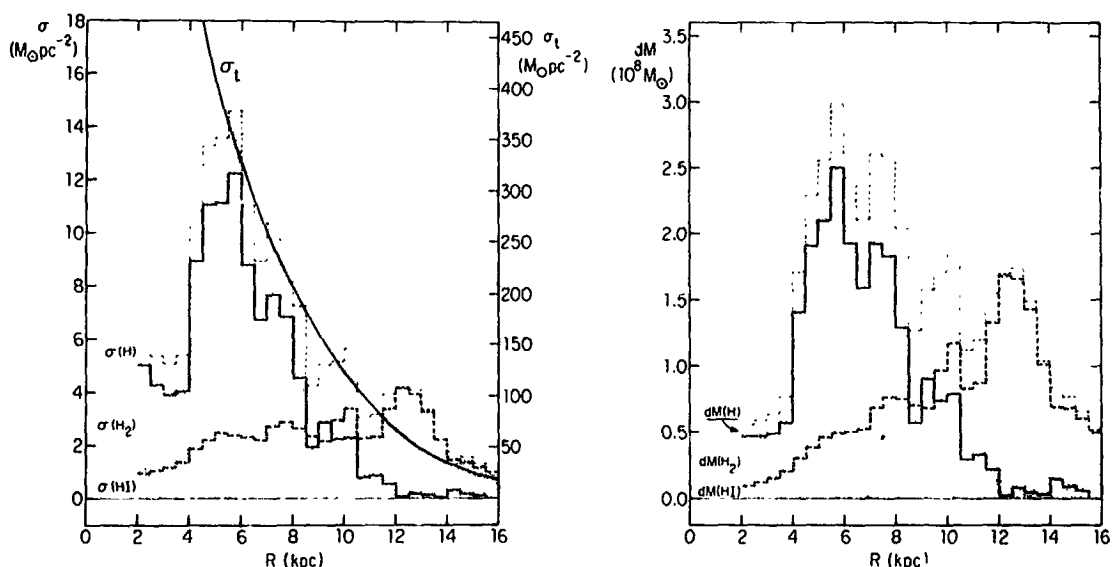
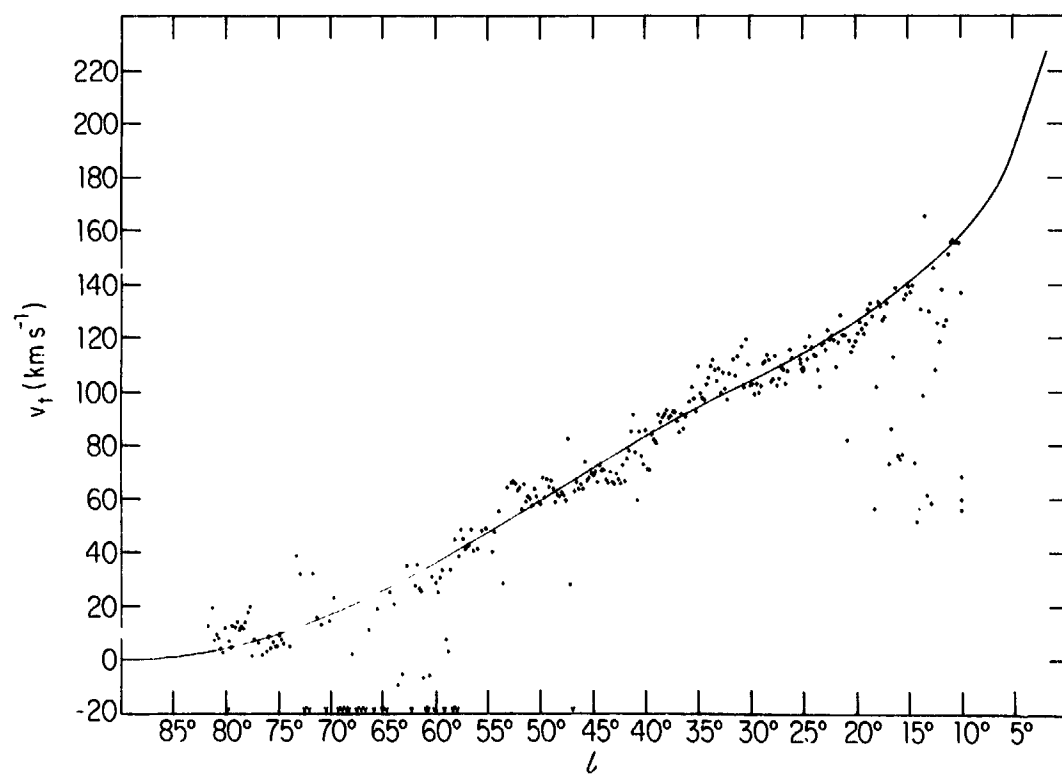
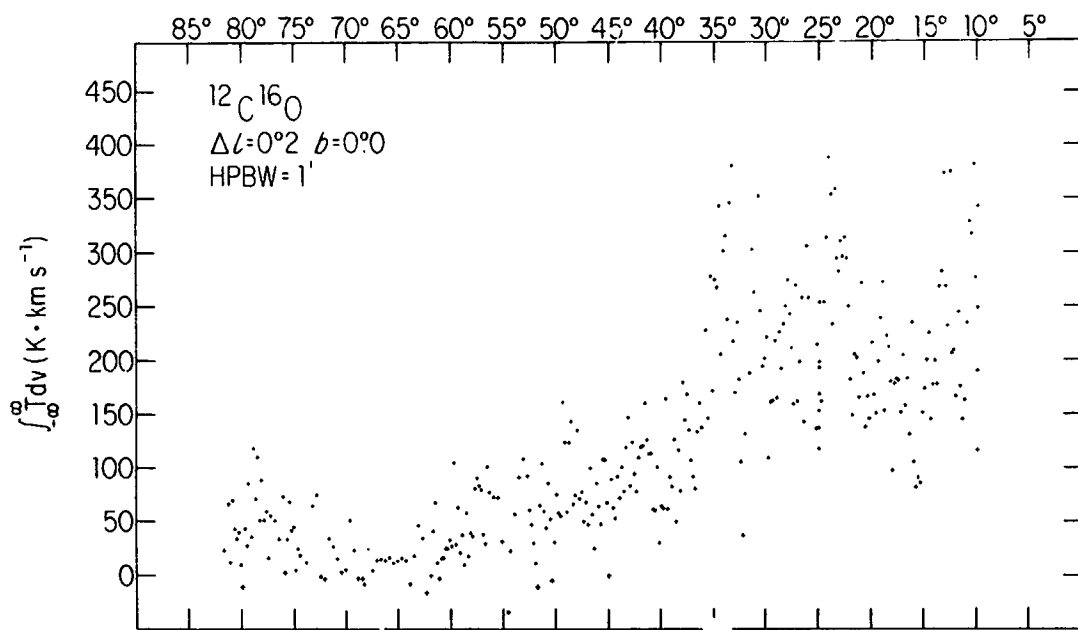
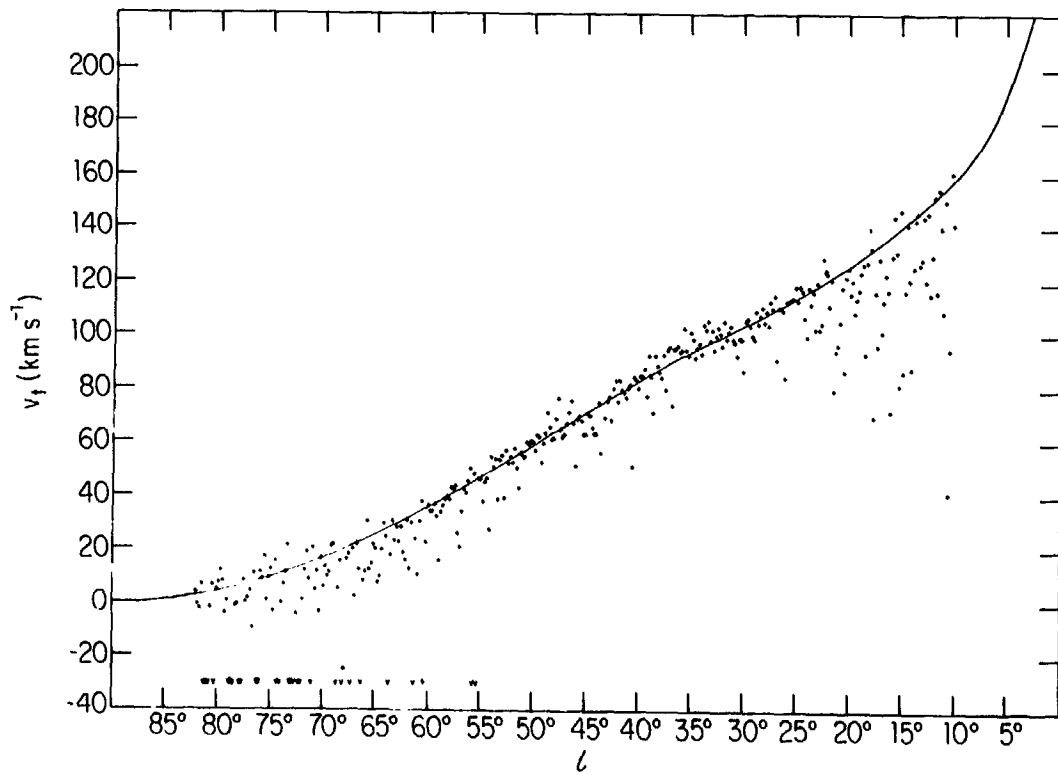
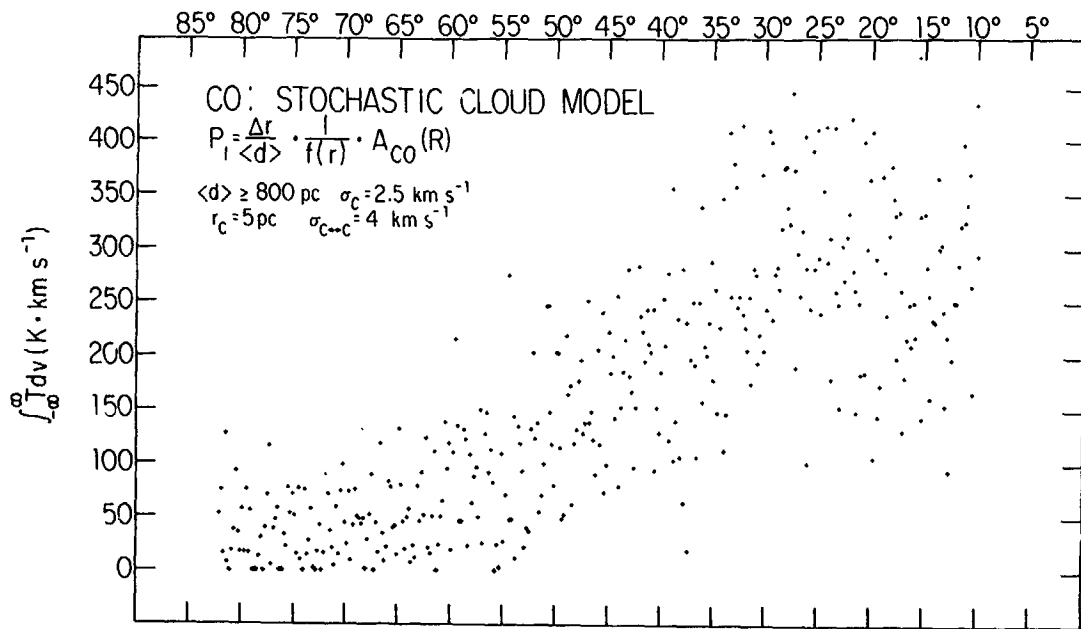


Figure 10. Radial distribution of projected surface densities and differential masses of atomic and molecular hydrogen. This figure is from Gordon and Burton (1976a), where the several important uncertainties inherent in the derivation of H_2 densities from observations of CO are summarized. Also shown is the total-mass surface density σ_t predicted dynamically by Innanen (1973).

Figure 11. Upper panel: Variation with longitude of the total-velocity integrals $\int T dv$ calculated from the CO observations of Figure 7. Lower panel: Variation with longitude of the CO terminal velocities. Comparison with the HI terminal velocities plotted in Figure 2 shows that the compressed molecular material is characterized by the same overall kinematics as characterize the much more ubiquitous atomic hydrogen.





servations, features extending over many beamwidths are nevertheless common. The CO observations show few extended features. The small-scale irregularities in Figure 11 mainly represent characteristics of the CO distribution, not measurement errors. The characteristic appearance in the CO spectra of isolated features allows estimates to be made of the characteristic size and separation of the emitting clumps. Burton and Gordon (1976a,b) have modelled the CO observations by generating synthetic profiles corresponding to a stochastic assemblage of dark clouds (see Baker and Burton 1975). The stochastic distribution is governed by the probability of finding a cloud in a particular interval, of length Δr , along the line of sight:

$$P_i = \frac{\Delta r}{\langle d \rangle} \frac{1}{f(r)} A_{CO}(R) .$$

Here $A_{CO}(R)$ is the (normalized) radial distribution of CO plotted in Figure 8, $f(r)$ is the telescope beam-filling factor, and $\langle d \rangle$ is the average separation between clouds at the mode of the $A_{CO}(R)$ distribution. The kinematics of the clouds are governed by circular galactic rotation and a motion of one cloud with respect to another characterized by a dispersion $\sigma_{c \leftrightarrow c}$. Each cloud has an internal velocity dispersion of σ_c . Using preliminary determinations of these parameters, Burton and Gordon (1976a) have modelled several characteristics of the CO observations. Figure 12 shows that the small-scale irregularities in the synthetic-profile integrals and the modelled terminal velocities are approximately the same as those observed. The model assemblage consists of clouds each having a diameter of 5 pc, an excitation temperature of 16 K, a representative optical depth of 5, an internal dispersion of 2.5 km s^{-1} , a cloud-to-cloud motion of 4 km s^{-1} , and a cloud-to-cloud separation of 200 pc at the peak of the $A_{CO}(R)$ distribution.

7. The Distribution of Carbon Monoxide within 10° of the Galactic Center from T. M. Bania's Observations. The $J = 1 \rightarrow 0$ rotational transition of the $^{12}\text{C}^{16}\text{O}$ isotope of carbon monoxide has been surveyed at $\ell = 0^\circ$ in the inner region of the Galaxy by Bania (1976). The observations, which extend over the range $10^\circ \geq \ell \geq 352^\circ$, are shown in Figure 13 in the form of a velocity-longitude contour diagram. Also shown in the figure is the observed velocity-longitude behavior of 21-cm neutral hydrogen emission for the same region of the Galaxy. Although the telescope beamwidths for the CO and HI observations are quite different, being $1'$ and $20'$ of arc, respectively, the angular sampling resolution

←
Figure 12. Longitude variations of the total-velocity integrals and of the terminal velocities calculated from synthetic line profiles constructed to mimic the CO observations. The model CO distribution consists of discrete clouds distributed stochastically as discussed in the text (see Burton and Gordon 1976a). The symbols v in Figures 11 and 12 refer to profiles for which no terminal velocity was determined because of the lack of an emission feature more intense than 1.2 K.

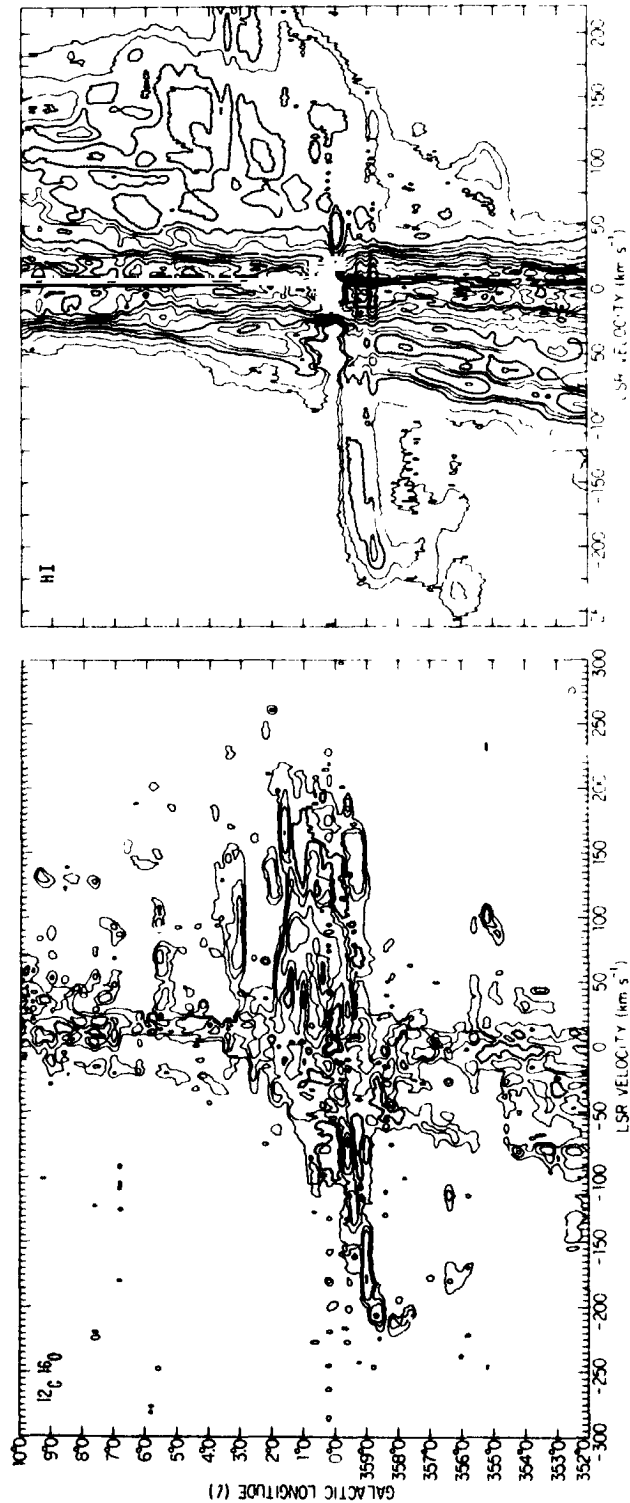


Figure 13. Longitude-velocity contour maps of carbon monoxide ($^{12}\text{C}^{16}\text{O}$) and neutral hydrogen (HI) in the inner Galaxy (Bania 1976). The data in both maps were taken at $b = 0^\circ$. Although the beamwidths of the CO and HI observations are $1'$ and $20'$ of arc, respectively, the data were both taken with the same angular sampling resolution ($\Delta\lambda = 0.2$). CO contour intervals correspond to antenna temperatures of 1.4, 3, 4, 10, 15, ... K; HI contours are drawn at antenna temperatures of 2, 3, 10, 15, 20, 30, 40, ... K.

Since the CO emission is collisionally excited by molecular hydrogen, the striking similarity of the CO and HI observations implies that the kinematics of atomic and molecular hydrogen are generally similar in the inner regions of the Galaxy. The CO observations in the region $|l| < 1^\circ$ are from Liszt et al. (1976).

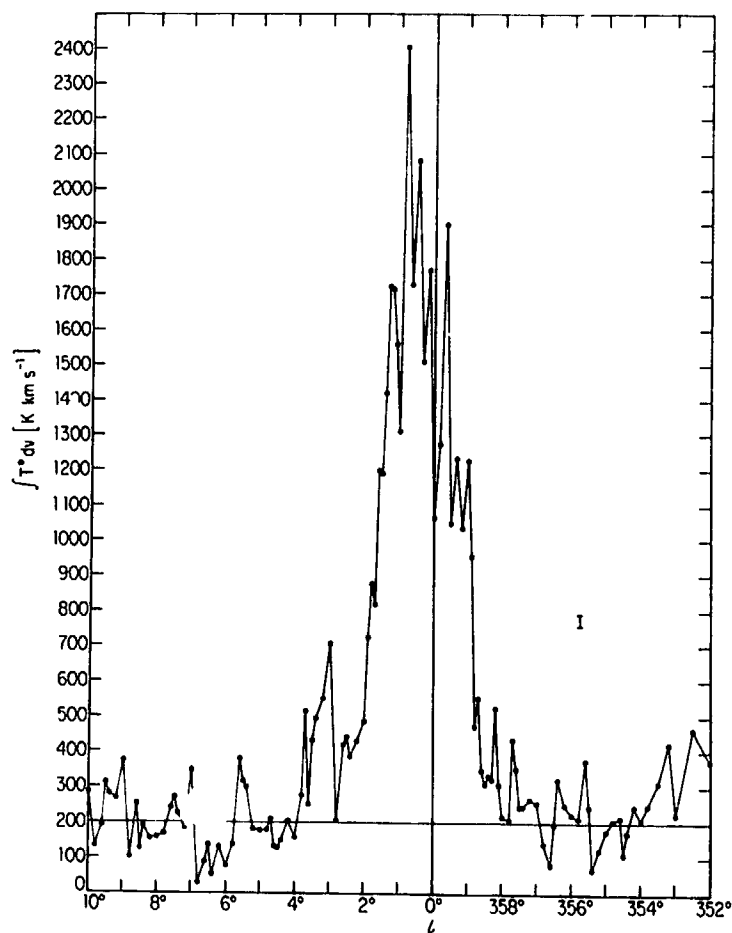


Figure 14. Observed longitude dependence of the integrated intensity of $^{12}\text{C}^{16}\text{O}$ emission in the inner Galaxy (Bania 1976). The symbol indicates the magnitude of a one standard deviation measurement error.

of both sets of observations, $\Delta l = 0.2$, is the same. The similarity of the distribution and kinematics of the CO and HI emission is striking. Apparently the regions wherein atomic hydrogen is converted to molecular hydrogen do not possess large velocity anomalies. The overall velocity-longitude behavior of both CO and HI is dominated by differential galactic rotation since the major portion of the emission observed occurs at positive velocities for $10^\circ \geq l \geq 0^\circ$ and at negative velocities for $352^\circ \leq l \leq 360^\circ$.

Some extended kinematic features common to both the CO and HI emission data and which are discussed in detail by Bania (1976) include (i) the 3-kpc arm; (ii) an anomalous cloud at $l = 355^\circ$, $v = 100 \text{ km s}^{-1}$, moving at a velocity forbidden by circular rotation; and (iii) the well-known nuclear disk feature.

The longitude dependence of the integrated intensity of $^{12}\text{C}^{16}\text{O}$ emission in the inner Galaxy is plotted in Figure 14 (Bania 1976). The intense peak near $l = 0^\circ$, with a half-width of about 1.5° , probably arises from CO lying within 350 pc of the galactic center (see Liszt et al. 1976). The background integrated intensity at the level indicated by the line in the figure at 200 K km s^{-1} is consistent with the accumulation along the line of sight of the annular disk of CO (see Figure 8), with no additional contribution from the region $R \lesssim 2 \text{ kpc}$.

8. The Galactic Distribution of Ionized Hydrogen from F. J. Lockman's Observations of the H166 α Recombination Line. Ionized hydrogen, in concentrations sufficiently dense to produce measurable radio recombination lines, is associated with very young, hot stars, and thus identifies sites of recent star formation in the Galaxy. In addition to the rather dense compact HII regions which have been studied in radio surveys of, for example, the H109 α recombination line, the interior part of the Galaxy contains larger regions of more moderate density ionized hydrogen. This lower density material is most easily observed in recombination lines at frequencies near 1 GHz, and although the emission is quite weak, it is seen at enough locations to be a useful tracer of both the velocity field and the overall level of star formation in the Galaxy. A survey of part of the galactic plane in the H166 α recombination line near 1.4 GHz has recently been completed (Lockman, 1976) and the gross distribution of this gas is reasonably well known.

Figure 15 shows the observed H166 α emission from a portion of the northern galactic plane, plotted in velocity-longitude coordinates. The lines from moderate density gas are detected at every observed position $4^\circ \leq l \lesssim 44^\circ$. The power in the line, averaged over 3° intervals, is plotted against longitude in Figure 16. Although these observations do not cover longitudes greater than 51° , a survey by Hart and Pedlar (1976) at Jodrell Bank indicates that there is virtually no H166 α emission between longitudes 52° and 70° . This, when considered with the absence of emission at small velocities (corresponding to locations near the sun) and the low level of emission at high positive velocity for low longitudes, indicates that most H166 α emission originates between galactocentric radii $4 < R < 8 \text{ kpc}$.

A quantitative description of the radial distribution of H166 α emission is shown in Figure 17, where the power in the line per kiloparsec derived under the assumption of pure circular galactic rotation is plotted against galactocentric radius R . The apparent emission at $R > 8 \text{ kpc}$ can be attributed to the broad nature of the features in the profiles since emission at each velocity has been separately assigned to the corresponding radius, and does not necessarily imply significant ionized gas at these radii. In contrast, it is quite likely that the apparent

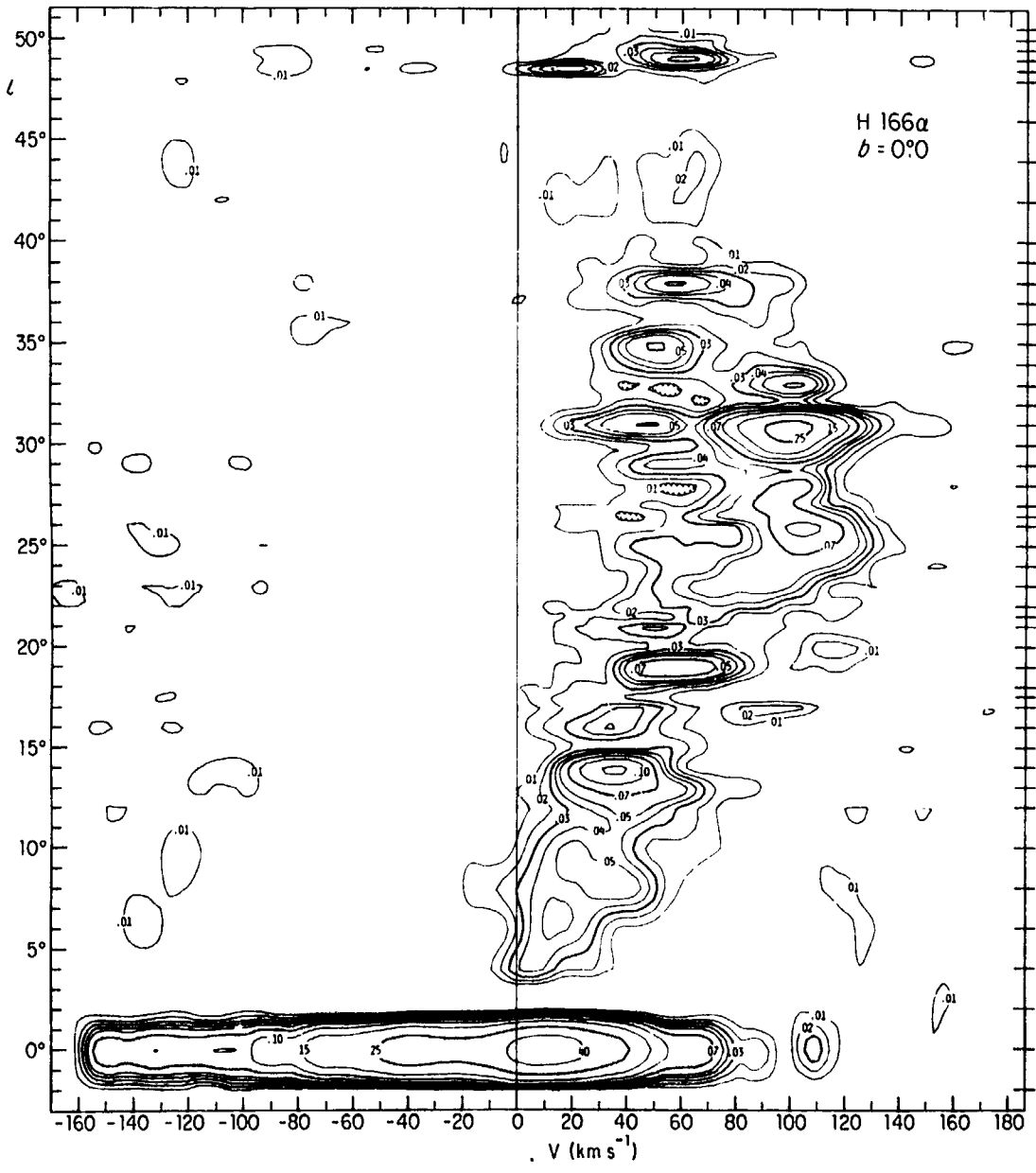


Figure 15. Distribution of H166 α antenna temperature in velocity-longitude coordinates (Lockman 1976). Marks through the right-hand border show the observed longitudes. Some of the weak emission at $v < 0 \text{ km s}^{-1}$ can be attributed to the C166 α recombination line of ionized carbon.

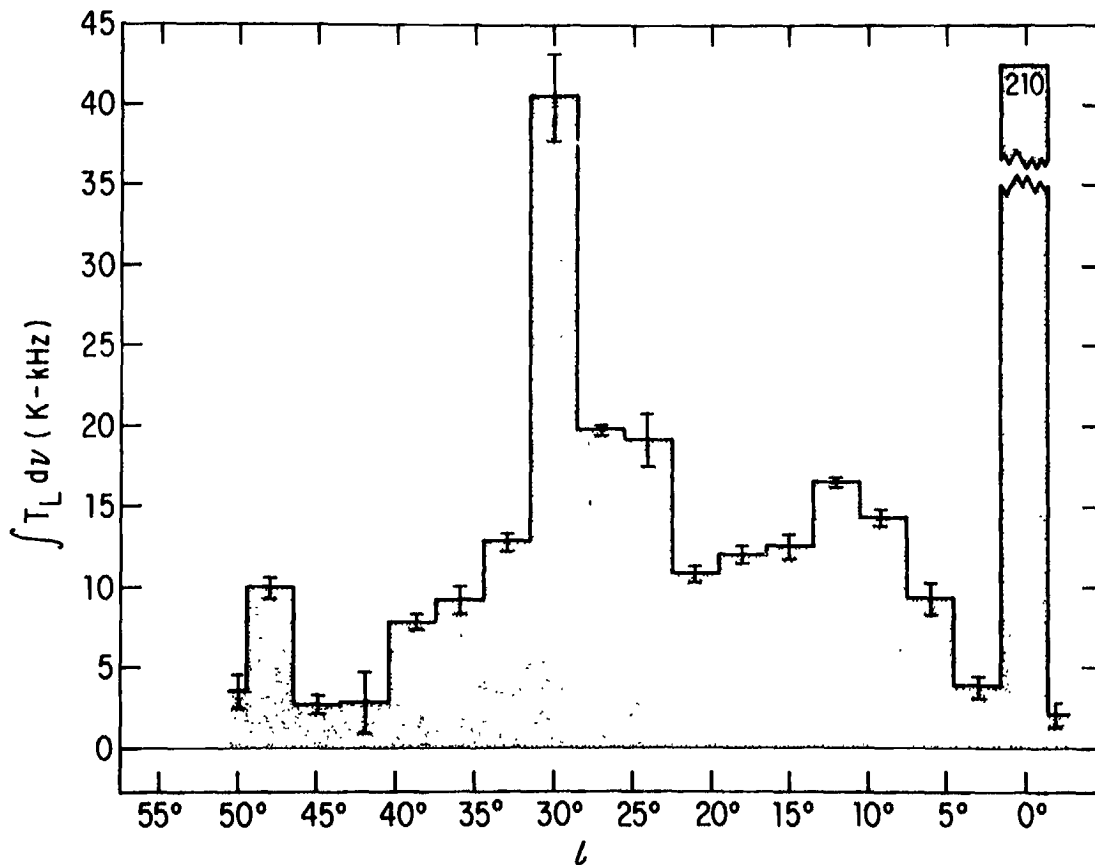


Figure 16. Total power in the H166 α line averaged over 3 $^\circ$ intervals as a function of longitude (Lockman 1976).

emission at $R < 4$ kpc is real, although the limited observations of this region cause large uncertainties in the analysis. A comparison with the radial distribution of neutral hydrogen (Figure 4) shows no strong correlation between the HI and the H166 α distributions, implying that the source of ionization must be distributed somewhat like the H166 α emission. Qualitatively the radial distribution of H166 α resembles that of CO (Figure 8) much more than that of HI. Although the exact nature of the regions giving rise to this recombination line emission is unclear, the ionized gas is so prevalent in the interior parts of the Galaxy that stars must be forming at a rate much larger than would be implied from observations made in the solar neighborhood.

Several of the topics discussed briefly in Sections 1-6 are dealt with in more detail in a chapter in Volume 14 of the Annual Review of Astronomy and Astrophysics. I am indebted to T. M. Bania and F. J. Lockman for providing the material in Sections 7 and 8, respectively.

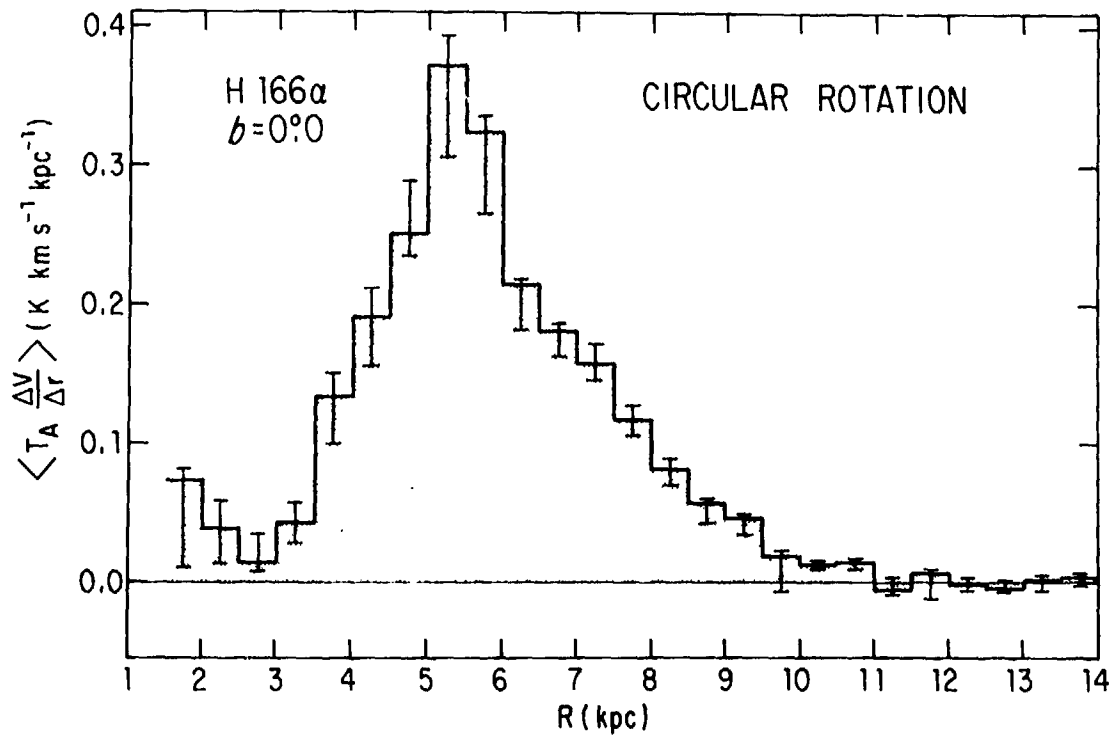


Figure 17. Power in the H166α line, per kiloparsec, derived under the assumption of pure circular galactic rotation, plotted against the galactocentric radius (Lockman 1976).

- Baker, P. L., and Burton, W. B. 1976, Ap. J., 198, 281.
- Baker, P. L., and Burton, W. B. 1976, in preparation.
- Bania, T. M. 1976, in preparation.
- Barbanis, B., and Woltjer, L. 1967, Ap. J., 150, 461.
- Bash, F. N., and Peters, W. L. 1976, Ap. J., 205, 786.
- Bottinelli, L. 1971, Astr. and Ap., 10, 437.
- Burton, W. B. 1971, Astr. and Ap., 10, 76.
- Burton, W. B. 1972, Astr. and Ap., 19, 51.
- Burton, W. B. 1973, Publ. Astr. Soc. Pac., 85, 679.
- Burton, W. B. 1974a, Galactic and Extragalactic Radio Astronomy, 82.
New York: Springer-Verlag.
- Burton, W. B. 1974b, Proc. I.A.U. Symp. 60, 551.
- Burton, W. B. 1976, Ann. Rev. Astr. and Ap., 14, in press.
- Burton, W. B., and Gordon, M. A. 1976a, Ap. J. (Letters), in press.
- Burton, W. B., and Gordon, M. A. 1976b, in preparation.
- Burton, W. B., Gordon, M. A., Bania, T. M., and Lockman, F. J. 1975,
Ap. J., 202, 30.
- Burton, W. B., and Shane, W. W. 1970, Proc. I.A.U. Symp. 38, 397.
- Carruthers, G. R. 1970, Ap. J. (Letters), 161, L81.
- Goldreich, P., and Kwan, J. 1974, Ap. J., 189, 441
- Gordon, M. A., and Burton, W. B. 1976, Ap. J., in press, Sept. 1 issue.
- Hart, L., and Pedlar, A. 1976, in press.
- Hollenbach, D. J., Werner, M. W., and Salpeter, E. E. 1971, Ap. J., 163,
165.
- Innanen, K. A. 1973, Ap. Space Sci., 22, 393.
- Kaplan, S. A., and Pikel'ner, S. B. 1975, Ann. Rev. Astr. and Ap., 12,
113.
- Kerr, F. J. 1968, Stars and Stellar Systems, VII, 575. Chicago:
University of Chicago Press.
- Kerr, F. J. 1969, Ann. Rev. Astr. and Ap., 7, 39.
- Kodaira, K. 1974, Publ. Astr. Soc. Japan, 26, 255.
- Lin, C. C., Yuan, C., and Shu, F. H. 1969, Ap. J., 155, 721.
- Liszt, H. S., Burton, W. B., Sanders, R. H., and Scoville, N. Z. 1976,
Ap. J., submitted.
- Lockman, F. J. 1976, Ap. J., in press, Oct. 15 issue.
- Lockman, F. J., and Burton, W. B. 1976, in preparation.
- Manake, S., and Miyamoto, T. 1975, Publ. Astr. Soc. Japan, 27, 35.
- Radhakrishnan, V. 1974, Proc. I.A.U. Symp. 60, 3.
- Roberts, M. S. 1974, Science, 183, 371.
- Roberts, W. W. 1972, Ap. J., 173, 259.
- Roberts, W. W. 1975, Vistas in Astr., 19, 91.
- Rots, A. H. 1975, Astr. and Ap., 45, 43.
- Scoville, N. Z., and Solomon, P. M. 1974, Ap. J. (Letters), 187, L67.
- Scoville, N. Z., and Solomon, P. M. 1975, Ap. J. (Letters), 199, L105.
- Shane, W. W., and Bieger-Smith, G. P. 1966, Bull. Astr. Inst. Nether-
lands, 18, 263.
- Simonson, S. C. 1974, Proc. I.A.U. Symp. 50, 511.
- Solomon, P. M., Wichramasinghe, N. C. 1969, Ap. J., 158, 449.
- Spitzer, L., et al. 1973, Ap. J. (Letters), 181, L116.

- Spitzer, L., and Jenkins, E. B. 1975, Ann. Rev. Astr. and Ap., 13, 133.
- Stecker, F. W. 1976, Nature, 260, 412.
- Strong, A. W. 1975, J. Phys. A., 8, 617.
- Tuve, M. A., and Lunderger, S. 1972, Astr. J., 77, 652.
- Weaver, H., and Williams, D.R.W., Astr. and Ap. Suppl, 8, 1.
- Westerhout, G. 1973, Maryland-Green Bank Galactic 21-cm Line Survey.
3rd ed. University of Maryland.
- Westerhout, G. 1976, Maryland-Bonn Galactic 21-cm Line Survey.
University of Maryland.
- Wielen, R. 1974, Publ. Astr. Soc. Pac., 86, 341.
- Yuan, C. 1969, Ap. J., 158, 871.

N76-29124

THE NON-THERMAL RADIATION IN THE GALAXY

J.E. Baldwin, Cavendish Laboratory, Cambridge, England

ABSTRACT

This paper does not attempt to review all aspects of the non-thermal continuum radiation in the Galaxy but concentrates on two topics of particular interest for gamma-ray studies:

- 1) The distribution of non-thermal emissivity with height z above the galactic plane. The main result here is that recent observations of the distribution of brightness at intermediate latitudes in the Galaxy and of the edge-on spiral galaxy NGC 891 indicate that the emissivity extends to heights of several kpc perpendicular to the plane.
- 2) The relationship between the non-thermal emissivity and the neutral gas. In several galaxies the angular distributions of neutral hydrogen and non-thermal emission are roughly coextensive and show similar features such as spiral structure. If radio galaxies and normal galaxies with strong nuclear radio sources are excluded, there appears to be a proportionality between their total HI content and their non-thermal radio luminosity.

1. Introduction. In the last few years there have been notable advances in observations of the non-thermal radiation from the Galaxy but almost no corresponding progress in our understanding of the phenomena in terms of physical processes taking place in the Galaxy. The observational advances can be summarised as:

i) Improved angular resolution. There are now several surveys with angular resolutions better than 10 arcmin at frequencies above 1 GHz, notably those initiated by Beard and Kerr (1969) at 2.7 GHz and continued by others. The highest angular resolution used has been 3 arcmin by Green (1974) at 408 MHz, where the galactic radiation appears to be fully resolved except for details of individual sources.

ii) Improved sensitivity. Surveys now extend to higher latitudes than previously at high frequencies. Good examples are the surveys by Hirabayashi et al. (1969) and Altenhoff et al. (1970).

iii) Observations at very high frequencies. The upper limit of frequency has now been extended to 15 GHz by Hirabayashi et al. (1972). This is extremely important for distinguishing the thermal component of the galactic background radiation.

iv) Surveys with identical angular resolutions have been made over a range of frequencies by Altenhoff et al. (1970).

v) The spectrum of the non-thermal radiation has been studied over a wide frequency range at low latitudes by many authors and with high accuracy at high galactic latitudes at frequencies up to 1.4 GHz by Sironi (1974) and Webster (1974).

vi) Whole sky surveys have been completed at lower frequencies (Landecker and Wielebinski, 1970) and are partially complete at 408 MHz (Haslam et al., 1974).

vii) Low frequency observations at 30 MHz by Jones and Finlay (1974) with an angular resolution of 0.8° provide important measures of the absorption coefficient due to ionised hydrogen close to the galactic equator.

viii) Observations of nearby spiral galaxies with high resolution and good sensitivity have revealed their disks and spiral structure in the non-thermal continuum (Pooley 1969; Mathewson et al. 1972; van der Kruit 1973) and have made possible the study of edge-on systems for measuring of the thickness of their disks and searching for galactic halos.

Of these advances, the one which has changed our viewpoint most is the extension of studies to nearby galaxies. It is still true that the actual properties of our Galaxy and no other are of the greatest importance for understanding the cosmic ray and gamma-ray data. But the freedom we gain by not being tied to model-making from a viewpoint inside one system is of crucial importance. Particularly so, since we can examine what relationship exists between the non-thermal emission and other constituents of galaxies in a way which is impossible with a sample of only one system.

In spite of these advances, the questions being asked 20 years ago are still with us. Do the radio observations provide evidence for a region of containment of cosmic rays in the Galaxy? What are the sources from which the cosmic ray electrons originate? What processes determine the shape of the radio spectrum and the corresponding shape of the electron energy spectrum? Of course there are answers to these questions, but which are we to believe?

In what follows I shall ignore many problems of importance and concentrate on two aspects of the non-thermal radiation which seem particularly important for this meeting. They are:

- a) The distribution of emission perpendicular to the galactic plane
- b) The relationship between the non-thermal radiation and the neutral gas.

First, we must review briefly the main properties of the distribution of non-thermal emission which are generally accepted.

2. The non-thermal disk. The distribution of brightness temperature, $T(l)$, in longitude, l , at $b = 0^\circ$ has been well known for many years. Improvements in angular resolution have revealed the presence of many HII regions and supernova remnants but have not changed the basic picture. The symmetry about the galactic centre is sufficiently good (Fig. 1a) that it is reasonable to make a circularly symmetric model of the radiation in the equatorial plane. I emphasize here, as in the past, that model-making is a reputable technique provided that one is good at guessing the correct model and that the model is a simple one. The procedure adopted in deriving the variation of the emissivity, $J(R)$, as a function of radius R from the galactic centre is straightforward. It differs slightly from many similar derivations in astronomy in that the Sun is situated in the disk itself and so $\{T(l) + T(l + 180^\circ)\}$ is the brightness temperature which would be observed from a point outside the Galaxy along a line of sight passing a distance $R_0 \sin l$ from the galactic centre. Notice that in this case we have no knowledge about the distribution of emission outside the

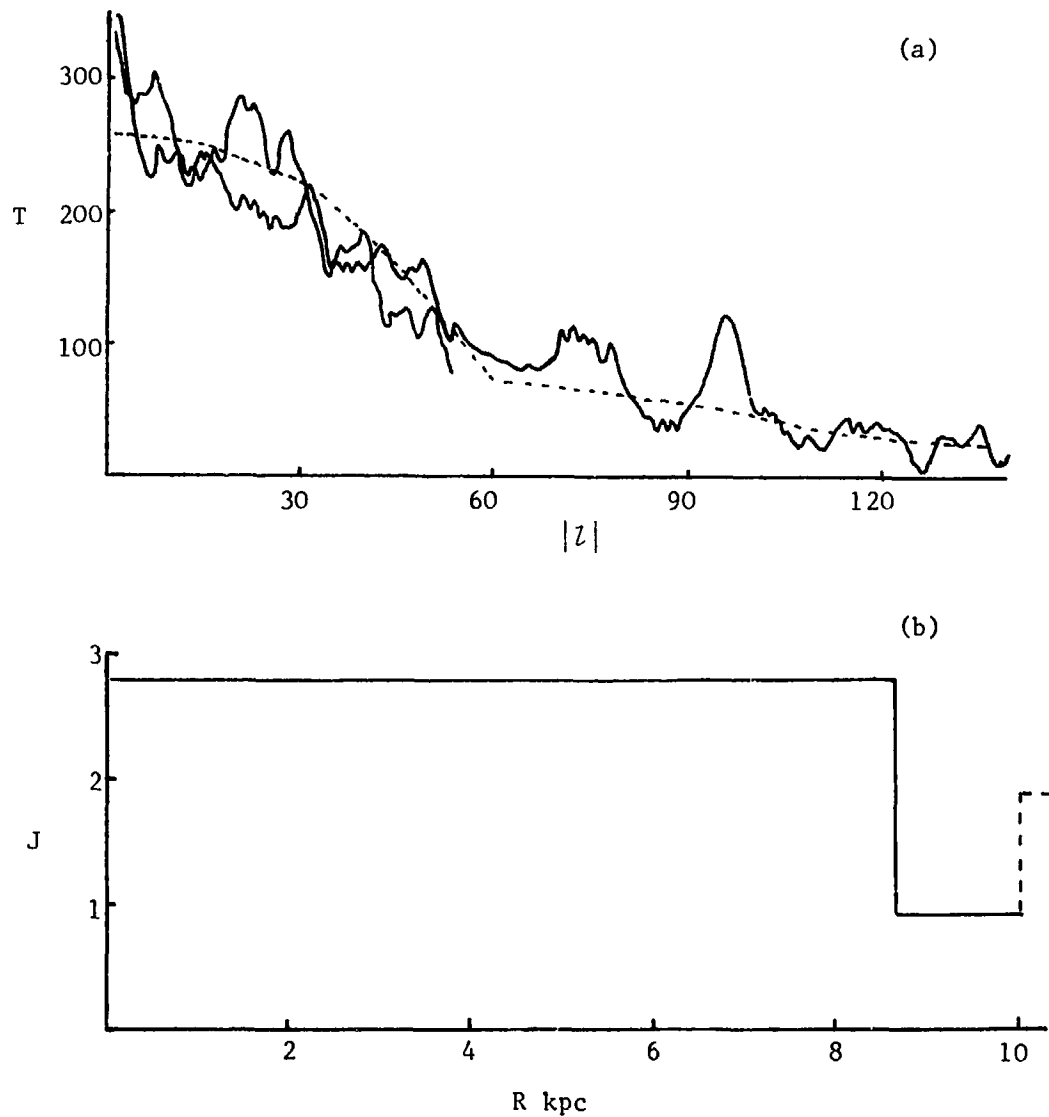


Fig. 1. (a) The distribution of brightness temperature with longitude at 408 MHz at $b = 0^\circ$ from Green (1974). The two halves of the curve have been reflected about $l = 0^\circ$ to show the departures from symmetry. The dotted line corresponds to the smooth model adopted.

(b) The variation of emissivity at 408 MHz with radius in the Galaxy derived from Fig. 1a. The units are $10^{-40} \text{ W m}^{-3} \text{ Hz}^{-1}$.

Sun's radius R_0 and are subject to appreciable uncertainties even just inside R_0 . The distribution of emissivity with radius, derived from the brightness temperatures in Fig. 1a, is shown in Fig. 1b. It is fairly similar to that derived, for instance, by Ilovaisky and Lequeux (1972) and by Baldwin and Pooley. The most important features of the curve are the fairly uniform value of the emissivity within $R = 8$ kpc and the rapid fall-off with radius near the Sun. The increase of emissivity with radius beyond R_0 is not shown by this technique but models of the local spiral arm (using data at high latitudes as well as at $b = 0^\circ$) strongly suggest that there is an increased emissivity in this arm.

The contours of brightness close to the galactic equator correspond very closely with those expected for a uniform thin disk of emission. The width in latitude between half intensity points is only 2° , very much smaller than the width in longitude, and the contours run remarkably parallel to the galactic equator for latitudes up to about 5° .

A long-standing problem is 'How much of this disk radiation is truly non-thermal?'. There is beyond doubt a thermal component from individual HII regions and also perhaps a smooth distribution of ionised hydrogen. Its magnitude has fluctuated from observer to observer. The reasons for this are simple. The extraction of a thermal component from several surveys at different frequencies depends on having observations with identical beam shapes and accurately determined zero levels. The zero levels, in particular, can be a potent source of error since they give rise to systematic variations of spectral index with latitude which mimic the behaviour expected from a narrow distribution of thermal emission along the galactic equator. In the first analysis of this kind, Westerhout (1958) found that, at 1420 MHz, about 50 per cent of the radiation at $b = 0^\circ$ was thermal. From the surveys by Altenhoff et al. (1970) at 1.4, 2.7 and 5.0 GHz, all with a resolution of 11 arcmin, Downes (Ph.D. thesis) concluded reluctantly that it was not possible to make the separation into thermal and non-thermal components because of uncertainties in one of the beam shapes. Jackson and Kerr (1971), who needed this result, were bolder using the same data and obtained a thermal component of 50 ± 25 per cent of the total brightness at $b = 0^\circ$ at 5 GHz. This value refers to a smooth distribution of thermal emission which has a total flux density far greater than that due to individual sources. The sources listed by Altenhoff et al. (1970) and by Reifenstein et al. (1970) have a combined flux density only about 5 per cent of the total flux density of the disk. Measurements of the galactic radiation at 15 GHz by Hirabayashi et al. (1974) are an important addition to our knowledge. For a number of points along the galactic equator, selected to be free of HII regions, they show spectra containing a very significant thermal component -

about 80 per cent of the total at 15 GHz. Taking a non-thermal temperature spectral index of -3 at high frequencies, this value would correspond to a 60 per cent contribution at 5 GHz, well within the errors in Jackson and Kerr's determination, and 30 per cent at 1.4 GHz which is only a small reduction on Westerhout's value. But a number of other authors have found a negligible contribution from thermal radiation even at 5 GHz. The resolution of this problem needs more serious measurements. At 408 MHz the effects of the thermal radiation can be neglected for most purposes. The distribution in latitude of the thermal component is narrower than for the non-thermal and it does not influence a discussion of the distribution of emission outside the plane of the disk.

3. The variation of emissivity with z . The evidence presented in the previous section suggests that the distribution of the non-thermal radiation is well represented by a plane stratified disk in which the emissivity is independent of R but may, however, have some dependence on z . If such a disk were of infinite extent and the Sun lay in its meridian plane, then the brightness temperature observed at any latitude b would be

$$T(b) = \int_0^{\infty} J(z) \operatorname{cosec} b \, dz$$

$$= \text{constant} \times \operatorname{cosec} b$$

Baldwin (1967) found that the best available data, which were at 400 MHz, fitted this law very closely for $20^\circ > b > 2^\circ$. Departures from the relation showed at lower latitudes but were perhaps affected by the angular resolution of the observations (about 50 arcmin). Under these circumstances it was only possible to derive a value of the equivalent thickness of the disk, $2 \int_0^{\infty} J(z) dz / J(0)$, of about 750 pc. The 150 MHz contour map of the whole sky assembled by Landecker and Wielebinski (1970) was used by Ilovaisky and Lequeux (1972) as the basis for fitting model disks as mentioned in section 2. They found it necessary to use two disks both having the same radius of about 10 kpc. The first had a thickness of 500 pc and an emissivity at 150 MHz of 200 K kpc^{-1} and the second a thickness of 2000 pc and an emissivity of 100 K kpc^{-1} . The method of fitting model contours to those observed is not described and it is hard to see which features in the observations led to the choice of disks used. The equivalent thickness of their disk which would be 1500 pc is in clear disagreement with Baldwin's value unless either it is due to the low resolution of the 150 MHz survey or there is a very rapid variation with frequency. An alternative explanation is that the old 400 MHz data were in error. Examination of modern data suggests that this may be so.

Improved angular resolution in the observations make it useful to reexamine the question of the z dependence of the emissivity. Jones and Finlay (1974) noted that, in the observations of Altenhoff et al. (1970), departures from the cosec b law occurred at $|b| \sim 1.5^\circ$, a much larger value than the resolution of 11 arcmin. Evidently this tells us something about the z distribution of emission. Consider now a disk of finite radius R which is in fact slightly less than R_0 . The

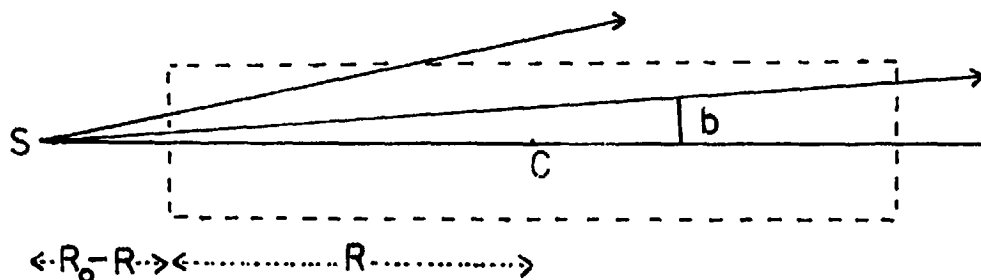


Fig. 2. Geometry of a thick disk with radius $R < R_0$.

situation is shown in Fig. 2. Then, taking $l = 0^\circ$ for simplicity, the brightness at latitude b will be

$$T(b) = \int_{(R_0 - R) \tan b}^{(R_0 + R) \tan b} J(z) \operatorname{cosec} b \, dz$$

For low latitudes $\tan b \sim b$. The change in $T(b)$ due to change in the lower limit of integration is to a good approximation $-(R_0 - R)J(0)$. This is just the emission lying very close to $z = 0$, present in the infinite disk and now missing in the case of the finite disk.

$$\text{So } b\{T(b) + (R_0 - R)J(0)\} = \int_0^{(R_0 + R)b} J(z) dz$$

$$\text{and } \frac{d}{db} b\{T(b) + (R_0 - R)J(0)\} = (R_0 + R)J((R_0 + R)b)$$

Thus in this model the departures of the brightness from the cosec b variation provide direct measurements of the emissivity at different heights. The behaviour is easily seen from Fig. 2. If the line of sight at latitude b emerges from the top face of the disk into a

region of zero emissivity before reaching the distant edge of the disk then the variation of brightness with latitude will vary as $\text{cosec } b$ (or $1/b$ for small latitudes). If the line of sight reaches the far edge of the disk whilst still in a region of finite emissivity, then the variation of brightness with latitude is slower than $\text{cosec } b$. In plotting the observational data the constant term $(R_0 - R)J(o)$ on the left hand side must be allowed for. It is about 7 - 8 per cent of the brightness temperature at $b = 0^\circ$ and at 408 MHz is roughly 25 K. The emissivity outside radius R is probably not zero but I think it likely that the value of the term must be at least 15 K. In practice there is a further constant term to be allowed for, since the observed value of $T(b)$ already includes a constant contribution from extragalactic sources and perhaps an almost constant term from any large extended radio halo of the Galaxy, neither of which have been mentioned in the model analysis. My best guesses of their combined value range from 6 K to 20 K at 408 MHz. Values from the 408 MHz survey of Haslam et al. (1974) are plotted directly in Fig. 3a making no allowance for either of these terms, on the basis that they exactly cancel. I adopted this as the most conservative view, i.e. that will lead to the lowest values of emissivity at large values of z . In fact it is probable that the term $(R_0 - R)J(o)$ will be the larger and will lead to larger emissivities at high z . Also plotted in Fig. 3a are data from the 1.4 GHz survey of Altenhoff et al. (1970). An allowance of 1 K has been made for the constant term $(R_0 - R)J(o)$. The zero level of their brightness temperature scale corresponded to the sky brightness at latitudes of $\pm 25^\circ$ which is certainly higher than the sum of extragalactic and possible halo contributions. Thus again the values plotted represent a conservative view of the emissivity at large z . The shape of the curve fits that of the 408 MHz data very closely. The variation of emissivity with z derived from the 408 MHz data is shown in Fig. 3b together with the model of Ilovaisky and Lequeux adjusted to 408 MHz with a temperature spectral index of -2.6.

The most interesting feature of the curve is the extensions to at least 3 kpc from the galactic plane. Since the constant terms in the brightness temperatures were chosen conservatively, the extensions are probably yet larger. The correctness of the result obviously depends on whether the model is correct. Tests which might justify it would be an analysis at all longitudes, including those where the edge of the disk is seen tangentially, but I have not yet completed these.

In the discussion so far I have avoided the use of the phrase 'radio halo'. It arouses antagonism in otherwise placid astronomers and many have sought to deny its existence including Burke (1967), Wielebinski and Peterson (1968), Yates (1966), Ilovaisky and Lequeux (1972) and Price (1974). The main feature of all these analyses is that features formerly associated with the presence of a halo can be

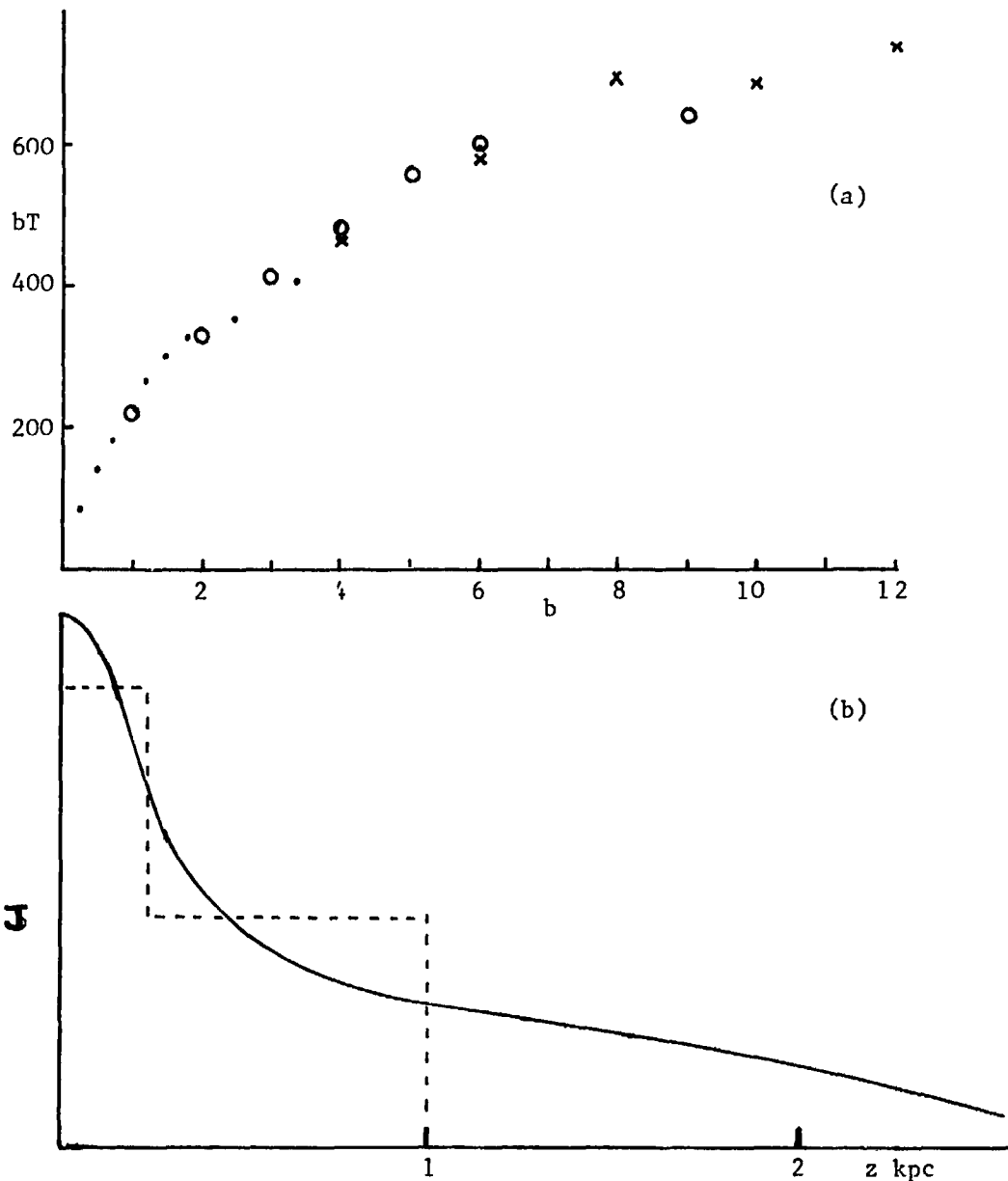


Fig. 3. (a) The variation of $bT(b)$ with galactic latitude. Dots are 1.4 GHz (Altenhoff et al. 1970) for $12^\circ < l < 17^\circ$. Crosses are 408 MHz (Haslam et al. 1974) $30^\circ < l < 40^\circ$, $b > 0^\circ$. Circles $b < 0^\circ$.

(b) The variation of emissivity $J(z)$ with height z above the galactic plane for a plane stratified disk model derived from the 408 MHz data in (a). The dotted line is Ilovaisky and Lequeux's emissivity adjusted to 408 MHz.

explained in terms of features in the disk but at the expense of leaving an embarrassingly large isotropic component which is presumed to be of extragalactic origin. The only recent supporter of halos has been Webster (1975) who showed that the distribution of the spectral index of the radiation at high latitudes was consistent with a model in which a spherical halo has a steeper spectrum than the disk radiation. The question of its existence seems to me to be still quite open, but hard to resolve. The main point to establish is the existence of emission at large values of z . The shape of the distribution seems to me a subsidiary refinement. Perhaps the compromise which would satisfy everyone would be if the Galaxy has a very thick disk as indicated by the preceding discussion. An independent line of evidence which suggests that it may be so comes from the study of other galaxies.

4. The edge-on spiral galaxy NGC 891. Studies of an edge-on spiral might settle unambiguously whether radio halos exist or not. Many negative searches made in the past did not in fact have sensitivities adequate to detect them. For several years M31 has been thought to possess one but Wielebinski (1976) has recently argued that it does not. The next best candidate we know is NGC 891. It is very close to edge-on. It is an Sb galaxy probably of slightly earlier type than the Galaxy but looking very similar optically to the wide-angle infra-red photographs of the Milky Way showing the central bulge of the Galaxy. It has slightly large dimensions than the Galaxy, is rather more massive and its intrinsic radio luminosity is a few times larger. Observations by Baldwin and Pooley (1973) at Cambridge indicated that the equivalent thickness of the disk was larger than in the Galaxy (4.8 kpc at the present distance of 14 Mpc) though in retrospect that determination was certain to err on the large side by an uncertain amount. More recent observations at Westerbork (Sancisi et al. 1974; Allen and van der Kruit 1976; Allen, Baldwin and Sancisi, in preparation) have provided a study at higher resolution and greater sensitivity over a range of frequencies from 610 MHz to 5 GHz. In these observations extensions of the emission above and below the galactic equator were detected to heights of 8 kpc at 21 cm. The most detailed profile of the emission normal to the plane was obtained at 5 GHz and is shown in Fig. 4. The width of the narrow component to half intensity points after correction for beam smoothing is 9.6 arcsec or 700 pc, rather similar to that in the Galaxy. The extensions seen out to ± 1 arcmin (4 kpc) in z also resemble those seen in the Galaxy.

One of the most interesting aspects of the results concerns the spectral variations over the galaxy. In the equatorial plane the spectral index α is uniformly -0.65 but the spectrum steepens with increasing z reaching values of α of -1 at heights of 4 kpc above the disk. Whether the steepening is associated with energy losses

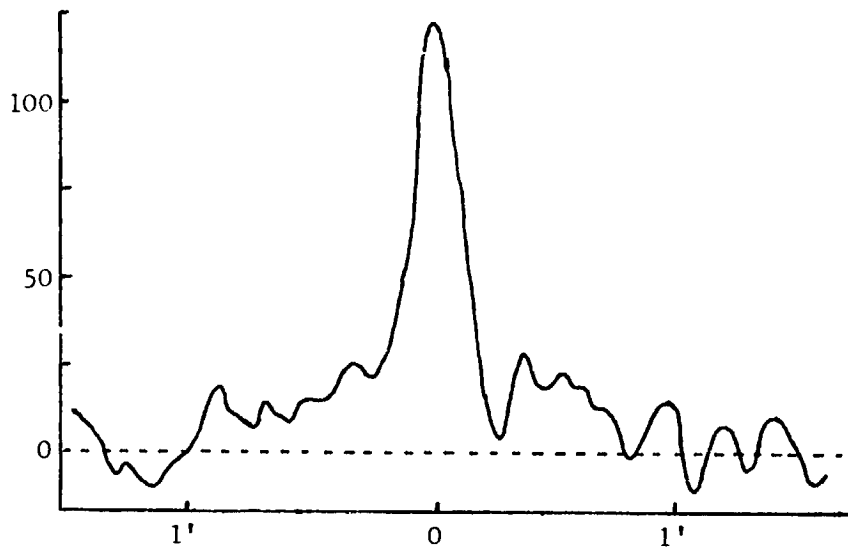


Fig. 4. The distribution of emission with z in NGC 891 at 5 GHz.

by the electrons contained for periods of about 10^8 years or is merely due to lower magnetic fields at large z is not yet known. The uniformity of the spectrum in the disk suggests either that the sources of the electrons are spread throughout the disk or that diffusion in the disk is relatively rapid.

The evidence discussed in section 3 makes it probable that the radio emission in the Galaxy resembles that in NGC 891 quite closely. It is of great interest to examine the variations in spectral index at high latitudes discussed by Webster (1975) in terms of a thick disk model rather than the spherical halo which he adopted for analysis but work on this has not yet started.

5. The relationship between the non-thermal radiation and the neutral gas. There are many reasons for expecting that there should be some correlation between the non-thermal emission and the gas in galaxies. For instance

i) If magnetic flux is frozen into neutral gas clouds then $B \propto n_H^{0.67}$. Since the non-thermal emissivity $J \propto B^{1-\alpha}$ and $\alpha \approx -0.7$, then $J \propto n_H^{1.1}$ if the cosmic ray electron density is uniform.

ii) Regions of high n_H give rise to star formation leading perhaps relatively quickly to supernovae which might provide a high flux of cosmic ray particles.

iii) Galaxies having a high gas content and rate of star formation should also have a high supernova rate and a generally high flux of cosmic ray particles not solely in the neighbourhood of a single supernova. At the other extreme dwarf elliptical galaxies with almost no gas may be very weak sources of cosmic ray electrons and also they are unlikely to have large scale magnetic fields which could trap particles for a long period.

If correlations do exist, they are evidently very important for our interpretation of the gamma-ray data. Correlations are hard to substantiate in the Galaxy because of the distance problems for both the HI and the continuum emission, except close to the Sun at high latitudes. There have been a number of discussions of this region, notably of the non-thermal spurs and loops (Berkhuijsen et al. 1971). Heiles (1974) has also drawn attention to some local features in the neutral hydrogen which are correlated with continuum features.

It must be clear that we are not seeking a one-to-one correlation of HI with non-thermal radiation. HI in the Galaxy extends radially well beyond the Sun but the non-thermal emission probably dies away quite rapidly beyond the local spiral arm; the z distribution of HI well may not be as wide as that of the continuum. It must also be clear that we are talking about the disk radiation associated with normal spiral galaxies, not radio galaxies or the nuclei of spirals. Finally we must recognise that any correlations we find may not imply a direct physical connection.

Similarities in the features of the distribution of HI and non-thermal radiation have been commented on for individual galaxies for a long time. For instance, the LMC and SMC (Mathewson and Healey 1964), M31 (Pooley 1969; Emerson 1974), M101 (Allen and van der Kruit 1976). Thermal radiation, which might well correlate with HI, is not the dominant in the continuum distributions, even in the LMC. In most cases the non-thermal continuum is more centrally condensed in the galaxy than the HI.

A direct comparison of the total HI content and the non-thermal radio luminosity is now possible for a large number of nearby galaxies. The data are presented in Fig. 5. They cover a wide range from the most massive spirals rich in gas such as M101 to the lowest mass of HI detected ($3 \times 10^5 M_{\odot}$) in recent measurements we have made of NGC 205, one of the dwarf companions of M31. The radio luminosities are based on flux densities measured at a wide range of frequencies but converted to 1420 MHz assuming a spectral index of -0.6 . Where possible the flux densities refer only to the disk component and have had any nuclear component subtracted. They are all small corrections for the values plotted. There is a very clear correlation in the diagram with a scatter of only about x2 about a

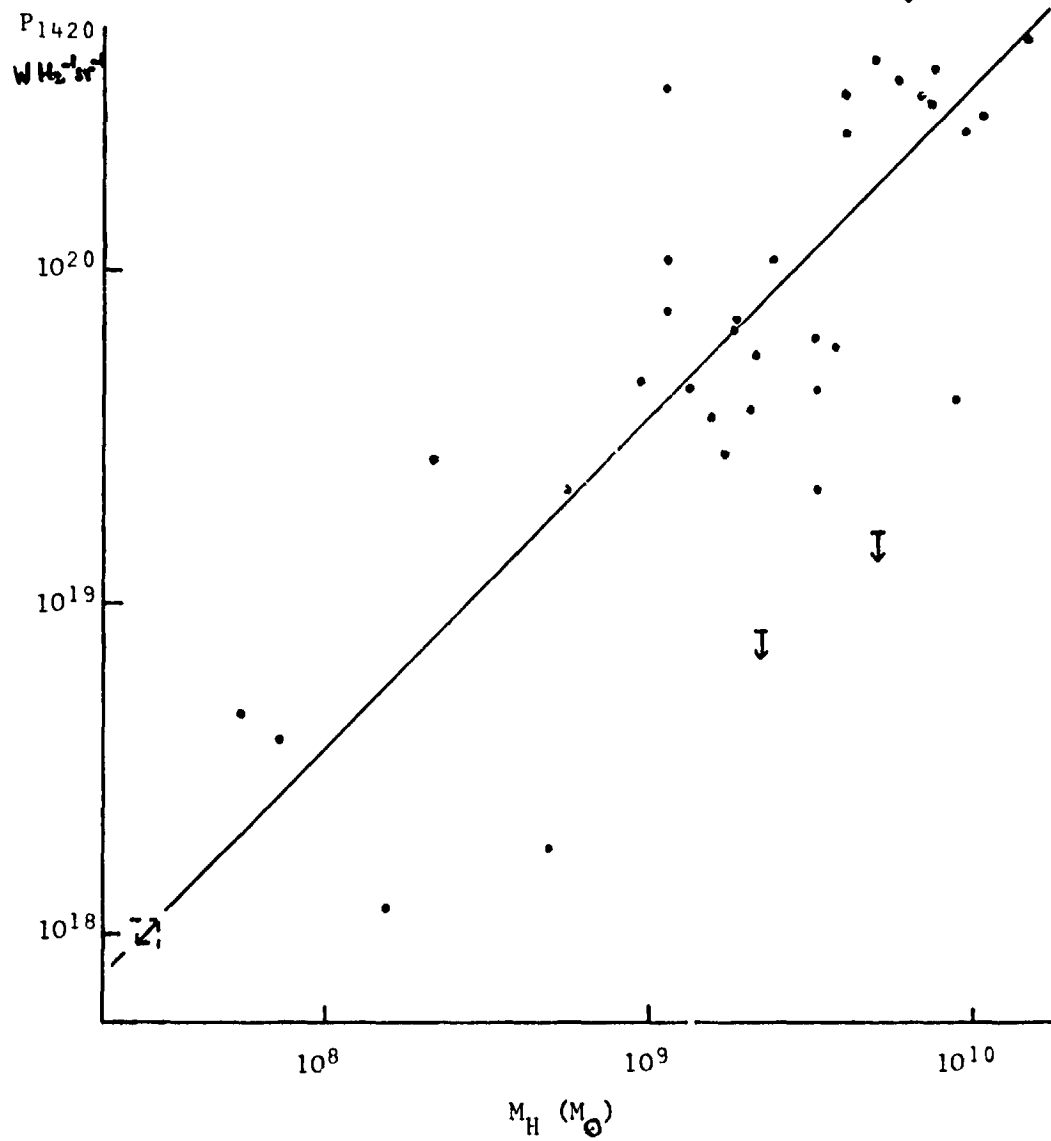


Fig. 5. The relationship between radio luminosity at 1420 MHz and the neutral hydrogen content of galaxies.

line of unit slope. Errors in distances merely slide points in a direction parallel to this line. The absence of points well above the line is very significant. Below the line we must beware. The data suffer from rather unknown selection effects. Values are plotted only when there are published measurements of both HI and continuum flux densities. Astronomers are notorious for not publishing negative results so that some genuinely interesting points which lie away from the line may be missing. The line drawn corresponds to a constant ratio of column density of HI to non-thermal brightness temperature at 1420 MHz, N_{H}/T_{1420} of 2.5×10^{25} atoms m^{-2} K^{-1} (2.5×10^{21} atoms cm^{-2} K^{-1}). It is clearly consistent with what we know for nearby galaxies which have been mapped, that the surface densities of HI are typically 10^{25} atoms m^{-2} (10^{21} atoms cm^{-2}) and they have brightness temperatures of about 0.4 K. Our Galaxy would lie well on the line if observed from outside.

It would be easy, but perhaps idle, to speculate on the significance of the correlation until one understands why some galaxies lie off the line with abnormally low values of continuum emission. Prominent examples are NGC 3109 and NGC 4244, both late type, perhaps Sc or Irr I galaxies. It seems to me that if we understood what is peculiar about such objects we might gain some important clues about the origin of cosmic rays.

6. Observational needs. In the fields I have discussed there are two very clear opportunities for improved observations:

i) Measurements of continuum flux densities of galaxies with high sensitivity. We are engaged in a survey which is sensitive to sources of low surface brightness at 150 MHz at present which we hope will cover most of the northern sky. I hope others are undertaken at higher frequencies.

ii) Measurements of the galactic non-thermal continuum at high frequencies (> 1 GHz) with the aim of extending the surveys to higher galactic latitudes. Such observations would be important in establishing any systematic variation of spectral index with z .

References

- Allen, R.J. and van der Kruit, P.C. 1976. *Ann. Rev. Astr. and Ap.* 14,
14,
Altenhoff, W.J., Downes, D., Goad, L., Maxwell, A. and Rinehart, R.
1970. *Astr. and App. Suppl.* 1, 319.
Baldwin, J.E. 1967. *IAU Symposium No. 31. Radio Astronomy and the
Galactic System.* p. 337.
Baldwin, J.E. and Pooley, G. 1973. *M.N.R.A.S.* 161, 127.
Beard, M. and Kerr, F.J. 1969. *Aust. J. Phys. Suppl.* No. 11.

- Berkhuijsen, E.M., Haslam, C.G.T. and Salter, C.J. 1971. *Astr. and Ap.* 14, 252.
- Burke, B.F. 1967. IAU Symposium No. 31. *Radio Astronomy and the Galactic System.* p. 361.
- Emerson, D.T. 1974. *M.N.R.A.S.* 169, 607.
- Green, A.J. 1974. *Astr. and Ap. Suppl.* 18, 267.
- Haslam, C.G.T., Wilson, W.E., Graham, D.A. and Hunt G.C. 1974. *Astr. and Ap. Suppl.* 13, 359.
- Heiles, C.E. 1974. IAU Symposium No. 60. *Galactic Radio Astronomy.* p. 625.
- Hirabayashi, J., Ojina, T. and Morimoto, M. 1969. *Nature* 223, 49.
- Hirabayashi, H., Yokoi, H. and Morimoto, M. 1974. *Nature Phys. Sci.* 237, 54.
- Ilovaisky, S.A. and Lequeux, J. 1972. *Astr. and Ap.* 20, 347.
- Jackson, P.D. and Kerr, F.J. 1971. *Ap. J.* 168, 29.
- Jones, B.B. and Finlay, E.A. 1974. *Aust. J. Phys.* 27, 687.
- Landecker, T.L. and Wielebinski, R. 1970. *Aust. J. Phys. Ap. Suppl.* No. 16.
- Mathewson, D.S. and Healey, J.R. 1964. IAU/URSI Symposium No. 20. *The Galaxy and the Magellanic clouds.* p. 283.
- Mathewson, D.S., van der Kruit, P.C. and Brouw, W.N. 1972. *Astr. and Ap.* 17, 468.
- Pooley, G.G. 1969. *M.N.R.A.S.* 144, 101.
- Pooley, G.G. 1969. *M.N.R.A.S.* 144, 143.
- Price, R.M. 1974. IAU Symposium No. 60. *Galactic Radio Astronomy.* p. 637.
- Reifenstein, E.C., Wilson, T.L., Burke, B.F., Mezger, P.G. and Altenhoff, W.J. 1970. *Astr. and Ap.* 4, 357.
- Sancisi, R., Allen, R.J. and van Albada, T.S. 1974. *Colloques Internationaux du Centre National de la Recherche Scientifique* No. 241. *La Dynamique des Galaxies Spirales.* p. 295.
- Sironi, G. 1974. *M.N.R.A.S.* 166, 345.
- van der Kruit, P.C. 1973. *Astr. and Ap.* 29, 231.
- Webster, A.S. 1974. *M.N.R.A.S.* 166, 355.
- Webster, A.S. 1975. *M.N.R.A.S.* 171, 243.
- Westerhout, G. 1958. *Bull. Astr. Ned.* 14, 215.
- Wielebinski, R. 1976. *Astr. and Ap.* 48, 155.
- Wielebinski, R. and Peterson, C.E. 1968. *Observatory*, 88, 219.
- Yates, K.W. 1968. *Aust. J. Phys.* 21, 147.

N76-29125

INFRARED ASTRONOMY AND HIGH ENERGY ASTROPHYSICS

G.G. Fazio, Center for Astrophysics, Harvard College
Observatory and Smithsonian Astrophysical Observatory,
Cambridge, Mass. 02138

ABSTRACT

Observations of the diffuse far-infrared flux from the galactic plane as well as far-infrared measurements of the properties of dense molecular clouds, when combined with recent high-energy gamma-ray measurements and radio observations of carbon monoxide, can yield new information about the total mass of molecular clouds, the large scale structure of the inner galaxy, and the density of cosmic rays.

1. Introduction. Our picture of the distribution of interstellar gas in the galaxy has been changing rapidly, with important implications for galactic structure theory.

Earlier studies of the interstellar gas distribution depended on studies of diffuse optical light, radio continuum and 21-cm radiation. Recently, observations of absorption lines in the ultraviolet spectra of reddened stars have yielded information on the density of molecular hydrogen, but only within a distance of about 1 kpc of the sun. However, recent changes in our knowledge of large scale galactic structure have come about as a consequence of two new and important observations: (1) The detection, at millimeter wavelengths, of carbon monoxide in molecular clouds; in particular, the ground-based observations of the 2.6-mm line associated with the rotational transition ($J = 1 \rightarrow 0$) in CO. (2) The satellite observations of γ -radiation from the galactic plane (in particular the SAS-2 and COS-B results for γ -rays greater than MeV).

The CO measurements yield the molecular cloud abundance in the galaxy, which can then be indirectly related to the molecular hydrogen density (Scoville and Solomon, 1975; Gordon and Burton, 1976). Emission of the 2.6-mm rotation line of CO ultimately results from collisions of H_2 and CO. Hence the CO observations can yield information on the H_2 density and temperature.

The gamma-ray measurements, assuming the radiation arises either from electron bremsstrahlung or π^0 -meson decay, yield information on the product of the interstellar gas density and the cosmic-ray intensity.

The CO surveys show that the molecular cloud abundance in the galaxy exhibits a strong radial dependence with a broad maximum in the 5 to 6 kpc region. A strong increase in the γ -ray emissivity, peaking in the 5 to 6 kpc region, has now been associated with the increase in molecular cloud concentration (Stecker et al., 1974; Puget and Stecker, 1974). The consequence of these observations and their interpretation is that molecular hydrogen is by far the most abundant form of gas in the inner galaxy.

Thus, observations of the mm CO line and the galactic γ -ray flux are related, in that they both give similar distribution of radiation and both lead to a determination of the molecular hydrogen density in the galaxy. Although they complement each other, both require independent analysis in obtaining the molecular hydrogen density, each with different uncertainties.

With this in mind, I would like to suggest an alternative technique, far-infrared observations, for exploring the physics and galactic distribution of interstellar gas, particularly cold molecular clouds and molecular hydrogen.

Specifically, in connection with high-energy astrophysics, I would like to suggest two explicit observations that could yield new and important information on the gas density and cosmic-ray density in the galaxy:

(1) measurement of the diffuse far-infrared flux and spectrum from the galactic plane (Fazio and Stecker, 1976);

(2) measurement of the γ -ray flux from dense molecular clouds in the galaxy (Black and Fazio, 1973).

2. Diffuse Far-Infrared Flux. The basic source of far-infrared radiation in a molecular cloud or HII region is the reradiation of dust heated by light from early type stars or young stellar associations. Judging from measurements of CO excitation temperatures in the molecular clouds (Scoville and Solomon, 1975, for example), the dust temperature in them is expected to be of the order of 10-25 K so that they are expected to radiate most of their energy in the wavelength range $\geq 100 \mu\text{m}$ in distinct contrast to the hotter strong infrared sources at shorter wavelengths ($< 100 \mu\text{m}$) which are primarily associated with HII regions. Stein (1966), Pipher (1973), and Andriesse (1974) have previously proposed the existence of a diffuse infrared flux from the galactic plane due to thermal radiation by dust grains, but the recent CO observations now permit a more detailed prediction of the properties of this radiation.

For this discussion we will assume that the ratio of total gas to dust is roughly the same as that in more diffuse atomic clouds (Ryter *et al.*, 1975) and that the physical properties of the dust are roughly uniform throughout the Galaxy. We will then propose a framework for future

far-infrared surveys by suggesting some basic numerical relations for predicting flux distributions and emissivities. Using dust temperatures derived from CO and other measurements, we can then predict the diffuse far-infrared flux distribution in the galactic plane as a function of galactic longitude ℓ in the range $4^\circ < \ell < 90^\circ$ and the far-infrared emissivity distribution as a function of galactocentric distance.

a) Galactic Plane Emission

If we assume the dust is at an equilibrium temperature, T_d , and radiates with an absorbtivity, Q_{IR} , then the energy emitted in the wavelength interval $d\lambda$ per unit volume of the dust cloud per second is given by

$$J_{IR}(\lambda)d\lambda = 4\pi^2 a^2 n_d Q_{IR}(\lambda) B_\lambda(T_d) d\lambda \quad (1)$$

where a is the radius of the dust grain, n_d the density of dust particles, and $B_\lambda(T)$ is the Planck function.

The value of n_d is related to the total hydrogen density by

$$n_d = (3m_H/4\pi\rho a^3) (M_d/M_H) n_H \quad (2)$$

where m_H is the mass of the hydrogen atom, n_H the total hydrogen density ($n_H = 2n_{H_2} + n_{HI}$), ρ is the grain density, and M_d/M_H the dust-to-gas mass ratio. The column density $N_H = \int n_H ds$ in any direction can be related to the CO emission in that direction as follows:

$$N_H = 4.6 \times 10^{20} I_{CO} \text{ cm}^{-2} \quad (3)$$

where $I_{CO} = \int T_A dv$ is the integrated CO intensity in units of $K \text{ km s}^{-1}$ (Solomon, 1973; Scoville and Solomon, 1975; Gordon and Burton, 1976)¹.

¹ Based on the CO measurements alone, eq. (3) is uncertain by a factor of 5 (Scoville and Solomon, 1975). However, arguments taking into account infrared and X-ray absorption measurements reduce this uncertainty to within a factor of 2 (Stecker *et al.*, 1975).

The dust parameters are ρ , a , and Q_{IR} . The value of ρa can be determined using a hydrogen column density at $l=0^\circ$ (excluding the galactic nucleus) of $7 \times 10^{22} \text{ cm}^{-2}$ (Stecker et al., 1975) and an optical depth in that direction $\tau_V = 2.8$, (Becklin and Neugebauer, 1968; Spinrad et al., 1971). Then

$$\tau_V = 0.92 A_V = \pi a^2 Q_V N_d \quad (4)$$

where A_V is the visual extinction in magnitudes, Q_V is the extinction efficiency at visible wavelengths and N_d is the column density of the dust. If we assume the canonical values $(M_d/M_H) = 10^{-2}$ and $Q_V = 1$, we find

$$\rho a = 3.1 \times 10^{-5} \text{ g cm}^{-2} \quad (5)$$

This is consistent with the values given by Allen (1973) of $\rho = 1 \text{ g cm}^{-3}$ and $a = 3 \times 10^{-5} \text{ cm}$ estimated from Q_V and which we now adopt. We then obtain from eq. (?)

$$N_d = 1.4 \times 10^{-13} N_H \quad (6)$$

The value of Q_{IR} is assumed to be of the form $A_1 \lambda^{-1}$ with $A_1 = 4.5 \times 10^{-5} \text{ cm}$ (Pottasch, 1973)². The optical depth of the dust is then

$$\tau_{IR} = Q_{IR} \pi a^2 N_d = 8.2 \times 10^{-6} \lambda_{\text{cm}}^{-1} I_{CO} \quad (7)$$

For the range of values for I_{CO} given by Scoville and Solomon (1975) and taking $\lambda = 300 \text{ } \mu\text{m}$, it is found that the galaxy is optically thin at far-infrared wavelengths.

From equations (1) and (3) the infrared brightness can be computed as a function of galactic longitude l

² The dependence $Q_{IR} \propto \lambda^{-n}$ with $n=1$ is somewhat uncertain at long wavelengths. Pottasch (1973) and Soifer et al. (1972) find evidence in favor of an overall dependence given by $n \approx 1$. Scoville and Kwan (1975) and Leung (1975) suggest the dependence may be better represented by $n \approx 1.5$ for $\lambda \gtrsim 30 \text{ } \mu\text{m}$, although Leung also gives several examples of grains for which $n \approx 1$. Andriesse (1974) suggests that $n = ?$ for $\lambda > \lambda_c$ with λ_c between $50 \text{ } \mu\text{m}$ and $200 \text{ } \mu\text{m}$.

$$I_{IR} d\lambda = \frac{d\lambda}{4\pi} \int J_{IR} ds = 0.97 \times 10^{-10} \quad (8)$$

$$\times \{I_{CO}(\ell) d\lambda \lambda^{-6} (\exp(1.44/\lambda T) - 1)^{-1}\}$$

$$\text{erg cm}^{-2}\text{s}^{-1}\text{Sr}^{-1}$$

with λ in cm. The total infrared brightness is

$$I_{IR} = \int_0^{\infty} I_{IR} d\lambda = 3.8 \times 10^{-13} T_d^5 I_{CO}(\ell) \text{wm}^{-2}\text{Sr}^{-1} \quad (9)$$

The total emission per grain is

$$\epsilon_g = n_d^{-1} \int J_{IR} d\lambda = 7.7 \times 10^{-24} T_d^5 w \quad (10)$$

The temperature of the dust can be derived by relating it to the CO kinetic temperature, T_{CO} . Goldreich and Kwan (1974) and Scoville and Kwan (1975) have investigated the thermal coupling between radiatively heated dust and ambient molecular gas (H_2) and indicate that the gas will approach thermal equilibrium with the dust ($T_{H_2} \rightarrow T_d$) via collisions of H_2 with grains for $n_{H_2} > 10^4 \text{ cm}^{-3}$. However, at $n_{H_2} = 10^4 \text{ cm}^{-3}$ the collision rate is sufficient to give only $T_{H_2} = 1/2 T_d$. Observational evidence, however, suggests the coupling may be stronger. Scoville and Solomon derive an average value of T_{CO} of 6.6K. We shall assume that a lower limit to T_d is 7K.

An upper limit to the dust temperature can be derived by assuming the dust particle absorbs all the incident visible and ultraviolet radiation and reradiates it in the infrared. At equilibrium:

$$4\pi^2 a^2 \int_0^{\infty} Q_{IR} B_{\lambda}(T_d) d\lambda = \pi a^2 c u_{\gamma} \quad (11)$$

where u_γ is the density of radiation in interstellar space $\approx 7 \times 10^{-13}$ erg/cm³ (Allen, 1973). Solving for T_d , we get $T_d = 15K$. Kaplan and Pikelner (1970) and Greenberg (1971) obtain similar estimates. u_γ may vary somewhat throughout the galaxy, but eq. (11) gives only a $u_\gamma^{0.2}$ dependence for T_d .

In presenting our results in graphical form, we shall assume a value $T_d = 10K$. In figure 1 we have plotted the total infrared brightness, I_{IR} as a function of galactic longitude derived from eq. (9) using the data of Scoville and Solomon for I_{CO} and excluding the galactic center. Of particular importance is the predicted large peak at $\ell = 30^\circ$ tangent to the maximum interstellar gas density near 5 kpc.

A further consequence of our model which can be used as an experimental test is the prediction that the width of the galactic far-infrared disk should be comparable with that of the molecular cloud disk. The full width of the cloud disk is given by Scoville and Solomon to be ~ 130 pc corresponding to a full width in galactic latitude of $\sim 1^\circ$ at $\ell \sim 30^\circ$.

The infrared spectrum can be obtained from equation (8). The maximum in the spectral curve is given by

$$\lambda_m \approx (hc/5.98kT_d) \approx 0.21 T_d^{-1} \text{ cm} \quad (12)$$

where for $T_d = 10K$, $\lambda_m = 240 \mu\text{m}$. In general, with Q_{IR} of the form $A_n \lambda^{-n}$ ($n \geq 0$),

$$\lambda_m = hc/\{(n+5)kT_d\} \approx \frac{1.44}{(n+5)T_d} \text{ cm} \quad (13)$$

In the Rayleigh-Jeans approximation, $hc \ll \lambda kT$, the far-infrared spectrum takes the power-law form

$$I_{IR} d\lambda \propto \lambda^{-(4+n)} d\lambda \quad (14)$$

It follows from eq. (11) (also Andriess (1974)) that assuming $n > 1$ would result in higher T_d estimates and

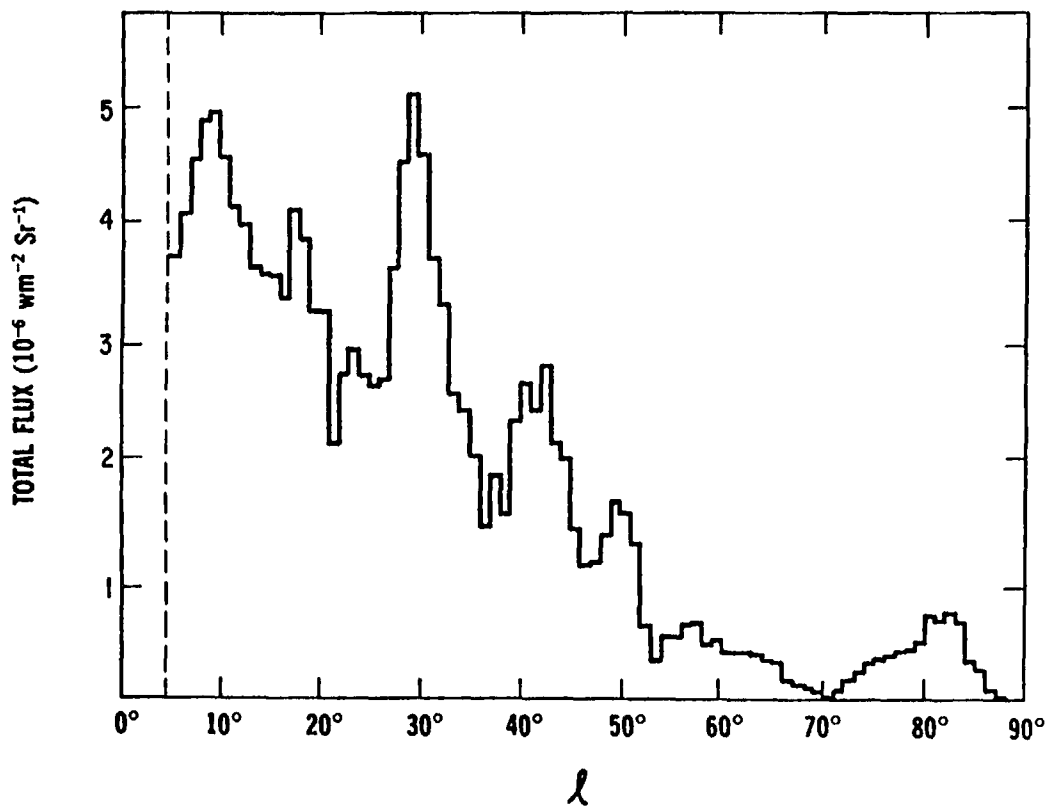


Fig. 1. Predicted longitude dependence of the galactic far-infrared flux based on the model in equation (9) using the CO data of Scoville and Solomon (1975) and a temperature of 10K.

smaller differential fluxes at long wavelengths, although the total infrared flux integrated over all λ as shown in the figures remains unchanged (Greenberg, 1971). For example, Andriessse (1974) with $n = 2$, obtains $T_d \sim 24K$ with $\lambda_m \sim 85 \mu m$. For the intermediate case, $n = 1.5$, $\lambda_m \sim 150-200 \mu m$. Future spectral measurements over the galactic plane in the far-infrared could thus help determine the wavelength dependence of Q_{IR} .

Using the relations derived by Stecker *et al.* (1975) in conjunction with equations (6) and (10) and employing the data of Scoville and Solomon on the molecular cloud distribution in the galaxy, the total far-infrared emissivity from molecular clouds as a function of galactocentric distance was calculated. The results are given in figure 2.

(b) Galactic Center Region

In the galactic center region $|l| < 3^\circ$, Scoville, Solomon and Jefferts (1974) have already shown that a correlation exists, as a function of galactic longitude, between the 100 μm flux and the maximum CO brightness temperature at each longitude. These authors conclude that the CO and dust coexist in nearly thermal equilibrium.

The CO measurements indicate that the molecular cloud disk surrounding the galactic nucleus has a radius of ~ 250 pc and that the total mass of molecular gas, mostly H_2 , within the cloud is $\sim 5 \times 10^7 M_\odot$.

In accordance with our assumed gas-to-dust ratio, the implied dust mass is then $M_d \sim 5 \times 10^5 M_\odot$ or about 10^{39} g. The total number of grains is then

$$N_g = (3M_d/4\pi a^3 \rho) \sim 10^{52} \quad (15)$$

and, from equation (10), the total luminosity of the galactic center source is estimated to be

$$L_{G.C.} = N_g \epsilon_g \sim 8 \times 10^{28} T_d^5 w \quad (16)$$

which, using the data given by Hoffman, Frederick and

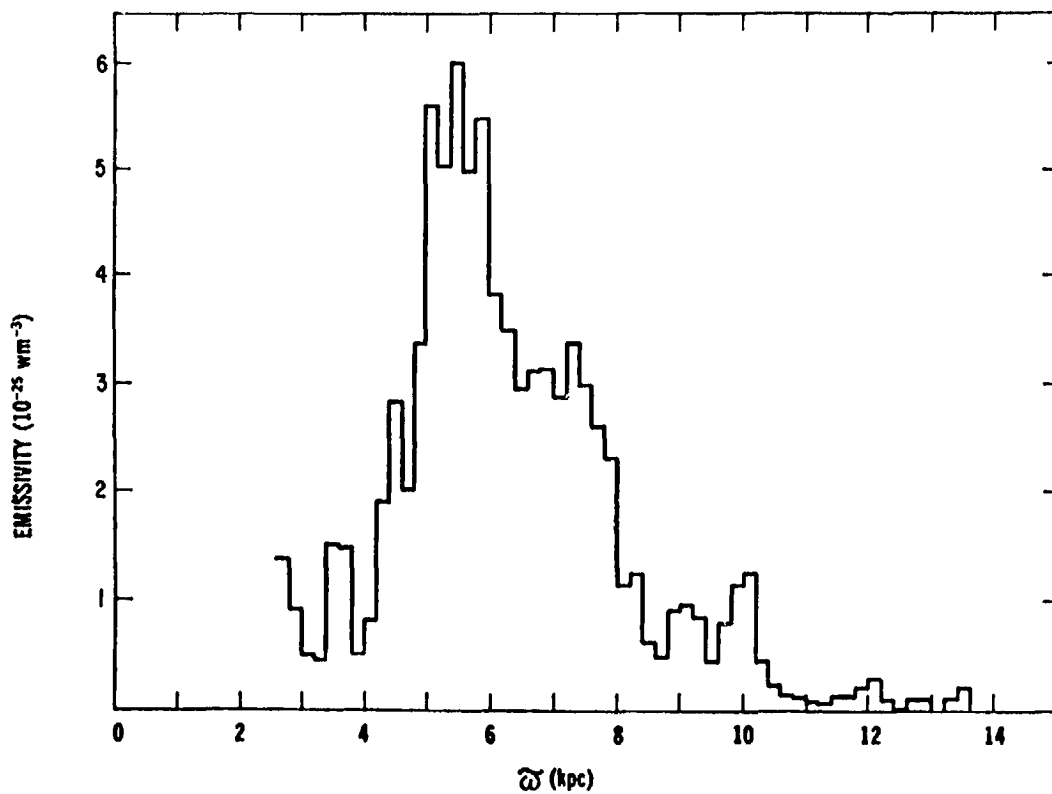


Fig. 2. Predicted galactic far-infrared emissivity distribution using equations (6) and (10) together with the data of Scoville and Solomon (1975) and the values for n_{H_2} derived by Stecker *et al.* (1975). Again, a cloud of $T = 10\text{K}$ has been assumed.

Emery (1971), yields an estimated temperature $T_{d,g.c.}$ of the order of 25 K. The mean temperature of the CO gas, expected to be somewhat cooler, is of the order of 20 K (Scoville, Solomon and Jefferts, 1974) so that our model gives reasonable results for the galactic center source.

(c) Conclusions

Our results indicate that much can be learned about the physics and conditions of interstellar dust and molecular clouds as well as the galactic dust and cloud distribution by making far-infrared studies of the galactic plane. In the inner galaxy, most of the interstellar medium is in the form of the cold clouds. Far-infrared surveys, in conjunction with other observations, will enable us to get better estimates of quantities like n_H , N_d and T_d . We have predicted the intensity, angular distribution and spectrum of the diffuse far-infrared radiation over that region of the galactic plane where sufficient CO data are available ($4^\circ < \ell < 10^\circ$) using the data of Scoville and Solomon (1975). Comparison of our model with 100 μ m observations of the galactic center source, which is expected to be about three times hotter than the average galactic molecular cloud, gives us confidence in the basic relations given in this paper. We believe the flux estimates calculated here to be reasonable predictions, however, one should bear in mind the assumptions made, in particular the wavelength dependence of Q_{IR} , the uncertainty in the relationship between I_{CO} and n_H and the assumption of a uniform value of $T_d = 10$ K since the predicted flux has a steep temperature sensitivity.

(d) Other Infrared Experiments

Recently other infrared experiments have been proposed to study galactic structure. Ito *et al.* (1976) have observed the diffuse near-infrared radiation (2.4 microns) from the galactic plane and observed a correlation with the longitude distributions of CO molecular clouds, thermal radio emission, neutral hydrogen and γ -ray emission. The authors predict that models of the galactic mass distribution should be improved by these observations.

Puget *et al.* (1975) have discussed the general distribution of Interstellar reddening within ~ 1 kpc of the sun

and find a correlation with the distribution and column density of nearby dense molecular clouds. From this mass distribution the nearby cosmic γ -ray flux can be predicted and subtracted from the measured flux to obtain the true γ -ray flux from the inner galaxy. This true flux then yields the large scale cosmic-ray distribution in the galaxy.

3. The Gamma-Ray Flux from Dense Interstellar Clouds. In 1973 John Black and I (Black and Fazio, 1973) predicted that dense interstellar clouds could be detectable discrete sources of γ -rays (> 100 MeV), produced by cosmic-ray interactions with the gas in the cloud, particularly molecular hydrogen. The gamma-ray flux from a discrete cloud of mass M at a distance R_{pc} (parsec) is given by the simple expression:

$$F_{\gamma} (> 100 \text{ MeV}) \approx 1.3 \times 10^{-6} \left(\frac{1}{R_{pc}} \right)^2 \left(\frac{M}{M_{\odot}} \right) \text{ photons/cm}^2 \text{ sec}$$

This formula assumes the cosmic ray intensity is uniform in the galaxy, with the same intensity as observed at the Earth.

Recently near- and far-infrared observations, as well as radio molecular line emission, of dense dark clouds have yielded new information on the density, extent, and central position of these clouds. Hence better estimates of the cosmic γ -ray fluxes can now be predicted. Also the SAS-2 has now provided the most extensive and highest sensitivity survey of γ -rays from these clouds. It is necessary, therefore, to reinvestigate this problem.

The dark cloud south of the star ρ Oph is perhaps the largest and densest of the nearby molecular clouds. It is also one of the best observed clouds at infrared wavelengths (Vrba, Strom, Strom, and Grasdalen, 1975; Fazio, Wright, Zeilik, and Low, 1976) and in microwave line emission (Encrenaz et al., 1975). Using a gas density of $\sim 10^4 \text{ cm}^{-3}$ in the cloud, and $D \sim 3 \text{ pc}$, gives a total mass of $4 \times 10^3 M_{\odot}$. The distance to the cloud is about 190 pc. Hence the predicted γ -ray flux is 1.4×10^{-7} photons/cm² sec. The SAS-2 observations of this source yield only an upper limit (95% confidence level) to the γ -ray flux above 100 MeV of $2 \times 10^{-6} \text{ cm}^{-2} \text{ sec}$ (Kniffen, Lamb, Fichtel, and Thompson, 1976). Thus the present sensitivity is about a factor of 10 above the predicted flux. Other possible sources have also been investigated, with negative

results. These results are summarized in Table 1.

As Black and Fazio (1973) pointed out earlier, the molecular cloud ring around the galactic center, which is at a radius of 250 pc and moving radially outward, should be a detectable gamma-ray source. For a total mass of $\sim 10^8 M_{\odot}$ and a distance of 10 kpc the predicted flux is $\sim 1.3 \times 10^{-6}$ photons/cm sec, and the predicted size is $\sim 3^{\circ}$ along the plane and $\sim 0.5^{\circ}$ perpendicular to the plane. However this source is presently obscured by the more intense radiation from the 5 kpc ring and the lack of sufficient angular resolution.

Further high-energy gamma-ray experiments with increased angular resolution and sensitivity are obviously needed before important new information can be obtained on the discrete molecular cloud sources and the density of cosmic rays in the galaxy.

It is interesting to note that although no discrete sources were observed, that a plot of the positions of the center of mass of dark clouds along the plane, as given by B.T. Lynds (1962), shows an inclination to the plane, above it in the 0° to 150° region and below it in the 150° - 250° region. This inclination is the same as bright B stars and indicates that these clouds are associated with Gould's Belt. The SAS-2 gamma-ray flux measurements exhibit a similar asymmetry to the plane, and although no discrete dark cloud was observed, the cumulative effect of many smaller clouds could be important.

I am particularly indebted to the SAS-2 group of D.A. Kniffen, R.C. Lamb, C.E. Fichtel and D.J. Thompson for their rapid analysis of the gamma-ray observations of discrete molecular clouds.

TABLE 1
UPPER LIMITS TO THE GAMMA-RAY
FLUX FROM DENSE MOLECULAR CLOUDS

MOLECULAR CLOUD SOURCE	GAMMA-RAY FLUX (> 100 MeV) UPPER LIMIT (photons/cm ² sec)*
Oph DARK CLOUD	2.0×10^{-6}
R Cor A DARK CLOUD	6.7×10^{-7}
Taurus DARK CLOUD	3.1×10^{-6}
IC 1848-1	2.0×10^{-6}
Orion A	1.1×10^{-6}
Orion I-2	1.3×10^{-6}
B 227	$5.0 \times 10^{-6} \dagger$
L 134	5.4×10^{-7}
L 121	1.1×10^{-6}
B 335	2.1×10^{-6}
B 163	2.0×10^{-6}
NGC 1333	2.0×10^{-6}
M 78	1.1×10^{-6}

* Upper limits to the flux are at the 95% confidence limit; results are from SAS-2 observations (Kniffen, Lamb, Fichtel, and Thompson, private communication).

† This flux limit is high due to confusion with the gamma-ray sources NP0532 and $\gamma(193+3)$. Whether this cloud could be the latter source should be investigated further.

REFERENCES

- Allen, G.W. 1973, Astrophysical Quantities, 3rd ed.,
Athlone Press, London.
- Andriessse, C.D. 1974, *Astr. and Ap.* 37, 257.
- Becklin, E.E. and Neugebauer, C. 1968, *Ap. J.* 151, 145.
- Black, J.H. and Fazio, G.G. 1973, *Ap. J. (Letters)* 185, L7.
- Burton, W.B. 1976, *Ann. Rev. Astr. and Ap.*, in press.
- Burton, W.B., Gordon, M.A., Baina, T.M., and Lockman, F.J.
1975, *Ap. J.* 202, 30.
- Encrenaz, P.J., Falgone, E., and Lucas, R. 1975, *Astron.*
and *Ap.* 44, 73.
- Fazio, G.G., and Stecker, F.W. 1976, *Ap. J. (Letters)*, in press.
- Fazio, G.G., Wright, E.L., Zeilik II, M. and Low, F.J.
1976, *Ap. J. (Letters)*, to be published.
- Fichtel, C.E., Hartman, R.C., Kniffen, D.A., Thompson,
D.J., Bignami, G.F., Ögelman, H., Özel, M.F., and
Tümer, T. 1975, *Ap. J.* 198, 163.
- Greenberg, J.M. 1971, *Astr. and Ap.* 12, 240.
- Goldreich, P. and Kwan, J. 1974, *Ap. J.* 187, 243.
- Gordon, M.A. and Burton, W.B. 1976, preprint.
- Hoffman, W.F., Frederick, C.L., and Emery, F.J. 1971, *Ap.*
J. (Letters) 164, L23.
- Ito, K., Matsumoto, T., and Uyama, K. 1976, preprint.
- Kaplan, S.A. and Pikelner, S.B. 1970, The Interstellar

- Medium, Harvard U. Press, Cambridge, Mass.
- Kniffen, D.A., Lamb, R.C., Fichtel, C.E., and Thompson, D.J. 1976, (private communication).
- Leung, C.M. 1975, Ap. J. 199, 340.
- Lynds, B.T. 1962, Ap. J. Suppl. 7, 1.
- Paul, J., Cassé, M. and Cesarsky, G.J. 1976, preprint.
- Pipher, J.L. 1973, Interstellar Dust and Related Topics, p. 559 (J.M. Greenberg and H.C. van de Hulst, eds.) Reidel Pub. Co. Holland (IAU Symp. No. 52).
- Pottasch, S.R. 1974, Astr. and Ap. 30, 371.
- Puget, J.K., Ryter, C.E., Serra, B. and Bignami, G. 1976, Astron. and Ap., in press.
- Puget, J.L. and Stecker, F.W. 1974, Ap. J. 191, 323.
- Ryter, C.E., Cesarsky, C.J. and Audouze, J. 1975, Ap. J. 198, 103.
- Scoville, N.Z., and Kwan, J. 1975, Ap. J. in press.
- Scoville, N.Z., and Solomon, P.M. 1975, Ap. J. (Letters) 199, L105.
- Scoville, N.Z., Solomon, P.M., and Jefferts, K.B. 1974, Ap. J. (Letters) 187, L63.
- Soifer, B.T., Pipher, J.L., and Houck, J.R. 1972, Ap. J. 177, 315.
- Solomon, P.M. 1973, Physics Today 26, 32.
- Solomon, P.M. and Stecker, F.W. 1974, Proc. ESLAB Symp. on

- the Context and Status of γ -ray Astronomy, Frascati
(ESRO SP-106) p. 253.
- Spinrad, H., Liebert, J., Smith, H.E., Schweitzer, F.,
and Kuhl, L. 1971, Ap. J. 165, 17.
- Stecker, F.W. 1976, Nature, 260, 412.
- Stecker, F.W., Puget, J.L., Strong, A.W., and Breckamp,
J.H. 1974, Ap. J. (Letters), 188, L59.
- Stecker, F.W., Solomon, P.M., Scoville, N.Z., and Ryter,
C.E. 1975, Ap. J. 201, 90.
- Stein, W. 1966, Ap. J. 144, 318.
- Vrba, F.J., Strom, K.M., Strom, S.E., and Grasdalen, G.L.
1975, Ap. J. 197, 77.

N76-29126

"ULTRAVIOLET OBSERVATIONS OF LOCAL GAS"

E. B. Jenkins, Princeton University Observatory, Princeton, New Jersey
08540 U.S.A.

ABSTRACT

From satellite measurements of ultraviolet spectra of stars, an average density of approximately 1.1 cm^{-3} for hydrogen atoms, in both atomic and molecular form, is estimated for regions of space along the galactic plane within about 1 kpc of the sun. About 20% of the atoms are bound in molecular form although this figure is uncertain since the ultraviolet measurements avoid the very dense interstellar clouds. Discrete values for this percentage are observed to vary markedly; regions with less than average density seem to have fractional abundances of H_2 several orders of magnitude lower than average. A ratio of CO/H which ranges from 10^{-9} to 10^{-6} is observed for regions in front of stars observed by the Copernicus satellite.

I. Introduction

A basic theme which underlies many of the contributions to the study of galactic structure is the complementarity of information derived from such diverse observables as diffuse gamma ray emission, radio continuum fluxes, 21-cm and CO line emissions, and counts of pulsars and supernova remnants. Against the backdrop of these methods, studies on the distribution and properties of interstellar matter from observations in the ultraviolet seem relatively myopic, since only about one percent of the volume of the galactic disk can be surveyed by present-day orbiting telescopes. The primary factor which limits ultraviolet studies to regions within a few kpc of the sun is the strong attenuation of ultraviolet radiation by the intervening interstellar dust. In spite of this restriction of range, we shall see in the discussion which follows the special contributions which arise from viewing interstellar absorption features in the ultraviolet. In particular, one obtains unique information on the general behavior of atoms and molecules in space, which is of value in the interpretations of data from other areas of research. Also, we can ascertain average densities of various gaseous constituents in the local part of our galaxy, and such measurements serve as a benchmark for calibrating the broader scale mappings of interstellar matter which are quantitatively uncertain.

II. Background

Just over ten years ago, the development of attitude control systems for Aerobee sounding rockets triggered the beginning of the age of ultraviolet stellar spectroscopy, since the spectrographs could be stabilized with enough precision to record exposures of bright stars during the vehicle's coasting trajectory above the atmosphere. Owing to the moderate wavelength resolutions of the early observations (typically a few Angstroms), much of the research concentrated on the properties of stellar features, rather than absorption features produced by the intervening gas in space. These early rocket flights were able to provide, however, two important contributions which furthered our understanding of the local interstellar gas. First, a number of observations of Ly α absorption by interstellar H I established that the average densities toward most of the stars observed were substantially lower than expected in our region of the galaxy from studies of 21-cm emission, suggesting that a good fraction of the volume of space within several hundred pc of the sun had densities lower than the overall mean density (Jenkins 1970). The second main achievement in the study of the interstellar medium was the discovery of absorption by molecular hydrogen (Carruthers 1970, Smith 1973), a form of matter long suspected to be an important constituent of the

gas, but one which until then had been tantalizingly elusive to detect.

The spectrometer aboard the first orbiting astronomical observatory OAO-2 permitted us to survey at 12 Å resolution the L α absorption for a substantial number of stars (Savage and Jenkins 1972). While 21-cm radio line observations provide a rich backlog of information on the distribution and kinematics of interstellar gas, several important differences in the way the gas is measured establish a unique value to the L α data. First, the volume sampled toward a star has a definite length and virtually infinitesimal width, while the radio beam samples a cone-shaped space of unlimited extent. Also, corrections for saturation are unnecessary for the L α line, since it is already heavily saturated, so much so that the damping wings are the principal contributors to the absorption. Hence the line strength is governed purely by the column density of the gas rather than a complex inter-relationship between the amount, velocities and spin temperatures of atoms along a line of sight. Finally, the L α measurements allow one to compare directly the abundances of H I to other species observed toward the same stars, such as interstellar Na I, Ca II and K I (seen by absorptions in the visible spectrum) and also interstellar dust grains (revealed by continuous absorption).

In the discussions which will follow, we will draw heavily upon the inference from the OAO-2 L α survey that hydrogen gas column densities and obscuration by dust (as revealed by B-V color excesses) are well correlated with each other, and that measurements of E(B-V) toward a star can be used with reasonable accuracy to predict the total amount of gas present (Jenkins and Savage 1974). The colocation of gas and dust has also been demonstrated in analyses of radio data (e.g. see references cited in Jenkins (1970) and also recent work by Grayzeck and Kerr 1974, Heiles 1976, and Heiles and Jenkins 1976).

Over the past four years the successful operation of the Copernicus satellite, the last of the OAO's, has brought about a climax in the study of the interstellar gas, since absorption by strong resonance lines from the ground states of important constituents could be studied in detail. Much has been learned about the composition and physical state of interstellar gases from the Copernicus observations; however it is out of place to summarize the broad spectrum of conclusions here, especially since much of the material has already been reviewed in the literature (Spitzer and Jenkins 1975, Snow 1976). Instead, we shall focus on two topics which have a special relevance to the study of cosmic gamma rays and galactic structure. First, the ultraviolet observations can give an independent determination of the average density of both atomic and molecular hydrogen, against which we can compare the representative densities derived from larger scale observations at a galactocentric distance $R = 10$ kpc. The second area of interest is a study of the relative abundances of CO and H₂ in the interstellar medium, since it enables us to calibrate the H₂ densities

in terms of CO radio measurements for gas outside the dense molecular clouds.

III. Average Density of H I and H₂

a) Observational Selection

Our objective in analyzing the surveys of H I and H₂ column densities (which we denote as N(H I) and N(H₂)) is to arrive at a representative average for the space densities within the overall sampling volume. If the stars chosen for the survey are widely enough distributed and represent a truly random sample of directions in the sky, one can total all the column densities and divide by the sum of the distances r to give a measure of average space density along all of the lines of sight. If we draw upon the L α results of Savage and Jenkins (1972), Jenkins and Savage (1974)*, Bohlin (1975) and preliminary results from Bohlin, Drake and Savage (1976), we find for 130 stars an average value

$$\frac{\sum N(\text{H I})}{\sum r} = 0.32 \text{ cm}^{-3}$$

From the work of Spitzer et al. (1973), (1974) and Bohlin, Drake and Savage (1976) we find for 70 stars

$$\frac{\sum N(\text{H}_2)}{\sum r} = 0.043 \text{ cm}^{-3}$$

We must immediately realize, however, that these figures are far from representative, since the choice of stars is not random. A strong ^{bias against} reddened stars exists in all of the surveys. That such selection is a dominant effect follows from two main factors: first, the distribution of gas in space is highly irregular, and second, the extinction of star light is very strong at short wavelengths (York et al. 1973). Another contributing factor is that some of the stars are at large distances from the plane of the galaxy: 21% of the total sample path length has $z > 100\text{pc}$ and 10% is more than 200 pc away from the plane. Figure 1 shows a plot of color excess per unit distance $E(B-V)/r$ against distance r for all of the stars studied for L α or H₂ absorption.

*In all of our use of the data of Savage and Jenkins (1972) and Jenkins and Savage (1974), we have rejected the type B1.5 and B2 stars for which Savage and Panek (1974) estimated the stellar L α feature to be a significant part of the measured absorption.

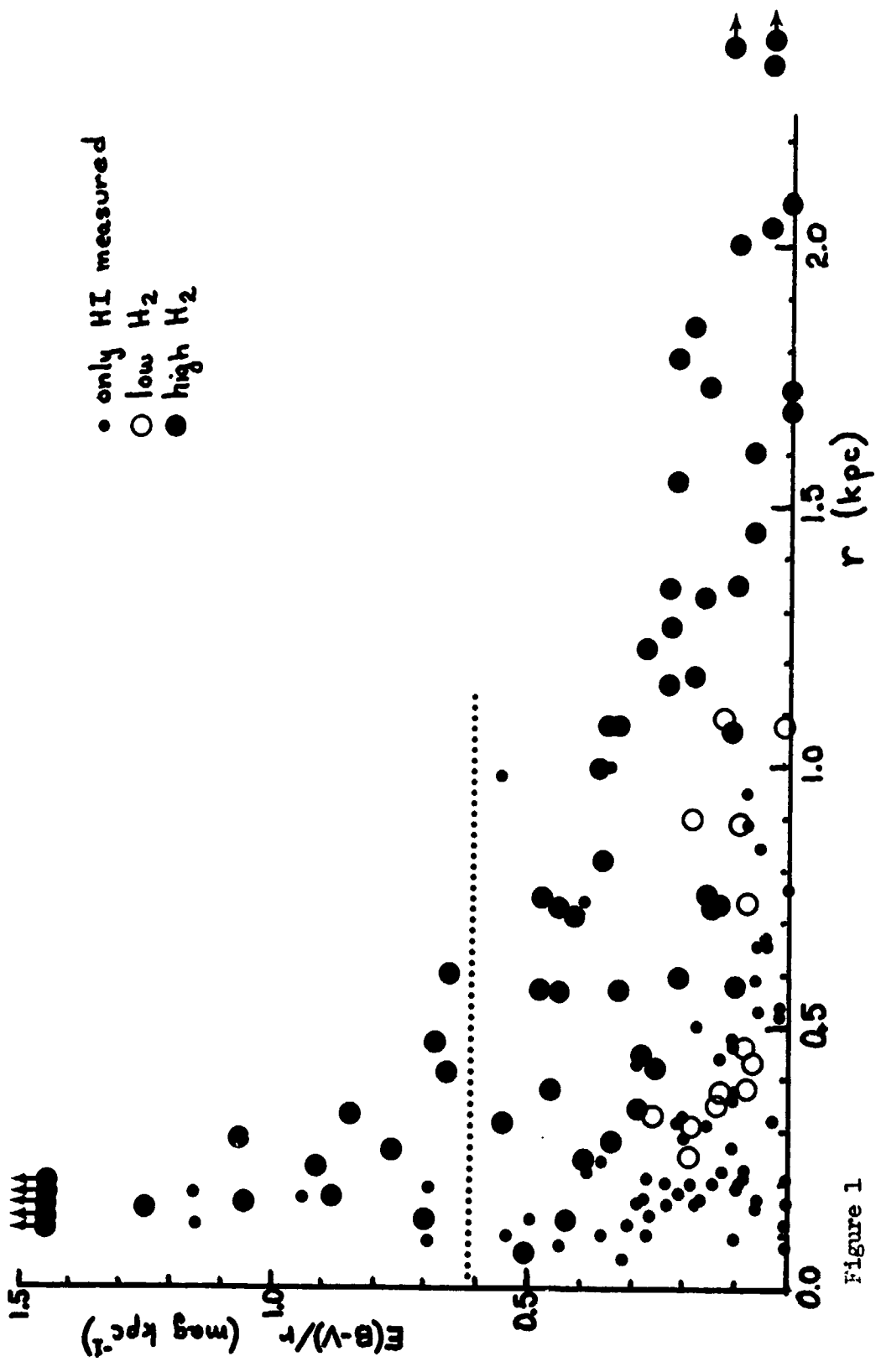


Figure 1

If one samples truly random regions of space in the plane of the galaxy within 1 kpc of the sun, one should have an average $E(B-V)/r$ of $0.61 \text{ mag kpc}^{-1}$ (Spitzer 1968), shown by the dotted line in the diagram (about half this value is obtained if stars are selected to a given magnitude limit in the visible). In the immediate vicinity of the sun (a few hundred pc or so), the actual reddening per unit distance is somewhat less than normal (FitzGerald 1968). Figure 1 shows us that for stars more distant than about 300 pc the sample represents lines of sight which avoid areas with normal reddening, and this bias becomes worse with increasing distance. For all of the stars shown on the diagram, $\Sigma E(B-V)/\Sigma r = 0.23 \text{ mag kpc}^{-1}$. Thus an interpretation of the H I and H₂ data must contain some compensation which overcomes the effects of this selection.

b) Ionization

Another effect which must be considered is the fact that every measurement is toward a star which is hot enough to photoionize a region of space around it. Thus, to varying degrees some of the gas will be removed from sight in a systematic manner, in addition to our having lines of sight which intersect by chance the ionization zones around other stars. One can assess how important the observed stars' ionization is to an overall result by the following analysis: under ideal circumstances we expect for each observation the equation

$$N(\text{H I}) + 2N(\text{H}_2) + (3N_L n_e / 4\pi\alpha)^{1/3} = R E(B-V)$$

to be valid, where R is the ratio of the total gas column density to the color excess (we treat R as an unknown, but whose value is constant everywhere). The third term in the equation is the expected column density of ionized hydrogen around a star emitting N_L Lyman limit photons per second in a region with a uniform electron density n_e . At 10^4 °K the recombination coefficient α to all levels of hydrogen except $n = 1$ is estimated to be $2.6 \times 10^{-13} \text{ cm}^3 \text{ s}^{-1}$ (Spitzer 1968), and values of N_L for stars of various spectral types are listed by Panagia (1973). We have no direct knowledge about values for n_e in the vicinity of most of the stars, but H α and radio continuum emission measures indicate typical densities ranging from 1 to 10 cm^{-3} , although some of the more conspicuous H II regions have much higher densities. For these two values of n_e , best solutions for R give $5.7 \times 10^{21} \text{ cm}^{-2} \text{ mag}^{-1}$ and $6.3 \times 10^{21} \text{ cm}^{-2} \text{ mag}^{-1}$, respectively, for all of the stars surveyed. A least-squares solution which allows both R and $n_e^{1/3}$ to vary as free parameters yields $n_e^{1/3} = 0.33 \text{ cm}^{-2/3}$ and

$R = 5.4 \times 10^{21} \text{ cm}^{-2} \text{ mag}^{-1}$. (1) If ionization were neglected we would have found $R = 5.2 \times 10^{21}$.

To summarize, the least-squares solution suggests ionization by the target stars reduces the amount of gas seen by only about 4%, but this fraction could be as large as 17% if n_e were typically 10 cm^{-3} . The fact that the least-squares solution for a representative $n_e^{1/3}$ is small may be an indication that the actual values for R inside the ionization zones are somewhat larger than in the general gas regions.

c) Evaluation of Overall Densities

In analyzing the behavior of the average volume density n along various lines of sight, it is instructive to study the relationship for different values of $E(B-V)/r$. For the 70 stars where both $N(\text{H I})$ and $2N(\text{H}_2)$ have been measured (see references cited in § IIIa), we see from Figure 2⁽²⁾ that the average total hydrogen densities $n(\text{H I}) + 2n(\text{H}_2)$ are linearly related to $E(B-V)/r$, although the points show some scatter. This scatter is worse if one plots just $n(\text{H I})$ versus $E(B-V)/r$, because of the large variability in the fraction of hydrogen in molecular form (see § IIIId).

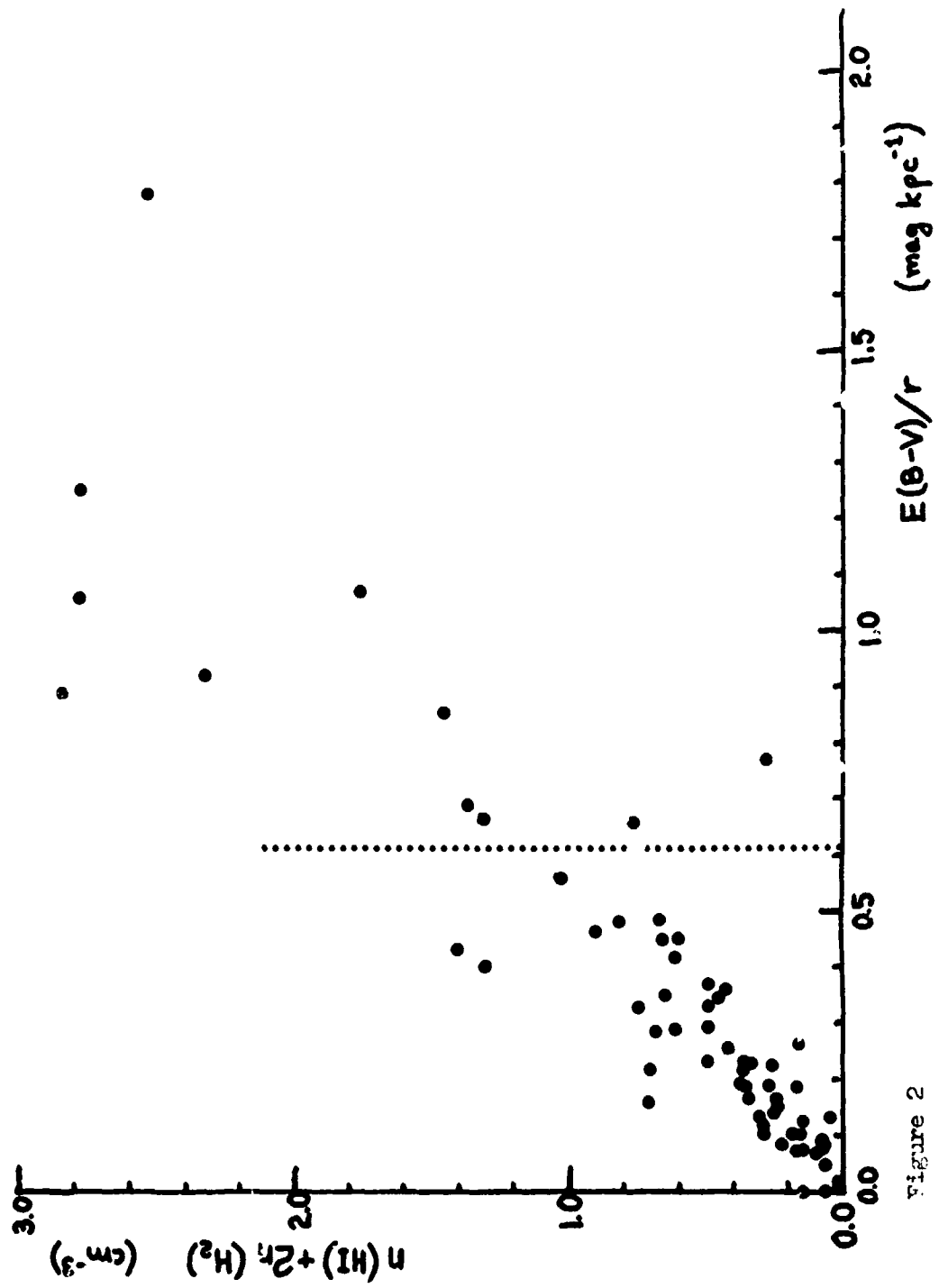
The lack of any gross irregularities in the relationship of total gas density to dust density suggests that a derivation of an average density, with a compensation for the selection discussed in § IIIa, is relatively straightforward. We may take the observed $\Sigma [N(\text{H I}) + 2N(\text{H}_2)] / \Sigma r$, multiply it by the true average reddening per unit

(1) The expression

$$\Sigma \epsilon^2 = \left\{ \left[N_t + 8720 N_L^{1/3} n_e^{1/3} - R E(B-V) \right]^2 / (N_t + R^2 E(B-V)^2)^{1/2} \right\},$$

where $N_t = N(\text{H I}) + 2N(\text{H}_2)$, was minimized by varying the parameters R and $n_e^{1/3}$. The error matrix terms $\partial^2 \Sigma \epsilon^2 / \partial R^2$, $\partial^2 \Sigma \epsilon^2 / \partial R \partial (n_e^{1/3})$ and $\partial^2 \Sigma \epsilon^2 / \partial (n_e^{1/3})^2$ are 0.35, -1.7×10^{20} and 3.2×10^{41} , respectively.

(2) The points for a few of the 70 stars are outside of the range of Fig. 2; they are reasonably in line with the average tendency but off beyond the upper right corner of the diagram.



distance, and divide by the observed $\Sigma E(B-V)/\Sigma r$. The resulting estimate for the overall density of hydrogen atoms, in both atomic and molecular form, is approximately 1.1 cm^{-3} , a figure which one might consider raising to 1.2 or 1.3 to compensate for the systematic losses from ionization discussed in § IIIb.

d) Behavior of H_2

If we concentrate on the distribution of H_2 , we find considerably more variability in the measurements. Early data from Copernicus suggested a bimodal distribution in H_2 column densities (see Fig. 4 of Spitzer and Jenkins, 1975); the more recent, extensive survey by Bohlin, Drake and Savage (1976) confirms that values for $n(\text{H}_2)$ are either around 10^{-6} cm^{-3} or are in the range 10^{-3} to 10^{-1} cm^{-3} for various lines of sight. (Cases with low and high molecular abundances are shown as different symbols in Fig. 1.)

This phenomenon may be qualitatively understood if one considers the formation and destruction of H_2 in space (Hollenbach et al. 1971). Since H_2 is probably formed as the atoms collide with dust grains and combine on the grain surfaces, the rate of H_2 production scales with the square of the density. The destruction of the molecules is primarily from photodissociation by starlight, and for reasonable densities and starlight fluxes the expected abundances are in accord with the very low values for $n(\text{H}_2)$ quoted above. An important feature of the photodissociation, however, is that it occurs by absorption in discrete, strong lines, rather than by a continuum. This process, originally proposed by Solomon (see Field et al. 1966), involves the absorption of an ultraviolet photon which raises the molecule to a higher level of electronic excitation, which is then followed by a spontaneous decay to the ground electronic level. Occasionally (about 11% of the time) the decays are to the vibrational dissociative continuum of the ground state, resulting in the destruction of the molecule. For moderate column densities of H_2 ($\sim 10^{17} \text{ cm}^{-2}$) the lines become optically thick, and thus for increasing interstellar cloud thicknesses self-shielding becomes important. As a result, an abrupt transition to high molecular density occurs, since photodestruction rates are markedly reduced in the cloud's interior.

For a given line of sight, we are unable to ascertain the details of cloud geometry, incident starlight fluxes, or other factors which govern the equilibrium between atoms and molecules. However, the measured $E(B-V)/r$ is a crude indicator of whether dense clouds are present. Figure 3 shows a plot of $2n(\text{H}_2)$ versus $E(B-V)/r$ for the same stars as shown in Figure 2. Instead of the direct proportionality we saw for the total hydrogen density, the observed relationship of molecules to dust suggests that for $E(B-V)/r \lesssim 0.1$ molecules have difficulty in accumulating, but as $E(B-V)/r$ exceeds this value the

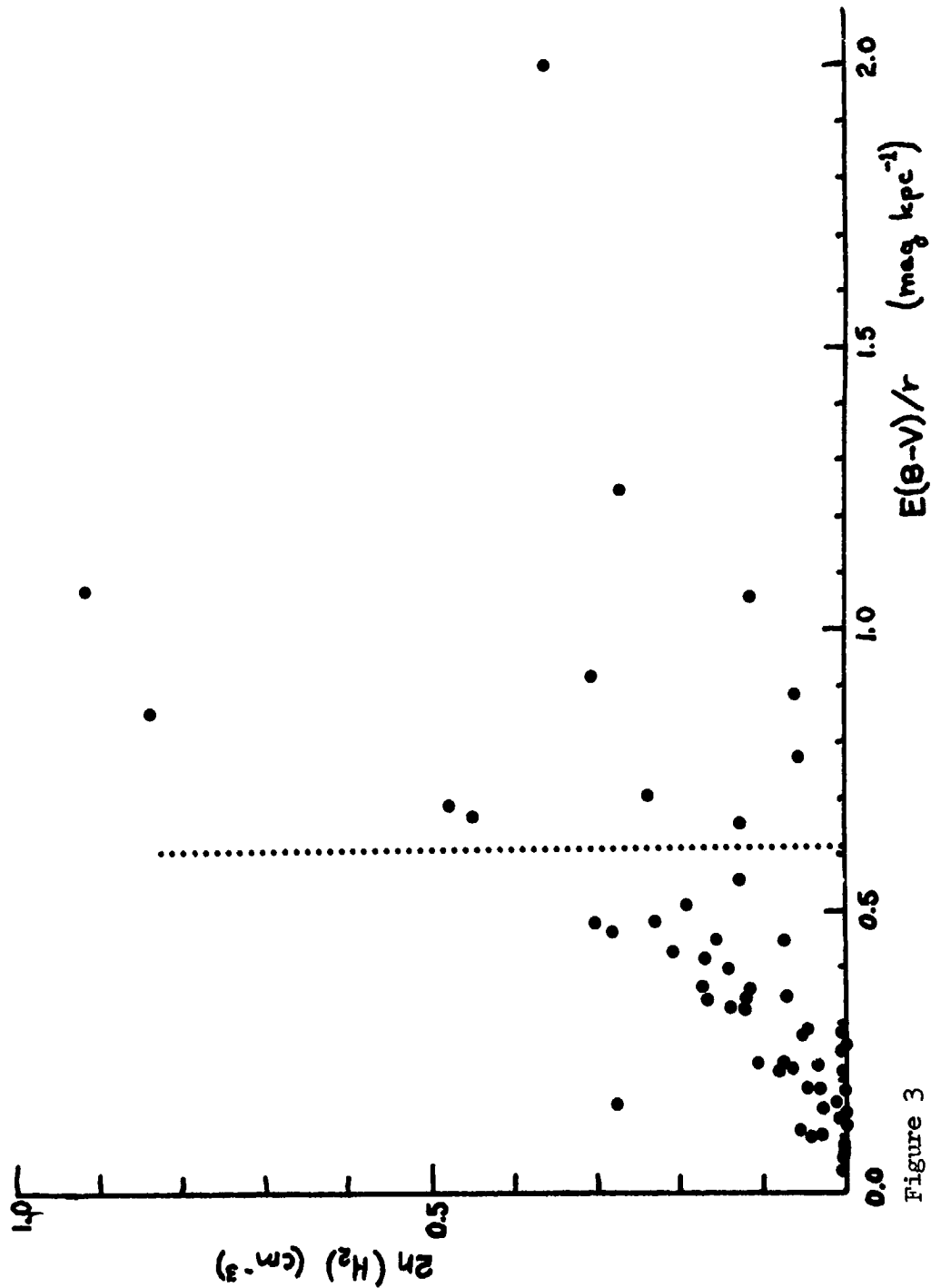


Figure 3

shielding becomes important and the average molecular densities begin to grow with increasing amounts of material present. We note that the scatter of points is larger here than in Figure 2, this is also probably a consequence of the unusual evolution for molecular regions.

Because of the nonlinearity in the growth of molecules, it is harder for us to derive an overall average for $n(\text{H}_2)$ which has the compensation for observational selection. In essence, we must know a frequency distribution for the true $E(\text{B-V})/r$ for small volumes of space in our part of the galaxy, rather than just a mean value. A crude estimate for the best value of $n(\text{H}_2)$ can be made by assuming the intersection of the dotted line ($0.61 \text{ mag kpc}^{-1}$) with the trend of points in Figure 3 gives an indication of the average conditions, under the assumption that when we observe this amount of reddening per unit distance, the distribution of material is typical of more general regions of space. A value of 0.1 cm^{-3} seems to be a good estimate for a representative H_2 density; from the spread of points we see this number could easily be in error by a factor of two. Combining this result with the total density derived in § IIIc, we find that roughly 20% of the neutral atoms are bound in molecular form.

IV. THE RATIO OF CO TO H_2

In addition to measuring column densities of H I and H_2 , the Copernicus satellite can scan absorptions by CO molecules in front of a star. While this offers us some insight on the formation of CO in space, measurements of the ratio of CO to H I and H_2 are also of interest to compare with the adopted ratios used to derive H_2 densities from radio measures of CO. The radio observations are, of course, of prime importance in mapping the distribution of molecular regions in our galaxy.

Figure 4 shows CO/H_2 density ratios, plotted against our familiar scale of $E(\text{B-V})/r$, for 21 stars which were analyzed by Jenkins and Shaya (1976) for CO and by Spitzer et al. (1973, 1974) and Bohlin, Drake and Savage (1976) for H_2 . The uncertainties in some of the ratios are as large as 50%, although many of the values are better defined than this. The sharp change in the abundance ratio shown here is reminiscent of the contrasts in H_2 abundances discussed in § IIIId. In fact, if we examine the ratio of CO to total hydrogen, as shown in Figure 5, we see that the variation of the CO to H_2 ratio is simply a result of the large changes in the fractional abundance of H_2 . In other words, the density of CO is governed more by the total density of gas than by the presence of H_2 . This conclusion is of relevance to theories on the formation of CO, since ion-molecule reaction chains, initiated by the presence of H_2 , are a popular explanation for the origin of CO in interstellar clouds (e.g., see Glassgold and Langer 1975). The apparent insensitivity of the

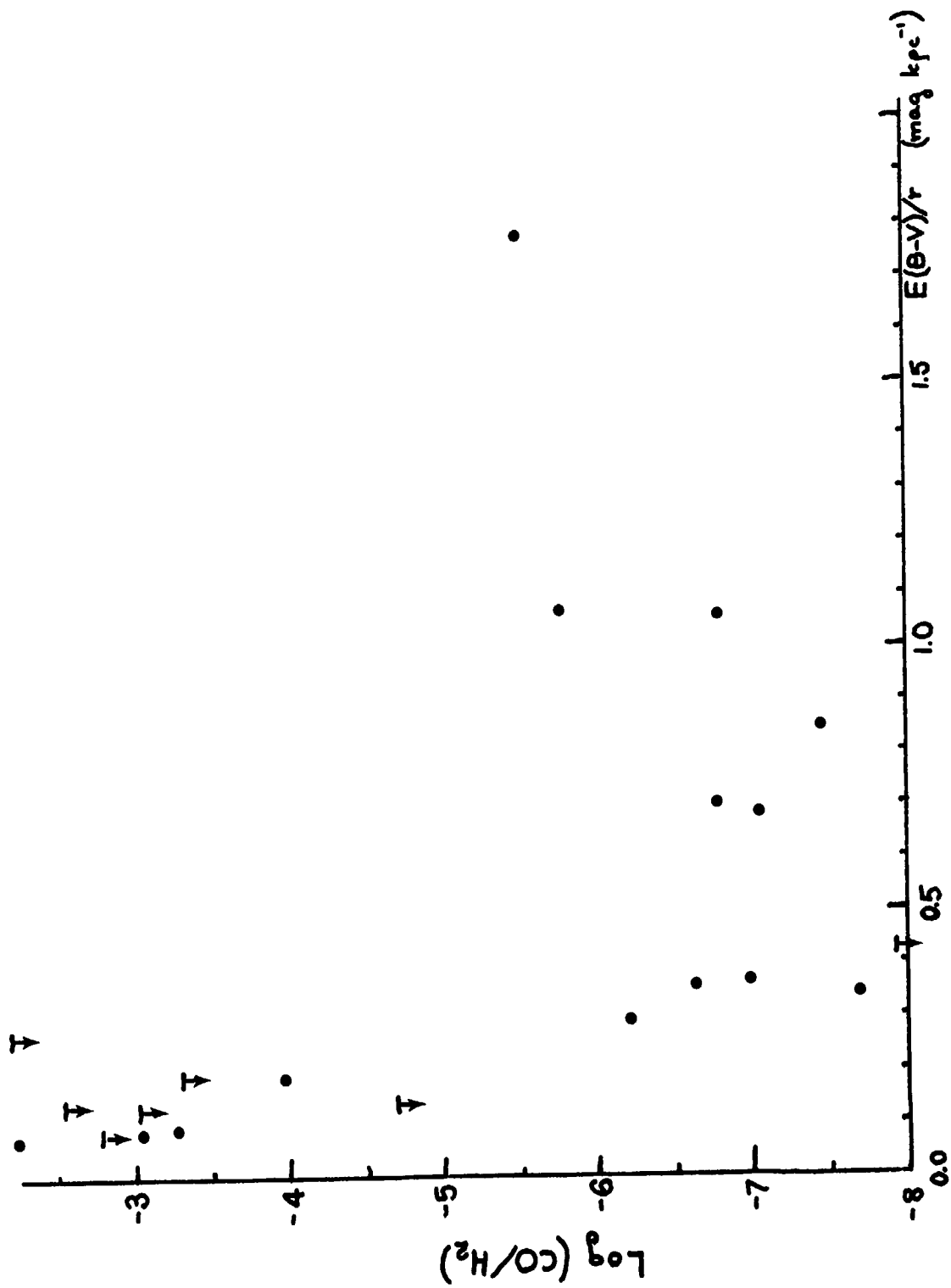


Figure 4

presence of CO to the amount of H₂ suggests that other mechanisms, such as direct formation of CO on grains, may be more important for the interstellar clouds observed here.

When relating the observed values of CO/H shown in Figure 5 to the radio observations, it is important to emphasize that the Copernicus results refer to interstellar material of much lower density than the classical "molecular clouds" identified by most radio observers. As suggested by the trend of points as E(B-V)/r increases, the relative amount of CO increases as larger densities are reached. Still, it is interesting to note that the ratios shown here are substantially lower than an estimate of $\log(\text{CO}/\text{H}) = -4.2$ sometimes adopted for the dense clouds (e.g., see Gordon and Burton 1976 and references cited therein), the latter being equivalent to roughly 10% of the available cosmic abundance of carbon being bound in the form of CO.

V. CONCLUSIONS

From the preceding discussion, we have seen that information gathered from ultraviolet telescopes covers several topics which are helpful in synthesizing our concepts of galactic structure. We have learned about some general properties of interstellar material, i.e., ratios of dust extinction and CO to H I and H₂, and we have evaluated the density of gas in our local part of the galaxy. Each of these studies help to place quantitative constraints on the interpretations of those observations which provide a more global outlook on the distribution of material in the galaxy.

From a survey of galactic 21-cm and CO line emission, Gordon and Burton (1976) mapped the distributions of $n(\text{H I})$ and $n(\text{H}_2)$ as a function of distance from the center of the galaxy. For a galactocentric distance $R = 10$ kpc they estimate both $n(\text{H I})$ and $n(\text{H}_2)$ to be about 0.4 cm^{-3} . On the other hand, the ultraviolet data suggest that $n(\text{H I}) \approx 0.9 \text{ cm}^{-3}$ and $n(\text{H}_2) \approx 0.1 \text{ cm}^{-3}$ within approximately one kpc of the sun. Some of the discrepancy can be attributed to systematic errors or unrealistic assumptions inherent in the interpretations of these two quite different modes of measurements. However, even without these inaccuracies, the differences would be understandable: how could we possibly expect the local density of gas to closely match the density found for a ring covering a wide azimuth at the same distance from the galactic center? In fact, we should expect reasonably strong density contrasts across arms of the galaxy. Hence, although there is some disagreement, it does not seem to unreasonable in view of the uncertainties in both evaluations and the variability we expect to have in the actual distribution of material.

When Gordon and Burton (1976) defined an absolute scale for $N(\text{H}_2)$ to accompany their molecular density distribution function, they

assumed a ratio $\log(\text{CO}/\text{H}_2) = -4.2$, a value considerably above the ratio we observe for clouds having up to one magnitude of visual extinction. It should be immediately apparent, however, that had they assumed $\log(\text{CO}/\text{H}_2) \sim -6$ or -7 , as suggested in Figure 4, they would have derived inordinantly high molecular densities toward the inner region of the galaxy. We should recall from the preceding discussion that their measurement of $n(\text{H}_2)$ of 0.4 cm^{-3} already seems a bit high for $R = 10 \text{ kpc}$. One can surmise, therefore, that unless there is some large and systematic error resulting from their assumptions used to convert antenna temperatures to CO densities, practically all (i.e., at least 99%) of the CO emission must come from clouds which are characteristically much more dense than we can observe in the ultraviolet. The marked irregularity in the distribution of CO emission in itself suggests dense clouds are primary sources of the radiation; we can presume that the more diffuse emission which fills in the spaces between the obvious clouds originates from smaller clouds which, while still very dense, are unresolved by the radiotelescope.

Finally, we have distilled from the Copernicus data a relation, which seems to be fairly universal under a variety of conditions, for the amount of gas associated with given amount of extinction by dust. The value quoted here, $[N(\text{H I}) + 2N(\text{H}_2)]/E(\text{B-V}) = 5.4 \times 10^{21} \text{ cm}^{-2} \text{ mag}^{-1}$, is somewhat lower than an earlier determination from OAO-2 data by Jenkins and Savage (1974) of $7.5 \times 10^{21} \text{ cm}^{-2} \text{ mag}^{-1}$. As shown by Savage and Panek (1974) and Bohlin (1975), some of the stars observed by OAO-2 had more than the expected contamination by stellar lines, and also Jenkins and Savage applied what appears to be too large a correction for ionization by the target stars.

We must bear in mind, of course, that the observed gas to dust ratio may vary from place to place in the galaxy if there are abundance gradients (i.e., an enhancement of the relative CNO abundances toward the galactic center; see the discussion by Stecker et al. (1975)). In addition, the character, and hence extinction properties of the dust grains may change as the interior densities of clouds increase.

The author is grateful to R. C. Bohlin, J. F. Drake and B. D. Savage for communicating preliminary results from their survey of H I and H_2 from data taken by the Copernicus satellite. Their results constituted the largest fraction of the data base upon which the conclusions were derived in this work. This research was supported by contract NAS5-1810 from the U. S. National Aeronautics and Space Administration.

References

- Bohlin, R. C. 1975, Ap. J., 200, 402.
- Bohlin, R. C., Drake, J. F. and Savage, B. D. 1976, private communication of preliminary data.
- Carruthers, G. R. 1970, Ap. J. (Letters), 161, L81.
- Field, G. B., Somerville, W. B. and Dressler, K. 1966, Ann. Rev. Astr. and Ap., 4, 207.
- FitzGerald, M. P. 1968, A. J., 73, 983.
- Glassgold, A. E. and Langer, W. D. 1975, Ap. J., 197, 347.
- Gordon, M. A. and Burton, W. B. 1976, Ap. J., in preparation.
- Grayzeck, E. J. and Kerr, F. J. 1974, A. J., 79, 368.
- Heiles, C. 1976, Ap. J., 204, 379.
- Heiles, C. and Jenkins, E. B. 1976, Astr. and Ap., 46, 333.
- Hollenbach, D. J., Werner, M. W. and Salpeter, E. E. 1971, Ap. J., 163, 165.
- Jenkins, E. B. 1970, Ultraviolet Stellar Spectra and Related Ground-Based Observations, ed. L. Houziaux and H. E. Butler (IAU Symp. 36) (Dordrecht: Reidel) p. 281.
- Jenkins, E. B. and Savage, B. D. 1974, Ap. J., 187, 243.
- Jenkins, E. B. and Shaya, E. 1976, in preparation.
- Panagia, N. 1973, A. J., 78, 929.
- Savage, B. D. and Jenkins, E. B. 1972, Ap. J., 172, 491.
- Savage, B. D. and Panek, R. J. 1974, Ap. J., 191, 659.
- Smith, A. M. 1973, Ap. J. (Letters), 179, L11.
- Snow, T. P. 1976, Earth and Extraterrestrial Sciences, in press.
- Spitzer, L. 1968, Diffuse Matter in Space (New York: Wiley Interscience).
- Spitzer, L., Cochran, W. D., and Hirshfeld, A. 1975, Ap. J. (Suppl.), 28, 373, No. 266.
- Spitzer, L., Drake, J. F., Jenkins, E. B., Morton, D. C., Rogerson, J. B. and York, D. G. 1973, Ap. J. (Letters), 181, L116.
- Spitzer, L. and Jenkins, E. B. 1975, Ann. Rev. Astr. and Ap., 13, 133.
- Stecker, F. W., Solomon, P. M., Scoville, N. Z., and Ryter, C. E. 1975, Ap. J., 201, 90.
- York, D. G., Drake, J. F., Jenkins, E. B., Morton, D. C., Rogerson, J. B. and Spitzer, L. 1973, Ap. J. (Letters), 182, L1.

SMALL SCALE LOCAL GAMMA-RAY FEATURES

J.L. Puget, Département d'Astrophysique Fondamentale, Observatoire
de Meudon, 92190 Meudon

C. Ryter, Centre d'Etude Nucléaire de Saclay, B.P. N°2, 91190 Gif-sur-
Yvette

G. Serra, Centre d'Etude Spatiale des Rayonnements, 31100 Toulouse

ABSTRACT

In order to draw implications from nearby γ -ray emission the different ways which can be used to obtain an estimate of the amount of matter on each line of sight are investigated. Then it is shown that within present uncertainties the cosmic ray intensity inside molecular clouds within 1 kpc from the sun is the same as the cosmic ray intensity measured at the sun. In the last part, what can be learnt from a comparison of far infra-red and gamma-ray data is discussed.

1. The importance of local features. The galactic plane is transparent to gamma-rays produced in the interaction of cosmic rays with interstellar matter so they are a good probe for the large scale structure of our galaxy. It has been shown that longitude profiles of gamma-ray intensity along the galactic plane can be unfolded, assuming cylindrical symmetry, to obtain the gamma-ray production rate as a function of galactocentric distance (Puget and Stecker, 1974). Nevertheless, due to poor resolution of gamma-ray detectors such profiles are averaged over several degrees in latitude and this gives relatively more importance to local features than distant ones for similar contributions to the column density. In consequence it is important to subtract the local contribution, which is very patchy due to the structure of the interstellar medium where most of the mass is gathered in dense clouds, in order to unfold meaningfully the longitude profile.

Solomon and Stecker (1974) pointed out the importance of molecular clouds and their large scale distribution in the galaxy for understanding of γ -ray production. This has been confirmed since by papers using different approaches : Stecker et al 1975, Paul et al 1976. The molecular clouds which contain most of the mass of the interstellar medium in the inner galaxy have been shown to be $10^{4-5} M_{\odot}$ clouds with radii of a few parsecs and typical column densities of 10^{22} cm^{-2} except for a dense core for which the column density can be up to 10^{23} cm^{-2} but which contains only a small fraction of the total mass. The question of the density of cosmic rays in such clouds compared to the density of cosmic rays in the surrounding interstellar medium is important for the interpretation of the large scale variations of the matter density vs cosmic ray density and the implication on the hydrostatic equilibrium of the gas disc (Wentzel et al 1975, Mouschovias 1975).

2. The matter column density. - The gas-to-dust ratio. In recent years, it has become apparent that a substantial fraction of the interstellar hydrogen is in molecular form, and that consequently, 21 cm observations are not necessarily faithful tracers of the total amount of interstellar gas. Here, we propose that interstellar reddening and absorption allows quantitative estimates of column densities to be made, at least within one kpc of the sun. This requires a prior knowledge of the gas-to-dust ratio.

Numerous studies of the gas-to-dust ratio can be found in published literature but the question does not seem to be understood in any detail (see for instance Heiles, 1974). Puget et al (1976) discussed the different estimates of this ratio made recently and showed that if all forms of hydrogen (atomic, molecular and ionized)

are included, it appears that the gas-to-dust ratio is constant in a wide range of densities, from a very tenuous, partly ionized medium to obscured regions with $E_{B-V} \approx 2$ mag, or $A_V \approx 6.5$ mag. Up to this value at least, one is able to assess the total matter column density by using interstellar reddening data and the gas-to-dust ratio: we adopt here the relation

$$N_H = 7 \times 10^{21} E_{B-V} \text{ H atoms cm}^{-2} \quad (1)$$

Some care, however, should be exercised when using equation (1) along with large scale reddening surveys. As is well-known, obscured regions frequently accommodate dense gas and dust clouds, with extinction in excess of 10 mag which practically escape detection in low angular resolution maps, as obtained by star counts. In other words, the very strong extinction in the clouds, which reaches 50 mag or more, does not contribute to the extinction when averaged in picture elements of a few tens of square degrees. In such cases, equation (1) provides only a lower limit to the true average column density. One should then rely on radio and far infrared observations (radiations for which the cores can be optically thin) to estimate the core contribution to the total mass. This contribution is negligible (within 10 % uncertainty limit) for a few molecular clouds for which a detailed comparison of molecular column densities and reddening have been made.

Star counts can be used to get the visual absorption on part of the line of sight for regions with up to 6 magnitudes extinction. This method was used by Encrenaz et al (1975) to show that the ratio N_{CO}/A_V is constant throughout the ρ Ophiucus cloud.

When one wants the extinction integrated over the whole line of sight the only way to get data covering completely large areas of the sky is to use galaxy counts. For directions around the galactic center data can be obtained only for latitudes b such that $|b| > 5^\circ$. In the anticenter direction if averages are taken on wide enough longitude ranges meaningful values can be obtained even down to $b = 0$.

Another question one must ask is how good is the gas-to-dust ratio when one looks at regions far away from the sun. This can be investigated by comparing latitude distributions for H I (Daltabuit and Meyer, 1972), reddening (Fitzgerald, 1968) and visual absorption from galaxy counts (Shane and Wirtanen, 1967, Kiang, 1969). 4 such profiles are shown on figure 1 for different longitude ranges around the anticenter direction. For $|b| \approx 5^\circ$ the column densities deduced from reddening or absorption (in good agreement within uncertainties) are larger than the column densities deduced from 21 cm data. On the other hand, at $b = 0$ they are significantly smaller. Puget et al (1976) have argued that gas to dust ratio is a well defined quantity

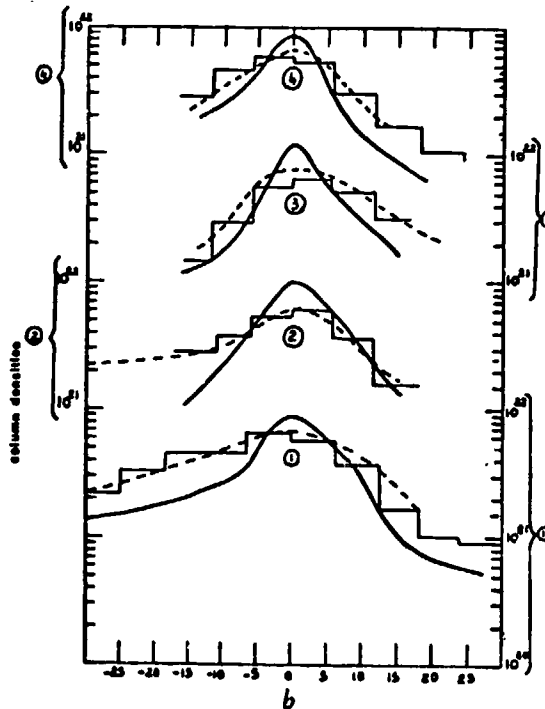


FIGURE 1 .

Evidence for gas-to-dust gradient in the outer region of the galactic disc.

Solid line : atomic hydrogen

Histogram : total gas column density deduced from star reddening

Interrupted line : the same deduced from galactic counts.

- ① $210 < l < 240$, ② $160 < l < 170$,
 ③ $120 < l < 160$, ④ $170 < l < 210$

only when all forms of hydrogen are included so we should take into account molecular hydrogen (H_2 is negligible). Gordon and Burton (1976) give 48 % of hydrogen in molecular form for the interstellar gas at 10 kpc from the center and 34 % on the line of sight at $b = 0$ in the anticenter direction. So once again it is found that near the sun ($b \approx 7^\circ$) with $N_H \sim 2 N_{HI}$ on the average, equation (1) gives the right column density. At $b = 0$ we find $\langle E_{B-V} \rangle = .95$, $\langle N_{HI} \rangle = 9.8 \cdot 10^{21} \text{ cm}^{-2}$. Assuming $\langle N_H \rangle = 1.34 \langle N_{HI} \rangle = 1.3 \cdot 10^{22} \text{ cm}^{-2}$. This implies a gas-to-dust ratio twice as large on the average than the value adopted in equation (1) or a 20 % decrease per kiloparsec of the relative amount of dust.

Such a gradient compares well with the metal abundance gradients deduced from observations of H II regions in external galaxies (Searle, 1971), and in our galaxy, (Peimbert, Sivan, private comm.)

3. Gamma-ray emission. Most of the γ -ray emission above 100 MeV from the Galactic plane is attributed to the decay of neutral pions formed in the interaction of cosmic rays with interstellar matter.

The γ -ray intensity I_γ associated with a line of sight is given by

$$I_\gamma = 1.3 \times 10^{-25} N_H / 4\pi \text{ photon cm}^{-2} \text{ s}^{-1} \text{ sr}^{-1} \quad (2)$$

using the production rate per hydrogen atom for a cosmic ray density equal to that observed in the solar vicinity (Stecker, 1973). With equation (1) this relation becomes

$$I_{\gamma} = 7.25 \cdot 10^{-5} E_{B-V} (n_{CR}/n_{CRO}) \text{ photon cm}^{-2} \text{ s}^{-1} \text{ sr}^{-1} \quad (3)$$

where n_{CR} is the density of cosmic rays and n_{CRO} the value of this density in the solar neighbourhood. Their ratio is not expected to be very different from 1 when averaged over lines of sight at $|b| > 5^{\circ}$.

The latitude distribution of the intensity I_{γ} averaged between $l_{II} = 350^{\circ}$ and $l_{II} = 20^{\circ}$ is given by the COS-B caravane collaboration (these proceedings, p.). For $|b| > 5^{\circ}$ visual absorption deduced from galaxy counts is expected to give the best estimates of the total column densities as shown above. For $b > 5^{\circ}$, Shane and Wirtanen (1967) and Kiang (1969) have been used, for $b < 10^{\circ}$ we used the 5 galaxies per square degree contour from Harvard counts as quoted by Shane and Wirtanen (1967). The γ -ray fluxes are computed using (3) and

$$E_{B-V} = 0.4 \log (65/N) \quad (4)$$

where N is the number of galaxies per square degree. Considering the uncertainties in relation (4) and statistical errors in the counts of galaxies E_{B-V} is obtained with uncertainties of the order of 20 % and we conclude from the fair agreement obtained in figure 2, that,

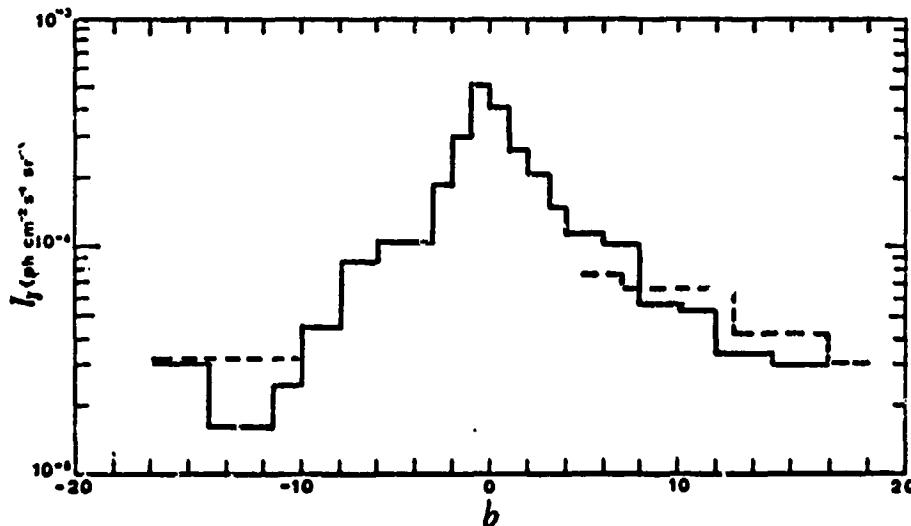


FIGURE 2 . Latitude distribution of the γ -ray emission in the galactic center region as measured by the COS-B satellite (solid line) and γ -ray emission predicted from the total column density deduced from galaxy counts (interrupted line).

within this precision range, cosmic ray intensity in these regions is on the average equal to the solar vicinity intensity. Mouschovias (1975) suggests that for the production of γ -rays in molecular clouds there will be a trade off between increased gas density and decreased cosmic ray intensity. About half of the gas on the line of sight is in molecular form so we can conclude that there is no strong depletion of cosmic rays in molecular clouds. This question can be investigated in more detail by comparing γ -ray isophotes and galaxy counts contours. The only published map of γ -ray isophotes is the one given by Kniffen et al (1975) for the anticenter direction. On figure 3 we compare the outermost isophote of this map with contours at l and b galaxies per square degree corresponding to E_{B-V} = respectively to 0.7 and 0.3 magnitudes.

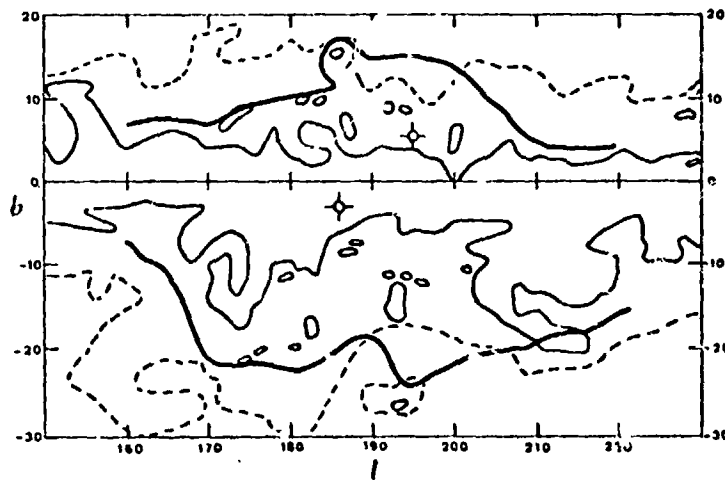


FIGURE 3. Gamma-ray emission and interstellar matter in the galactic anticenter region. Heavy line : outer contour of the γ -ray map obtained from SAS-2 satellite. Light solid line : contour of the $E_{B-V} \approx 0.7$ mag region. Interrupted line : contour of the $E_{B-V} \approx 0.3$ mag region. Crosses : the two γ -ray sources Tau γ -1 and 195 + 1.

We estimate the γ -ray intensity associated with this isophote by normalisation the total flux of the Crab pulsar above 35 MeV which shows very clearly on this map. We assumed the flux to be 60 % pulsed from variation of the pulsed fraction with energy and the pulsed flux is $6.2 \cdot 10^{-6}$ photons $\text{cm}^{-2} \text{s}^{-1}$ (Kniffen et al, 1975). This leads to an intensity of $3.2 \cdot 10^{-5}$ $\gamma \text{ cm}^{-2} \text{s}^{-1} \text{Sr}^{-1}$ which would be associated with lines of sight with $E_{B-V} = 0.44$. From the relative positions of the γ isophote, the $E_{B-V} = 0.3$ and $E_{B-V} = 0.7$ contours one can say that there is no evidence for depletion of cosmic rays in molecular clouds as far as the envelopes are concerned (Nothing can be said about cores).

On figure 4 the same galaxy counts contours are shown for the whole galactic plane and should compare well with γ -ray isophotes at $5 \cdot 10^{-5}$ and $2 \cdot 10^{-5} \gamma \text{ s}^{-1} \text{ sr}^{-1} \text{ cm}^{-2}$.

4. Galactic far infra-red emission. Another probe for large scale structure in the galaxy is far infra-red radiation emitted by dust. Here again the study of individual clouds and comparison of infra-red emission and γ -rays can help to disentangle matter distribution and cosmic ray distribution. Assuming known the gas to dust ratio the infra-red intensity might be a tracer of interstellar matter. For any realistic dust model and for $\lambda > 70 \mu\text{m}$ the Galaxy is optically thin. The integrated far infra-red intensity relies also on the energy density of the exciting field. Ryter and Puget (1976) have shown that the power radiated by the dust mixed to the gas in clouds is about a factor 20 larger than the power that can be accounted for by the usual star light density $u \approx 0.5 \text{ eV cm}^{-3}$. This implies that strong power sources are imbedded in the clouds and are obviously attributed to new born stars.

The amount of dust and the source of the power (related to the star formation rate) can be separated if sufficient spectral information is obtained. The total power radiated by the dust can be evaluated and expressed as a radiated power normalized per hydrogen atom L_{IR}^{H} . On the other hand, the temperature can be deduced from multi-colour photometry. Based on a realistic dust model (a mixture of ice and silicates) Ryter and Puget find the approximate relation

$$L_{\text{IR}}^{\text{H}}(T) = 5 \times 10^{-39} T^{5.8} W(\text{H atom})^{-1} \quad (5)$$

where T is the dust temperature. The general result is that for a sample of clouds located between the sun and the 5 kpc ring, the temperatures needed to explain the total power radiated (through (5)) are in good agreement with the colour temperatures. We can then use those results in the following way. The temperature can be obtained precisely from (5) if the total power is measured and can be used to infer the column density of dust from the infra-red intensity at wavelengths such that the Rayleigh Jeans approximation is valid. The different physical parameters n_{HI} , n_{H_2} , n_{dust} , n_{CR} , T_{dust} and gas temperatures are all physically related and the understanding of the physics implies the confrontation of γ -ray, far infra-red and radio data for which dense molecular clouds and the whole galactic plane are optically thin.

9-4

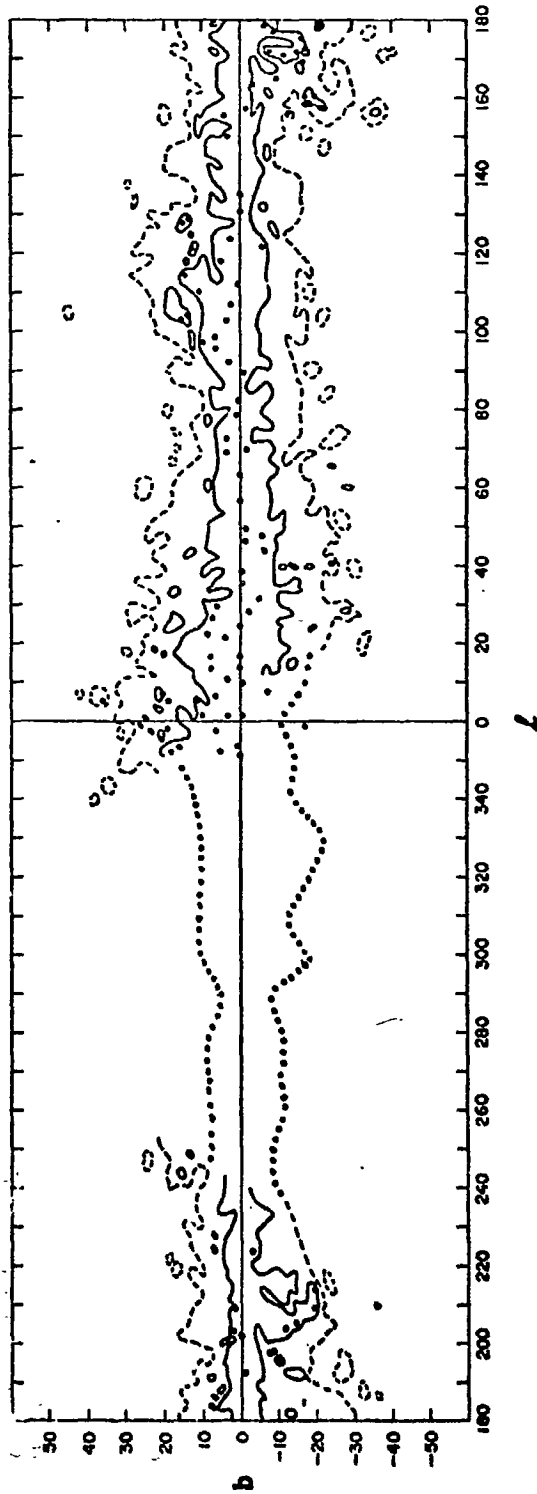


FIGURE 4 . Contours of the interstellar extinction deduced from galaxy counts (Kiang 1969).
 Solid line : $E_{B-V} \geq 0.7$ mag, i.e. zero to one galaxy per square degree. Interrupted line :
 $E_{B-V} \approx 0.3$ mag, i.e. 10 galaxies per square degree. Dotted line : $E_{B-V} \approx 0.45$ mag, i.e.
 5 galaxies per square degree (Harvard counts as quoted by Shane and Wirtanen 1967).
 Filled circles : molecular clouds observed.

References.

- Daltabuit, E. and Meyer, S. 1972, *Astron. and Astrophys.*, 20, 415.
- Encrenaz, P.J., Falgarone, E. and Lucas, R. 1975, *Astron. and Astrophys.*
- Fitzgerald, M.P. 1968, *Astron. J.*, 73, 983.
- Gordon, M.A. and Burton, W.B. 1976, preprint.
- Heiles, C., 1974, in *Galactic Radio Astronomy*, IAU Symp. N°60, p. 625
ed. Kerr, F.J. and Simonson, D.C. III, Reidel, Dordrecht
(Holland).
- Kiang, T. 1969, *Dunsink Observatory Publications*, 1, N°5.
- Kniffen, D.A., Bignami, G.F., Fichtel, C.E., Hartman, R.C., Ügelman,
H., Thomson, D.J., Üzel, M.E. and Tümer, T., 1975, 14th Int.
Conf. on Cosmic Rays, Munich, Aug. 15-29.
- Mouschovias, T.C., 1975, *Ap.J. Lett.* 202, L1.
- Paul, J., Cassé, M., and Césarsky, C.J., 1975, 14th Int. Conf. on
Cosmic Rays, Munich, Aug. 15-29.
- Puget, J.L. and Stecker, F.W., 1974, *Ap.J.* 191, 323.
- Puget, J.L., Ryter, C., Serra, G. and Bignami, G., 1976, *Astron. and
Astrophys.*, in press.
- Ryter, C. and Puget, J.L., 1976, preprint.
- Solomon, P.M. and Stecker, F.W., 1974, *ESRO Symp. Context and Status
of Gamma-Ray Astronomy*, Reidel, in press.
- Searle, L., 1971, *Ap.J.* 168, 327.
- Solomon, P.M. and Stecker, F.W., 1974, *ESRO Symp. Context and Status
of Gamma-Ray Astronomy*, Reidel, in press.
- Stecker, F.W., 1973, *Ap.J.* 185, 499.
- Stecker, F.W., Solomon, P.M., Scoville, N.Z. and Ryter, C.E., 1975,
Ap.J. 201, 90.
- Shane, C.D. and Wirtanen, C.A., 1967, *Pub. of the Lick Obs.* 22, 1.
- Wentzel, D.G., Jackson, P.D., Rose, W.K. and Sinha, R.P., 1975,
Ap.J. (Letters), 201, L5.

N76-29127

DIFFUSE GALACTIC GAMMA RAY LINES

R.E. Lingenfelter, Department of Astronomy and Department of Geophysics & Space Physics, University of California, Los Angeles, California 90024*

R. Ramaty, NASA/Goddard Space Flight Center, Laboratory for High Energy Astrophysics, Greenbelt, Maryland 20771

ABSTRACT

We have studied the origin and observability of diffuse gamma ray line emission from our galaxy. We find that such lines could be formed by nuclear excitation interactions of low energy cosmic rays with both interstellar gas and dust grains. The gamma ray emission lines from deexcitation of grain nuclei are sharp with Doppler widths of the order of 10 keV or less; the lines from gas nuclei are also relatively sharp with widths of the order of ~ 100 keV for the most intense line $^{12}\text{C}^{*4.439}$, and of the order of a few keV for the $^{56}\text{Fe}^{*0.847}$ line; and the lines from cosmic ray nuclei are broad with widths of the order of several hundred keV.

We present here a detailed evaluation of the production rate of the 4.44 MeV line for a variety of assumed cosmic ray spectra. We compare these results with reported galactic gamma ray line intensities and conclude that the measurements are consistent with a low energy cosmic ray density which increases toward the galactic center in proportion to the molecular gas density.

An exciting possibility for the future would be the detection of nuclear gamma ray lines from interstellar dust grain nuclei using a solid state detector with energy resolution of a few keV or better.

*This research was supported in part by National Science Foundation grant AST67-08178.

1. Introduction. We have calculated the gamma ray line emission expected to result from cosmic ray nuclear interactions with interstellar gas and dust in the galaxy. This emission consists of a sharp line component from deexcitation of interstellar grain nuclei, a relatively narrow line component from deexcitation of gas nuclei, and a broad line component from deexcitation of cosmic ray nuclei. These three components can in principle be separated in measured spectra permitting study of both the interstellar medium and the cosmic rays.

In the study of galactic structure the sharp line component of nuclear gamma ray emission offers the first opportunity to determine the composition and spacial distribution of interstellar grains. The narrow line component also appears to offer a better opportunity than either atomic or molecular line emission for determining the spacial distribution and composition of interstellar gas because of the high transparency of even very dense interstellar clouds to gamma radiation, and the lack of dependence of the gamma ray emissivity on the chemical state of the matter.

In addition the broader gamma ray line component provides the best opportunity available so far for studying the low energy cosmic rays which are important not only in conjunction with understanding the origin and propagation of cosmic rays but also in the study of galactic structure where the role of low energy cosmic rays in heating of the interstellar gas and in nucleosynthesis of the light elements is not yet understood.

At present galactic gamma ray line astronomy is only in a rudimentary stage, but it has already produced surprising results. Emission in several gamma ray lines from the direction of the galactic center have been reported for balloon experiments by Haymes et al. (1975) and possibly confirmed at least for the 4.4 Mev line in a preliminary analysis of Apollo experiments by Trombka (private communication, 1976). The intensities of these lines are roughly two orders of magnitude higher than would be predicted assuming uniform density and composition of the interstellar gas and cosmic rays throughout the galaxy. If these observations are correct, then these intensities suggest strong spacial variations in both the density and composition of interstellar gas and cosmic rays.

Very little systematic study has been made of gamma ray line production by low energy cosmic rays in the galaxy, although there have been extensive theoretical studies (e.g., Ramaty et al., 1975) of gamma ray line production by solar flare particles at the sun.

Fowler et al. (1970) first estimated the combined line emission of gamma rays of energy greater than 1 Mev as a possible limitation on the production of LiBeB in the interstellar medium by low energy cosmic rays. Meneguzzi and Reeves (1975), pursuing this problem further, have calculated some individual line emissivities but only for a very limited class of low energy cosmic ray spectra.

Ramaty and Boldt (1971) also estimated the gamma ray line emission at 4.4 and ~ 6.2 Mev as a possible limit on their model of heating the Gum Nebula by low energy cosmic rays from the Vela supernova.

The first measurements of broad line emission at slightly less than 0.5 Mev from the direction of the galactic center by Johnson et al. (1972) and Johnson and Haymes (1973) led Fishman and Clayton (1972) to suggest the possibility of gamma ray emission at 0.478 and 0.431 Mev resulting from excitation and spallation of low energy cosmic ray ${}^7\text{Li}$ nuclei. Kozlovsky and Ramaty (1974) also considered the contribution to this emission from production of excited ${}^7\text{Li}$ and ${}^7\text{Be}$ in low energy alpha particle interactions with helium.

The most general study of the problem of gamma ray line emission resulting from low energy cosmic ray interactions with the interstellar gas was made by Rygg and Fishman (1973). They considered a larger number of nuclear excitation processes and a wider range of possible low energy cosmic ray spectra than were previously considered. They predicted significant emission in the 1 to 2 Mev range which seems to have been observed by Haymes et al. (1975). But they calculated only direct excitation of low energy cosmic ray nuclei by interstellar hydrogen, ignoring the broadening of excited cosmic ray emission lines and the production of excited nuclei by spallation reactions. They also apparently only estimated the contribution from the excitation of cosmic ray nuclei by interstellar helium and the excitation of the interstellar gas nuclei by cosmic ray protons and alpha particles. The production by these processes is very sensitive to the assumed energy spectrum and should be calculated

explicitly.

In the present study all of these processes are considered, as well as additional direct excitation processes. We also explore a much wider range of possible low energy cosmic ray spectra and possible galactic spacial variations in both cosmic ray and interstellar gas compositions in the hopes of better assessing the usefulness of gamma ray line observations for studies of galactic structure and composition, the role of cosmic ray heating and light element nucleosynthesis in the interstellar medium, and of course the nature, origin and propagation of the low energy cosmic rays.

The full results of these calculations will be given in a forthcoming paper. Here we will present only a sampling of these calculations relating to the strongest single line, that is the line at 4.44 Mev resulting from deexcitation of the first excited nuclear level in ^{12}C . This is also currently the best measured line and we will discuss the implications of these measurements in the light of our calculations.

2. Gamma Ray Line Emission. There is an enormous variety of nuclear interactions between cosmic rays and the interstellar gas and dust which lead to gamma ray line emission. The relative intensities of different lines depend on the excitation cross sections, the cosmic ray energy spectrum and composition, and the interstellar gas and dust composition. The various gamma ray deexcitation lines which we consider, together with their nuclear excitation interactions, are listed in Table 1.

For each of these lines we calculate a gamma ray emission rate or emissivity. In general the production rate of excited nuclei, which will emit deexcitation gamma rays of energy ϵ_k , produced by cosmic ray interactions with the interstellar gas may be simply written:

$$q_k = \sum_{ij} \int_0^{\infty} dE n_i \phi_j(E) \sigma_{ijk}(E) \quad (1)$$

where E is the cosmic ray kinetic energy per nucleon; n_i is the density of interstellar gas nuclei of isotope i ;

TABLE 1
GAMMA RAY LINES

GAMMA RAY ENERGY (MeV)	DEEXCITATION PROCESS	EXCITATION REACTION	GAMMA RAY ENERGY (MeV)	DEEXCITATION PROCESS	EXCITATION REACTION
0.431	$^7\text{Be}^{*0.431}\text{-g.s.}$	$^4\text{He}(^7\text{He},\text{n})^7\text{Li}^{*0.431}$ $^4\text{He}(^7\text{He},\text{n})^7\text{Li}^{*0.431}$ $^7\text{Li}(p,\text{n})^7\text{Be}^{*0.431}$ $^7\text{Li}(p,\text{n})^7\text{Be}^{*0.431}$ $^{10}\text{B}(p,\text{n})^7\text{Be}^{*0.431}$	0.921	$^{48}\text{Tl}^{*0.921}\text{-g.s.}$	$^{56}\text{Fe}(p,\text{n})^{48}\text{V}(e^{*})^{48}\text{Tl}^{*0.921}$
0.477	$^{55}\text{Fe}^{*1.408}, ^{55}\text{Fe}^{*0.931}$	$^{56}\text{Fe}(p,2n)^{55}\text{Co}(e^{*}), ^{55}\text{Fe}^{*1.408}$ (128) $^{56}\text{Fe}(p,\text{pn})^{55}\text{Fe}^{*1.408}$	1.023	$^{10}\text{B}^{*1.740}, ^{10}\text{B}^{*0.717}$	$^{10}\text{B}(\text{p},\text{p}')^{10}\text{B}^{*1.740}$
0.478	$^7\text{Li}^{*0.478}\text{-g.s.}$	$^3\text{He}(^7\text{Li},\text{p})^7\text{Be}(e^{*})^7\text{Li}^{*0.478}$ (128) $^3\text{He}(^7\text{Li},\text{p})^7\text{Be}(e^{*})^7\text{Li}^{*0.478}$ $^3\text{He}(^7\text{Li},\text{n})^7\text{Be}(e^{*})^7\text{Li}^{*0.478}$ (128) $^7\text{Li}(p,\text{p}')^7\text{Li}^{*0.478}$ $^7\text{Li}(p,\text{n})^7\text{Be}(e^{*})^7\text{Li}^{*0.478}$ (128) $^7\text{Li}(^7\text{Li},\text{p})^7\text{Li}^{*0.478}$ $^{14}\text{N}(p,\text{x})^7\text{Be}(e^{*})^7\text{Li}^{*0.478}$ (128) $^{12}\text{C}(p,\text{x})^7\text{Be}(e^{*})^7\text{Li}^{*0.478}$ (128) $^{12}\text{C}(p,\text{x})^7\text{Li}^{*0.478}$	1.042	$^{18}\text{O}^{*1.042}\text{-g.s.}$	$^{18}\text{O}(p,\text{n})^{18}\text{O}^{*1.042}$
0.511	$^4\text{He}^{*0.511}$ Annihilation	$^{10}\text{B}(p,\text{n})^{10}\text{C}(e^{*})$ $^{12}\text{C}(p,\text{pn})^{11}\text{C}(e^{*})$ $^{12}\text{C}(p,\text{x})^{10}\text{C}(e^{*})$ $^{12}\text{C}(^7\text{Li},\text{pn})^{11}\text{C}(e^{*})$ $^{14}\text{N}(p,\text{x})^{11}\text{C}(e^{*})$ $^{16}\text{O}(p,\text{pn})^{15}\text{O}(e^{*})$ $^{16}\text{O}(p,\text{x})^{11}\text{C}(e^{*})$ $^{16}\text{O}(p,\text{x})^{11}\text{C}(e^{*})$ $^{16}\text{O}(^7\text{Li},\text{pn})^{15}\text{O}(e^{*})$ $^{19}\text{F}(p,\text{x})^{16}\text{O}(e^{*})$ $^{24}\text{Mg}(p,\text{x})^{22}\text{Ne}(e^{*})$ $^{28}\text{Si}(p,\text{x})^{22}\text{Ne}(e^{*})$ $^{56}\text{Fe}(p,\text{n})^{56}\text{Co}(e^{*})$ $^{56}\text{Fe}(p,2n)^{55}\text{Co}(e^{*})$ $^{56}\text{Fe}(p,\text{x})^{52}\text{Ni}(e^{*})$	1.121	$^{46}\text{Tl}^{*2.010}, ^{46}\text{Tl}^{*0.889}$	$^{56}\text{Fe}(p,\text{x})^{46}\text{Sb}(e^{*})^{46}\text{Tl}^{*2.010}$
0.717	$^{10}\text{B}^{*0.717}\text{-g.s.}$	$^{10}\text{B}(p,\text{p}')^{10}\text{B}^{*0.717}$ $^{10}\text{B}(p,\text{n})^{10}\text{C}(e^{*}), ^{10}\text{B}^{*0.717}$ $^{10}\text{B}(^7\text{Li},\text{p})^{10}\text{B}^{*0.717}$ $^{11}\text{B}(p,\text{pn})^{10}\text{B}^{*0.717}$ $^{12}\text{C}(p,\text{x})^{10}\text{C}(e^{*}), ^{10}\text{B}^{*0.717}$ $^{16}\text{O}(p,\text{x})^{10}\text{B}^{*0.717}$	1.238	$^{56}\text{Fe}^{*2.085}, ^{56}\text{Fe}^{*0.947}$	$^{56}\text{Fe}(p,\text{p}')^{56}\text{Fe}^{*2.085}$ $^{56}\text{Fe}(p,\text{n})^{56}\text{Co}(e^{*}), ^{56}\text{Fe}^{*2.085}$ $^{56}\text{Fe}(^7\text{Li},\text{pn})^{56}\text{Fe}^{*2.085}$
0.744	$^{52}\text{Cr}^{*3.119}, ^{52}\text{Cr}^{*2.370}$	$^{56}\text{Fe}(p,\text{x})^{52}\text{Ni}(e^{*}), ^{52}\text{Cr}^{*3.114}$ (855)	1.266	$^{31}\text{P}^{*1.266}$	$^{31}\text{P}(p,\text{p}')^{31}\text{P}^{*1.266}$ $^{12}\text{Si}(p,\text{pn})^{11}\text{C}(e^{*}), ^{31}\text{P}^{*1.266}$ $^{32}\text{S}(p,\text{pn})^{11}\text{C}(e^{*}), ^{31}\text{P}^{*1.266}$
0.811	$^{58}\text{Fe}^{*0.811}\text{-g.s.}$	$^{56}\text{Fe}(^7\text{Li},\text{pn})^{58}\text{Co}(e^{*}), ^{58}\text{Fe}^{*0.811}$	1.273	$^{29}\text{Si}^{*1.273}\text{-g.s.}$	$^{32}\text{S}(p,\text{x})^{29}\text{Si}(e^{*}), ^{29}\text{Si}^{*1.273}$
0.835	$^{54}\text{Cr}^{*0.835}\text{-g.s.}$	$^{56}\text{Fe}(p,\text{x})^{54}\text{Ni}(e^{*}), ^{54}\text{Cr}^{*0.835}$	1.275	$^{22}\text{Ne}^{*1.275}\text{-g.s.}$	$^{22}\text{Ne}(p,\text{p}')^{22}\text{Ne}^{*1.275}$ $^{23}\text{Na}(p,\text{n})^{22}\text{Ne}(e^{*}), ^{22}\text{Ne}^{*1.275}$ $^{24}\text{Mg}(p,\text{x})^{22}\text{Ne}(e^{*}), ^{22}\text{Ne}^{*1.275}$ $^{28}\text{Si}(p,\text{x})^{22}\text{Ne}(e^{*}), ^{22}\text{Ne}^{*1.275}$
0.847	$^{56}\text{Fe}^{*0.847}\text{-g.s.}$	$^{56}\text{Fe}(p,\text{p}')^{56}\text{Fe}^{*0.847}$ $^{56}\text{Fe}(p,\text{n})^{56}\text{Co}(e^{*}), ^{56}\text{Fe}^{*0.847}$ $^{56}\text{Fe}(^7\text{Li},\text{pn})^{56}\text{Fe}^{*0.847}$ $^{56}\text{Fe}(^7\text{Li},\text{pn})^{56}\text{Co}(e^{*}), ^{56}\text{Fe}^{*0.847}$	1.312	$^{48}\text{Tl}^{*2.295}, ^{48}\text{Tl}^{*0.983}$	$^{56}\text{Fe}(p,\text{x})^{48}\text{V}(e^{*}), ^{48}\text{Tl}^{*2.295}$
0.889	$^{46}\text{Tl}^{*0.889}\text{-g.s.}$	$^{56}\text{Fe}(p,\text{x})^{46}\text{Sb}(e^{*}), ^{46}\text{Tl}^{*0.889}$	1.369	$^{24}\text{Mg}^{*1.369}\text{-g.s.}$	$^{24}\text{Mg}(p,\text{p}')^{24}\text{Mg}^{*1.369}$ $^{24}\text{Mg}(p,\text{x})^{24}\text{Ne}(e^{*}), ^{24}\text{Mg}^{*1.369}$ $^{24}\text{Mg}(^7\text{Li},\text{pn})^{24}\text{Mg}^{*1.369}$ $^{27}\text{Al}(p,\text{x})^{24}\text{Mg}^{*1.369}$ $^{27}\text{Al}(p,\text{x})^{24}\text{Ne}(e^{*}), ^{24}\text{Mg}^{*1.369}$ $^{27}\text{Al}(^7\text{Li},\text{pn})^{24}\text{Mg}^{*1.369}$ $^{28}\text{Si}(p,\text{x})^{24}\text{Mg}^{*1.369}$ $^{28}\text{Si}(p,\text{x})^{24}\text{Ne}(e^{*}), ^{24}\text{Mg}^{*1.369}$
0.931	$^{55}\text{Fe}^{*0.931}\text{-g.s.}$	$^{56}\text{Fe}(p,\text{pn})^{55}\text{Fe}^{*0.931}$ $^{56}\text{Fe}(p,2n)^{55}\text{Co}(e^{*}), ^{55}\text{Fe}^{*0.931}$ (766)	1.395	$^{21}\text{Ne}^{*1.746}, ^{21}\text{Ne}^{*0.351}$	$^{23}\text{Na}(p,2p)^{21}\text{Ne}^{*1.746}$
0.936	$^{52}\text{Cr}^{*2.370}, ^{52}\text{Cr}^{*1.434}$	$^{56}\text{Fe}(p,\text{x})^{52}\text{Ni}(e^{*}), ^{52}\text{Cr}^{*2.370}$	1.408	$^{56}\text{Fe}^{*1.407}\text{-g.s.}$	$^{56}\text{Fe}(p,\text{p}')^{56}\text{Fe}^{*1.408}$ $^{56}\text{Fe}(^7\text{Li},\text{pn})^{56}\text{Fe}^{*1.408}$
0.937	$^{18}\text{O}^{*0.937}\text{-g.s.}$	$^{18}\text{O}(p,\text{n})^{18}\text{O}^{*0.937}$	1.408	$^{55}\text{Fe}^{*1.408}\text{-g.s.}$	$^{56}\text{Fe}(p,\text{pn})^{56}\text{Fe}^{*1.408}$ $^{56}\text{Fe}(p,2n)^{55}\text{Co}(e^{*}), ^{55}\text{Fe}^{*1.408}$ (171)
			1.434	$^{52}\text{Cr}^{*1.434}\text{-g.s.}$	$^{56}\text{Fe}(p,\text{x})^{52}\text{Ni}(e^{*}), ^{52}\text{Cr}^{*1.434}$
			1.571	$^{18}\text{O}^{*2.551}, ^{18}\text{O}^{*1.982}$	$^{18}\text{O}(p,\text{p}')^{18}\text{O}^{*3.55}$
			1.622	$^{14}\text{N}^{*3.945}, ^{14}\text{N}^{*2.313}$	$^{14}\text{N}(p,\text{p}')^{14}\text{N}^{*3.945}$ $^{16}\text{O}(p,\text{x})^{14}\text{N}^{*3.945}$
			1.634	$^{20}\text{Ne}^{*1.634}\text{-g.s.}$	$^{20}\text{Ne}(p,\text{p}')^{20}\text{Ne}^{*1.634}$ $^{20}\text{Ne}(^7\text{Li},\text{pn})^{20}\text{Ne}^{*1.634}$ $^{24}\text{Mg}(p,\text{x})^{20}\text{Ne}^{*1.634}$ $^{27}\text{Al}(p,\text{x})^{20}\text{Ne}^{*1.634}$ $^{28}\text{Si}(p,\text{x})^{20}\text{Ne}^{*1.634}$
			1.636	$^{23}\text{Ne}^{*2.076}, ^{23}\text{Ne}^{*0.440}$	$^{23}\text{Ne}(p,\text{p}')^{23}\text{Ne}^{*2.076}$ $^{24}\text{Mg}(p,\text{pn})^{23}\text{Ne}^{*0.440}$
			1.772	$^{56}\text{Fe}^{*3.857}, ^{56}\text{Fe}^{*2.085}$	$^{56}\text{Fe}(p,\text{p}')^{56}\text{Fe}^{*3.857}$ $^{56}\text{Fe}(p,\text{n})^{56}\text{Co}(e^{*}), ^{56}\text{Fe}^{*3.857}$

REPRODUCIBILITY OF THE ORIGINAL PAGE IS POOR

TABLE I
GAMMA RAY LINES
(continued)

GAMMA RAY ENERGY (MeV)	DEEXCITATION PROCESS	EXCITATION REACTION	GAMMA RAY ENERGY (MeV)	DEEXCITATION PROCESS	EXCITATION REACTION
1.774	$^{28}\text{Si}^*1.774$	$^{28}\text{Si}(p,p')^{28}\text{Si}^*1.774$ $^{28}\text{Si}(n,\alpha')^{28}\text{Si}^*1.774$ $^{32}\text{S}(p,pp)^{28}\text{Si}^*1.774$	4.438	$^{12}\text{C}^*4.438$ -g.s.	$^{12}\text{C}(p,p)^{12}\text{C}^*4.438$ $^{11}\text{B}(p,\gamma)^{12}\text{C}^*4.438$ $^{12}\text{C}(p,p')^{12}\text{C}^*4.438$ $^{12}\text{C}(n,\alpha')^{12}\text{C}^*4.438$ $^{14}\text{N}(p,n)^{12}\text{C}^*4.438$ $^{15}\text{N}(p,\alpha)^{12}\text{C}^*4.438$ $^{16}\text{O}(p,pp)^{12}\text{C}^*4.438$ $^{16}\text{O}(n,\alpha)^{12}\text{C}^*4.438$
1.809	$^{26}\text{Mg}^*1.809$ -g.s.	$^{26}\text{Mg}(p,p')^{26}\text{Mg}^*1.809$ $^{26}\text{Mg}(p,n)^{26}\text{Al}(e^+)^{26}\text{Mg}^*1.809$ $^{27}\text{Al}(p,2p)^{26}\text{Mg}^*1.809$ $^{27}\text{Al}(p,pp)^{26}\text{Al}(e^+)^{26}\text{Mg}^*1.809$ $^{28}\text{Si}(p,\alpha)^{26}\text{Al}(e^+)^{26}\text{Mg}^*1.809$	4.443	$^{11}\text{B}^*4.444$ -g.s.	$^{11}\text{B}(p,\gamma)^{11}\text{B}^*4.444$ $^{11}\text{B}(p,p')^{11}\text{B}^*4.444$ $^{11}\text{B}(n,\alpha')^{11}\text{B}^*4.444$ $^{12}\text{C}(p,2p)^{11}\text{B}^*4.444$ $^{12}\text{C}(n,\alpha)^{11}\text{B}^*4.444$
1.982	$^{18}\text{O}^*1.982$ -g.s.	$^{18}\text{O}(p,p')^{18}\text{O}^*1.982$ $^{18}\text{O}(n,\alpha')^{18}\text{O}^*1.982$	4.741	$^{11}\text{B}^*9.186,^{11}\text{B}^*4.444$	$^{11}\text{B}(n,\alpha)^{11}\text{B}^*9.186$
1.995	$^{11}\text{C}^*1.995$ -g.s.	$^{11}\text{B}(p,n)^{11}\text{C}^*1.995$ $^{12}\text{C}(p,pp)^{11}\text{C}^*1.995$ $^{12}\text{C}(n,\alpha)^{11}\text{C}^*1.995$ $^{16}\text{O}(p,n)^{11}\text{C}^*1.995$ $^{16}\text{O}(p,\alpha)^{11}\text{C}^*1.995$	4.830	$^{11}\text{B}^*9.275,^{11}\text{B}^*4.444$	$^{11}\text{B}(n,\gamma)^{11}\text{B}^*9.275$
2.124	$^{11}\text{B}^*2.124$ -g.s.	$^{11}\text{B}(p,p')^{11}\text{B}^*2.124$ $^{11}\text{B}(n,\alpha')^{11}\text{B}^*2.124$ $^{12}\text{C}(p,2p)^{11}\text{B}^*2.124$ $^{12}\text{C}(n,\alpha)^{11}\text{B}^*2.124$	5.180 5.241	$^{15}\text{O}^*5.181$ -g.s. $^{15}\text{O}^*5.242$ -g.s.	$^{12}\text{C}(n,n)^{15}\text{O}^*5.181$ & 5.242 $^{16}\text{O}(p,pp)^{15}\text{O}^*5.181$ & 5.242 $^{16}\text{O}(n,\alpha)^{15}\text{O}^*5.181$ & 5.242
2.184	$^{17}\text{O}^*2.055,^{17}\text{O}^*0.871$	$^{17}\text{O}(p,p')^{17}\text{O}^*2.055$	5.270 and 5.298	$^{15}\text{N}^*5.271$ -g.s. $^{15}\text{N}^*5.299$ -g.s.	$^{12}\text{C}(p,p)^{15}\text{N}^*5.271$ & 5.299 $^{15}\text{N}(p,p')^{15}\text{N}^*5.271$ & 5.299 $^{16}\text{O}(p,2p)^{15}\text{N}^*5.271$ & 5.299 $^{16}\text{O}(n,\alpha)^{15}\text{N}^*5.271$ & 5.299
2.313	$^{14}\text{M}^*2.313$ -g.s.	$^{12}\text{C}(n,\alpha)^{14}\text{M}^*2.313$ $^{13}\text{C}(p,\gamma)^{14}\text{M}^*2.313$ $^{14}\text{N}(p,p')^{14}\text{M}^*2.313$ $^{14}\text{N}(p,n)^{14}\text{O}(e^+)^{14}\text{M}^*2.313$ $^{14}\text{N}(n,\alpha')^{14}\text{M}^*2.313$ $^{16}\text{O}(p,n)^{14}\text{M}^*2.313$ $^{16}\text{O}(p,\alpha)^{14}\text{M}^*2.313$	6.129	$^{16}\text{O}^*6.131$ -g.s.	$^{16}\text{O}(p,p')^{16}\text{O}^*6.131$ $^{16}\text{O}(n,\alpha)^{16}\text{O}^*6.131$ $^{20}\text{Ne}(p,pp)^{16}\text{O}^*6.131$ $^{20}\text{Ne}(n,\alpha)^{16}\text{O}^*6.131$
2.365	$^{13}\text{M}^*2.365$ -g.s.	$^{10}\text{B}(n,\alpha)^{13}\text{M}^*2.365$ $^{12}\text{C}(p,\gamma)^{13}\text{M}^*2.365$ $^{12}\text{C}(pn)^{13}\text{M}^*2.365$	6.176	$^{15}\text{O}^*6.177$ -g.s.	$^{12}\text{C}(n,n)^{15}\text{O}^*6.177$ $^{15}\text{N}(p,n)^{15}\text{O}^*6.177$ $^{16}\text{O}(p,pp)^{15}\text{O}^*6.177$ $^{16}\text{O}(n,\alpha)^{15}\text{O}^*6.177$
2.741	$^{16}\text{O}^*8.872,^{16}\text{O}^*6.131$	$^{16}\text{O}(p,p')^{16}\text{O}^*8.872$	6.322	$^{15}\text{N}^*6.324$ -g.s.	$^{12}\text{C}(n,p)^{15}\text{N}^*6.324$ $^{15}\text{N}(p,p')^{15}\text{N}^*6.324$ $^{16}\text{O}(p,2p)^{15}\text{N}^*6.324$ $^{16}\text{O}(n,\alpha)^{15}\text{N}^*6.324$
3.086	$^{13}\text{C}^*3.086$ -g.s.	$^{12}\text{C}(p,p')^{13}\text{C}^*3.086$	6.478	$^{11}\text{C}^*6.480$ (g.s.)	$^{12}\text{C}(p,pp)^{11}\text{C}^*6.480$
3.365	$^{10}\text{Be}^*3.366$ -g.s.	$^{10}\text{Be}(p,p')^{10}\text{Be}^*3.366$ $^{11}\text{B}(p,2p)^{10}\text{Be}^*3.366$	6.741 and 6.791	$^{11}\text{B}^*6.743$ -g.s. (708) $^{11}\text{B}^*6.791$ -g.s. (718)	$^{11}\text{B}(p,p')^{11}\text{B}^*6.743$ & 6.791 $^{11}\text{B}(n,\alpha')^{11}\text{B}^*6.743$ & 6.791 $^{12}\text{C}(p,2p)^{11}\text{B}^*6.743$ & 6.791
3.561	$^6\text{Li}^*3.562$	$^6\text{He}(^3\text{He},p)^6\text{Li}^*3.562$ $^6\text{He}(n,\alpha)^6\text{Li}^*3.562$ $^6\text{Li}(p,p')^6\text{Li}^*3.562$ $^6\text{Li}(n,\alpha')^6\text{Li}^*3.562$ $^7\text{Li}(p,pp)^6\text{Li}^*3.562$ $^9\text{Be}(p,\alpha)^6\text{Li}^*3.562$ $^{12}\text{C}(p,n)^6\text{Li}^*3.562$	6.786	$^{15}\text{O}^*6.780$ -g.s.	$^{16}\text{O}(p,pp)^{15}\text{O}^*6.780$ & 6.788
3.684	$^{13}\text{C}^*3.684$	$^{12}\text{C}(n,n)^{13}\text{C}^*3.684$ $^{12}\text{C}(p,p')^{13}\text{C}^*3.684$ $^{12}\text{C}(n,\alpha')^{13}\text{C}^*3.684$ $^{16}\text{O}(p,n)^{13}\text{C}^*3.684$	6.917	$^{16}\text{O}^*6.919$ -g.s.	$^{16}\text{O}(p,p')^{16}\text{O}^*6.919$ $^{16}\text{O}(n,\alpha')^{16}\text{O}^*6.919$
3.853	$^{13}\text{C}^*3.854$	$^{12}\text{C}(n,n)^{13}\text{C}^*3.854$ $^{12}\text{C}(p,p')^{13}\text{C}^*3.854$ $^{12}\text{C}(n,\alpha')^{13}\text{C}^*3.854$ $^{16}\text{O}(p,n)^{13}\text{C}^*3.854$	7.117	$^{16}\text{O}^*7.118$ -g.s.	$^{16}\text{O}(p,p')^{16}\text{O}^*7.118$ $^{16}\text{O}(n,\alpha')^{16}\text{O}^*7.118$

$\phi_j(E)$ is the flux of cosmic ray nuclei of isotope j as a function of energy; $\sigma_{ijk}(E)$ is the cross section for the interaction of nuclei i and j producing an excited nucleus which at rest emits a gamma ray of energy ϵ_k .

If the excited nuclei were at rest with respect to the observer the energy spectrum of the gamma ray emission would be essentially a series of delta functions at energies ϵ_k . But since the excited nuclei have either some residual or recoil velocity after the nuclear interaction, the observed gamma ray emission will be Doppler shifted. This Doppler shifted energy, ϵ is given by the transformation

$$\epsilon = \epsilon_k [\gamma - (\gamma^2 - 1)^{1/2} \cos\theta]^{-1} \quad (2)$$

where γ is the Lorentz factor of the excited nucleus in the rest frame of the observer, and θ is the angle between the direction of motion of the excited nucleus and the line of sight between it and the observer. Then given a distribution of the Lorentz factor of the excited nuclei $P(\gamma)d\gamma$ and assuming the distribution of directions is isotropic, the observed distribution of gamma ray energies

$$P(\epsilon) = \int_{\gamma^*}^{\infty} d\gamma P(\gamma) \frac{1}{2\epsilon_k (\gamma^2 - 1)^{1/2}} \quad (3)$$

where $\gamma^* = (\epsilon_k^2 + \epsilon^2)/(2\epsilon\epsilon_k)$ is the minimum Lorentz factor which the excited nucleus must have in order to Doppler shift the gamma ray of energy ϵ_k to energy ϵ .

The observed gamma ray emissivity, as a function of energy, including all lines k , is then

$$q(\epsilon) = \sum_{ijk} \int_0^{\infty} dE \phi_j(E) \sigma_{ijk}(E) \int_{\gamma^*}^{\infty} d\gamma' \frac{P_{ijk}(E, \gamma')}{2\epsilon_k (\gamma'^2 - 1)^{1/2}} \quad (4)$$

noting that $P_{ijk}(E, \gamma')$ is the probability that the excited nucleus, resulting from the interaction of nuclei i and j and energy E , will have a Lorentz factor γ' at the time of deexcitation.

The gamma ray line emission resulting from these interactions tends to fall into three components: sharp line emission by excited interstellar dust grain nuclei; narrow line emission by excited interstellar gas nuclei; and broad line emission by excited cosmic ray nuclei. Excited nuclei of dust grains lose most if not all of their recoil kinetic energy before deexcitation so that their emission line widths primarily reflect the bulk motions of the grains in the galaxy leading to Doppler widths of the order of 10 keV or less. The small recoil energies of the excited interstellar gas nuclei cause the gamma ray lines emitted by them to have a typical Doppler broadening of only ~ 100 keV, and the gamma ray lines emitted by the excited cosmic ray nuclei, which lose little kinetic energy in these interactions, have a typical Doppler broadening of several hundred keV. A typical gamma ray line profile from deexcitation of interstellar gas and cosmic ray nuclei is shown in Figure 1.

Measurements of the integral intensity of individual lines have much better statistical significance and a comparison of these with calculated integral intensities provides the greatest information on the density, composition and energy spectra of the cosmic rays and interstellar gas.

The integral emissivity for a particular gamma ray line, k , can be obtained by integrating the emissivity (Equation 4) over a gamma ray energy range of $\pm \Delta \epsilon$ around ϵ_k . If $\Delta \epsilon$ is larger than the broadening of the line emission from the excited interstellar gas and dust nuclei, then the integral emissivity $q(\epsilon_k \pm \Delta \epsilon)$ becomes,

$$\begin{aligned}
 q(\epsilon_k \pm \Delta \epsilon) = & \sum_{i^*j} \int_0^{\infty} dE n_i \phi_j(E) \sigma_{ijk}(E) + \\
 & \sum_{ij^*} \int_0^{E^*} dE n_i \phi_j(E) \sigma_{ijk}(E) + \\
 & \sum_{ij^*} \int_{E'}^{\infty} dE n_i \phi_j(E) \sigma_{ijk}(E) \frac{\Delta \epsilon}{\epsilon_k (\gamma^2 - 1)^2} \quad (5)
 \end{aligned}$$

where

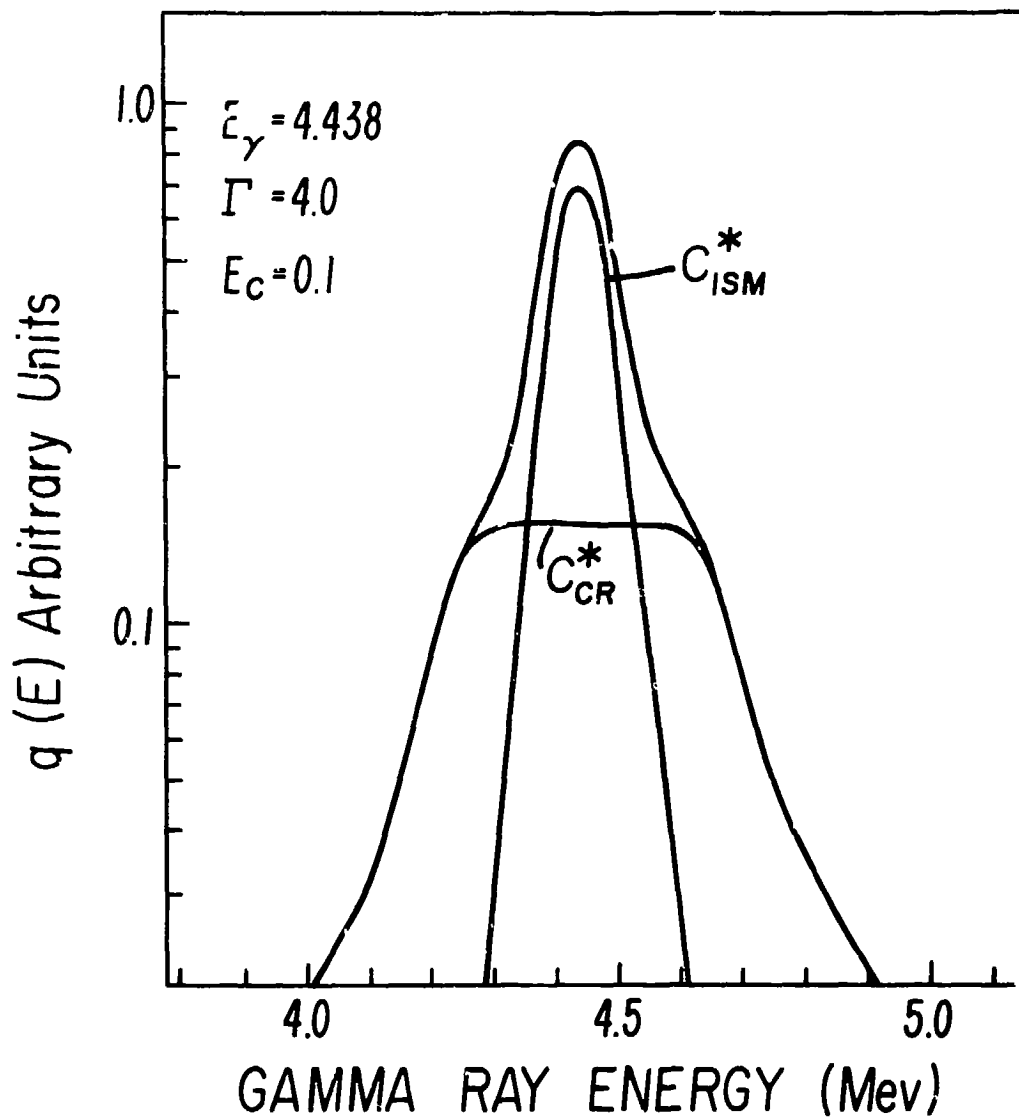


Figure 1. A typical gamma ray line profile showing the narrow line emission spectrum of excited interstellar gas nuclei and the broad line emission of cosmic ray nuclei.

$$E' \equiv mc^2 \left[\left\{ 1 + \left(\frac{\Delta\varepsilon}{\varepsilon_k} \right)^2 \right\}^{1/2} - 1 \right], \quad (b)$$

is the incident cosmic ray energy per nucleon at which the width of the broadened line emission from the excited cosmic ray nucleus equals $2\Delta\varepsilon$.

Since either the energy density of the cosmic rays, or the instantaneous energy loss rate of the cosmic rays can be more easily related to other properties of the interstellar medium than the intensity $\phi_j(E)$, we normalize the gamma ray line emissivity to these parameters. Thus we calculate the emissivity per unit cosmic ray energy density, $q(\epsilon)/w$, in photons $\text{sec}^{-1} \text{ev}^{-1}$ and the emissivity per unit energy loss, $q(\epsilon)/\dot{w}$, in photons erg^{-1} . The cosmic ray energy density, in ev cm^{-3} , is

$$w = 10^6 \sum_j \int_0^\infty dE A_j \phi_j(E) E / c\beta \quad (7)$$

where A_j is the atomic number of cosmic ray nuclei j and the instantaneous cosmic ray energy loss rate,

$$\dot{w} = \sum_{ij} \int_0^\infty dE \phi_j(E) \left(\frac{dE}{dx} \right)_i \quad (8)$$

where the energy loss rate dE/dx is taken from Barkas and Berger (1964).

From the above equations we can thus calculate gamma ray line emissivities for the interstellar medium based on measured, or in some cases calculated, cross sections, an assumed cosmic ray energy spectrum, and cosmic ray and interstellar gas abundances.

The energy dependent excitation cross sections used in these calculations for the various interactions listed in Table 1 will be published in a forthcoming paper. Most of the measurements on which they are based are summarized in the extensive review papers on charged particle reactions by McGowan and Milner (1972, 1973a, 1973b, 1975). The energy dependent excitation cross sections for some of these interactions have also been presented and discussed in Ramaty et al. (1975) and Meneguzzi and Reeves (1975).

The cosmic ray energy spectrum in interstellar space is not known below about 500 Mev/nucleon because the interplanetary magnetic field and solar wind exclude lower energy particles from the inner part of the solar system. Thus we must consider a range of different energy spectra

and then try to place some bounds on the spectral shape from a comparison of the relative emissivities of various lines calculated for each spectrum with the observations of relative line intensities.

For these calculations we have assumed that the cosmic ray intensity is a power law in energy per nucleon with a spectral index $-\Gamma$ down to some cutoff energy E_c below which the intensity is constant, i.e. the intensity of cosmic ray particles j has the form

$$\phi_j(E) = \phi_{0j} \text{ for } E < E_c \quad (9)$$

and

$$\phi_j(E) = \phi_{0j} (E/E_c)^{-\Gamma} \text{ for } E_c < E < E_s \quad (10)$$

where

$$E_s = \Gamma mc^2 / (2.7 - \Gamma) \text{ for } \Gamma < 2.7 \text{ and } E_s = \infty \text{ for } \Gamma \geq 2.7$$

so that the flatter spectra join smoothly at high energies into a power law in total energy with the observed spectral index of -2.7 , giving

$$\phi_j(E) = 14.61 \phi_{0j} (2.7 - \Gamma)^{\Gamma - 2.7} \left(\frac{E_c}{\Gamma mc^2}\right)^{\Gamma} \left(\frac{mc^2}{E + mc^2}\right)^{2.7} \quad (11)$$

for $E > E_s$.

For the relative elemental and isotopic abundances in the combined interstellar gas and dust we have used the solar system abundances compiled by Cameron (1973). Although these may be representative of the local interstellar medium, the recent work of Searle (1971), Shields (1974), Smith (1975) and D'Odorico et al. (1976), studying abundances in galactic nebulae suggest large radial gradients in the abundances of He, N and O relative to H across our galaxy. Such gradients in these and other elements, such as C, are expected from galactic evolutionary models (e.g. Talbot and Arnett, 1975). The

present observations allow only very preliminary modeling of the spacial dependence of the relative abundances but gamma ray line observations may be able to contribute significantly to our understanding of this problem.

For the relative elemental and isotopic abundances of the cosmic rays we have used the measurements of elemental abundances of Smith et al. (1973) at energies >1.5 Gev/nucleon except for the more recent iron abundance measurement of Garcia-Munoz et al. (1975) and the relative isotopic abundance measurements summarized by Meyer (1975). For the initial calculations we have assumed that these abundances are energy independent. There is however a significant energy dependence in the relative abundance of some nuclei especially those elements and isotopes which are mainly of secondary origin. If the composition of cosmic rays reflects in any way the gross composition of matter in the region of their source we must also consider the possibility of cosmic ray abundance gradients related to those in the interstellar gas and dust.

3. Calculated Emissivity. With these relative abundances we have calculated the gamma ray line emissivities for a variety of possible cosmic ray energy spectra (Equations 9 to 11) characterized by a spectral index $-r$ and a cutoff energy E_c .

The emissivity per unit cosmic ray energy density, q/w , for the combined gamma ray line emission from the nuclear excited states $^{12}\text{C}^*4.439$ and $^{11}\text{B}^*4.444$ at energies of 4.44 ± 0.44 Mev is shown in Figure 2, calculated from Equations 5 and 7 for the interactions listed from those lines in Table 1. This is then the emissivity in the local interstellar medium for an average hydrogen density of 1 atom cm^{-3} and assuming a total cosmic ray energy density of 1 ev cm^{-3} . The emissivity q/w for this line is roughly linear in the C/H ratio for changes of an order of magnitude or less, if C/O is constant.

The peak in emissivity for essentially all spectra at a cutoff E_c of ~ 10 Mev/nucleon reflects a peak in the excitation cross sections at roughly that energy. Thus spectra which carry most of their energy in particles of around 10 Mev/nucleon are most efficient in producing

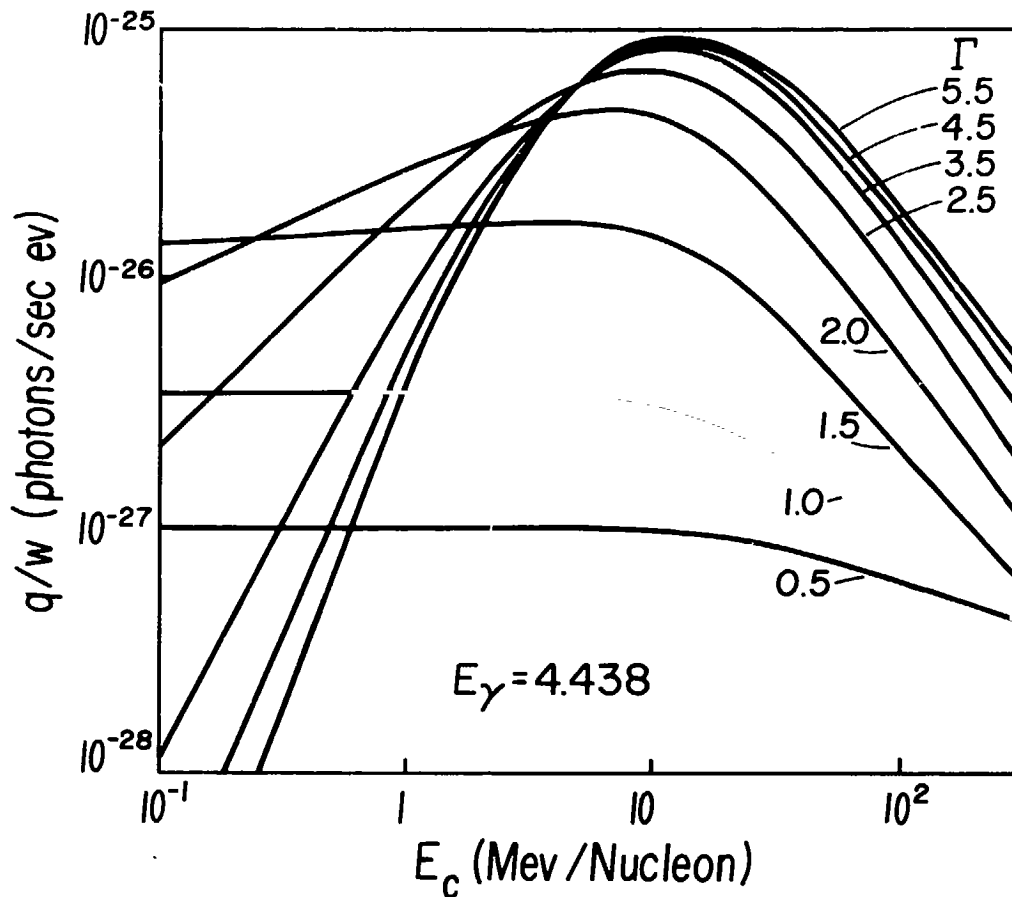


Figure 2. The 4.44 ± 0.44 Mev gamma ray emissivity per unit cosmic ray energy density as a function of the assumed cosmic ray energy spectral index $-\Gamma$ and the cut-off energy E_c defined in Equations 9 to 11.

$12_{C*4.439}$. The fraction of the emissivity in the narrow line component of excited interstellar gas and dust depends strongly on the spectral shape but for cases with E_c of ~ 10 Mev/nucleon, which give the maximum emissivity, roughly half is in the narrow line component within 4.44 ± 0.05 Mev. Note also that for $E_c > 3$ Mev/nucleon the emissivity per unit energy density is rather insensitive to the spectral index Γ so long as it is greater than about 2.5.

These emissivities for the 4.44 Mev line are between 1.4 and 20 times larger than those calculated for that

line by Rygg and Fishman (1973), depending on spectral index, and are the same to two times higher than those of Meneguzzi and Reeves (1975). Both differences result primarily from our inclusion of additional excitation interactions.

The emissivity per unit cosmic ray energy loss rate, q/\dot{w} , for the same line is shown in Figure 3 calculated

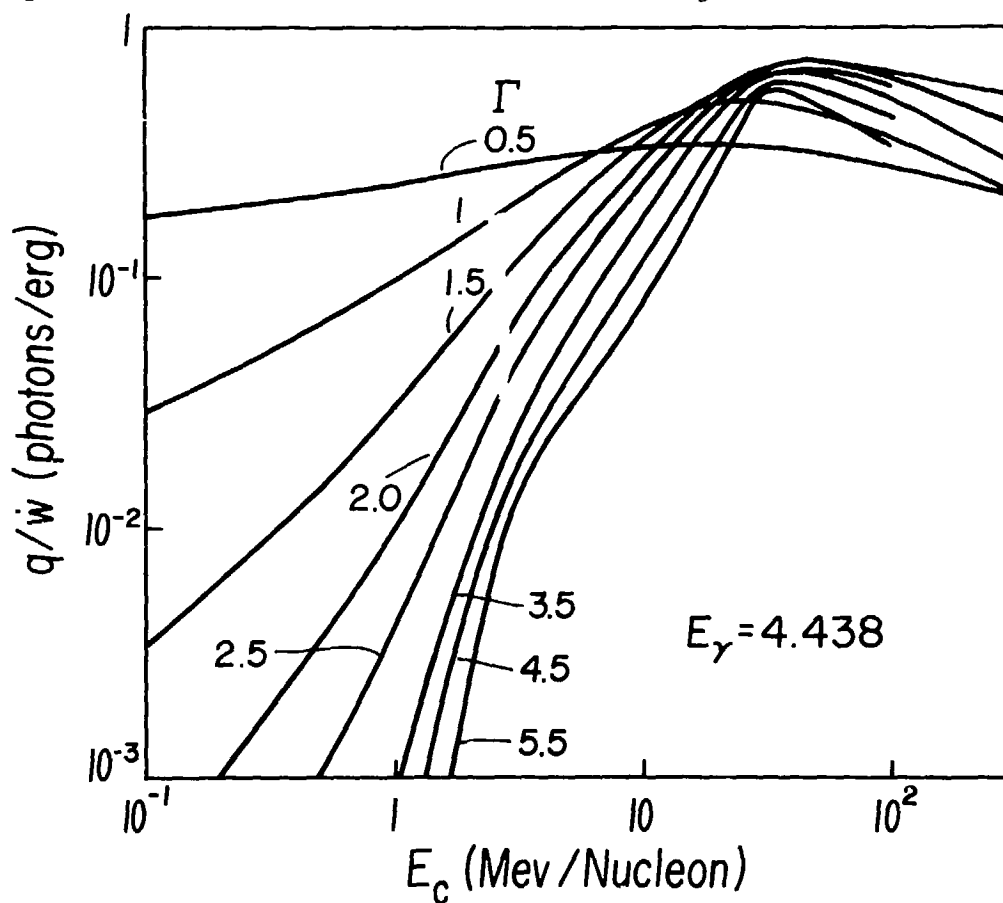


Figure 3. The yield of 4.44 ± 0.44 Mev gamma rays per erg of cosmic ray energy dissipated in ionization and nuclear interactions with the interstellar medium as a function of the assumed cosmic ray spectral parameters.

from Equations 5 and 8. This is the yield of 4.44 Mev gamma rays per erg of energy dissipated by ionization and nuclear interactions in an ambient medium of solar composition. This emissivity is also roughly linear in C/H for

constant C/O. As can be seen the yield is greatest for cutoff energies $E_c \gtrsim 10$ Mev/nucleon and it is not strongly dependent on the spectral index for these cases.

In addition to the 4.44 Mev line there are a number of other lines which, depending on the assumed cosmic ray spectral shape and composition, can have comparable emissivity. The combined emissivity per unit cosmic ray energy density of all gamma ray lines listed on Table 1 with gamma ray energies >0.8 Mev is shown in Figure 4, for the same conditions as above.

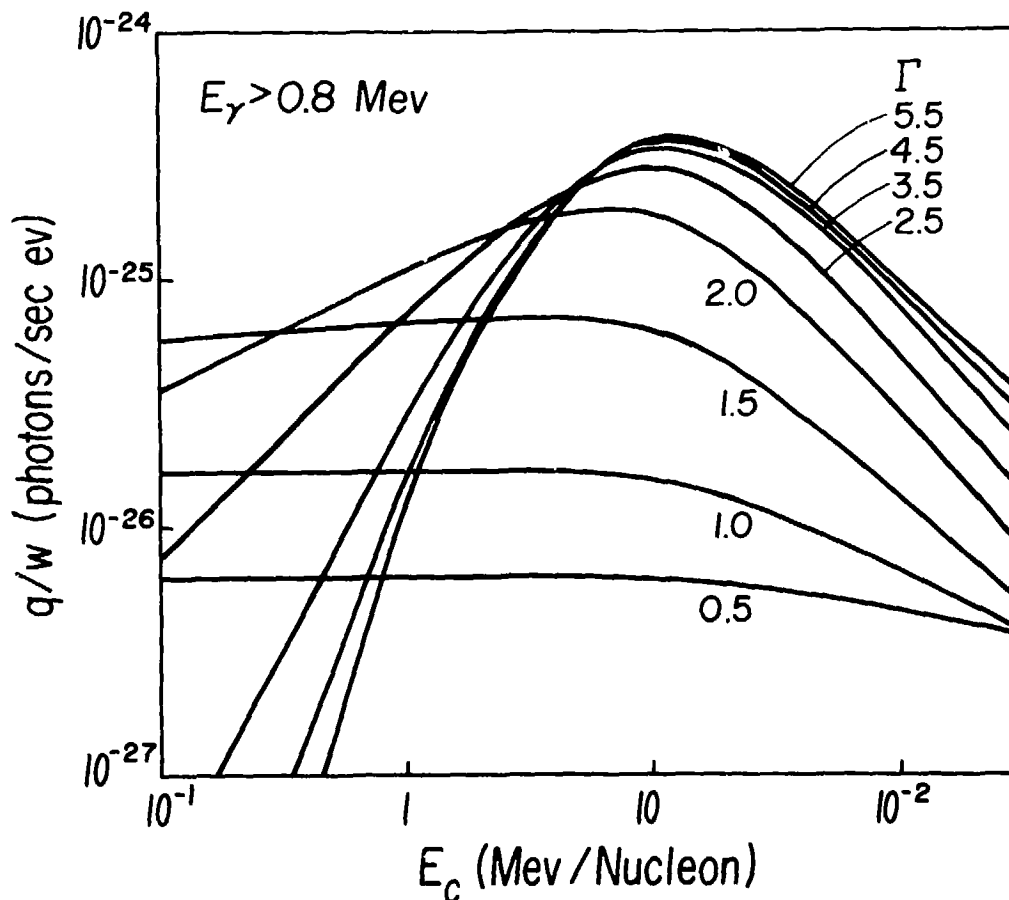


Figure 4. The combined gamma ray line emissivity per unit cosmic ray energy density of all of the gamma ray lines of energy >0.8 Mev listed in Table 1, as a function of the assumed cosmic ray energy spectral parameters.

As can be seen by comparison with Figure 2, the combined gamma ray line emissivity is roughly 4 times that of the

4.44 Mev line alone. This ratio is essentially independent of the assumed shape of the cosmic ray energy spectrum. Haymes et al. (1975) in fact report a total gamma ray line intensity above 0.8 Mev that is about 4.1 ± 0.8 times that of the 4.4 Mev gamma rays.

If the reported gamma ray flux at about 4.4 Mev (Haymes et al., 1975, and Trombka, private communication, 1976) is of galactic origin then unresolved line emission at energies >0.8 Mev may make a significant contribution to the apparent flattening of the diffuse gamma ray background at these energies.

4. Galactic Gamma Ray Line Intensity. From these emissivities we can estimate the expected galactic gamma ray line intensity, assuming some distribution of the interstellar gas, dust and cosmic rays. If the density and composition of the cosmic rays, gas and dust were uniform throughout the galaxy with $n_H = 1 \text{ atom cm}^{-3}$ and $w = 1 \text{ ev cm}^{-3}$ and solar composition then the expected local galactic intensity of even the narrow line component of 4.44 \pm 0.05 Mev gamma rays would be $\lesssim 3 \times 10^{-5} \text{ photons cm}^{-2} \text{ sec}^{-1}$. This intensity, as was previously noted by Meneguzzi and Reeves (1975), could not be detected above the diffuse gamma ray background of $\sim 10^{-3} \text{ photons cm}^{-2} \text{ sec}^{-1}$ in that energy interval.

But this is not the case, for the density and composition of the interstellar gas and dust are now known to vary significantly across the galaxy. The details of these spacial dependences, however, are not yet fully understood. The neutral hydrogen distribution in the galaxy is fairly well determined from 21-cm observations recently reevaluated by Burton et al. (1975). But estimates of the molecular hydrogen distribution based on the observed CO distribution (Scoville and Solomon, 1975; Burton et al., 1975; and Gordon and Burton, 1976) necessarily reflect the uncertainties in possible C/H and O/H abundance variations. However, for the purpose of calculating the narrow line component of 4.44 Mev gamma ray emission from deexcitation of carbon in the interstellar gas and dust, we shall assume that the spacial distribution of the carbon and oxygen density in the galaxy is directly proportional to that deduced for CO molecules at galactic radii $>2 \text{ kpc}$ (Gordon and Burton, 1976), ignoring for the moment any contribution from the galactic nucleus.

Then if the cosmic ray energy density were uniform throughout the galaxy with $w = 1 \text{ ev cm}^{-3}$ the local galactic gamma ray intensity of the narrow line component at $4.44 \pm 0.05 \text{ Mev}$ could be as much as $10^{-4} \text{ photons cm}^{-2} \text{ sec}^{-1}$ which is still only 10% of the diffuse background.

However we might also expect the cosmic ray energy density in the galaxy to vary because of a nonuniform distribution of cosmic ray sources. Observations of the spacial distribution of likely cosmic ray sources such as supernovae (Ilovaisky and Lequeux, 1972) and pulsars (Hulse and Taylor, 1974, 1975) show a strong dependence on galactic radius. These distributions are qualitatively similar (Burton et al., 1975) to that of CO molecules. If we thus assume that the cosmic ray energy density is also proportional to the CO distribution of Gordon and Burton (1976) with a local value of 1 ev cm^{-3} then the expected galactic gamma ray intensity in the narrow line component at $4.44 \pm 0.05 \text{ Mev}$ could be as large as $\sim 0.6 \times 10^{-3} \text{ photons cm}^{-2} \text{ sec}^{-1}$ which should be resolvable above the background. In a preliminary analysis of measurements with an omnidirectional detector on Apollo 16 Trombka (private communication, 1976) reports seeing a 4.4 Mev gamma ray line intensity of $\sim 1.5 \pm 0.75 \times 10^{-3} \text{ photons cm}^{-2} \text{ sec}^{-1}$, although part of this flux is background due to neutron activation of the detector. Further analysis of the background is required before it can be established that diffuse gamma ray line emission has been observed.

5. Gamma Ray Line Emission from the Galactic Nuclear Ring. A significant fraction of the intensity reported by Trombka (private communication, 1976) may also come from the direction of the galactic center from which Haymes et al. (1975) report a spectral feature at about 4.4 Mev with an intensity of $(0.95 \pm 0.27) \times 10^{-3} \text{ photons cm}^{-2} \text{ sec}^{-1}$. This emission could also result from cosmic ray interactions in a dense ring of interstellar gas, deduced from molecular line observations to lie in the nuclear disc of the galaxy at a radius of about 270 pc from the center (Kaifu et al., 1972; Scoville, 1972; and Robinson, 1974). The hydrogen density in this ring must be $>10^3 \text{ cm}^{-3}$ in order to excite the observed CO and NH_3

emission lines and the total mass of the ring is estimated to be between 10^8 and $10^9 M_{\odot}$, corresponding to a volume of $\sim 10^{62} \text{ cm}^3$. This should be compared to estimates of the total mass of gas in the galaxy of $\sim 4 \times 10^9 M_{\odot}$ (Gordon and Burton, 1976).

The local gamma ray line intensity coming from such a ring is simply

$$\phi = \frac{qn_{\text{H}}V}{4\pi r^2} \quad (12)$$

where q is the emissivity, $n_{\text{H}}V$ is the total number of hydrogen atoms in the ring, equal to 10^{65} to 10^{66} for a ring mass of 10^8 to $10^9 M_{\odot}$, and r is 10 kpc, the distance of the sun from the galactic center. With these values the reported 4.4 Mev gamma ray intensity ϕ of 10^{-3} photon $\text{cm}^{-2} \text{ sec}^{-1}$ would require an emissivity q of 10^{-22} to 10^{-23} photons $\text{cm}^{-3} \text{ sec}^{-1}$. Assuming, as discussed above, that the C/H and O/H ratios in the galactic nuclear ring are an order of magnitude greater than solar values, then we could expect q/w to be as much as 10^{-24} photons $\text{sec}^{-1} \text{ ev}^{-1}$. The reported emission could thus be produced by cosmic ray interactions with the gas in the nuclear ring if the cosmic ray energy density were between 10 and 10^2 ev cm^{-3} . This is comparable to cosmic ray energy densities already suggested for a nuclear region by Sanders and Wrixon (1973) who estimated that either a magnetic field or a cosmic ray pressure, or energy density, of the order of 10 ev cm^{-3} was required to keep the gas from collapsing into the galactic equatorial plane. It is also much less than might be expected if the cosmic ray energy density were assumed to be roughly proportional to the C and O density which is at least $\sim 10^4$ times larger in the nuclear ring than locally. The total energy in such low energy cosmic rays in the ring is only 10^{51} to 10^{52} ergs which could in principle be produced by a single supernova.

From the calculated q/\dot{w} for the 4.44 Mev line shown on Figure 3 we also see that the maximum gamma ray photon yield per erg of cosmic ray energy lost in ionization and nuclear interactions is on the order of unity for the local C/H ratio. Hence it could be as much as 10 in the gas in the nuclear ring, if the C/H ratio there is 10 times higher. The reported intensity ϕ of 10^{-3} photons $\text{cm}^{-2} \text{sec}^{-1}$ implies 4.4 Mev gamma ray luminosity of $4\pi r^2 \phi = 10^{43}$ photons sec^{-1} for the nuclear ring. The above q/\dot{w} further implies a total energy loss rate for the cosmic rays in the ring of 10^{42} ergs sec^{-1} . This is comparable to the infrared luminosity of the galactic nucleus (Hoffman et al., 1971). If the total cosmic ray energy is between 10^{51} and 10^{52} ergs, then the mean life of such cosmic rays w/\dot{w} is between 30 and 300 years. Since the estimated mass of molecular gas in the ring is between 3% and 30% of the molecular gas in the galaxy (Gordon & Burton, 1976) we might expect the relative frequency of occurrence of supernovae in the ring and in the galaxy to be similar. A galactic supernova rate of one every 25 years (Tammann, 1974) could thus give a supernova rate of one every 75 to 750 years in the nuclear ring. If each supernova produced a few times 10^{51} ergs in low energy cosmic rays, this rate could supply the required cosmic ray energy a substantial fraction of the time, producing a variable gamma ray source on time scales of the order of the cosmic ray energy loss time.

6. Summary. We have evaluated the production rate of the most significant nuclear gamma ray lines from 0.4 to 7 Mev, produced in cosmic ray interactions with the interstellar material. Each of these lines consists of three components with different line widths. There is a sharp line component with a Doppler width of the order of 10 kev or less emitted on deexcitation of interstellar grain nuclei which should be easily observed by solid state detectors with energy resolution of a few kev or less. Studies of this component can give the first measurement of the composition and spacial distribution of interstellar grains throughout the galaxy. There is also a relatively narrow gamma ray line component with a width of the order of 100 kev for the most intense line, $^{12}\text{C}^*4.439$, and of the order of a few kev for the $^{56}\text{Fe}^*0.847$ line, emitted on deexcitation of interstellar gas nuclei, and lastly a broad line component with a

width of several hundred kev, emitted on deexcitation of low energy cosmic ray nuclei.

Here we have presented a detailed evaluation of the production rate of the 4.44 Mev line for a variety of assumed cosmic ray spectra. Comparing these results with reported (Haymes et al., 1975; Trombka, private communication, 1976) galactic gamma ray line intensities, we conclude that the measurements are consistent with a low energy cosmic ray density which increases toward the galactic center in proportion to the molecular gas density.

7. Acknowledgements: We particularly wish to thank Helen Lee for her aid with the machine computations.

8. References

- Barkas, W.H., and Berger, J.J., 1964, Tables of Energy and Ranges of Heavy Charged Particles, NASA SP 3013.
- Burton, W.B., Gordon, M.A., Banis, T.M., and Lockman, F. J., 1975, Ap. J., 202, 30.
- Cameron, A.G.W., 1973, in Explosive Nucleosynthesis, D.S. Schramm and W.D. Arnett eds. (Austin: Univ. of Texas Press) p. 3.
- D'Odorico, S., Peimbert, M., and Sabbadin, F., 1976, Astron. Astrophys., 47, 341.
- Fishman, G.J., and Clayton, D.D., 1972, Ap. J., 178, 337.
- Fowler, W.A., Reeves, H., and Silk, J., 1970, Ap. J., 162, 49.
- Garcia-Munoz, M., Juliusson, E., Mason, G.M., Meyer, P., and Simpson, J.A., 1975, Ap. J., 197, 489.
- Gordon, M.A., and Burton, W.B., 1976, Ap. J., in press.
- Haymes, R.C., Walraven, G.D., Meegan, C.A., Hall, R.D., Djuth, F.T., and Shelton, D.H., 1975, Ap. J., 201, 593.
- Hoffman, W.F., Frederick, C.K., and Emery, R.J., 1971, Ap. J. Lett., 164, L23.
- Hulse, R.A., and Taylor, J.H., 1974, Ap. J., 191, L59.

- Hulse, R.A., and Taylor, J.H., 1975, Ap. J., 201, L55.
- Ilovaisky, S.A., and Lequeux, J., 1972, Astron. Astrophys., 18, 169.
- Johnson, W.N. III, Harnden, F.R. Jr., and Haymes, R.C., 1972, Ap. J. Lett., 172, L1.
- Johnson, W.N. III, and Haymes, R.C., 1973, Ap. J., 184, 103.
- Kaifu, N., Kato, T., and Iguchi, T., 1972, Nature, 238, 015.
- Kozlovsky, B., and Ramaty, R., 1974, Ap. J. Lett., 191, L43.
- Meneguzzi, M., and Reeves, H., 1975, Astron. Astrophys., 40, 91.
- Meyer, J.P., 1975, 14th Internat. Cosmic Ray Conf. Papers, 11, 3698.
- McGowan, F.K., and Milner, W.T., 1972, Nuclear Data Tables, 11, 1.
- McGowan, F.K., and Milner, W.T., 1973a, Charged Particle Reaction List 1948-1971 (New York: Academic Press), 547 pp.
- McGowan, F.K., and Milner, W.T., 1973b, Atomic Data and Nuclear Data Tables, 12, 499.
- McGowan, F.K., and Milner, W.T., 1975, Atomic Data and Nuclear Data Tables, 15, 189.
- Ramaty, R., and Boldt, E.A., 1971, The Gum Nebula and Related Problems (NASA X 683-71-375), 97.
- Ramaty, R., Kozlovsky, B., and Lingenfelter, R.E., 1975, Space Sci. Rev., 23, 198.
- Robinson, B.J., 1974, I.A.U. Symposium No. 60. Galactic Radio Astronomy, F.J. Kerr and S.C. Simonson, eds. (Dordrecht: Reidel), p. 521.
- yyg, T.A., and Fishman, G.J., 1973, Proc. 13th Internat. Cosmic Ray Conf. (Denver), 1, 472.

Sanders, R.N., and ... G.T., 1973, Astron. Astrophys.,
26, 365.

Scoville, N.Z., 1972, Ap. J., 175, L127.

Scoville, N.Z., and Solomon, P.M., 1975, Ap. J. Lett.,
199, L105.

Searle, L., 1971, Ap. J., 168, 327.

Shields, G.A., 1974, Ap. J., 193, 335.

Smith, H.E., 1975, Ap. J., 199, 591.

Smith, L.H., Buffington, A., Smoot, G.F., and Alvarez, L.
W., 1973, Ap. J., 180, 987.

Talbot, R.J., Jr., and Arnett, W.D., 1975, Ap. J., 197,
551.

Tammann, G.A., 1974, in Supernovae and Supernova Remnants,
C.B. Cosmovici, ed. (Dordrecht: Reidel), p. 155.

CONTRIBUTED PAPERS

June 3, 1976 P.M.

1. Steepening of the γ -Ray Background Spectrum From Local γ -Ray Production, K. Thielheim, Institut für Reine and Angewandte Kernphysik, Universität Kiel, W. Germany

Reference: R. Schlickheiser and K. O. Thielheim, 1976, Nature 261, 478.

2. Production Spectrum of π^0 -Mesons in the Galaxy, S. A. Stephens, NASA/Johnson Space Flight Center, Houston, Texas 77058.

Reference: No preprint available.

3. Carbon Monoxide Kinematics in the Inner Galaxy, T. M. Bania, National Radio Astronomy Observatory, Edgemont Road, Charlottesville, VA 22901.

Reference: T. M. Bania, Carbon Monoxide Kinematics in the Inner Galaxy, Bull. AAS 8, 334 (1976).

4. CO Observation of the Scale Height and Distribution of Molecular Clouds in the Galactic Plane, Richard Cohen, Columbia University and Goddard Institute for Space Studies, 2880 Broadway, New York, NY. 10025.

Reference: No Preprint available

5. A Survey of Ionized Hydrogen in the Plane of the Galaxy, F. J. Lockman, National Radio Observatory, Edgemont Rd., Charlottesville, VA. 22901.

Reference: F. J. Lockman, A Survey of Ionized Hydrogen in the Plane of the Galaxy, Ap. J. in press.

6. Angular Distribution of Low Energy γ -Ray Flux as Observed on Apollo 16, David Gilman, Dept. of Astronomy, Cornell University, Ithaca, N.Y.

Reference: No preprint available.

7. 0.3-10 MeV Diffuse γ -Ray Spectrum From Measurements Obtained During the Apollo 15, 16 and 17 Missions, Jacob Trombka, Goddard Space Flight Center.

Reference: J. Trombka, C. W. Dyer, L. G. Evans, M. J. Bielfeld, S. M. Seltzer and A. E. Metzger, Bull. Am. Phys. Soc. 21, 562 (1976).
Also: Reanalysis of the Apollo Cosmic γ -Ray Spectrum in the 0.3-10 MeV Region, J. Trombka, C. W. Dyer, L. G. Evans, M. J. Bielfeld, S. M. Seltzer and A. E. Metzger, GSFC Preprint X-682-76-128.

8. Cosmic Diffuse γ -Ray Angle and Energy Distributions from 2 to 30 MeV, R. S. White, S. Moon, J. Ryan, R. Wilson, A. D. Zych and B. Dayton, Physics Dept. U. of California, Riverside, CA 92502.

Reference: Cosmic Diffuse γ -Ray Angle and Energy Distributions From 2 to 30 MeV, R. S. White, S. Moon, J. Ryan, R. Wilson, A. D. Zych and B. Dayton, Bull. Am. Phys. Soc. 21, 56a (1976).

CONTRIBUTED PAPERS
June 4, 1976 A.M.

1. Cosmic Ray Propagation in a Closed Galaxy, Bernard Peters, Danish Space Research Institute, Lyngby, Denmark.

Preprint: Cosmic Ray Propagation in a Closed Galaxy, B. Peters and N. J. Westergaard, Danish Space Research Institute, Lyngby, Denmark.

2. Distribution of Cosmic Ray Nuclei in the Galaxy, Arnold Wolfendale, Physics Department, University of Durham, England.

Preprint: Distribution of Cosmic Ray Nuclei in the Galaxy, D. Dodds and A. W. Wolfendale, Physics Department, University of Durham, England.

3. The Source Function for the Inverse Compton Process in the Solar Vicinity, Giovanni Bignami, Istituto di Science Fisiche, Aldo Pontromeli, Via Celoria 16, Milano, Italy 20133.

Reference: The Source Function for the Inverse Compton Process in the Solar Vicinity, G. Piccimotti and G. F. Bignami, to be published in Astron. and Astrophysics.

N76-29128

GAMMA RAYS AND SUPERNOVA EXPLOSIONS

W. David Arnett, Department of Astronomy, University of Illinois,
Urbana, Illinois 61801

ABSTRACT

The detection of gamma rays from supernovae will provide interesting tests of current theory. This discussion will review some current ideas on the expected gamma ray flux, as modified by recent theoretical results.

1. Continuum Emission. After the explosion high energy electromagnetic radiation may be produced by an uncovered pulsar or by the interaction of the ejected debris with the interstellar medium. Here we will consider instead the radiation associated with the explosion itself, especially with high temperatures.

It appears that most of the radiation from type II supernovae is thermal radiation. To produce copious gamma radiation of this sort requires high temperature. The observational data is well represented by low temperatures ($T \lesssim 20,000$ °K). Thus $kT \lesssim 10$ ev which certainly is not favorable for gamma emission. A detailed discussion for SN 1969L is given by Falk and Arnett (1976). Most of the luminosity seems to be due to the diffusive release of imprisoned radiation by an expanding plasma. There is a "first burst" due to the arrival of the supernova shock at the stellar surface. It is not clear just how high the temperatures get in this brief stage ($\Delta t \lesssim 1$ day). The calculations give $T_{\max} \approx 40,000$ °K; it is unlikely that this is off by orders of magnitude. Consequently it appears that type II supernovae do not release very much of their energy as gamma ray continuum radiation.

There is a simple reason for this result. A massive star of, say, $10 M_{\odot}$ develops a large radius, $r \approx 5 \times 10^{13}$ cm, after helium burning. The observed luminosity at peak, which looks like a black body, has $L \approx 10^{43}$ erg, so if we allow for some expansion,

$$\sigma T_e^4 = L/4\pi r^2 \lesssim 10^{43}/\pi \times 10^{28}$$

or $T_e \lesssim 50,000$ °K. Doppler shifts in absorption lines of up to about 10^9 cm/sec are observed. The radius doubles in a time

$$t \approx r/v \approx 5 \times 10^{13}/10^9 \approx 5 \times 10^4 \text{ sec} \approx 1/2 \text{ day,}$$

and in two days $r \approx 2 \times 10^{14}$ cm so $T_e \approx 25,000$ °K and it continues to cool. When the photospheric temperature drops below about $6,000$ °K the opacity decreases due to recombination and one sees in to deeper, hotter regions. Thus T_e decreases below $6,000$ °K only slowly.

When will the temperature throughout the envelope drop low enough to cause transparency? First the initial (post shock) temperature must be estimated. For $10 M_{\odot}$ and an average velocity of $6,000$ km/sec gives

a kinetic energy of 3.6×10^{51} ergs, a value in accord with that estimated as necessary to explain the nature of galactic supernova remnants. This energy can fill a sphere of radius $r = 5 \times 10^{13}$ cm with black body radiation at a temperature $T \simeq 1.0 \times 10^6$ °K.

Is the expansion approximately adiabatic? It seems possible; observed supernova luminosities, integrated over the outburst give energies of order 10^{50} ergs. The diffusion time is

$$\tau \simeq 3r^2/\lambda c \simeq 3r^2 \rho \kappa / c .$$

Now most of the stellar mass is in an extended, almost constant density envelope, so

$$\rho \simeq 3M/4\pi r^3$$

and the diffusion time is

$$\tau \simeq 2 \times 10^8 \text{ sec} \left(\frac{10^{14} \text{ cm}}{r} \right) \left(\frac{\kappa}{0.4 \text{ cm}^2/\text{g}} \right) \frac{M}{M_{\odot}} .$$

This equals $t \sim r/v$ only for $r \simeq 10^{16}$ so the dominant effect is expansion.

For quasi-adiabatic expansion, $\rho \sim T^3$ so we have

$$T/10^6 \text{ °K} \simeq 5 \times 10^{13} \text{ cm} / (10^9 \text{ cm/sec } t) ,$$

so for $T \simeq 6000$ °K,

$$t \simeq 80 \text{ days} .$$

After this time a significant fraction of the envelope becomes transparent (This is sufficiently long to hide many gamma lines; see Table 1 below). More complex calculations support these simple arguments.

It is not clear how high the energy densities associated with the "burst" in type I supernovae become. They may be similar to SN II. The Morrison - Sartori (1969) model requires fairly hard (UV) radiation, in large amounts (energies $> 10^{52}$ ergs). While Lasher (1975) has explained the shape of the visual light peak of SN I, his models do not yet explain the hard UV pulse. It is not at all obvious that a hard UV pulse, even if it exists, means that significant gamma radiation will result. Such radiation is difficult to rule out entirely for all (as yet unspecified) models.

Colgate (1975) assumes that the supernova shock has a high temperature precursor. If instead the matter is accelerated by radiation pressure (Falk and Arnett 1976) then the reason for expecting a strong gamma-ray burst disappears. Until the physics of the "peak" in SN I is well understood and agreed upon it seems wise to regard the theoretical situation as unclear.

Because of many underlying similarities it is beginning to appear that both SN I and SN II may be the result of explosions in extended stars. More condensed objects may explode and give rise to higher effective temperatures and gamma radiation. Such events would not correspond to those events astronomers term supernovae.

2. Line Emission. The last stable nucleus with $Z = N$ is ^{40}Ca . In stars the thermonuclear synthesis of heavier nuclei tends to form $Z = N$ nuclei which are unstable toward electron capture or positron emission. Radiative decay from excited states of the daughter nucleus gives rise to gamma ray lines. This process is particularly important because a lot of mass - the iron group - is formed this way. Similarly nuclear processing in proton rich, or neutron rich environments can also produce unstable nuclei whose decay may give gamma lines.

a. The "typical zone" approach. To be useful for the experiment-er a theory of such processes should be able to predict gamma line emission. To date most predictions have relied on detailed analysis of thermonuclear processing in "typical zones". One specifies a set of initial conditions (temperature, density and composition) and an expansion time scale, then solves the coupled nonlinear equations (reaction network) for the evolution of the abundances. For a clear review of the gamma line problem from this viewpoint see Clayton (1973).

Table 1 summarizes these results, and gives a few comments on the problems with some of the proposed sources.

The astrophysical aspects of a single zone approximation are clearly oversimplified. Stars are not homogeneous; they have structure. Further, stars of different mass behave in very different ways. The net result of all this complexity may be different in some important details from a set of typical zones which reproduce some of the dominant features.

Table 1. Gamma Line Prospects (After Clayton)

Nucleus	X_{\odot}	Progenitor	$T_{1/2}$	Atoms/SN (Clayton's estimate)	Process and Comments
^{56}Fe	1.3×10^{-3}	^{56}Co	77d	3.6×10^{54}	e-process; Si burning; good prospect
^{56}Co	1.3×10^{-3}	^{56}Ni	6.1d	3.0×10^{54}	e-process; Si burning; good prospect
^{48}Ti	2.3×10^{-6}	^{48}Cr , ^{48}V	16d	6.2×10^{51}	e-process; Si burning; good prospect
^{44}Ca	1.9×10^{-6}	^{44}Ti , ^{44}Sc	48 yr	5.6×10^{51}	Not produced at solar value in any network calculation to date (?!)
^{60}Ni	2.0×10^{-5}	^{60}Fe	3×10^5 yr	4.4×10^{52}	Hypothetical result of neutron capture during explosive carbon burning
		^{60}Co	5.26 yr	(?)	
^{22}Ne	1.2×10^{-4}	^{22}Na	2.6 yr	(?!)	rapid $^{14}\text{N}(\alpha, \gamma)^{18}\text{F}(\alpha, \gamma)^{22}\text{Na}$ in exploding He zone; most ^{22}Ne <u>not</u> formed this way.
^{238}U (example)	1.3×10^{-10}	(r-process)	4.5×10^9 yr	1.3×10^{47}	r-process; relatively little matter is processed this way

b. The Stellar Model Approach. Some preliminary work which attempts to go beyond the one zone approach has just been completed. The evolution of the cores of stars of mass $10 \leq M_{\odot} \leq 95$ have been evolved to dynamical instability. They all develop a nickel-iron core which exceeds the Chandrasekhar mass and contracts toward the neutron star state (or beyond). The remaining matter is loosely bound in a surrounding mantle. It is assumed that this mantle is explosively ejected from the star and that this process corresponds to at least some observed supernovae (see Arnett 1975a). The circumstantial evidence for this point of view is fairly strong. The precise mechanism for the explosion is unclear (see papers by Wilson, et al., Colgate, Arnett, Schramm and Bruenn in the Seventh Texas Symposium, 1975).

1.) The Nucleosynthesis Yield per Star. The evolutionary calculations dealt with helium cores of mass M_{α} . To correlate these with the masses M of main sequence stars (with which the initial mass function, the IMF, deals) the carbon burning cores were compared with carbon burning models of Paczynski (1970) and Lamb, Iben and Howard (in preparation). These models were more complete and consistent than those of the other authors which were examined. The first two columns in Table 2 give the derived transformation for M_{α} and M .

The other columns give the fractions by mass of the star in the form of ${}^4\text{He}(\alpha)$, ${}^{12}\text{C}$, ${}^{16}\text{O}$, ${}^{20}\text{Ne}$, ${}^{24}\text{Mg}$ and "Si + Fe". The latter entry is the matter which has been processed through oxygen burning but not silicon burning. It is expected that this matter, which lies just outside the collapsing core, will undergo silicon burning upon ejection, hence the notation "Si + Fe". These entries for a given mass do not sum to unity; the "missing mass" is the collapsing core. The values shown were taken when γ became less than $4/3$, that is, when dynamical collapse began. Some nuclear rearrangement may yet occur during the explosion, especially among the inner regions (higher Z nuclei).

2.) The Nucleosynthesis yield per Generation. To get the net yield we must weight the results in Table 2 by the (number x mass) of stars having a given mass M . This weighting is discussed in detail in Talbot and Arnett (1973) and references therein. If $X_i(m)$ is the fraction by mass of a star of mass m , that is ejected (see Table 2) then the yields are

$$q_i = \int_1^{\text{max}} \psi(m) X_i(m) dm$$

where we use a Salpeter IMF,

$$\psi(m) = \zeta(\mu - 1) m^{-\mu}$$

Table 2. Yield per Star

Masses		Abundances by Mass					
M_{α}	M	α	C	O	Ne	Mg	"Si + Fe"
3	10	5.08(-1)	1.59(-2)	1.30(-3)	--	--	--
4	12	5.11(-1)	4.80(-2)	4.18(-2)	1.01(-2)	1.64(-2)	2.53(-2)
6	16	4.30(-1)	4.80(-2)	1.29(-1)	7.10(-2)	4.23(-2)	4.42(-2)
8	22	3.87(-1)	7.10(-2)	2.07(-1)	9.61(-2)	3.38(-2)	4.24(-2)
12	28	2.99(-1)	1.02(-1)	3.20(-1)	8.67(-2)	2.59(-2)	3.53(-2)
16	35	2.54(-1)	1.01(-1)	3.85(-1)	8.90(-2)	2.52(-2)	6.12(-2)
24	50	2.09(-1)	9.57(-2)	4.88(-1)	8.22(-2)	2.60(-2)	3.89(-2)
32	75	2.07(-1)	6.40(-2)	5.19(-1)	7.33(-2)	3.03(-2)	3.73(-2)
48	95	1.70(-1)	5.84(-2)	6.32(-1)	7.01(-2)	3.26(-2)	7.09(-3)

for $m > 1 M_{\odot}$, where $\mu = 4/3$ and the lower end of the IMF has been corrected for Weistrop's dwarfs ($\zeta = 0.25$, see Talbot and Arnett 1973). This choice is probably the most straightforward at present. Table 3 gives these yields per generation.

Table 3. Yield per Generation

Z	q_z	$q_z/1-f$	X_{\odot}
α	2.2(-2)	2.5(-2)	2.4(-1)
C	4.4(-3)	5.3(-3)	4.5(-3)
O	1.7(-2)	2.0(-2)	1.1(-2)
Ne	4.2(-3)	4.9(-3)	1.2(-3)
Mg	1.7(-3)	2.0(-3)	5.6(-4)
"Si + Fe"	1.9(-3)	2.2(-3)	2.0(-3)

Galactic evolutionary models must be consistent with the paucity of metal-poor low-mass stars. The identification of Pu^{244} , I^{129} and ^{26}Al as extinct radioactivities demands that nucleosynthesis be an on-going process in our galaxy. Those currently interesting models which can satisfy these constraints predict that the abundance of a species i approaches

$$X_i \rightarrow q_i / (1 - f)$$

where f is the fraction of matter returned to the interstellar medium by stars of $M > 1 M_{\odot}$ ($f \approx 0.15$). This is true for infall models, inhomogeneous models, or metal-enhanced star formation models. It is not true for initial burst models.

These predicted abundances are compared with solar system abundances in Table 3. Except for ^4He (which is thought to be produced cosmologically anyway) the agreement is good. Uncertainties due to further processing in the explosion, to errors in the IMF, and to errors in the input physics will give rise to variations of factors of two in these numbers. Larger variations are possible. Still it is encouraging that the most straightforward prediction of the absolute yield of stellar nucleosynthesis comes out so well.

3.) Implications for Gamma lines. These results have several important implications for gamma-line astronomy.

a) Our ideas of explosive nucleosynthesis, and hence our predictions of gamma line luminosities, can be put on a firmer foundation.

b) By filling in the gaps between "typical zones", the production of important nuclei like Ti^{44} and Sc^{44} can be understood (see Table 1).

c) By pinning down the explosive conditions we can see how much of such nuclei as ^{60}Fe , ^{60}Co and ^{22}Na are produced (see Table 1).

d) We will be able to predict luminosities from particular events rather than be forced to consider a "typical supernova".

e) The more realistic approach to the problem may give rise to some surprises!

This research has been supported in part by the National Science Foundation.

REFERENCES

- Arnett, W. D. 1975a, Ap. J., 195, 127.
- Arnett, W. D. 1975b, Ann. N. Y. Acad. Sci., 262, 47.
- Bruenn, S. W. 1975, Ann. N. Y. Acad. Sci., 262, 80.
- Clayton, D. D. 1973, Explosive Nucleosynthesis, ed. Schramm, D. N. and Arnett, W. D. (Univ. Texas Press: Austin), 264.
- Colgate, S. A. 1975, Ann. N. Y. Acad. Sci., 262, 34.
- Falk, S. W. and Arnett, W. D. 1976, submitted.
- Lasher, G. 1975, Ap. J.,
- Morrison, P. and Sarrori, L. 1969, Ap. J., 158, 541.
- Paczynski, B. 1970, Acta Astr., 20, 47.
- Schramm, D. N. 1975, Ann. N. Y. Acad. Sci., 262, 65.
- Talbot, R. J. Jr. and Arnett, W. D. 1973, Ap. J., 186, 51.
- Wilson, J. R., Couch, R., Cochran, S., Le Blanc, J. and Barkat, Z. 1975, Ann. N. Y. Acad. Sci., 262, 54.

N 76-29129

GALACTIC DISTRIBUTION OF PULSARS

J.H. Seiradakis
Max-Planck-Institut für Radioastronomie, Auf dem Hügel 69,
5300 Bonn 1, W. Germany

ABSTRACT

The density distributions of pulsars in luminosity, period, Z-distance and galactocentric distance have been derived using a uniform sample of pulsars detected during a 408 MHz pulsar survey at Jodrell Bank. There are indications of a "fine scale" structure in the spatial distribution and evidence that there is a general correlation with other galactic populations and the overall spiral structure. The electron layer in our Galaxy is shown to be wider than the pulsar layer and uniform on a large scale. The number of pulsars in the Galaxy has been estimated and used to derive the pulsar birthrate.

1. Introduction

This paper attempts to establish the distribution of pulsars in luminosity, period and position within the Galaxy. Obviously, any such attempt is limited not only by the small number of pulsars (149) so far discovered, but also by the fact that these have been discovered by many observatories, at many different frequencies and using widely different techniques. Table I summarises the observatories and the means by which pulsars have so far been discovered.

Observatory	Pulsars discovered	Technique
Arecibo (Puerto Rico)	45	Periodicity searches, de-dispersion
Bologna (Italy)	5	Paper charts
Cambridge (U.K.)	6	Paper charts
Jodrell Bank (U.K.)	42	Dispersion & periodicity technique
Molonglo (Australia)	32	Paper charts, de-dispersion
NRAO (U.S.A.)	6	Dispersion & periodicity technique
Ootacamund (India)	3	Paper charts ?
Parkes (Australia)	9	Periodicity searches
Puschino (U.S.S.R.)	1	Paper charts

Table I. Observatories and techniques by which pulsars have been discovered.

It is obvious that any attempt to statistically analyse pulsar data should take into account the uncertainties of the search techniques and thus try to concentrate on a smaller sample with well defined selection effects.

Large (1971) studied the distribution of 29 pulsars observed at Molonglo and was able to deduce the period, luminosity and galactic Z-distance distributions from his data. Using this information it became clear that a considerably more sensitive search confined to a limited region close to the galactic plane would reveal a large number of pulsars. In fact such a survey carried out at Jodrell Bank at 408 MHz, has yielded 51 pulsars of which 31 were new discoveries (Davies, Lyne and Seiradakis 1972, 1973). Because of the greater sensitivity of the survey, these pulsars are generally rather more distant than those obtained at Molonglo and show the distribution on a larger galactic scale. The results of a statistical analysis of these pulsars show a number of features which had not been previously detected. The galactocentric distribution has been derived, which combined with the

Z-distribution, gives a good view of the distribution of pulsars in the Galaxy.

2. The Observations

The observing system employed during the survey was similar to that described by Davies, Large and Pickwick (1970). The observations were made at 408 MHz using the 76-m MkIA radiotelescope at Jodrell Bank. The total intensity of radiation from each beam area in the sky was obtained by adding the outputs of two receivers, each sensitive to one hand of circular polarisation. The receivers had excess noise temperature of 110 K and bandwidths of 4 MHz. The overall system gave 1.2 K per Jy for a source at the beamcentre. The half-power beamwidth of the telescope was 0.7° at this frequency.

The detected receiver output was sampled in an on-line Ferranti Argus 400 computer over 16384 intervals of 40 ms (a total of about 11 minutes) and stored for further analysis. While one such observation was in progress, the computer processed previously acquired data, the analysis time for one observation taking about 10 minutes.

The main properties of the search system are summarized in Table II.

Telescope	:	MkIA
Frequency	:	408 MHz
Bandwidth	:	4 MHz
Beamwidth	:	0.75°
Sensitivity	:	1.2 K/Jy
Technique	:	Periodicity Search
Integration Time	:	$10^m 55^s$
Sampling Interval	:	40 msec
Method of Analysis	:	Fast Folding Algorithm
Period Range	:	0.16 to 4 sec
Other Characteristics	:	On-line analysis, gave about 2 pages of output per integration

Table II. The Jodrell Bank Pulsar Search System

Periodic signals having periodicities in the range $0.16 < P < 4$ seconds were detected using a Fast Folding Algorithm (FFA) specially adapted for a pulsar search. The basic algorithm has been described by Staelin (1969). It amounts to cross correlating the data with pulse trains of varying period and phase, having duty cycles between $12\frac{1}{2}\%$ and 25 %. The system was therefore equally sensitive to all pulsars within a large range of dispersion measures which would be expected to lengthen the pulses in the receiver bandwidth. For pulsars having dispersion measures up to about $500 \times P \text{ pc. cm}^{-3}$, where P is the period in seconds, the minimum detectable mean flux near the centre of the beam was about 0.010 Jy for regions away from the galactic plane, where the total system temperature was at a minimum. Figure 1 shows how the sensitivity of the system varied as a function of pulsar period and dispersion measure.

The area of the sky surveyed was systematically observed by setting the telescope to track each position for 11 minutes and then moving it to another. This area was chosen in order to study both the galactic longitude and latitude distribution of pulsars.

Figure 2 indicates the region of the galaxy surveyed. It covers the areas with longitude extending from the galactic centre to $l^{\text{II}} = 240^\circ$ and latitude $|b^{\text{II}}| < 5^\circ$. The latitude coverage for areas with low longitude ($l^{\text{II}} < 115^\circ$) was extended to $|b^{\text{II}}| < 10^\circ$. The survey was made in two sessions. In the first, the whole area was surveyed on a primary grid of points having 1° spacing and centred on the half degrees of both longitude and latitude. Since the beamwidth was only 0.7° , the observed region was considerably undersampled ($\sim 40\%$ coverage). In order to improve the statistics for the interesting regions (at longitudes below 115°), in the second session, observations were made at the interstices of the grid, i.e. at the integral degree points in longitude and latitude. These observations were essentially independent of those at the primary grid points. About 80% of the area where the two sessions overlap was covered. This area is shown shaded in Figure 2.

If during the search procedure there were any indications of the presence of a periodicity in the data, or if the observation was spoiled by interference, a further observation was made at the same position and the new observation was checked for periodicities close to any obtained in the first observation. If no coincidence was found, a negative observation was recorded. About 15% of the observations were repeated in this way. If there was a coincidence, a pulsar was likely to be in the beam and the area was then searched by scanning across the grid point using a simple pulsar observing programme which folded the data using the periodicity determined from the search observations. This generally confirmed the presence of a pulsar and allowed a more

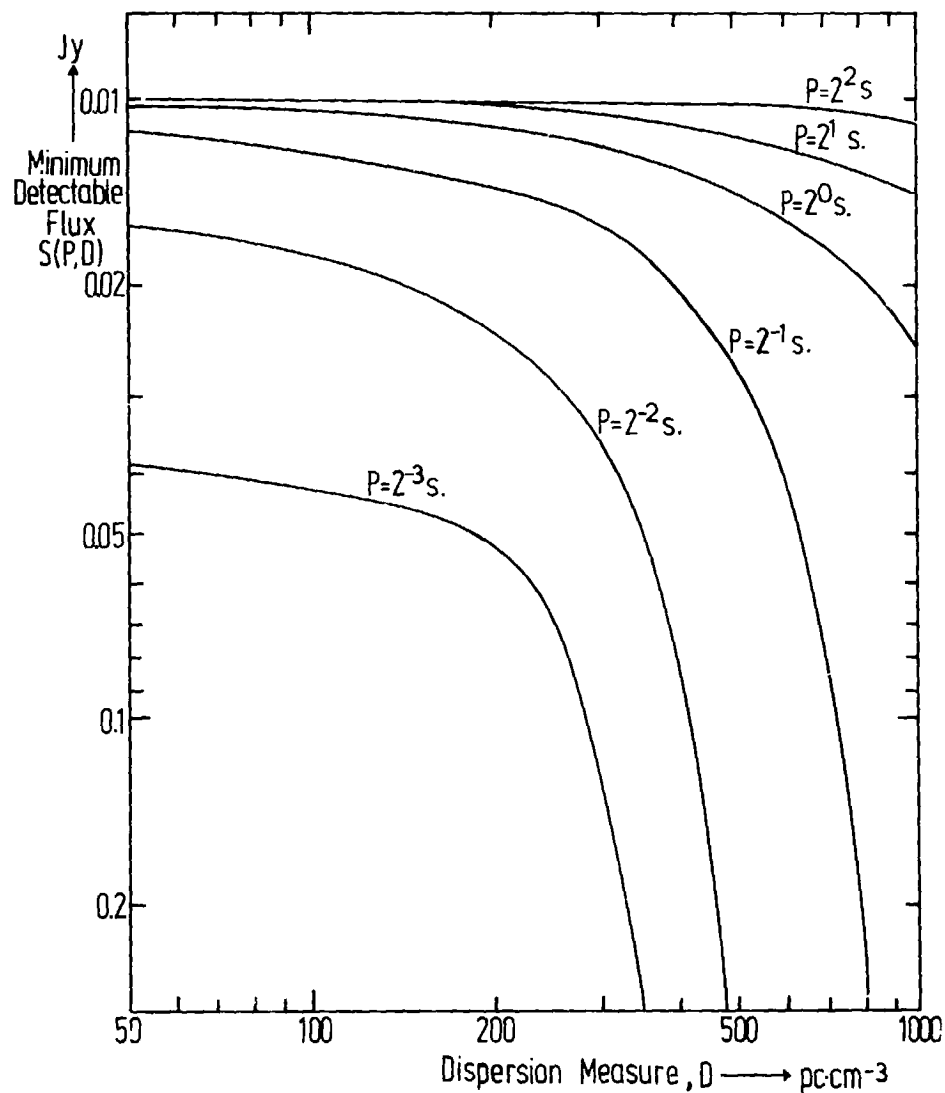


Figure 1. The system sensitivity as a function of pulsar period and dispersion measure.

precise determination of the period and the position of the pulsar.

During the survey 51 pulsars were detected, of which 31 were previously unknown. Only one previously known pulsar which lay within the survey area, PSR 1915+13, was not detected using the procedure described above.

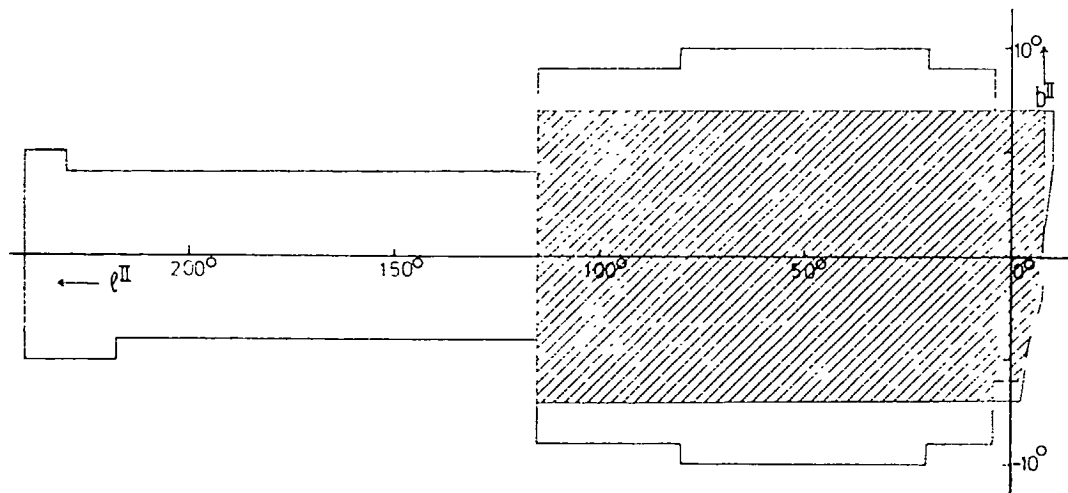


Figure 2. The area searched. The coverage in the shaded area was 80% and in the rest it was 40%.

Table III presents the data of the 51 pulsars which were detected. The first seven columns give the observed parameters. The integrated equivalent width quoted in this table is the ratio between the area beneath the pulse profile and the peak of the profile. The last three columns give derived parameters which will be discussed later.

3. The Analysis

When the survey had finished about 5000 beam areas along the galactic plane had been investigated in which 51 pulsars had been detected. The sky background temperature in each beam could be found from the literature, e.g. Seeger, Westernout, Conway and Hoekama (1965), and the sensitivity of the search system, $S(P,D)$, was also available.

Assuming that the spatial distribution of pulsars in the Galaxy is cylindrically symmetrical, each of the 51 pulsars occupies a point in a 4-dimensional space of luminosity ($L = SD^2$), period (P), galactic Z-distance ($Z = D \sin b^{II}$) and galactocentric distance projected on the plane of the Galaxy ($R = (D^2 \cos^2 b^{II} + D_{GC}^2 - 2DD_{GC} \cos b^{II} \cos l^{II})^{1/2}$). Here the dispersion measure, D , has been used directly as a measure of distance and D_{GC} is the dispersion measure corresponding to the

TABLE III

PSR	ℓ II deg.	b II deg.	P sec.	DM pc. cm ⁻³	S_{408} Jy	M_E deg.	R pc. cm ⁻³	Z pc. cm ⁻³	$L_{408-3,2}$ Jy (pc. cm ⁻³) ²
0105+65	124.6	3.3	1.284	30	0.025	7.8	268	1.73	23
0153+63	130.5	0.2	2.352	60	0.013	5.0	293	0.21	47
0329+54	145.0	-1.2	0.715	27	2.27	4.5	273	-0.56	1655
0355+54	148.2	0.8	0.156	57	0.056	8.1	300	0.90	182
0540+23	184.4	-3.3	0.246	72	0.030	13.7	322	-4.14	156
0611+22	188.8	2.4	0.335	97	0.048	11.0	346	4.06	452
1700-32	351.7	5.4	1.212	103	0.092	12.5	149	9.69	976
1717-29	356.5	4.3	0.620	45	0.030	15.7	205	3.37	61
1718-32	354.5	2.5	0.477	120	0.095	12.1	131	5.23	1368
1730-22	4.0	5.8	0.872	45	0.031	16.0	205	4.55	63
1749-28	1.5	-1.0	0.563	51	1.07	4.5	199	-0.89	2783
1813-26	5.2	-4.8	0.593	90	0.026	26.6	161	-7.53	211
1818-04	25.5	4.7	0.598	85	0.15	7.5	178	6.96	1084
1819-22	9.4	-4.3	1.874	140	0.022	10.0	115	-10.50	431
1822-09	21.5	1.4	0.769	21	0.025	6.5	231	0.48	11
1826-17	14.5	-3.3	0.307	210	0.085	20.8	71	-12.09	3748
1831-04	27.0	1.8	0.290	68	0.081	54.0	192	2.14	375
1831-03	27.7	2.3	0.687	230	0.067	8.5	117	9.23	3544
1845-04	28.9	-1.0	0.598	142	0.055	16.0	143	-2.48	1109
1845-01	31.3	0.1	0.659	163	0.057	20.6	139	0.57	1514
1846-06	26.7	-2.4	1.451	152	0.031	4.9	133	-6.37	716
1859+03	37.2	-0.6	0.655	402	0.074	11.0	253	-4.21	11959
1900-06	28.5	-5.6	0.432	180	0.016	13.8	126	-17.56	518
1900+01	35.8	-1.9	0.729	228	0.103	7.5	148	-7.56	5354
1906+00	35.1	-3.9	1.017	111	0.026	2.7	171	-7.55	320
1907+02	37.6	-2.7	0.495	190	0.015	13.9	153	-8.95	542
1907+10	44.8	1.0	0.284	144	0.061	16.0	179	2.51	1265
1910+?J	54.0	5.0	2.233	84	0.010	2.9	212	7.32	71

TABLE III (contd)

PSR	ℓ II deg.	b II deg.	P sec.	DM pc. cm ⁻³	S ₄₀₈ Jy	W _E deg.	R pc. cm ⁻³	Z pc. cm ⁻³	Jy (pc. cm ⁻³) ² L ₄₀₈
1911-04	31.3	-7.1	0.826	89	0.074	3.2	180	-11.00	586
1917+00	36.5	-6.2	1.272	85	0.034	5.2	189	-9.03	246
1918+19	53.9	2.7	0.821	135	0.038	28.6	202	6.36	693
1919+21	55.8	3.5	1.337	12	0.056	6.8	244	0.73	8
1920+21	55.3	3.0	1.078	220	0.048	6.9	220	11.51	2323
1929+10	47.4	-3.9	0.227	3	0.61	9.1	248	-0.20	6
1933+16	52.4	-2.1	0.359	158	0.36	6.1	198	-5.79	8987
1944+17	55.3	-3.5	0.441	16	0.033	19.0	241	-0.98	8
1946+35	70.7	5.1	0.717	129	0.12	5.7	240	11.24	1997
1952+29	65.9	0.8	0.427	8	0.020	17.0	247	0.10	1
2002+31	69.0	0.0	2.111	225	0.014	3.6	270	0.18	709
2016+28	68.1	-4.0	0.558	14	0.29	9.6	245	0.98	57
2020+28	68.9	-4.7	0.343	25	0.25	7.0	242	-2.05	156
2021+51	87.9	8.4	0.529	23	0.31	12.0	250	3.36	164
2106+44	86.9	-2.0	0.415	129	0.038	20.0	275	4.50	632
2111+46	89.0	-1.3	1.015	142	0.19	10.0	285	-2.97	3831
2148+63	104.3	7.4	0.380	125	0.025	20.5	305	16.10	391
2217+47	98.4	-7.6	0.538	44	0.063	6.0	260	-5.82	122
2223+65	108.6	6.9	0.683	100	0.038	18.0	298	12.18	380
2255+58	108.8	-0.5	0.368	148	0.042	12.2	329	-1.81	920
2305+55	108.6	-4.2	0.475	45	0.023	18.3	268	-3.30	47
2319+60	112.1	-0.6	2.256	96	0.07	10.4	299	-1.01	645
2324+60	112.9	0.0	0.234	120	0.041	21.9	317	0.06	590

distance of the centre of the Galaxy. This use of the dispersion measure implies a uniform electron density throughout the region of interest. If the electron density is averaged over long path lengths, this assumption has been shown to be satisfied in the local neighbourhood of the Sun (Prentice and ter Haar 1969), and there are strong indications that over greater distances, and throughout the volume containing the observed pulsars, the same assumption is true (Guélin 1974, Lyne 1974).

The aim of this work is to obtain from the observed distribution of pulsars in L, P, Z and R, which contain a number of selection effects, an estimate of their true density distribution.

The number of pulsars observed, having luminosity L, period P, lying at a distance Z away from the galactic plane and at a distance R from the galactic centre can be written

$$N(L,P,Z,R) dL dP dZ dR = V(L,P,Z,R) \rho(L,P,Z,R) dL dP dZ dR \quad (1)$$

where $V(L,P,Z,R)$ is the volume of the Galaxy explored and $\rho(L,P,Z,R)$ is the true pulsar density and dL , dP , dZ and dR are intervals in L, P, Z and R. Thus, in principle, it is possible to deduce an estimate of $\rho(L,P,Z,R)$ from the observed distribution of pulsars, $N(L,P,Z,R)$ and a knowledge of the volume searched.

Unfortunately, $N(L,P,Z,R)$ is not a continuous function and is everywhere zero except for δ functions corresponding to the positions of the pulsars, and it is clear that equation (1) cannot be solved without some simplifying assumptions. In this we follow Large (1971) and assume that the variables are independent in density, and we write:

$$\rho(L,P,Z,R) = \rho(L) \rho(P) \rho(Z) \rho(R) \quad (2)$$

This separation of the variables would not, of course, be justified if there were any correlation between them. It is shown, however later, that no significant correlation exists, and hence the variables can be treated as completely separable.

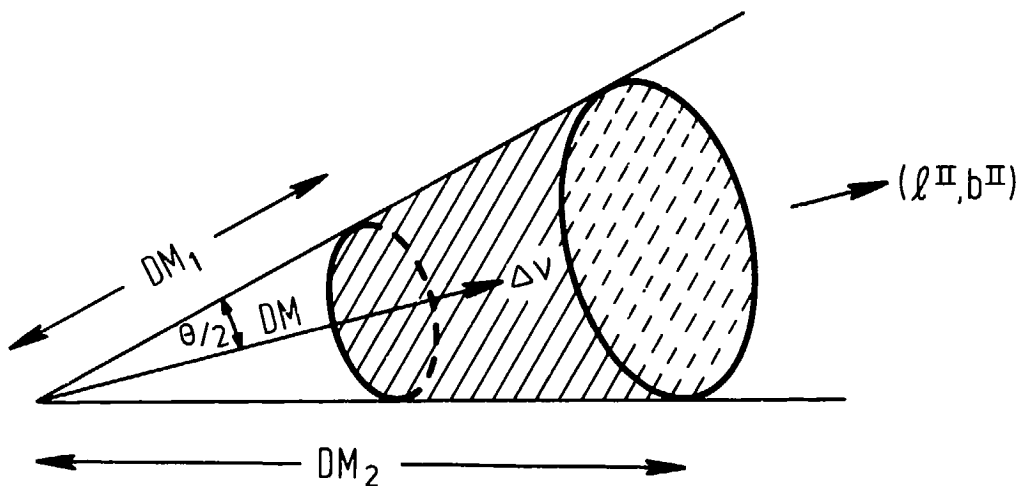
Combining equations (1) and (2) one gets:

$$\rho(L) = \frac{\iiint N(L,P,Z,R) dL dP dZ dR}{\iiint \rho(P) \rho(Z) \rho(R) V(L,P,Z,R) dP dZ dR} \quad (3)$$

and three similar equations for $\rho(P)$, $\rho(Z)$ and $\rho(R)$. If $V(L,P,Z,R)$ is known, the four equations can be solved iteratively using the observed distribution of pulsars $N(L,P,Z,R)$.

The calculations for the volume, $V(L,P,Z,R)$ are illustrated in Figure 3.

THE CONE FORMED BY THE BEAM OF THE TELESCOPE



$$\Delta V = \frac{\pi}{12} \theta^2 (DM_2^3 - DM_1^3)$$

$$L_{\min} = \left(\frac{T_{BG} + 120}{30 + 120} \right) \cdot (DM)^2 \cdot 0.01 \cdot \frac{B(p)}{1 - A(p) \cdot DM}$$

Figure 3. The explored volume calculations.

Each of the 5000 beams that were observed explored a region of the (L,P,Z,R) space. The volume of the Galaxy searched for each element in this space was obtained by considering the telescope beam, which occupies a conical volume of width θ , to consist of a number of segments at distance D (dispersion measure) of length δD and diameter θD , so that for each segment the volume searched is:

$$\delta V(L,P,Z,R) = \frac{\pi}{4} \theta^2 D^2 \delta D .$$

Knowing the sky background temperature and the sensitivity of our system, it was possible to calculate the minimum luminosity L_{\min} , that a pulsar with period P and dispersion measure D would need to be detectable.

$$L_{\min} = D^2 \frac{0.01}{S(P,D)} \frac{T_s}{140 \text{ K}}$$

T_s consists of the sum of the receiver excess noise temperature (110 K) and the sky background temperature which varied over the sky between about 30 K and several hundred K.

Thus, for this survey, P and L were incremented by small steps in the range $2^{-3} \leq P \leq 2^2$ s and $10^0 \leq L \leq 10^5$ Jy (pc. cm⁻³)², and we set $\Delta V = 0$ for $L < L_{\min}$ or $\Delta V = \int_{DM_1}^{DM_2} \delta V = \frac{\pi}{12} \theta^2 (DM_2^3 - DM_1^3)$ for $L \geq L_{\min}$ (see Figure 3).

By carrying out this procedure on all conical segments which form the telescope beam for D incremented by small steps in the range $0 < D < 1000$ pc. cm⁻³ and for all the beam positions observed during the survey, it was possible to estimate the volume of the Galaxy searched for each point in the (L,P,Z,R) space.

4. The Results

The four distributions shown in Figures 4, 5, 6 and 7 are the density distributions of pulsars in luminosity, period, Z-distance and galactocentric distance. The units employed are arbitrary and are as follows:

$\rho(R)$ and $\rho(Z)$ are chosen to be unity in the solar neighbourhood
 $\rho(P)$ is unity for periods in the range $2^{-3/4} < P < 2^{-1/4}$, i.e. at $P = P_{\max}$
 and $\rho(L)$ is the number of pulsars per cubic dispersion measure unit, per semidecade in luminosity, having period $P = P_{\max}$, in the solar neighbourhood.

This choice of units is convenient for estimating the true pulsar density in any volume of the 4-dimensional space (L,P,Z,R).

The error bars in the above mentioned figures have been calculated assuming that the number of pulsars observed in each interval is small-samples-Poisson distributed. They give the 20% confidence limits of the presented distributions.

4.1 The Luminosity Distribution

Figure 4 shows that the number of pulsars per unit volume in the Galaxy decreases rapidly with luminosity. A best fit to the data gives a power law

$$\rho(L) = \rho(L_0) L^{-b}$$

with $b = 2 \pm 0.2$. This is in excellent agreement with Large's (1971)

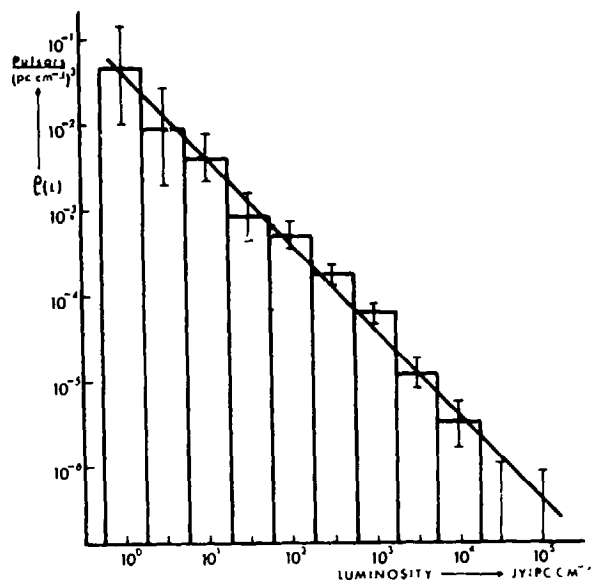


Figure 4. The luminosity distribution of pulsars.

results and the most recent analysis of the Arecibo survey data (Roberts 1976). The errors of the less luminous classes are quite large and the possibility of a turnover at the faint pulsar end can not be excluded. In fact, the high sensitivity pulsar search in Arecibo (Hulse and Taylor 1974, 1975), in which a boundary to the spatial distribution of pulsars was detected, didn't discover pulsars that were intrinsically less luminous than the ones in our sample. Their pulsars were fainter only because they were more distant. The fact that they didn't discover many more intrinsically faint nearby pulsars indicates that a turnover in the luminosity distribution should be placed at about 1 Jy (pc. cm⁻³)². This statement is corroborated by the negative results of a low frequency (151 MHz) pulsar search at Jodrell Bank in which a large portion of the northern hemisphere was covered using a fairly sensitive system.

4.2 The Period Distribution

The median of the period distribution of pulsars is at 0.55 ± 0.09 seconds with a standard deviation of about 1.0 in $\log_2 P$. The distribution shows a marked decrease in pulsar density for either short or long period pulsars. This is not due to any instrumental effects but is a genuine property of pulsars. The decrease of the density of pulsars at periods of around 1 second is independent of the period interval chosen and has been confirmed by the Arecibo search (J.H. Taylor, private communication). This is a result that needs further investigation.

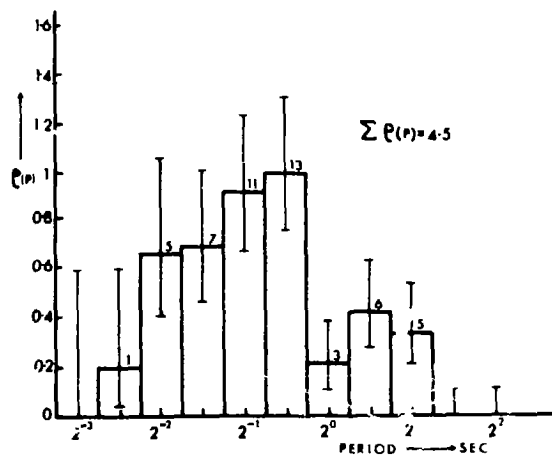


Figure 5. The period distribution of pulsars.

4.3 The Z-distance distribution

The pulsar Z-distance distribution can be adequately described by a Gaussian function:

$$\rho(Z) = \rho(Z_0) e^{-\frac{(Z - 0.5)}{134.2}}$$

where Z is in dispersion measure units and $\rho(Z_0)$ is the pulsar density on the galactic plane. Figure 6 shows this distribution. It was found convenient to describe our spatial distributions in dispersion measure units (pc. cm^{-3}). These are the units used in the horizontal scale. The scale height is $\sigma = 8.2 \text{ pc. cm}^{-3}$. Assuming a uniform electron density of $0.025 \text{ electrons/cm}^3$, extending beyond the pulsar layer, the full width of the pulsar Z-distance distribution to half

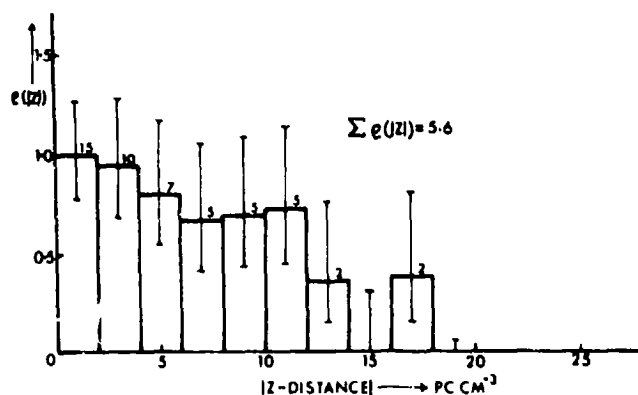


Figure 6. The Z-distance distribution of pulsars.

power points can be calculated to be 650 pc. The pulsar layer seems to be considerably wider than that of any other class of young population objects. In particular, it is much wider than the supernova remnants layer (Jlovaisky and Lequeux 1972, Kodaira 1974), but one should carry in mind that this may simply reflect the effect of pulsar high velocities as reported by several authors.

Recent observations (Falgarone and Lequeux 1973) suggest that the full width of the electron layer is of the order of 1 kpc or greater. This is much wider than the pulsar layer. In fact, a careful inspection of Table III shows that no pulsar at such high Z-distance was detected (assuming an electron density of 0.025 electrons/cm³, 1 kpc corresponds to 25 pc. cm⁻³). Some further comments on the electron layer are made later.

Our results, although heavily affected by statistical ambiguities, give evidence that the median of the Z-distribution occurs at -0.5 pc. cm⁻³ (with a standard error of 1.5 pc. cm⁻³). Assuming a mean electron density of 0.025 electrons/cm³, this corresponds to -20 pc from the plane. In other words, the suggestion that the Sun lies 20 pc north of the galactic plane (e.g. Elvis 1965) has also been revealed by our pulsar observations.

4.4 The galactocentric distribution

Figure 7 illustrates our best estimate for pulsar galactocentric distribution. The horizontal scale is, as explained in the previous section, in dispersion measure units (to convert into pc, divide by the electron density, i.e. 0.025 electrons/cm³).

The distribution of pulsars in galactocentric distance shows a marked decrease away from the galactic centre. The median of the distribution is at 161 ± 13 pc. cm⁻³ (6.4 ± 0.5 kpc). No pulsar with $R < 70$ pc. cm⁻³ (~ 3 kpc) was detected but the errors of the intervals in the inner region are so large that the possibility that the pulsar density may still be quite high near the galactic centre can not be excluded. On the other side, towards the anticentre there is a genuine decrease of the number of pulsars. The density distribution becomes practically zero after the Perseus arm (~ 13 kpc), in excellent agreement with the spatial boundary found by the Arecibo search.

Among the pulsars which were detected, PSR 1826-17 was the closest to the galactic centre (~ 3 kpc) and PSR 0611+22 - the IC 443 pulsar - was the furthest away (~ 14 kpc).

In the distribution shown in Figure 7 there are indications of spiral structure. The tangential points of the Norma-Scutum, the Sagittarius and the Perseus arms are shown and it is obvious that the

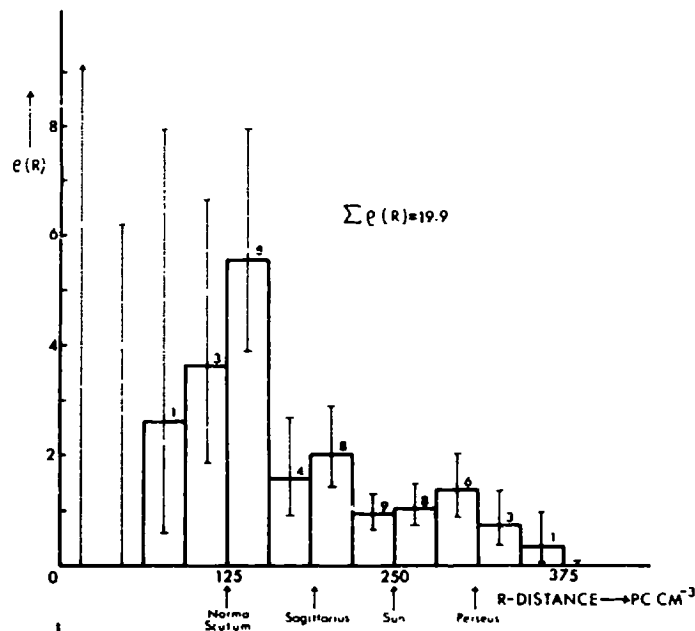


Figure 7. The galactocentric distribution of pulsars.

pulsar density follows this pattern quite closely. The large statistical errors of the present distribution do not allow any conclusive statement to be made.

In order to investigate the significance of the spiral structure found, we scaled our Galaxy differently and, using the same procedure, tried to fit the observations to the new model. If the spiral structure originally found was due to periodicities created by the analysis procedure, they should show up again. Figure 8 shows the results of such an exercise. The galactic centre distance has been taken to be 400 pc. cm^{-3} (16 kpc). No other change to our data or analysis procedure was made. It is obvious that any trace of spiral structure has disappeared. The other distributions (luminosity, period and Z-distance) did not change by more than 0.1%. This was expected unless there was some significant degree of correlation among them.

The existence of a definite cut-off in pulsar density and the indications of (a) the off-set of the Sun's position by 20 pc and (b) the spiral structure revealed, suggests that pulsars may prove to be a very powerful tool in studying the spiral structure of our Galaxy. Their built-in measure of distance (the dispersion measure), the independent measure of distance that can be obtained by hydrogen absorption measurements and the fact that they can be observed at much greater distances than optical observations allow, make them unique in

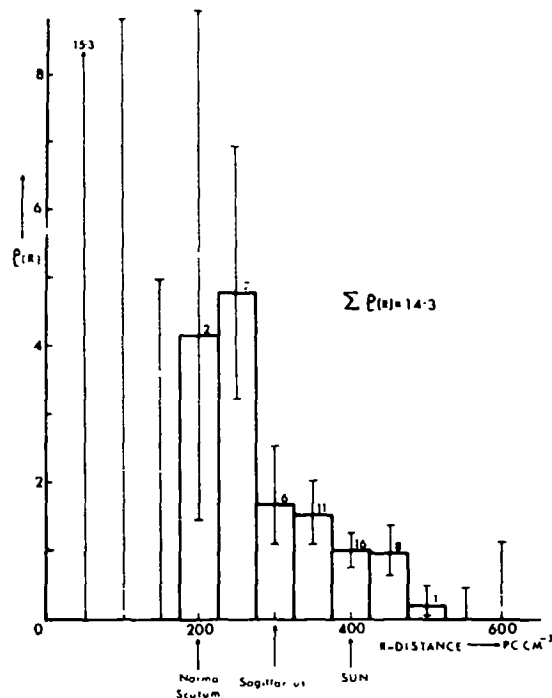


Figure 8. The hypothetical galactocentric distribution of pulsars assuming that the distance to the galactic centre is 16 kpc.

this field. A more sensitive survey than the one presented here should reveal many more pulsars, as indicated by their luminosity distribution (Figure 4) and confirmed by the Arecibo search.

5. Discussion

Throughout the analysis, the dispersion measure of pulsars has been taken as a measure of distance. This assumption is justified only if the electron layer is (a) wider than the pulsar layer and (b) uniform on a scale comparable to the interval scale used during the analysis.

Many authors have contributed to the understanding of these problems. Falgarone and Lequeux (1973) give a comprehensive review of the relevant arguments. They show that the width of the ionised layer is ~ 1000 pc, i.e. wider than the pulsar layer. This result is further corroborated by the pulsar Z-distance distribution shown in Figure 6. This shows a monotonic decrease in density with Z-distance. If the ionised layer was substantially thinner than the pulsar layer, this would have been indicated by a peak at non-zero Z-distance. (For more details see Gould 1971). Such an effect has not been found.

Inhomogeneities in the distribution of thermal electrons are expected to occur in the interstellar medium. Not only is a correlation with the spiral structure expected, but also local variations of the electron density due to the different components of the interstellar gas will inevitably upset a uniform distribution. However, Gomez-Gonzales and Guélin (1974), Lyne (1974) and other authors have shown that the electron density near the galactic plane may be regarded as uniform when averaged over a pathlength of a few kiloparsecs. The mean electron density suggested is ~ 0.025 electrons/cm³. Figure 9 illustrates the above arguments. It shows the dispersion

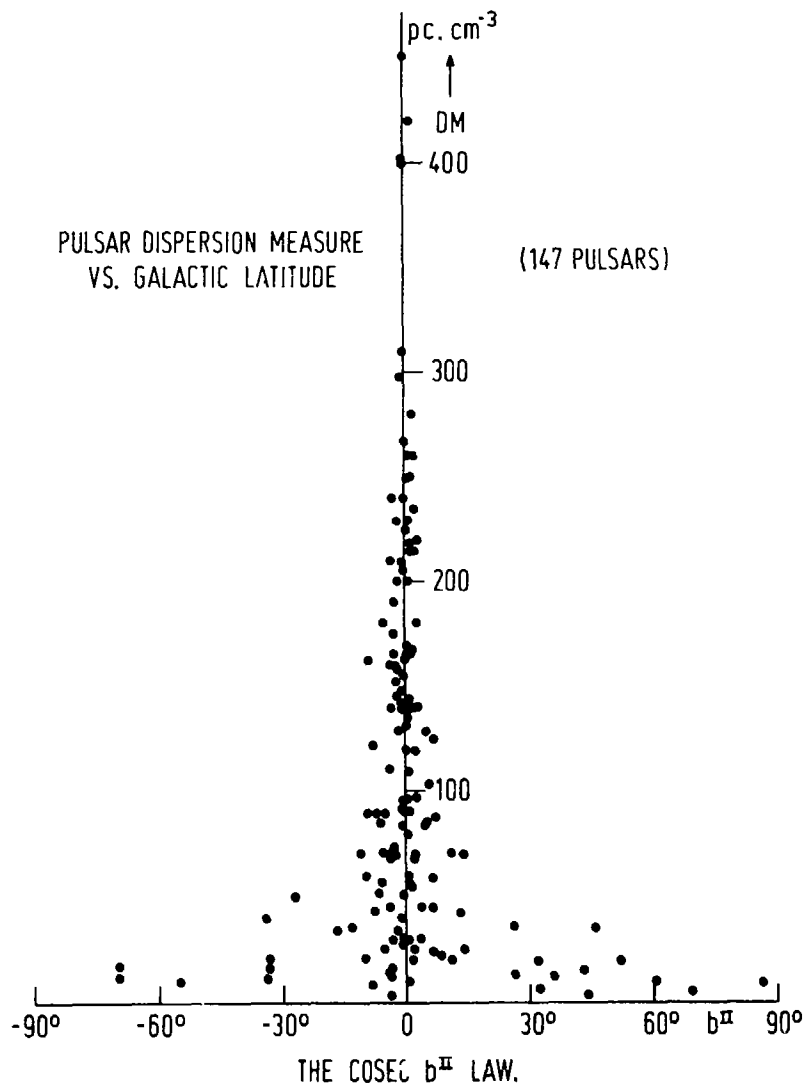


Figure 9. Pulsar dispersion measures as a function of galactic latitude.

measure of 147 pulsars plotted as a function of galactic latitude. It indicates that if one uses the dispersion measure as a measure of distance, pulsars do follow the cosec b^{II} law predicted by a uniform disk-shaped distribution of sources, having distances greater than a few hundred parsecs.

A justification of the assumption of the independence of the examined distributions was mentioned in § 4.4. In order to further investigate this an other method was devised.

From the previously derived distribution of pulsars and a knowledge of our system sensitivity it was possible to calculate the number of pulsars expected to be observed in each range of the 4-dimensional space (L,P,Z,R). Assuming that there were no digitization errors and no correlation between the examined distributions, this number should be very close to the observed number of pulsars. Any correlation between the distributions would upset this result. Table IV presents χ^2 -tests for the observed and expected two dimensional

Table IV

Distribution	Classes (n)	χ^2	P (%)
R - Z	4	0.379	93.5
R - P	4	0.564	82.5
R - L	3	0.222	81.5
Z - P	4	0.305	95.8
Z - L	3	1.493	71.9
P - L	4	1.053	78.9

distributions. The first two columns give the distribution to be tested and the number of classes into which it was divided. The last two show the statistic (χ^2) and the result (P) of the test. It is obvious that no discrepancy between expected and observed numbers was found, which suggests that the assumption of no correlation between the examined distributions is correct.

Recombination line observations, e.g. Matthews, Pedlar and Davies (1972), indicate the existence of a dense ionised bulk of material in the inner region of the Galaxy ($R < 5$ kpc). The effect of such a region on pulsar observations would be of great importance. Dispersion and scintillation broadening would make pulsars practically undetectable in such a region. The effect would be a kind of "brick wall" where the observed pulsars show first a sudden increase of their dispersion measure and then a sharp cut off of their number density.

Our observations indeed show such a sharp cut off at about

130 pc. cm⁻³ (~ 5 kpc, Figure 7). However, we claim that this is due to limitations in our sensitivity and it is quite independent of any "brick wall" effect. Only if the observed number of pulsars in a certain region was significantly different from the expected number (calculated by the method mentioned above) could it be said that an effect which had not been taken into account had been discovered. In this survey, no such region was found. The "brick wall" effect was not detected.

However, what was detected is an enhancement of pulsar density in the region 5 to 6 kpc (Figure 7). This is in excellent agreement with the distribution of many important constituents of our Galaxy, such as molecular clouds, HII regions, supernova remnants, cosmic rays and γ -rays (see Stecker 1976). In particular, HII regions (a good indicator of the distribution of massive hot stars) appear to correlate very well with the distribution of pulsars. As explained earlier, pulsars which happen to lie in dense ionised regions would be practically undetectable. However, high pulsar velocities would result in the bulk of pulsars escaping from their birthplaces. They would then surround their parent population, and thus still be detectable. All of the above mentioned constituents are associated with the formation and destruction of young OB stars in our Galaxy. As explained by Stecker (1976) the correlation of these components can be physically explained.

Of course, the mean Z-distance of pulsars is much wider than the mean Z-distance of any of these populations. However, one should bear in mind that this only reflects high pulsar velocities. On the other hand, these high velocities, in conjunction with the indications of spiral structure found (Figure 7), support other evidence that pulsar true ages do not exceed $\sim 5 \times 10^6$ years (Lyne, Ritchings and Smith 1975). A mean age of $\sim 10^7$ years and a typical velocity of ~ 200 km/sec would have resulted in the disappearance of any spiral structure.

6. Conclusions

The distributions illustrated in Figures 4 to 7 are, to our best estimate, independent of selection effects due to either pulsar position or system sensitivity. They describe the density distribution of pulsars in luminosity, period, Z-distance and galactocentric distance.

Using these distributions and equation (1), it is possible to calculate the total number of pulsars in the Galaxy. It is reasonable to use a lower limit of 1 Jy (pc. cm⁻³)² for the luminosity distribution, i.e. the luminosity of the least luminous pulsar observed. However, it must be pointed out that the error bars of the last two luminosity intervals in Figure 4 indicate that the uncertainties are about one order of magnitude. These uncertainties become the largest

source of error in the estimation of the total number of pulsars. The unknown distribution of pulsars in the inner region of the Galaxy (Figure 7) does not give rise to significant errors since the corresponding volume of space decreases rapidly at this region. The calculated number of pulsars does not vary by more than 20% if one assumes a) a uniform distribution with space density 5.6 units (see Figure 7) and b) a distribution extending to the maximum value indicated by the error bars in the range $0 < R < 70 \text{ pc. cm}^{-3}$.

The estimated number of pulsars in the Galaxy with luminosity exceeding $1 \text{ Jy (pc. cm}^{-3})^2$ and period in the range $2^{-3} < P < 2^2$ seconds, is $(6 \pm 5) \times 10^4$. The errors are mainly due to uncertainties in the luminosity distribution. No beaming factor has been taken into account.

Assuming a two beam model, the probability of a pulsar being observable is given by $f = \psi \sin \theta$, where θ is the angle between the rotation and the magnetic axes and ψ is the integrated pulse width. If the rotation and magnetic axes are randomly distributed, then $\langle \sin \theta \rangle = \pi/4$ and taking a value of $\psi = 20^0$, it is found that $f = 0.25$. Taking into account this beaming factor, we find that the number of pulsars in the Galaxy is

$$N = 2 \times 10^5$$

in good agreement with Large's (1971) estimate of 5×10^5 pulsars.

Taking a mean age of 5×10^6 years for pulsars (Lyne, Ritching and Smith 1975, Manchester, Taylor and Van 1974), we find a pulsar birth-rate of

1 pulsar every 25 years.

This is in good agreement with previous publications and the rate of occurrence of supernovae, e.g. Tammann (1973). However, supernovae and pulsar birthrates are subject to many assumptions (distances, lifetime, beaming factor etc.) and hence they are not very reliable.

It is my pleasure to thank Professor J.G. Davies and Dr. A.G. Lyne for their continuous help during this work.

References

- Davies, J.G., Large, M.I., Pickwick, A.C. 1970, *Nature*, 227, 1123.
Davies, J.G., Lyne, A.G., Seiradakis, J.H. 1972, *Nature*, 240, 229.
Davies, J.G., Lyne, A.G., Seiradakis, J.H. 1973, *Nature Phys. Sci.*, 244, 84.
Elvis, T. 1965, "Stars and Stellar Systems" (ed. Blaauw, A. and Schmidt, M.), University of Chicago Press, 5, Chapter 3.
Falgarone, E., Lequeux, J. 1973, *Astron. Astrophys.*, 25, 253.
Gomez-Gonzales, J., Guélin, M. 1974, *Astron. Astrophys.*, 32, 441.
Gould, R.J. 1971, *Astrophys. and Space Sci.*, 10, 265.
Guélin, M. 1974, *IAU Symp. No. 60*, 51.
Hulse, R.A., Taylor, J.H. 1974, *Astrophys. J. (Letters)*, 191, L59.
Hulse, R.A., Taylor, J.H. 1975, *Astrophys. J. (Letters)*, 201, L55.
Ilovaisky, S.A., Lequeux, J. 1972, *Astron. Astrophys.*, 18, 169.
Kodaira, K. 1974, *Publ. astr. Soc. Japan*, 26, 255.
Large, M.I. 1971, *IAU Symp. No. 46*, 165.
Lyne, A.G. 1974, *IAU Symp. No. 60*, 87.
Lyne, A.G., Ritchings, R.T., Smith, F.G. 1975, *M.N.R.A.S.*, 171, 579.
Matthews, H.E., Pedlar, A., Davies, R.D. 1973, *M.N.R.A.S.*, 165, 149.
Prentice, A.J., ter Haar, D. 1969, *M.N.R.A.S.*, 146, 423.
Roberts, D.H. 1976, *Astrophys. J. (Letters)*, 205, L29.
Seeger, C.L., Westerhout, G., Conway, R.G., Hoekama, T. 1965, *Bull. astr. Inst. Netherlands*, 18, 11.
Stecker, F.W. 1976, *Nature* 260, 412.
Tammann, G.A. 1973, "Supernovae and Supernovae Remnants", *Astrophys. and Space Sci. Library*, Vol. 45.

N76-29130

COSMIC RAY PROPAGATION AND CONTAINMENT

E. N. Parker, Laboratory for Astrophysics and Space
Research, 933 E. 56th Street, Chicago, Illinois 60637

ABSTRACT

The cosmic rays are an active gaseous component of the disk of the galaxy, and their propagation and containment is a part of the general dynamics of the disk. The sources of cosmic rays are a matter of speculation. The disk is inflated by the cosmic ray gas pressure P comparable to the magnetic pressure $B^2/8\pi$, but the rate of inflation is unknown. The time spent by the individual cosmic ray particles in the disk is inversely proportional to the cosmic ray production rate and may be anything from 10^5 years to more than 10^7 years. It is evident from the decay of Be^{10} that the cosmic rays circulate through a volume of space perhaps ten times the thickness of the gaseous disk, suggesting a magnetic halo extending out ~ 1 kpc from either face of the disk. The cosmic rays may be responsible for the halo by inflating the magnetic fields of the disk. Extension of the fields to 1 kpc would imply a high production rate and short life ($< 10^7$ years) of cosmic rays in the dense gaseous disk of the galaxy. But the dynamical questions, including the role of the tunnels of superhot gas produced by supernovae, cannot yet be answered in any unique way. The purpose of this review is to outline the problem as it faces us at the present time.

INTRODUCTION

There has accumulated in the last three decades a body of detailed information on the properties of the galactic cosmic rays as they show themselves at the present time in the solar system. From this information we now believe, with some confidence, that cosmic rays are a permanent feature of the galactic environment, with an intensity that has not varied much over the last 10^4 - 10^9 years. Information is beginning to be available on the relative abundances and the energy spectra of the many isotopes that make up the cosmic rays. The abundances probably vary with time, reflecting the activity of nearby sources. Some cosmic ray isotopes are collision products, some are synthesized in the neutron rich environment before acceleration, and some are just the "natural" isotopes found in all matter. The measurements of relative abundances, and the variation of those abundances with energy, are our strongest tool for probing the origin of cosmic rays.

At the same time there has become available considerable, but by no means complete, information on the gas and fields through which the cosmic rays move in the gaseous disk of the galaxy. The galactic nonthermal radio emission has been mapped, presumably giving a picture of the distribution of cosmic ray electrons across the celestial sphere, and, finally γ -ray observations are available, mapping the collisions of the cosmic ray protons with the interstellar gas.

These observational facts and inferences have been explored with a multitude of theoretical models, so that today we have an idea of the possibilities for the origin and behavior of cosmic rays in the galaxy. It is the task of the present review to sift from our heap of knowledge and interpretations those ideas and principles that seem to be basic for understanding the role played by cosmic rays in the galaxy.

Now the complex observational and theoretical pictures of cosmic rays in the galaxy are far from complete, and so are ambiguous. Hence it is possible to form a summary opinion only by looking at the overall picture with a not unjaundiced eye. This review is, then, to be understood as a view of cosmic rays through tinted eyeglasses.

Whenever confronted with alternatives, I choose what seems to be the simpler. The choice that I make will, therefore, not always be the most interesting choice. And I stand ready to amend an opinion whenever observational or theoretical facts suggest a simpler.

I should emphasize that it is possible to put together a "plausible" picture of cosmic rays only because so many workers have had the patience, determination, and ingenuity to explore so many alternatives. It is not possible in the available time to give proper credit to all those whose efforts have made an opinion possible.

Consider, then, the circumstances in which we find cosmic rays in the galaxy. They appear to be a permanent fixture, at about their present level in the solar neighborhood. γ -ray observations, on which others will speak at length, suggest somewhat greater and smaller cosmic ray intensities elsewhere in the gaseous disk of the galaxy. The cosmic rays are trapped in the general galactic magnetic field and the field is embedded in the gaseous disk. Without the weight of the interstellar gas to confine the field, the field and the cosmic rays would expand out of the galaxy and disappear. The basic point of departure for understanding cosmic rays in the galaxy is their role in the local dynamics of the galactic disk. The cosmic rays, the magnetic field, and the interstellar gas shape each other, so that the propagation and containment of cosmic rays in the galaxy are inseparable from the dynamical theory of the disk.

Considering the individual cosmic ray proton at the median energy of 10 Gev we note that its cyclotron radius in the mean azimuthal field of $3-4 \times 10^{-6}$ gauss (Hiltner, 1956; Manchester, 1972) is 10^{13} cm. This is so small compared to the characteristic thickness 10^{21} cm (300 pc) of the gaseous disk and field that the particle may be considered tied to the local lines of force. Scattering across the field by any conceivable field irregularities (say, one scattering through a large angle every cyclotron period of 2×10^3 sec) is negligible over the $10^6 - 10^8$ year life of the particle in the galaxy, as are the gradient and curvature drifts of 10^3 cm/sec in the observed large fluctuations in the field, with scales of 30-150 pc (Jokipii and Lerche, 1969; Jokipii, Lerche, and Schommer, 1969). So a cosmic ray particle is a permanent companion of the flux tube in which it is born, condemned to roam this one dimensional space until it dies by collisions or until the tube is convected out of the galaxy.

So far as motion along the line of force is concerned, note that cosmic rays of 1-10 Gev are scattered principally by field variations with scales of $10^{12} - 10^{13}$ cm. These scales lie in the large and unknown interval between the strong fluctuations at 10^{11} cm, determined from pulsar scintillation studies, and the strong fluctuations at scales of 3×10^{18} cm and larger, observed directly with instruments on telescopes. Whether there are fluctuations in the range of $10^{12} - 10^{13}$ cm determines whether cosmic rays are significantly scattered back and forth along the magnetic lines of force, or whether they stream unhindered along the lines. Scattering is not necessary to understand the observed behavior of cosmic rays, so far as we are able to tell. But it is a necessary condition for Fermi acceleration in interstellar space, so the question must be settled if we are to decide the role of interstellar Fermi acceleration. The reader is referred to a recent paper by Lee and Jokipii (1976) where the problem of cosmic ray propagation and interstellar density and field fluctuations is reviewed.

But we should not think of the propagation and containment of cosmic rays in terms of the individual particle. The individual particles do not interact directly with each other but, nonetheless, they constitute a fluid constituent of the disk. They form a relativistic gas with a density of about $10^{-10}/\text{cm}^3$ (or $3 \times 10^{45}/\text{pc}^3$), and with a pressure P (equal to one-third their energy density,) of about 0.5×10^{-12} dynes/cm². Their pressure is as large as the Reynolds stresses of the mean turbulent motion of the interstellar gas, as large as the magnetic pressure of the galactic field, and very much larger than the mean thermal pressure of the interstellar gas.

Observations of the gaseous disk of the galaxy show a mean gas density of some 2 hydrogen atoms/cm³ over a thickness of 300 pc. The disk is thinner toward the center of the galaxy and considerably thicker farther out. The gas is distributed very inhomogeneously in cloud complexes separated by distances of the order of 500 pc. There is an irregular magnetic field embedded in the gas. The mean field is in the azimuthal direction around the disk (Hiltner, 1956) with a local strength of $3-4 \times 10^{-6}$ gauss (Manchester, 1972). The fluctuations ΔB are as large as the mean field B , with a characteristic correlation length of 10^2 pc (Jokipii and Lerche, 1969; Jokipii, Lerche, and Schommer, 1969).

The magnetic field is observed only within the dense gaseous disk of the galaxy, of course, where there is enough dust to polarize the passing starlight and enough free electrons to give a measurable Faraday rotation. Hence we have no direct information on the lines of force as they extend outside the gaseous disk. We can say, however, that the external magnetic field of any astrophysical body tends toward the lowest energy state available to it, and that is a closed configuration, of the form of a dipole for a globular object like the sun or the Earth. The closed configuration is rapidly achieved by dynamical line cutting (neutral point annihilation). So we expect to find astrophysical fields to be largely closed on themselves (Parker, 1973a, b; Jokipii, 1973). In some cases, of course, there is an active outflow of gas from the body that forces the field open. The solar wind extends the magnetic lines of force of the sun out through the solar system; there may be a galactic wind from the nucleus of the galaxy (Burke, 1968; Johnson and Axford, 1971) which forces open the magnetic field of the nucleus. But there is no evidence of an outflow of gas from the surface of the thin gaseous disk. So we suggest that the local galactic magnetic field is largely closed. Hence most of the magnetic lines of force extending out of the disk in the local irregularities are reentrant nearby.

Altogether, then, the cosmic rays below some 10^{16} ev/nucleon are tied to the lines of force and the lines have a closed topology. The cosmic rays are bottled up and are not free to escape individually from the surface of the galaxy. This view forces us to the conclusion that, if they escape at all, it must be as a consequence of the group pressure inflating the field and pushing outward from the galaxy. The 10 Gev particles escape along with the 10^4 Gev particles, etc. (Parker 1965, 1966, 1968b, 1969, 1975). The cosmic rays "bubble" out of the galaxy, if they escape at all (see below).

Other possibilities have been contemplated, in which the lines of force of the galactic magnetic field are presumed open to the outside in some way. In that case the cosmic rays are confined by scattering from the fluctuations in the field, their theoretical escape rate determined by whatever mean cosmic ray age seems appropriate. Thus, for instance, if the distance to the exit is $L = 1 \text{ kpc} = 3 \times 10^{21} \text{ cm}$ and we believe that the cosmic ray age is $t = 2 \times 10^6$ years, the scattering must reduce cosmic ray transport along the magnetic field to the effective diffusion coefficient $\eta_{\parallel} \approx L^2/t = 2 \times 10^{29} \text{ cm}^2/\text{sec}$.

The various options and possibilities have been thoroughly explored (see, for instance, Ramaty, Reames, and Lingelfelter, 1970; Jokipii, 1973; Ramaty, 1974). If cosmic rays are generated within the disk at a suitably high rate, then, there is also the possibility that the cosmic rays are scattered, and their escape limited, by the Alfvén waves caused by their own rapid streaming (Wentzel, 1968, 1969, Kulsrud and Pearce, 1969).

The ideas invoking an open magnetic topology are faced with the problem of explaining the turbulent spectrum and the gas density variations in just such a way that all energies from 1-10⁷ GeV have about the same diffusion coefficient (Kulsrud and Cesarsky, 1971; Skilling, 1971; Cesarsky and Kulsrud, 1973; Skilling, McIvor, and Holmes, 1974; Holmes, 1974; Jokipii, 1976). We might expect that the more energetic particles, being fewer in number and having higher rigidity, would escape more freely along the magnetic lines of force, so that the cosmic ray spectrum would cut off rather sharply above 10² or 10³ GeV. The fact that the spectrum extends as $E^{-\alpha}$ with $\alpha \approx 2.6$ all the way to 10⁷ GeV indicates that the very high energy particles are locked up in the same box as the particles at 10 GeV. Thus we interpret the absence of a high energy cut off as direct evidence that the galactic magnetic field topology is closed. It remains to be seen, then, whether cosmic rays are significantly scattered as they move as individuals, or stream in bulk, along the galactic magnetic field. There is no evident theoretical need for scattering, nor are observations able to come to grips with the magnetic fluctuations over the scales 10¹² - 10¹³ cm that are relevant for the median energy (10 GeV) particles. It is the accumulated effects of the small angle scattering of these magnetic fluctuations that may reduce the effective mean free path to 10¹⁸ - 10²⁰ cm. Insofar as the individual cosmic rays are scattered as the cosmic ray gas flows slowly along the lines of force, the theoretical treatment would presumably combine diffusion with the focusing effects of the large-scale field, as pointed out by Earl (1974a, b, 1975), to give a realistic treatment of the stochastic and ordered components of the particle motion in the stochastic lines of force of the general field.

If we are to think of cosmic rays as a hot gas inflating the gaseous disk, there are several obvious questions that come to mind, such as their source and their ultimate destination. Is the cosmic ray gas streaming by the solar system on its way to escape from the galaxy? A relative bulk velocity u leads to an anisotropy in the

frame of the solar system. The fractional intensity difference recorded by a detector with a fixed energy window looking first upstream and then downstream is $\Delta I/I = 2(2+\alpha) v/c$ for the differential energy spectrum $E^{-\alpha}$. This result can be applied to the protons (above about 500 Gev) that penetrate to the orbit of Earth without being too greatly deflected by the interplanetary magnetic field. A bulk streaming velocity of 10^2 km/sec yields $\Delta I/I = 3 \times 10^{-3}$. The Earth and its daily rotation can be used to scan around the directions perpendicular to the axis of Earth. It is a difficult experimental task, but possible in principle, to detect such small intensity differences. One needs a suitably large, stable detector at a sufficient depth underground. There must be enough atmospheric information available to make suitable corrections for the height and density variations of the air overhead. It is a complicated undertaking with a long and troubled history, but there is some reason to think that the major pitfalls have been discovered and understood, so that such efforts as the Utah experiment (Bergeson, Groom, and West, 1975) will soon have definite results. The work done already shows that the anisotropy is small, of the order of 10^{-3} or less. (See the summary of results in Osborne, 1975).

There is no experiment of which I am aware that can look for $\Delta I/I$ in the direction parallel to the axis of Earth. So a null result from the sidereal diurnal variation above 500 Gev proves nothing. Indeed, Jones (1970) has pointed out that whatever the variable streaming of cosmic rays in the galaxy, the single most probable result of a measurement of $\Delta I/I$ is zero. We have every right to expect that $\Delta I/I$ is not zero, however, and look forward to a positive answer.

Lacking a direct measurement of the local bulk streaming of the cosmic rays, what can we deduce about their origin and their ultimate fate? What is the source of the cosmic ray gas that inflates the interstellar medium? The simplest assumption is that the cosmic rays are produced here in the galaxy, although it has been fashionable in some circles to argue other more spectacular possibilities. Supernovae, flare stars, and the turbulence of the interstellar gas and field are among the obvious possible accelerators. The enormous energy ($10^{51} - 10^{52}$ ergs) of the type II supernova, the copious supply of relativistic particles observed in the remnant after the explosion, and the large relative abundance of heavy elements within the exploding star, are the circumstantial evidence on which the supernova is considered to be a major source (Ginzberg,

1958; Ginzburg and Syrovatskii, 1964). The recent work of Schramm and Arnett (1975) on neutral current interactions indicates that enough of the heavy elements in the interior of the supernova can be blasted outward in the explosion to supply the observed heavy elements. The spinning neutron star (pulsar) left behind, and the interstellar blast wave produced by the supernova, may accelerate the individual nuclei to relativistic energies (Pacini, 1968; Gunn and Ostriker, 1969; Kulsrud, Ostriker, and Gunn, 1972; Mertz, 1974; Scott and Chevalier, 1975; Jodogne, 1975). One of the outstanding theoretical obstacles, however, is the injection of the accelerated particles into the surrounding interstellar magnetic field. First of all, fast particles remaining for long within the expanding blast wave (the supernova remnant) are rapidly decelerated by the expansion. So they must leave quickly and enter the interstellar field outside the expanding remnant. But, on the other hand, it has been pointed out (Wentzel, 1968, 1969, 1974; Kulsrud and Pearce, 1969; Tadamaru, 1969; Lee, 1972) that the bulk streaming of cosmic rays along a magnetic field is limited to a few times the Alfvén speed computed in the ionized component of the thermal gas. Faster streaming generates transverse fluctuations in the magnetic field (Alfvén waves) that scatter the individual cosmic ray particles and strongly impede their flow. A single supernova must produce some $10^{49} - 10^{51}$ ergs of relativistic particles at the time of the explosion and/or in the next thousand years or so in the active remnant (Woltjer, 1972) if one supernova every 50 years in the galaxy is to supply most of the cosmic rays. How can so many fast particles be absorbed quickly into the surrounding interstellar gas and field? It is not obvious that escape into the interstellar medium is possible (see, for instance, the discussion of Cowsik and Wilson, 1975). Hence, the possibility that there are other major sources of cosmic rays cannot be ignored. The flare stars are a popular alternative (Cowsik, 1975). They are cool subdwarfs of small mass, roughly one thousandth or less as bright as the sun, commonly occurring throughout the galaxy. Some few of them have been observed to flare every few hours with outbursts one thousand times larger than the big cosmic ray flares on the sun (see, for instance, Moffet, 1974). But even if all red subdwarfs were as active as the more extreme cases, there would be barely enough total energy available. The local cosmic ray energy density of 1.6×10^{-12} ergs/cm³ with a nominal replacement time of 10^7 years, requires an input of 0.5×10^{-26} ergs/cm³ sec. If there is one active flare star in each 4 pc^3 (10^{56} cm^3) then each such flare star must supply relativistic particles at a rate of 0.5×10^{30} ergs/sec. This

is 10^{-1} the total luminosity of the flare star. The acceleration mechanism on the flare star must be very efficient indeed. It would appear that the flare stars are a contributor, but not the major source.

The general feeling on the subject is that both flare stars and supernovae produce cosmic rays, but how much is an open question (see, for instance, Cowsik, 1975). By analogy to solar flares, we may guess that the flare star contributes heavily at the low energy end of the spectrum, below, say, 10^9 ev per nucleon. The study of isotopic abundances among cosmic rays is the principal tool for getting at these questions. The problem is complicated by the local solar modulation and by competition between the spallation and fragmentation of cosmic ray nuclei within the source and while in transit in interstellar space. A number of authors have worked for many years now conducting numerical experiments on parameterized hypothetical models of the cosmic rays and galactic field, exploring the consequences at Earth of a variety of cosmic ray energy spectra and nuclear compositions at the sources, the distribution of sources in space, the mean cosmic ray life or path length before arrival at Earth, the interstellar scattering mean free paths, the interstellar gas density distributions, and finally the unknown modulation of the cosmic rays by the solar wind, necessary to account for the observed energy spectra and abundances of the nuclear species presently observed (see, for instance, Ramaty, Reames, and Lingenfelter, 1970; Lingenfelter, Ramaty, and Fisk, 1971; and the review by Osborne, 1975). A number of preliminary suggestions are already available, but, to carry the task through to completion, the isotopic observations must be extended to more massive nuclei. Whatever the outcome of the isotopic studies, a host of possible sources, from young massive stars to old black holes, must be considered. Presumably the sources are concentrated in the dense gaseous disk. The old idea, that there may be a strong contribution to cosmic ray acceleration from the turbulence in the interstellar gas (Fermi, 1949, 1954; Morrison, Olbert, and Rossi, 1954, Parker, 1955) has surfaced again. As noted above, an interstellar energy input of the order of 10^{-26} ergs/cm³ sec to the cosmic rays is required, so that significant interstellar cosmic ray acceleration would be a major sink of energy for the turbulence of the interstellar gas. And it would occur only if there were strong turbulence over scales of 10^{12} - 10^{13} cm.

The work on cosmic ray propagation in the galaxy has come a long way from the early days when the concept was

first pointed out (Fermi, 1949, 1954). In those days we thought of the field as wholly chaotic, with cosmic ray transport a matter of random walk through space (Morrison, Olbert, and Rossi, 1954) to free escape at the "surface" of the disk. The general ordered pattern of the mean galactic field of some $3-4 \times 10^{-6}$ gauss is now an observational fact of life (Hiltner, 1956; Manchester, 1972). But, noting that the scattering of most cosmic ray particles ($E \leq 10^{13}$ ev) across the magnetic field is completely negligible, the random walk of the magnetic lines of force (Getmantsev, 1963; Jokipii 1966; Jokipii and Parker, 1969a, b; Parker, 1969; Jones, 1971, 1972) is the principal transport of cosmic ray particles from the interior to the surface of the disk of the galaxy. It is the random walk of the lines of force, described by the mean square transverse displacement $\langle \Delta z^2 \rangle$ of the line per unit length Δs along the field, that permits the cosmic rays to diffuse across the disk and escape. The correlation length λ for the field fluctuation ΔB is of the order of 100 pc and $\langle (\Delta B / B)^2 \rangle^{1/2} \sim 0.5$ (Jokipii and Lerche, 1969; Jokipii, Lerche, and Schommer, 1969). Hence, in order of magnitude $\langle \Delta z^2 \rangle / \Delta s \sim 0.5 \lambda$. The scale height of the disk is of the order of $\Lambda = 1.5 \lambda$ so that a magnetic line of force wanders the distance Λ from the center to the "surface" of the disk in a distance s where

$$s \langle (\Delta z)^2 \rangle / \Delta s = \Lambda^2$$

from which it follows that $s = 4.5 \lambda = 500$ pc, in order of magnitude. Thus escape follows in distances of 0.5 kp $= 1.5 \times 10^{21}$ cm. A mean life of $t = 10^7$ years implies a mean streaming velocity of $u = s/t = 50$ km/sec, or an anisotropy of $\Delta I / I \approx 1.5 \times 10^{-3}$.

The diffusion of cosmic ray particles, batted back and forth along the stochastic lines of force, has been explored in the literature under the name of "compound diffusion." (Lingenfelter, Ramaty, and Fisk, 1971; Allen, 1972).

It is possible to obtain information on the electron component of the cosmic rays as they progress out from their sources in the disk by looking at the nonthermal galactic radio emission (Ginzburg and Syrovatskii, 1964, 1965).

Badhwar and Stephens (1975) have put together a self consistent model including hydrostatic equilibrium of the disk and the nonthermal radio emission (presumed to be

from the cosmic ray electrons in the galactic field B). The requirement for mean hydrostatic equilibrium of the gas pressure p and density ρ , the field pressure $B^2/8\pi$ and the cosmic ray pressure P in the local gravitational acceleration g of the galactic disk, is (Parker, 1966, 1969)

$$\frac{d}{dz} \left(p + \frac{B^2}{8\pi} + P \right) = -\rho g,$$

while the nonthermal radio emission (synchrotron emission) is proportional to the square of the energy of the individual electrons and to the energy density of the magnetic field (Ginzburg and Syrovatskii, 1964, 1965). The calculations of Badhwar and Stephens lead to a model of broad extent, with the gas, field and cosmic rays extending out a kpc on either side of the disk, in order to account for the observed radio emission from directions perpendicular to the plane of the disk. Webster (1975) has suggested a weaker broader halo, of some 10 kpc extent, containing relativistic electrons with a steeper energy spectrum, based on radio data alone. The reconciliation, or the relation, of these halo models has yet to be straightened out.

The broad distribution of gas, field, and cosmic rays implied by this theoretical model is most interesting in view of the recent measurements of the low Be^{10} abundance and the implications for the existence of a cosmic ray halo around the galaxy.

The recent observational determination (Garcia-Munoz, Mason, and Simpson, 1975a, b) of the nearly complete absence of the spallation product Be^{10} has direct implications for the region of space occupied by the cosmic rays. Garcia-Munoz, et al, point out that, if interpreted in terms of the usual ideas of cosmic ray production within the disk, followed by escape from the galaxy after penetrating 4-5 gm/cm^3 , the very low abundance of Be^{10} indicates a low average spallation rate of the heavy nuclei. That is to say, the cosmic rays circulate through a volume of space in which the mean density is one tenth or less the mean value of 2 hydrogen atoms/ cm^3 in the gaseous disk. Since the cosmic rays are observed here among the dense gases of the disk, they must spend ten times as long in some other region of much lower density ($N \lesssim 0.1$ atom/ cm^3). Evidently the cosmic rays circulate freely through the disk and an extensive magnetic halo surrounding the disk to a distance of 1 kpc or more on either side. Presumably

the magnetic fields of the gaseous disk are inflated to form magnetic bubbles extending outward for 1-2 kpc from either surface of the disk so that the galaxy has a significant halo of magnetic field and cosmic rays (Parker, 1965, 1968b, 1969). In view of the fundamental importance of the result an independent direct determination in space is desirable (see, for instance, the balloon work of Preszler, Kish, Lezniak, Simpson, and Weber; 1975 Hagen, Fisher, Ormes, and Arens, 1975; Fisher, Hagen, Maehl, Ormes, and Arens, 1976).

Now we have learned from the development of the many parametrized models of cosmic ray diffusion and spallation that the possibilities range all the way from the minimum cosmic ray life of 10^5 - 10^6 years before escaping from the gaseous disk of the galaxy (just enough time to penetrate the 4 - 5 gm/cm² to account for the observed spallation in interstellar space and/or in the source. See, for instance, Ramaty, Reaves, and Lingenfelter, 1970; Silberberg and Tsao, 1973, Shapiro and Silberberg, 1975, Shapiro, Silberberg, and Tsao, 1975) to the opposite extreme that cosmic ray particles never escape but knock around in the disk for 10^7 - 10^8 years before losing their energy and becoming diluted with fresh particles (Rasmussen and Peters, 1975). These views have various fundamental consequences for the dynamics of the cosmic rays and the gaseous disk. First of all, the calculated production rate is profoundly affected. A life of only 10^6 years averages out to an energy input of 5×10^{-26} ergs/cm³ sec, or 1.5×10^{41} ergs/sec over an estimated volume of 3×10^{66} cm³ for the gaseous disk of the galaxy, whereas the production rate need be only 0.03 as large if the cosmic rays do not escape. Second, the high production, short life cosmic ray model implies that the galactic magnetic field is rapidly inflated by the cosmic ray gas produced in the disk, blowing magnetic bubbles out the sides of the disk at some 10^2 km/sec (Parker, 1965, 1966, 1968b, 1969). The cosmic rays are a major source of activity in the interstellar medium, and it would appear unlikely therefore that the interstellar turbulence could be the source of significant cosmic ray acceleration. The tail cannot be expected to wag the dog. We would expect to find cosmic rays streaming at 1 - 2×10^2 km/sec along the field in the disk, producing a local anisotropy possibly as large as $\Delta I/I = 3 \times 10^{-3}$. The dynamical limitations to cosmic ray streaming pointed out by Wentzel and Kulsrud would come into play, so that the cosmic rays would often be strongly scattered as they move along the galactic field ($\kappa_{||} \approx 10^{29}$ cm²/sec).

On the other hand, the long life model leads to little or no blowing of magnetic bubbles, to very little streaming of cosmic rays, to low anisotropy $\Delta I/I \sim 10^{-4}$, and to no large contribution from cosmic rays to interstellar turbulence. The activity of the interstellar gas and field would be largely a consequence of the formation, passage, and explosion of massive stars within the interstellar gas.¹ Significant Fermi acceleration in interstellar space (say 0.3×10^{-26} ergs/cm³ sec) is then a real possibility in the long-life model. It needs only to be shown that the cosmic ray particles are strongly scattered back and forth along the magnetic field by the local turbulent fluctuations.

From the purely theoretical point of view, the controlling effect is the production rate of cosmic rays within the disk of the galaxy. For a given cosmic ray density, the life within the disk is inversely proportional to the production. So long as their strength is not negligible, the sources build up the cosmic ray pressure until it becomes comparable to the magnetic pressure $B^2/8\pi$. Thus, over a wide range of source strength $P \approx B^2/8\pi$ and the cosmic ray density is fixed by the strength of the field. Hence, we do not learn much from the observational fact that $P \approx B^2/8\pi$ (Parker, 1968b). Instead we try to determine the age of the local cosmic rays, hoping that it represents the mean life of the cosmic rays in the disk. The age is inferred from the abundance of spallation products and the decay of those spallation products that are radio active, such as Be¹⁰. The source strength is then assumed to be inversely proportional to the estimated age.

These issues are the principal questions concerning the containment and propagation of cosmic rays in the galaxy: Are cosmic rays generated so rapidly in the disk of the galaxy that they escape in only a few times 10^6 years, with considerable dynamical agitation of the magnetic fields of the disk, or are they generated slowly, so that escape is negligible and they slowly die through collisions while remaining captive within the galaxy? It appears that cosmic rays circulate freely through a volume of space an order of magnitude thicker than the disk. Is that volume anything more than the magnetic bubbles

1. Incidentally, the recent observational work of Hobbs (1976) shows that, whatever the cosmic ray life may be, the interstellar gas is heated principally by dissipation of turbulence and by the UV from hot stars (Oort and Spitzer, 1955; Parker, 1968a) rather than by a high intensity of low energy cosmic rays.

extended out the side of the disk by the pressure of the cosmic rays? It should be noted that a large ($\sim 10^{-3}$) local cosmic ray anisotropy would imply a high production rate and a short life. A measured small anisotropy (in a direction perpendicular to the axis of Earth) would imply nothing (Jones, 1970). As already noted, isotopic studies are the principal means for getting at the ages, and hence the source strengths. As a working hypothesis we suppose that all abundances represent steady-state mean values when it comes to working out their implications. But it must be kept in mind that, although there is observational evidence that the mean overall cosmic ray intensity (made up largely of protons) has not fluctuated much, we have no proof that the various spallation products do not vary (over periods of $10^4 - 10^6$ years). The different energies and isotopes may be the transient products of different nearby sources.

There is some possibility that the high energy electrons may shed light on cosmic ray life in the galaxy (with the usual assumption that the electrons have the same origin as the protons, of course). The point is that the very high energy electrons ($10 - 10^3$ Gev) lose energy rapidly by synchrotron emission, with the characteristic life diminishing with increasing particle energy. The power emitted is proportional to the square of the electron energy. Thus, the electron spectrum is depressed at high energies (relative to the source spectrum) by the synchrotron losses. It has been hoped that a careful study of the spectrum might reveal the energy at which the losses become severe, giving an indication of the time the electrons have been in the galactic magnetic field since their acceleration to the energies of which they are observed. For a thorough review of the present state of knowledge of the electron component, the reader is referred to Ramaty (1974) and Meyer, (1974, 1975). The other side of this picture is the point of Ginzburg and Syrovatskii already noted, that the synchrotron emission is observed as the principal component of the galactic nonthermal radio emission, giving us the product of the number of electrons per unit volume, their mean square energy, and the magnetic field energy density integrated along the line of sight. Unfortunately it is difficult, from our position near the central plane of the gaseous disk, to disentangle the contribution of relativistic electrons trapped in the strong fields of supernova remnants from the general background of the cosmic ray electrons. The nonthermal emission from directions perpendicular to the plane of the disk is more reliably employed (see, for instance, Badhwar and Stephens, 1975) than the intense hodge-podge that is

seen from the directions of low galactic latitude, along lines of sight that traverse long distances through the disk.

Finally it should be mentioned that the most direct view of cosmic rays in the gaseous disk is provided by the γ -ray observations, which are thoroughly discussed by several other speakers at this Symposium. The γ -rays give the integral of the products of the gas density and the cosmic ray intensity along the line of sight. Hence, unfortunately, their sensitivity falls off rapidly when we look to the galactic halo, because of the small gas density there. It is difficult to separate the small halo contribution from the massive signal from the dense gaseous disk.

There is a lot of theoretical work to be done yet, based on the studies of magnetohydrostatic equilibrium of the cosmic rays and the gaseous disk already available (Parker, 1966, 1968a, 1969; Lerche 1967a, b; Mouschovias, 1974; Mouschovias, Shu, and Woodward, 1974; Badwar and Stephens, 1975) showing the structure of the gas concentrations with the expanded field between. Appenzeller (1971) has observations of the compressed configuration of the field where it is weighed down in regions of dense gas. The full problem is not static, of course, but dynamical, because the equilibrium of the interstellar gas, field, and cosmic rays is unstable, over dimensions of 500 pc along the magnetic field. The dynamical instability is the major factor in the formation of the large cloud complexes, and the bulging magnetic bubbles in between. The bulges are inflated by the cosmic rays and the inflation, at whatever rate it may occur, provides the escape of cosmic rays from the disk of the galaxy. The inflated loops of field may extend 500 pc or more out from the disk, providing the halo indicated by the very low abundance of Be^{10} in the cosmic rays. Fig. 1 shows a formal example of the inflated magnetic field, (Parker, 1968b) above the surface of the disk, on which the normal component of the field is specified as $B_0 \sin kx$ and the cosmic ray pressure is $\epsilon (B_0^2/8\pi) \cos^2 kx$ with $\epsilon = 0.9$. The field outside the disk is extended by about a factor of three beyond the normal magnetostatic form in the absence of cosmic ray pressure. Noting the neutral sheets between successive bulges and the possibility for rapid reconnection of the lines of force, it seems to us that, if the extensive (1 kpc) halo is to be accounted for by inflation by cosmic rays, then the inflation of the loops of field must proceed at a lively pace (~ 100 km/sec) or the loops, with the dynamical instability (Parker, 1975) would not

survive to such great distance. We suggest, then, that the simplest explanation of the absence of Be^{10} is a high cosmic ray production rate, so that the mean dwell time in the disk is closer to 10^6 years than to 10^7 . If the cosmic ray life is, in fact, very long ($> 10^7$ years), then some other dynamical origin of an extended (1 kpc) magnetic halo must be imagined.

A variety of effects need yet to be fitted into the overall picture. The implications of extensive tunnels of very hot gas (Cox and Smith, 1974; Scott, 1975; Jones, 1973) from supernova remnants are estimated to occupy fully half of interstellar space. Their properties, and their consequences to the dynamics of the gaseous disk, have not yet been fully explored. We should begin thinking about the problem because the enormous scale height of the hot gas (10^6 °k) suggests that it plays a dynamic, rather than a static, role in the disk. The formation of the tunnels from supernova remnants to occupy half of the interstellar space must have a cooling effect on the cosmic rays inside, and a warming effect on the cosmic rays in the interstellar medium outside. The superheated tunnel gas is tenuous ($\leq 10^{-2}/\text{cm}^3$) and buoyant, representing a bubble relative to the surrounding "normal" traditional two-phased interstellar medium. The tunnels rise out of the gaseous disk in characteristic times 2×10^7 years or less, which is a little shorter than the estimated cooling time. Hence the escaping tunnels of hot gas contribute a corona of gas and field around the gaseous disk of the galaxy. The magnetic fields in the expanded tunnels would be expected to be very weak, so that they are more likely to permit free escape, than effective confinement, of the cosmic ray gas within them. It is not obvious, therefore, that they contribute to the cosmic ray halo around the galaxy. The tunnels of supernova remnants are one more complex reason why it is so difficult to form a unique picture of the dynamical life of the cosmic ray gas in the galaxy.

Finally, we should not fail to note that the galactic magnetic field appears to be generated by the nonuniform rotation of the gaseous disk in concert with the local cyclonic turbulence of the disk (Parker, 1971a; Stix, 1975). Hence the origin of the field is closely tied to the motions in the disk to which the cosmic rays may make a significant contribution. Apart from some very much idealized examples (Parker, 1971b) this larger problem has not been explored at all.

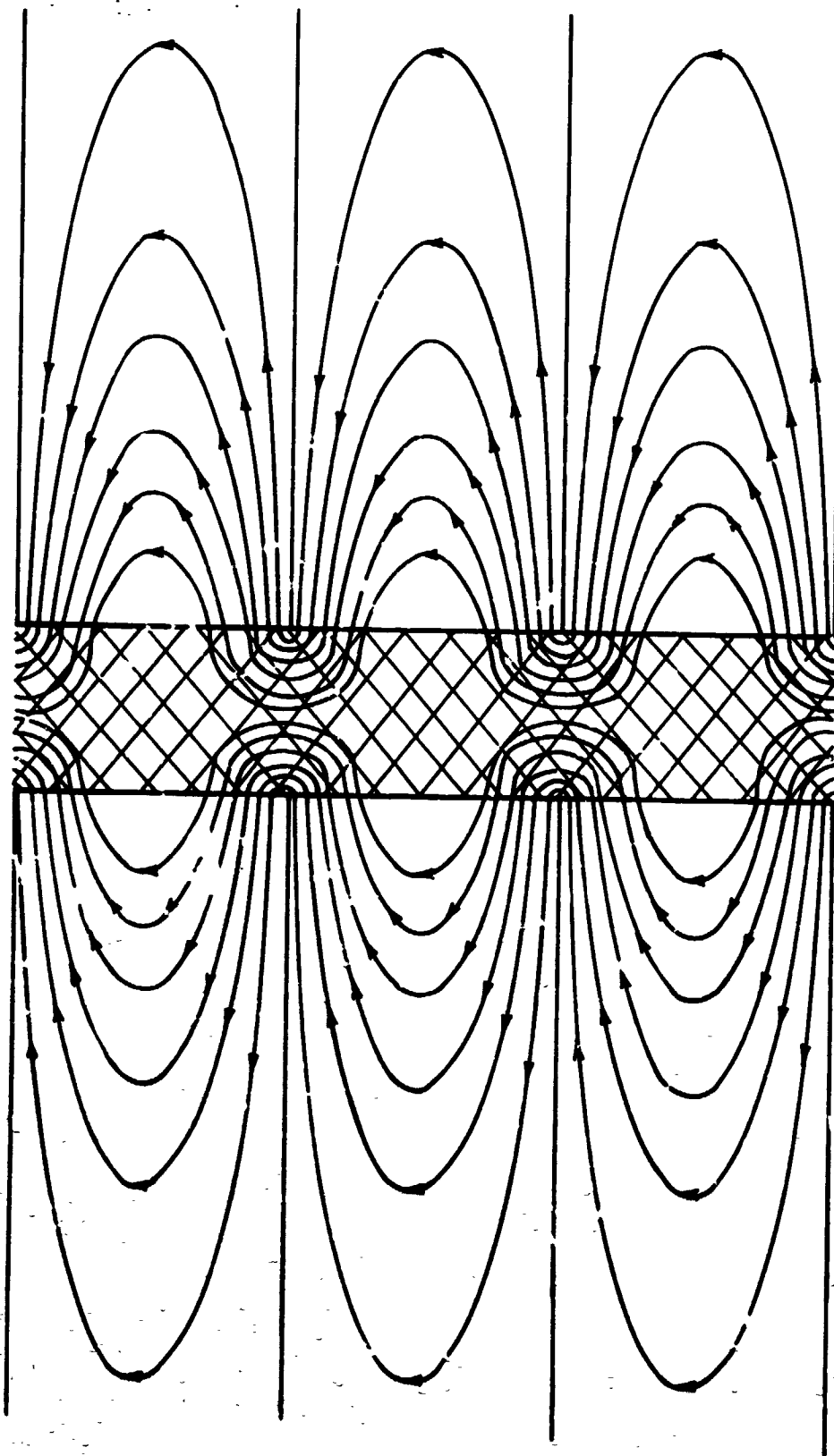
REFERENCES

- Allen, H. R. 1972, Astrophys. Letters, 12, 237.
- Appenzeller, I. 1971, Astron. Astrophys., 12, 313.
- Badhwar, G. D. and S. A. Stephens, 1975. Proc. 14th Intern. Conf. Cosmic Rays, 2, 639 (Munich, August).
- Bergeson, H. E., D. E. Groom, and W. J. West 1975, Proc. 14th Intern. Conf. Cosmic Rays, 2, 581 (Munich, August 1975).
- Burke, J. A. 1968, Mon. Not. Roy. Astron. Soc., 140, 241.
- Cesarsky, C. J. and R. M. Kulsrud 1973, Astrophys. J., 185, 153.
- Cowsik, R. 1975, Proc. 14th Intern. Conf. Cosmic Rays, 11, 3758 (Munich, August).
- Cowsik, R. and L. W. Wilson 1975, Proc. 14th Intern. Conf. Cosmic Rays, 2, 475. (Munich, August 1975).
- Cox, D. P. and B. W. Smith 1975, Astrophys. J. Letters, 189, L105.
- Earl, J. A. 1974a, Astrophys. J., 188, 379.
- Earl, J. A. 1974b, ibid, 193, 231.
- Earl, J. A. 1975, Proc. 14th Intern. Conf. Cosmic Rays, 5, 1733. (Munich, August).
- Fermi, E. 1949, Phys. Rev., 75, 1169.
- Fermi, E. 1954, Astrophys. J., 119, 1.
- Fisher, A. J., F. A. Hagen, R. C. Maehl, J. F. Ormes, and J. F. Arens 1976, Astrophys. J., (May).
- Garcia-Munoz, M., G. M. Mason, and J. A. Simpson, 1975a, Proc. 14th Intern. Conf. Cosmic Rays, 1, 325, 331. (Munich, August).
- Garcia-Munoz, M., G. M. Mason, and J. A. Simpson 1975b, Astrophys. J. Letters, 201, L141.
- Getmantsev, G. G. 1963, Soviet Astron. A.J., 6, 477.
- Ginzburg, V. 1958, Prog. in Elementary Particles and Cosmic Ray Physics, 4, Chap. 5. (Amsterdam: North Holland Pub. Co.)
- Ginzburg, V. L. and S. I. Syrovatskii 1964, Origin of Cosmic Rays, (New York: Pergamon Press).
- Ginzburg, V. L. and S. I. Syrovatskii 1965, Ann. Rev. Astron., 3, 297.
- Gunn, J. and J. Ostricker 1969, Phys. Rev. Letters, 22, 728.
- Hagen, F. A., A. J. Fisher, J. F. Ormes, and J. F. Arens 1975, Proc. 14th Intern. Conf. Cosmic Rays, 1, 361 (Munich, August).
- Hiltner, W. A. 1956, Astrophys. J. Suppl., 2, 389.

- Hobbs, L. M. 1976, Astrophys. J., 203, 143.
- Holmes, J. A. 1974, Mon. Not. Roy. Astron. Soc., 166, 155.
- Jodogne, J. C. 1975, Proc. 14th Intern. Cosmic Ray Conf., 2, 435 (Munich, August 1975).
- Johnson, H. E. and W. I. Axford 1971, Astrophys. J., 165, 381.
- Jokipii, J. R. 1966, Astrophys. J., 146, 480.
- Jokipii, J. R. 1973, Comments Astrophys. Space Sci., 5, 125.
- Jokipii, J. R. 1976, Astrophys. J., (in press).
- Jokipii, J. R. and I. Lerche 1969, Astrophys. J., 157, 1137.
- Jokipii, J. R., I. Lerche, and R. A. Schommer 1969, Astrophys. J. Letters, 157, L119.
- Jokipii, J. R. and E. N. Parker 1969a, Astrophys. J., 155, 777.
- Jokipii, J. R. and E. N. Parker 1969b, ibid., 799.
- Jones, E. M. 1975, Astrophys. J., 201, 377.
- Jones, F. C. 1970, Phys. Rev. Letters, 25, 1534.
- Jones, F. C. 1971, Astrophys. J., 169, 477.
- Jones, F. C. 1972, ibid., 172, 525.
- Kulsrud, R. M. and C. Cesarsky 1971, Astrophys. Letters, 8, 189.
- Kulsrud, R. M., J. P. Ostricker, and J. E. Gunn 1972, Phys. Rev. Letters, 28, 638.
- Kulsrud, R. and Pearce, W. 1969, Astrophys. J., 156, 445.
- Lee, M. 1972, Astrophys. J., 178, 837.
- Lee, L. C. and J. R. Jokipii 1976, Astrophys. J. (in press).
- Lerche, I. 1967a, Astrophys. J., 148, 415.
- Lerche, I. 1967b, ibid., 149, 553.
- Lingenfelter, R. E., R. Ramaty, and L. A. Fisk 1971, Astrophys. Letters, 8, 93.
- Manchester, R. N. 1972, Astrophys. J., 172, 43.
- Mertz, L. 1974, Astrophys. Space Sci., 30, 43.
- Meyer, P. 1974, Phil. Trans. R. Soc. London A, 277, 349.
- Meyer, P. 1975, in Origin of Cosmic Rays, (Dordrecht-Holland: D. Reidel Pub. Co.) ed. by J. L. Osborne and A. W. Wolfendale, p. 233.
- Moffett, T. J. 1974, Astrophys. J. Suppl., No.273, 29, 1.
- Morrison, P., S. Olbert, and B. Rossi 1954, Phys. Rev., 94, 440.
- Mouschovias, T. Ch. 1974, Astrophys. J., 192, 37.
- Mouschovias, T. Ch., F. H. Shu, and P. R. Woodward 1974, Astron. Astrophys., 33, 37.
- Oort, J. H. and L. Spitzer 1955, Astrophys. J., 121, 6.
- Osborne, J. L. 1975, in Origin of Cosmic Rays, (Dordrecht-Holland: D. Reidel Pub. Co.) ed. by J. L. Osborne and A. W. Wolfendale p. 203.
- Pacini, F. 1968, Nature, 219, 145.

- Parker, E. N. 1955, Phys. Rev., 99, 241.
- Parker, E. N. 1965, Astrophys. J., 142, 584.
- Parker, E. N. 1966, ibid, 145, 811.
- Parker, E. N. 1968a, ibid, 154, 57, 875.
- Parker, E. N. 1968b, Stars and Stellar Systems, Vol. VII, Nebulae and Interstellar Matter (Chicago: University of Chicago Press) ed. by B. M. Middlehurst and L. H. Aller, Chap. 14, Section 7.4.
- Parker, E. N. 1969, Space Sci. Rev., 9, 651.
- Parker, E. N. 1971a, Astrophys. J. 163, 255; 166, 295.
- Parker, E. N. 1971b, ibid, 168, 239.
- Parker, E. N. 1973a, Astrophys. Space Sci., 22, 279.
- Parker, E. N. 1973b, ibid, 24, 279.
- Parker, E. N. 1975, Astrophys. J., 202, 523.
- Preszler, A. M., J. C. Kish, J. A. Lezniak, G. Simpson, and W. R. Webber 1975, Proc. 14th Intern. Conf. Cosmic Rays, 12, 4096.
- Ramaty, R. 1974, in High Energy Particles and Quanta in Astrophysics (Cambridge, Massachusetts: MIT Press) ed. by F. B. McDonald and C. E. Fichtel, Chap. III.
- Ramaty, R., D. V. Reames, and R. E. Lingenfelter 1970, Phys. Rev. Letters, 24, 913.
- Rasmussen, I. L. and B. Peters 1975, Proc. 14th Intern. Conf. Cosmic Rays, 12, 4102.
- Schramm, D. N. and W. D. Arnett 1975, Astrophys. J., 198, 629.
- Scott, J. S. 1975, Nature 258, 58.
- Scott, J. and R. Chevalier 1975, Astrophys. J. Letters, 197, L5.
- Shapiro, M. M. and R. Silberberg 1975, Phil. Trans Roy. Soc. London A, 277, 317.
- Shapiro, M. M., R. Silberberg, and C. H. Tsao 1975, Proc. 14th Intern. Cosmic Ray Conf., 2, 532.
- Silberberg, R. and C. H. Tsao 1973, Astrophys. J. Suppl. 25, 315.
- Skilling, J. 1971, Astrophys. J., 170, 265.
- Skilling, J., J. McIvor, and J. A. Holmes 1974, Mon. Not. R. Astron. Soc., 167, 87.
- Stix, M. 1975, Astron. Astrophys., 42, 85.
- Tademaru, E. 1969, Astrophys. J., 158, 959.
- Webster, A. 1975, Mon. Not. Roy. Astron. Soc., 151, 243.
- Wentzel, D. G. 1968, Astrophys. J., 152, 287.
- Wentzel, D. G. 1969, ibid, 157, 545.
- Wentzel, D. G. 1974, Annual Rev. Astron. Astrophys., 12, 247.
- Wottler, E. 1972, Annual Rev. Astron. Astrophys., 10, 247.

Fig. 1. An idealized plot of the inflated magnetic lines of force outside the galactic disk. The gaseous disk is represented by the cross hatched horizontal region with a thickness of 300 pc, indicated by the scale on the right hand side. The normal component of the field is specified as $B_0 \sin kx$ at the surface of the disk, inflated by a cosmic ray pressure $0.9 (B_0^2/8\pi) \cos^2 kx$. The lines within the disk are drawn in a completely arbitrary form. Presumably the massive interstellar cloud complexes are confined in the pockets of field sketched within the disk.



1400 pc
1200
1000
800
600
400
200
0

N76-29131

GAMMA RAYS AND LARGE SCALE GALACTIC STRUCTURE

D. A. Kniffen, C. E. Fichtel and D. J. Thompson
NASA/Goddard Space Flight Center
Greenbelt, Md. 20771

ABSTRACT

Recent γ -ray observations have provided a new means of studying large scale galactic structure. Many theoretical models have been developed in an attempt to explain the spatial structure in the observed emission which results from interactions of energetic cosmic rays with the interstellar gas. Bignami and Fichtel (1974) and Bignami et al. (1975) have pointed out that the peaks in the observed distribution are remarkably well correlated with longitudes corresponding to tangential directions to known spiral arm features. Based on theoretical and experimental arguments, they assumed that on the scale of galactic arms the cosmic rays are more intense where the mass of the gas to which they are coupled is greatest. Refining this model with the results of recent surveys of the interstellar gas (Gordon and Burton, 1976) as interpreted by the Simonson model (1976) of the galactic structure, a good fit to the observations is obtained whether the cosmic rays are confined to the spiral arms in the disk or are more evenly confined as in a flat halo model. A universal cosmic ray distribution leads to a distribution which disagrees with the observations but this interpretation is subject to the large uncertainties in the molecular hydrogen densities deduced from the observations of the 2.6 mm carbon monoxide line.

1. Introduction. Gamma-ray astronomy is now emerging as an important observational technique for the study of the structure and content of our galaxy. The intensity of the radiation stands clearly above the diffuse celestial background, and the fluctuations in the spatial distribution provide important information on the dynamic conditions in the galaxy. Furthermore, the highly penetrating nature of the γ -radiation makes it a valuable probe across the densest regions of interstellar space without the uncertainties introduced when absorption corrections are required.

The question of the origin of the galactic plane emission has been the object of intensive study since the first clearly positive observation of galactic γ -rays by Kraushaar et al. (1972) which indicated a general galactic disk enhancement with a peak intensity toward the galactic center. It has been recognized for some time (Pollack and Fazio, 1963; Stecker, 1971) that cosmic rays in the Galaxy interact with the interstellar gas, leading to high energy γ -rays. Kraushaar et al. (1972) pointed out that the observations were not consistent with a uniform cosmic-ray distribution.

Strong et al. (1973) assumed that the cosmic-ray density has a distribution which increases smoothly toward the galactic center. Using the galactic magnetic field model of Thielheim and Langhoff (1968) they developed a model in which the cosmic rays were assumed to vary proportionally to the magnetic field to the first and second powers. Although the model failed to produce some of the detail in the distribution, it was the first to assume a variable cosmic-ray intensity and gave improved results over previous models. Many attempts have subsequently been made to develop models which yield the longitude distribution of γ -radiation above 100 MeV observed by SAS-2. With the greater sensitivity and the improved spectral and spatial resolutions available with the SAS-2 observations (Fichtel et al., 1975) and with the recent radio surveys of interstellar atomic and molecular hydrogen densities (Burton et al., 1975; Gordon and Burton, 1976), it is possible to study the details of the conditions in the emission region.

2. Development of Theoretical Models. Kniffen et al. (1973) suggested that the large intensity increases in the longitude distribution of γ -radiation above 100 MeV over a broad 70° to 90° galactic interval toward the galactic center are possibly due predominantly to radiation from galactic features, especially from the spiral arm segments,

Following the initial report of the SAS-2 galactic γ -ray observations, several theoretical models were developed in an attempt to explain the details of the spatial distribution. Bignami and Fichtel (1974) proposed that the cosmic rays were enhanced where the interstellar gas to which the cosmic rays are coupled is more dense. Since the production of γ -rays is proportional to the product of the cosmic-

ray intensity and gas density, the resulting γ -ray emission tends to be higher within the galactic spiral arms, with the longitude distribution showing an overall enhancement toward the central galactic region with peaks in the directions tangential to the spiral arms.

An approach similar to that of Strong et al. (1973) has been taken by Schlickeiser and Thielheim (1974a,b) and Thielheim (1975). They also note that the cosmic rays should be dynamically coupled to some portion of the matter through galactic fields. Assuming a power law dependence of the cosmic-ray-interstellar gas density product on the magnetic field strength, they determine the relationship which gives the best fit to the γ -ray distribution. Using the spiral shaped galactic magnetic field model of Thielheim and Langhoff (1968) reasonable agreement with the observations is obtained by assuming a third to fourth power dependence of this product on the magnetic field.

Paul et al. (1974, 1975) using the same galactic magnetic field distribution have used the observation of synchrotron radiation to deduce the cosmic-ray distribution and again find it consistent with the assumption of proportionality with the interstellar gas density. They also note that the confinement region is more important to γ -ray production than is the distribution of sources.

Stecker et al. (1975) have used the distribution of molecular hydrogen inferred from the carbon monoxide observations of Scoville and Solomon (1975). They determine that the best agreement to the γ -ray distribution is obtained with cosmic rays proportional to the 0.3 power of the gas density. As an alternate approach, Stecker (1975) has assumed that the supernova distribution obtained by Kodaira (1974) is representative of the galactic cosmic ray distribution and again, using the carbon monoxide observations obtains a good fit to the observations. However this interpretation is subject to the experimental uncertainties in the observed interstellar gas and γ -ray distributions and conversion of these observations to galactocentric radial distributions, as well as the uncertainties in the determination of supernova remnant distributions (Ilovaisky and Lequeux, 1972; Kodaira, 1974; Clark and Caswell, 1976). A significant contribution from the inverse Compton production of high energy γ -rays on the enhanced starlight density at the galactic center is required to produce the observed intensities in the 0° - 30° galactic longitude range for both of these models. Galactic plane surveys do not yet exist for the southern hemisphere, so this theory is developed only for the 0° - 180° longitude range and cannot yet speak to the 180° - 360° range where the evidence of spiral structure is most pronounced in the γ -ray distribution. Fuchs et al. (1975) have performed an analysis similar to that of Stecker et al. (1975) with different estimates of the atomic and molecular hydrogen and reach the conclusion that no power of the cosmic ray-gas density relationship gives a particularly good fit to the observations.

The resolution of the open questions on the distribution and relative influence of the interstellar hydrogen, especially the molecular component where the values are obtained from the rather uncertain interpretation of the 2.6 mm line of carbon monoxide, and the form of the coupling of the cosmic rays to the various gas components must await more and better observations both in radio and γ -ray astronomy. In addition, the resolution of the question of the contribution of discrete sources to the γ -ray distribution depends on γ -ray observations with better angular resolution.

This brief summary of some of the models currently being used to explain the observed distribution of high energy γ -rays is not intended to be a complete review, but to set the background for a more complete discussion of the model of Bignami et al. (1975) and Fichtel et al. (1976) for explaining the observed distribution of high energy galactic γ -rays and the importance of making observations in the medium energy (8-50 MeV) γ -ray energy range.

3. The Model. In this section a model is developed for the emission of γ -radiation from the galactic disk. To introduce the model the original work of Bignami and Fichtel (1974) and Bignami et al. (1975) for explaining the observed spatial distribution of galactic γ -radiation above 100 MeV is briefly discussed. The importance of making observations at medium γ -ray energies for studying the galactic cosmic ray electron distribution and its relationship to these concepts will be discussed. Finally, the most recent survey of the interstellar gas densities is used to update the calculations.

As already discussed, Bignami and Fichtel (1974) proposed a model which assumed that the cosmic rays were proportional to the interstellar gas to which they are coupled. Assuming that the cosmic rays and magnetic fields are galactic in nature, this hypothesis is supported by the following considerations. Bierman and Davis (1960) and Parker (1966) in more detail have shown that the expansive pressures of the magnetic fields, the kinetic motion of matter and the cosmic rays, can only be balanced by the gravitational attraction of the matter. In particular the only matter which is relevant to the portion of the expansive pressure due to the cosmic rays and magnetic fields is that through which the magnetic fields penetrate. Moreover, the galactic cosmic-ray energy density cannot substantially exceed that of the magnetic fields, or the cosmic ray pressure will push a bubble into the fields, ultimately allowing the cosmic rays to escape. Locally the energy density in each of the expansive pressures discussed above appears to be approximately the same and the total of the three together is about equal to that allowed by the gravitational attraction of the gas. This suggests that the cosmic-ray density may generally be as large as would be expected under quasi-equilibrium conditions. This concept is

given some theoretical support by the calculated slow diffusion rate of cosmic rays (Parker, 1969; Lee, 1972; Wentzel, 1974).

Based on these concepts and the trial assumption that cosmic rays are coupled to the interstellar gas on the scale of galactic arms, Bignami and Fichtel (1974) and Bignami et al. (1975) calculated the expected longitude distribution of the γ -rays with energies above 100 MeV principally from the production of γ -rays by the decay of neutral pions produced in cosmic ray-gas collisions. Bignami et al. (1975) have pointed out that the enhancements in the γ -ray longitude distribution seen by SAS-2 at l values of about 35° , 0° , 345° , 330° , and 315° (Fichtel et al., 1975) are remarkably well correlated with the galactic longitude directions tangent to the major spiral arm features in Simonson's model of galactic structure. The Simonson model, shown in Figure 1, is based on the density wave theory with an arm to inter-arm contrast of about 3 to 1. The enhanced γ -ray intensities seem to

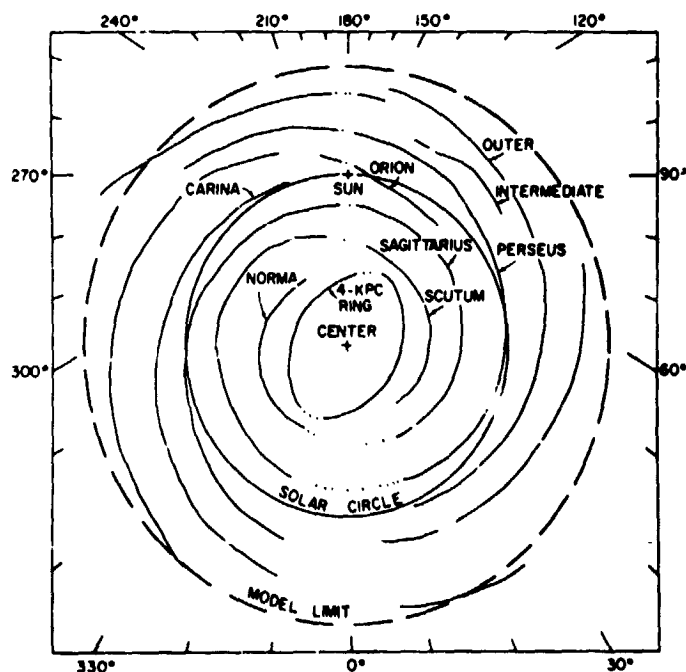


Figure 1. A smoothed spatial diagram of the ridges of the gas density deduced from 21-cm measurements of HI and the density wave theory (Simonson, 1976).

be correlated with the directions of the Scutum (35°), 4 kpc (345°), Norma (330°), and again the Scutum (315°) arm. The strong correlation with these features led Bignami et al. (1975) to adopt a model for the total galactic gas distribution based on 21 cm observations of neutral atomic hydrogen as interpreted by the Simonson model. The γ -ray intensity is then determined by the expression

$$\Phi(E_\gamma, l) = \frac{1}{4\pi} \int S(E_\gamma) g(r, l, b) N(r, l, b) dr db$$

where $S(E_\gamma)$ is the local source function for the production of γ -rays of energy E_γ . $S(E_\gamma)$ is dominated by the decay of neutral pions formed in collisions of the cosmic rays with the interstellar gas whose total density is $N(r, l, b)$. $g(r, l, b)$ is a factor which takes into consideration the spatial dependence of the source function due to the variation of the cosmic-ray density. r is the radial distance from the Sun and l and b are galactic longitude and latitude. As a trial assumption, based on the arguments given above, a linear dependence on the gas density was assumed.

In the model of Bignami et al. (1975) it is assumed that the spiral structure is common to both the atomic and molecular hydrogen. Although the question of the degree of spiral structure in our Galaxy is still an open question, recent studies (Georgelin and Georgelin, 1976; Clark and Caswell, 1976) give strong new evidence for a spiral structure in the distribution of HI, HII and supernova remnants, hence the assumption of a common distribution for HI and H₂ seems reasonable. A density of molecular hydrogen equal to that of the atomic hydrogen (Spitzer et al., 1973; Jenkins and Savage, 1974) as observed locally is assumed throughout the inner galaxy with a forty percent contribution beyond the solar cycle. The resulting calculation reproduces the essential features of the distribution with a direct calculation involving no normalization.

The discussion to this point has been based on the production of galactic γ -rays above 100 MeV. Fichtel et al. (1976) have pointed out the significant new information obtainable from observations at somewhat lower energies. In the 10-30 MeV energy range, additional important production mechanisms include bremsstrahlung production by energetic cosmic ray electrons traversing the interstellar gas, Compton emission of cosmic-ray electrons colliding with interstellar photons and the synchrotron emission of electrons interacting with the galactic magnetic fields. "Local" source functions for each of these mechanisms for the production of medium (10-30 MeV) and high (> 100 MeV) γ -radiation are given in Table I. The bremsstrahlung source function is calculated using the cross sections of Koch and Motz (1959), integrated over the interstellar spectrum deduced by Daugherty et al.

(1975), and the secondary electron spectrum calculated by Ramaty (1974). The density of higher z elements in the interstellar gas is more important in this case because of the $Z(Z+1)$ dependence on charge. This increases the production rate by a factor of 0.55. The Compton and synchrotron cross sections are given by Ginzburg and Syrovatskii (1964). The pion decay source mechanism is taken from the work of Stecker (1971).

Table I -- Source Functions in Solar Vicinity

SOURCE MECHANISM	VALUE OF SOURCE FUNCTION ($\text{cm}^{-3} \text{sec}^{-1}$)	
	10-30 MeV	> 100 eV
Neutral Pion Decay*	6.5×10^{-27}	13.0×10^{-26}
Electron Bremsstrahlung*	1.2×10^{-25}	3.5×10^{-26}
Compton Scattering (starlight)	0.6×10^{-26}	0.2×10^{-26}
Compton Scattering (3°K)	1.0×10^{-26}	0.2×10^{-26}
Synchrotron Radiation	1.0×10^{-30}	0.2×10^{-30}

*Assuming 1.05 hydrogen nuclei/ cm^3 locally in the galaxy, a helium to hydrogen ratio of 0.1 and heavy nuclei to hydrogen ratio of 0.01.

Electron Spectrum: $J(E_e) = (6.8 \times 10^{-3}) E_e^{-1.8}, E_e \leq 2 \text{ GeV}$
 $J(E_e) = (1.4 \times 10^{-3}) E_e^{-2.8}, E_e > 2 \text{ GeV}$

Photon Energy Densities: (starlight) $\approx .45 \text{ eV/cm}^3$
 (3°K) $\approx .25 \text{ eV/cm}^3$

The Table shows clearly the shift from a nucleonic mechanism at higher energies to an electron mechanism in the medium energy range. However, the cosmic-ray--gas interactions dominate over other processes in all energy ranges for regions except where the starlight photon/interstellar gas density ratio, $N_{ph}(r, \ell, b)/N(r, \ell, b)$, is much larger than its local value. This condition is expected to exist throughout the galaxy except possibly at the center. There is no direct evidence pertaining to the photon density in the region of the galactic center,

so this possibility remains an open question. The 3°K black universal blackbody radiation is a source of Compton produced γ -radiation, but this contribution is only a significant γ -ray producer where the interstellar gas density is much lower than it is locally.

The γ -ray intensity applicable to this more general case is given by

$$\begin{aligned}
 I(E_\gamma, \ell) = & \frac{1}{4\pi} \int_0^{\infty} dr db [S_{\gamma n}(E_\gamma, r=0) g(r, \ell, b) \frac{N(r, \ell, b)}{N(r=0)} \\
 & + S_{\gamma e_p}(E_\gamma, r, \ell, b) \\
 & + S_{\gamma e_s}(E_\gamma, r, \ell, b)] .
 \end{aligned} \tag{1}$$

$S_{\gamma n}$ represents the γ -rays created per second by the decay of pions produced in interactions of nucleonic cosmic rays (with the intensity and spectral distribution in the solar vicinity) with the interstellar gas. $S_{\gamma e_p}$ and $S_{\gamma e_s}$ are similar functions for primary and secondary cosmic ray

electrons, respectively. Fichtel et al. (1976) have shown that the primary cosmic ray electrons contribute to the γ -ray production in proportion to N^2 times a function which decreases the strength of the dependence to some degree. At the same time the secondary cosmic ray electrons contribute as N^3 times a term which somewhat decreases the strength of the dependence. Hence, the secondaries become somewhat more significant in high density regions, but remain a minority contribution within the range of densities considered here.

As in the nuclear cosmic ray case, the electron contribution to the γ -radiation from a specific direction can be calculated by performing the appropriate integral of the cosmic ray--gas density product for a given galactic longitude. The calculated 10-30 MeV emission gives a longitude distribution similar, though not exactly the same as the high energy distribution. The outstanding feature of the resulting emission can be seen from the spectral distribution for the direction $\ell = 335^\circ$, $b = 0^\circ$ shown in Figure 2 taken from Fichtel et al. (1976). This calculation uses the model of Bignami et al. (1975) although the basic features of the spectrum are not very model dependent. The dramatic shift from the bremsstrahlung mechanism at lower energies to the pion decay mechanism at higher energies is evident. Thus, comparing the longitude distribution of medium energy γ -ray observations with those at higher energies provides a test of the hypothesis that

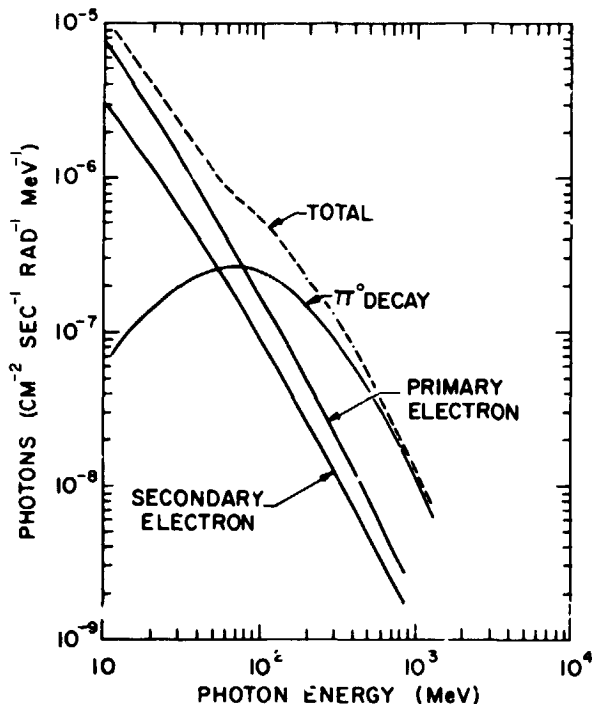


Figure 2. Expected γ -ray spectrum for $l=335^\circ$, $b=0^\circ$. Dashed line includes total of contributions from cosmic-ray--interstellar gas interactions and bremsstrahlung emission from both primary and secondary electrons. This spectrum should be typical except near the galactic center where a substantial Compton component may be present.

cosmic ray electrons are predominantly primary in origin and produced in the same sources and in the same proportion as the nucleonic component.

There are very few experimental data with which to compare the medium to high energy γ -ray emission over the galaxy. A comparison of the Share et al. (1974) observations of the galactic center with those of SAS-2 (Fichtel et al., 1975) tend to confirm the spectral shape shown in Figure 2. A comparison of high energy γ -ray observations with radio observations of synchrotron emission are inconclusive because of the difficulty of interpretation due to the lack of a detailed knowledge of the interstellar fields.

Rasmussen and Peters (1975) have recently reexamined the closed-galaxy model for cosmic rays and shown that, under certain assumptions, it can explain the observed nuclear composition and flux of cosmic rays near the earth. One interesting prediction of this model as noted by Ramaty and Westergaard (1976) is that the cosmic ray electron bremsstrahlung would be larger relative to the cosmic ray nucleon π^0 γ -ray flux than in the more recently popular model discussed here wherein there is significant cosmic-ray leakage from the galaxy. An accurately measured γ -ray energy spectrum can clearly help to resolve the question of whether this alternate theory is correct.

4. Interstellar Gas Distribution. A crucial input to any model of galactic γ -ray production due to cosmic ray interactions is the distribution of the interstellar gas. The most recent large scale galactic

survey of the 21 cm line of atomic hydrogen of which the authors are aware is the work of Burton (1976) and Gordon and Burton (1976). Recent surveys of the 2.6 mm line of carbon monoxide from which the densities of molecular hydrogen are inferred include those of Scoville and Solomon (1975), Burton et al. (1975), and Gordon and Burton (1976). The limited data on disk thicknesses indicate that the molecular hydrogen with a scale height of about 50 pc is apparently more closely confined to the disk (Burton and Gordon, 1976) than is the neutral atomic hydrogen which has a scale height of 120 pc inside the solar circle, increasing linearly beyond the sun to about twice this value at about 15 kpc (Baker and Gordon, 1975). These scale heights somewhat reduce the dominance of the molecular hydrogen at galactocentric radii observed in the surveys. Unfortunately these surveys do not cover the entire galactic plane, since the observations were made from the northern hemisphere. Hence, any model attempting to explain the γ -ray emission over the entire plane from these data must necessarily infer the densities for the galactic longitude region from 180 to 360 degrees. Furthermore, the densities of molecular hydrogen depend on a rather uncertain evaluation of the CO/H₂ ratio in interstellar space.

The model of Bignami et al. (1975) has been applied to these recent observations of the interstellar constituents. The data have been interpreted in terms of the Simonson model of galactic structure (1976). The arm densities are estimated by modulating the radial distribution of both atomic and molecular hydrogen given by Gordon and Burton (1976). The modulation provides a 3 to 1 arm to interarm contrast with a peak at the galactocentric radius of the arm and with an average value consistent with the radial distributions obtained from the surveys. For the portions of the plane where observations ($270 \leq l \leq 360$) do not exist the densities in the extension of a given arm were reduced by 20 percent to reflect the larger galactocentric distances. The height dependence of each constituent is taken to be a gaussian with the scale heights given by Baker and Burton (1975) and Burton and Gordon (1976). As before, the cosmic rays were assumed to be coupled linearly to the total gas density with a scale height similar to that of the atomic hydrogen. The contributions to the galactic γ -ray distribution were calculated in the same manner as described before.

Figure 3 indicates the γ -ray distribution calculated for this model. As in the previous model, most of the major features of the observed distribution are reproduced, with an excellent intensity fit for most cases. The success of the model in reproducing the γ -ray distribution for the portion of the plane where the gas densities are observed indicates the validity of the reasonable assumption of a linear coupling between the cosmic rays and the interstellar gas. For comparison, Figure 4 indicates the distribution expected for a thick, or fat "disk" model of the galactic cosmic rays in which the cosmic rays are still confined by the galactic magnetic fields anchored

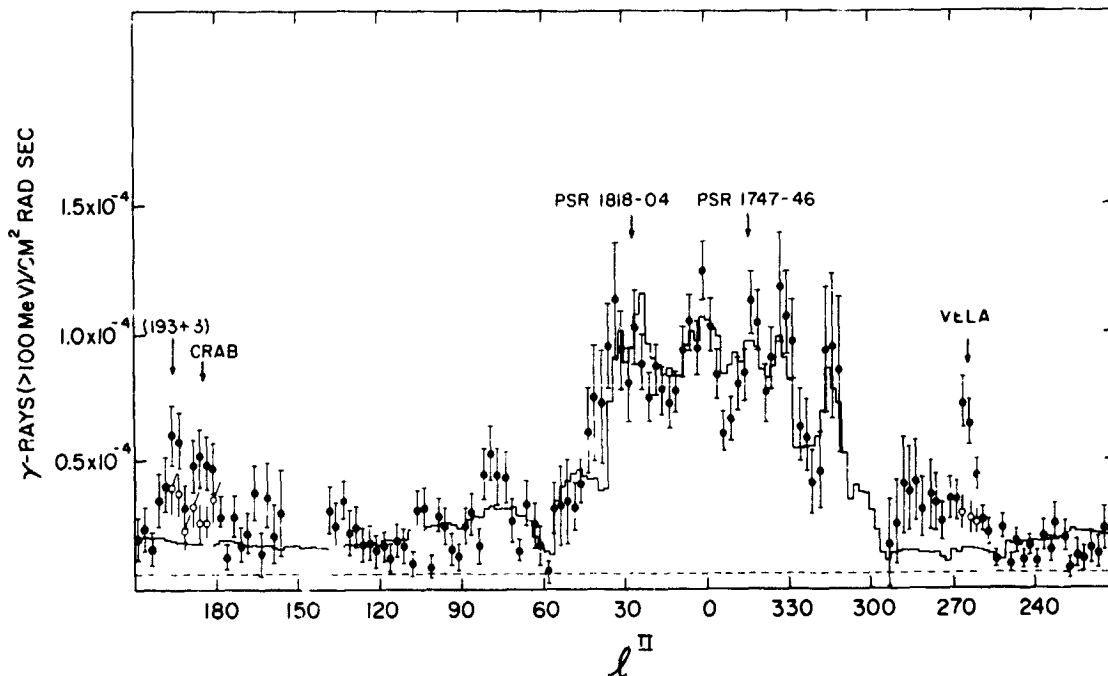


Figure 3. The solid line represents the longitude distribution of the calculated γ -ray emission above 100 MeV summed from -10° to $+10^\circ$ in galactic latitude. The distribution obtained by applying the model of Bignami et al. (1975) to the recent HI and H₂ distributions of Gordon and Burton (1976) as interpreted by the Simonson model (1976) of galactic structure. The cosmic rays are assumed to have the same scale heights as the HI. The SAS-2 data is shown for comparison. Open circles represent the residual intensities with known point source contributions removed.

in the spiral arms but have a scale height, 500 pc, much greater than that of the gas. Within the experimental uncertainties an equally good fit is obtained to the observed γ -ray distribution.

Figure 5 indicates the γ -ray longitude distribution expected for a model in which the cosmic-rays are constant throughout the galaxy with a value equal to that observed near the Sun. Clearly this distribution is inconsistent with the SAS-2 observations, and would seem to offer evidence against the universality of cosmic rays. Unfortunately, the uncertainty in the measured interstellar molecular hydrogen densities weakens this interpretation.

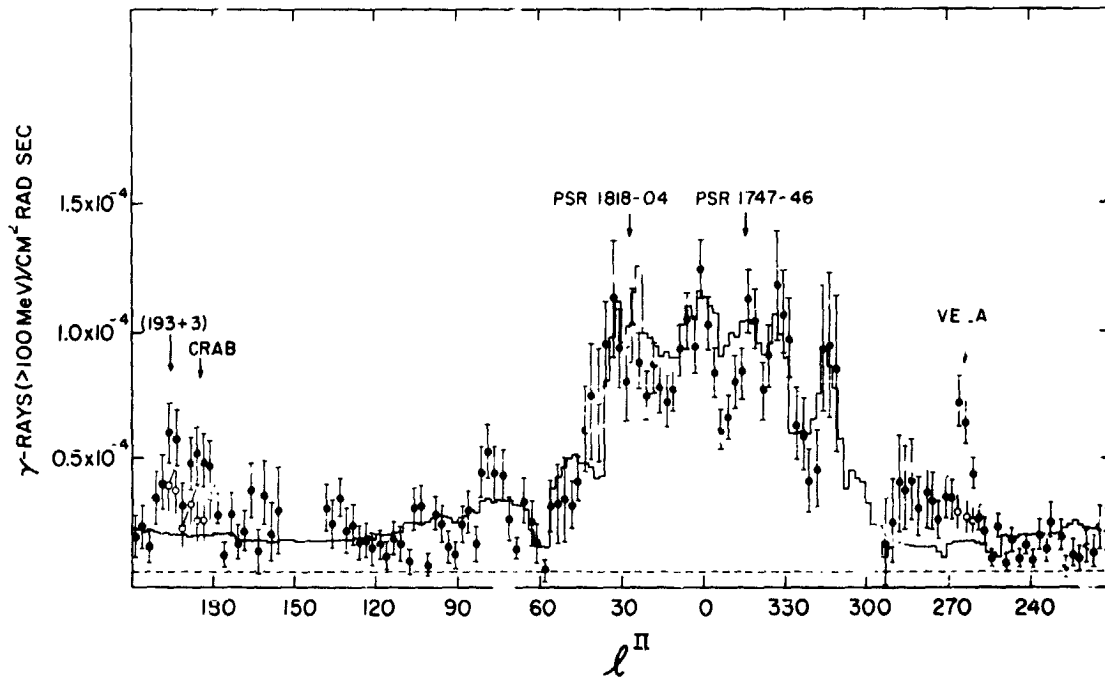


Figure 4. Same as Figure 3 with a thick "disk" model for the cosmic rays. A scale height of 500 pc is assumed.

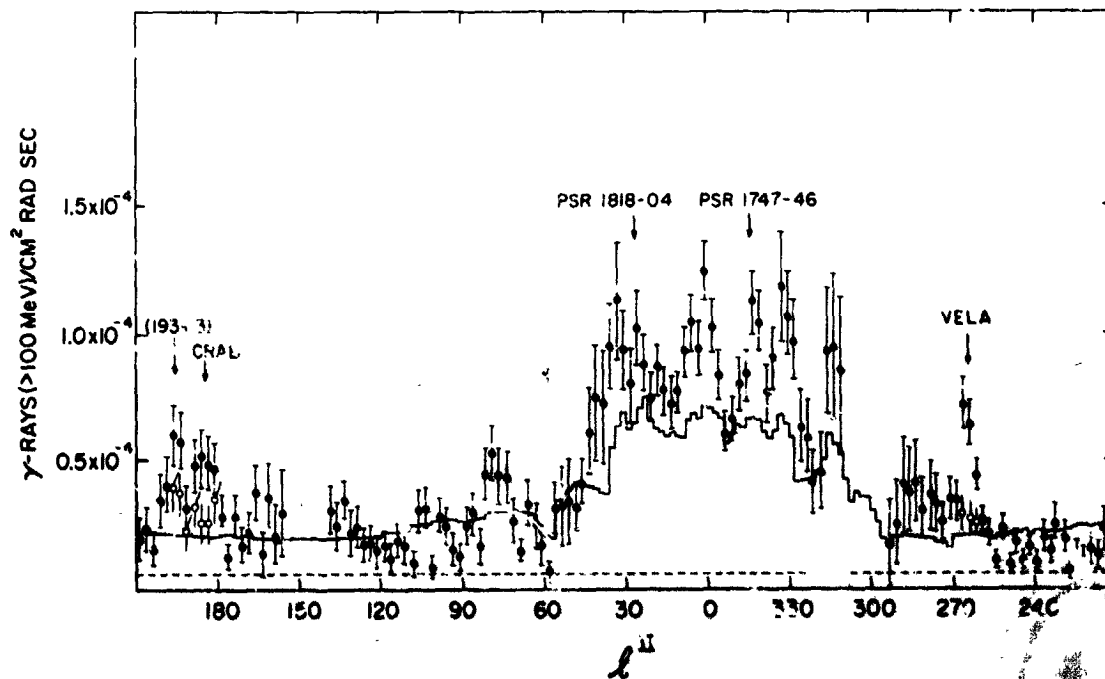


Figure 5. Same as Figure 4 for a constant cosmic ray model with an intensity as measured near the Sun.

5. Conclusion. γ -ray astronomy is now beginning to provide a new look at galactic structure, and the distribution of cosmic rays, both electrons and nucleons, within the galaxy. The observations are consistent with a galactic spiral arm model in which the cosmic rays are linearly coupled to the interstellar gas on the scale of the spiral arms. The agreement between the predictions of the model and the observations for regions of the plane where both 21 cm and 2.6 mm CO surveys exist emphasizes the need to extend these observations to include the entire plane. Future γ -ray observations with more sensitivity and better angular resolutions combined with these radio surveys should shed new light on the distribution of cosmic rays, the nature of the galaxy and the location and intensity of the spiral arms.

C-5

REFERENCES

- Baker, P. L. and Burton, W. B. 1975, Ap. J. 198, 281.
- Bierman, L. and Davis, L. 1960 Zs. F. Ap. 51, 19.
- Bignami, G. F. and Fichtel, C. E. 1974, Ap. J. 189, L65.
- Bignami, G. F., Fichtel, C. E., Kniffen, D. A. and Thompson, D. J. 1975, Ap. J. 199, 54.
- Burton, W. B. 1976, to be published.
- Burton, W. B., Gordon, M. A., Bania, T. M., and Lockman, F. J. 1975, Ap. J. 202, 30.
- Burton, W. B. and Gordon, M. A. 1976, submitted to Astrophysical Letters.
- Clark, D. H. and Caswell, J. L. 1976, Mon. Not. R. Astr. Soc. 174, 267.
- Daugherty, J. K., Hartman, R. C., and Schmidt, P. J. 1975, Ap. J. 198, 493.
- Fichtel, C. E., Hartman, R. C., Kniffen, D. A., Thompson, D. J., Bignami, G. F., Ugelman, H., Özel, M., and Tümer, T. 1975, Ap. J. 198, 163.
- Fichtel, C. E., Kniffen, D. A., Thompson, D. J., Bignami, G. F., and Cheung, C. Y. 1976, Ap. J. in press.
- Fuchs, B., Schlickeiser, R., and Theilheim, K. O. 1975, Proc. 14th Int. Cos. Ray Conf. 1, 83.
- Georgelin, Y.M. and Georgelin, Y.P. 1976, Astron. and Astrophys. 49, 57.
- Ginzburg, V. L. and Syrovatskii, S.I. 1964, The Origin of Cosmic Rays, (Oxford, Pergaman Press).
- Gordon, M. A. and Burton, W. B. 1976, Ap. J., to be published.
- Ilovaisky, A. and Lequeux, J. 1972, Astron. and Astrophys. 20, 347.
- Jenkins, E. B. and Savage, B. D. 1974, Ap. J. 187, 243.
- Kniffen, D. A., Hartman, R. C., Thompson, D. J., and Fichtel, C. E. 1973, Ap. J. 186, L105.

- Koch, M. W. and Motz, J. W. 1959, Rev. Mod. Phys., 31, 920.
- Kraushaar, W. L., Clark, G. W., Garmire, G. P., Borken, R., Highbie, P., Leong, V., and Thorsos, T. 1972, Ap. J. 177, 341.
- Lee, M. A. 1972, Ap. J. 183, 837.
- Parker, E. N. 1966, Ap. J. 145, 811.
- Parker, E. N. 1969, Space Science Reviews 9, 654.
- Paul, J., Cassé, M., and Cesarsky, C. J. 1974, Proc. 9th ESLAB Symposium, ESRO SP-106, 246.
- Paul, J., Cassé, M., and Cesarsky, C. J. 1975, Proc. 14th Int. Cos. Ray Conf. 1, 59.
- Pollack, J. B. and Fazio, G. G. 1963, Phys. Rev. 131, 2684.
- Ramaty, R. 1974, High Energy Particles and Quanta in Astrophysics, ed. F. B. McDonald and C. E. Fichtel (Cambridge: MIT Press), Chapter III.
- Ramaty, R. and Westergaard, N. J., 1976, "Electrons in a Closed Galaxy Model of Cosmic Rays," Astr. and Sp. Science (in press).
- Rasmussen, I. L. and Peters, B. 1975, Nature 258, 412.
- Reames, D. V. 1974, High Energy Particles and Quanta in Astrophysics, ed. F. B. McDonald and C. E. Fichtel (Cambridge: MIT Press) Chapter II.
- Schlickeiser, R. and Thielheim, K. O., 1974a, Physics Letters 53B, 369.
- Schlickeiser, R. and Thielheim, K. O., 1974b, Astron. and Astrophys. 34, 167.
- Scoville, N. Z. and Solomon, P. M. 1975, Ap. J. 199, L105.
- Share, G. H., Kinzer, R. L., and Seeman, N. 1974, Ap. J. 187, 45.
- Simonson, S. C. III 1976, Astron. and Astrophys. 46, 261.
- Spitzer, L., Drake, J. F., Jenkins, E. B., Morton, D. C., Rogerson, J. B., and York, D. V. 1973, Ap. J. 181, L116.

Stecker, F. W. 1971, Cosmic Gamma Rays, Mono (Baltimore).

Stecker, F. W. 1975, Phys. Rev. Letters 35, 188.

Stecker, F. W., Solomon, P. M., Scoville, N. W., and Ryter, C. E.
1975, Ap. J. 201, 90.

Strong, A. W., Wdowczyk, J., and Wolfendale, A. W. 1975, ed. F. W.
Stecker and J. I. Trombka (Washington: U. S. Government Printing
Office) 259.

Thielheim, K. O. 1975, Origin of Cosmic Rays, ed. J. L. Osborne and
A. W. Wolfendale, (Dordrecht-Holland, Reidel Pub. Co.), 165.

Thielheim, K. O. and Langhoff, W. 1968, J. Phys. A. (Proc. Phys.
Soc.) Ser. 2, 1, 694.

Wentzel, D. G. 1974, Ann. Rev. of Ast. and Astr. 12, 71.

GAMMA RAYS, COSMIC RAYS AND GALACTIC STRUCTURE

F. W. Stecker, Theoretical Studies Group, Goddard Space Flight Center,
Greenbelt, Maryland 20771

ABSTRACT

Working primarily from the recent SAS-2 observations of galactic γ -rays, the relation of these observations to the large scale distribution of cosmic rays and interstellar gas in the galaxy is reviewed and re-examined. Starting with a discussion of production rates, the case for π^0 decay being the predominant production mechanism in the galactic disk above 100 MeV is reestablished and it is also pointed out that Compton γ -rays can be a significant source near $l = 0^\circ$. To facilitate discussion, the concepts of four distinct galactic regions are defined, viz. the nebulodisk, ectodisk, radiodisk and exodisk. Bremsstrahlung and π^0 decay γ -rays are associated with the first two (primarily the first) regions and Compton γ -rays and synchrotron radiation are associated with the latter two regions. On a large scale, the cosmic rays, interstellar gas (primarily H_2 clouds in the inner galaxy) and γ -ray emissivity all peak in a region between 5 and 6 kpc from the galactic center. This correlation is related to correlation with other population I phenomena and is discussed in terms of the density wave concept of galactic structure. The singular nature of the HI distribution has led to the concept of population 0. The deduced cosmic-ray distribution appears to follow the supernova remnant and pulsar distributions in the galaxy. This fact, together with the fall-off of cosmic rays in the outer galaxy favors a galactic origin theory for most cosmic rays.

Correlations with arm features do not appear to be evident at longitudes $0^\circ \leq l \leq 180^\circ$. Between 180° and 360° some evidence for correlation with arm features may or may not exist but arguments against confinement of cosmic rays in spiral arms (with $I_{CR} \propto n_{gas}$) are given on the basis of γ -ray evidence, lifetime of cosmic rays, isotropy, etc. The galactic γ -ray and non-thermal radio distribution are compared with similarities and differences noted. Finally, the contribution of high-latitude γ -rays to the observed cosmic background is discussed and this contribution is shown to reasonably account for the observed spectrum of high-latitude γ -rays between 35 and 200 MeV.

1. Introduction. The pioneering work of Kraushaar, et al. (1972) with their OSO-3 satellite experiment showed that the Milky Way dominates the sky at γ -ray wavelengths and that the galactic γ -radiation is much more intense in directions toward the galactic center than away from it. With the advent of the successful SAS-2 satellite detector (Fichtel et al. 1975) we have our sharpest view yet of the galaxy in γ -rays. In addition, new data from the European COS-B satellite is now becoming available. Although we still do not have many of the answers we want regarding galactic γ -rays we are now in a position to allow us to start asking questions about what γ -ray astronomy tells us about the galaxy and to begin answering them in a cautious way. In order to find plausible answers, we must consider the new information provided by the γ -ray observations together with related information from other branches of astronomy. I will attempt here a review and reexamination of some of these questions in order to basically clarify some of the answers.

2. Data. We start with a summary of the general features of the SAS-2 observations which are as follows:

(1) On a large scale, the cosmic γ -ray radiation can be considered as consisting of two components; there is a general cosmic background radiation coming from all directions which may be cosmological in origin (Stecker 1971, 1975a, Stecker et al. 1971) and also a bright band of radiation coinciding with the galactic plane or Milky Way which is, relative to the background components, both much more intense and harder.

(2) The galactic γ -radiation is most intense in the region within $\pm 40^\circ$ from the galactic center where it is almost an order of magnitude stronger than in directions away from the galactic center.

(3) Two young nearby pulsars, viz., the Vela pulsar and the Crab Neutron pulsar (NP0532) stand out strongly in the observations at galactic longitudes 264° and 185° respectively. In addition, another γ -ray source, as yet unidentified has been reported at 193° longitude (Kniffen et al. 1975).¹

(4) There are indications of more fine-scale structure in the observations possibly due to such causes as (a) more distant discrete sources such as pulsars, (b) "hot spots" due to supernova remnants and gas clouds, and (c) possible general correlations due to spiral structure.

¹Evidence for γ -ray emission from two other pulsars, PSR 1747-46 and PSR has now been reported by the SAS-2 group (see Thompson, these proceedings). 1975-04

In order to arrive at an understanding of these observations, we must first plausibly establish what the predominant mechanism is which produces the observed galactic γ -rays. In addition to the production of γ -rays in discrete galactic objects such as pulsars, there are three main mechanisms by which high energy (greater than 100 MeV) radiation is produced by high energy interactions involving cosmic rays in interstellar space. These processes which produce what may be called "diffuse galactic γ -rays" are (a) the decay of π^0 mesons produced by interactions of cosmic ray nucleons with interstellar gas nuclei, (b) the bremsstrahlung radiation produced by cosmic-ray electrons interacting in the Coulomb fields of nuclei of interstellar gas atoms, and (c) Compton interactions between cosmic ray electrons and low energy photons in interstellar space.

3. Production Mechanisms and Spectra. For the γ -ray region above 100 MeV, it is easy to show that π^0 decay γ -rays dominate over bremsstrahlung γ -rays in the galaxy since one knows the relevant cross sections and the estimates of the cosmic ray electron-nucleon ratio are good enough for this conclusion to be reached (Stecker 1968, 1971, 1975). (Of course, the reverse is true for lower energy γ -rays since the π^0 decay differential spectrum turns over at ~ 70 MeV.) The above conclusion is valid independent of the gas density distribution in the galaxy if the cosmic ray electrons and nucleons have similar distributions since both production processes are proportional to the total gas density. Thus, one would therefore expect similar γ -ray emissivity distributions in the galaxy in both cases.

Using recent estimates of the demodulated cosmic-ray electron spectrum in the solar vicinity of the galaxy (Goldstein, et al. 1970, Daugherty et al. 1975, Daniel and Stephens 1975) and a canonical total mean hydrogen density in the solar vicinity of $n_H = 1 \text{ cm}^{-3}$, the integral and differential production rates of γ -rays at 10 kpc from the various processes have been calculated and are shown in Figures 1 and 2. The π^0 decay production rate is taken from Stecker (1970). The bremsstrahlung and Compton production rates have been calculated using the formulas for a KE^{-1} differential electron spectrum

$$q_B(E_\gamma) = \frac{4.33 \times 10^{-25}}{\Gamma - 1} n_H KE^{-\Gamma} \text{ cm}^{-3} \text{ s}^{-1} \text{ MeV}^{-1} \quad (1)$$

and

$$q_c(E_\gamma) = \frac{8\pi}{3} \sigma_T \rho_{ph} (m_e c^2)^{1-\Gamma} \left(\frac{4}{3} \langle \epsilon \rangle \right)^{(\Gamma-3)/2} KE_\gamma^{(\Gamma+1)/2} \quad (2)$$

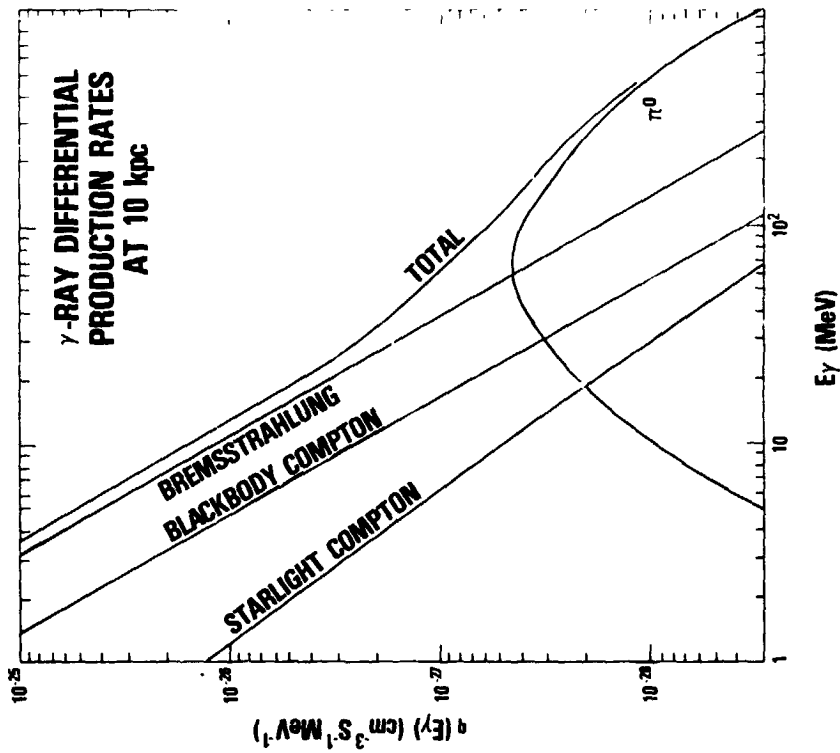


Figure 2. Local galactic γ -ray differential production rate for a total gas density of 1 atom per cm^3 and starlight radiation density of 0.44 eV/cm^3 . The π^0 -decay rate is from Stecker (1970).

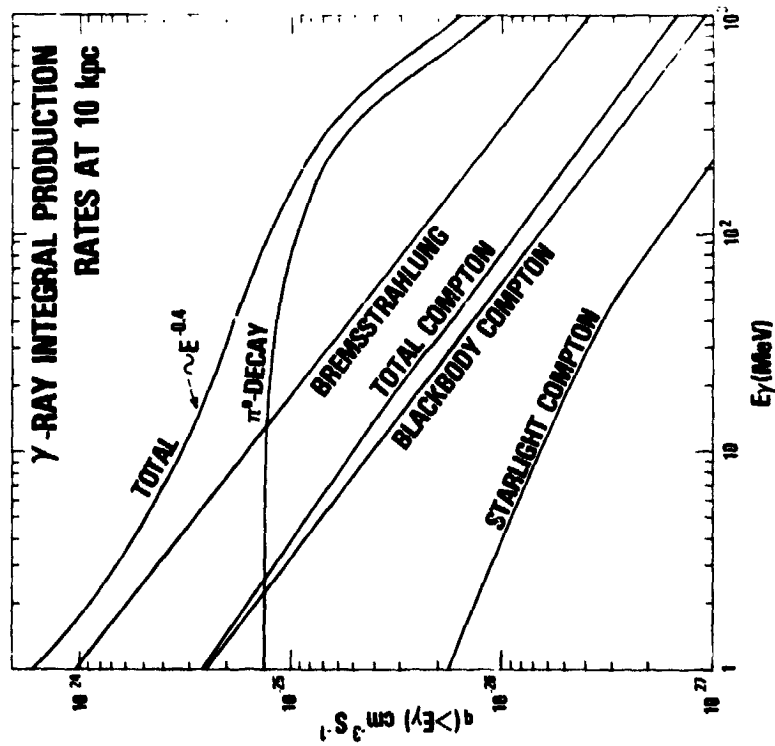


Figure 1. Local galactic γ -ray integral production for a local total gas density of 1 atom per cm^3 and starlight radiation density of 0.44 eV/cm^3 . The π^0 -decay rate is from Stecker (1970).

(see, e.g. Ginzburg and Syrovatskii 1964, Stecker, 1971, 1975a). The bremsstrahlung rate is given specifically for the cosmic mixture of H and He based on the cross sections for these elements given by Dovzhenko and Pomanskii (1964). In the equations n_H is the hydrogen atomic density, σ_T is the Thomson cross section equal to $6.65 \times 10^{-25} \text{ cm}^2$, ρ_{ph} is the photon energy density and $\langle \epsilon \rangle$ is the mean photon energy such that

$$\frac{4}{3} \langle \epsilon \rangle = 3.1 \times 10^{-4} T(\text{eV}) \quad (3)$$

Equations (1) and (2) are accurate to within a few percent. For the Compton process, Ginzburg and Syrovatskii (1963) give a correction factor $f_c(\Gamma)$ dependent on the differential electron spectral index Γ , such that $f_c(2) = 0.86$, $f_c(3) = 0.99$ and $f_c(4) = 1.4$. For bremsstrahlung, using the formulas given by Blumenthal and Gould (1970), I find the correction factor to be

$$f_B \approx 1 - \frac{2}{3} \frac{(\Gamma - 2)}{\Gamma(\Gamma + 1)} \quad (4)$$

so that $f_B(2) = 1$, $f_B(2.5) = 0.96$ and $f_B(3) = 0.94$. (The local bremsstrahlung rate calculated here is similar to that given by Fichtel et al. (1976) and Ramaty and Westergaard (1976)). The Compton production rate was calculated for a 2.7K blackbody background and a two component starlight model of total radiation density 0.44 eV cm^{-3} (Allen 1973) consisting of a 10^4 K graybody component of energy density 0.22 eV cm^{-3} and a $5 \times 10^3 \text{ K}$ graybody component of equal energy density 0.22 eV cm^{-3} (Lillie, quoted by Greenberg 1971). The 10^4 K component will hereafter be referred to as the Population I component since it is due primarily to Population I stars and the $5 \times 10^3 \text{ K}$ component will be referred to as the Population II component. Although these components contribute approximately equally at a galactocentric distance of 10 kpc, it is expected that the Population I component will be negligible at the galactic center region, which, we will see, is the only region where Compton interactions are expected to play a significant role (Stecker et al 1975).

The Population I component produces a break in the starlight Compton spectrum at a critical energy $E_{C,I} \approx 60 \text{ MeV}$, for the Population II component, $E_{C,II} \approx 30 \text{ MeV}$. The total starlight Compton spectrum is shown in the figures.

A comparison of the pion-decay and Compton processes throughout the galaxy is not as straightforward as the comparison with bremsstrahlung since, in this case, the Compton process scales like the low-energy photon density in

the galaxy whereas the pion-decay process scales like the gas density distribution. There is also the possibility, pointed out by Cowsik and Voges (1975), that Compton production takes place throughout a greater volume of the galaxy since starlight is expected to exist at higher distances from the galactic plane than gas. Therefore, for the purposes of further discussion, I will introduce the useful concepts of various galactic disk regions with different thicknesses as shown in Figure 3. These disks are defined as follows:

(a) The nebulodisk is defined as the region where most of the dust clouds and molecular clouds are found. Its thickness is of the order of 130 pc (Scoville and Solomon 1975, Burton and Gordon 1976).

(b) The ectodisk is the domain of the more diffuse atomic hydrogen (HI). Its thickness is of the order of 260 pc (Burton et al. 1975).

(c) The radiodisk, about 500 pc thick, is the region from which most of the synchrotron emission in the galaxy originates according to the interpretation of Ilovaisky and Lequeux (1972) of the 150 MHz data of Landecker and Wieblinski (1970). For conceptual purposes, I will consider this as the diffusion-trapping region of most cosmic rays. Trapping in a more extensive "halo" will tend to wipe out radial gradients in the cosmic-ray intensity which are necessary to an explanation of the γ -ray measurements (Stecker 1975b, Dodds et al. 1975, Stecker et al. 1975), as will be discussed in more detail in section 8. In any case, recent observations appear to rule out significant trapping in a halo-type region (Webster 1975).

(d) The exodisk, here tentatively identified with a disk about 2 kpc thick from which some synchrotron emission is also occurring according to the interpretation of Ilovaisky and Lequeux. I call this the exodisk because cosmic rays may be escaping from the galaxy primarily from this region (see the discussion of Jokipii 1976).

Using this language, γ -rays from bremsstrahlung and pion decay originate in the nebulodisk and ectodisk whereas those from Compton scattering originate in the radiodisk and exodisk. Even so, the theoretical estimates shown in Figures 1 and 2 indicate that in typical regions of the galactic disk (excluding the galactic nuclear region we will be discussing separately) pion-decay dominates over Compton scattering even if the Compton-producing disk is an order of magnitude thicker than the gas disk. Furthermore, the latitude distribution of galactic γ -rays obtained by SAS-2 shows that the galactic γ -ray disk is thinner than the radiodisk whereas dominant Compton production would imply that the γ -ray disk should be comparable in width to the radiodisk. Stronger evidence for the thinness of the γ -ray disk has been reported by Samami et al. (1974)

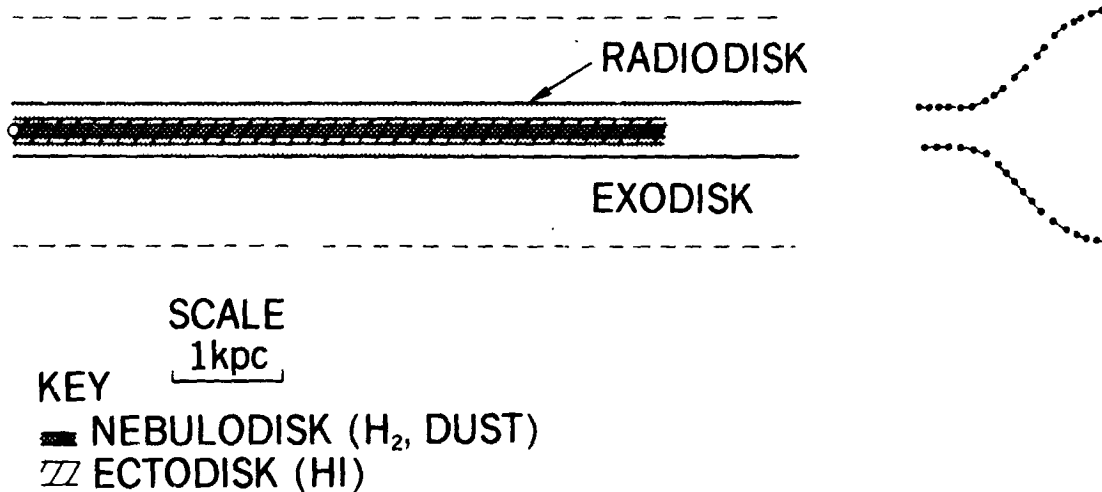


Figure 3. Regions of the galaxy as defined in the discussion given in the text.

which place this width at 3° whereas the SAS-2 resolution can only place an upper limit of about 1° on this width.² The asymmetry in the latitude distributions of γ -rays in the center and anticenter directions is further found to correlate well with the gas distribution again arguing for the dominance of pion-bremsstrahlung processes (Fichtel et al. 1975, Stecker et al. 1975, Puget et al. 1976).

4. Compton γ -Rays from the Galactic Center. The observed angular distribution of galactic γ -rays does not exclude the possibility of a significant Compton component being produced near the galactic center which is far enough away so that only a small angle is subtended by the galactic bulge. With a half angle of 0.1 rad ($\sim 5^\circ$), a source of 2 kpc thickness will be consistent with the γ -ray observations at the galactic center. Assuming that the starlight radiation density varies as the total mass distribution of Perek (1962) as suggested by Cowsik and Voges (1974), but with the radiation density at 10 kpc taken to be 0.44 eV/cm^3 (Allen 1973), I have recalculated the galactic Compton γ -ray flux as a function of galactic longitude assuming a cosmic-ray electron flux equal to its value at 10 kpc. The results are shown in Figure 4 for two different values of the γ -ray disk half-width h as indicated. For γ -ray production in the inner galaxy, where the detector beam covers the whole source, the line intensity is simply proportional to h and is given by

$$I_\gamma(\ell) = \frac{h \cos \ell}{2\pi} \int_{\sin^2 \ell}^{(R_m/10)^2} \frac{2x dx Q_\gamma(x)}{(1-x^2)(x^2 - \sin^2 \ell)^{1/2}} \text{ where } x = R/10. \quad (5)$$

R is the galactic radius in kpc and R_m is taken to be ~ 9 kpc. (Puget and Stecker 1974).

²The COS-B results in the 300-2000 MeV range reported here place an upper limit of 4° on this width.

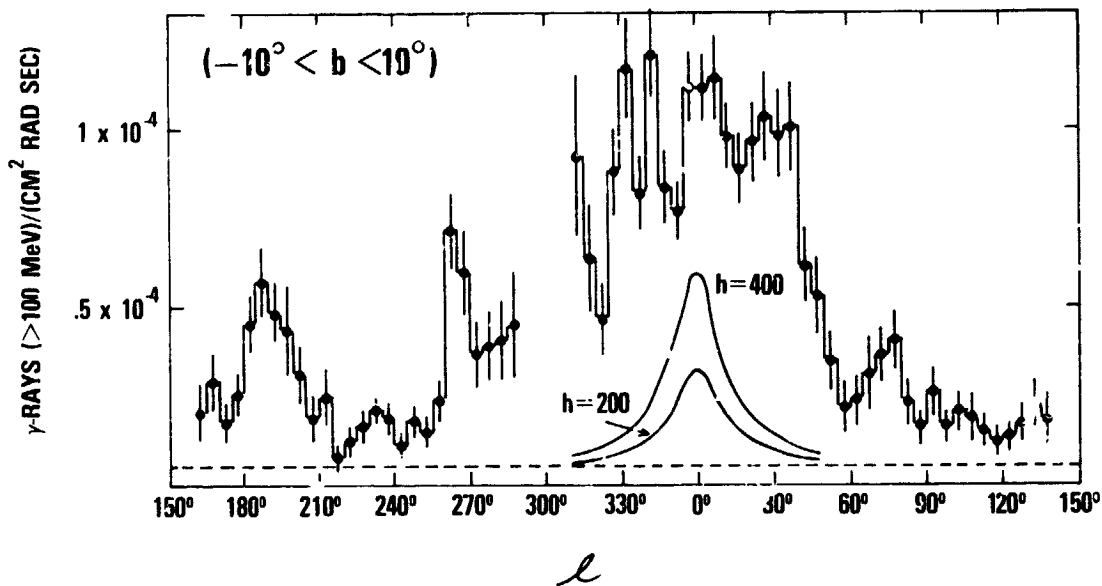


Figure 4. Compton production rate calculated using the method of Puget and Stecker (1974) for two values of half-thickness of the production disk $h = 200$ pc and 400 pc. These rates are shown together with the SAS-2 data reported by Fichtel et al. (1975).

It can be seen that, given an increased cosmic-ray electron intensity near the galactic center or a large enough value of h , it is possible for Compton scattering to provide a significant, or even major portion of the γ -ray flux near the galactic center as suggested by Cowsik and coworkers, contrary to the conclusions of Shukla et al. (1975). However, at longitudes less than 10° or 15° from the galactic center, the Compton contribution to the galactic γ -ray flux becomes relatively unimportant. This calculation is essentially in agreement with that of Dodds et al. (1975) for $h = 115$ pc. Stecker et al. (1975) pointed out that because of the relative lack of both HI and H_2 gas inside of 3 kpc (except at the galactic nucleus) not enough pion-decay and bremsstrahlung γ -rays could be produced to account for the flux at the galactic center but pointed out that the inclusion of Compton γ -rays could adequately account for the observed flux distribution and intensity.

One may ask whether the observed spectrum of γ -rays coming from the galactic center region can tell us the production source. Using a 5×10^3 K (Population II) photon field in the central region of the galaxy, and based on the radio synchrotron data, one would expect a differential γ -ray spectral index of 1.8 from Compton produced γ -rays in the 35-200 MeV energy range. The pion-bremsstrahlung spectrum shown in Figures 1 and 2 has an average index of 1.4 in this energy range. The observations (Fichtel et al. 1975) yield a mean index of about 1.65 ± 0.25 which is, unfortunately, not accurate enough to tell us whether Compton or pion-bremsstrahlung γ -rays provide the dominant contribution.

5. γ -Rays in the Galactic Disk. As was discussed earlier, it is expected that cosmic-ray-gas interactions (pion-bremsstrahlung) are more important than Compton interactions in producing γ -rays in most of the galactic disk. There remains the question of whether most of the galactic γ -rays are produced by diffuse processes or point sources. Here, the lines are not clearly drawn but two arguments seem to favor diffuse processes (a) only three significant point sources have been found by SAS-2, two of which are relatively nearby pulsars; moreover they have steeper spectra than the general galactic γ -radiation, and (b) by analogy with the case of the nonthermal radio radiation from cosmic ray electrons in the galaxy, one may argue that it is expected that the γ -rays also should be produced mainly by cosmic rays after they have left their sources and are in interstellar space rather than when they are still at the source (Lequeux 1971).

Since, therefore, it is most likely that most galactic γ -rays with energy above 100 MeV result from the decay of π^0 -mesons which were produced in interstellar interactions of cosmic-ray nucleons with interstellar gas nuclei, it follows that by studying the γ -ray emissivity distribution in the galaxy, one may learn about the distribution of cosmic-rays, mainly 1-10 GeV protons (Stecker 1973), and gas in the galaxy. We thus turn our attention, in the rest of this article, to a discussion of the implication of the SAS-2 observations of galactic γ -rays for determining new information about the distribution and origin of cosmic rays and about the structure and composition of the galaxy.

It was first deduced by Stecker et al. (1974) (later supported in calculations by Puget and Stecker (1974), Strong (1975), and Puget et al. (1976)) that the SAS-2 observations imply that γ -ray emission is highly nonuniform in the galaxy and that the emissivity distribution peaks in the region of the galaxy about halfway between the sun and the galactic center. My analysis of the latest version of the SAS-2 data with more events and smaller longitude bins (see paper of Kniffen, these proceedings) using the method of Puget and Stecker (1974) places this peak emissivity in the region between 5 and 6 kpc from the galactic center for the positive longitude side of the galaxy ($0^\circ \leq l \leq 180^\circ$) and at ~ 5 kpc for the "negative" longitude side ($180^\circ \leq l \leq 360^\circ$) (See Figures 5 and 6 and section 7). The correlation between the CO and γ -ray distribution is excellent for the range $0^\circ \leq l \leq 180^\circ$; unfortunately, there is presently no CO data yet available for the range $180^\circ \leq l \leq 360^\circ$. The new γ -ray unfolding is in good agreement with that of Puget et al. (1976) for the range $0^\circ \leq l \leq 180^\circ$, however there are some differences in the range $180^\circ \leq l \leq 360^\circ$ due mainly to differences in the data used and the subtraction of a pulsar contribution at 345° .

It was noted by Solomon and Stecker (1974) that the γ -ray emissivity distribution bears a strong similarity to the distribution of molecular clouds in the

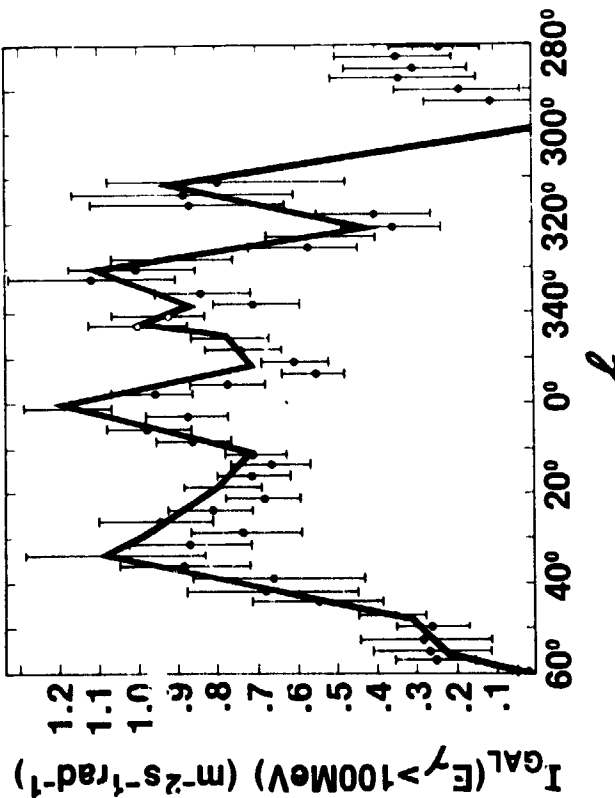


Figure 5. Most recent SAS-2 longitude data with more events reported in 2.5° longitude bins shown for the inner region of galactic longitude with the two points shown by the open circles having the contribution of pulsar PSR 1747-46 subtracted out (Kniffen, personal communication). The solid line shows the approximation to the distribution used in the unfolding calculation, the results of which are given in Figure 6.

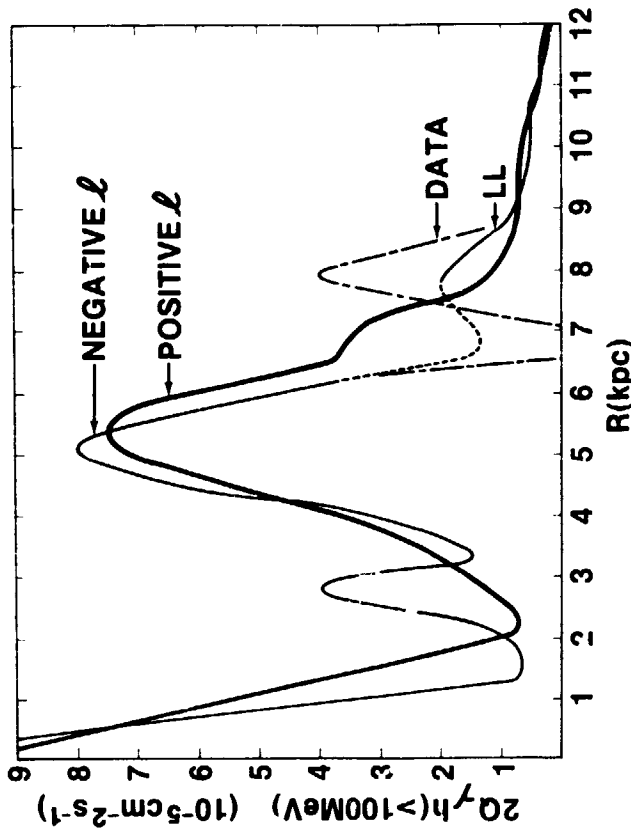


Figure 6. Radial distribution of galactic γ -ray emission obtained from unfolding the longitude distribution of Figure 5 for the ranges $0^\circ \leq l \leq 180^\circ$ (positive longitudes and $180^\circ \leq l \leq 360^\circ$ (negative longitudes). For negative l , the unfolding using the data points in the range $310^\circ \leq l \leq 317.5^\circ$ is shown by the dot-dashed curve; that obtained using the lower limits to the statistical error bars is shown by the curve marked LL. The emissivity at the galactic center ($R = 0$) is approximately $1.5 \times 10^{-4} \text{ cm}^{-2} \text{ s}^{-1}$.

galaxy which also peaks in the 5 to 6 kpc region (Scoville and Solomon 1975, Burton et al. 1975). This similarity, coupled with the lack of enough gas in atomic form to explain the γ -ray measurements led to the supposition that H_2 is far more abundant in the inner galaxy than HI and that H_2 plays the major role in producing galactic γ -rays (Solomon and Stecker 1974, Burton et al. 1975, Stecker et al. 1975). In fact a γ -ray emissivity which scales like the more uniform HI distribution will not explain the observations. An alternative explanation for the γ -ray observations is to assume that the cosmic rays increase by more than an order of magnitude in intensity in the inner galaxy (Stecker et al. 1974) but this alternative encounters difficulties in producing instability in the galactic gas disk (Wentzel et al. 1975). The remaining problem has been to determine the absolute amount of H_2 in the galaxy as well as its distribution. This can be estimated both by using the UV observations of H_2 in the local galactic neighborhood as typical of the H_2 at a galactocentric distance of 10 kpc and by using the infrared and x-ray absorption measurements in the direction of the galactic center to estimate the total column density of gas in that direction. Stecker et al. (1975) used the data shown in Table 1 to estimate a total column density of $\sim 7 \times 10^{22} \text{ cm}^{-2}$. Gordon and Burton (1976) worked directly from their CO data to determine the H_2 density. Both these methods yield consistent results and indicate that the volume averaged density of H_2 is of the order of 2 molecules per cm^3 in the 5 to 6 kpc region (Stecker et al. 1975, Gordon and Burton 1976) and drops off dramatically inside of 4 kpc and in the outer galaxy. At 10 kpc, at least half of the interstellar gas is probably in atomic form and there is a negligible amount of H_2 in the outer regions of the galaxy (Scoville and Solomon 1975, Burton et al. 1976). The gas distributions obtained are shown in Figures 7 and 8. A subsequent deduction of the implied cosmic ray distribution indicates that the cosmic rays increase (relative to the local intensity) by about a factor of two (Stecker et al. 1975) or slightly more (Puget et al. 1976) at a maximum coinciding with the maximum in the gas density in the 5 to 6 kpc region and that the cosmic rays drop off rather rapidly in the outer galaxy (Stecker et al. 1975, Dodds et al. 1975). Dodds et al. (1975) have calculated the latitude distribution of γ -rays in detail under the "extragalactic" hypothesis (uniform cosmic ray intensity) and "galactic" hypothesis (reduced cosmic ray intensity in the outer galaxy) and compared the results with the SAS-2 observations as shown in Figure 9.

Stecker (1975b) has shown that the cosmic-ray distribution deduced using the γ -ray observations in conjunction with the deduced variation of total gas (HI + H_2) in the galaxy is, within experimental error, identical to the distribution of supernova remnants (Ilovaisky and Lequeux 1972, Kodaira 1974) and pulsars (Lyne 1974, Hulse and Taylor 1975, Sieradakis, these proceedings). The similarity of the deduced cosmic ray distribution and the distribution of supernova remnants provides our strongest evidence to date that the observed cosmic ray nucleons, which make up 99% of the cosmic rays, originate in galactic supernovae either in the explosion or the resulting pulsars. It supports other evidence

Table 1. Column Densities of Hydrogen at $l = 0^\circ$ Excluding the Galactic Nucleus ($\times 10^{-22}$) (cm^{-2}) ($N_{\text{G.C.,}\odot}$)

$\langle N_{\text{HI}} \rangle$	$\gtrsim 0.6$ to 1.5	Daltabuit and Meyer (1972)
from 21 cm radio	~ 2	Kerr and Westerhout (1965)
	≤ 1.2	Clark (1965)
$\langle 2N_{\text{H}_2} \rangle$	3 to 10	Scoville and Solomon (1975)
from CO		
$\langle 2N_{\text{H}_2} + N_{\text{HI}} \rangle$	$\lesssim (11.5 \pm 2)$	this work ($I_{\text{CR}} \gtrsim I_\odot$)
from SAS-2 γ -ray flux		
$\langle 2N_{\text{H}_2} + N_{\text{HI}} \rangle$	6.5 to 9	$\sigma_{\text{H}_2}/2\sigma_{\text{HI}} \leq 1.7$ (Kaplan and Markin 1973) as verified by the measurements of Crasemann et al. (1974).
from x-ray absorption		
$\langle 2N_{\text{H}_2} + N_{\text{HI}} \rangle$	5 to 7.5	Ryter, et al. (1975)
from IR absorption		

from measurements of abundance ratios of heavy nuclides (see, e.g. Reeves, 1975).

Figure 9 shows the rough distributions of supernova remnants and total gas in the galaxy and Figure 10 shows the implied γ -ray longitude distribution calculated by Stecker (1975b) with Compton interactions included at the galactic center. Also shown is the observed longitude distribution (Fichtel et al. 1975).

6. Implication of the Large-Scale Galactic Distributions. On an overall large scale, there appears to be an excellent correlation between several important constituents of the galaxy in terms of their distributions as a function of galactocentric distance. These constituents are molecular clouds, HII regions (ionized hydrogen), cosmic rays, γ -rays, supernova remnants and pulsars. All of these constituents of the galaxy seem to be most dense in the 5 to 6 kpc region and appear to drop off sharply inside of 4 kpc and in the outer galaxy. They all can be associated with the formation and evolution of the so-called Population I stars in the galaxy and are known to have a Population I distribution. They are associated with the formation and destruction of hot young O and B stars in the galaxy which delineate arms in other spiral galaxies. That the correlation of

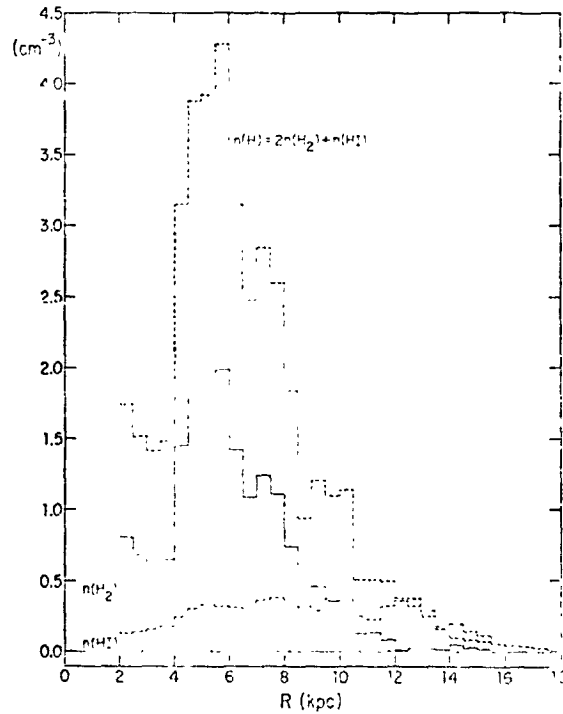


Figure 7. Volume density of interstellar hydrogen as a function of galactic radius given by Gordon and Burton (1976).

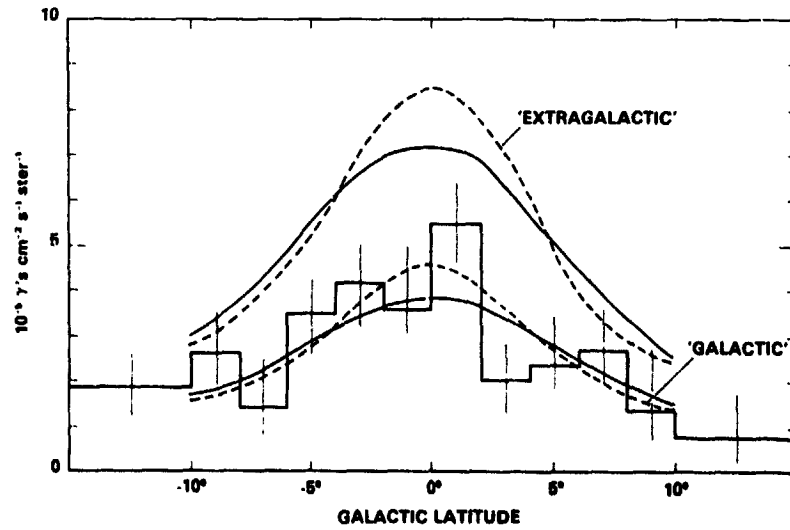


Figure 8. Calculated galactic latitude distributions of γ -rays for the "extragalactic" (uniform cosmic-ray flux) and "galactic" (falloff of cosmic rays in the outer galaxy) hypotheses as given by Dodds et al. (1975) together with SAS-2 data of Fichtel et al. (1975).

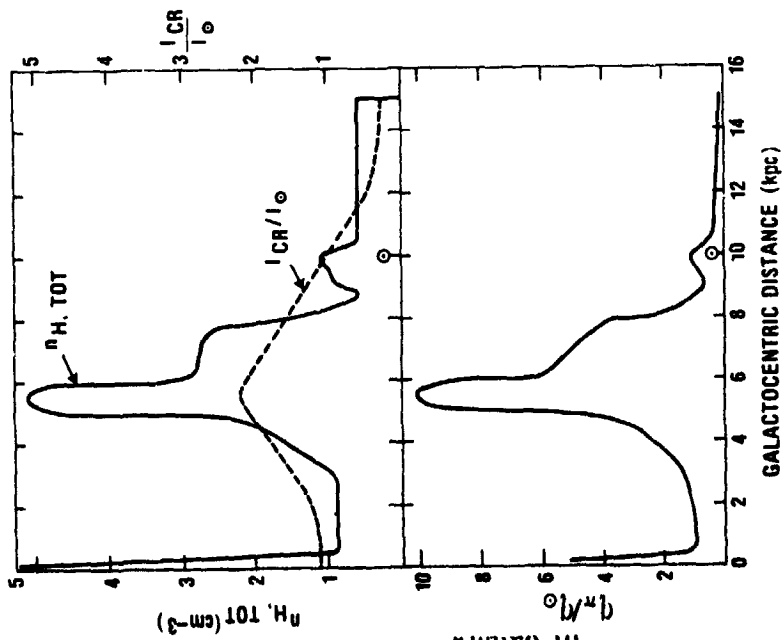


Figure 9. Volume density of interstellar hydrogen given by Stecker (1975) as deduced using the CO data of Scoville and Solomon (1975) together with the relative large-scale galactic cosmic-ray distribution, assumed proportional to the supernova remnant distribution deduced by Kodaira (1974) (top); the implied relative γ -ray emissivity from π^0 -decay is also shown (bottom).

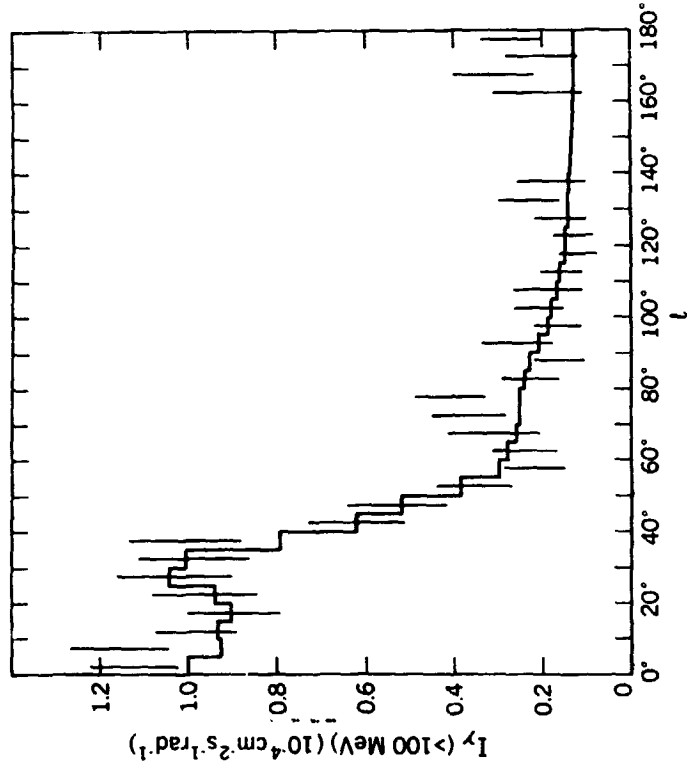


Figure 10. Longitude distribution of galactic γ -rays for $-10^\circ \leq b \leq 10^\circ$ averaged over 5° intervals calculated using the π^0 -decay emissivity distribution given in Figure 9 and including effect of bremsstrahlung from secondary electrons and Compton γ -rays at the galactic center (Stecker 1975). The Compton contribution at the galactic center, calculated using a local electron flux and a value of $h = 100$ pc, may be underestimated. The calculations are only valid for $0^\circ \leq l \leq 180^\circ$ and are shown by the histogram together with the data given by Fichtel et al. (1975), shown by the vertical lines.

figure 10.

these components is natural can be seen in Figure 11. The gravitational collapse of molecular clouds is expected to lead to the formation of OB associations containing the massive, hot, short-lived O and B stars whose ultraviolet radiation causes the formation of zones of ionized gas around them (HII regions). The massive O and B stars, after a few million years, terminate their existence as supernovae which in turn leads to the generation of cosmic rays. It has also been suggested that the supernova explosions can trigger the formation of new OB associations in a feedback effect (Öpik, 1953, Ögelman and Maran 1975). The compound effect of cosmic rays and molecular clouds being enhanced in the same region of the galaxy then leads to an even stronger enhancement in the γ -ray emissivity in the enhanced region. In addition, an increase in the flux of sub-relativistic cosmic rays may help lead to an additional increase in the amount of ionized gas in the region around 5 kpc as indicated in recent surveys (Mezger 1970, Lockman 1976).

As a final note, Hayakawa et al. (1976) have recently reported a correlation between their observed $2.4 \mu\text{m}$ infrared flux and CO emission on a galactic scale. The shape of the longitude distribution given by Hayakawa et al. (see Figure 12) implies a strong maximum near 5 kpc which, one can argue, points to the emission originality in very young Population I objects. Thus, one may speculate that a major contribution comes from circumstellar shells surrounding pre-main sequence stars such as T Tauri stars or close surrounding Be stars (see e.g., the review of Neugebauer, et al. 1971). A similar galactic distribution of diffuse far-infrared ($100 \mu\text{m}$ - $300 \mu\text{m}$) emission originating in dust in molecular clouds has been predicted by Fazio and Stecker (1976).

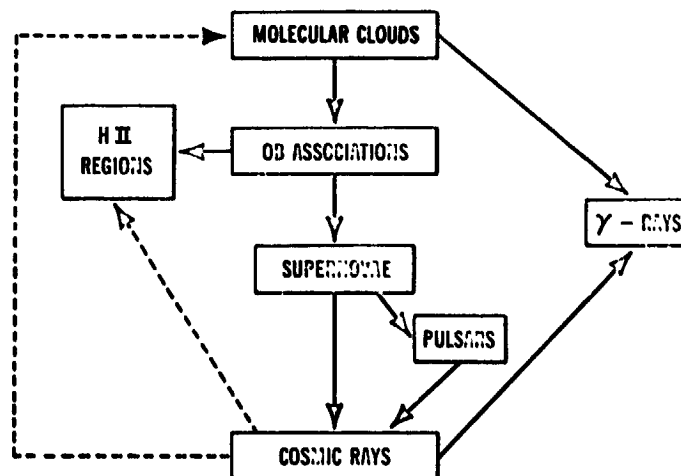


Figure 11. Plausible generic relations between various "Population I" galactic constituents (Stecker 1976).

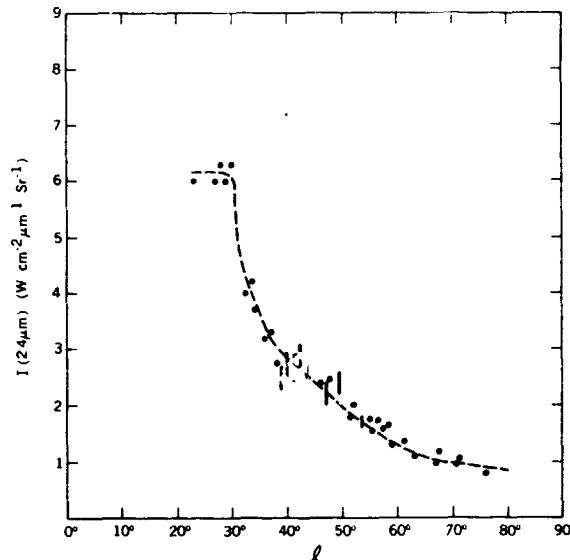


Figure 12. Galactic longitude distribution of 2.4 μm infrared mission reported by Hayakawa et al. (1976).

Whereas all of the components of the galaxy just discussed have correlated large-scale galactic distributions with maximum densities in the 5 to 6 kpc region, 21 cm radio observations of HI indicate a relatively constant overall density distribution of atomic hydrogen between 4 and 14 kpc from the galactic center with no evidence for a significant enhancement in the 5-6 region (Kerr and Westerhout 1965, Burton et al. 1975). This implies that the H_2 distribution is much more sensitive to the compression effects expected in density wave models of galactic structure than the more diffuse HI with the ratio H_2/HI having a radial galactic dependence somewhat similar to that of HII/HI as discussed by Shu (1973).

The density wave models have the attractive feature of explaining the persistence of spiral arms in galaxies over time periods for which the differential rotation of these galaxies would destroy material arms. In these models, a spiral perturbation on the overall gravitational field of a galaxy results in excess gas accumulating in troughs of gravitational potential where star formation will then preferentially take place leading to the young OB associations and associated HII regions which stand out in optical surveys of external galaxies and delineate spiral arms. In this case then, one is only seeing the wave of new star formation rather than the real bulk of existing stars (approximately 95% as they move around the galactic center. The density wave models provide a plausible framework in which to consider the structure of spiral galaxies, but they are not complete in that they do not explain the origin of the spiral wave pattern itself

or the energy input required to maintain it. In the context of the density wave theories, however, a crowding of the wave pattern and an increase in the frequency of gas shocking in the region of the inner arms would naturally lead to an increased density of molecular clouds, young stars, supernovae and HII regions in the 5 to 6 kpc region. The question of the details of spiral structure in the Galaxy is, however, more difficult. Our Galaxy apparently shares with other spiral galaxies a lack of gas of all types in the innermost region (radius less than 4 kpc with the exception of the galactic nucleus). Similar structural characteristics have been found in other spiral galaxies (Roberts 1974).

However, there is a large variation in structural details among spiral galaxies. This range of detail, from those with long thin well developed arms and high surface brightness (van den Bergh type I) to those with only a bare hint of arm structure (van den Bergh type V) has been incorporated into the general framework of density wave theory by Roberts et al. (1975). The galaxies with well developed arms and high surface brightness with an implied high star formation rate are found to satisfy the condition $(W_{10}/a) > 1$ where W_{10} is the velocity component of basic rotation normal to the spiral arms and a is the effective acoustic speed of the interstellar gas. Within galaxies themselves there can exist in the inner regions, zones of strong nonlinear compression where $(W_{10}/a) > 1$ and in the outer regions, zones of weak linear compression where $(W_{10}/a) < 1$ Burton (1976) has estimated the interface between these two zones in our own Galaxy to occur at a galactocentric radius $R \sim 10$ kpc (see paper of Roberts, these proceedings).

Figure 13 shows the smoothed radial distribution of mean surface density of the atomic and molecular components of interstellar gas in our Galaxy based on recent data of Burton et al. (1975) where the H_2 density is normalized according to the methods of Stecker et al. (1975) with a scale height of ~ 65 pc for the molecular clouds (Scoville and Solomon 1975, Burton and Gordon 1976). Also shown are the regions of weak and strong compression. It can be seen that the transition region near 10 kpc is one in which the total surface density is roughly constant but where larger and larger amounts of gas are converted from HI to H_2 as R decreases.

All of these recent observational and theoretical developments regarding galactic structure³ prompted Stecker (1976) to suggest the following changes in the Baade (1944) classification scheme for galactic objects:

(I) The classification "Population II" which consists of old disk stars ("high velocity" stars) nuclear bulge stars, halo stars and globular cluster stars stays the same.

³See also the summary and discussion of Burton (1976).

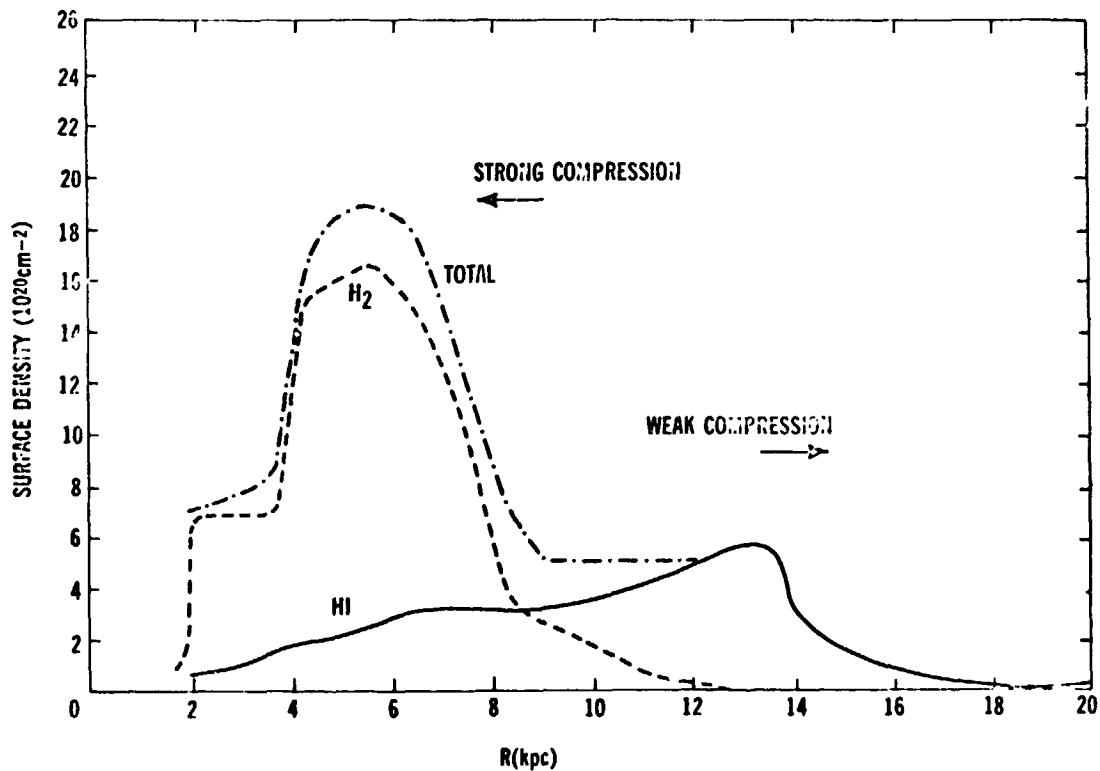


Figure 13. Surface density distribution of HI, H₂ and total gas, derived as described in the text, shown with regions of weak (linear) and strong (nonlinear) density wave compression as determined by Burton (1976). The figure is from Stecker (1976).

(II) The classification "Population I" should be expanded to include all galactic objects narrowly confined to the galactic plane and associated with the formation of Population I stars. Thus the set of galactic population I objects will include molecular clouds, OB associations, HII regions, dark nebulae, dust, supernovae and even associated radiation fields such as infrared (Fazio and Stecker 1976) synchrotron and π^0 -decay γ -radiation from molecular clouds. This population is expected to predominate in regions of the galaxy where $(W_{10}/a) > 1$ (strong compression).

(III) I define a new population class, "Population 0" consisting of the more diffuse atomic hydrogen which is now considered not to play a primary role in star formation. (In the case of some of the denser HI clouds there may be some blurring of definition). This population will be important in regions where $(W_{10}/a) < 1$ (weak compression). The main distinction between population 0 and I stems from the effects of compression and with the higher compression stemming from the nonlinear density waves. Two basic differences between the

galactic distributions of the population I and Population 0 components are shown in Table 2.

Table 2

Population	Scale height perpendicular to plane	Galactocentric Radius of Maximum Surface Density
Population I	~ 50 to 70 pc (nebulodisk)	5 to 6 kpc
Population 0	≥ 110 pc (ectodisk)	12 to 13 kpc

The population I component is thus associated with the nebulodisk and the population 0 component with the ectodisk. It is found that in late-type spiral galaxies it is characteristic for the neutral hydrogen density to peak well outside the visible radius of the galaxy. (Roberts 1974). This is illustrated by Figures 14 and 15 from the work of Rots and Shane (1975) which shows clearly that for M81 the 21 cm emission peaks outside the optical disk of the galaxy. The above classification, with population 0 removed from a primary role in the star formation process, naturally accommodates this hitherto somewhat mysterious fact.



Figure 14. Optical image of M81 together with 21 cm contours (Rots and Shane 1975).

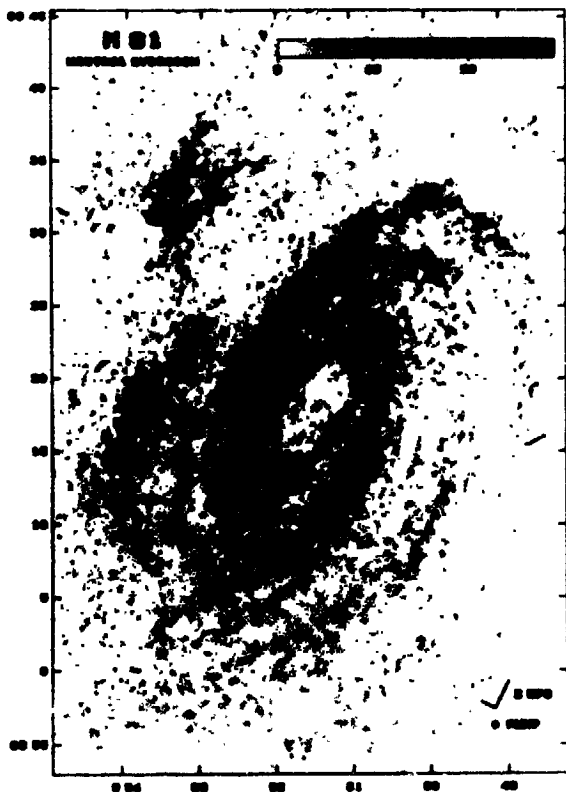


Figure 15. 21 cm radio map of M81 showing regions of neutral atomic hydrogen. The scale is the same as for Figure 14. It can be seen that the peak HI density lies at the outside of the optical image of the galaxy. (Rots and Shane 1975.)

7. Spiral Features and "Solid Arm" Models. As has been discussed above, there is a large variation in structural details among spiral galaxies, ranging from a bright and well defined arm structure (the so-called grand design) in galaxies such as M51 and M101, to the more crowded complex and nondescript features of galaxies such as M33. (Roberts, et al. 1975, Sandage 1961). In the latter cases, ordered spiral features extending over distances of the order of several kpc would be difficult, if not impossible to determine from a point within the galactic disk.

This brings us to the question of what can be learned about the "small scale" structure of the galaxy (i.e. spiral density perturbations) from the recent γ -ray observations.

In considering the question of looking for evidence of spiral structure in the γ -ray observations, two points must be kept in mind: the limited resolution of the SAS-2 telescope and the ambiguous interpretation of data from other types of astronomical observations as to the character of the spiral features of our Galaxy (Simonson 1970, Burton 1974). Burton (1974) has pointed out that 21 cm features associated with spiral arms could be due mainly or in part to kinematic

effects. In addition, while the overall distribution of "Population I" material can be understood in terms of density wave models of the Galaxy, one is on much shakier ground when it comes to analyzing the detailed structural features such as reconstructing spiral arms.

Attempts have been made to interpret the SAS-2 γ -ray data based on grand-design spiral models of the galaxy (Simonson 1976) with large arm-interarm ratios of both gas and cosmic rays (Bignami and Fichtel 1974), Bignami et al. 1975, Paul et al. 1976).

Because of the lack of CO data at negative longitudes, Bignami et al. constructed models based on 21 cm studies of atomic hydrogen. These models did not fully utilize the emerging implications of recent molecular cloud observations with regard to the galactic H_2 component in the inner galaxy. The models of Bignami et al. had therefore required unrealistically high amounts of HI at locations which have been attributed to arm features (see Figure 16) and proportionally large amounts of cosmic rays relative to the solar intensities ($I_{CR} \propto n_H$) in order to obtain fluxes of γ -rays to compare with the observations in the range $|\ell| \leq 40^\circ$. These models also assumed that H_2 was proportional to HI everywhere in the galaxy so that $(n_{H_2} + n_{HI})/n_{HI} = K$ with (in the recent model of Bignami et al. (1975)) $K = 2$. Then since the γ -ray emissivity is proportional to the product $I_{CR} n_H$ with I_{CR} assumed proportional to n_H , $I_\gamma \propto (Kn_{HI})^2 \propto 4n_{HI}^2$. With this sensitive density dependence, the assumptions about n_{HI} shown in Figure 16 with $\langle n_{HI} \rangle$ above the recently observed values took on critical importance. Therefore, Kniffen et al. (these proceedings) have reexamined this model including the implications of the recent CO data. The model of Paul et al. (1976) has sought to relate the radio data to the γ -ray data by making the additional assumptions $I_{CR} \propto I_e \propto n_H \propto B^2$. They themselves point out, however, that the b distribution of the radio-synchrotron and γ -ray emission are different (see Figure 17). Also, there is only a rough relation between the longitude distributions of the two components which mainly reflects the overall structural features discussed earlier (see also section 9).

Passing on then from specific spiral arm models one may still consider the general question of whether the γ -ray observations provide evidence of spiral features. In this context, I previously noted that the expanding "3 kpc" arm, observed by its distinct separation on velocity-longitude plots of both HI and CO emission, has insufficient material either in atomic or molecular form to account for the largest peak in the observed galactic γ -ray distribution at $340^\circ \leq \ell \leq 345^\circ$ shown in Figure 4 as proposed by Bignami et al. The new longitude distribution reported here no longer has such a prominent feature as shown in Figure 5 with a $\sim 5\%$ contribution from PSR 1747-46 subtracted out (see Hartman, these proceedings). The unfolding of the new SAS-2 data shown in Figure 6 is compatible with emission from the 3 kpc feature, however, the explanation of a superimposed nearby source together with statistical fluctuations cannot be ruled out.

ATOMIC HYDROGEN DENSITY DISTRIBUTION IN THE GALAXY

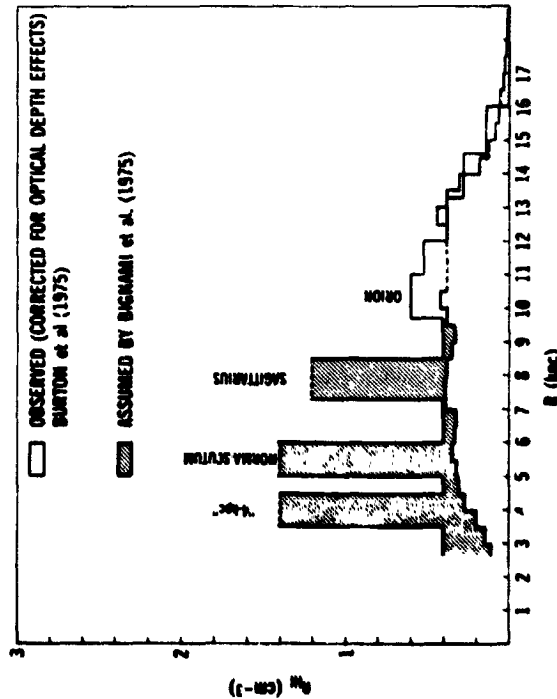


Figure 16. Mean HI density as a function of galactic radius as obtained from 21 cm surveys (Burton et al. 1975) and assumed in the recent spiral arm model of Bignami et al. (1975). This model further assumes that H₂ has the same galactic distribution as HI (contrary to the observations of Scoville and Solomon (1975) and Burton et al. (1975)). It is assumed in the model that $n_{TOT} = KN_{HI}$ with $K = 2$ (Bignami et al. (1975)). Circular symmetry is not assumed in the model and the figure only represents typical positions for the arm features. The model appears to overestimate the volume averaged density of HI (regardless of structural details) as determined by the 21 cm observations (see Stecker et al. (1975) for further discussion).

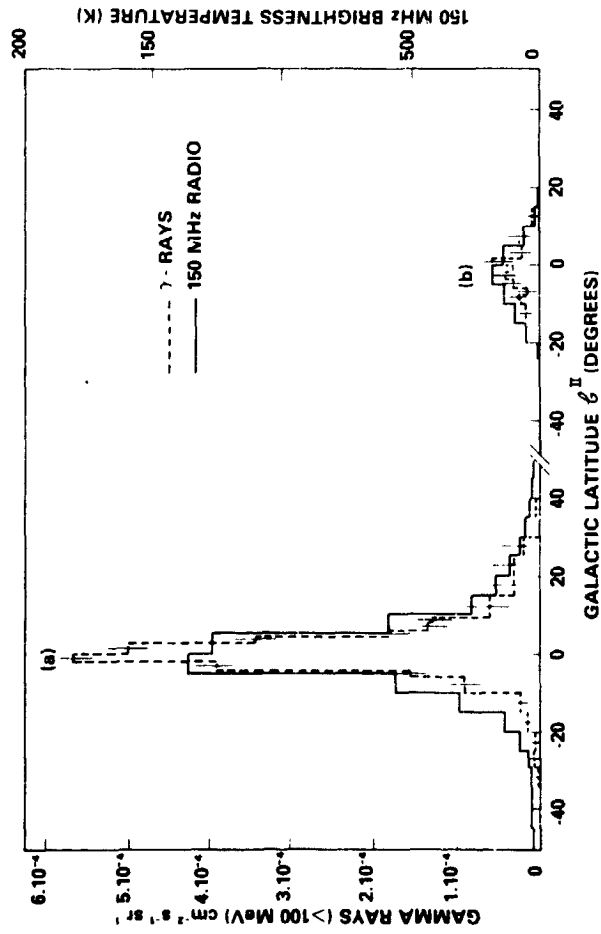


Figure 17. Comparison of latitude distribution of γ -rays (unresolved) and 150 MHz nonthermal emissions in the galaxy for the cen. r (a) and anticenter (b) directions (Paul et al. 1976).

The large peak in the data in the range $310^\circ \leq l \leq 315^\circ$ has been associated by the SAS-2 group (Fichtel et al. 1975) with the "Scutum arm" feature as interpreted by some 21 cm observers. However, the narrow profile of this feature is hard to reconcile with that expected from a spiral arm. An ideal uniform spiral arm will fill in at longitudes closer to the galactic center than the tangential longitude so that it traces out a characteristic longitude distribution shaped somewhat like a shallow letter M. The inside slope of this pattern as calculated by the SAS-2 group in this model should be shallower than that actually observed. Looking at it another way, if one tries to unfold the longitude data for $180^\circ \leq l \leq 360^\circ$, it requires a negative γ -ray emissivity for $R \simeq 7$ kpc (see the dot-dashed curve in Figure 6) in order to obtain the steep slope inside of 315° on the longitude distribution. Since this is clearly nonphysical, one must look for an alternate explanation. One such explanation is to assume that the true flux is near the low end of the statistical error bars. The unfolding then results in the solid line shown in Figure 6 with a relatively small arm type feature at $R \simeq 7.7$ kpc which may be associated with the "Scutum arm." Such a feature is compatible with the mean gas density falling outside of 6 kpc. Another possibility is point source contamination. In order to truly resolve this problem and the whole problem of gas density on the "negative longitude" side of the galaxy, we must await further γ -ray observations with better statistics near 310° and filling in the data gap in the range $290^\circ \leq l \leq 315^\circ$. We also need CO observations from a millimeter wave facility in the southern hemisphere which will have access to this half of the galactic plane, and we also could make use of related far infrared observations (Fazio and Stecker, 1976).

In summary, neither the γ -ray nor CO observations provide clear evidence of arm features at positive longitudes, but an overall larger scale structure, fairly symmetric vis-a-vis positive and negative longitudes, indicating a maximum emissivity in the 5 to 6 kpc region is seen (see Figure 6). Possible evidence of arm features if found at negative longitudes (Fichtel et al. 1975) which may be associated with the complex distribution of HII regions at those longitudes (Puget et al. 1976) but which does not correspond to the flat $\langle n_{\text{HI}} \rangle$ distribution seen in 21 cm observations, even modulated with a large arm-interarm ratio. Such a model will not give the proper intensity or distribution of galactic γ -rays unless the H_2 cloud distribution is taken into account (Stecker et al. 1975). Further evidence for this may be seen in the lack of a "Sagittarius arm" feature at $l = 50^\circ$ which is absent in both the CO observations (Scoville and Solomon 1975, Burton et al. 1975) and the SAS-2 γ -ray observations (Fichtel et al. 1975). A strong Sagittarius arm would also be inconsistent with the γ -ray latitude observations of Samimi et al. (1974). The small γ -ray enhancement in the Cygnus region ($65^\circ \leq l \leq 80^\circ$) has been identified with the Orion arm by the SAS-2 group, however, the existence of the Orion arm is in serious question from the kinematical evidence of HI gas in that region (Burton and Bania 1974) and known

clumpiness of gas with relatively large amounts of CO emission in that region, together with supernova remnants in that direction may help account for the observed γ -ray enhancement.⁴ Additional evidence against cosmic ray confinement in a local ("Orion") arm comes from the lack of cosmic-ray anisotropy in this direction as well as the long-term constancy of the cosmic ray flux (Brecher and Burbidge 1972). New evidence of a possible 2×10^7 yr lifetime for cosmic-rays in the solar neighborhood (Garcia-Munoz et al. 1975) would rule out strict cosmic-ray confinement in arms with a γ -ray production rate proportional to n_H^2 as suggested by Bignami and Fichtel (1974) and Paul et al. (1976). Such a lifetime, although still uncertain (O'Dell et al. (1973), Hagen et al. 1975), would argue for diffusion of cosmic-rays in a larger region of the galaxy (Jokipii 1976) as will be discussed in more detail in the next section, and will support a weaker cosmic-ray correlation with larger scale galactic features as argued by Stecker et al. (1975) on the basis of the CO data.⁵ These authors note that an approximate relation $I_{CR} \propto n_{TOT}^\alpha$ holds in the inner galaxy where $n_{TOT} \approx n_{H_2}$ and $0.2 \leq \alpha \lesssim 0.5$.

8. Implications of a 20 My Lifetime for Cosmic-Rays on Interpretation of the γ -Ray Data. It has been established earlier that there must be a positive overall correlation between cosmic-rays and matter in the galaxy in order to explain the γ -ray production rate. On the other hand, should it be established that cosmic rays have a mean lifetime $\sim 2 \times 10^7$ yr. as obtained by Garcia-Munoz et al. (1975), this would imply a relatively small mean gas density seen by cosmic-rays throughout their lifetime. Studies of cosmic-ray secondaries have revealed that cosmic rays travel through an average of 1.5 to 3×10^{24} atoms/cm² throughout their lifetime in the galaxy. Taking that lifetime to be 6×10^{14} s implies

$$\langle n_H \rangle_{\text{cosmic ray confinement volume}} = \frac{(1.5 - 3) \times 10^{24} \text{ cm}^{-2}}{(3 \times 10^{10} \text{ cm}^3/\text{s}) (6 \times 10^{14} \text{ s})} \approx 0.1 - 0.2 \text{ cm}^{-3} \quad (6)$$

Jokipii (1976) has pointed out that the γ -ray evidence argues against their being trapped in "tunnels" in the galactic disk as suggested by Scott (1975). The other alternative, arguing against confinement in spiral arms, is that the cosmic rays spend considerable time in regions where $n_H \lesssim 0.2 \text{ cm}^{-3}$ as well as those where $n > 0.2 \text{ cm}^{-3}$, and in a region thicker than the gas disk such as the radio-disk or exodisk (see Figure 3). Confinement in a large halo would require a $\sim 10^8$ yr trapping time (Ginsburg and Syrovatskii 1974) and appears not to be

⁴Much of the Cygnus enhancement has now been associated with Cygnus X-3 (Thompson, these proceedings).

⁵Arm effects in the γ -ray longitude profile can, of course, be caused by density and source perturbations alone without invoking cosmic-ray confinement.

consistent with the radio evidence (Webster 1975). In addition confinement in such a large region would tend to wipe out any radial gradient in the cosmic-ray flux as suggested by the γ -ray observations (Stecker 1975, Dodds et al. 1975). Thus, one might presently favor an "exodisk" concept as suggested by Jokipii (1976) and as perhaps as illustrated by the radiodisk studies of some spiral galaxies in the observation of Ekers and Sancisi (1976). An example from these observations is NGC4631 shown in Figure 18. As can be seen from the figure, a fat disk or flat halo type region of synchrotron emission surrounds NGC4631; such a region may also exist around our own galaxy. An even more apt example may be the spiral NGC891 which shows a radiodisk of thickness ~ 4 kpc (Van der Kruit and Allen 1976) and a gas disk, seen in 21 cm, of thickness $\lesssim 500$ pc (Sancisi, quoted by Ekers 1975). (See paper of Baldwin, these proceedings).

9. Comparison of Radio and γ -Ray Longitude Distributions. Paul et al. (1976) have constructed a model of γ -ray emission in our Galaxy based in part on the assumption of the relation $I_e B^2 \propto I_{CR} n_H$ which implies $I_{sync} \propto L_\gamma$. It is my own philosophy that one should eliminate such a priori assumptions and work from the data as much as possible. One can learn from comparisons of the distributions of various galactic emissions, both from their similarities and their differences. It has already been remarked that the 150 MHz radio and γ -ray emissions have different latitude distributions. Figure 19 shows that similarities and differences also exist in the longitude distributions. The SAS-2 γ -ray data is shown by the histogram and the radio data is taken from Price (1974) with the positions of the tangents of 21 cm features shown by the arrows. Note that the γ -ray distribution is generally wider in the inner galaxy than the radio distribution. Both are enhanced in the Cygnus region ($l \simeq 80^\circ$) and in the longitude range near 310° . Note, however, that in the later case, the reported γ -ray emission is relatively much more intense than the 150 MHz emission, supporting the suggestion made earlier in this paper regarding the 310° feature (see Figure 6). The peak in the γ -ray distribution at $\sim 260^\circ$ can be attributed to the Vela pulsar and the enhancement in the anticenter direction is due primarily to the Crab pulsar and another γ -ray source at $l \simeq 193^\circ$.

10. The Galactic Contribution to the High-Latitude γ -Ray Background. The revised Apollo data shown in Figure 20 (Trombka et al. 1976) are consistent with other data in the ~ 1 MeV range and are consistent with cosmological redshifted π^0 -decay processes proposed by the author in the past (Stecker 1969, 1971, Stecker et al. 1971, Stecker 1974, 1975a) which predict a shelf-like feature near ~ 1 MeV and a steep spectrum $\sim E^{-3}$ above 10 MeV. At energies between 35 and 200 MeV, the observed spectrum at high galactic latitudes ($b > 30^\circ$) appears to be flatter than at lower energies, $\sim E^{-(2.4 \pm 0.2)}$ (Fichtel et al. 1975). This can be readily explained as high latitude galactic background emission due to the finite thickness of the galactic γ -ray disk. Taking a typical SAS-2 path length

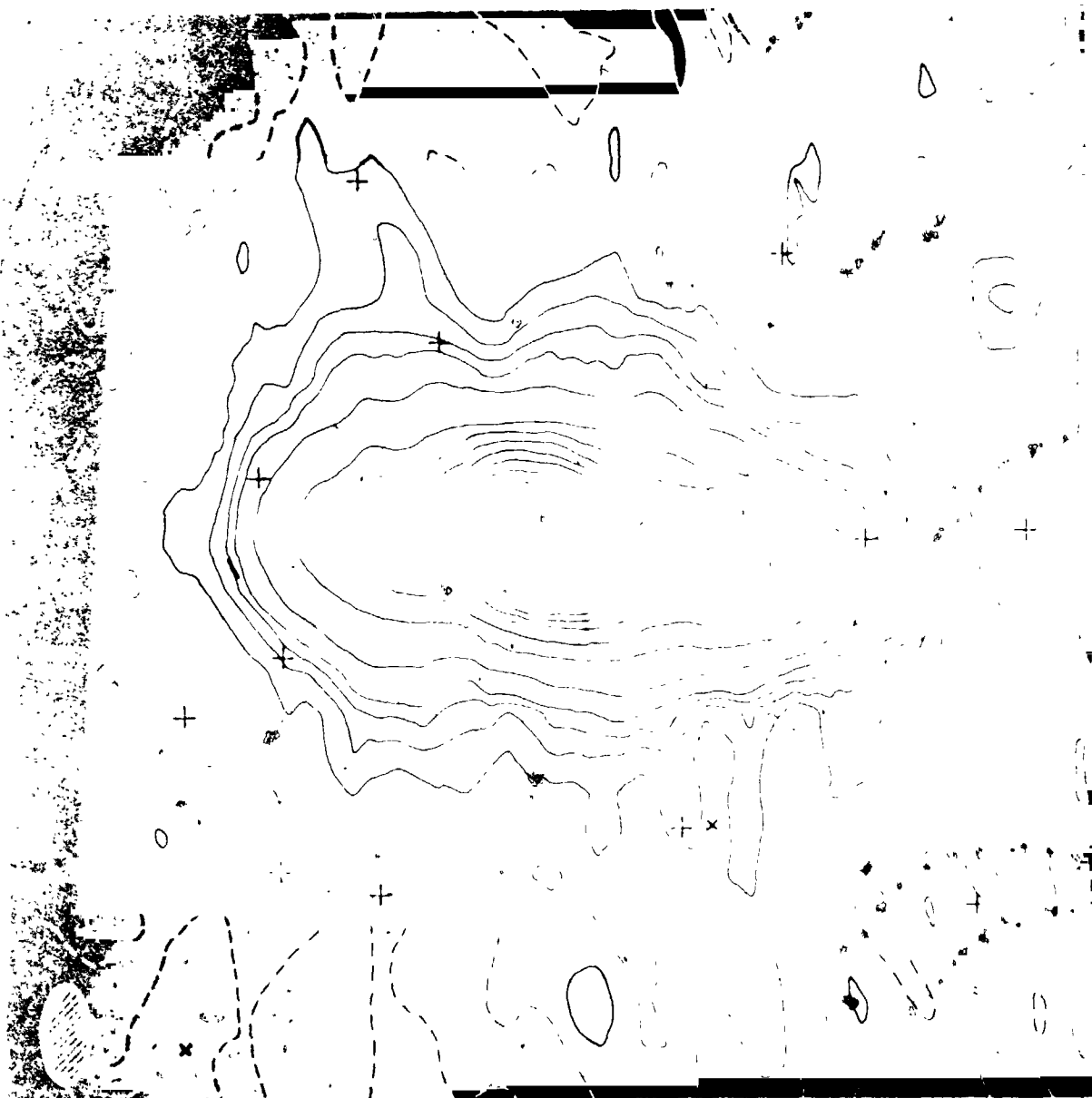


Figure 18. Optical image of the edge-on spiral galaxy NGC 4631 together with preliminary 50 cm radio contours obtained with the aperture synthesis array at Westerbork by Ekers and Sancisi (personal communication).

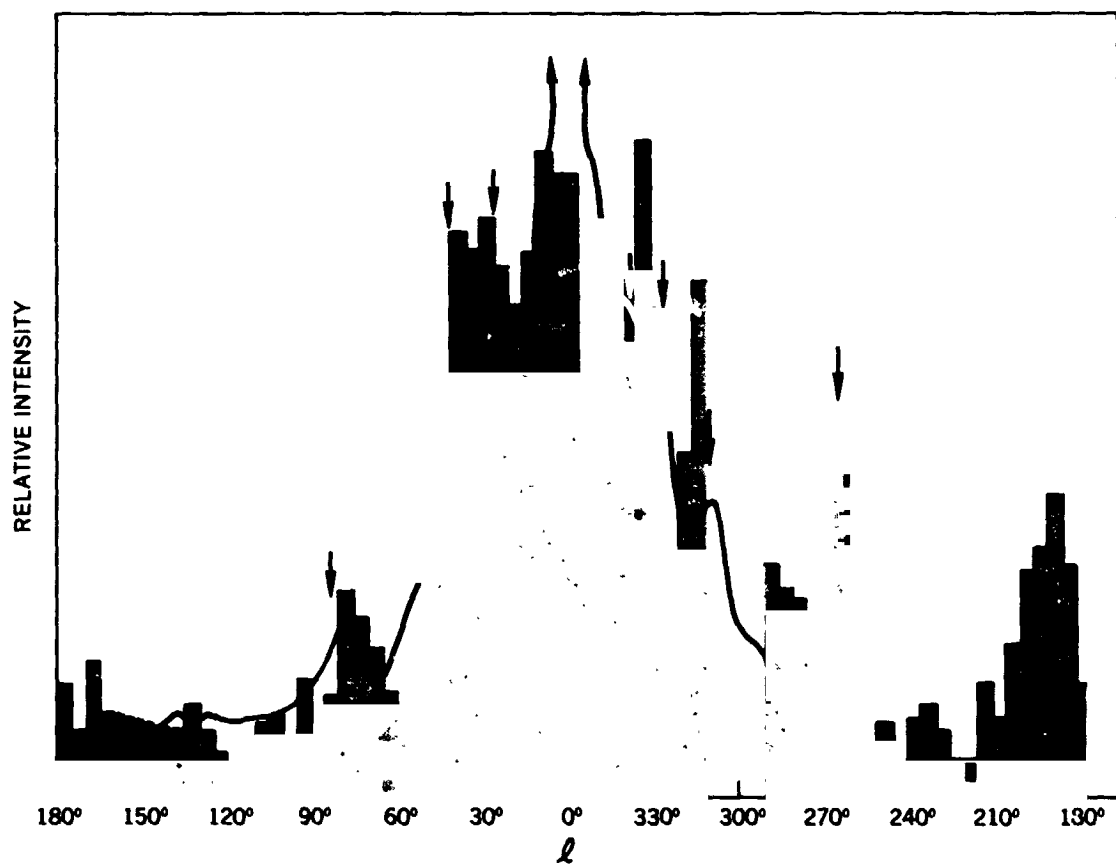


Figure 19. Comparison of longitude distributions of γ -rays (Fichtel et al. (1975) and 150 MHz radio emission (Price 1974).

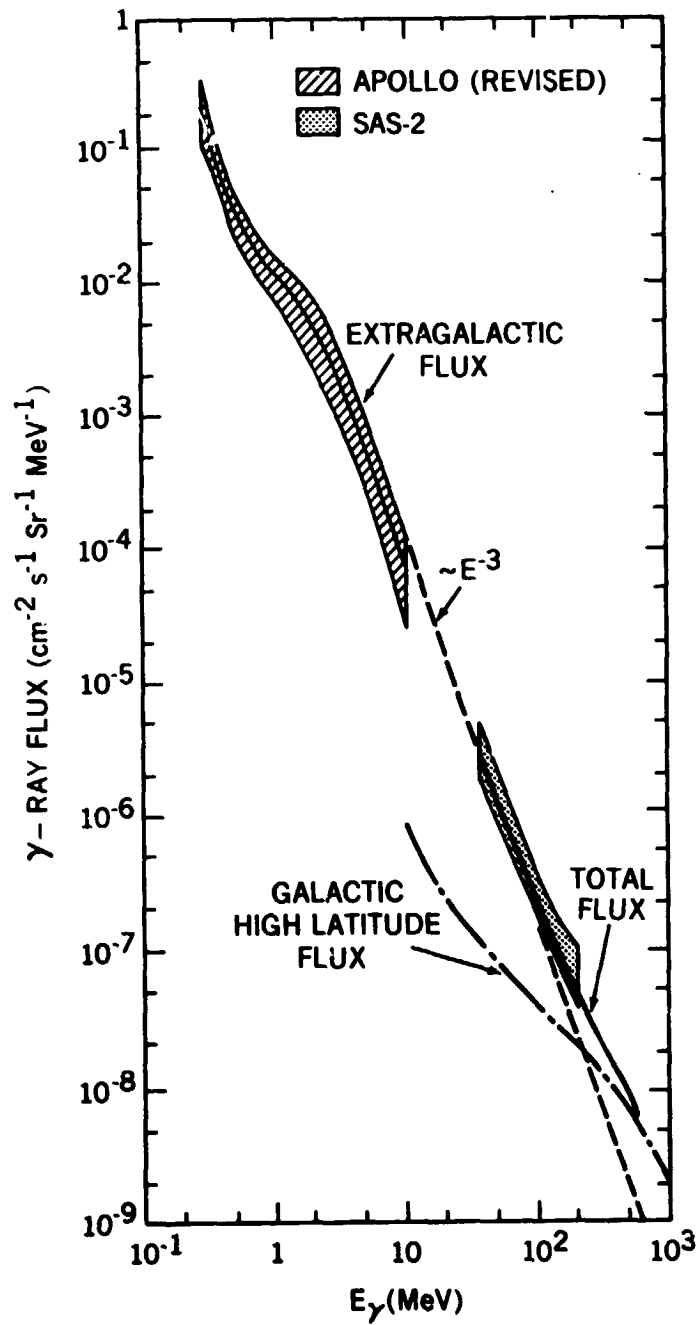


Figure 20. Revised background γ -ray observations from Apollo 15 (re-corrected for intrinsic spurious events (Trombka, personal communication) and high latitude SAS-2 observations (Fichtel et al. 1975). The cosmological background is expected to have a E^{-3} form above ~ 10 MeV from the π^0 -decay models (see Stecker 1975 for discussion and review). The contribution from the high-latitude galactic flux, as calculated in this work, is sufficient to flatten the total spectrum to the shape observed by SAS-2 with an approximate $E^{-2.4}$ form at energies between 35 and 200 MeV. The galactic Compton contribution at high latitudes used here may be underestimated (a larger scale height may be more appropriate.) But this does not significantly change the total flux or shape of the spectrum calculated.

of 3×10^{20} csc b cm^{-2} (Falgarone and Lequeux 1973) with $b = 40^\circ$, and using the differential production rate shown in Figure 2. Choosing an E^{-3} power law above 10 MeV which runs through both the SAS-2 and Apollo data (shown in Figure 20 by a dashed line) and adding in the galactic flux, the total flux expected is shown by the solid line. This can be seen to be flatter than the pure extragalactic background component and consistent with the SAS-2 data. The effect of the galactic contamination can be reduced ideally by $\sim 33\%$ by making observation at $b = 90^\circ$. However, it should be noted that the galactic background can still be expected to dominate at energies above 300 MeV making a proposed test (Stecker 1974, 1975) between the cosmological π^0 -decay models of the γ -ray background invalid.⁶

11. γ -Rays and Galactic Structure: An Approach for the Future. The early optimistic hope of 21 cm observers to delineate the spiral structure of the Galaxy has been dimmed by complications in the analysis of even the most thorough velocity-longitude plots due to kinematic (velocity streaming) effects, nonuniformities within arm features (fragmentation, branching, etc.) and strong non-circular gas velocities as evidenced at $l = 0^\circ$. At the same time, high-resolution 21 cm surveys of external spirals, such as the Rots and Shane (1975) work on M81 shown in Figure 14, have shown that large-scale spiral structure exists in the gas in spiral galaxies, as we know it exists in other components such as dust clouds, HII regions and OB associations. The CO observations of our Galaxy, which should reflect arm structure in young molecular clouds even more strongly than the 21 cm observations, have not revealed such structure in the $0^\circ \leq l \leq 180^\circ$ range. However, they have excitingly revealed a larger scale overall galactic structure which shows a broad maximum in the 5-6 kpc region. The existence of this structure is supported by the γ -ray observations. Strong correlations with other Population I phenomena in the galaxy suggest that a new picture of overall galactic structure is emerging and will lead to new understandings of the nature of the Galaxy.

Some γ -ray observers have exhibited the optimism shown in the early 21 cm work in looking for spiral features. However, it should be remembered that γ -ray observations have some difficulties in their analysis as do 21 cm observations. Three problems inherent to the interpretation of γ -ray observations and not the 21 cm observations are (1) no velocity information to help determine from where in the galaxy emission at a specific longitude originates (2) relatively poor angular resolution in the present data, which restricts fine-scale structure

⁶Theoretical difficulties have arisen with regard to various aspects of the Omnes model for baryon-antibaryon separation in the early universe. At present, the author considers these difficulties to be intrinsically no worse than those with the standard "big-bang" cosmology (see e.g., Gunn and Tinsley 1975). The possibility of some mechanism of baryon separation on a large scale as an explanation for the γ -ray background should not be prematurely discarded at this time.

studies and (3) the fact that the γ -ray emission is proportional to the product of gas density and cosmic-ray intensity integrated along the line-of-sight so that assumptions must be made to separate these two quantities or, preferably, other observations must also be used to determine the gas density.

Of course, the γ -ray observations have their advantages. Optical depth corrections are entirely unnecessary. And, to the extent that the gas density distribution can be obtained by other means (using as much of the electromagnetic spectrum as possible, e.g., radio, microwave and far-infrared observations (Fazio and Stecker (1976)) the galactic cosmic-ray nucleon distribution can then be deduced. Indeed, 100 MeV γ -ray observations are unique in their potential for determining information about the large-scale distribution of galactic cosmic-ray nucleons. Using the above approach, large-scale structure in both the interstellar gas and the cosmic-ray distributions is now becoming apparent. Higher resolution γ -ray observations should enable us to study important unresolved questions about small-scale and spiral structure features. A concerted "synoptic" approach to galactic surveys by observers at all wavelengths should enable us in the future to take advantage of complementary observations and improve our understanding of the structure and dynamics of the galaxy.

References

- Allen, C. W. 1973. Astrophysical Quantities (3rd Ed.), Athlone Press, London.
- Baade, W. 1944. Ap. J. 100, 137.
- Bignami, G. F. and Fichtel, C. E. 1974. Ap. J. (Letters) 189, L65.
- Bignami, G. F., Fichtel, C. E., Kniffen, D. A. and Thompson, D. J. 1975. Ap. J. 199, 54.
- Blumenthal, G. R., and Gould, R. J. 1970, Rev. Mod. Phys. 42, 237.
- Brecher, K. and Burbidge, G. 1972. Ap. J. 174, 253.
- Burton, W. B. 1974. Galactic Radio Astronomy (ed. F. J. Kerr and S. C. Simonson, III) Reidel Pub. Co., Dordrecht, Holland, 551.
- Burton, W. B. 1976. Ann. Rev. Astr. Ap. 14, in press.
- Burton, W. B., and Bania, T. M. 1974. Astr. and Ap. 33, 425.
- Burton, W. B. and Gordon, M. A. 1976. Ap. J. (Letters), in press.
- Burton, W. B., Gordon, M. A., Bania, T. M., and Lockman, F. J. 1975. Ap. J. 202, 30.
- Cowsik, R. and Voges, W. 1974. Proc. ESLAB γ -Ray Symposium, Frascati, ESRO SP-106, 229.
- Daniel, R. R. and Stephens, S. A. 1975. Space Sci. Rev. 17, 45.
- Daugherty, J. K., Hartman, R. C., and Schmidt, P. J. A. 1975. Ap. J. 198, 493.
- Dodds, D., Strong, A. W. and Wolfendale, A. W. 1975. Mon. Nat. RAS. 171, 569.
- Dovzhenko, O. I. and Pomanskii, A. A. 1964. Sov. Phys. JETP 18, 187.
- Ekers, R. D. 1975. Structure and Evolution of Galaxies (ed. G. Setti) Reidel Pub. Co., Dordrecht, Holland, 217.
- Ekers, R. D. and Sancisi, R. 1976. in preparation.

- Falgarone, E. and Lequeux, J. 1973. *Astr. and Ap.* 25, 253.
- Fazio, G. G. and Stecker, F. W. 1976. *Ap. J. (Letters)* 207, in press.
- Fichtel, C. E., Hartman, R. C., Kniffen, D. A., Thompson, D. J., Bignami, G. F., Ögelman, H., Özel, M. E. and Tümer, T. 1975. *Ap. J.* 198, 163.
- Fichtel, C. E., Kniffen, D. A. Thompson, D. J., Bignami, G. F. and Cheung, C. Y. 1976. *Ap. J.* in press.
- Garcia-Munoz, M., Mason, G. M. and Simpson, J. A. 1975. *Proc. 14th Cosmic Ray Conf.* 1, 221.
- Ginzburg, V. L. and Syrovatskii, S. I. 1964. Origin of Cosmic Rays, MacMillan Co., New York.
- Goldstein, M. L., Fisk, L. A. and Ramaty, R. 1970. *Phys. Rev. Lett.* 25, 732.
- Gordon, M. A. and Burton, W. E. 1976. *Ap. J.*, in press.
- Greenberg, J. M. 1971. *Astr. and Ap.* 12, 240.
- Gunn, J. E. and Tinsley, B. M. 1975. *Nature* 257, 454.
- Hagen, F. A., Fisher, A. J., Ormes, J. F. and Arens, J. F. 1975. *Proc. 14th Cosmic Ray Conf. Munich* 1, 361.
- Hayakawa, S., Ito, K., Matsuda, T., Ono, T., and Uyama, K. 1976. *Nature* 261, 29.
- Hulse, R. A. and Taylor, J. H. 1975. *Ap. J. (Letters)* 201, L55.
- Ilovaisky, A. and Lequeux, J. 1972. *Astr. and Ap.* 20, 347.
- Jokipii, J. R. 1976. preprint.
- Kerr, F. J. and Westerhout, G. in Galactic Structure, Stars and Stellar Systems 5 (ed. A. Blaauw and M. Schmidt) U. Chicago Press.
- Kodaira, K. 1974. *Pub. Astr. Soc. Japan* 26, 255.
- Kniffen, D. A., Bignami, G. F., Fichtel, C. E., Hartman, R. C., Ogelman, H. Thompson, D. J., Özel, M. E. and Tümer, T. 1975. *Proc. 14th Cosmic Ray Conf.* 1, 100.

- Kraushaar, W. L., Clark, G. W., Garmire, G. P., Borken, R., Higbie, P., Leong, C. and Thorsos, T. 1972. *Ap. J.* 177, 341.
- Landecker, T. L., and Wieblinski, R. 1970. *Austr. J. Phys. Suppl.* 16, 1.
- Lequeux, J. 1971. *Astr. and Ap.* 15, 42.
- Lockman, F. J. 1976. *Ap. J.*, in press.
- Lyne, A. G. 1974. in *Galactic Radio Astronomy* (ed. F. J. Kerr and S. C. Simonson, III) Reidel Pub. Co., Dordrecht, Holland, 87.
- Mezger, P. A. 1970. *Proc. IAU Symp. No. 38*, Basel, Switzerland (ed. W. Becker and G. Contopoulos) Reidel Pub. Co., Dordrecht, Holland, 107.
- Neugebauer, G., Becklin, E. and Hyland, A. R. 1971. *Ann. Rev. Astr. Ap.* 9, 67.
- O'Dell, F. W., Shapiro, M. M., Silberberg, R. and Tsao, C. H. 1973. *Proc. 13th Cosmic Ray Conf., Denver*, 1, 490.
- Ögelman, H. B. and Maran, S. P. 1975. *Ap. J.*, in press.
- Opik, E. 1953. *Irish Astr. J.* 2, 219.
- Paul, J. Cassé, M. and Cesarsky, C. J. 1976. *Ap. J.*, in press.
- Perek, L. 1962. *Advances in Astron. and Ap.* 1, 165.
- Price, R. M. 1974. *Galactic Radio Astronomy* (ed. F. J. Kerr and S. C. Simonson, III) Reidel Pub. Co., Dordrecht, Holland, 637.
- Puget, J. L. and Stecker, F. W. 1974. *Ap. J.* 191, 323.
- Puget, J. L., Ryter, C. E., Serra, G. and Bignami, G. F. 1976. *Astr. and Ap.* in press.
- Ramaty, R. and Westergaard 1976. preprint.
- Reeves, H. 1975. *Origin of Cosmic Rays* (ed. J. L. Osborne and A. W. Wolfendale) Reidel, Dordrecht, Holland, 135.
- Roberts, M. S., 1974. *Science* 183. 371.

- Roberts, W. W., Jr., Roberts, M. S., and Shu, F. H. 1975. *Ap. J.* 196, 381.
- Rots, A. H. and Shane, W. W. 1973. *Astr. and Ap.* 45, 25.
- Samimi, J., Share, G. H. and Kinzer, R. L. 1974. *Proc. ESLAB γ -Ray Symp., Frascati, ESRO SP-106*, 211.
- Sandage, A. 1961. *The Hubble Atlas of Galaxies*, Carnegie Inst., Washington, D. C.
- Scott, J. S. 1975. *Nature* 258, 58.
- Scoville, N. Z. and Solomon, P. M. 1975. *Ap. J. (Letters)* 199, L105.
- Shu, F. J. 1973. *The Interstellar Medium* (ed. K. Pinkau) Reidel Pub. Co., Dordrecht, Holland, 219.
- Shukla, P. G., Casse, M. and Ceasarsky, C. J. 1975. *Proc. 14th. Cosmic Ray Conf., Munich* 1, 65.
- Sierdakias, J. 1976. in preparation.
- Simonson, S. C., III, 1970. *Astr. and Ap.* 9, 163.
- Simonson, S. C., III, 1976, *Astr. and Ap.* 46, 261.
- Solomon, P. M. and Stecker, F. W. 1974. *Proc. ESLAB γ -Ray Symp., Frascati ESRO SP-106*, 253.
- Stecker, F. W. 1968. *Thesis, Harvard University Library.*
- Stecker, F. W. 1969, *Ap. J.* 157, 507.
- Stecker, F. W. 1970. *Astrophys. and Space Sci.* 6, 377.
- Stecker, F. W. 1971. *Cosmic Gamma Rays*, Mono. Book Co., Baltimore.
- Stecker, F. W. 1973. *Ap. J.* 185, 499.
- Stecker, F. W. 1974, *Proc. ESLAB γ -Ray Symp., Frascati, ESRO SP-106*.
- Stecker, F. W. 1975a. *Origin of Cosmic Rays* (ed. J. L. Osborne and A. W. Wolfendale) Reidel Pub. Co., Dordrecht, Holland, 267.

Stecker, F. W. 1975. Phys. Rev. Lett. 35, 188.

Stecker, F. W. 1976. Nature 260, 412.

Stecker, F. W., Morgan, D. L. and Bredekamp, J. H. 1971. Phys, Rev. Lett. 27, 1469.

Stecker, F. W., Puget, J. L., Strong, A. W. and Bredekamp, J. H., 1974. Ap. J. (letters) 188, L59.

Stecker, F. W., Solomon, P. M., Scoville, N. Z., and Ryter, C. E. 1975. Ap. J. 201, 90.

Strong, A. W. 1975. J. Phys. A 8, 617.

Trombka, et al. 1976. in preparation, also presented at this symposium.

Van der Kruit, P. C. and Allen, R. J. 1976. Ann. Rev. Astr. Ap. 14, in press.

Webster, A. 1975. Mon. Not. RAS 171, 243.

Wentzel, D. G., Jackson, P. D., Rose, W. K. and Sinha, R. F. 1975. Ap. J. (Letters) 201, L5.

GSFC Symposium Registered Participants

Prof. W. David Arnett
Enrico Fermi Institute
University of Chicago
Chicago, IL. 60637

Dr. C. Ayre
The Harrison M. Randall Lab. of Physics
The University of Michigan
Ann Arbor, Michigan 48109

Dr. T. Bai
Code 660
NASA/GSFC
Greenbelt, MD 20771

Dr. V. K. Balasubrahmanyam
Code 661
NASA/GSFC
Greenbelt, MD 20771

Dr. John E. Baldwin
Cavendish Laboratory
Madingley Road
Cambridge, England 66477

Dr. W. Baldwin
Department of Astronomy
University of Virginia
Charlottesville, Va.

Dr. T. M. Bania
National Radio Astronomy Obs.
Edgemont Road
Charlottesville, VA. 22901

Dr. B. Beron
High Energy Physics Laboratory
Stanford Univ.
Stanford, California 94305

Dr. David Bertsch
Code 662
NASA/GSFC
Greenbelt, MD 20771

Dr. G. F. Bignami
Universita Di Milano
Istituto Di Science Fisiche
Aldo Pontromeli
Via Veloria 16
Milano, Italy 20133

Dr. Albert Boggess
Code 673
NASA/GSFC
Greenbelt, MD 20771

Dr. Ralph Bohlin
Code 672
NASA/GSFC
Greenbelt, MD 20771

Dr. E. Boldt
Code 661
NASA/GSFC
Greenbelt, MD 20771

Dr. R. Buccheri
Universita di Palermo,
Istituto Fisica Universita,
Via Archirafi 36,
Palermo, Italy

Dr. W. B. Burton
National Radio Astronomy Obs.
Edgemont Road
Cherlottesville, VA 22901

Dr. E. L. Chupp
Physics Department
University of New Hampshire
Durham, NH 03824

Dr. J. F. Clark
Code 100
NASA/GSFC
Greenbelt, MD 20771

Dr. Thomas L. Cline
Goddard Space Flight Center
Code 661
Greenbelt, MD 20771

Dr. Richard Cohen
NASA Goddard Institute for Space Studies
2880 Broadway
New York, N.Y 10025

Dr. John T. Cowan
Astronomy Program
University of Maryland
College Park, MD 20742

Dr. Carol Crannell
Code 682
NASA-GSFC
Greenbelt, MD 20771

Dr. Glen Dahlbacka
Lawrence Livermore Lab
L-32
Livermore CA 94550

Dr. Upendra Desai
Code 663
NASA/GSFC
Greenbelt MD 20771

Dr. M. Dubin
Code 680
NASA/GSFC
Greenbelt, MD 20771

Dr. L. Dunkelman
Code 673
NASA/GSFC
Greenbelt, MD 20771

Dr. P. Durouchoux
CEA-CEN Saclay
DPH/EP
BP 2
Gif sur Yvette 31
France

Dr. C. Dyer
Code 682
NASA/GSFC
Greenbelt, MD 20771

Dr. Engel
Imperial College of Science
and Technology
Prince Consort Road
London SW72AZ, England

Mr. Charles Ehrmann
Code 663
NASA/GSFC
Greenbelt, MD 20771

Dr. L. Evans
Code 682
NASA/GSFC
Greenbelt MD 20771

Dr. G.G. Fazio
Smithsonian Astro
60 Garden ST
Cambridge MA 02138

Dr. Carl Fichtel
Code 660
NASA/GSFC
Greenbelt, MD 20771

Dr. Richard Fahey
Code 671
NASA/GSFC
Greenbelt, MD 20771

Mr. D. Galasso
Code 682
NASA/GSFC
Greenbelt, MD 20771

Dr. D. Gilman
Clark Hall
Cornell University
Ithaca, NY 14850

Dr. M. Goldstein
Code 692
NASA/GSFC
Greenbelt, MD 20771

Prof. K. Greisen
Dept Phys. Clark Hall
Cornell Univ
Ithaca NY 14850

Dr. J.E. Grindlay
Harvard College Observatory
60 Garden Street
Cambridge, Massachusetts 02138

Dr. R.C. Hartman
Code 662
NASA/GSFC
Greenbelt MD 20771

Dr. Michael Hauser
Code 661
NASA/GSFC
Greenbelt MD 20771

Prof. R.C. Haymes
Space Science Department
Rice University
Houston, Texas 77001

Dr. W. Hermsen
Cosmic-Ray Working Group Huygens Labororium
Leiden, The Netherlands

Dr. E.B. Hughes
High Ener Phys Lab
Stanford Univ
Stanford CA 94305

Dr. W.L. Imhof
Lockheed Palo Alto Research Laboratory
3251 Hanover Street
Palo Alto, CA 94304

Dr. A. Ito
Dept. of Physics and Astronomy
Univ. of MD
College Park, MD 20771

Dr. Allen S. Jacobson
183-901 Jet Propulsion Laboratory
California Institute of Technology
Pasadena, CA 91103

Dr. E.B. Jenkins
Princeton University Observatory
Princeton, NJ 08540

Dr. W.N. Johnson
Naval Research Lab Code 7128
Washington, D.C. 20375

Dr. Frank Jones
Code 602
NASA/GSFC
Greenbelt, MD 20771

Dr. G. Kanbach
Max Planck Institute fur Physik
und Astrophysik
Institute fur Extraterrestrische Physik
8046 Garching-bei-Munchen, Germany

Dr. F.J. Kerr
Astronomy Program
University of Maryland
College park, MD 20742

Dr. R. Kinzer
Code 7120 13
Naval Research Lab
Washington D C 30475

Dr. A. Klimas
Code 692
NASA/GSFC
Greenbelt, MD 20771

Dr. Donald A. Kniffen
Code 662
NASA/GSFC
Greenbelt, MD 20771

Dr. Fred Knight
University of California
San Diego
Dept of Physics, Code-011
La Jolla CA 92093

Dr. David Koch
American Science & Engineering
955 Massachusetts Avenue
Cambridge MA 02139

Dr. L. Koch
Service d'Electronizue
Centre D'Etudes Nucleaires de Saclay
Gif-sur-Yvette
France

DR. J. Kurfess
Code 7122
Naval Research Lab
Washington, D.C 20375

Dr. Richard Lamb
Code662
NASA/GSFC
Greenbelt, MD 20771

Dr. L. C. Lee
Code 002
NASA/GSFC
Greenbhl, MD 20771

Dr. Marvin Leventhal
Room 1C-302
Bell Telephone Lab Inc.
Murray Hill NJ 07974

Dr. James Ling
Jet Propulsion Laboratory
California Institute of Technology
Pasadena, CA 91103

Dr. R. B. Lingenfelter
University of California
Department of Astronomy
Los Angeles, CA 90024

Dr. F. J. Lockman
National Radio Astron. Obs.
Edgemont Rd.
Charlottesville, VA 22901

Dr. Crawford MacCallum
Sandia Laboratories
Albuquerque, NM 87115

Dr. Glenn Mason
Fermi Inst. Nuclear Studies
University of Chicago
Chicago, IL 60637

Dr. Mather
Code 661
NASA/GSFC
Greenbelt, MD 20771

Dr. Christian Matzler
Code 660
NASA-GSFC
Greenbelt, MD 20771

Mr. G. Maurer
Code 682
NASA/GSFC
Greenbelt, MD 20771

Dr. H. A. Mayer-Hasselwander
Max-Planck-Institute for Extraterrestrische Physik
8046 Garching bei
Munchen, Germany

Dr. Brian McBreen
Department of Physics
University College
Dublin Ireland

Dr. F. McDonald
Code 660
NASA/GSFC
Greenbelt, MD 20771

Dr. Jaylee Mead
Code 671
NASA/GSFC
Greenbelt, MD 20771

Dr. Charles Meegan
Marshall Space Flight Center
Code ES-22
Huntsville, AL 35812

Dr. T. Montmerle
Centre d'Etudes Nucleaires de Saclay
Division de la Physique Service d'Electronique
Physique
Boite Postal No. 2
91190 Gif-sur-Yvette
France

Prof. Philip Morrison
Mass Institute of Tech. 6 308
Cambridge MA 02139

Dr. G. Morfil
Max Planck Institute fur Physik und Astrophysik
Institute fur Extraterrestrische Physik
8046 Garching bei Munchen
West Germany

Dr. L. Moskaleva
Institute of Geochemistry and Analytical Chemistry
USSR Academy of Sciences
Moscow, USSR

Dr. M. Mustafa
Code 682
NASA/GSFC
Greenbelt, MD 20771

Dr. George H. Nakano
Organ 52-12 Bldg. 205
3251 Hanover Street
Palo Alto CA 94304

Dr. Naraman
Tata Institute of Fundamental Research
Bombay 400-005
India

Dr. Hakki Ogelman
Faculty of Science-Dept. of Theoretical Physics
Middle East Technical University
Ankara, Turkey

Dr. K. Omidvar
Code 602
NASA/GSFC
Greenbelt, MD 20771

Dr. E. N. Parker
Fermi Institute for Nuclear Studies
University of Chicago
Chicago, IL 60637

Dr. J. Paul
Centre d'Etudes Nucleaires de Saclay
BP 2,91 Gif-sur-Yvette,
FRANCE

Dr. Charles Pellerin
Code 662
NASA/GSFC
Greenbelt, MD 20771

Dr. George F. Peiper
NASA/GSFC Code 600
Greenbelt MD 20771

Dr. Bernard Peters
Danish Space Research Inst.
LUNDLOFTEVEJ 7
2800 LYNGBY
Denmark

Dr. J. L. Puget
Department d'Astrophysique Fondamenrale
DAF Observatoire de Meudon
France

Dr. R. Ramaty
Goddard Space Flight Center
NASA Code 660
Greenbelt MD 20771

Dr. William Roberts Jr.
Dept. of Applied Math & Computer Science
University of Virginia
Charlottesville, VA 22901

Dr. Nancy Roman
NASA Headquarters Code S.G.
Washington DC 20546

Dr. Herman Rothermel
Code 662
NASA/CSFC
Greenbelt, MD 20771

Dr. Arnold Rots
National Radio Astronomy Observatory
Edgemont Rd.
Charlottesville, VA 22901

Dr. L. Scarsi
Universita di Palermo, Istituto Fisica Universita
Via Archirafi 36
Palermo, Italy

Dr. E. Schatzman
Institute Dastrophysique
98 Bis Bldg. Arago
Paris 14
France

Dr. W. Schmidt
Code 660
Goddard Space Flight Center
Greenbelt, MD 20771

Dr. V. Schonfelder
Max Planck Institut fur Extraterrestrische Physik
8046 Garching bei Munchen
Germany

Dr. N. Z. Scoville
Dept. of Physics and Astronomy
Univ. of Mass.
Amherst MA 01002

Dr. Nathan Seeman
Code 7025
Naval Res. Lab
Washington, DC 20375

Dr. John Seiradakis
Max-Planck Inst. fur Radioastronomie
Auf dem hugel 69
53 Bonn 1
West Germany

Dr. Maurice M Shapiro
Naval Research Lab
Cosmic Ray Physics 7020
Washington, DC 20390

Dr. A. Schardt
Code 660
NASA/GSFC
Greenbelt, MD 20771

Dr. Gerald H. Share
Code 7120 14
Naval Research Lab
Washington, DC 20375

Dr. P. Shukla
Service d'Electronique Physique
Centre D'Etudes Nucleaires de Saclay
Gif-sur-Yvette
France

Dr. R. Silberberg
Cosmic Ray Physics Lab
Naval Research Lab Code 7028
Washington, DC 20375

Dr. G. Simpson
Space Science Center
Univl. of New Hampshire
Durham, NH 03824

Dr. R. P. Sinha
Astronomy Program
Univ. of MD
College Park, MD 20742

Dr. Barham Smith
Code 660.1
NASA/GSFC
Greenbelt, MD 20771

Dr. P. M. Solomon
Earth and Space Sciences Dept.
State Univ. of New York
Stony Brook, NY 11714

Dr. Lyman Spitzer
Princeton University Observatory
Princeton, NJ 08540

Dr. T. Stecher
Code 672
Goddard Space Flight Center
Greenbelt, MD 20771

Dr. Floyd Stecker
Code 602
NASA-GSFC
Greenbelt, MD 20771

Dr. Gary Steigman
Yale University Observatory
Box 2023 Yale Sta.
New Haven, CT 06520

Dr. S. A. Stephens
Johnson Space Flight Center
T N 2
Houston, TX 77058

Dr. P. A. Sturrock
Insti. Plasma Res.
Stanford Univ.
Stanford CA 94305

Dr. Yu. A. Surkov
Institute of Geochemistry and Analytical Chemistry
USSR Academy of Sciences
Moscow, USSR

Dr. B. N. Swanenburg
Cosmic Ray Working Group, Huygens Laboratorium
Leiden , The Netherlands

Dr. Jean Swank
Code 661
NASA/GSFC
Greenbelt, MD 20771

Dr. B. Taylor
Space Science Dept. (ESLAB)
ESTEC, Noordwijk
The Netherlands

Dr. B. Tægarden
Code 661
NASA/GSFC
Greenbelt, MD 20771

Prof. K. Thielheim
Institut für Reine und
Angewandte Kernphysik der
Universität Kiel
Kiel, West Germany

Dr. Dave Thompson
Code 662
NASA-GSFC
Greenbelt, MD 20771

Dr. Hugh S. Tornabene
6012 Westchester Park Dr # T1
College Park MD 20740

Dr. J. Trair-o
Code 663
NASA-GSFC
Greenbelt, MD 20771

Dr. J. Trombka
Code 682
NASA-GSFC
Greenbelt, MD 20771

Dr. Melville P. Ulmer
SAO/HCO
Center for Astrophysics
60 Garden Street
Cambridge MA 02138

Dr. A. Underhill
Code 670
Goddard Space Flight Center
Greenbelt, MD 20771

Dr. M. S. Vardya
Code 671
NASA/GSFC
Greenbelt, MD 20771

Larry Varnell
183-401
Jet Propulsion Lab.
Pasadena, CA 91106

Dr. G. Vedrenne
Centre d'Etude Spatiale
des Rayonnements
Complexe Aerospatial de Toulouse-Lespinet 31 Toulouse
France

Dr. C. Wende
Code 601
NASA/GSFC
Greenbelt, MD 20771

Dr. C. Wentz
Code 682
NASA/GSFC
Greenbelt, MD 20771

Dr. G. Westerhout
Astronomy Program
University of Maryland
College park, MD 20742

Dr. William A. Wheaton
Center for Space Research MIT
Cambridge, Mass. 02139

Dr. R. Stephen White
Department of Physics
University of California
Riverside CA 92502

Dr. J. Willett
183-901
Jet Propulsion Laboratory
Calif. Inst. of Technology
4800 Oak Grove Dr.
Pasadena, CA 91103

Dr. R. D. Wills
Space Science Dept. (ESLAB)
ESTEC, Noordwijk
The Netherlands

Dr. P. Yasskin
Code 602
NASA/GSFC
Greenbelt, MD 20771

Dr. A. Zych
Inst. Geophys/Planetary Science
Calif. Univ. at Riverside
Riverside CA 92502